DIGITAL CONTROL OF RECTIFIER FIRING ANGLES FOR THE ZERO GRADIENT SYNCHROTRON (ZGS) RING MAGNET POWER SUPPLY*

Martin J. Knott, Lloyd G. Lewis, and Herbert H. Rabe
Argonne National Laboratory
Argonne, Illinois

Abstract

The heart of the new control system for the ZGS ring magnet power supply is a counter that counts from 0 to 3600 each voltage cycle of the main generator. This provides an electrical degree scale that is synchronized with the generator voltage wave by a phase-lock feedback loop. Digital gates compare the number in the counter with the desired angle forfiring each of the 12 rectifier phases. At eauality, a pulse is generated and applied to the control grids of the appropriate mercury vapor rectifiers. Fast digital arithmetic adder circuits upclate the desired firing angles for each of the 12 phases in response to commands from the ZGS programmer and in response to feedback signals from beam spill monitors and from $\dot{B}$ pickup coils on the ring magnet. Separate digital arithmetic adders and selectors provide individual adjustment of each phase in order to reduce low frequency ripple. This system has greatly reduced 50-, 100-, and 150-cycle ripple on the ring magnet field on flattop and on porches, has provided fast action to permit spill control when the RF accelerating cavity is off, and has provided stable operation in full rectify for the accelerating part of the ZGS cycle.

Introduction

The new slow resonance extraction system for the ZGS provides two simultaneous beams that have *no* RF structure. The system accomplishes this by turning off the RF accelerating cavity early in flattop and then, after the beam has debunched, by moving the beam to the $\nu_r = 2/3$ extraction point with the ring magnet control system. The rate of extraction is then controlled through manipulation of the ring magnet field.

This magnetic spill mode places specific demands on the control system for the ring magnet power supply. One of these demands is that the system must be able to rapidly change the voltage applied to the ring magnet. The required speed and accuracy are determined by the amount of beam steering needed to start and maintain the extraction at a selected rate.

A second demand is that the control system for the ring magnet minimizes the generation of low frequency ripple. This is important because the ripple produces modulation of the extracted beam intensity.

An additional requirement is that the ring magnet control system be capable of operating in full rectify; that is with natural commutation from phase to phase. This provides the minimum accelerating time and the desired conditions for beam injection into the ZGS.

ZGS Ring Magnet

The ZGS ring magnet circuit contains eight magnets and eight power supplies connected in a series circuit with four-fold symmetry.[1] The result is the equivalent of a 12-phase supply in each quadrant of the ring magnet.

The rectifiers in each of these eight supplies are mercury vapor tubes. The excitation arc operates continuously so that firing control is provided by two grids placed between the cathode arc and the anode.

Each of the eight supplies is provided with a low pass LC filter. The filter has a rolloff of 40 dB/decade and a corner frequency of about 40 Hz. The filter is underdamped with a damping ratio of about 0.3.

Ripple Amplitudes

Ripple amplitudes produced by the ZGS ring magnet power supply were measured in two ways. The first was to use the fast gauss clock in the ZGS programmer. The clock output was sent to a digital-to-analog (D—A) converter and to an oscilloscope. The gauss pictures from the oscilloscope showed that most of the ripple produced by the original analog control system was at low frequencies. Amplitudes at ~ 50 cycles (generator frequency) were of the order of 1 or 2 G. The 12th harmonic was not readily observed on this display.

The second method was to look at the dc voltage across one pair of ring magnets. This was a more convenient signal for ripple studies since the relative amplitudes of the several harmonics were more favorable for measurement.

The relatively large low frequency ripple (at less than the 12th harmonic) results from a variety of causes. One cause is the incorrect spacing of rectifier firing pulses. A second cause is the characteristics of the low pass filter which attenuates poorly at the low frequencies. Additional causes include possible errors in the number of turns on the polyphase transformer windings, variations in the leakage inductance from one phase winding to another, lack of symmetry in circuit resistances, and imbalances between phases of the generator voltage.

The effects of some of these causes of low frequency ripple can be cancelled on flattop by properly retarding or advancing the firing time of one or several of the 12-phase rectifiers with respect to the others. From this, it is apparent that exactly uniform spacing of the firing pulses to the rectifiers will not produce minimum ripple.

Firing Accuracy

The bias voltages *to* the unijunctions in the original firing control system were readjusted to produce a significant change in the ripple at the generator frequency. These changes in firing angles were measured with the digital phase-angle meter used for routine monitoring of the ZGS ring magnet supply.

The data showed that substantial reductions in the low frequency ripple could be obtained if the firing

*Work performed under the auspices of the U. S. Atomic Energy Commission.

angles of the 12-phase rectifiers were reproducible to 1/10 of an electrical degree. This is far beyond the accuracy and stability of conventional analog ramp type control systems. For this reason, a digital control system was designed and installed at the ZGS.

Rectifier Grid Drive

The control of firing angles to 0.1° electrical corresponds to controlling the turn-on of a rectifier to about 5 μs. Any variation in the turn-on time of a single rectifier must be smaller than this if the control accuracy is to be achieved. In a similar way, variation in the average time delay from one rectifier to another must be shorter than 5 μs.

High voltage switch-transistors were used to provide the drive to the grids of the rectifier tubes. The firing pulse from the control circuit was coupled through a well insulated pulse transformer to a drive module that operated at rectifier cathode potential. The 1/2 μs pulse was lengthened to 4 ms by a single shot amplifier located at cathode potential. This lengthened pulse was applied to switch-transistors that supplied the grid drive signal.

The grids were switched to *t300* V with respect to the cathode with a rise time of 600 ns. Under these conditions, the tube turn-on was about 1 μs at low currents and also at high currents when the tube was first used. At high currents, the time delay and the jitter increased during the first two minutes. At equilibrium, the delay varied from a minimum of about *2* μs to a maximum of about 5 μs. We believe that this increase in turn-on delay is caused by outgassing of the electrodes under high current loads.

Turn-off of the rectifier by removal of the positive anode voltage left a plasma in the space between the grids and the cathode arc. This caused grid currents that lasted long enough to influence the next turn-on. For this reason, a switch-transistor was used to clamp grid #1 to a negative bias when the tube was off. This bias swept out the ions left in the interelectrode space in about 1/2 ms.

Number System and Logic

The digital parts of the control system shown in the block diagram of Fig. 1 use the binary number system. This was chosen since the input from the ZGS programmer is in one's complement form and because of convenience in construction.

The DISPLAY system uses LED numeric display elements driven by a binary coded decimal counter. This is convenient for checkout by the maintenance personnel.

The digital logic utilizes 7400 series TTL-MSI integrated circuits. About 250 integrated circuit chips are mounted in dual in-line packages and are interconnected by wire-wrap wiring. The propagation delays for this logic series vary from package to package but are of the order of a few tens of ns.

Phase Lock Loop

The generator voltage wave varies in frequency during the ZGS cycle and is very distorted. Rectifier commutation produces notches in the generator voltage wave that are as large as 25% of the peak voltage. For this reason, a zero crossing type of reference is not suitable even when the input wave is heavily filtered. This is true because the filters that were tried produced variable phase shifts and/or large transients when entering flattop and invert. The phase-lock loop shown in the upper right portion of Fig. 1 was found to operate satisfactorily.

In this loop, a dc tachometer voltage from the main generator and the output voltage from the filter are added in an operational amplifier. The resultant voltage drives a voltage-to-frequency (v—f) converter that produces a sawtooth wave. This sawtooth drives a binary that divides the frequency by two and produces a square wave with ±10 V output levels.

It is well known that the mathematical product of two sine waves of the same frequency but different phases produces a dc component plus a second harmonic component. The dc component depends on the phase difference between the two sine waves.

In a similar way, the product of a square wave and a distorted sine wave of the same period produces a dc component that is a function of the phase difference between the two waves. This fact is utilized in the loop in Fig. 1 by feeding the distorted sine wave from the generator bus and the square wave from the frequency divider to a transconductance type analog multiplier. The output which contains dc and ac components is fed to the low-pass filter to complete the feedback loop.

This loop would operate without the dc tachometer input; but since the maximum loop gain is finite, the phase difference between the ac reference and the square wave in locked operation would vary with generator speed. The dc tachometer input amplitude is adjusted so that the dc output of the filter is nearly zero in the locked condition. In this way, the phase difference between the ac reference and the square wave is made very nearly 90° and independent of generator speed.

Main Counter Loop

The MAIN COUNTER and its associated feedback loop are shown in the upper left part of Fig. 1. The function of this counter is to provide a digital degree scale that has 360.0° per generator cycle and that is phase synchronized with the square wave from the phase-lock loop. Its operation is described below.

The dc tachometer voltage, shown in the upper left of Fig. 1, is multiplied by a constant in the SERVO CONTROL. The product is then applied to the input of the v—f converter. The gain constant is adjusted to give very nearly 160 counts per electrical degree of the generator wave. In this way, the main counter receives very nearly 16 x 3600 counts each generator cycle, without the feedback loop's correction. This makes the action of the feedback loop almost independent of generator speed.

The main counter is provided with gates that clear the counter to zero each time the total count reaches 16 x 3600. The gates generate a ROLLOVER pulse at the same time that the counter is cleared. No other input clears the counter, thus assuring 360.0° per main counter cycle.

The main counter is synchronized with the phase-lock loop in the following way. The positive-going edge of the square wave from the phase-lock loop ÷ 2 loads a register with the number from the main counter. This number is then subtracted from a reference number, obtained by adding a BIAS to the number contained in the RECTIFY D.S. digital switch. This difference is the digital servo-loop error signal and represents the amount that the main counter is ahead or behind the reference square wave from the phase-lock loop. The difference is loaded into a second register that feeds a d—a converter, thus furnishing a voltage error signal.

This voltage error signal feeds a proportional and an integral network in the servo control. The effect is to speed up or slow down the v—f converter *so* that the number transferred from the main counter is equal to the reference number.

Full Rectify Adjustment

The main counter control loop contains a reference number that may be changed to adjust the firing pulse times for full rectify. At full rectify (000.0° from the programmer), the RECTIFY D.S. is changed in 0.1° increments until the firing pulses are correctly timed. The digital phase angle meter is used to check this. At correct adjustment, the RECTIFY D.S. plus the BIAS has a nominal value of 180.0°. Small variations are caused by the effects of noise on the phase-lock loop.

Preset Counter

Under ideal conditions at full rectify, rectifier #1 turns on when the number in the main counter is 30°, rectifier #2 when the number is 60°, etc., and rectifier #12 when the number is 360°. At invert, each rectifier turn-on is delayed up to 155° so that several of the rectifier turn-on angles will occur in the following cycle of the main counter. The logic problems associated with this situation are avoided by using the PRESET COUNTER shown below the main counter in Fig. 1.

The preset counter counts by 0.1° steps and has a range of 819.1°. It is not cleared to zero but is preset to the number in the main counter at a specific time each cycle. The PRESET CONTROL logic operates so that in effect, the time for the presetting is after rectifier #12 has turned on and also is after the rollover of the main counter. If rollover has not occurred before turn-on of rectifier #12, the preset control in effect locks out the unwanted comparator output pulses generated between the time of rectifier #12 turn-on and the time of rollover.

The range of the preset counter and the method of presetting it require that the "B" input to the comparator has the following ranges:

Rectifier #1 varies from 15° to 200°
Rectifier #2 varies from 45° to 230°
Rectifier #3 varies from 75° to 260°
. . . . . .
Rectifier #12 varies from 345° to 530°

Lag Register

In normal operation, the ZGS programmer makes the major part of the changes in rectifier firing angles. This is done through the programmer input to the SELECTOR at the bottom of Fig. 1. The number of degrees of firing delay is put in the 0005 register at any time. The number is then transferred to the 0005' register under internal timing control.

The number in the LAG REGISTER is subtracted from the number in the 0005' register. The difference is divided by 256 and the quotient added to the initial value of the number in the lag register. The lag register then approaches the number in the 0005' register along a digitally generated "exponential." The time constant is controlled by the RATE logic and is selected from the *ZGS* programmer. The output "L" is thus made to change slowly enough to prevent arc faults in the rectifiers and to prevent distortions in the ring magnet field that would reduce the beam intensity.

Under fault conditions, the safety interlocks switch the selector from programmer input to a steady invert angle.

Maximum Invert Angle

The rectifier arc fault rate is dependent on the amount of firing delay used. Less delay is permissible at high magnet currents than at low currents. The control system is therefore provided with logic that limits the firing delay.

The MAXIMUM INVERT adjustment digital switch is shown at the lower left of Fig. 1. The hold button on the register permits changes during operation of the ring magnet. The digital switch angle is added to a fixed 108.8° to get the total maximum angle.

The CURRENT COMPENSATION input at the lower left of Fig. 1 is a voltage obtained from a magnet current transductor. This voltage is fed to a sample and hold (S/H) and then to an a—d converter. The number in the associated register is proportional to magnet current. The amplifier gain may be changed to adjust the amount of compensation.

The current compensation angle is subtracted from the maximum invert angle to give a limit "M" that varies with magnet current. This value "M" and the lag register number "L" go to a COMPARATOR and SELECTOR that make the number at "G" equal to the smaller of these two inputs to the comparator.

Phase Counter

The phase counter (φCNT), located in the lower right of Fig. 1, controls the distribution of firing pulses to the several rectifiers and determines the angular increments between the rectifier firings. The operation is as follows.

Consider the φCNT to be in the first of its 12 states. The counter output and DECODE gates condition DRIVER #1 to transmit the next comparator pulse to rectifier #1. The counter output causes the 30°INC generator output "C" to be zero and connects D. S. 1 digital switch to the E input to the adder. The output of this adder can be adjusted between 0° and 30° by adjusting D. S. 1.

If the programmer input is 0^{o} (full rectify) and if the FEEDBACK is not in use ($F=15^{o}$), the B input to the comparator may be from 15^{o} to 45^{o} depending on the D.S. 1 setting.

As soon as the number in the preset counter equals or exceeds the number B, a comparison pulse is generated. This pulse is transmitted to rectifier #1 and causes the ϕCNT to advance to the second state.

In this second state, D.S. 2 digital switch is connected by the selector to output E and driver #2 is conditioned. In this case, the 30^{o}INC generator output has a value of 30.0^{o}.

This process continues to fire each of the 12 rectifiers in the proper sequence. The ϕCNT is self-synchronizing at startup of the system because of the equal to or greater than action of the comparator.

Feedback

The digital control system is provided with a fast channel that may be used in conjunction with other control systems such as the $\dot{B}$ feedback control and the external beam intensity control.

The feedback system, located at the bottom of Fig. 1, consists of an input amplifier, a S/H, an a—d converter, and a register (REG). The input voltage range is -20 to t20 V. The a—d converter has an output range of 0^{o} to 30.0^{o}. When the feedback input is not in use. the REG is held at 15.0^{o}.

Model

Dynamic checks of the digital control of the rectifier firing angles are done through use of the MODEL. This model contains two small 6-phase transformers supplied from the generator bus. One transformer has a delta primary and the other a wye connected primary. The secondaries connect to 12 small photo-coupled SCR's that are operated by the 12 drivers of Fig. 1. The rectified voltage is fed to an operational amplifier analog model of the ZGS passive filter and ring magnet system. Magnet voltage, magnet current, and current through the filter inductor are available. Model current and magnet voltage are transmitted to the power house display system for the operators' inspection.

Discussion

The control system has been in routine use since November 1973. Initial startup was with all the digital switches, D.S. 1 - D.S. 12, set for equal intervals between rectifier firings. No particular problems with arcbacks were encountered.

Readjustments of the individual rectifier angles were made to minimize ripple. This was done with the aid of the control computer using the PHASOR[2] program. The amplitudes of the first, second, and third harmonics were reduced to values that were about a factor of 20 smaller than with the old analog ramp control system. This was done without the feedback input.

The amplitude of the sixth harmonic could be minimized but remained large. The minimum was fairly broad, and the values of D.S. 1 - D.S. 12 indicated that the delta and wye connected transformers did not produce voltage waves that are 30^{o} apart. It appears that the angles are about 28^{o}.

The feedback connection is used with the B coil on the ring magnet to control the slope of the magnet flat-top for energy loss extraction. In this mode, increased ripple amplitudes appear on the ring magnet voltage. These are at low frequencies and are not reproducible from cycle to cycle. It appears that low frequency noise is picked up in the $\dot{B}$ system. Even so, the ripple is less than with the old control system.

The feedback input is used during resonant extraction to control the extraction rate.[3] The signal is supplied from beam monitoring devices to magnetically program the beam position during extraction.

Acknowledgments

Many people have enthusiastically contributed to the digital firing control system project. Their efforts have made the system operational in a remarkably short time.

We wish to thank Mr. Ray Kickert for his efforts, especially during the measurements of the dynamic characteristics of the mercury vapor rectifiers and during debugging and testing of the system.

The ring magnet power group, under Mr. George West, did an outstanding job of constructing many of the circuit modules and making the many changes in the control and interlock circuits. We wish to thank P. Bertucci, L. Johns, P. Roth, E. Kulovitz, W. Welch, and the whole ring magnet power group.

References

1. J. F. Sellers, E. F. Frisby, W. F. Praeg, and A, T. Visser, Ring Magnet Power System for the Zero Gradient Synchrotron, 1965 Particle Accelerator Conference, Washington, D. C., March 10 to 12, 1965, IEEE Transactions on Nuclear Science, Volume NS-12, No. 3, p. 338 (1965)

2. Lloyd G. Lewis and Anthony D. Valente, Argonne National Laboratory, PHASOR: A Control Computer Method for Displaying Amplitude and Phase of Ripple Components in the Ring Magnet Voltage, IXth International Conference on High Energy Accelerators, Stanford, California, May 2 to 7, 1974.

3. Y. Cho, E. A. Crosbie, L. G. Lewis, C. W. Potts, and L. G. Ratner, Argonne National Laboratory, Slow Resonance Extraction of Two Simultaneous Beams without RF Structure, IXth International Conference on High Energy Accelerators, Stanford, California, May 2 to 7, 1974.

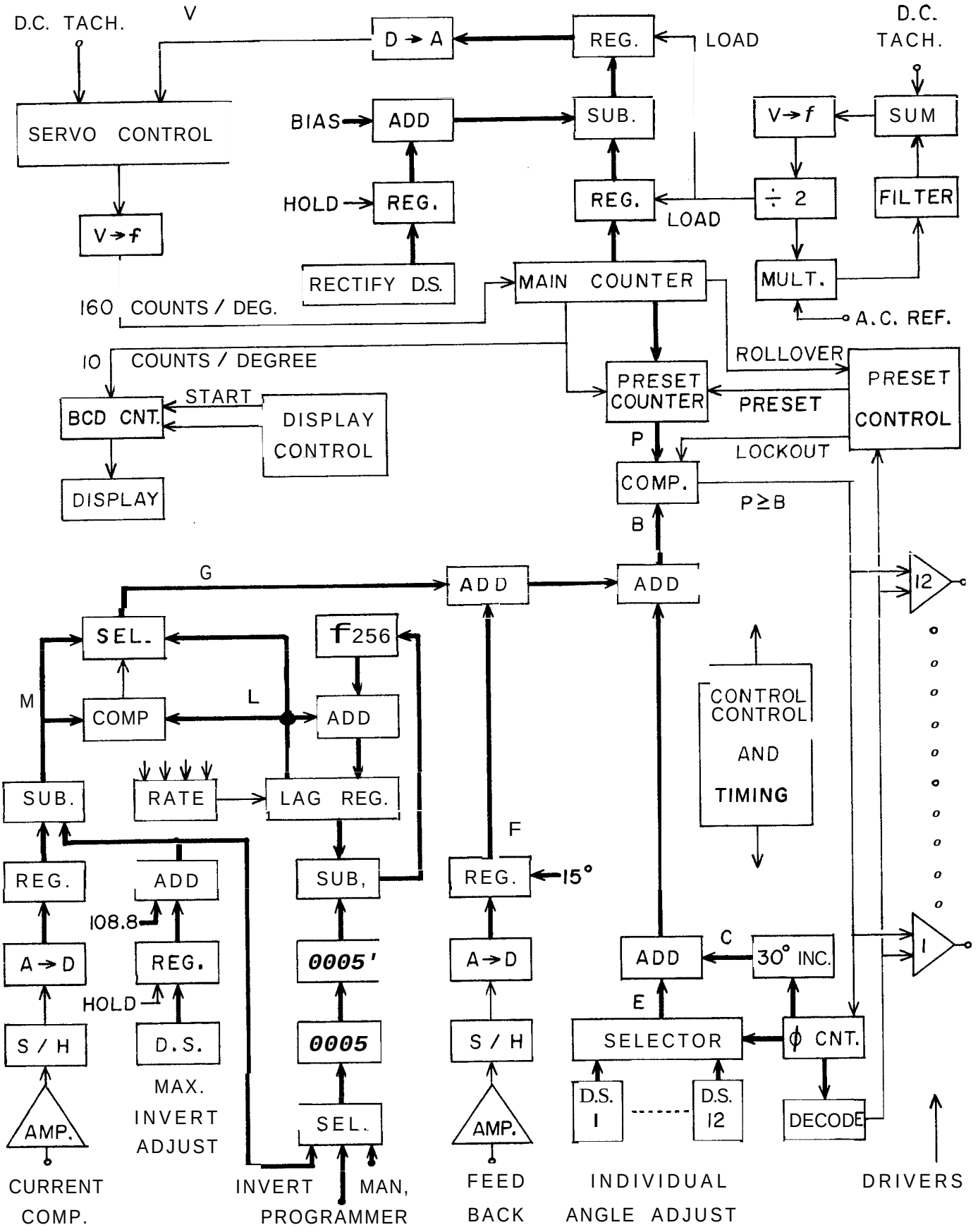

FIG. 1 – DIGITAL FIRING ANGLE CONTROL SYSTEM BLOCK DIAGRAM

PHASOR: A CONTROL COMPUTER METHOD FOR DISPLAYING AMPLITUDE AND PHASE OF RIPPLE COMPONENTS IN THE RING MAGNET VOLTAGE*

Lloyd G. Lewis and Anthony D. Valente
Argonne National Laboratory
Argonne, Illinois

Abstract

Deviations of 12-phase generator-transformer-rectifier systems from ideal performance result in the generation of ring magnet ripple at the fundamental and at low harmonics of the generator frequency. Analysis and display of the amplitude and phase of each of these harmonic components makes it possible for the systems engineer to minimize the ripple by readjusting the control system. The Zero Gradient Synchrotron (ZGS) control computer samples both the filtered voltage on the ring magnet and a reference voltage produced by a phase-lock loop connected to the generator bus. Data are taken during a selected interval of the *ZGS* cycle and are then analyzed. Computer driven graphic displays plot the raw ripple data, amplitude and phase bar graphs for each harmonic component, reconstructed ripple data for checking, and graphs for comparing ripple components under different operating conditions. Numerical information is also displayed. The PHASOR program corrects the phase angles for the phase shifts produced by the ZGS passive filter. These corrected angles indicate which of the 12-phase firing angles should be retarded or advanced to reduce the ripple.

Introduction

Power supplies for synchrotron ring magnets usually consist of phase-controlled rectifiers operated from an ac power line or from ac generators. The number of ac phases is often high to minimize the ripple. The ripple on the magnet is reduced even more in some systems by inserting a low-pass filter between the rectifiers and the ring magnet.

In a 12-phase system with a low-pass filter, the amplitude of the ripple component at the fundamental frequency of the power line may exceed the amplitude of the 12th harmonic. This is caused in part by the filter's attenuation being larger at the higher frequency. Additional causes include errors in the number. of turns on the polyphase transformer windings, variation in the leakage inductance from one phase winding to another, lack of symmetry in circuit resistances, and imbalances between phases of the power line or generator.

The magnitude of the low frequency ripple components may be reduced on flattop by properly retarding or advancing the firing time of each of the 12-phase rectifiers with respect to the others.

Proper adjustment of the firing delays of each of the 12 phases is extremely difficult by trial and error methods and an optimum is difficult to determine by eye. For these reasons, analytical methods are required.

A swept frequency spectrum analyzer was used in an attempt to analyze the ripple during a 700 ms flattop of the ZGS ring magnet. At the low ripple frequencies, 50-600 Hz, the sweep rate for the required resolution was so low that an analysis could not be performed in the length of the flattop, In addition, no phase angle information is given by such an instrument.

The ZGS control computer system was used in conjunction with the program PHASOR to analyze the ripple and display the results. The program is of the interactive type where the computer operator directs the logic flow after observing the results of each section of the program.

Data Input

The reference for all phase angles was a square wave produced by a phase-lock loop that had one phase of the generator voltage as its input. This loop acted as a filter for the distortions in the generator voltage wave and gave sharp indications of corresponding points in each generator voltage cycle. The loop was adjusted so that the positive-going square wave transitions were at 90° on the generator voltage sine wave and were independent of generator voltage and frequency.

This square wave, shown in Fig. 1A, was the input to an analog integrator that was voltage limited at ± 10 V. The waveform from this is shown in Fig. 1B. The rise and fall times were adjusted to be slightly longer than the control computer data sampling interval. In this way, the computer was assured of one data point on the rise even through the computer was not synchronized to the generator.

The second input to the ZGS control computer data station was a voltage containing the magnet ripple information. It was obtained by capacitively coupling the voltage which was across one quadrant of the ring magnet to an amplifier with a high common mode rejection. Zener diode networks eliminated most of the dc component.

Data Taking

The manual keyboard at the computer driven scope was used to specify the point in the ZGS cycle lor the start of data taking (e.g. 250 ms after the start of flattop). The keyboard was then used to enter the number of data samples of the ripple voltage that are to be taken. The computer then generates requisitions for all of the data points. Measurements are made at 100 us intervals and alternate between the reference wave and the ripple wave.

When the operator pushes the DISPLAY NEW SET key, a new set of data is taken on the next *ZGS* cycle. These data are then displayed on the scope screen. Figure 3 top plots the samples taken on the reference wave. The points that are circled are on the rising and falling slopes of the reference. Figure 3 bottom plots the samples taken on the ripple wave.

*Work performed under the auspices of the U. S. Atomic Energy Commission.

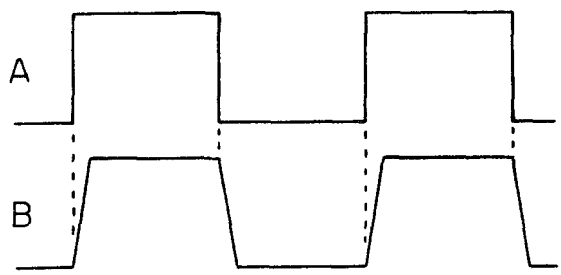

Fig. 1 Phase Lock Loop Waveforms

The computer operator, by inspection of the scope display, determines that the amplitude range of the data is acceptable and that enough points are taken. He may then proceed to analyze the data by pushing the ANALYZE button on the scope.

Analysis

A finite, periodic function V(t) may be written as

$$V(t) = \sum_{n} \left(A_n \cos n\omega t + B_n \sin n\omega t \right) \qquad (1)$$

where

$$n = 0, 1, 2, 3 \ldots \text{ and } \omega = \frac{2\pi}{\tau}$$

and the coefficients are given by

$$A_n = \frac{2}{\tau} \int_{-\frac{\tau}{2}}^{+\frac{\tau}{2}} V(t) \cos n\omega t \, dt \qquad (2)$$

$$n = 0, 1, 2 \ldots$$

$$B_n = \frac{2}{\tau} \int_{-\frac{\tau}{2}}^{+\frac{\tau}{2}} V_t \sin n\omega t \, dt$$

where $B_0 = 0$ and A_0 = twice the dc value of the signal.

If we make k measurements during one period of the function V(t), we may approximate the integrals (2) and (3) by the following:

$$a = \frac{2}{k} \sum_{d=1}^{k} V_d \cos(r\theta_d) \quad r = 0, 1, 2, 3 \ldots \qquad (4)$$

$$b = \frac{2}{k} \sum_{d=1}^{k} V_c \sin(r\theta_d) \qquad (5)$$

$$\text{Then } V(t) = \frac{1}{2} a_0 + a_1 \cos \omega t + a_2 \cos 2\omega t + \ldots + b_1 \sin \omega t + b_2 \sin 2\omega t + \ldots \qquad (6)$$

or

$$V(t) = \frac{1}{2} a_0 + c_1 \sin(\omega t + x_1) + c_2 \sin(\omega t + x_2) + \ldots \qquad (7)$$

where

$$c_r = \sqrt{a_r^2 + b_r^2} \text{ and } x = \arctan\left(\frac{b_r}{a_r}\right) \qquad (8)$$

with the restriction $-180^\circ \le x_r \le +180^\circ$.

The first step in the analysis is to assign an angle θ_d to each of the data points. The computer searches the reference wave data points, Fig. 3 top, to locate all the positive-going edges. It counts the number of data points in each cycle and calculates the fractional intervals at the beginning and end of each cycle. These fractional intervals are calculated from the position of the circled points, Fig. 3 top. The total number of intervals is then divided into 360 to get the number of degrees per interval. θ_d for the first data point in each cycle and the frequency of each cycle are displayed on the scope screen. A value of θ_d for each data point is then assigned.

The computer uses the equations (4), (5), and (8) to compute the amplitude and phase of the first 12 harmonic components. The sums, equations (4) and (5), may be extended over more than one cycle if the operator so specifies.

The phase angles, x_r of equation (7), are then corrected for the phase shifts produced by the ZGS passive filter, shown in Fig. 2. The results give the phase angle of each frequency component at the output of the rectifier.

Display Derived Ripple

The operator may push the DISPLAY DERIVED RIPPLE button to check the computation. In this mode, the computer uses the phases and amplitudes of the ripple components derived from the data to calculate V(t) at each value of θ_d. The graph is shown in Fig. 3 center. The amplitudes and phase angles of the components are given in the table at the bottom of Fig. 3.

A measure of the error is given by a number labelled FIT. This number is found by taking the difference between each measured ripple voltage and the voltage calculated from the phases and amplitudes of the ripple. This difference is divided by the measured voltage at each point and the ratio is squared. The number FIT is one minus the mean of this ratio.

Graph Phasor Set

The operator may see the results of the harmonic analysis by pushing a button labelled GRAPH PHASOR SET. This activates a subroutine that constructs the graphic display that is shown in Fig. 4.

The top lines on the right of Fig. 4 give the date and time of day for starting to take the set of data. The remaining lines on the right give the point in the ZGS cycle at which the data taking began. In this case it was 400.0 ms after the start of block 16 (flattop).

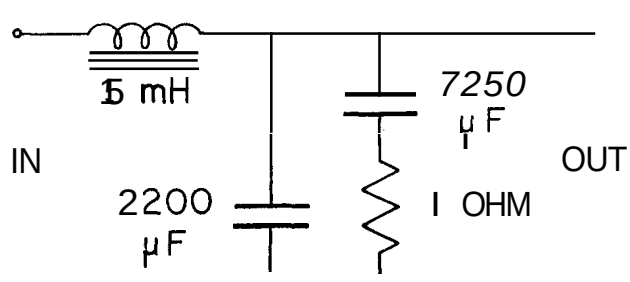

Fig. 2 ZGS Passive Filter

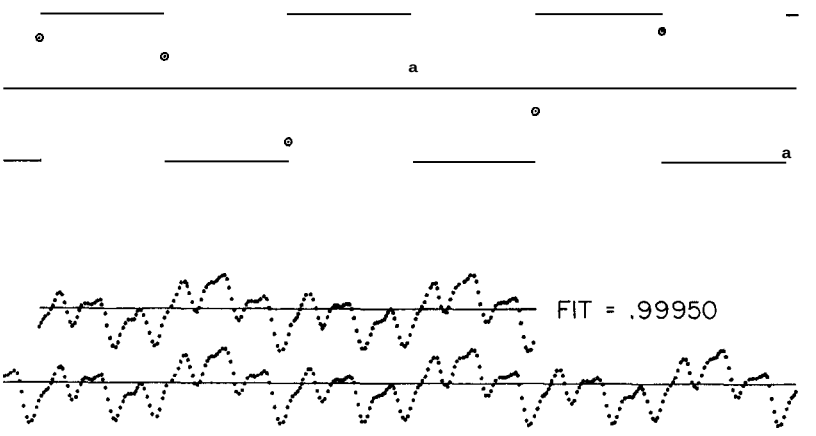

PHASOR

15 NOV. 1973
21 : 04 : 36

START AT 16 400.0
300 SAMPLES TAKEN

2 PERIOD ANALYSIS

	HZ	1ST THETA
1	50.15	4.82
2	50.10	2.28

ALPHA SET			AMP.	PHASE		AMP.	RETAINED SET PHASE	ALPHA	SET	
0	0	0	-.2	0	dc	0	0	0	0	0
			1.1	29.3	1	0	0			
0	0	0	1.1	-111.7	2	0	0	0	0	0
			.2	-112.0	3	0	0			
0	0	0	.3	-130.1	4	0	0	0	0	0
			.1	-145.9	5	0	0			
0	0	0	1.4	- 76.6	6	0	0	0	0	0
			.1	- 82.1	7	0	0			
0			.0	138.0	8	0	0	0		
			.0	11.1	9	0	0			
			.0	47.8	10	0	0			
			.0	- 5.9	11	0	0			
			.6	15.6	12	0	0			

Fig 3. Display New Set and Derived Ripple

Three hundred data samples were taken and two periods were analyzed. The first period had a frequency of 50.15 Hz, while the second had 50.10 Hz. This difference is caused by the slowing down of the generator during the ZGS cycle. The angle θ_d for the first data point in each cycle was 4.82° and 2.27°.

The top graph gives the reconstructed ripple data that was calculated from the amplitudes and phases of the derived ripple components. The FIT number is also given. This graph is included in Fig. 4, as well as in Fig. 3, for identification purposes and because many people get a better "feel" for the data from an analog type display.

The upper bar graph of Fig. 4 plots the dc component and the amplitudes of the first 12 harmonics of the generator frequency. The vertical scale for this plot is shown above and to the left of the bar graph. The scale factor in volts per inch is changeable at will through the scope keyboard. These amplitudes are for the filtered voltage applied to the ring magnet.

The lower bar graph of Fig. 4 plots the phase angles x_r for the first 12 harmonics. The range of angles is fixed at $\pm 180°$ to $-180°$ in accordance with the restriction on x_r in equation (8). These angles have been corrected for the phase shifts produced by the passive filter of Fig. 2. They are, therefore, the phase angles of the harmonic components at the output of the rectifiers. This is done to make it possible to determine which rectifier firing angles should be retarded or advanced to reduce the amplitudes of the ripple components.

The lower part of Fig. 4 lists several sets of numeric data. The column in the center lists dc and phases 1-12. The two columns to the left of center give the amplitudes in volts and the phase angles in degrees for the 12 phases and the amplitude of the dc component. These are the values used to calculate the derived ripple plotted at the top of Fig. 4.

The table of numbers at the lower left records the alpha angle settings for the 12 phases and in addition, the full rectify setting. These are the settings of the ZCS control system that produced the ripple reconstructed at the top of Fig. 4. The numbers are in octal code and represent deviations from the ideal uniform spacing of rectifier firing angles. These numbers are recorded in the exact format in which they appear on the control panel of the digital firing angle control system.

These numbers are entered through the use of the ENTER/MODIFY ALPHA SET subroutine, and can be used by the operator when desired.

Retained Set

The operator may save a set of results, such as that presented in Fig. 4, by pushing the button labelled RETAIN THIS PHASOR SET. This activates a subroutine that stores the information in computer memory for comparison with future data.

The operator may then analyze a new set of data and call for GRAPH PHASOR SET. The result is the generation of a display such as shown in Fig. 5.

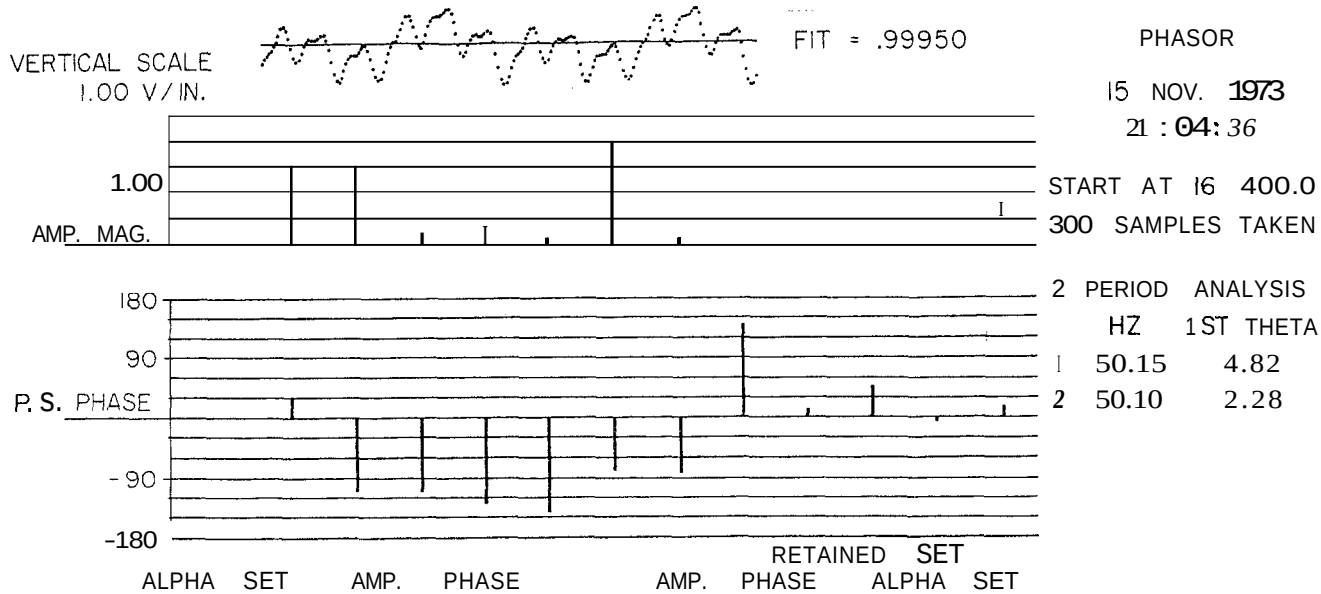

ALPHA SET			AMP.	PHASE		RETAINED SET AMP.	PHASE	ALPHA SET		
77	36	77	.2	0	dc	0	0	0	0	0
			1.1	29.3	1	0	0			
37	76	36	1.1	-111.7	2	0	0	0	0	0
			.2	-112.0	3	0	0			
76	36	77	.3	-130.1	4	0	0	0	0	0
			.1	-145.9	5	0	0			
36	74	36	1.4	- 76.6	6	0	0	0	0	0
			.1	- 82.1	7	0	0			
472			.0	138.0	8	0	0	0		
			.0	11.1	9	0	0			
			.0	47.8	10	0	0			
			.0	- 5.9	11	0	0			
			.6	15.6	12	0	0			

Fig. 4 Graph PHASOR Set

The numeric information at the top right of Fig. 5 is similar to that of Fig. 4 except it is for the new set of data. The derived ripple curve and the FIT number are also for the new set of data.

The bar graph for the amplitude now has two lines at each harmonic location. The left line in each pair gives the amplitude of that harmonic component in the new set of data, while the right line in each pair gives the amplitude of that harmonic component in the retained set. In this way, the amplitudes may be compared visually *to* determine the effect of the changes in the firing angles.

The bar graph for the phases also has a pair of lines at each harmonic location. The left line in each pair gives the phase angle for that harmonic component in the new set of data, while the right line gives the phase angle of that harmonic component in the retained set.

The numeric information, at the bottom of Fig. 5 on the right, gives the amplitude and phase angles for the retained set and in addition the alpha set that produced them, The numeric information, at the bottom on the left, gives the amplitude and phase angles for the new set of data and the corresponding alpha set.

output

The program PHASOR is an interactive one so that most of the output is through visual observation of the computer driven scope display. Several options in the interaction can produce copies of the scope display on 8½" x 11" photographic paper. These include:

COPY NEW SET -- similar to Fig. 3,
COPY LEFT SHIFTED -- that portion of Fig. *3* that was analyzed,
COPY DERIVED -- derived ripple,
COPY PHASOR & ALPHA SET -- similar to Fig. 4, 5.

The 'hard-copy" unit can produce a print in about ten seconds. No line printer output is provided.

Calibration

The effects produced by changes in rectifier firing angle were experimentally investigated. For example, the firing angle of phase number 1 was advanced several electrical degrees to produce a large ripple on flattop. PHASOR was then used to measure the amplitude and phase of the harmonic components of the ripple thus produced. This procedure was repeated for several combinations of changes in firing angles of selected rectifiers.

The calibration data were useful in predicting which of the 12 rectifier groups should have their firing angles altered to reduce a given observed ripple.

Discussion

Analyses of ripple data were made for a variety of firing angle combinations during the calibration runs and for many actual operating conditions while ripple reduction adjustments were made. In all cases, the bar graphs similar to Figs. 4 and 5 showed very small or no amplitudes for the 5th, 7th, 8th, 9th, 10th, and 11th harmonics. The phase angles computed for these

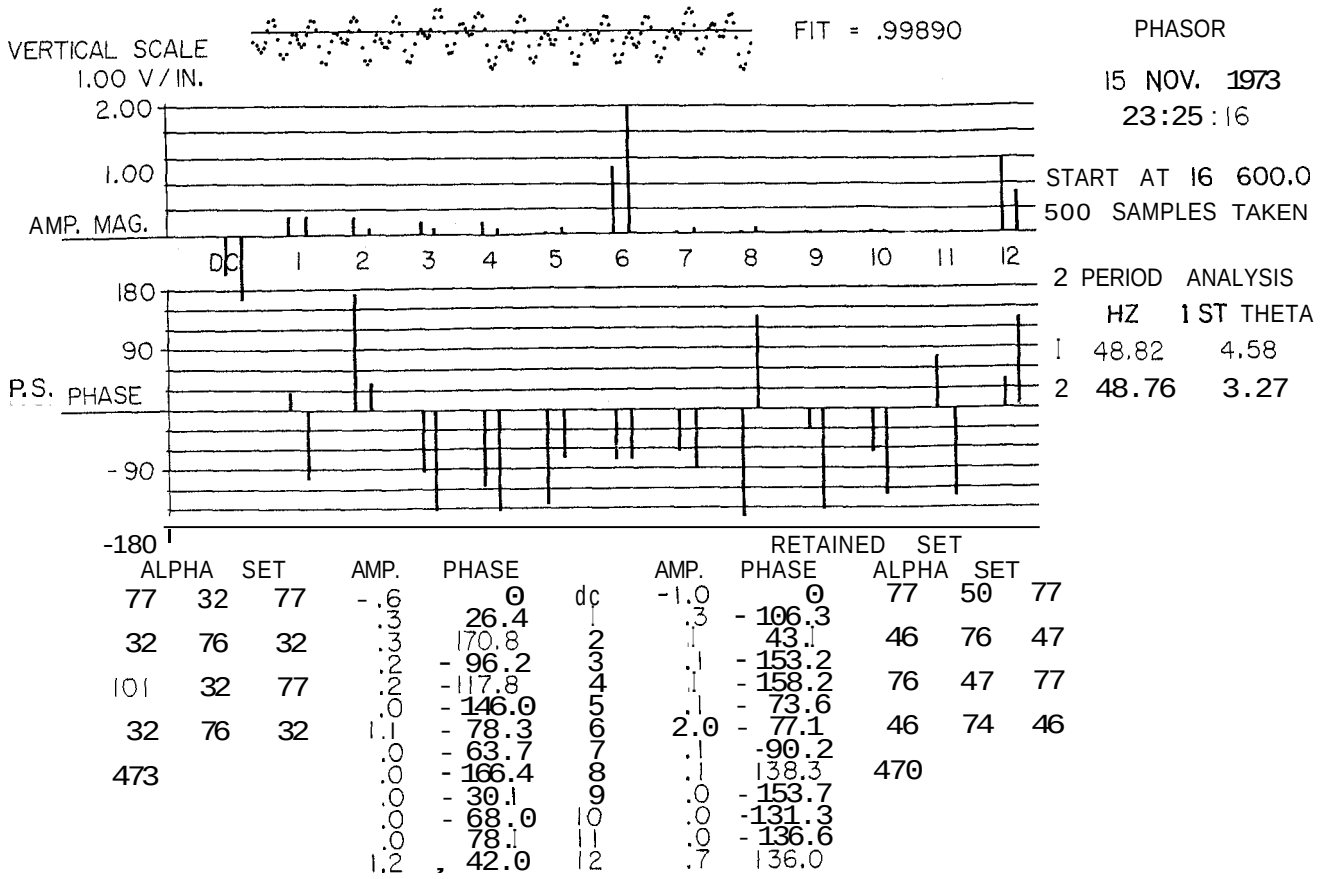

Fig. 5 Graph PHASOR Set With Retained Set for Comparison

harmonic components varied widely from one data set to the next which leads us to the conslusion that these harmonic components are largely the result of "noise" or inaccuracies in the input data.

We were not able to find a combination of rectifier firing angles that produced large **or** significant amounts of 5th, 7th, 8th, 9th, 10th, and Ilth, harmonics. We therefore have amplitude and phase meaaurements at harmonic numbers l, 2, 3, 4, 6, and 12 for **a** total of 12 measurements.

The control system has adjustments for each of the 12 phases but only 11 of these are independent variables as far as ripple is concerned. The 12th phase control and the "full rectify" control adjust the slope of the flattop. This slope is adjusted to zero before the ripple measurements are made.

Some thought was given to writing a program that would compute new firing angle settings from the ripple component amplitudes and phase angles. There appear to be enough measurements to permit the solving of a set of 12 equations. No adequate algorithm for this was developed in the very limited effort expended.

Inspection of the problem indicates that the ripple may be reduced one component at a time. **This** is the procedure used.

A perfect rectifier system will produce only the 12th harmonic, therefore this cannot be eliminated or effectively reduced by adjusting firing angles. On the other hand, the 6th harmonic can be increased or decreased in only one way. That is, all even numbered phases should be advanced an equal amount and all odd numbered phases retarded by the same amount. This method reduced the 6th harmonic amplitude to a minimum but would not make it vanish. The data indicate that the phase shift between our delta and wye connected transformers is only 28° rather than the theoretical 30°.

The first harmonic amplitude may be reduced by changing all of the 12 angles. In this case, the changes are distributed sinusoidally with the peak of the distribution determined by the phase angle of the 1st harmonic of the ripple. The 2nd harmonic may be reduced by a similar procedure except that the sinusoid for the distribution is the 2nd harmonic.

This program was used successfully to reduce the flattop ripple at the *ZGS* with the distributions for alpha angle changes determined manually. It is hoped that additional subroutines can soon be added to permit the computer to calculate the alpha settings that will minimize the ripple.

INITIAL EXPERIENCE WITH A MULTI-PROCESSOR CONTROL SYSTEM

K. B. Mallory
Stanford Linear Accelerator Center
Stanford, California

The SLAC accelerator has now been controlled through a system of two linked computers far a year. In the first four months of 1974 nine additianal CPU's have been linked into the system. Figure 1 shows the present configuration. It is time to review the problems encountered in computer-control of the accelerator and to discuss their solutions--installed, pending and proposed.

BACKGROUND

When SLAC was built, an SDS-925 computer was installed in the switchyard's data assembly building, now the Main Control Center (MCC). Its functians were to monitor interlocks and to control a few of the switchyard magnets. There was no cmputer asssciated with the accelerator itself. Four years later a PDP-9 was installed in the Central Control Roam (CCR) to log klystron performance and to help automatically select spare klystrons to replace failures. By making maximum use of existing relay multiplexers the PDP-9 was csnnected to nearly all accelerator control, analog and status signals within six months. As a result, however, it vas limited to executing sne control or analog readsut at a time.

It was then proposed functionally to move CCR to MCC by linking the computers and using "touch-panel" displays (Refs. 1,2), without physically moving hardware. The pattern generator for defining multiple-beams was the last interface to be completed, early in 1973. Operations from MCC started shortly thereafter.

INITIAL PERFORMANCE

From the outset, nearly all of the accelerator control and monitoring signals could be made available at 1he touch panel display units. Operators designed their own panel:, using a convenient software "panel. compiler". However, the system could only operate control at a time, just as was the case at a single control position In CCR. It presented analog signals only when the operator explicitly asked for them by name. Its only alarm annunciator was a "scroll" of the last fifteen messages resulting from detected changes. Since a major fault is normally followed by a number of consequent faults, the most important message often was rolled off the "scroll" before the operator realized any-thing had happened.

In our operating system (*Ref'.* 3), *each* status change and button-push creates one or more tasks. The PDP-9 can handle up to roughly 5C or more tasks at a time; the 925 can support twice as *many*. Nevertheless, there are many occasions when multiple changes create far too many tasks for tne system to manage which, at first, caused *many* system crashes. The solution was to cause various kinds of tasks to be deleted before the system was swamped. To give an extreme example, rist so rare as we would like, a fault can occasionally dump the entire RF system. This causes some 800 status changes to appear at the PDP-9 within two or three seconds. When *too many status* changes occur, the PDP-9 stops reporting individual changes and instead, with a single task, sends a total update of accelerator status to the 925. Similarly, *most* messages across the link can be aborted if there are too many tasks already in the system.

Since the computer system essentially replaces a pre-existing manual control system, there has been considerable pressure to "give us back what we had before." The annunciator problem was the first to bo attacked. There are now several new *programs* that (1) display the status of all 245 klystrons on one panel, (2) display status of a system (e.g. personnel protection or vacuum) and soon, (3) display a list of accelerator faults in order of priority. This last list displays current status, rather than changes, and is thus independent of occasional missed tasks, (4) multiple scrolls so that messages of different types can be directed to different displays.

RECENT IMPROVEMENTS

These software changes have made the system mare reliable and have imprsved its operation, but software alone cauld do nothing about the me-at-2-time control and very little about the slaw analog acquisition. The original proposal far improving controls required 30 special-purpose pracessors in the gallery, with circuits to store a command and then drive local relays while the PDP-9 transmitted control signals to other sectors. These processors at first were very complicated; but even when all of the timing and much of the special lsgic was deleted, they cost as much as putting a computer into every fourth sector, and increased the amount of work to be done by the PDP-9. Since an analog multiplex system and a method to restructure the addressing of some of the control channels were also desired, the special-purpsse processors never got off the drawing board. We bought nine PDP-8's instead.

The first of the PDP-8's arrived a year ago. An executive program similar to the one in the PDP-9 and *925* had been written and tested in a. simulator in the IBM 360. A terminal.-emulator prsgram was written for the PDP-8; it asked the 360's text-editor Cor a binary "listing" of the executive program, loaded it into core, and we were in business. By August, the eight gallery processors had been linked to the one in CCR, in October the link into the PDP-9 was established, and we were waiting primarily for fabrication and installation of interface hardware in the gallery. (Fig. 2) Programs to control the new hardware rind a program in the PDP-9 to store the PDP-8 programs on its disk were completed this winter. During this conference we have installed remote restart switches, as a pacifier to the operators who know that any system can go down occasionally.

By the end of this conference, when the accelerator is being started up, we expect eight of the *nine* computers to be fully operational, and to have 28 channels of control to the accelerator instead of the one we had before. The ninth csmputer is being used to test the analog multiplexing hardware as it comes out of the shop. We expect to have a form of analog multiplex system operating in September.

DEVELOPMENTS FOR THE FUTURE

I suggesred above that we were restructuring our control addresses. The original control addressing scheme required the operator first ti select a sector and then push a button for the desired control signal. When we installed pulsed beam guidance, we subdivided individual control addresses for adjusting up to six preset levels of a device. For manual operations, pushing one butt-n at a time, it made no difference to an operator what the addressing hierarchy might be in the hardware.

But we now have three independent operating positions in the Main Control Room, and arc talking *about*

adding automatic controls that might be initiated by the computer. The operator now selects which beam he wishes to tune on his touch panel (subdevice address). Then he selects what function he wishes to control (control address, e.g. beam loading or vertical steering). Finally he selects the particular location (sector) where he will make his adjustment. Thus our addressing logic has been turned completely upside-down. In particular, far instance, the controls for beam current and spectrum sharpening of all beams share three control addresses at the injector, which are accessed only by one of the new PDP-8 channels. Thus operators could still find themselves interfering with each other.

We plan to install special interfaces to allow parallel control of selected multilevel devices. The first was scheduled for installation in July, but it now appears that parallel control for "phase closure" (spectrum sharpening) and for fine energy control *may* become operational before the end of May.

When the analog multiplexing system comes into operation, a new problem will arise: the amount of link traffic is expected to be at best doubled, perhaps trebled from what it is now. Two pstential solutions are being studied -- a mare-efficient message-switching system for the PDP-8 in CCR (which will not do much to reduce link traffic from the PDP-9 to the 925) or a new data link, for analog signals only, direct from the PDP-8's t> an auxiliary processor at the 925.

Eventually, we will prsbably have to replace the 925, reliable though it be now. We are proposing to install new minicomputers to buffer several of the 1/0 devices now connected to the 925, and later to connect them to a new major processor which can first share and later, if necessary, take over the tasks of the veteran - the original cmputer installed for control of the BSY at SLAC.

REFERENCES

1. D. Fryberger and R. Johnson, "An Innovation in Control Panels for Large Computer Systems," Particle Accelerator Conference, Chicago, Illinois, March 1971.

2. S. Howry et al., "SLAC Control Room Consolidation - Software Aspects," Particle Accelerator Conference, Chicago, Illinois, March 1971.

3. S. Howry, "An Operating System for Process Control," 3rd ACM Symposium on Operating Systems Principles, Stanford, October 1971.

4. K. B. Mallory, "Some Effects of (Now Having) Computer Control for the Stanford Linear Accelerator Center," Particle Accelerator Conference, San Francisco, California, March 1973.

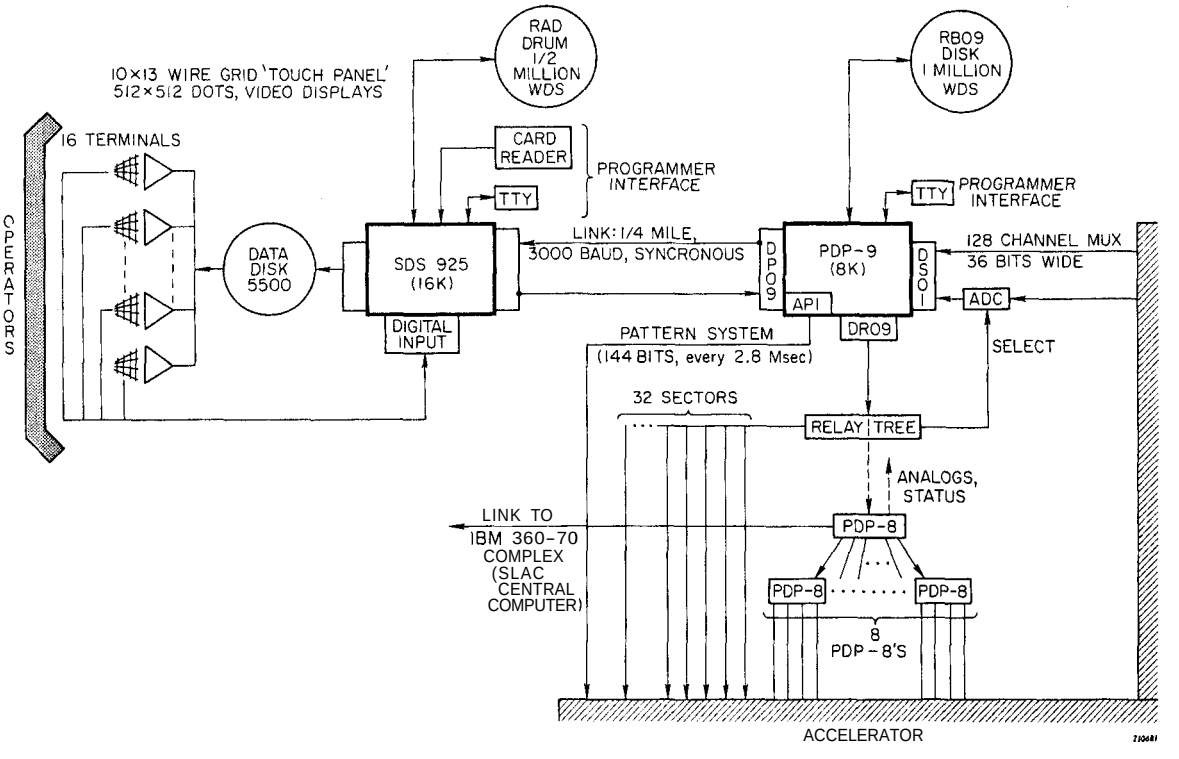

Fig. 1

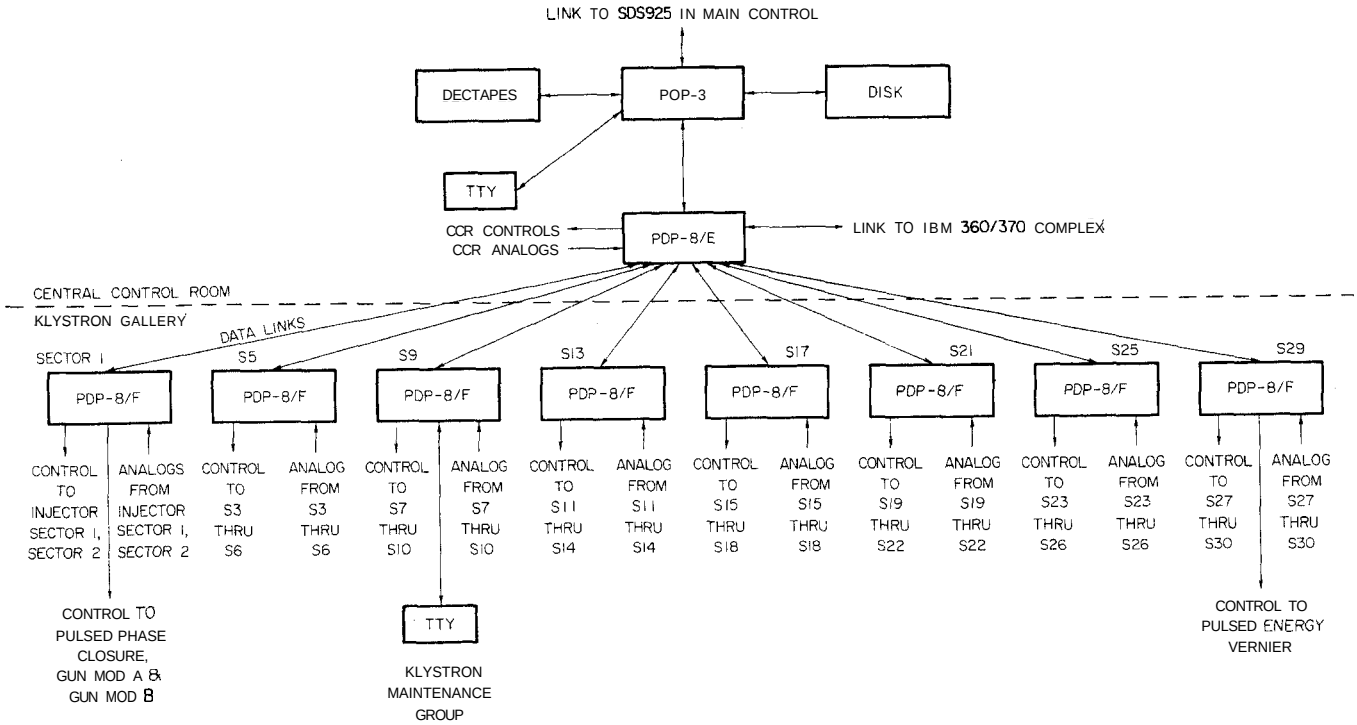
LINK TO SDS925 IN MAIN CONTROL
DECTAPES
POP-3
DISK
TTY
CCR CONTROLS
CCR ANALOGS
PDP-8/E
LINK TO IBM 360/370 COMPLEX
CENTRAL CONTROL ROOM
KLYSTRON GALLERY
DATA LINKS
SECTOR 1
S5
S9
S13
S17
S21
S25
S29
PDP-8/F
CONTROL TO INJECTOR SECTOR 1, SECTOR 2
ANALOGS FROM INJECTOR SECTOR 1, SECTOR 2
CONTROL TO S3 THRU S6
ANALOG FROM S3 THRU S6
CONTROL TO S7 THRU S10
ANALOG FROM S7 THRU S10
CONTROL TO S11 THRU S14
ANALOG FROM S11 THRU S14
CONTROL TO S15 THRU S18
ANALOG FROM S15 THRU S18
CONTROL TO S19 THRU S22
ANALOG FROM S19 THRU S22
CONTROL TO S23 THRU S26
ANALOG FROM S23 THRU S26
CONTROL TO S27 THRU S30
ANALOG FROM S27 THRU S30
CONTROL TO PULSED PHASE CLOSURE, GUN MOD A & GUN MOD B
TTY
KLYSTRON MAINTENANCE GROUP
CONTROL TO PULSED ENERGY VERNIER

Fig. 2

THE CPS IMPROVEMENTS 1965–1973
AN ASSESSMENT

THE CPS STAFF
CERN, Geneva, Switzerland

Summary

In 1965, plans were made to increase the beam intensity delivered by the CPS by a factor of ten or more. The first stage, involving a new power supply for the main magnet and more than doubling the cycle repetition rate, was completed in 1968. In the second stage, which is now essentially complete, the major items was the construction of an 800 MeV slow-cycling booster injector. Many other modifications were included. The Linac current had to be increased by an order of magnitude to supply the Booster, and the higher beam intensities required a more powerful RF accelerating system. Besides the 800 MeV injection elements, quadrupole lenses were installed to avoid longitudinal dilution at transition, and multipoles to counteract instabilities. In addition, the chamber vacuum was improved by a factor of ten, shielding and radiation resistance increased where necessary, and beam-equipment interaction reduced. Adequate instrumentation and control facilities had to be provided, and the efficiency of fast and slow extraction systems improved. Perturbations due to various collective phenomena had to beovercome.

The performance obtained during the first physics runs is reported.

1. Introduction

After a few years of operation, the CPS had reached a maximum intensity of 1 Tp/pulse* and, in view of space-charge effects, a further factor of two seemed the most that could be expected. The motor-generator set supplying the main magnet limited the duty cycle to a typical value of 10%at 19 GeV/c (200 ms flat-top with a 2 s repetition time) and even less at higher energies (100 ms flat-top every 3 s at 24 GeV/c). The experimental facilities comprised two halls, with a total area of 4000 m^2, fed by internal targets and a single fast extraction channel.

In 1964, an improvement programme was launched with the object of increasing the average accelerated beam intensity by a factor of 10 to 15[1]. This was to be achieved in two stages :

i) raising the repetition rate to gain a factor of 2 or 3, depending on energy and flat-top length, by constructing a new magnet power supply;

ii) raising the injection energy (factor ∿ 5 in intensity per pulse). Two possible methods were investigated in detail; a 200 MeV Linac[2] and a 600 MeV twin slow cycling booster synchrotron[3], A comparative study[4] showed that although both schemes could produce the required intensity increase, the higher space-charge limit of the booster allowed a greater potential for future development. Further studies finally led to an 800 MeV booster with 4 superposed rings[5]. In addition to the new injector, this part of the programme involved a number of complementary improvements to the 50 MeV Linac and the main proton synchrotron, which are detailed below.

* Tp = 10^{12} protons (Teraproton).

The programme was balanced by a comparable expansion of experimental areas and facilities (West Hall with the Omega spectrometer and the Big European Bubble Chamber (BEBC) and neutrino facility with Gargamelle), which took place simultaneously.

2. Main Magnet Power Supply

The new power supply[6] was designed to more than double the duty cycle.

The magnet voltage was increased from 5.4 to 10.8 kV, which approximately halved the rise and fall times of the magnetic field. In order to avoid increasing the maximum voltage to ground, limited by the winding insulation, a second rectifier set was inserted in the middle of the magnet circuit, with the output voltages of both rectifier sets symmetrical to ground. Keeping the same maximum current (6400 A) as before, the higher magnet voltage implies a higher peak power, namely 95 MVA in place of 46 MVA.

The increase in duty cycle raises the average power and the losses in the magnet. Mean power rose from 18 to 46 MVA and power dissipation in the magnet from 1.6 to 3 MW. The magnet cooling system had to be adapted to the new conditions.

The new power supply has a more flexible control system, which provides a wider choice of magnet cycles, including the possibility of two "flat-tops" at different energies. The distribution of accelerated protons between users is thereby simplified; a common example of such a complex cycle is : acceleration to 26.3 GeV/c, ejection of 4 bunches to ISR, deceleration to 24 GeV/c, then slow extraction shared with an internal target over a 400 ms burst.

The reduction obtained in the ripple voltage (20 V peak to peak instead of 100) and the better reproducibility of the magnet field ($4\ 10^{-4}$) are important factors in producing a satisfactory slow extracted beam.

Reliability has proved to be very good (2 h downtime per 1000 hours of operation in 1973).

An important additional implication was the need to increase the mean power and the rate of rise of the auxiliary power supplies. These modifications were carried out progressively, and still continue today, as each auxiliary sub-system proves to be a bottle-neck for an increase in the machine overall efficiency and has, in its turn, to be matched to the main power supply capability or modified to improve the control of beam dynamics effects.

3. Linac

Since the original 50 MeV Linac had also to serve as injector for the new Booster synchrotron, its performance required substantial improvement. This involved increasing the pulse length to 100 μs, for multiturn injection up to 15 turns; more current (100 mA) within a specified emittance and energy spread (30 π mm mrad

and ± 150 keV); and a higher repetition rate (2 s^{-1}) so that alternate pulses could be sent down a pair of new beam measuring lines. Besides increasing the duty cycle of several components (ion source, pre-accelerator, pulsed quadrupoles, etc.), a major problem was cavity beam loading and its compensation. This was tackled by installing for each of the three tanks an additional RF amplifier using more powerful tubes. However, the beam loading compensation is very difficult to adjust with adequate stability for long pulses at peak intensity, and it has been necessary to limit the beam to 50 mA, to achieve stable operation and reproducible beam quality.

4. 800 MeV Injection System

After injection at 50 MeV from the Linac and acceleration in the Booster, the 800 MeV beam is injected into the PS over one turn, and the bunches are trapped directly in synchronized buckets. The injection system together with the associated beam observation devices and low energy magnetic corrections is described elsewhere[7]. An incoming beam within the specified characteristics is trapped with barely detectable losses.

5. Accelerating System

The reduction of the magnetic field rise time also implies an increase of the energy gain per turn, and it was initially intended to achieve this with a set of three additional narrow-band second-harmonic cavities'. These would have been switched on 80 ms after injection when a remaining frequency swing of only 10%was needed to reach top energy. Although prototype units were developed and successfully tested with the beam, the project was dropped when, during the second stage of the improvement programme, it became clear that the whole RF system would have to be rebuilt.

An additional requirement was the desire to be able to trap the 20 Booster bunches in 10 of the PS buckets as a means of increasing the ISR luminosity. After investigating several alternatives[8], it was decided to build a new acceleration system capable of coping both with the faster rate of rise brought about by the new magnet power supply (section 2) and the higher beam intensity.

The new RF system[10] comprises ten units spaced around the ring. Each unit has two identical ferrite-tuned cavity resonators, working over the frequency range 2.5 - 10 MHz, providing a peak accelerating voltage of 2 x 10 kV. The available power output is 90 kW per unit, which is adequate, under the worst conditions, for an intensity of 1.5 Tp per PS bucket. The pair of resonators is connected in parallel, which simplifies tuning current control and allows a larger tolerance for the power tube output capacitance. The accelerating gaps are short-circuited by vacuum relays at the end of the acceleration phase of the cycle, so that they show a low impedance to the beam and re-bunching is avoided.

The power amplifier is a neutralized 70 kW tetrode, operating with grounded cathode in class B. It is housed in the cavity compartment to provide isolation between the varying cavity impedance and the feed cable, and is built as a plug-in assembly for rapid exchange; the rest of the system is in the centre of the ring where it is always accessible. All sub-assemblies are easily interchangeable and, apart from the final stages, fully transistorized.

The beam control system has also been replaced to meet the more stringent operational requirements (automatic phase programme, adapted pick-up sensitivity, beam-derived frequency programme, synchronization with the Booster, single bunch acceleration).

6. Vacuum System

It has long been known that residual gas could be a source of beam instabilities, and therefore set a lower limit on ultimate performance than simple gas scattering effects would indicate. Furthermore, the prospect of increased radiation damage, and therefore reduced reliability of vacuum seals made of organic materials, was an additional reason for redesigning the vacuum system[11].

The 82 oil diffusion pump groups have been replaced by about 130 sputter-ion pumps (200 or 400 ℓ/s pumping speed according to the local load) and 14 turbomolecular pump groups (260 ℓ/s) for pumping down to the 10^{-5} Torr range. All the rubber seals have been replaced by metallic types, and new bellows-sealed valves installed.

The completion of this project has reduced the mean pressure by a factor of ten, namely from 2-3 10^{-6} Torr down to 2-3 10^{-7} Torr. Recent beam dynamics experiments[12] have shown that at the intensity level of 2 Tp/p a return to the old pressure level immediately lowered the intensity by 50%. It should also be noted that, in spite of the longer pump down time, the time lost due to vacuum system faults has gone down from 20 h to 10 h per 1000 h of operation.

7. Extraction Systems

Efficient sharing of accelerated protons between an increasing number of users demanded the development of new extraction systems and components. Limitation of the intensity permissible on internal targets, to avoid both overheating of the target head and radiation damage to adjacent components, places a premium upon methods of slow extraction which can simultaneously share the beam without unduly increasing losses. A resonant extraction system of this kind is now in operation[13]. Generally, the use of higher intensities implies the necessity for improvements in extraction efficiency.

This problem has been tackled in two ways; firstly, by the development of extraction system components with wider apertures for the same deflecting power; secondly, by the use of devices ahead of the extractor magnet which enhance the separation of the protons-to-be-ejected whilst providing the minimum obstruction in the machine aperture (septa). Brief descriptions of these components follow.

i) A Full Aperture Kicker (FAK), to replace the plunging partial aperture devices which could only handle beam of pre-booster dimensions.
The new system consists of 9 ferrite transmission line magnet modules of 15 Ohm characteristic impedance. With a pulse voltage of 40 kV (80 kV on the pulse generator), the flux density in the 53 mm gap is 630 Gauss and the total kick strength at 26 GeV/c gives a displacement of 19 mm at the septum extractor magnet location with a 55 ns (10 to 90%) rise time. These parameters have been chosen taking into consideration the expected larger transverse emittance and the longer bunch length of the high intensity beam. The system was commissioned in 1973 and has performed well up to

26 GeV/c (nearly 100%efficiency) with the maximum beam injected so far (6 Tp/p).

ii) Electrostatic septum deflector as first stage of the slow extraction beam channels".
This unit has a 0.1 mm molybdenum foil grounded anode (the septum) with an anodized aluminium cathode. Field strengths of 100 to 110 kV/cm are currently achieved over a 10 to 20 mm gap. No adverse effects are observed when the proton beam hits the septum even at 6 Tp/p, but it is necessary to avoid grazing the cathode.
Among the major difficulties was the effect of secondary ions, which had to be screened off to avoid excessive sparking, and electromagnetic coupling of the septum with the beam, which had to be damped to avoid exciting strong beam oscillations.
The successful operation of the electrostatic septum was the main factor in reducing slow extraction losses to 3-5%[16].

iii) As intermediate element in the slow extraction channel, a 1.5 mm thick septum magnet[17], capable of giving a 1.5 mrad deflection (0.115 T at 24 GeV/c), was built and installed, and has been operating reliably for two years.

iv) Large aperture septum extractor magnets are being developed to accommodate the bigger beams. A vertical aperture of 30 mm (instead of 15-20 mm) is now necessary. For slow extraction, the 10%duty cycle initially specified had to be raised to 30% to match the capability of the new main magnet power supply (section 2).
The 30x50mm aperture magnet for fast and slow extraction from a long straight section has three 76 cm modules with 6 and 9 mm septa giving 30 mrad deflection (0.9 and 1.3 T at 26 GeV/c); although performing electrically and magnetically as intended, it has suffered from several mechanical failures (water/vacuum seals and has had to be modified.
Large aperture magnets for fast extraction from a short straight section[19] (30 x 45 mm aperture with a 19 mrad deflection at 26 GeV/c given by 1.8 T) are being built and will be installed this year. Because of their vertical dimensions, these new models can no longer fit between the upper and lower main magnet coils, and therefore have to be significantly shorter (105 instead of 140 cm).

8. Corrections for Beam Quality Preservation

The low-energy corrections are discussed elsewhere[7], as well as the y-transition jump system to avert longitudinal blow-up when passing through transition" energy.

At energies above transition, two types of correction are used :

i) programmed octupoles increase the spread in betatron frequencies in order to avoid the vertical head-tail instability. This effect is discussed in another paper[21]. It is expected to become stronger with increasing intensity. More powerful and more compact lenses (to fit into the restricted straight section space) have been built[22].

ii) the RF voltage is carefully programmed to provide enough Landau damping to suppress longitudinal instabilities[23].

In addition it is intended to install pulsed sextupoles in the near future, in order to program chromaticity and thus reduce the growth rate of the head-tail instability. The use of pulsed quadrupoles to correct the betatron tune dynamically during acceleration is also planned.

Extensive research into the coupling characteristics of various machine components which might interact with the beam is being conducted[24].

9. Instrumentation and Controls

The CPS instrumentation has been a key element in understanding beam behaviour and in obtaining rather rapidly the performance summarized in section 11 below. The main techniques used in the PS ring and for extraction systems have been reviewed elsewhere[25]. The special devices developed for the injection of the Booster beam are described in ref. 7.

In parallel with the improvements to the major components of the CPS, a control system centered around an IBM 1800 has been built up. This computer system serves the Booster and many sub-systems of the Linac and PS. Computer driven consoles with interactive control are used by the operating staff in the Main Control Room[26].

A multi-computer system is being built around several intercommunicating PDP-11/45[27], to facilitate operation under the even more demanding future conditions.

10. Radiation Problems and Beam Dumping

Although the proportion of accelerated protons wasted has been steadily reduced by increasing efficiency in their distribution, the increase in intensity has nevertheless created problems because of radiation damage; the higher levels of induced activity render "in situ" maintenance more difficult.

Most of the organic materials near the beam have been replaced by metal, ceramic or oxide-coated components, designed for faster servicing and quicker exchange. The major source of concern was the main PS magnet[28]. Several units have already had to be replaced, the weak points being the adhesive holding the laminations together and the poleface windings. The magnet blocks can be mechanically clamped, but the poleface windings will have to be replaced by a new version. An evaluation of the situation in the experimental areas of the CPS with regard to induced activity and radiation damage has also been made[29].

The roof shielding above targets was reinforced, and the earth shielding over the remainder of the ring increased to the structural load limit. An evaluation of the effects of various modes of operation on site radiation has been made, and this is one of the criteria used in establishing long-term programmes. There is a continued effort to keep down unnecessary losses.

In the operation of an accelerator such as the CPS, a certain amount of beam dumping is inevitable. This occurs, for example, during beam studies, or when one part of a complex distribution cycle has to be temporarily suppressed.

The CPS lattice makes it very difficult to design

an efficient general purpose fast dumping system, capable of absorbing the total expected intensity (10 Tp/p) for several hours, as has been done for newer machines such as the ISR, NAL or the SPS.

The policy[30] is therefore to use the external beam channels as often as possible for this purpose, and to provide a dump in each of them. Nevertheless, internal dumping cannot altogether be avoided. Internal dump targets, capable of localizing the losses in a limited region of the machine and of withstanding the thermal stresses caused by the higher intensity are being designed, and the feasibility of a fast dumping kicker is being investigated.

11. Performance

The peak intensity reached so far, as a result of the improvement programme, is over 6 Tp/pulse at 26 GeV/c. A much more important outcome is that the PS has been operating stably for regular scheduled high energy physics runs, at 26 GeV/c with 5 to 6 Tp/p at a 2 s repetition time. The beam was extracted by the full-aperture kicker system with losses barely above the threshold level of the beam loss monitoring system.

A longitudinal emittance of 9 mrad* (in units of RF radians x $\Delta p/m_o c$) was maintained at 6 Tp/p from trapping at 800 MeV up to transfer to the ISR at 26 GeV/c, thanks to the y-transition jump system. With the octupole corrections and the programming of the RF voltage along the cycle, all the harmful instabilities can be kept under control.

There is still some transverse mismatch and dilution during the first phase of acceleration due to the (not yet quite optimum) matching of the Booster-PS transfer line, to differences between the beam from the four PSB rings, and to the present somewhat limited flexibility of the low field corrections.

There are no measurable injection losses when the PSB beam is reduced to the specified emittance (E_V = 12 π mm mrad; E_H = 33 π mm mrad at the CPS entrance), i.e. during machine studies, but when it is not collimated, injection losses of about 10% have been observed.

It is not planned to use high intensity beam for "counter physics" experiments until the East experimental area is re-arranged in 1975[31] but slow extraction has been tested, and, although not. optimized, showed losses of only 7 to 10%.

The PS beam is at present distributed over some 20'000 m^2 of experimental areas, and to the ISR. Later, the machine will also act as injector for the 400 GeV SPS under construction nearby.

Typical cycles in current use have a 2.5 s repetition time, with fast extraction at 26 GeV/c for the ISR and bubble chambers, followed by a 500 ms flat-top at 24 GeV/c for counter experiments.

---

* 1 rad = 15.6 eVs for the CPS.

References

1. Germain, P., Contribution to CERN/SPC/189, "Studies in progress on possible improvements to the PS and its experimental equipment", October 1964.
   - Standley, P.H., "The CPS improvement programme", Proc. of 5th Int. Conf. on High Energy Accel., Frascati, 1965, pp. 80-85.
2. Taylor, C.S., private communication.
3. Hardt W., "Slow cycling injection method for intensity improvement of the CPS (TART Scheme)", Proc. of 5th Int. Conf. on High Energy Accel., Frascati, 1965, pp. 1.51-153.
4. Barbalat O (editor), "Comparison between two possible CPS injectors", CERN internal report DIR/TM/14, 1966, and CERN/SPS-227, 1966.
5. *MPS* Staff, "The second stage CPS improvement study", CERN internal report MPS/Int. DL/B 67-19.
   - Bovet C., Reich K.H., "The CERN proton synchrotron Booster", Proc. of 6th Int. Conf. on High Energy Accel.. Cambridge, 1967, pp. 315-319.
   - PSB Staff, "The CERN PS Booster, Design expectations confronted with reality, t-o years after start-up", Proc. of this Conference.
6. Bayard O., "La nouvelle alimentation de l'aimant du synchrotron à protons du CERN", CERN 71-10 (Part 1) and 71-20 (Part 2), 1971.
7. D. Boussard et al, "Injection and trapping of the beam at 800 MeV in the CERN PS", Proc. of this Conference.
8. Fischer H., "Proposed accelerating units for doubling the rise of the magnetic field at 80 ms after injection" CERN internal report MPS/RF/64-13.
9. Pirkl W., "Price estimates for 12 different versions of a new CPS accelerating system", CERN internal report MPS/RF 67-4.
10. Pirkl W., private communication.
11. Riboni P., "PS vacuum system improvement", CERN internal note MPS/ML/Note 69-3.
12. Möhl D., "Effect of vacuum pressure on beam instabilities", CERN internal note MPS/DL/Note 72-34.
13. Kubischta W., "Multiple target extraction sharing scheme at the CPS", Proc. of 8th Int. Conf. on High Energy Accel., CERN, Geneva, 1971, pp. 110-112.
14. Fiander D.C., "A design proposal for a full aperture kicker system for the CPS", CERN internal note MPS/SR/Note 71-3.
15. Bleeker J et al., "Development of an electrostatic septum at CERN", Proc. of 5th Int. Symp. on Discharges and Electrical Insulation in Vacuum, Poznan, 1972.
16. Kubischta W., private communication.
17. Bloess D., "Specification for the thin septum magnet for slow ejection 16", CERN internal note MPS/SR/Note 70-3.

18. Keyser R.L., "The development of large aperture septum magnets for slow ejection", CERN internal report MPS/SI/Int. MAE 72-5.

19. Bertolotto R., "Proposition pour la construction de nouveaux aimants à septum pour l'éjection rapide", CERN internal note MPS/SR/Note 72-4.

20. Hardt W., "Gamma-transition-jump scheme of the CPS", Proc. of this Conference.

21. -Gareyte J., Sacherer F., "Head-tail type instabilities in the CERN PS and Booster", Proc. of this Conference.
-Sacherer F., "Transverse bunched beam instabilities - Thaory", Proc. of this Conference.
-Möhl D., Schönauer H., "Landau damping by non-linear space-charge forces and octupoles", Proc. of this Conference.

22. Gyr M., "Studies on the PS octupoles", CERN internal note MPS/SR/Note 71-16/Corr.

23. Boussard D., Gareyte J., "Damping of the longitudinal instabilities in the CERN PS", Proc. of 8th Int. Conf. on High Energy Accel., CERB, 1971, pp. 317-320.

24. -Möhl D., "Equipment responsible for transverse beam instability in the PS", CERN internal note MPS/DL/Note 74-6.
-Faltens H, Umstätter H.H., "Longitudinal couplings impedances at insulated PS vacuum chamber flanges", CERN internal note MPS/LIN/Note 74-5.

25. Agoritsas A. et al, 'Techniques for measuring beam parameters", Proc. of 2nd USSR National Conf. on Part. Accel., Moscow, 1970.

26. Carpenter B., "Experiments with interactive control software at the CERN PS", Proc. of IEE Conf. on Software for Control, Warwick, England, 1973.

27. Madsen J.H.B., "The expansion of the PS control system", CERN internal note MPS/CO/Note 72-42.

28. Gouiran R., "La radioactivité de l'aimant du CPS et son influence sur la maintenance de l'anneau - Statistiques et prévisions", CERN internal report CERN/MPS/SR 73-5.

29. Coet P., "The work in highly radioactive experimental areas of the PS", CERN internal report CERN/MPS/MU-EP/72-2.

30. Steinbach Ch., "Beam dumping, the situation in January 1974", CERN internal note MPS/OP/Note 74-4.

31. Hoffmann L., "East hall transformation project", CERN internal note MPS/MU/Note EP/73-12/Rev.

SIMULTANEOUS STEERING OF H^+ AND H^- BEAMS AT LAMPF*

by

K. R. Crandall and W. E. Jule

University of California
Los Alamos Scientific Laboratory
Los Alamos, New Mexico

Summary

Based on analysis and computer simulations, it has become apparent that two kinds of doublet steering are necessary for linear acceleration of H^+ and H^- beams simultaneously. The respective advantages of steering by electrically "tilting" and "displacing" a system of doublets are described. Single dipole steering for simultaneous beams and the effect of the earth's magnetic field on oppositely charged beams is also considered. Finally, the implementation of this kind of steering at LAMPF is discussed.

Theory

Conventional steering superposes a dipole field to counteract any mechanical misalignment of a quadrupole. If one is dealing with a single quadrupole, this steering field can be applied in a manner which electrically moves the magnetic center of the quadrupole from its mechanical center to the correct design position. In Fig. 1 are shown force versus displacement diagrams for focussing and defocussing quads. A particle displaced a distance, x, from the quad center would feel a force, f,, as defined by the solid line. A steering field superposed on the quad field simply translates the solid line to the dashed line, and moves the magnetic center of the quad to point B. This type of displacement works for beams of opposite charge, since, while a quadrupole changes from focussing (F) to defocussing (D) when the sign of the beam changes, the steering field also reverses direction, The situation becomes more complicated when one considers two quadrupoles positioned close together which act as a doublet. In the standard approach, a series steering coil is wound on the two quadrupoles and the same steering field is applied to both magnets. From the above argument on how to electrically displace a quadrupole's magnetic center, one might conclude that equal fields applied in this way would electrically displace the doublet (both magnets are housed in the same case). Fig. 2 shows that this type of steering does not produce the desired effect.

Dipole steering fields applied in this way will electrically "tilt" the doublet, not displace it. This kind of steering, which we will call "tilted doublet steering" (TDS), works well for a single beam, but Fig. 2 shows that oppositely charged beams feel equal and opposite forces in traversing a tilted doublet; one beam would be steered onto the machine axis while the oscillation amplitude of the other beam is increased.

This difficulty can be overcome in the following manner. Consider only the horizontal plane for simplicity and consider a doublet which is FD for a positively charged beam. The force diagrams for this arrangement are shown in Fig. 3. It is evident that an electrical displacement of the doublet from A to B requires that equal and opposite forces be applied to the quadrupoles. We can accomplish this by applying equal and opposite steering fields to the ends of the doublet. This is called "displaced doublet steering" (DDS).

Now consider the force diagrams (Fig. 4) for a negatively charged beam. The first quadrupole is now D and the second quadrupole is F and the steering fields reverse their signs. So we see that DDS electrically corrects for misalignments of the doublet for negatively as well as positively charged beams. Hence the most versatile steering coil configuration is one which allows independent dipole fields to be superposed in both planes on each quadrupole. If economics, or other considerations dictate less versatile configurations of steering magnets, or the associated position sensing equipment, analytic techniques are effective in determining the best steering strategy.

Practice

At LAMPF there are 134 quadrupoles in the Alvarez linac and 103 doublets in the side-coupled structure. Since it would require two power supplies per quadrupole for electrical alignment, it is reasonable to investigate steering configurations which minimize transverse oscillations for a small number of steering positions. Hence, the first goal during construction is to attain the best doublet alignment possible. The doublets in the side-coupled structure are aligned to $\pm$ .007" and $\pm$ .4mr. Numerical simulations show that a .010" displacement has approximately the same effect as a 0.25mr doublet axis tilt. The alignments in the side-coupled linac are comparable to these, and hence it is necessary to have a combination of TDS and DDS.

In the side-coupled structure, one doublet per module is wired to provide a combination of TDS and DDS. However, each doublet has steering in only one plane. Based on numerical simulations, which also consider the number and location of position monitors, it has been found that steering in one plane in two sucessive modules and then in the other plane for the next two modules (i.e., the pattern is HHVV and then repeats) is an effective configuration.

The effect of the earth's magnetic field has also been considered. It is shown in reference 1 that the earth's field displaces the equilibrium orbit. Experimental results imply that this displacement is 0.15 cm in the side-coupled structure. The equilibrium orbit is displaced equally and oppositely for oppositely charged beams, hence to minimize transverse oscillations, it is necessary to steer so that the beams are positioned at their respective equilibrium orbits rather than at the design center of the linac.

In the Alvarez linac, there is not enough position information to establish that an off axis equilibrium orbit exists. However, it is expected that the effect of the earth's field would be small because of the steel in the tank wall which is not present in the side-coupled linac.

If one wishes to do effective steering, the position information should not be separated from the steering

*Work performed under the auspices of the U. S. Atomic Energy Commission.

magnet by too many intervening quadrupoles. If there are many misaligned quadrupoles before the position information, then the position information is not very useful. The best configuration seems to be to have position information in two successive cells after the steering magnet.

Acknowledgement

I would like to thank Don Swenson for suggesting the use of the force diagrams.

References

1. D. A. Swenson and K. R. Crandall, Los Alamos Scientific Laboratory, Private Communication, July, 1968.

2. D. A. Swenson, Los Alamos Scientific Laboratory, Private Communication, August 1968.

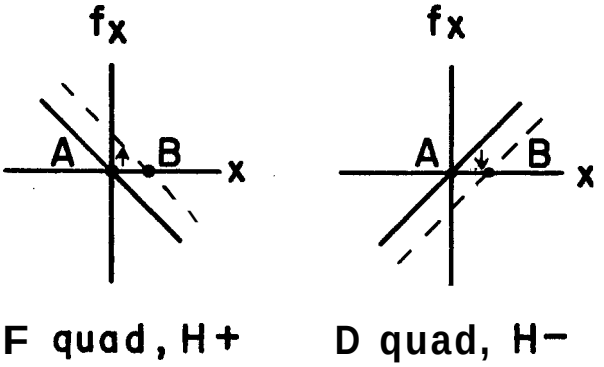

FIG. I

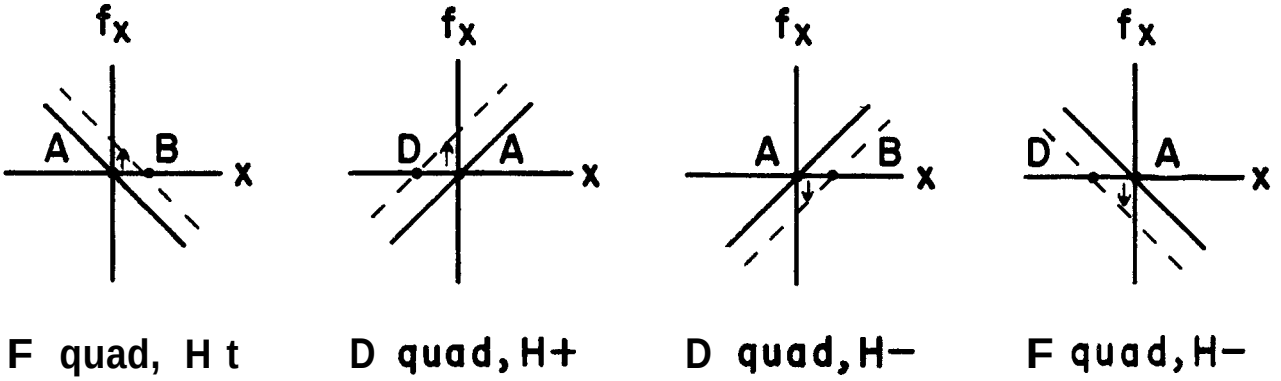

FIG. 2

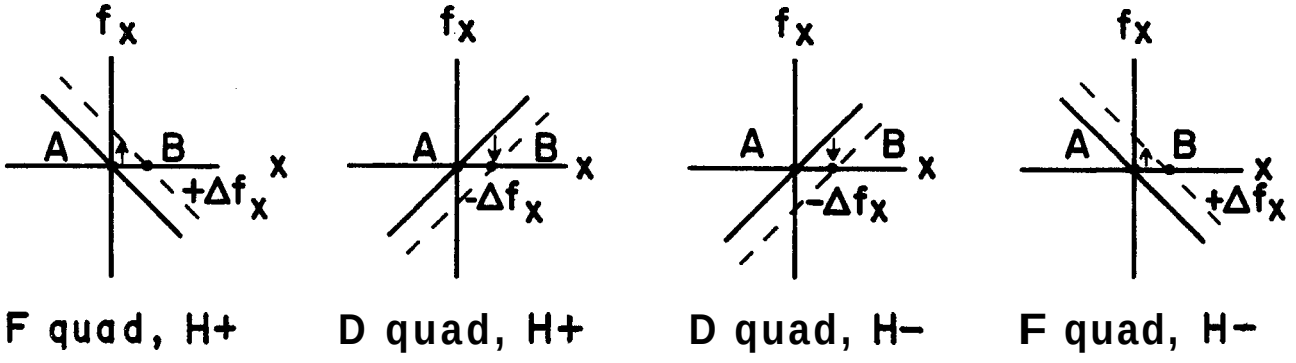

FIG. 3

FIG. 4

FUSION REACTIONS IN COLLIDING BEAMS*

John P. Blewett
Brookhaven National Laboratory
Upton, N.Y. 11973

Abstract

Two colliding beam configurations are presented in which fusion reactions can take place between deuterons and tritons. The first is a linear system in which the ion beams travel in the same direction and are focused by a collinear electron beam. In the second configuration the ions travel in a spiral path in a strong magnetic field and are focused by electrons travelling along the lines of force of the magnetic field. The first system yields very little power but the second appears to merit further attention.

1. Introduction

Students of controlled thermonuclear reactions tend to divide feasibility experiments using electromagnetic containment into "ordered" and "equilibrium" systems. The latter category includes virtually all of the magnetically contained plasma systems with which we are familiar. The former category, to which I propose to address myself, is generally regarded with disfavor; it is expected to reduce itself speedily to an equilibrium system by space-charge forces and by coulomb scattering. Furthermore, it usually includes a disproportionate amount of stored energy which, after the order in the system is lost, cannot be recovered.

In this paper I shall present two ordered systems. To the first all the above objections apply. The second seems to be less objectionable, and I present it herewith in the hope that some one will consider it further.

Many fusion reactions are possible candidates for use in production of power. The favorite, on which I shall concentrate, is:

Deuteron + triton → α particle + neutron + 17 MeV. This reaction goes at a relatively low temperature; the reaction cross section has a maximum of about 5 barns at about 100-keV energy for a deuteron bombarding a triton at rest. Most of the energy produced – about 14 MeV – accompanies the neutron.

First, we review briefly the arithmetic of fusion reactions in colliding beams. We consider colliding beams of deuterons with density ρ_D travelling at velocity v_D and tritons with density ρ_T travelling at velocity v_T. Densities are in coulomb per cubic meter; velocities are in meters per second.

In one cubic meter of the triton beam there are $6 \times 10^{18}\ \rho_T$ ions. These present to the deuteron beam a cross section of $6 \times 10^{18}\ \rho_T\sigma$, where σ is the fusion cross section. The rate of arrival of deuterons in the triton system is $6 \times 10^{18}\ \rho_D(v_D - v_T)$ per second. Hence the number of collisions per second per cubic meter is

$$36 \times 10^{36}\ \rho_T\rho_D\sigma(v_D - v_T) \qquad (1)$$

and the fusion energy liberated is

$$36 \times 10^{36}\ \rho_T\rho_D\sigma(v_D - v_T)E \text{ watts per cubic meter,} \qquad (2)$$

where E is the fusion energy liberated per collision.

For 100-keV deuterons bombarding tritons at rest the cross section σ has a maximum value of about 5×10^{-28} m^2. The fusion energy liberated per collision is 17 MeV or 2.7×10^{-12} joules. We assume that the velocities of deuterons and tritons correspond to a relative energy of about 100 keV, whence $v_D - v_T = 3 \times 10^6$ m/sec. We assume further that the densities of the two beams are equal so that $\rho_D = \rho_T = \rho_o$. With these assumptions we find that the fusion power is

$$1.46 \times 10^5\ \rho_o^2 \text{ watts per cubic meter.} \qquad (3)$$

If, for example, the system is to yield a fusion power of 1 megawatt per cubic meter, the charge density required is 2.6 coulombs per cubic meter, or about 1.5×10^{13} ions per cubic centimeter.

2. Linear Colliding Beams

The first example we present will be linear colliding beams. The results to be presented will be so absurd that the example will have value only as an indication of problems to be solved.

Suppose that two collinear beams of deuterons and tritons are brought into collision, each having a velocity of 1.5×10^6 m/sec. Going somewhat beyond the state of the art, we assume that both are 1000-ampere beams and that both have cross sections of 1000 square centimeters. This leads to a charge density of 6.7×10^{-3} coulombs per cubic meter and hence, to a fusion yield [from Eq. (3)] of 6.5 watts per cubic meter, or of 0.65 watts per meter of distance along the colliding beams. This seems a depressingly small yield, particularly when we realize that almost 60 MW have gone into producing the two colliding beams.

To improve the situation we make two changes:

a) We will make the two beams travel in the same direction at much higher energy.

b) The beams will be focused by an electron beam travelling in the opposite direction.

By these means the beam will be concentrated in a small cross section and the power level will be increased to more interesting levels.

It will be required that the deuterium and tritium ions differ in velocity by 3×10^6 m/sec as noted in the Introduction. Also the ions will be required to have the same energy so that both beams can come from the same ion source and so that the unreacted ions in both beams can be retarded by the same field to regain their kinetic energy.

These two requirements set velocities of 1.6×10^7 and 1.3×10^7 m/sec for deuterons and tritons respectively; both will have an energy of about 2 MeV.

Space charge and current fields produce a repulsive radial force in the ion beam of

$$E_r - vB_\theta = 2\ Ir(1 - \beta^2)/(\varepsilon_o \beta c r_o^2) \text{ volts/m} , \qquad (4)$$

*Work performed under the auspices of the U.S. Atomic Energy Commission.

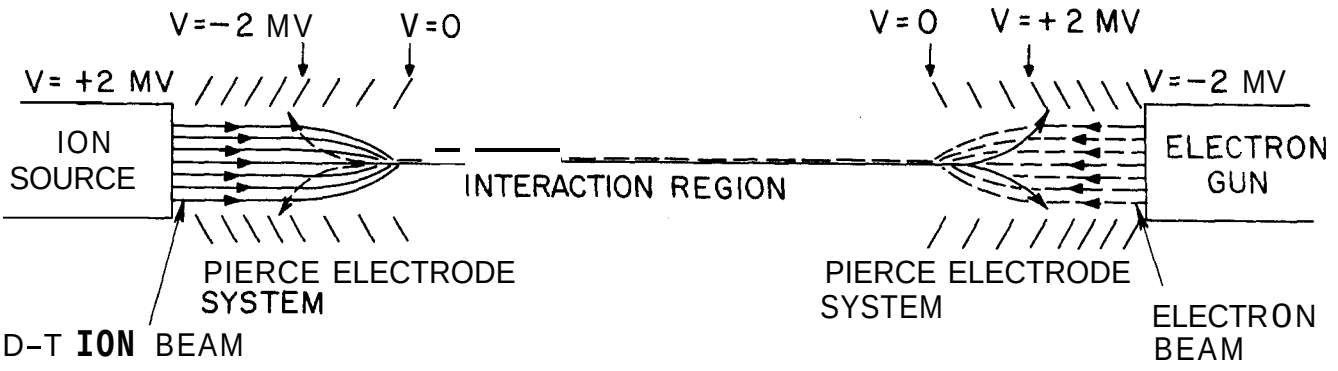

Fig. 1. Linear colliding beam system.

where I is total current (2000 amperes),
βc is ion velocity (about 1.5 X 10')
ϵ_o is the dielectric constant of free space (1.1×10^{-10} F/m)
r_o is the radius of the beam.

Approximately this force is

$$E_r - vB_\theta = 1200\ Ir/r^2 \text{ volts/m} \qquad (5)$$

If a relativistic electron beam of I_e amperes is now introduced, collinear with the ion beam but travelling in the opposite direction, it will contribute a focusing force of

$$2I_e r(1+\beta\beta_e)/(\epsilon_o \beta_e c r_o^2) \cong 60\ I_e r/r_o^2 \text{ volts/m}, \qquad (6)$$

where $\beta_e c$ is the electron velocity (assumed approximately equal to c). The internal forces in a relativistic beam approximately cancel each other and the electron beam will experience a focusing force due to the ion beam of approximately the strength given by Eq. (5). If the inward forces on ions and electrons are set equal, the electron current required proves to be about 80,000 amperes.

Under the forces just discussed, both beams will collapse to a small diameter determined by the original values of their emittances. If we assume (optimistically) an emittance of 100π cm·mrad for the ion beam, the final beam radius proves to be 1.4 mm. The charge density in each ion beam is about 11 coulombs/m^3 and the fusion power is now 17 MW/m^3. But the beam has become so small that the actual power generated per meter of beam is barely over 100 watts.

In Fig. 1 we present a configuration of electrodes for the linear colliding beam system. This arrangement makes possible the generation of 2-MeV beams of ions and electrons and the deceleration of both beams for recovery of the energy stored. One can safely conclude from the parameters just presented that such a system will never be built.

3. Proposed Configuration

What evidently is required to make a colliding beam system viable is a method for storing the ion beams until they interact. If this can be done the input ion currents become quite reasonable. For an output of 1 MW of fusion power all that is required is an input of 60 mA each of deuterons and tritons.

We note further that a prime requirement of the system is that it include strong restoring forces which will prevent coulomb scattered ions from leaving the system before they have time to take part in a fusion reaction.

The system to be proposed includes coincident deuteron and triton beams of the same momentum circulating in approximately circular paths in a rather high magnetic field, focused by a cylindrical beam of electrons travelling along the lines of force of the field. Figure 2 is a cross-section sketch of the geometry.

To satisfy the relative velocity criterion and to have the same momentum the deuteron energy must be 845 keV; the triton energy will be 564 keV. The deuteron velocity will be 9×10^6 m/sec; the triton velocity will be 6×10^6 m/sec. In a field of 6 tesla, the radius of curvature of these beams will be 3.0 cm.

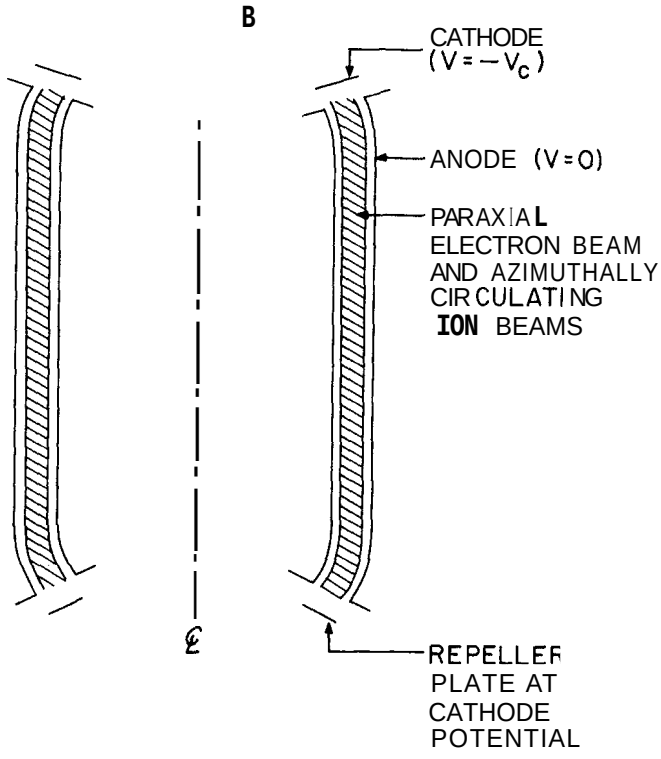

Fig. 2. Cross section through cylindrical colliding beam system.

4. Dynamics of the Electron Beam

We consider first the behavior of the electron

beam in the absence of the ion beams. The potential distribution in the beam must satisfy Poisson's equation

$$\frac{1}{r}\frac{\partial}{\partial r}\left(r\,\frac{\partial V}{\partial r}\right)+\frac{\partial^2 V}{\partial z^2}=\frac{4\pi\rho}{\epsilon}\ . \tag{7}$$

How the space-charge forces distribute themselves depends on two factors:

First is the boundary conditions. If, for example, we choose to concentrate the space-charge forces in the z-direction we use the continuity of space-charge condition and arrive at the classical $z^{4/3}$ potential distribution. In the present case, however, we choose to eliminate or at least minimize z-variations of potential due to space-charge fields; we can accomplish this by introducing electrodes which hold the outer and inner boundaries of the beam at zero potential (see Fig. 2). Now the primary potential distribution is radial and we can forget the second term on the left-hand side of Eq. (7).

The second factor to be considered is the dependence of electron energy on the potential distribution. If the electrons travel without deviation along the lines of force of the magnetic field, the high retarding space-charge field in the center of the beam will increase the density of the space charge in that region and this fact will need to be taken into account in the solution of Poisson's equation. This problem we shall bypass, and still hope to obtain significant results, by assuming that the electron source has infinitesimal radial extent but that, due to its finite emittance, all electrons are circulating about the lines of force of the magnetic field. The electron orbits will be considered further later in this section. This assumption will permit us to assume a charge density independent of radius and will simplify the solution of Poisson's equation. This solution, with the conditions that it must vanish at the inner radius (r_1) and the outer radius (r_2) of the beam, is rather easily obtained. It is:

$$V=\frac{\pi\rho}{\epsilon}\left\{r^2-\frac{(r_2^2-r_1^2)\ln r+r_1^2\ln r_2-r_2^2\ln r_1}{\ln(r_2/r_1)}\right\}\ . \tag{8}$$

If we assume that the radial extent of the electron beam is small we can simplify the expression for the potential by setting

$$r=r_o(1+\delta)$$
$$r_1=r_o(1-$$
$$r_2=r_o(1+\delta_2)\ .$$

Here r_o is a radius lying near the middle of the beam, to be defined more precisely later. With these assumptions, neglecting higher orders of the δ's, Eq. (5) becomes:

$$V=\frac{2\pi\rho\ r_o^2(\delta+\delta_1)(\delta-\delta_2)}{\epsilon} \tag{9}$$

The maximum value of V, to this order of approximation, will be for $\delta=(\delta_2-\delta_1)/2\ (\cong 0)$.

For example we assume an electron layer 1 mm thick extending from $r_1=2.95$ cm to $r_2=3.05$ cm. For reasons to be presented later we choose a value of ρ of 11.7 coulombs per cubic meter that leads to fusion yields of 20 MW/m^3; substituting for ϵ the value 1.11×10^{-10} F/m we find that the maximum value of the potential is 165,000 volts. Evidently the primary energy of the electron beam must be a little above this,

The motion of individual electrons is described by the following equations of motion:

$$m\ddot{r}-mr\dot{\theta}^2=eE_r+er\dot{\theta}B_z \tag{10}$$

$$\frac{1}{r}\frac{d}{dt}(mr^2\dot{\theta})=-e\dot{r}B_z \tag{11}$$

$$\dot{z}=\pm\sqrt{2eV_c/m}\ . \tag{12}$$

Here

E_r = [from (9)] $\dfrac{2\pi\rho r_o}{\epsilon}(2\delta+\delta_1-\delta_2)$ (13)

B_z = constant (6 T for the example to be considered)

V_c = cathode potential (greater than 165 kV in the example given).

The plus or minus sign in Eq. (12) depends on whether the electron is on a primary or reflected path.

From (11)

$$\dot{\theta}=-\frac{eB_z}{2m}\left(1-\frac{r_o^2}{r^2}\right)\ , \tag{14}$$

where r_o is the radius, somewhere near the middle of the electron sheet, where $\dot{\theta}=0$. If we write $r=r_o(1+\delta)$ etc., Eq. (14) becomes

$$\dot{\theta}=-\frac{eB_z\delta}{m}\ . \tag{15}$$

Substituting (15) in (10) we obtain

$$mr_o\ddot{\delta}-mr_o(1+\delta)\left(\frac{eB_z\delta}{m}\right)^2 = \frac{2\pi\rho r_o e}{\epsilon}(2\delta+\delta_1-\delta_2)-\frac{e^2B_z^2r_o}{m}\delta(1+\delta)\ . \tag{16}$$

Keeping only first order terms (16) becomes

$$\delta+\delta\left|\left(\frac{z}{\quad}\right.\right. \qquad \text{——} \qquad \text{——}$$

A first integration gives

$$\dot{\delta}^2+\delta^2\left[\left(\frac{eB_z}{m}\right)^2-\frac{4\pi\rho e}{\epsilon m}\right] = \frac{4\pi\rho e}{\epsilon m}\delta(\delta_1-\delta_2)+\text{integration constant.} \tag{18}$$

If $\delta=0$ for $\delta=\delta_2$ then the integration constant has the value

$$\delta_2\left[\left(\frac{eB_z}{m}\right)^2\delta_2-\frac{4\pi\rho e}{\epsilon m}\delta_1\right]$$

and

$$\dot{\delta}^2+(\delta-\delta_2)\left\{(\delta+\delta_2)\left(\frac{eB_z}{m}\right)^2-\frac{4\pi\rho e}{\epsilon m}(\delta+\delta_1)\right\}=0\ .$$

The other value for which $\dot{\delta}=0$ must be given by

$$\delta=\frac{-\left(\frac{eB_z}{m}\right)^2\delta_2+\frac{4\pi\rho e}{\epsilon m}\delta_1}{\left(\frac{eB_z}{m}\right)^2-\frac{4\pi\rho e}{\epsilon m}} \tag{19}$$

Evidently singularities will appear in this relation, and the electron sheet will become unstable if $(4\pi\rho/\epsilon)\cdot(m/eB_z^2)$ approaches unity. For the example we

have assumed (B_z = 6 T, ρ = 11.7 coulombs/m^3), this dimensionless quantity has the value 0.21 and the value of δ given by (19) is 0.26 δ_1 - 1.26 δ_2. If $\delta_1 \cong \delta_2$, the other value of δ for which δ = 0 is approximately - δ_1.

For those familiar with the notation of plasma physics, the quantity $(4\pi\rho/\epsilon)(m/eB_z^2)$ can be recognized as an analog of the plasma β function which is a measure of the ratio of plasma pressure to magnetic pressure. In a plasma @ must be kept below unity.

5. Dynamics of the Deuteron and Triton Beams

We assume, initially, that a small number of deuterons and tritons are injected into the space-charge field calculated in the preceding section for the electron sheet. These ions are to move in a flat spiral with negligible velocity in the z-direction. The method of injection into this orbit will be described in the next section.

Motion of the ions will be governed by

$$m_i \ddot{r} - \frac{m_i v_i^2}{r} = eE_r + ev_i B_z \quad , \qquad (20)$$

where m_i is the ion mass,
v_i is the ion velocity, given by $m_i v_i = - B_z e r_o$,
E_r is given by (13) above.

In the coordinates of the preceding section (20) becomes

$$\left(\frac{\quad}{\quad}\right) \frac{\quad}{1+\delta} = \frac{\quad}{\epsilon m_i} (2\delta + \delta_1 - \delta_2) - \left(\frac{\quad}{m_i}\right) \quad , \qquad (21)$$

whence

$$\ddot{\delta} + \delta \left[\left(\frac{B_z e}{m_i} \right)^2 - \frac{4\pi\rho e}{\epsilon m_i} \right] = \frac{2\pi\rho e}{\epsilon m_i} (\delta_1 - \delta_2) \qquad (22)$$

whose solution is

$$\delta = \delta_o \sin(\omega t + \varphi) - \frac{2\pi\rho e}{2} (\delta_1 - \delta_2) \quad ,$$

where

$$\omega^2 = \left(\frac{B_z e}{m_i} \right)^2 - \frac{4\pi\rho e}{\epsilon m_i}$$

δ_o and φ are determined by initial conditions.

We note that, since ρ represents the density of an electron space charge, the two terms in ω^2 both have the same sign. For deuterons

$$\omega = (8.33 \times 10^{16} + 6.33 \times 10^{19})^{\frac{1}{2}} = 7.96 \times 10^9 \quad .$$

The wavelength of this "betatron oscillation" is 0.71 mm (for deuterons). For tritons, ω = 6.50 x 10^9 and the betatron wavelength is 0.87 mm. This very short wave oscillation has its frequency determined almost completely by the density of the electronic space charge.

The very strong restoring force provided by the electron cloud should be effective in restoring to their orbits, ions that have undergone coulomb scattering either by other ions or by electrons. This topic is not analyzed in this report but must be given attention in future studies of this device.

6. Ion Injection

Deuterons and tritons are to be injected in such a fashion that they will continue to circulate in the magnetic field and will be unable to escape. During injection they will be given as little axial momentum as possible. Escape of ions at the ends of the devices will be prevented by a local increase in magnetic field The local increase in axial field will be accompanied by introduction of a radial field component which will serve to reverse the paraxial velocity of the ion beam. Field bumps of this type will be included at both ends of the device as indicated in Fig. 2.

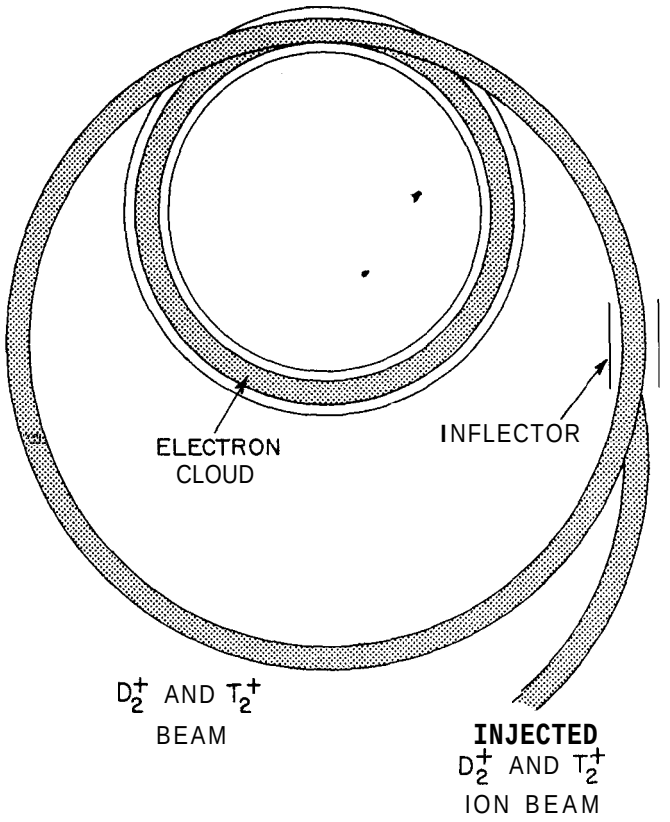

Fig. 3. Injection for cylindrical colliding beam system.

Several methods of injection will occur to the reader. One possible method is illustrated in Fig. 3. This method utilizes molecular ions which pass through an inflector to be deflected onto an orbit that intersects the electron cloud. Something of the order of 10%of the molecular beam should be stripped by electron collisions to become atomic ions which then will switch to orbits through the electron cloud (we assume a stripping cross section of the order of 10^{-16} cm^2). The remainder of the molecular ions will continue on circular orbits and return to the inflector. To prevent their loss by a second deflection, they will make their first entry into the inflector with a small component of paraxial velocity. The inflector is to have a finite axial extent and the paraxial velocity of the ions will be such as to allow the beam to miss the inflector on the second and later revolutions. Thus the molecular beam will re-enter the electron cloud several times

until virtually all of the beam has been reduced to atomic ions. This scheme has the virtue of allowing continuous injection. Pulsed injection procedures may, however, prove to be simpler and less demanding of extra magnetic field volume.

Another possible injection method would involve injection of neutral atoms produced by acceleration and stripping of negative ions. These techniques are well established for use in injection into the AGS. The neutral atom beam would be injected tangent to the electron cloud where a fraction of the order of 10% would be ionized and proceed on the desired circular orbits.

The procedure for initially combining the deuteron and triton beams into a single beam involves electrostatic deflection. The two beams, having the same momenta but different energies can be combined by deflection in an electrostatic field.

7. Procedure with High Density Lon Beams

The preceding sections dealt with the motion of ion beams of low intensity in a dense sheet of electrons. It has been shown that, to the first order, the motion of both electrons and ions is stable. There are large restoring forces on the ions which can serve to counteract the undesirable effects of coulomb scattering.

If, now, the electron density is doubled and the ion density is raised to the level of the original electron density, the net density and the electric field pattern will be unchanged. Only the distribution of B_z will be affected by the circulating ion current. For the densities quoted, B_z will drop by about 0.1 T through the thickness. This drop is too small to affect perceptibly the electron or ion motions.

The procedure to increase density would be to raise the injected ion currents. The potential maximum in the electron sheet would then drop and the electron current supply would automatically add electrons to restore the maximum value of the potential.

When the ion density has reached 11.7 coulombs/m^3, the fusion reactions will yield 3600 watts of fusion power per meter length of the system. The deuteron and triton supplies are required to provide only about 200 μA each to maintain this yield.

It would appear that the procedure of pushing ion current and electron current up, maintaining a constant difference between their charge densities, can be continued indefinitely to yield higher and higher levels of fusion power. No doubt, however, instabilities will put a stop to this. The point at which this happens will be difficult to predict theoretically and might more easily be determined experimentally.

DISCUSSION

V. Kelvin Neil (LLL): Your atoms are held in the device electrostatically rather than magnetically?

Blewett: *Yes.*

V. Kelvin Neil: And each one of these reactions which you're trying to get produces the helium?

Blewett: Yes.

V. Kelvin Neil: And the helium is also then electrostatically held? I'm trying to get to one of the problems in TOKOMAC where the helium is contained and, in effect, quenches the reaction.

Blewett (restating the question): The containment system is essentially an electrostatic containment system and that one of the products of the reaction would be a helium ion and will the helium ions do the same poisoning of the reaction as they do in TOKOMAC reactors? I don't think I can give a very good answer to that, except to say that the helium ions have about 4 MeV of energy which should be enough to kick them out of this region.

Leon Katz (University of Saskatchewan): Is this being proposed as a source of energy or as a source of neutrons for breeders?

Blewett: These are *sort* of interchangeable, aren't they? I should say that it is being proposed only as an experiment.

Arie Van Steenbergen (BNL): Charge exchange injection of accelerators is not an established fact.

WILL NEGATIVE HYDROGEN ION SOURCES SOON REPLACE PROTON SOURCES IN HIGH ENERGY ACCELERATORS?*

Th. Sluyters and K. Prelec
Brookhaven National Laboratory
Upton, New York

Although charge exchange injection into circular accelerators and storage rings has been proposed quite some time ago, the application of this attractive method has not been widespread because of low intensities of negative hydrogen beams available until recently. For synchrotrons and storage rings multiturn injection of protons via stripping of negative ions offers a better and simpler alternative to the present injection schemes by increasing the phase space density of the coasting beam. For cyclotrons injection of protons via stripping of relatively high energy neutral particles (obtained by partial stripping of negative ions) may alleviate the space charge problem during the early part of acceleration. However, beam intensities of negative hydrogen ions obtained by direct extraction from standard sources such as duoplasmatrons and Penning sources were seldom higher than several milliamperes, which was not sufficient for most of present circular accelerators. Indirect method of producing negative ion beams via charge exchange of protons, although at that time promising with respect to the intensity, had a disadvantage of yielding beams of a too low quality and requiring a too complex mechanical structure.

During the last year or so several papers and reports appeared describing two new approaches to the production of negative hydrogen beams extracted directly from a plasma. One of them was the hollow discharge duoplasmatron,[1,4,5] developed from a standard source by placing a rod along the main axis and reaching into the anode discharge region. A 100 μs pulsed beam of 6 mA was obtained with a normalized emittance less than 0.1 cm-mrad. An accompanying electron current of 0.5 A, a relatively low ion current density of 0.1 A/cm^2 and a high arc current of 100 A were features still to be improved.

The second approach was the use of the racetrack magnetron.[2,3,4] Even when operated with hydrogen gas only, the source yielded considerably higher H^- currents than a duoplasmatron. From an extraction slit of 1 mm × 10 mm, pulsed H^- currents ranged up to 75 mA, which corresponds to a current density of 0.75 A/cm^2. Even higher densities were obtained when cesium was injected into the source. The maximum reported[3] current density was 3.7 A/cm^2. These high current densities have been explained by an efficient production of negative ions at the cathode surface, especially when covered by a layer of cesium, and by decreasing the distance negative ions have to travel between the cathode and the extraction slit.

Prototypes of both sources have been built at BNL. With the hollow discharge duoplasmatron and hydrogen as the operating gas up to 8 mA of H^- current was obtained, corresponding to an ion current density of 0.25 A/cm^2. The normalized emittance was 0.3 cm-mrad and the pulse length 1 ms.

A significant improvement was achieved by injecting cesium through the hollow center tube. The beam intensity increased to 18 mA and the emittance remained about the same.

Two models of a magnetron source were also built at BNL. While the first of them already showed a behavior similar to the original source, there were several weak points in the construction and a new improved model was designed. By using a narrow extraction slit (0.5 mm × 10 mm) and with hydrogen as the operating gas, extracted H^- currents reached 17 mA, with normalized emittances in two directions of 0.44 and 0.60 cm-mrad at an extraction voltage of 8 kV. A dramatic change was observed after cesium was injected into the source. The extracted current of negative hydrogen ions increased to 100 mA, which corresponds to a current density of 2.0 A/cm^2. The normalized emittance measured in the direction of the extraction slit was 1.2 cm-mrad.

The new developments in the production of negative ion beams from sources using the direct extraction method have made their application more attractive in several fields. Current densities and phase space areas are becoming comparable to those of standard proton sources presently used in preaccelerators. Achievement of such characteristics seems to eliminate one of the main objections to the charge exchange injection into circular accelerators.

Acknowledgments

The assistance of many AGS staff members is greatly appreciated, especially V. Buchanan, R. Larson and L. Repeta in the design of the sources, power supplies and diagnostics and R. Clipperton and E. McKenna for the technical assistance and every-day operation of the ion source laboratory.

References

1. V.P. Golubev, G.A. Nalivaiko, and S.G. Tsepakin, Proc. Proton Linear Accel. Conf. (Los Alamos Report No. $4-5115, 1972), p. 356.
2. Iu.I. Bel chenko, G.I. Dimov, and V.G. Dudnikov, Novosibirsk Report No. 66-72, 1972 (in Russian).
3. Iu.I. Bel'chenko, G.I. Dimov, V.G. Dudnikov, and A.A. Ivanov, Novosibirsk Report No. 81-72, 1972 (in Russian).
4. K. Prelec and Th. Sluyters, Rev. Sci. Instrum. 44, 1451 (1973).
5. Th. Sluyters and K. Prelec, Nucl. Instrum. Methods 113, 299 (1973).

* Work performed under the auspices of the U.S. Atomic Energy Commission.

ISABELLE DESIGN STUDY OF INTERSECTING STORAGE ACCELERATORS*

H. Hahn
Brookhaven National Laboratory
Upton, New York

Summary. The present status of the ISABELLE design study for 200 x 200 GeV proton Intersecting Storage Accelerators at Brookhaven is presented. The most prominent features of this machine are the high center-of-mass energy of at least *400* GeV, the high luminosity of up to 10^{33} cm^{-2}sec^{-1}, the flexibility of the experimental insertions, and the use of superconducting magnets for bending and focusing of the beams. A general description of the design considerations and the main parameters is given. The possibility of future options, in particular the addition of a 15-GeV electron ring, is discussed.

I. Introduction

The advantage of using colliding beams to overcome the relativistic limitation in achieving the highest center-of-mass energies rather than beams from conventional accelerators striking stationary targets had been recognized early in accelerator history by Wideröe.[1] The original work at MURA on the stacking of many pulses[2] in each beam was fundamental for the achievement of adequate luminosity, and led directly to the design of the CERN ISR[3] which is at present the only proton-proton colliding beam device.

The construction of storage rings at the Brookhaven AGS had been considered previously in response to the recommendations made by the Ramsey panel.[4,5] A summer study was held at Brookhaven in 1963 to discuss the relative merits of accelerators and storage rings.[6] It was concluded that storage rings at AGS energies would be feasible, and a fir t parameter list for colliding beams was worked out.' At the same time it was pointed out by Jones[7] that storage rings of two or three times the circumference of the AGS could be used to accelerate the stacked protons to higher energies from 70 to 100 GeV. However, finally a decision was made not to construct storage rings, because it was thought that they lacked the versatility of a single proton accelerator of the same equivalent energy.

The idea of building storage rings at Brookhaven was revived in 1970 by Blewett[8] and this time it was greeted with enthusiasm. It soon received the endorsement of the Fitch committee which recommended that BNL apply its pioneering development work in superconducting magnets to build two proton intersecting storage accelerating rings to operate in the neighborhood of 200 GeV.[9] A study group was set up under Mills which issued a preliminary design study[10] (the "Gray Book") in 1972. The ISABELLE design has undergone a number of metamorphoses as documented in a series of publications.[10-15] However, the study has now advanced to a point where a revised version of the "Gray Book" is being edited.[16] A construction proposal will be submitted to the AEC in the near future. If funded in FY 1976 the ISA could be operational in 1981 providing an exciting facility for particle physics research.

The LSA design incorporates a series of innovations which will make it the frontier of high energy physics and accelerator technology. Its most prominent features are the high center-of-mass energy of *400* GeV, the high luminosity of up to 10^{33} cm^{-2}sec^{-1}, the flexibility of the experimental insertions, and the use of superconducting magnets for bending and focusing of the beam. This paper describes the present status of the ISABELLE design study, explains the basic design choices which had to be taken, gives a qualitative description of the machine components and the final parameter list, and concludes with an outlook on possible future additions to the basic proton-proton rings.

*Work performed under the auspices of the U.S. Atomic Energy Commission.

II. Basic Design Choices

Center-of-Mass Energy

The usefulness of the machine under consideration depends on many factors. One of these, the center-of-mass energy (usually designated by $\sqrt{s}$), is the single most important parameter in particle physics. The *400* GeV center-of-mass energy of the ISA is equivalent to that of a conventional accelerator of 86 TeV. In the U.S., the NAL accelerator, at *400* GeV, provides a center-of-mass energy of 28 GeV. The highest center-of-mass energies presently available is at the CERN ISR with an energy of 61 GeV. This is equivalent to a 2 TeV accelerator. The ISA will allow almost an order of magnitude increase in center-of-mass energy.

The choice of the ISA design energy is less obvious than that of the Bevatron, which was conceived to produce antiprotons. Current theoretical ideas give some indication as to the minimum energy desirable for the next machine. Simplifying greatly, one may state that there are two energy scales which a new machine should reach or exceed.[17] The first is set by the energy for which the strength of weak interactions equals that of electromagnetic interactions. Theories which would unify the Fermi theory of weak interactions and quantum electrodynamics have been proposed and postulate the existence of intermediate vector bosons (W), with rest masses above 37 GeV. Storage rings with 100 x 100 GeV would be adequate to produce these particles. In fact, the failure to observe W-production at center-of-mass energies larger than 100 GeV would cause difficulty for theories of this class. Another energy scale is given by the unitarity limit which for lepton-lepton interactions is about 300 GeV, but for hadron interactions may be near 600 GeV. It is clear, that with the weak, electromagnetic and strong interactions beginning to have the same effective strength at ISA energies, substantial new physics can be expected to appear before reaching the unitarity limit.

Another approach to choose the design energy would be to look at the historical progress of the accelerator field. The traditional step in center-of-mass energy has been a factor of *4* (AGS to NAL) to 8 (CERN PS to ISR). This would indicate a desired energy range from about 100 x 100 GeV to 250 x 250 GeV. The design energy of 200 GeV would thus appear to be justified from most points of view.

Luminosity

A design parameter as important as the energy is the luminosity of storage rings. The luminosity is determined by parameters of the machine such as the circulating current, beam emittance, geometry of the beam crossing region, tolerable beam-beam tune shift, etc. The design luminosity of the ISA has been fixed at

10^{33} cm^{-2}sec^{-1} per interaction region.

The ISA luminosity is expected to be more than two orders of magnitude above the values currently achieved at the CERN proton storage rings. This high value can be obtained by exploiting low-beta insertions, head-on (or small angle) collisions of the protons and, especially, the small emittance and high phase space density of the AGS at Brookhaven. An informative expression for the optimum luminosity of proton storage rings has been derived by Keil,[18]

$$L_{opt} = \frac{4}{3}\gamma\left(\frac{I}{e\,c\,r_p}\,\frac{\pi}{\epsilon_{inv}}\,\Delta\nu_{max}\,\ell\right)^{\frac{1}{2}}$$

which is obtained by adjusting the amplitude function at the crossing point to the value

$$\beta^*_{opt} \cong \left(\frac{ec}{8r_p I}\,\frac{\epsilon_{inv}}{\pi}\,\ell\Delta\nu_{max}\right)^{\frac{1}{2}} .$$

Here I is the current stacked in one ring, $\epsilon_{inv} = \beta\gamma\epsilon$ is the invariant transverse emittance which is assumed equal in the horizontal and vertical planes, ℓ is the unshielded free space between magnets around the collision region, $\Delta\nu_{max}$ is the linear tune shift due to the space-charge forces of the beam-beam interactions, e is the electronic charge, c is the velocity of light and, r_p is the classical proton radius.

The luminosity depends strongly on the current which can be stored and, in the case of the ISA, accelerated. An estimate of the more serious current limitations due to the beam induced gas pressure rise[19] and the transverse resistive wall instability (CERN's brick wall effect[20]) indicates that 10 A is a realistic figure for the ISA. The beam-beam tune shift tolerable in proton storage rings is not firmly established, but there seems to be agreement that $\Delta\nu_{max} \cong 5 \times 10^{-3}$ is a conservative limit. The present design provides a free space between magnets of ℓ = 40 m; this value could easily be halved at a later time if higher luminosities should be desired. The optimum luminosity depends directly on the emittance achievable; the AGS, with an $\epsilon_{inv} \cong 12.5\ \pi\ 10^{-6}$ m·rad, is ideally suited as an injector for a proton storage ring. The optimum luminosity in the ISA is obtained with β^*_{opt} = 0.7 m and reaches the level of $L_{opt} = 3 \times 10^{33}$ cm^{-2}sec^{-1}, a value which is comfortably above the design requirement.

Experimental Insertions

The anticipated experiments at the ISA differ in their specific requirements as to luminosity, tolerable momentum spread, shape and size of the crossing region, radiation background, etc. A number of experiments have been conceptually designed and the constraints on the experimental insertions have been established. It was concluded that only the small-angle scattering experiment requires an unusual straight section configuration to provide the desirable angular resolution of 25 μrad or better. Most experiments studied can be performed adequately in a general-purpose experimental insertion with a total of 40 m of free space around the crossing point and adjustable optical parameters. To preserve complete four-fold symmetry during commissioning of the machine, all four experimental insertions will be made identical. After having gained experience with the operation of the ISA, it will be possible to introduce other experimental insertions, also fully matched but in all likelihood no longer identical, which are better suited to experiments with special requirements. This concept provides considerable flexibility in the layout of the experiments, approaching that of a conventional accelerator.

Superconducting Magnets

The use of superconducting magnets has a significant impact on the expected performance of the ISA. The study of performance limitations due to collective effects indicates that most limitations become worse for a machine with a large radius and small vacuum chamber dimensions. Superconducting magnets are beneficial on both accounts:

i) Operation at fields of 40 kG, as assumed in the ISA design, reduces the machine radius by a factor of two when compared to a conventional machine of equal maximum energy. Superconducting 40 kG magnets using commercially available NbTi composite wires have been built and operated at Brookhaven, reliably and economically.[21,22]

ii) Operation of large-gap conventional magnets is prohibitive in terms of the electric power consumption. Economically designed conventional magnets limit the luminosity of storage accelerators, otherwise comparable to the ISA, to values of about 10^{32} cm^{-2}sec^{-1} which is an order or magnitude below the present design value.[23]

The use of superconducting magnets obviously necessitates the generation and maintenance of a low-temperature environment, 4.5 K in the case of NbTi conductors. The need for a dewar, refrigerator and liquid helium distribution system presents an economic burden which must be compensated for by savings in the construction cost due to the smaller tunnel size, vacuum equipment, and other field-dependent items, but also by savings due to reduced operating cost owing to lower electric power consumption. A comparison of the ISA with the low-luminosity conventional magnet ISA described in Ref. 23 shows that the initial capital expenditures would be at most 10% Less for the conventional magnet ISA. The annual electric power consumption, on the other hand, is clearly in favor of the superconducting machine: 35 GWh vs 90 GWh/year. At the rate of 2.8¢/kWh predicted for December 1974 this represents an annual savings of about $1.5 M in operating funds.

Performance and economical considerations point towards the superconducting solution. In arriving at a decision, the advantages must be balanced against the risk inherent in the application of a new technology. Superconducting magnet technology has advanced to a point that the performance of magnets, i.e. their peak field, field quality, and random errors due to fabrication tolerances, can be predicted with an accuracy equal to that for conventional magnets. Questions regarding the behavior of superconducting magnets in radiation environments have been proven manageable based on the experience gained from the operation of the 8° bend in the high-intensity proton beam to the North Area of the AGS.[22] Refrigeration systems of the capacity required have demonstrated their reliability in commercial use. It is our judgment that the technical know-how for the execution of thisproject is at hand.

Further advances in this field conceivably in time for the construction of the ISA are anticipated from the development of new materials of the A15 type such as Nb_3Sn or Va_3Ga which would bring 60 kG magnets into reach. These would be translated into an increase of the energy of about 300 GeV and a further reduction of the electric power consumption without essentially changing the financial scope of the project,

III. General Description

Ring Structure

The geometric configuration of the storage accelerator is essentially that of a circle expanded by four,

symmetrically located experimental straight sections, in which the beams are brought together in a horizontal small-angle or collinear collision region (Fig. 1). The total circumference of the rings is 2690 m corresponding to exactly 3-1/3 times the circumference of the AGS. Shown in Fig. 1 are the four experimental halls to be constructed from the start around the four collision points. The ISA consists of two intersecting magnet rings located one above the other in a common tunnel, the cross section of which is shown in Fig. 2. The AGS will be used as the source of 28.5 GeV protons which will be ejected into the beam line now feeding the North Area and the 7 ft bubble chamber, and which would be extended to the proposed location of the ISA. The area north of the AGS is reasonably level and the Brookhaven site provides ample space for future expansion.

The separated function lattice structure initially will have complete four-fold symmetry. The regular part of the ring contains *48* normal cells. The regular cell structure is broken into octants by adding four 250 m long (200 m straight) experimental insertions and four 110 m long (50 m straight) service insertions with the latter satisfying the machine requirements of injection, fast protective ejection, rf system, etc. The vertical separation of the beams will be 46 cm allowing a common dewar for the magnets of the upper and lower rings. The elements of a typical half cell are shown in Fig. 3. On the other hand, both rings are electrically and magnetically separated to permit experiments with unequal energies and to accommodate the antiproton option.

The normal cell uses a simple FODO sequence with two 4.25 m long (iron face-to-face) dipoles and one 1.3 m long (iron face-to-face) quadrupole per half cell. The total length of a normal cell is 25.40 m leaving a distance between magnets of about 1 m. The maximum amplitude function, horizontally and vertically, is β_{max} = *43* m and the maximum horizontal momentum dispersion is X_p = 1.7 m in the normal cell.

The service insertions are fully matched to the regular lattice and exhibit zero dispersion in the center while keeping the amplitude function at low values, $\beta_{vmax} \leq 110$ m (Fig. *4*).

Conflicting design requirements prohibit the use of a unique insertion for all experiments and a number of fully-matched experimental insertions have been worked out in detail: A general purpose modest-beta insertion, a high luminosity low-beta insertion, a small-angle elastic scattering insertion, and a multipurpose spectrometer insertion where the beams interact within a bending magnet. Initially, during the commissioning of the ISA, four general purpose modest-beta insertions ($\beta_v^* = 6$ m) will be installed to keep β_{max} to safe values, say below 300 m. Luminosities of 5×10^{32} cm^{-2}sec^{-1} at each crossing point should be achievable. In this insertion the crossing angle is adjustable from 0 to 6 mrad by means of horizontal steering magnets. To achieve the design luminosities a low-beta insertion ($\beta_v^* = 2.2$ m, $X_p = 0$ m) will be required imposing higher β_{max} and larger chromaticity (Fig. *5*). Further improvements in luminosity resulting from an even lower beta (the theoretical optimum is $\beta_v^* = 0.7$ m) and shorter free space between magnets, down to 20 m, are conceivable.

Beam Transfer

A number of schemes for transferring the AGS beam at 28.5 GeV to the ISA have been studied. The method of energy stacking now used at the CERN ISR has been adopted in view of its numerous advantages:

i) Operation of the AGS can be optimized for highest transverse phase-space density (instead of highest intensity) which is a prerequisite to achieving the highest luminosities. The intensity in the ISA is then simply built up by a larger number of AGS pulses.

ii) No modifications or additions to the AGS are required. Prior to ejection the total rf peak voltage in the AGS will be reduced from *400* kV to approximately 36 kV in order to match the AGS bunch shape to the bucket of the ISA stacking system. Existing equipment for fast ejection of the beam to the North Area would be retained for the beam transfer to the ISA.

iii) Aperture requirements for injection purposes are well matched to the available vacuum chamber aperture of 8 cm which has been determined by vacuum considerations.

The beam transport equipment from the AGS to the ISA is more economical if conventional magnets are used since it only needs to be energized during the stacking process. The ISA stacking rf system operates on the same frequency as the AGS *(4.45* MHz) and is designed for a peak voltage of 12 kV. To prevent self-bunching and dilution of the stacked protons, the impedance seen by the beam must be kept below 100 Ω, which is achieved by an appropriate feedback system.[24] The AGS pulse, with its intensity reduced to 2.3×10^{12} protons in 10 bunches, is captured directly by the stacking system, decelerated, slowly debunched and deposited into the unbunched stack. The AGS pulse fills only a fraction (⅓) of the ISA circumference; dilution of the stack is prevented by designing a stacking rf system with suppressed buckets. The design current of 10 A (or 5.6×10^{14} protons) will be reached in about one hour by repeating this cycle 250 times or more. Assuming a total longitudinal phase space dilution of 2 (which according to the CERN-ISR experience is not unrealistic) the momentum spread of the stacked beam will be $\Delta p/p = 0.7\%$, and its dimensions 2.0 × 0.8 cm in horizontal and vertical direction respectively. Estimates show that the design current of 10 A does not exceed the limits set by coherent transverse instabilities,[25] and the beam induced pressure rise,[26] if appropriate precautions are taken.

Acceleration System

In order to accelerate the stacked beam it will be rebunched by an rf system operating at the second harmonic, f = 223 kHz. Adiabatic rebunching can be done, in principle, without phase-space dilution or loss of particles but the 700 Ω impedance of the acceleration rf system necessitates a rebunching in the relatively short time of about 100 msec and some degradation of the beam must be expected (note that the accelerating gaps are shorted during the stacking procedure). The peak rf voltage, which is determined by the momentum spread of the stacked beam to be *40* kV, is provided by four ferrite loaded cavities. The energy gain per turn of 12.5 keV during the 2 minute acceleration cycle is well within the capabilities of the rf system. No insurmountable difficulties with accelerating the beam *of* 10 A are expected: The choice of the 2nd harmonic shculd make the beam essentially stable against longitudinal bunched beam instabilities;[27] estimates of the transverse resistive wall instability indicate that the bunched beam will remain stable if the unbunched beam was stable; diffusion from a repeated crossing of the 5th order resonance during the acceleration cycle was numerically computed and found to be inconsequential, 3rd or 4th order resonances, however, must be avoided at all times even when the momentum spread (and tune spread) is increased to about 2% as a result of the bunching.[28] After the acceleration cycle, the rf is switched off, the cavities are shorted again, and the beam is allowed to debunch retaining the 0.3% momentum spread of the bunched beam.

Superconducting Magnet and Dewar System

A program to develop superconducting magnets for use in accelerators and beam transport lines has been going on at Brookhaven for ten years and has led to the construction of dipole models which satisfy most of the important design criteria of the ISA magnets. The experience gained from the two identical 1 m long ISA models[21] and the two 1.8 m long dipoles for the so-called 8° bend[22] used in the extracted primary proton beam line to the AGS neutrino area will be described elsewhere in this paper. As will be substantiated there, the results have provided conclusive information concerning the question of stability, magnetic field precision (i.e. systematic errors), reproducibility (i.e. random errors), reliability, and behavior in a radiation environment.

Stability of the magnets, with the absence of quenching (transition to the normal state) or training effects (higher fields can be reached only after repeated quenching), is essential in the application of superconducting magnets to accelerators. The Brookhaven magnets have shown a remarkable degree of stability and, in fact, operation in the resistive region above the short sample critical current (defined by a resistivity of 10^{-12} Ω-cm), has been possible.

Systematic deviations from field uniformity (actually the dipoles will need a sextupole term for adjustment of the chromaticity) must be avoided at all field levels encountered during operation (6 to *40* kG). One requires roughly that the prescribed field shape of the magnets is accurate to within a few parts in 10^5 over the entire aperture of the vacuum chamber (8 cm diameter representing 67% of the magnet coil aperture). Systematic errors which are the same from magnet to magnet, may be introduced by the conductor arrangement, by the construction of the coil ends, by iron saturation effects, by diamagnetic effects in the superconductor itself, and by rate-dependent eddy currents. Saturation and magnetization effects are field dependent and require special attention. The results from the various models indicate that a single sextupole tuning coil is sufficient to compensate all important magnet errors. However, additional tuning coils must be incorporated to provide full control over the working line in the presence of space-charge effects.

Random errors, or deviations from magnet to magnet, are mainly caused by fabrication tolerances in the position of the conductors or the concentricity of the coils in the iron shield, by a nonsymmetrical gap in the median plane of the iron shield, and possibly by other causes. Closed orbit deviations, gradient errors and imperfection stopbands are caused by random errors. Briefly, one requires differences in the dipole fields of $\Delta B/B \leq 5 \times 10^{-4}$ rms and in the quadrupole gradients of $\Delta G/G \leq 10^{-3}$ rms. Estimates of the permissible random field errors indicate that tolerances on the conductor position of ≤ 50 μm rms are required. Measurements confirmed that these tolerances can be achieved with the particular construction technique employed in the ISA models. Multipurpose correction windings will be installed in all magnets to provide compensation of random field errors at least up to the decapole component.

The reliability of superconducting magnets, that is the absence of changes over long operating periods or changes due to thermal cycling, is being tested in an ongoing life test; after 5000 pulses simulating 10 years of normal ISA operation no indication of changes has been detectable.

The effects of radiation on the materials used in the magnet construction certainly requires consideration The critical current density of NbTi is essentially unaffected by particle fluxes up to[29,30] 10^{17}/cm^2 so that it is unlikely that the superconductor will be degraded in normal operation. Care must be taken to avoid plastics which are most sensitive to radiation damage; epoxy-impregnated fiberglass will, therefore, be used almost exclusively in the windings. Quenches may be initiated by localized heating from beam spills, but the 8° bending magnet has demonstrated that a properly cooled magnet is able to withstand a fair amount of beam heating without destruction of the superconducting state. An accidental beam spill of the entire stored beam may present a serious problem, this being the case for superconducting and normal magnets alike.

The study of the recent literature on superconducting magnets proves that a number of different designs have been successfully employed. At Brookhaven two alternate styles, the window-frame and the cosine magnets, have been tried. In order to be definite, the design and cost estimate of the ISA have been based on the cosine magnet. It is well known that a pure dipole field is provided by coils of circular cross section with a cosine current density distribution. In the actual construction, shown in Fig. 6, the ideal current distribution is approximated by six current blocks per quadrant, of different azimuthal widths, but equal current density. Exact positioning of the blocks is determined in a way to suppress the five lowest harmonics. The current blocks are built up with a single layer of wide flat braid (about 2.1 cm x 0.05 cm). The braid is composed roughly of 100 twisted composite wires, 0.3 mm in diameter, each containing, typically, *400* superconducting NbTi filaments of 10 μ diameter. The wires in the braid have a CuNi jacket to increase the coupling resistance between wires and thus decrease eddy current effects to tolerable levels during pulsing. The iron core tightly surrounds the coil, and as an integral part of the construction, must also be at liquid helium temperature. The physical length of the dipoles is 4.25 m, that of the quadrupoles is 1.3 m. The inner diameter of the coil is 12 cm, the outer diameter of the iron is 40 cm. The stored energy per dipole is 465 kJ at 40 kG, there are 256 dipoles per ring, and the total stored energy is about 120 MJ per ring. Since the vacuum chamber is warm, adequate thermal insulation must be installed between the vacuum chamber and the magnet coil. Special requirements on this insulation are established by the need for outgassing the vacuum chamber at 2000 C.

Two magnets, one from the upper and one from the lower ring, will be contained in one dewar (Fig. 7). This configuration has the advantages that all vacuum joints are directly accessible for leak tests at room temperature, but it may lead to higher heat loads unless special precautions are taken. Heat loads from current leads will be minimized by having cold connections between all dipoles of one octant of the ISA ring. In this arrangement, the current in the dipoles can be chosen almost arbitrarily. In the ISA dipole it is 3.3 kA at full field to keep voltages induced during a quench within tolerable bounds. However, for the purpose of magnet protection during a quench, it is necessary to provide current leads from every other magnet which are connected to shunting diodes. Since these leads are normally not in use, they can be designed for lower current carrying capacity (here 1000 A). The quadrupoles will be designed for a current of 500A at the highest gradient of *6.6* kG/cm and a pair of leads for each quadrupole is foreseen.

The ISA design calls for *40* kG superconducting magnets. This choice is based on the present-day availability of NbTi filamentary superconducting wires from commercial sources in this country and the experience with magnet models at Brookhaven and at

other laboratories. It is conceivable that improvements of magnet design and construction techniques will result in magnets which can be operated reliably at 60 kG. The reduced current carrying capability of NbTi superconductor at 60 kG must be compensated by a larger conductor cross section resulting in increased superconductor cost. But, since the superconductor represents only a fraction of the total magnet cost, the price increase for 60 kG is not significant when compared to the total cost of the project. Work is in progress to test the concept for 60 kG magnets.[31] The prospects for early development of new superconducting materials, such as Nb_3Sn or V_3Ga, are encouraging. These materials would have an impact on the ISA design in two ways: First, their high critical temperature (18 K in the case of Nb_3Sn versus 9.5 for NbTi) makes operation at temperatures in the range from 8 - 9 K possible, resulting in substantial savings in the electric power consumption of the refrigeration system. Second, the critical current of these materials is higher by an order of magnitude considerably simplifying the design of 60 kG magnets. Filamentary Nb_3Sn or Va_3Ga wires are not yet available commercially in the U.S. because these compounds are brittle and must be fabricated in ways different from the drawing process used for NbTi. A diffusion technique has been developed at Brookhaven by which conductor samples have been produced.[32] In view of their great potential, the development of Nb_3Sn conductors will be emphasized and the construction of a 1 m long dipole model using this material has been initiated. First results from Nb_3Sn magnets are expected in less than a year. A final decision on the choice of the magnet for the ISA can he delayed until one year after approval of the project without affecting the orderly progress of the construction.

Refrigeration System

All components of the refrigeration system required to generate the cold environment for the superconducting magnets are conventional as to their design which is similar to that used in large helium liquefiers in gas fields. Their sizes are comparable to the industrial liquid nitrogen or natural gas liquefiers which have an established record of reliability. The operating temperature of the superconducting magnets was specified at ≤ 4.5 K which can only be achieved by pool boiling of liquid helium. Some consideration has been given to the optimum choice of the operating temperature. Earlier studies of the GESSS (General European Superconducting Synchrotron Study)-group[33] seemed to favor lower temperatures down to 3.5 K. Our analysis showed, however, that the greater cost and complexity of a refrigeration system designed for subatmospheric pressure does not seem to be commensurate with the gains made possible in the magnetic design. Furthermore, operation at lower temperatures increases the electric power consumption, thus providing a compelling argument for temperatures at or above 4.2 K.

The refrigeration system of the ISA must function in a variety of situations: normal operation, cooldown, bake-out of vacuum chamber, etc. The system's requirements are set by the normal operating condition with all magnets excited to full field. The total accelerator heat load in this case is about 20 kW, of which only 15% represents excitation-dependent ohmic losses. The total refrigerator capacity of 23 kW is provided by a system consisting of a central six-unit four-stage compressor station and eight 2.9 kW refrigerator cold boxes which are installed close to each octant. The refrigerator units are designed with four expansion engines, with the final expansion employing either a wet engine or a Joule-Thompson valve. The electric power requirements at the compressor motors are 9.5 MW with J-T valves or 7.5 MW if wet engines are used. Since available information about the reliability of wet engines is insufficient it is planned to install a parallel J-T valve, which could be put into operation if the wet engine fails. For greatest operational simplicity, the refrigeration system is designed entirely without liquid nitrogen usage. A total of 136 000 liters of liquid helium is contained in the filled dewars of the ISA. Nevertheless, it will be possible to cool and fill the entire ISA in less than 1 week,

The response of the refrigeration system to a number of faults has been analyzed in detail and precautions to prevent possible loss of refrigerant have been incorporated into the design:

i) The quench of a single magnet may lead to a quenching of all magnets in one half-cell which are cryogenically coupled. The release of the 1.8 MJ during the quench will result in the evaporation of 800 liters of liquid helium which will be vented into a low-pressure buffer device, The dewars will be refilled and ready for operation after about ½ hour.

ii) Shutdown of one of the 8 refrigerator units can be tolerated during normal operation of the ISA, since the system was sized so that 7 units are adequate to carry the Pull load. The helium distribution system is interconnected around the entire ring, and the computer control system assures equal loads in the refrigerator units.

iii) Unscheduled loss of electric power would cause transfer of the liquid helium to liquid storage vessels by pressure build-up in the dewars. A loss of 15% of the helium must be expected if the electric power remains off for longer than 10 hours. By providing an emergency diesel-powered compressor this loss of refrigerant can be prevented.

iv) The worst fault would occur if the protective beam dump fails and the beam with its 20 MJ energy is spilled into the magnets. This would evaporate, in a short time, over 8000 liters of liquid helium which could not be recovered.

Magnet Power Supply

The demands on the magnet power supply are modest as a result of the slow two-minute acceleration cycle. The total energy stored in the bending magnets of each ring is about 120 MJ. Therefore, a 2 MVA rated power supply is adequate. With the peak dipole current of 3.3 kA the required power supply voltage is about 600 V. These are ideal parameters for solid-state rectifiers-inverters. The power supply will be a six-phase SCR system including a passive inductance-capacitance filter to reduce the ripple to the required $\Delta I/I \leq 10^{-6}$. The quadrupoles, sextupole and correction element windings, and the magnets in the experimental insertions, will be supplied by similar power supplies at much lower power levels.

The large total stored energy makes it important to include fault protection in case of a magnet quench. For this purpose shunting power diodes are included across the magnets in each dewar. These operate below their voltage threshold for current conduction under normal operation but provide a current path in case of a quench.

Vacuum System

The density of residual gas molecules in proton storage rings must be lower by several orders of magnitude than in conventional accelerators. This is necessary to reduce beam blow-up from multiple Coulomb scattering or inelastic nuclear scattering and the accom anying background radiation. The design, therefore, calfs for a pressure of 10^{-10} Torr in the circular

quadrants of the ring and 10^{-11} Torr in the experimental insertions. Electrons and negative ions trapped in the Coulomb field of the beam must be removed with suitable clearing electrodes.

Experience with the CERN ISR shows that the most serious current limitation is set by the beam-induced gas pressure rise (pressure bump phenomena).[19] Qualitatively, this effect is caused by ionized residual gas molecules being propelled electrostatically against the vacuum chamber and liberating adsorbed molecules in sufficient quantity to increase the gas pressure. At some value of the current, this pressure leads, avalanche-like, to the destruction of the beam. For the geometry of the ISA vacuum system (8 cm i.d. circular vacuum chamber, 5 m distance between pumps, each with 500 ℓ/sec pumping speed) the theory26 yields the limit $\eta I_{cr} \leq 30$ A where η is the desorption coefficient. The desorption coefficient of typical chamber materials at room temperature depends, predominantly, on the bake-out temperature and the surface condition. A desorption coefficient of $\eta < 3$ (permitting $I > 10$A) is expected with a bake-out temperature of 200° C and an argon discharge cleaning prior to assembly. The use of a vacuum chamber operating at liquid helium temperatures has been considered, but adandoned in view of experiment indicating desorption coefficients of several thousand.[35] Experiments to simulate the pressure bump effect are in progress and will allow an early verification of the assumptions used in the design of the ISA vacuum system.

The ISA vacuum chamber will be made of aluminum whose good thermal conductivity will prevent cold spots in the center of the cold magnets. The good electrical conductivity will alleviate resistive wall instabilities. The pumping will be provided by conventional Ti-sublimation pumps and ion-sputter pumps for non-getterable gases. The dewar construction provides direct access to all vacuum joints and pumps resulting in an almost conventional UHV system.

Control System

It is planned to operate the whole ISA-AGS accelerator complex from a central control center. This maximizes the information interchange between the two accelerator systems and minimizes the operating crew required. The various functions encountered in the operation of the machines, such as data collection, analysis and display, beam monitoring, or execution of operator instructions will be carried out by a carefully designed computer-based control system. If computers are considered as integral parts of the control system from the inception, a powerful system of great flexibility at relatively moderate cost will result.

ISA Shielding

Many of the considerations regarding the shielding requirements of conventional accelerators are equally applicable to storage rings. There are, however, important differences which had to be taken into account in the layout of the ISA shielding. Adequate shielding is required here for radiation protection against accidental beam spills, whose location and occurrence are unpredictable. The basic requirement is that a person outside of the shield will not receive a radiation dose exceeding 100 mrem in the worst case of 10^{15} protons dumped at any point. This will be satisfied by an earth cover extending to 160 m in any tangent direction in the plane of the accelerator and providing 6 m of earth in any transverse direction over the ring tunnel. The skyshine dose at the site boundary has been estimated to be 10^{-3} mrem per 10^{15} protons dumped. It is concluded that an off-site point would never accumulate the permissible annual dose equivalent of 1 mrem. At the end of its useful life span of typically one day, the beam will be dumped in a controlled fashion into a beam stop consisting of a metal block shield 4 m long and 1 m wide. Special requirements in regard to shielding will exist in the experimental areas, which are not related to safety considerations and can, therefore, be worked out after the machine has been put into operation.

IV. Future Options

A number of options have been investigated which could be added to the basic ISA at a later stage. The most attractive from the standpoint of physics research would be the addition of a facility for ep collisions.[36,37] Electrons would first be accelerated to 4 GeV in the AGS, they would then be accelerated to 15 GeV, providing high center-of-mass energies for ep collisions. This second acceleration could take place in an additional electron ring located either inside the ISA tunnel or, to minimize interference with the ongoing pp work, in a separate tunnel to the east of the ISA. Another more economical possibility is to accelerate the electrons in one of the ISA rings. The vacuum chamber in one, or perhaps both, ISA rings would be designed to allow water cooling on one side to carry away the large amounts of energy radiated from the electron beam. However, further studies are required to ascertain the feasibility of this approach. It is estimated that the luminosity of ep collisions would be greater than 10^{33} $cm^{-2}sec^{-}$ at electron energies up to 7 GeV (cm energy = 75 GeV) and then drop to 5×10^{31} $cm^{-2}sec^{-1}$ at the maximum electron energy of 15 GeV (cm energy = 109 GeV).

Special care was taken in the design of the basic ISA so as not to preclude the deuteron and antiproton option. Acceleration and storage of deuterons[38] should not present any particular problems and would make it possible to study proton-neutron and neutron-neutron cross sections with luminosities of about 7×10^{32} $cm^{-2}sec^{-1}$. Antiprotons39 can be produced by using one ring as a 200 GeV accelerator and the other as storage ring, providing $p\bar{p}$ collisions with a luminosity approaching 10^{29} $cm^{-2}sec^{-1}$.

V. A Two-Stage Approach to ISABELLE

A preliminary design study of a 100 GeV storage accelerator has been carried out in sufficient detail to provide the information required for a rough cost estimate.[40] In a situation where available funds limit the size of a project it may be necessary to consider a proton storage ring of lower energy and lower luminosity. The minimum energy of the next generation proton storage rings should represent a reasonable step beyond the CERN ISR and permit to test the region where the strength of weak and electromagnetic interactions are about equal. The opinion has been expressed that an ISA capable of 100 X 100 GeV at a luminosity of 10^{32} $cm^{-2}sec^{-1}$ is admittedly less attractive than the full ISABELLE but nevertheless fully justifiable in terms of the physics as presently understood and a natural step towards a superconducting 300 GeV ISA. The particular design was therefore done for a storage ring using the ISA tunnel. Here it is indicated to use conventional magnets at about 15 kG, with the exception of the 70 or so dipoles in the experimental insertions which should be superconducting to assure an optimum insertion design. The estimates show that the conversion penalty would be smaller than 20% of the ISABELLE cost. More objectionable, the physics program would have to be interrupted during a one year period.

Table I. Main ISABELLE Parameters

FINAL ENERGY	200 X 200 GeV
-Equivalent Accelerator	86 TeV
LATTICE (four-fold symmetry)	
-Circumference ($3\text{-}1/3 \times C_{AGS}$)	2690 m
-Experimental insertion length (straight)	4 X 250 (200) m
-Multipurpose insertions (straight)	4 X 110 (50) m
-Normal cell length	48 X 25.40 m
-Vertical distance between orbits	0.46 m
-Distance between magnets D-D (iron-iron)	0.90 m
-Distance between magnets D-Q (iron-iron)	1.0 m
GENERAL PURPOSE EXPERIMENTAL INSERTIONS (horizontal crossing, adjustable parameters)	
$-\beta^*_v$	2-6 m
$-\beta^*_h$	5-10 m
-Maximum β	1000 - 300 m
-Total free space around crossing point	40 m
-Crossing angle	0-6 m
-Interaction length	< 1 m
MAGNET SYSTEM	
-Bending field at 200 GeV	40 kG
at 28.5 GeV	5.9 kG
-Number of normal dipoles/ring	256
-Dipole length magnetic	4.11 m
physical (iron-iron)	4.25 m
-Peak current in dipole	3.3 kA
-Stored energy at 40 kG/dipole	465 kJ
-Vacuum chamber aperture (warm bore)	8 cm
-Main coil i.d.	12 cm
-Operating temperature (pool boiling)	$\leq$ 4.5 K
-Quadrupole gradient	6.6 kG/cm
-Peak current in quadrupole	500 A
-Stored energy/quadrupole	30 kJ
-Quadrupole length magnetic	1.16 m
physical (iron-iron)	1.30 m
CRYOGENIC SYSTEM	
-Total heat load at 4.5 K	$\approx$ 20 kW
-Total refrigeration capacity	8 X 2.9 kW
-Power requirements of compressors	7.5 MW
-Total liquid helium	136 000 liter
INJECTION	
-AGS energy	28.5 GeV
-Number protons/AGS pulse (10 bunches)	2.3×10^{12}
-AGS emittance $\epsilon_h = \epsilon_v$	$0.4\ \pi \times 10^{-6}$ m·rad
-Longitudinal phase space per bunch, A	0.36 eV·sec
-ISA current/ring	10 A
-Number protons/ring	5.6×10^{14}
-Number AGS pulses stacked	$\approx$ 250
-Stacked beam size	2.0 cm X 0.8 cm
-Momentum spread	0.7 %
-rf frequency stacking system	4.45 MHz
-rf voltage	12 kV
-Impedance (with feedback)	400 (40) Ω
ACCELERATION	
-Duration	2 min
-rf frequency (h = 2)	223 kHz
-Energy gain/turn	12.5 kV
-Peak rf voltage	40 kV
-Momentum spread at 200 GeV	0.3 %
LUMINOSITY	
L_{pp} (200 GeV, unbunched, β^*_v = 2 m, $\Delta\nu_{max} = 5 \times 10^{-3}$)	$\geq 10^{33}$ cm-2sec-1
$-p\bar{p}$ option, $L_{p\bar{p}}/L_{pp}$	$\leq 10^{-4}$
-dp option, L_{dp}/L_{pp}	$\cong$ 0.7
-dd option, L_{dd}/L_{pp}	$\cong$ 0.7
-ep option	
Maximum e-energy	15 GeV
Number of electrons	8.2×10^{12}
Maximum luminosity at 7 GeV-electrons	10^{33} cm^{-2}sec^{-1}
Luminosity at 15 GeV-electrons	5×10^{31} cm^{-2}sec^{-1}

Acknowledgments

This paper is adapted from the new ISABELLE design study report and thus summarizes the work of many members of the Brookhaven Accelerator Department. The study was coordinated by the ISA Parameter Committee composed of H. Hahn, Chairman, M.Q. Barton, J.P. Blewett, R.W. Chasman, E.D. Courant, J.G. Cottingham, G.K. Green, M. Month, M. Plotkin, I. Polk, R.R. Rau, J. Sandweiss, R.P. Shutt, and J. Spiro. The physics input to the design study was provided by the ISA Experimental Coordinating Group under the guidance of J. Sandweiss and R.P. Shutt, co-chairman, with C. Baltay, E.W. Beier, D. Berley, A.S. Carroll, W.E. Cleland, G.T. Danby, R.M. Edelstein, E. Engels, G. Finocchiaro, K.J. Foley, M.L. Good, P. Grannis, H. Jostlein, J. Kirz, J.T. Lach, D.M. Lazarus, L.M. Lederman, W. Lee, Y.Y. Lee, S.J. Lindenbaum, I.R. Linscott, R.I. Louttit, A.K. Mann, J.N. Marx, A. Maschke, J. Orear, S. Ozaki, R.B. Palmer, R.F. Peierls, J. Peoples, R.H. Phillips, L. Rosenson, C. Rubbia, J.S. Russ, N.P. Samios, W. Selove, L.W. Smith, G.A. Snow, M.W. Strovink, S.C.C. Ting, F. Turkot, C.L. Wang, W.J. Willis and the ex-officio members H.W.J. Foelsche, H. Hahn, V. Radeka, R.R. Rau, A.M. Thorndike, and J. Weneser. Further direct contributions to the design study were made by H.J. Halama, C. Lasky, H. McChesney, P. Mohn, W. Moore, G. Morgan, G. Parzen, E.C. Raka, W.B. Sampson, A. Schlafke, Th. Sluyters, and A. van Steenbergen, but also by many members of the Brookhaven Accelerator Department whose names had to be omitted here. Last but not least, the design study profited enormously from the comments made by our colleagues from universities and other accelerator centers during and after the 1972 Summer Study. It is a pleasant duty to thank the many contributors without whose efforts there would not be an ISABELLE design report.

References

1. R. Wideroe, BRD Patent 876279 (priority September 8, 1943).
2. J.W. Kerst, F.T. Cole, H.R. Crane, L.W. Jones, J.L. Laslett, T. Ohkawa, A.M. Sessler, K.R. Symon, K.M. Terwilliger, and N.W. Wilson, Phys. Rev. 102, 590 (1956).
3. K. Johnsen, Nucl. Instrum. & Meth. 108, 205 (1973).
4. E.D. Courant, BNL Report EDC-51 (1963).
5. J.P. Blewett, Proc. Intern. Conf. High Energy Accelerators, Dubna 1963, p. 75.
6. J.W. Bittner, Ed., Proc. 1963 Summer Study on Storage Rings, Accelerators and Experimentation at Super-High Energies, Brookhaven 1963.
7. L.W. Jones, ref. 5, p. 300.
8. J.P. Blewett, BNL Reports AADD-169 (1970) and AADD-175 (1971).
9. V.L. Fitch, Chairman, J.P. Blewett, R.L. Cool, E.D. Courant, M.L. Good, G.K. Green, V.W. Hughes, L.M. Lederman, S.J. Lindenbaum, F.E. Low, A.K. Mann, B.D. McDaniel, F.E. Mills, A. Pevsner, R.R. Rau, N.P. Samios, R.D. Sard, M. Schwartz, R. Serber, J.C. Street, A.M. Thorndike, M.G. White, and W.J. Willis.
10. J.P. Blewett and H. Hahn, Eds., BNL Report 16716 (1972).
11. J.P. Blewett. Proc. 8th Intern. Conf. High-Energy Accelerators, CERN 1971, p. 501.
12. E.D. Courant, Proc. 3rd All-Union Conf. Charged Particle Accelerators, Moscow, 1972, Vol. 1, p. 367.
13. F.E. Mills, IEEE Trans. Nucl. Sci. NS-20, No. 3, 1036 (1973).
14. J.P. Blewett, Proc. US-Japan Seminar High-Energy Accelerator Science, Tokyo and Tsukuba, 1973 (in press).
15. R.R. Rau, Comments on Nuclear and Particle Physics, (in press).
16. H. Hahn and M. Plotkin, Eds., "Design Study of 200 GeV Intersecting Storage Accelerator" (in press).
17. T.D. Lee, Phys. Today 25, No. 4, 23 (1972).
18. E. Keil, Report CERN/ISR-TH/73-48 (1973).
19. E. Fischer, ref. 12, p. 101.
20. K. Hubner, E. Keil, and B. Zotter, ref. 11, p. 295.
21. W.B. Sampson, P.F. Dahl, A.D. McInturff, K.E. Robins, this conference.
22. J. Allinger, G. Danby, B. DeVito, H.W.J. Foelsche, S.Y. Hsieh, J.W. Jackson, and A.G. Prodell, this conference.
23. W.J. Willis, G. Danby, H. Hahn, H.J. Halama, A.W. Maschke, M. Month, G. Parzen, and I. Polk, BNL Report CRISP 74-6 (1974).
24. E. Keil and B. Zotter, Particle Accelerators, 3, 11 (1972).
25. M. Month and K. Jellett, Nucl. Instrum. & Meth. 113, 453 (1973).
26. O. Grobner and R.S. Calder, ref. 13, p. 760.
27. F. Sacherer, ref. 13, p. 825.
28. R. Chasman, A. Garren, R. Gluckstern, and F.E. Mills, this conference.
29. K. Wohlleben, J. Low Temp. Phys. 13, 269 (1973).
30. W. Maurer, ref. 12, p. 222.
31. J. Allinger, G. Danby, and J. Jackson, this conference.
32. M. Suenaga and W.B. Sampson, Appl. Phys. Lett. 20, 443 (1972).
33. D.B. Thomas, ref. 12, p. 176.
34. S.K. Erents and G.M. McCracken, J. Appl. Phys. 44, 3139 (1973).
35. J.W. Bittner and H.J. Halama, ref. 12, p. 191.
36. R. Chasman and G.A. Voss, ref. 13, p. 777.
37. R. Chasman, Proc. DESY Seminar ep and ee Storage Rings, Hamburg 1973 (in press).
38. S. Ohnuma and Th. Sluyters, Proc. 1972 Proton Linear Accelerator Conf., Los Alamos, p. 191.
39. C. Baltay, R. Chasman, H.W.J. Foelsche, H. Hahn, M. Month, and A. van Steenbergen, this conference.
40. M. Month, L.N. Blumberg, R. Chasman, J. Claus, H. Hahn, H.J. Halama, G.H. Morgan, G. Parzen, I. Polk, E.C. Raka, and J. Spiro, BNL Report CRISP 74-8 (1974).

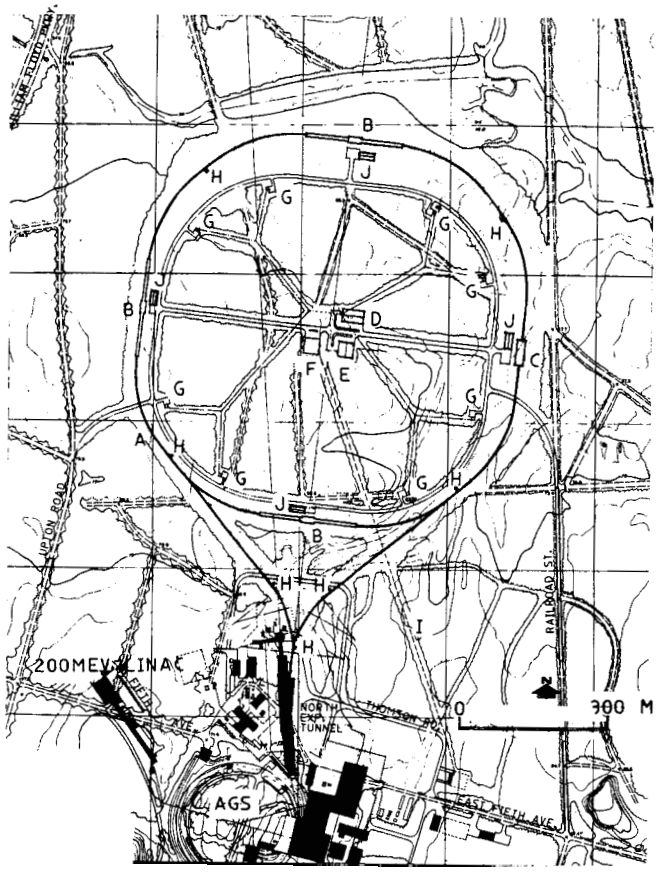

Fig. 1. ISA Site Plan. Legend: A-main magnet enclosure, B-large experimental halls, C-small experimental hall, D-compressor building, E-service building, F-69 kV substation, G-refrigerator buildings, H-exit buildings, 1-69 kV overhead line, J-assembly buildings.

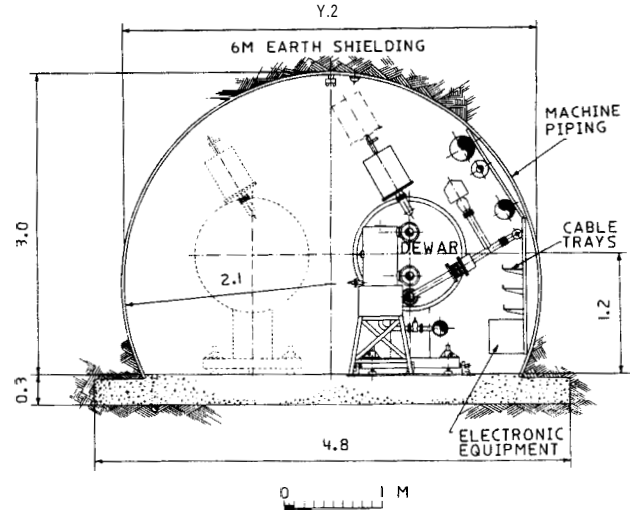

Fig. 2. Tunnel cross section (dimensions in m).

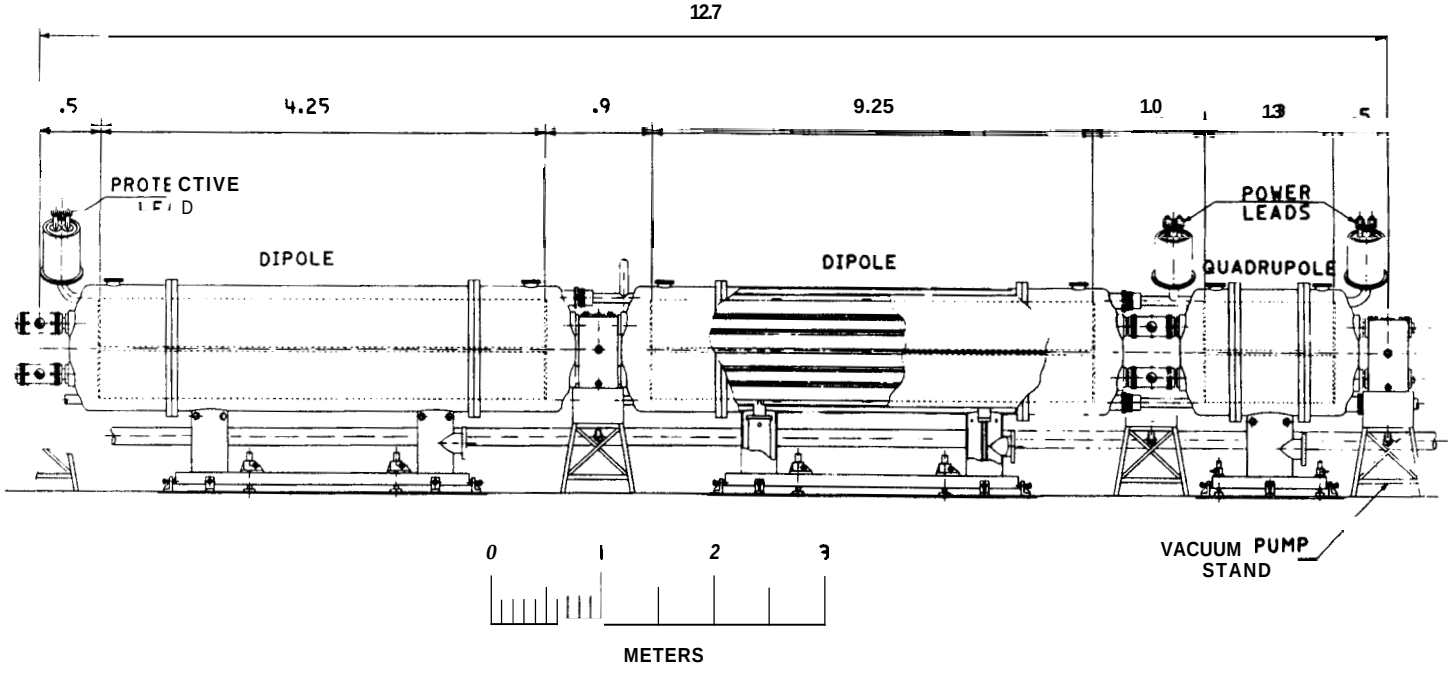

Fig. 3. Components of normal half cell (dimensions in m).

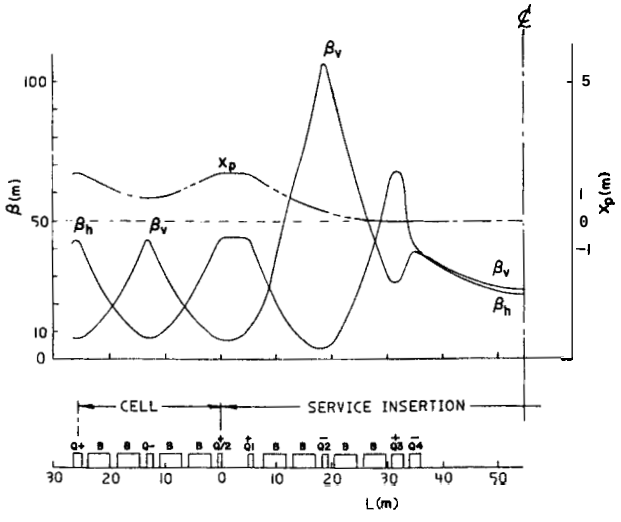

Fig. 4. Normal cell and service insertion.

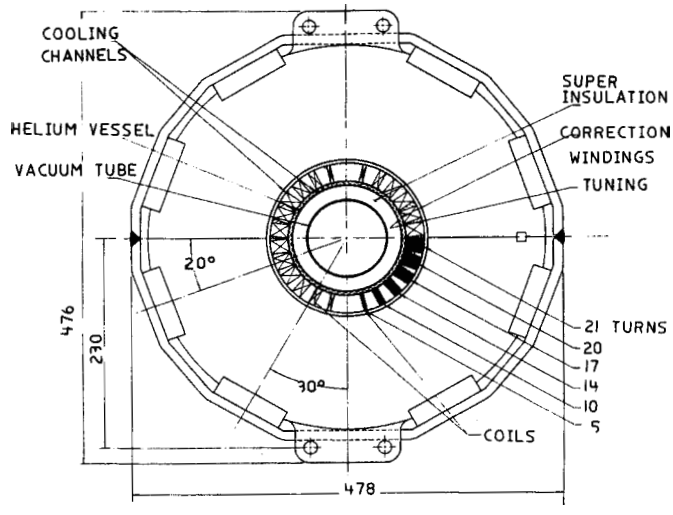

Fig. 6. Cross section of ISA dipole (dimensions in mm). Main parameters are aperture 8 cm, main coil i.d. *12* cm, main coil o.d. 16.2 cm, iron core i.d. 16.85 cm, iron core o.d. *40.6* cm, length *4.25* m, weight *4280* kg, current 3300 A at *40* kG.

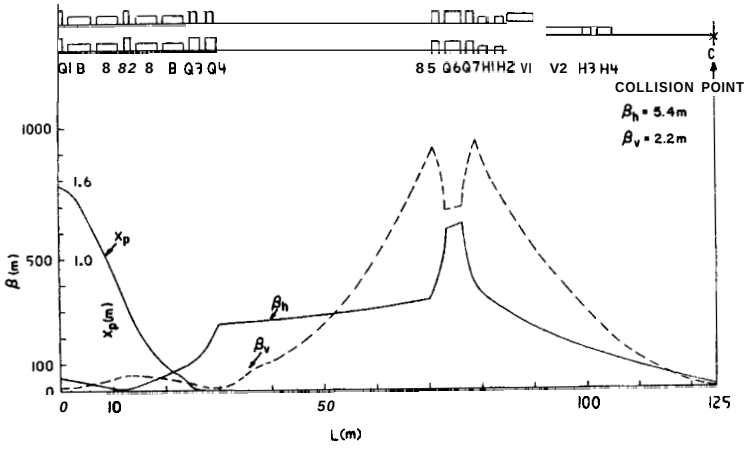

Fig. 5. Low-beta insertion. The same magnet configuration with modified quadrupole settings can be used as general-purpose modest-beta insertion.

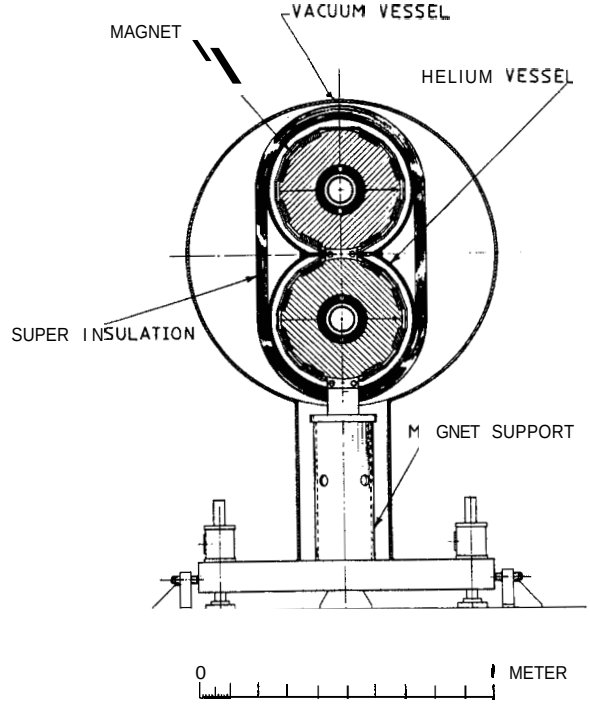

Fig. 7. Dewar cross section.

Paul Reardon (NAL): Have you done vacuum experiments in your prototype magnets?

Harold Hahn (BNL): No, but we have a very intensive vacuum program separate from the magnet program. When we still were thinking of a cold vacuum tube, we developed cryosorption pumps and tested their behavior with very good results. The design has changed in the meantime and we are now investigating the outgassing rate of aluminum after various treatments like argon discharge, bake-out at a certain temperature, and chemical polishing. We are convinced that the outgassing rate of aluminum after a heat treatment at 200° C is about an order of magnitude lower than required in the ISA. We have not yet completed a simulation experiment of the pressure bump phenomena. Results from this experiment should be available, I think, in summer.

Mark Barton (BNL): I would like to comment on Reardon's question. The vacuum problem has not been examined in the magnet, but the warm bore feature has. The Model II has warm bore.

Reardon: The bake-out of this special superinsulation is really an interesting question.

Hahn: The bake-out would be done, of course, while the machine is not in operation. Therefore, the heat leak from the bake-out can be compensated by the lack of a heat leak from the current leads. At least from the point of straight heat load, there is no problem.

Martin Donald (Rutherford): Do you have to cross transition energy?

Hahn: No. The transition energy is below the injection.

Rolfe Wideroe (SIN): Did you say how much the first phase of the project will cost?

Hahn: I didn't mention the cost. It will be official very soon; it's 126.5 million dollars.

Kjell Johnsen (CERN): You have in each beam a stored energy of about 20 MJ. Have you thought about how to get rid of it as a whole and what precautions do you take against dumping small fractions of it into the superconducting magnets?

Hahn: The present design foresees an internal beam dump, essentially the same system you have in the ISR. I would suspect that the real machine will be equipped with an external dump while keeping the internal beam dump as a protective device. We are aware of the importance of the beam dump. Does that answer your first question?

Johnson: I guess so, but our internal beam dump would explode if 20 MJ were dumped into it.

Hahn: To solve the problem caused by beam loss, we will use beam scrapers at well chosen locations around the ring. We have many straight sections far away from the experimental insertions and the idea is to scrape and dump small amounts of the beams at these locations. In addition, the experience with our superconducting magnets exposed to a full intensity beam from the AGS has shown that they can tolerate more radiation than at least some people thought they could.

Richard B. Neal (SLAC): I heard about a phased approach to ISABELLE. Could you describe what you have in mind?

Hahn: Clearly what we have in mind is what I have been describing today. Any other approach would have to be suggested by financial limitations by the AEC or some other "force majeure." But I think it could be implemented easily if required, and we have discussed a 100-GeV machine in the same ISA tunnel with conventional magnets to be replaced later by superconducting magnets. At this time, one would go most likely to 60-kg magnets and 300 GeV. The obvious question in such an approach is the conversion penalty which we estimate at not more than 20% of the total initial project. It also would provide us with magnets already usable for the electron ring. The interruption of the experimental program might be more serious, of course, and I would like to state again that what we want to build is what I have described in this talk.

David Thomas (Rutherford): This is a comment on magnets. In my talk, I said that all magnets are bad and I stick by that. I think no superconducting magnet will operate exactly at the design field and therefore one hasn't really licked the design problem. But having said that, I would like to put the record straight by saying the best of the bad designs on the basis of the performance specifications given here is certainly the Brookhaven magnet.

DESIGN AND STATUS OF EPIC

EPIC Machine Design Study Group of the
Rutherford* and Daresburyt Laboratories, United Kingdom

Presented by G H Rees

Introduction

The origins of EPIC date from the time when a study was undertaken of possible future machines for the national high energy physics laboratories in Britain. The new facilities were to replace the Rutherford and Daresbury accelerators NIMROD and NINA at the end of their useful lives. A few people from the two laboratories evaluated some storage ring machine designs[1], and one such design was described in an internal report[2]. This was based on a proposal made by Pellegrini et al. at the 1971 International Accelerator Conference[3].

The studies were given further impetus in the Autumn of 1972 by visits to the Stanford Linear Accelerator Centre of Professor Flowers, the then chairman of the British Science Research Council and Dr Stafford, director of the Rutherford Laboratory. The thoughts of Professors Panofsky and Richter of SLAC on the physics potential of high energy electron-positron and electron-proton colliding beam systems were communicated to their visitors. Before the end of 1972 an EPIC machine design study group had been established. From the outset it was a combined study between Rutherford and Daresbury Laboratories, for it was appreciated that only by pooling the resources of the two high energy laboratories would it be possible to realise a complex of the size of EPIC.

The first nine months of 1973 were spent obtaining approximate cost estimates for a two ring machine complex, with a number of different options envisaged for the actual construction stages[4]. The complex consisted of a single conventional magnet ring providing electron-positron colliding beams at incident momenta up to 14 GeV/c, together with a second ring housed in the same tunnel which would be capable of accelerating and then storing high energy protons. The second magnet ring was evaluated both for superconducting missing magnet schemes and for conventional magnets. As an electron-proton colliding beam system the peak proton momentum for a full superconducting ring was 200 GeV/c. During the initial design and costing, the study group recognised the machine design uncertainties in predicting the luminosity for the electron-proton colliding beams.

The costings are given in Table 2 of the following section, and were reported at the DESY Storage Ring Symposium of October 1973. At about that time it was decided to concentrate the studies towards a more accurate evaluation of the single ring electron-positron system. The two ring scheme for electron-proton interactions, though now only a long term objective, is still considered an essential feature in the design of the initial ring.

By October 1974 the revised evaluation of the electron-positron ring will be completed. A machine proposal will then be submitted for approval to the Science Research Council, seeking funding to allow completion of a 14 GeV electron-positron storage ring by 1981.

Electron-Positron-Proton Initial Feasibility Study.

EPIC has many features in common with the early design of PEP, which was reported [3] at the 1973 US Accelerator Conference. A schematic diagram of the proposed EPIC complex is shown in Figure 1. The two ring colliding beam system has four interaction regions, each of which is 17 m maximum in length. The rings are contained in a common tunnel, with the proton ring magnets situated vertically above the magnets of the electron machine. A system of vertical bending magnets brings the separate paths of the electrons and protons into coincidence over the central regions of the long straight sections.

In Figure 2 is shown a proposed lay out of the machine at the Rutherford Laboratory. The use of as much as possible of the existing laboratory facilities has been taken into account. The present linac buildings, the Nimrod magnet hall, main control room and two experimental halls are all planned to be used in the few facility. The 100 MeV electron linac, positron converter and 200 MeV positron linac will be located in the hall that presently houses the Nimrod 15 MeV proton linac. The Nimrod magnet hall will house a debuncher for the 200 MeV positrons together with the linac-booster beam transfer lines. The booster will be sited in its own shielding enclosure, half in and half out of one of the existing experimental halls. Most of the components for the transfer lines from the booster to EPIC will be available from existing experimental hall equipment.

The proposed lay out of the components in an insertion is shown in Figure 3, and typical lattice β-functions in the insertion in Figure 5. The range of the minimum β_H values at the centre of the insertion is 0.4 to 1.2 m in the e-ring and 1.0 to 2.5 m in the p-ring. Correspondina values for β_V are 0.1 m to 0.3 m in the e-ring and 0.4 to 1.0 m in the p-ring. Collinear crossings of the electron and proton beams in the insertions are brought about by vertical bending magnets. The bend angles in the dipoles nearest to the interaction region are 3.7° for the electrons and there is a large associated radiation loss. The choice of such a large bend angle is made to enable the proton-ring high-6 quadrupoles to be located as close as possible to the centre of the insertion.

The maximum design luminosity for collisions between 14 GeV/c electrons and 100 GeV/c protons is approximately $5\ 10^{31}\ cm^{-2}\ sec^{-1}$, but with a measure of uncertainty because of the incomplete understanding of the effects of the beam-beam interaction. There is no damping mechanism for the betatron and synchrotron oscillations for the protons, and it remains to establish the maximum allowable space charge forces on the protons in the collision regions of storage rings. Parameters relevant to the initial feasibility study are given in Table 1, where the luminosity estimates correspond to the maximum momentum particles.

*J R J Bennett, H C Brooks, M H R Donald, D A Gray, M R Harold, J D Lawson, J D Lewin, B G Loach, J R M Maidment, G H Rees, P F Smith and W A Smith

†E A Hughes, N Marks, D E Poole, M W Poole, V P Suller, G Saxon, T Swain, K Tarry and D J Thompson

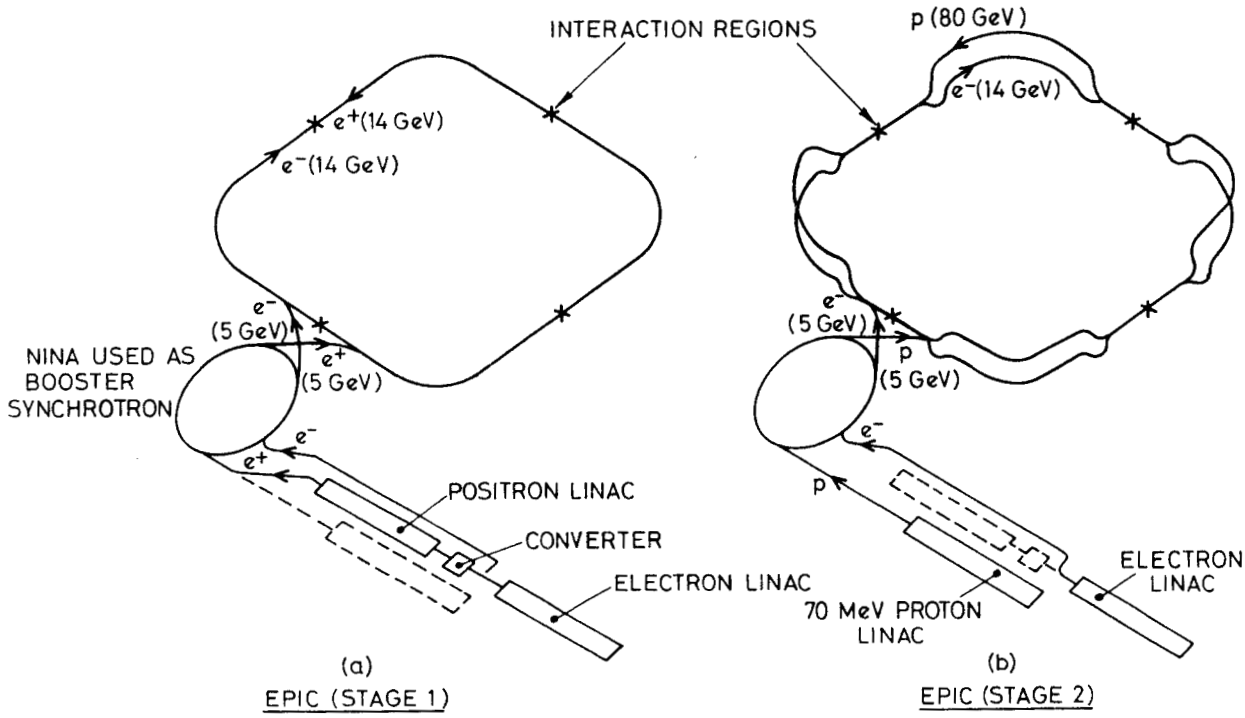

FIG.I. SCHEMATIC DIAGRAM **OF** EPIC (STAGE 1) FOR e^+e^- COLLISIONS AND EPIC (STAGE *2*) FOR **e p** COLLISIONS

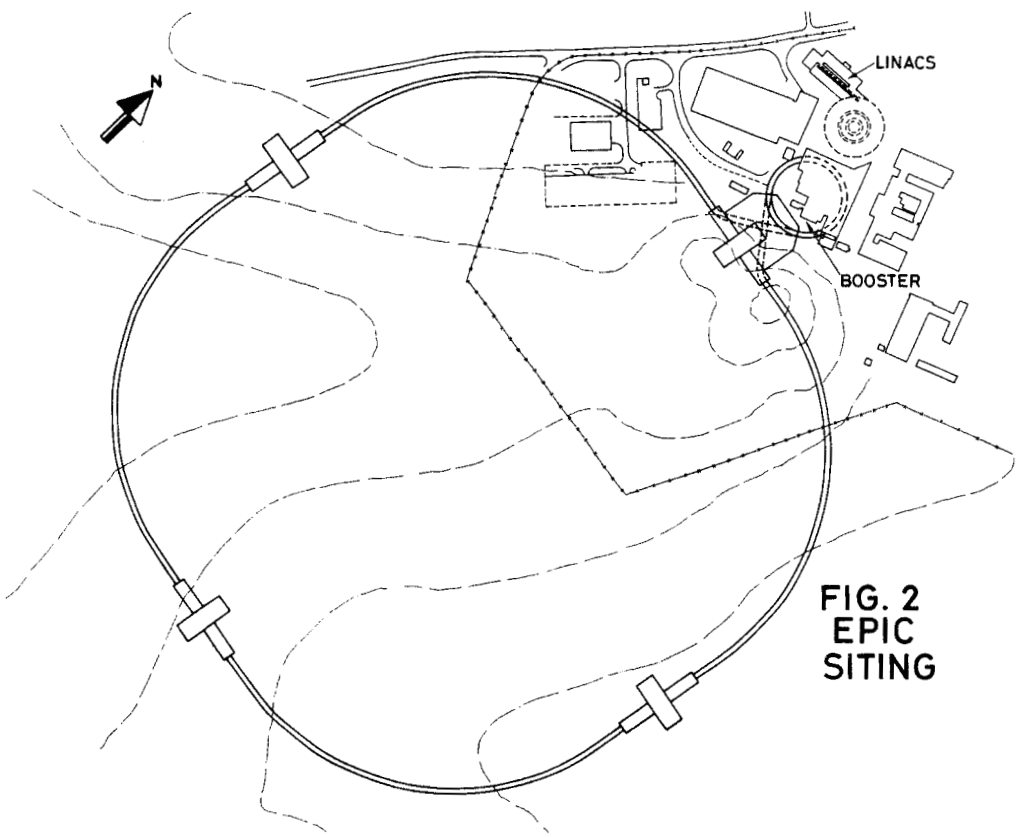

FIG. 2
EPIC
SITING

TABLE 1 - Selected Parameters
(Half-Full S/c Ring for Protons)

Ring circumference (metres)		2122.3	
No. of Interaction Regions		4	
Interaction region lengths (metres)		17.0	
Long st. section lengths (metres)		141.4	
No. of normal magnet cells		56	
No. of dispersion matching sections		8	
Machine tunes, Q		15.1-19.4	
	e-ring		p-ring
Maximum momentum (GeV/c)	14		100
Bending radius (metres)	168.1		74.5
Peak RF Voltage (Megavolts)	42.8		4.0
Peak radiated power (Megawatts)	2.5		0.0
No. of bunches/ beam for e-p	8		8
No. of particles/ bunch for e-p	$5\ 10^{11}$		$7.5\ 10^{11}$
e-p Luminosity ($cm^{-2}\ sec^{-1}$/Xn.)		$\sim 5\ 10^{31}$	
No. of bunches/ beam for e+ - e-	2		
No. of particles/ bunch for e+ - e-	$5\text{-}8\ 10^{11}$		
e+ - e- Luminosity ($cm^{-2}\ sec^{-1}$/Xn.)		$\sim 5\ 10^{31}$	

Preliminary investigation has shown that the vertical bending units may be used as spectrometer magnets for the detection of proton fragments which emerge from the electron-proton interactions at small angles. It is possible to place detection systems behind the common vertical dipoles which are downstream of the collision region for the proton ring. The shaded area of Figure 4 is an acceptance plot for the small angle fragments. The region marked (A) is related to an additional detector array installed normal to the beams at the location (A) of Figure 3. Similarly, (B) is realised by the use of a long septum magnet and further detectors at the corresponding point (B) in this figure. The use of machine components as spectrometer magnets is a feature missing from the PEP[5] and ISABELLE[7] e-p proposals.

A powerful RF accelerating system compensates for the synchrotron radiation energy losses of the electrons (and positrons). This leads to very short bunch lengths. For electron-positron collisions there are two bunches in each beam so that separation of the beams prior to collision is necessary only at the intersection regions. In the case of an electron-proton system there is the choice of using either bunched or unbunched proton beams. Provided that the problem of satisfactory bunch compression can be obtained and sustained for protons there are many advantages for the bunched option. The most important of these is the reduction in the total number of protons, easing the shielding requirements and the protection problems for superconducting magnet rings. In the EPIC design the choice is made of eight proton bunches together with eight electron bunches. The scheme for the required proton bunch compression is described in reference 2, and a method for separating the electrons and protons in the intersection region in reference 8.

Synchronisation is an essential feature of the collisions between bunched electron and proton beams. The increase of proton velocity with energy requires compensating path lengths in the particle orbits. Schemes considered for EPIC include: radial steering of the proton beam together with a number of different vertical 'dog-leg' insertions in the electron ring[9], continuously variable 'dog-leg' insertions[10] and moving the proton high-β quadrupoles to allow the electron energy to be changed at a given proton energy. Synchronisation becomes progressively more difficult at the lower proton energies and in the EPIC feasibility study the lowest proton momentum is restricted to 55 GeV/c.

A modified form of the Daresbury accelerator, NINA, will serve as a booster for EPIC. The combined function magnets are adequate for accelerating particles to a peak momentum of 5 GeV/c. The NINA repetition rate will be reduced from 53 Hz to 4 Hz, and an additional RF system will be installed. During the feasibility study it was considered that the booster could serve as an injector for electrons, positrons and protons. To this end, the gamma transition of the lattice was arranged to assist with proton bunch compression. Now there are reservations that the protons can be accelerated successfully in the presence of the electron RF systems. If a separate booster is developed for protons, it might also cater for deuterons. There is a strong physics case for studying electron-deuteron collisions[11] in EPIC in conjunction with electron-proton studies. However, the entire question of whether or not to use bunched proton beams must be reassessed if there is the additional requirement of providing deuteron beams.

The lattice design of EPIC is influenced by the need to provide an electron-positron radial beam size that satisfies luminosity requirements. It has been found that, to provide adequate values in the e-ring of gamma transition and radial beam size, it is necessary to provide a number of combined function magnets in a predominantly separated-function lattice. In each superperiod, two such units are included amongst the sixty bending magnets. This lattice feature is shown in Figure 6, together with the horizontal dispersion matching sections.

An important consideration for the electron-proton colliding beams is the choice of the radial to vertical beam aspect ratio at the interaction region. The ratio is chosen at four to one. If a choice had been made of a smaller ratio, the vertical magnet apertures would have been undesirably large, particularly as the conventional ring in the feasibility design had to cater for the possibility of storing 80 GeV/c protons in addition to 14 GeV/c electrons. This feature allowed for a possible proton-proton colliding beam option. The effect of horizontal-vertical space charge coupling between the electron and proton beams has not been assessed, but it is realised that this could affect the luminosity estimates. At electron energies below 14 GeV, the natural beam size may be too small, and two possible schemes have been considered to

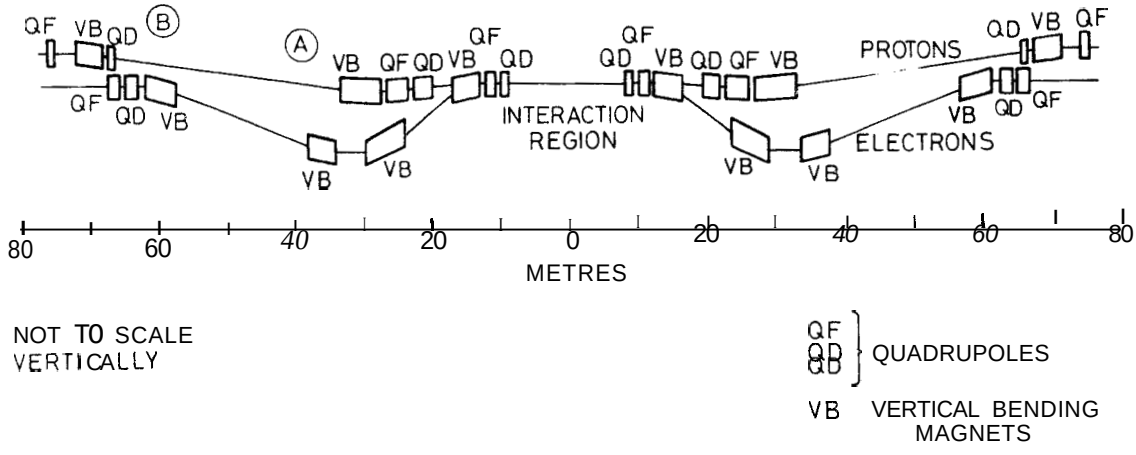

FIG. 3. e – p INTERACTION REGION GEOMETRY

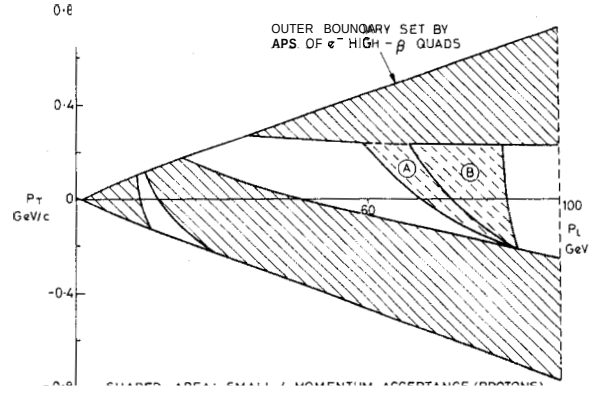

FIG. 4.

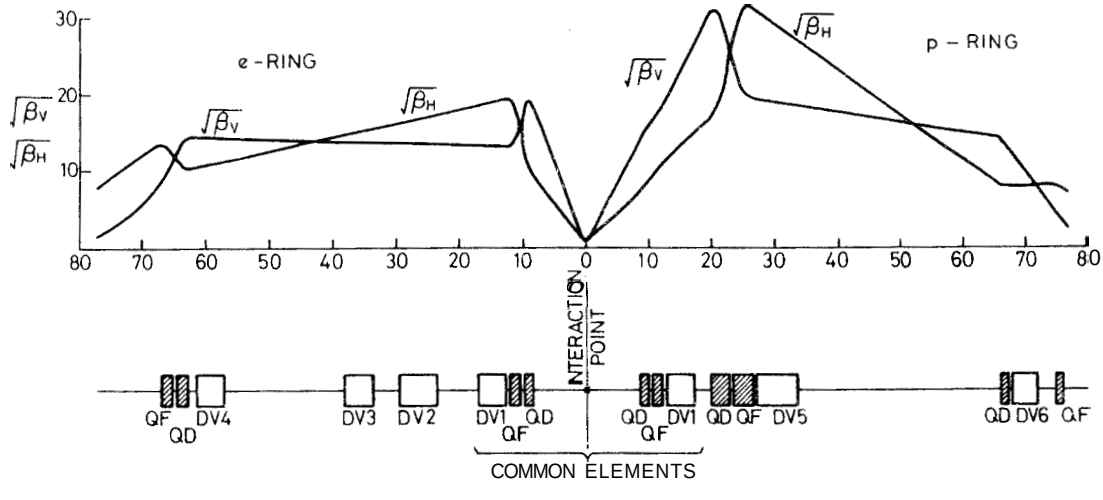

FIG. 5. e – p INSERTION (N.B BOTH RINGS ARE SYMMETRICAL ABOUT THE INTERACTION POINT)

overcome this effect. These include reducing the Q values of the machine and a further adjustment in the radial damping. If satisfactory enhancement is introduced, the luminosity will scale approximately as the product of the energies of the incident particles.

The approximate costings of the various options of the feasibility study are given in Table 2.

TABLE 2 - 1973 Cost Estimates of EPIC Options

Option	Rings	Cost
14 GeV e^+ - e^- Ring	Conventional (C)	£19.6M
14 GeV e^- - 80 GeV p	C + C	£35.1M
14 GeV e^- - 100 GeV p	C + Half-Full S/c	£43.7M
14 GeV e^- - 200 GeV p	C + Full S/c	£56.5M

Revised Design of Electron-Positron Ring

The ring circumference has been extended by 3% to provide increased straight section lengths. This will ease the design of a future proton ring in the event that it is built with all conventional magnet units.

The dipole magnets now proposed for the single ring are low field units, and costing is proceeding on the basis of using C-magnets. The open end of the C will face radially inwards to simplify the design of the vacuum system.

The magnet lattice has a high chromaticity as a consequence of the high β-values in the long insertions. The full range of the beam momentum spread is also large to ensure an adequate beam lifetime. To correct for the chromaticity, provision is made in the lattice to include sextupoles near to every quadrupole. Studies of the distribution and strengths of these sextupoles are still continuing and are proving to be a major design problem. Present studies treat the problem in linear approximation, but subsequent studies will include tracking over many machine revolutions.

As in the feasibility study the space between the high-β quadrupoles, which is completely free for experimental equipment, is set at 17 m. This may be revised if necessary as the insertion is longer than is required for the design of the electron-positron ring alone. However, there are restrictions on the maximum allowed β-values in the insertion, and the premium to be paid for increasing the central region is a decrease in the luminosity.

The variable damping feature has been mentioned in the previous section. Referring to Figure 6, the modified damping is introduced by combined-function focussing units, indicated DI/QF. On either side of these units are quadrupoles which may be adjusted to vary the local dispersion while still preserving the dispersion matching. Details of the scheme are given in reference 12. The damping time constant of the horizontal betatron oscillations of the electrons and positrons is given by:

$$T_x = [\, J_x P_\gamma / 2E \,]^{-1}$$

where P_γ is the average rate of synchrotron radiation energy loss, E is the energy of the circulating electrons or positrons and J_x, the partition coefficient, is a function of the magnet lattice. The horizontal beam size varies inversely as the square root of the coefficient, J_x. In a separated-function magnet lattice J_x is approximately equal to 1, while in the EPIC electron-positron ring it is adjusted to be approximately 0.4.

The beam aspect ratio at the interaction region is now under review. Recent studies of the beam-beam interaction for e^+ - e^- collisions indicate that a larger ratio than the previously considered value of four to one might be acceptable. These studies are reported in a subsequent section. The possible advantage for EPIC in increasing the beam aspect ratio is that the maximum horizontal β-value could then be decreased.

The revised ring parameters are given in Table 3. The luminosity will scale as E^2, provided satisfactory beam sizes are obtained by adjustments of machine tune and damping.

TABLE 3 - EPIC Electron-Positron Ring

Ring circumference (m)	2191.6
Long st. section lengths (m)	154.3
Maximum momentum (GeV/c)	14
Injection momentum (GeV/c)	4.8
Range of machine tunes, Q	15 1-19.4
Bending radius (m)	71.9
Max. energy loss/turn (MeV)	19.8
Peak RF Voltage (MV)	30.0
No. of bunches/beam	2
Max. no. of particles/bunch	$8\ 10^{11}$
Peak synch. rad'n. power (MW)	1.39
Rms. mom. spread at 14 GeV/c	$8\ 10^{-4}$
Rms. bunch length (cm)	1.8
Rms. bet. amp. (cm) at β_x = 42 m	0.33
Max. luminosity (cm^{-2} sec^{-1}/Xn.)	$\sim 5\ 10^{31}$

Injection Scheme for Electrons and Positrons

The specification for the total filling time of the EPIC ring is 15 minutes for two bunches of electrons and two bunches of positrons, with the maximum number of particles per bunch set at $8\ 10^{11}$. At the injection momentum of 4.8 GeV/c, the damping time constant of the radial betatron motion is approximately 0.6 sec, so that the maximum rate for filling an individual EPIC bunch is of the order of once per second. Accordingly, if individual bunches are filled in sequence, the repetition rate of the booster injector must be approximately 4 Hz, and the number of particles per booster pulse must be at least 10^9.

The scheme proposed to inject a full booster beam pulse into a single EPIC bunch is the following. The booster accelerates eight bunches, which are subsequently ejected bunch-by-bunch, one after every revolution period of the main ring. There is an interchange of the radial and vertical beam emittances in the transfer line, followed by radial multi-turn injection into EPIC. A requirement for this scheme is that the circumference of the booster is related to that of EPIC by the ratio $8/(2n+1)$, where n is an integer. The chosen value of n is 35.

The straight sections of NINA are increased in length when it is used as a booster for EPIC. The harmonic number, h, of the existing RF system is thus altered, and the ring size is adjusted to make the new value of h equal 336, a number which is

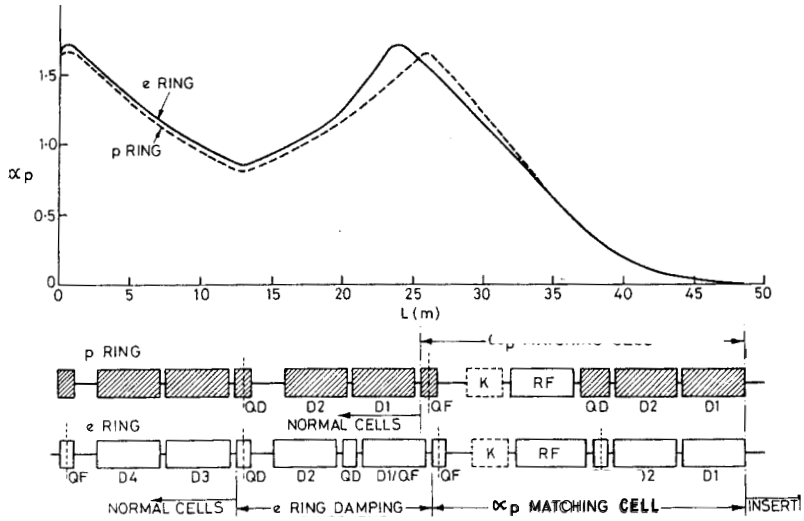

FIG. 6.
e-- p RINGS - α_p MATCHING SECTIONS - e RING DAMPING ADJUSTMENT

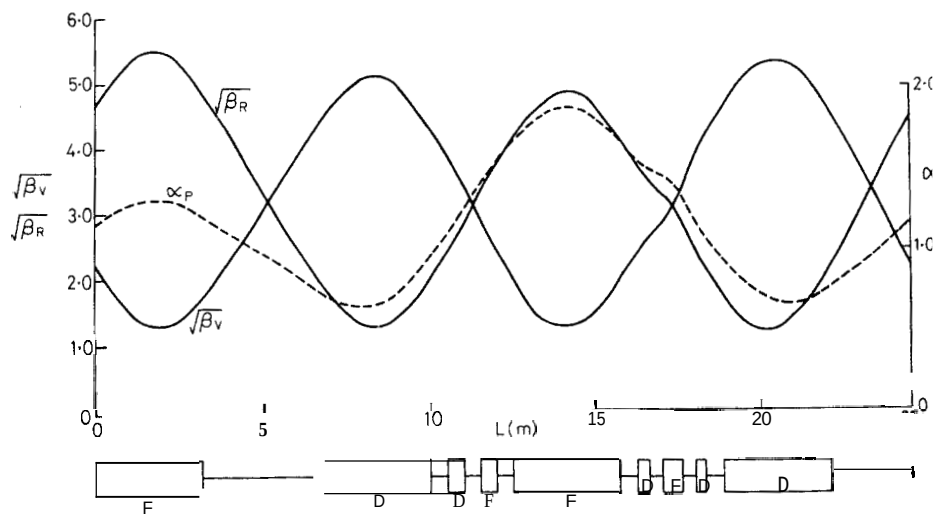

FIG.7. NINA BOOSTER-NORMAL PERIOD

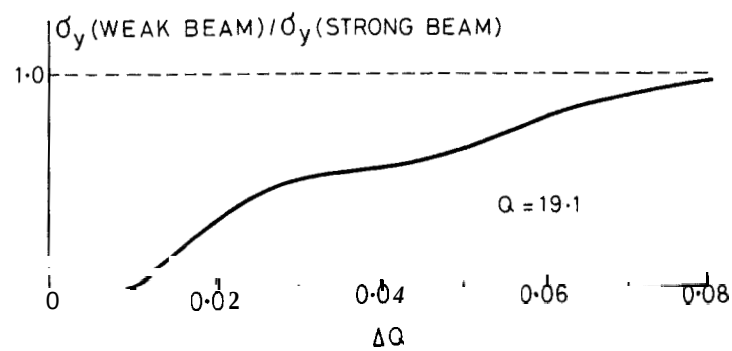

FIG. 8. BEAM-BEAM HORIZONTAL-VERTICAL COUPLING IN EPIC

divisible by 8. A second RF system is installed, with h = 48, to assist in initial trapping and bunch compression.

A further gain in overall capture efficiency is obtained by modulating the gun of the proposed 100 MeV electron linac injector[13]. Modulation at 9.71 MHz, with 10 nanosecond pulse lengths, leads to the filling of the required 8 booster bunches. This proposal is important for obtaining the required fluxes of injected positrons. If the average current in the electron linac is set at 400 mA for positron production, the peak current during the 10 ns pulses becomes 4A. The electron energy at the positron converter will be modulated by more than 10% during the pulse, but the output energy of the subsequent 200 MeV positron linac can be correctly stabilised.

It is planned to reduce the momentum spread of the 200 MeV positrons by means of a debuncher and correcting cavity. A scheme is under study which is similar to the one installed at the 300 MeV electron linac of Mainz University[14]. Studies of trapping in the booster indicate that the input momentum spread should be approximately $\pm$ 3.5 10^{-3}.

The proposed modifications for NINA include a new magnet power supply, the second RF system, new injection and fast extraction systems and the introduction of quadrupole doublets and combined function triplets into the magnet lattice. The lattice design is shown in Figure 7. The doublets introduce a range of Q-tuning, while the triplets provide damping of the horizontal betatron motion of the electrons and positrons. The damping magnets have a D-profile and are arranged to form a triplet of zero total bend by the use of a reversed field in the central unit.

The magnetic field in the booster has a reduced rate of rise at injection, an intermediate flat at a field level corresponding to 2.25 GeV/c and a flat top of approximately 20 ms duration. Trapping, and acceleration to 2.25 GeV/c are undertaken by the lower frequency RF system. During the intermediate flat, the beam damps in phase sufficiently to be captured by the high voltage, high frequency RF system, which then completes acceleration to 4.8 GeV/c. The beam phase is adjusted during the flat top for synchronisation with the EPIC main ring.

Electron-Positron RF System

Design is proceeding on the basis of a peak energy gain per turn in EPIC of 30 MeV, developed in 42 m of accelerating structure. At 14 GeV/c the energy loss per turn in synchrotron radiation is 19.8 MeV. The RF over-voltage provides a beam lifetime of 10^5 s for loss out of the phase stable region due to quantum fluctuation effects.

Beam loading of the RF cavities by the two electron and two positron bunches is being analysed in a manner similar to that proposed by Keil[15]. The tightly bunched beams excite the RF cavities not only at the fundamental resonant mode but also at the higher cavity modes. This is a consequence of having appreciable harmonic components of beam current up to quite high frequencies, together with a close spacing of the harmonics. The amplitude of the harmonics varies as $e^{-(\omega\Delta)^2/2}$, where Δ is the rms bunch duration. The spacing of the harmonics is at twice the bunch repetition frequency. Beam-cavity and beam-equipment interactions will affect the equilibrium bunch lengths and the synchrotron motion, and these effects remain to be determined.

The design of the RF system is thus provisional, and there may be future changes in the choice of RF harmonic number and type of accelerating structure. The present choice of harmonic number is 2944, corresponding to an RF frequency of 402.7 MHz. The proposed standing wave accelerating structure is of the type developed at Los Alamos for LAMPF, but at approximately half the frequency. The inner aperture of the proposed cavity is of diameter 12 cm. The re-entrant nose cones are adjusted to optimise the transit-time corrected shunt impedance (approximately 30 MΩ/m). As discussed in reference 16 there is mechanical complexity in Los Alamos type structures at 400 MHz. The addition of the side-mounted cavities, that give the resonant coupling and $\pi/2$ mode operation, is complicated by the cavity size.

There will be four RF buildings, one associated with each superperiod of the machine. These buildings will provide access for installing and removing ring components. The installed RF power at each building will be approximately 1 MW, CW. The accelerating structure adjacent to an RF building will be subdivided into two sections of approximate length 5 m. The number of feeder points for the 5 m sections will be determined by power characteristics of windows. In the event that the peak energy of the storage ring is subsequently increased, further RF buildings and accelerating structures will be installed.

Normal Cells

Each of the four superperiods contains 14 normal cells which are of a separated-function FODO design of length 24.8 m. Each half-cell contains two dipoles, a quadrupole, a sextupole, a correction dipole and a beam monitor.

The dipoles for the electron-positron ring are 4.5 m long while the quadrupoles are 1.0 m. There is a spacing of 0.4 m between the two dipoles of a half-cell. One section of vacuum chamber extends through the two dipoles, and a shorter section threads through the quadrupole, sextupole and correction dipole. Two pumping ports are included in the longer section, while the shorter section has a length of bellows and a beam monitor. An aluminium chamber is proposed as in the SPEAR design, with the necessary cooling channel along the length of the outer wall. There will be distributed pumps within the vacuum chamber in the dipoles.

Insertions

No vertical bending magnets are required in the insertions of the electron-positron ring. The quadrupoles are arranged as in the electron-proton configuration, Each half of an insertion has a pair of high-β quadrupoles together with a pair of matching quadrupoles. These doublets generate the low-β values at the centre of the insertion and provide betatron motions which are matched to those in the normal cells.

In one of the long insertions there are two injection systems, one for the electrons and one for the positrons. Each system has an injection septum magnet together with upstream and downstream fast kicker magnets.

Other elements contained in the long insertions are the RF systems, electrostatic beam separation plates, correction dipoles, sextupoles, octupoles and skew quadrupoles. The insertion sextupoles will be distributed relative to the chromaticity correction sextupoles so as to minimise third order resonances.

Beam-Beam Computer Simulation

A computer program has been developed that evaluates the motion of a weak beam in the presence of a strong beam for the case of electron-positron beam-beam interactions. The dimensions of the strong beam are assumed fixed, with Gaussian distributions in the two transverse phase planes. Representative particles of the weak-beam are introduced with the same radial distribution as the strong beam but with small initial vertical motions.

The program tracks particles of the weak beam through successive superperiods of the storage ring, assuming no magnet imperfections in the lattice components. For each superperiod transit, estimates are obtained for the radiation damping, the fluctations of the quantum excitations and the linear and non-linear forces of the beam-beam interaction. Random number generators are used to derive the quantum excitation terms. A number of different approximations have been used for the beam-beam space charge forces, but all have given essentially the same results. The possibility is now being considered of extending the program to include the added effects of imperfections in the ring magnets.

Initial tracking studies have been made for EPIC Q values of 19.1. Results are given in Figure 8 for a radial to vertical beam aspect ratio in the strong beam of four to one. The horizontal axis of the graph is the parameter ζ, which is approximately equal to the tune shift per interaction, **AQ**. The radial size of the weak beam remains unchanged, but the vertical dimension grows to reach that of the strong beam for $\Delta Q = 0.08$. Luminosity estimates for EPIC assume **AQ** values of 0.04.

A second set of results has been obtained for the same Q values but with a different beam aspect ratio for the strong beam. The aspect ratio at the collision region has been changed to 16:1 by doubling the radial dimension and halving the vertical. Though σ_y (strong), the rms beam height of the strong beam, is halved, it is found that σ_y (weak) again approaches the value of σ_y (strong) when **AQ** reaches 0.08. It is of interest to note that the beam-beam limits of operating storage rings occur at **AQ** values of this magnitude.

Results have also been obtained for EPIC Q values of 18.1. At this tune, the effect of the linear term in the space charge force is equivalent to reducing the minimum B-function at the point of collision. The simulation becomes approximate and the results difficult to interpret. Preliminary results indicate a reduced vertical growth of the weak beam at the interaction point, but an appreciable vertical size at the high-β quadrupoles.

Summary

The present status of the EPIC machine design has been outlined in this report. By October 1974 an improved cost estimate will be obtained for a 14 GeV electron-positron storage ring. The physics case for EPIC and a machine proposal will then be submitted to the Science Research Council, seeking funds to allow the ring to be built by 1981.

References

1 D A Gray (Editor). Proceeding of the Daresbury-Rutherford Accelerator Working Party, Rutherford Report RHEL.R 252 (1972) p.34.

2 G H Rees. Initial design aspects of storage rings as a possible future UK facility, Rutherford Report DRAG/SR1 (internal note), May 1972.

3 C Pellegrini et al., A high energy proton-electron-positron colliding beam system, Proceedings 8th International Conference on High Energy Accelerators, CERN(1971) p. 153.

4 M R Harold & G H Rees, Some EPIC parameters of interest to experimentalists, EPIC Report EPIC/MC/12 (internal note), March 1973.

5 T Elioff et al., Proton-Electron-Positron Design Study. Proceedings of the 1973 Particle Accelerator Conference, IEEE Trans. Nucl. Sc. NS-20, No.3 1039 (1973).

6 R Bangerter et al., PEP Lattice Design. Proceedings of the 1973 Particle Accelerator Conference, IEEE Trans. Nucl. Sc. NS-20, No. 3 786 (1973).

7 R Chasman & G A Voss. ISABELLE e-p Option. Proceedings of the 1973 Particle Accelerator Conference, IEEE Trans. Nucl. Sc. NS-20, No. 3 777 (1973).

8 J R M Maidment. Beam separation in the EPIC II e-p option. EPIC Report EPIC/MC/30 (internal note), August 1973.

9 G H Rees. Energy variation for e-p collisions in EPIC II. EPIC Report EPIC/MC/18 (internal note), May 1973.

10 J D Lewin. Path length adjustment for energy variations in EPIC. EPIC Report EPIC/MC/22 (internal note), June 1973.

11 P V Landshoff. Some physics questions about deep inelastic e-p. EPIC Report EPIC/WP3/3 (internal note), June 1973.

12 G H Rees. EPIC Updated: variable damping and tunes in the e± ring. EPIC Report EPIC/MC/39 (internal note), January 1974.

13 G Saxon. Injection Schemes for EPIC. EPIC Report EPIC/MC/41 (internal note), January 1974.

14 H Herminghaus & K Kaiser. Design, construction and performance of the energy compressing system of the Mainz 300 MeV electron linac. Nucl. Instr. & Methods, 113, (1973) p.189-194.

15 E Keil. The interaction between tightly bunched beams and RF cavities. CERN/ISR-TH/74-15. March 1974.

16 M A Allen & P B Wilson. Linac type RF structures for high energy storage rings. SLAC-PUB-1142, October 1972.

Phil Morton (SLAC): What is included in your cost estimate—salaries and so forth, or what?

Grahame Rees (Rutherford): No, never include salaries.

Matthew Allen (SLAC): The shunt impedance figures for the cavities seem awfully high. Are you sure of that number?

Rees: We assumed copper cavities, not aluminum cavities, and these were values obtained from Los Alamos type computer programs.

Allen: Losses in the coupling slots will reduce the value below the computed values.

Rees: Perhaps we have been a bit conservative in power estimates because of the large amount we've allowed for power dissipated in the higher modes—we've allowed as much as for the fundamental mode. I agree, we might have to evaluate this.

Ednor Rowe (University of Wisconsin): What fraction of the Dower loss due to svnchrotron radiation occurs in the dog legs in the interaction region?

Rees: About **30** - 40% at top energy.

Ernest Michaelis (CERN): Do you plan to vary the proton energy or is it fixed?

Rees: The usual way we thought to change energy would be to keep the ratio of electron and proton momenta constant so that the particles always come out of the vertical bending magnets at the same angle. We also thought it desirable to change the energies of the beams independently. This would be quite difficult in our design because one then has to change the position of the proton quadrupoles. But since the displacements required aren't large, this could be set up before a run at a given energy.

Melvin Month (BNL): You said that the synchrotron frequency goes up to a dangerous level if the tune drops below 15. Could you explain that statement?

Rees: Synchrotron frequencies are reaching 10% of the revolution frequency which has always been considered an undesirably high value. So we will have to look seriously at betatron-synchrotron coupling at modes higher than this.

THE PROTON-ELECTRON-POSITRON PROJECT - PEP*

L. Smith

LBL-SLAC Joint Study Group
Berkeley and Stanford, California

Introduction

In the summer of 1971, a group of physicists at LBL and SLAC, including visitors from CERN and Frascati, made an inquiry into the feasibility of a new colliding beam complex capable of producing collisions at higher energies than hitherto envisaged between electrons and positrons and also between electrons and protons and positrons and protons. They concluded that such a facility, which would consist of an electron storage ring and a proton storage ring, was quite possible and that no known physical limitation of the behavior of stored beams would prevent the achievement of luminosities sufficient to yield useful reaction rates for many important high-energy interactions. To illustrate these conclu ions, a conceptual design was described and analyzed.[1] The physics importance was later forcefully emphasized by an LBL-SLAC Physics Study Group.[2]

Subsequently, the collaborative study between LBL and SLAC grew, involving more people as the concepts and designs became more refined. A combination of a 15 GeV electron-positron ring and a 200 GeV superconducting proton ring, referred to as PEP, emerged as the preferred design. In the meantime, other laboratories began studying similar or related ideas in both the U. S. and Europe and their representatives came together at SLAC and LBL in the summer of 1973 to exchange ideas and work on common problems. By the end of 1973, a version of PEP suitable for location on the SLAC site had been developed and the two laboratories entered into a formal agreement to jointly propose and construct the electron-positron portion of the system, in a manner compatible with the subsequent addition of the proton ring to achieve the full PEP capability. This paper will describe the full PEP complex as presently visualized; the accompanying paper by John Rees[3] will describe the specific electron-positron system for which a formal proposal for construction is presently being submitted.

physics Potential

For electron-proton collisions with the maximum energies of the preferred design, the center-of-mass energy is 110 GeV which is the same as that which would be available with a 6000 GeV beam from a conventional accelerator incident on a stationary hydrogen target (there is no economically feasible way of reaching these energies with a conventional accelerator). The facilities of the present proposal are designed to be compatible with this addition. The future electron-proton system, together with the presently proposed electron-positron system, would comprise a total facility of unique capability for particle physics research which is briefly outlined below.

(a) Deep Inelastic Lepton Scattering ($e^-(e^+)p \rightarrow e\text{-}(e^+) + \text{hadrons}$)

Inelastic electron-proton scattering plays an essential and unique role in the investigation of the structure of the hadrons. The known electromagnetic field generated by the scattered electron interacts with the local electromagnetic current of the proton and thus can probe the structure of the nucleon at arbitrarily small distances. This local interaction is in sharp contrast to hadron-hadron scattering in which the basic interaction between the particles is more complex. By varying the energy and angle of the scattered electron it is possible to "tune" or vary the virtual photon's mass Q^2 over a large range. In particular, it is possible to achieve virtual photon masses whose square is negative and whose magnitude is much greater than the proton mass and therefore allows for collisions in an asymptotic region not available in accelerators using a fixed mass projectile.

Experiments on inelastic scattering at SLAC, where both the mass and energy of the virtual photon are large, have yielded profound and unexpected results. These results show that the cross sections do not depend independently on both the mass and energy of the photon, but instead on their ratio. This "scaling" behavior has led to major new concepts in our understanding of hadronic structure in terms of a possible substructure within the hadron that is composed of point-like constituents (partons). The greatly enhanced center-of-mass energy of a PEP facility would extend the measurements of deep inelastic scattering far into the unknown region. With the example parameters used here the virtual photon energy would reach to 6000 GeV and its mass to 110 GeV compared to an energy of 20 GeV and a mass of 5 GeV at the present SLAC frontier.

Confirmation of the scaling behavior at these larger values of energy and mass would give support to these new ideas while observation of violations of scaling would indicate a new energy scale for hadronic phenomena perhaps associated with the production of new particles and of a "size" for the constituents themselves. This point is emphasized by the surprising results of the recent SPEAR experiments in the time-like region which do not support these ideas of the quark-parton model, and in this respect make the further study of the inelastic electron reactions even more intriguing. Other general and fundamental features to be studied for large photon masses include the applicability of Regge theory analyses, the validity of sum rules based on current algebra, and the "fragmentation" of very massive virtual photons into jets of secondary hadrons.

Besides the electromagnetic inelastic electron scattering, it will be possible to observe the effects caused by weak neutral current of the type discovered in the recent CERN and NAL neutrino experiments. The effects of the neutral current would be observable as parity violations, charge conjugation violation, and possibly electromagnetic scaling violations. Since both energy and momentum transfer are easily determined, detailed knowledge as to the nature of these neutral current effects will be possible.

Thus, this unique feature of a PEP facility, the study of deep inelastic scattering, will yield results on one of the most significant problems in particle physics.

* Work supported by the U. S. Atomic Energy Commission.

(b) Weak Interactions ($ep \to \nu_e$ + hadrons)

If the scaling phenomena observed in deep inelastic scattering is assumed to hold also for the weak interactions, as would be implied at least in part by the conserved vector current (CVC) idea, then with the Fermi theory one is led to the conjecture that the total weak interaction cross section will continue to grow quadratically with the center-of-mass energy. This has the startling consequence that at energies in the PEP region the weak interactions with their inherent violation of parity and strangeness would have grown in strength to be comparable to the electromagnetic interactions. In fact in the region of the largest momentum transfer accessible for the particular example of PEP parameters used in this study, the scaling hypothesis indicates that the deep inelastic electromagnetic cross section is smaller than the weak process.

Experiments with PEP will show either that the weak interaction is no longer "weak" or that the Fermi theory in its simple form breaks down. The discovery of a failure in the Fermi theory would in itself be of the first magnitude in importance; additionally one could then entertain hopes of discovering the mechanism of breakdown. If a W boson, for example, were the source of a major failure of Fermi theory, its mass might be sufficiently low ($\approx$ 30 GeV) that W particles could be produced by PEP.

Thus, the exploration of weak interactions at PEP energies will present some of the most exciting possibilities for new discoveries. Information from experiments in this area could lead also to unifying principles for the basic forms of elementary particle interactions.

General Description

The goal of PEP is to provide collisions at energies ranging from 30 to 110 GeV in center-of-mass energy for electrons and protons, and from 10 to 30 GeV for electrons and positrons. A luminosity of 10^{32} $cm^{-2}sec^{-1}$ at the top energies, to be achieved simultaneously at a number of interaction points, is deemed adequate to support a vigorous and varied experimental program in both e–p and e^+e^- physics. In order to achieve that luminosity with a relatively modest number of stored particles, we have chosen to use bunched beams in head-on collision. The head-on collision scheme appears also to be more advantageous for experimental detectors as well as affording a greater simplicity in the insertion structure. We have furthermore adopted a six sided configuration, which provides five areas for physics experiments and one for accelerator physics investigations and monitoring.

The geometrical configuration of the two rings is shown schematically in Fig. 1. The six collision points are at the centers of 20 meter long straight sections at each crossing of the rings. The electron ring is placed alternately above and below the plane of the proton ring; this pattern eliminates vertical dispersion in the circular portions of the electron ring, and the attendant and undesirable quantum-excitation contribution to vertical emittance, and eliminates the need for a series of quadrupoles in the sloping sections (see Fig. 2) of the electron ring. As a result, the required insertions are shortened, overcrowding of magnet elements is avoided, and the electron path length can be varied in these sections to provide synchronization with the protons over the projected range of proton energies (50 to 200 GeV).

The circular arcs of both rings are made up of 48 conventional FODO cells (8 per sextant) operating at a nominal phase advance of about 90° per cell at maximum beam energies. In addition to insuring positive damping for the electrons, the separated function scheme simplifies the design of the super-conducting magnets in the proton ring and, in both rings, permits a wide range of focusing conditions useful for controlling beam size. To achieve matching between cells and insertions for the variety of conditions required in the interaction region, the quadrupoles in the insertions, the normal cells, and in the two cells on each side of each insertion are independently controlled.

The insertions, as presently conceived, are shown in Fig. 2, along with the adjacent cells. Starting from the interaction point, both beams go through the doublet, $Q_{1,2}$, which consists of conventional steel quadrupoles and which is strong enough to focus the electrons and/or positrons, but has little effect on the protons. The bending magnet, B_1, also conventional, serves to separate the two beams, deflecting the light particles toward the elevation of their next sextant. The small deflection given to the protons is compensated by three vertical bending magnets ($B_{2,3,4}$), which restore the protons to the median plane. The angle of deflection provided by B_1 is adjustable to permit the variation in total circumference of the electron ring needed for synchronization at different proton energies. On the basis of single particle beam dynamics, the subsequent bending magnets in the electron line could be wide aperture magnets fixed permanently in position. However, the electro-magnetic fields generated by a high-intensity beam in such a vacuum chamber configuration might make that scheme infeasible, in which case it would be necessary to move magnets or the vacuum chamber in this region when the proton energy is to be changed.

In the proton line, the doublet, $Q_{3,4}$, consists of super-conducting quadrupoles which focus the protons. Beyond $Q_{3,4}$ is a 28 meter long straight section; these straight sections, twelve in all, will be used to accommodate rf systems, injection hardware and other beam components. The twelve 20 meter long straight sections directly above or below in the electron ring will serve the same purposes for the light particles.

The choice of 20 meters free space around the interaction point represents a compromise between the desire for as much room as possible for experimental equipment and the machine physics requirement that β_{max} should be as small as possible because of aperture, chromaticity, and tolerance considerations. It appears that the straight section space assigned to major accelerator hardware is more than adequate; if this is really the case, one or more of the insertions could be modified to meet particular experimental requirements by extending the interaction region at the expense of the adjoining 28 and 20 meter straight sections. The vertical separation of 80 centimeters between the two rings appears to be adequate to accommodate the necessary equipment in both rings. The tunnel size adopted for the Stage I proposal[4] would permit the further addition of another electron ring, a feature which might prove to be extremely valuable in light of the fact that current experimental results are indicating that electron-electron collisions at high energy would yield significant additional information. A second electron ring would also make it possible to achieve higher luminosities for the e^+e^- system at lower energies by permitting an increased number of bunches.

Figure 3 shows an overall view of the rings on the SLAC site. We include it here only to give a general impression, since it is, of course, identical to the layout proposed for Stage I and will be discussed in detail in the following paper. Figure 4 shows tunnel cross sections in alternate sextants of the ring.

Operating Parameters

Tables I and II give the lattice parameters and typical operating parameters. Figures 5 and 6 show the betatron and off-momentum functions for the high energy mode of Table II. In contrast to an electron-positron system, in which emittances are determined by the Lattice configuration and particle energy (and the limitations on performance imposed by the beam-beam interaction are known empirically, if not understood theoretically), one must make assumptions concerning the behavior of protons in order to arrive at a set of operating parameters for an electron-proton system. Regarding emittances, there is sufficient experience with high energy accelerators to provide reasonable figures, but regarding the beam-beam effect, there is as yet no indication of the ultimate limitations. We must assume, however, that protons are subject to the same harmful effect, and, in the absence of radiation damping, are probably more sensitive than are electrons. We have therefore taken as design criteria that the linear beam-beam tune shift should not exceed 0.05 for the electrons (based on actual experience) or 0.005 for protons, the latter figure having also some justification on theoretical grounds.

The performance is then limited by this criterion, as in well-designed electron rings, and the interaction point parameters are determined by maximizing luminosity consistent with the above tune shifts while minimizing β_{max}, chromaticity, and restricting the total number of particles used. The number of protons required (3.6×10^{13}) is small compared to the number stored in the ISR (6×10^{14}), but it should be remembered that in our case they must be accelerated from a low energy and collected into short bunches. Thus, the intensity achieved at Brookhaven (10^{13}) and the design goal at Batavia (5×10^{13}) are better standards for comparison.

The assumed transverse emittances are somewhat larger than those achieved in existing synchrotrons, but here again the beam-beam limit precludes any advantage in striving for greater brightness.

The chromaticity is sufficiently low that it can be controlled by using two sextupoles in each of the FODO cells in both sings. This distribution is smooth enough to eliminate serious nonlinear resonances near the chosen working points while providing necessary control over head-tail instabilities.

Injection, Acceleration, and Bunching

The electrons or positrons would be handled in the same way as in Stage I, as described in the next paper. It should be noted that the vertical bends required to separate the rings in the full PEP configuration cause an increase in synchrotron radiation, so that, for the full configuration more rf power will be required.

For the protons, the procedure is more complicated. Referring to Table II, 24 bunches, each with 1.5×10^{12} protons, are required. The present concept is to accelerate 1.5×10^{12} protons first to about 5 GeV in a small proton synchrotron located, possibly, at the present SPEAR site, and then transfer them by single turn extraction to an existing bucket at the 96th harmonic in the PEP proton ring. This process would be repeated 24 times, filling every fourth bucket in the main ring. The protons would then be accelerated to the appropriate energy and the rf voltage increased until the bunches are short enough to fit into buckets at four times higher frequency (h = 384, f = 53 MHz). At this frequency, the voltage would be raised to compress the bunches to the desired length. Assuming a longitudinal emittance of 10π cm in ($\Delta p/p$, Δz) units, the final voltage would be about 6 MeV/turn for σ_ℓ = 25 cm.

Since this value of σ_ℓ is much less than the minimum-β values for the protons, the luminosity is not sensitive to proton bunch length but, unfortunately, the beam-beam tune shifts are sensitive since the electrons or positrons may encounter protons in regions of higher electron-ring-β if the proton bunches are longer. The voltage needed in the proton ring depends strongly on both longitudinal emittance and required bunch length; a final choice of voltage will require careful consideration of achievable emittance and the parametric dependence of the beam-beam effect.

After the proton bunches are formed, the electrons would be introduced into their ring already synchronized in azimuth and perhaps separated laterally in order to prevent particles from meeting each other except at low-β points. How long this situation can be maintained for experiments is difficult to predict for the electron-proton system, but judging from electron ring experience, we anticipate a need to refill every few hours. The remaining protons would be decelerated as far as possible and then dumped.

Machine Components

The electron-ring system would differ very little from that described in the next paper. The proton ring would have a number of unique features, some of which are described. below.

(a) Superconducting Magnet System

The magnet design incorporates intrinsically stable, fine filament, NbTi super-conductor. Cross sections of the magnets are shown in Fig. 7. The ultra-high vacuum region is enclosed by a nonmagnetic beam tube, upon which the multi-layered coil is wound. Circular symmetry is used in all inner regions to yield the best structural and magnetic properties.

The cryostat is continuous through a half-sextant of the ring with surrounding evacuated thermal insulation, an 80° temperature shield, and finally a room-temperature vessel. Helium at 4.4°K is introduced at the center of a sextant and forced in both directions to the ends, from whence it flows back at reduced temperature and pressure in the outer annular region of the cry stat, acting as a counter-flaw heat exchanger.? The only additional element in the tunnel is the transfer line from the surface, where the rest of the refrigeration equipment is housed. This scheme minimizes interference between refrigeration components and tunnel hardware, particularly with experimental apparatus near the interaction region.

The heat leak at 4.4°K is assumed to be 1.2W/meter, and that from room temperature to 80% is taken to be 2.5W/meter. Allowance is made for two pairs of electrical leads for the dipoles, six for the quadrupoles and, in addition, for quench leads and auxiliary beam equipment. The additional heat load due to eddy current heating and beam induced currents appears to be much less. The total load at 4.4°K is about 1500W per

sextant, requiring some 600 kW of installed power capacity at each of the six stations. The magnet power supply circuit would parallel the refrigeration system.

(b) Vacuum System in the Proton Ring

Much attention has been given in the recent past to the question of warm-bore versus cold-bore vacuum systems. A cold-bore system has many attractive features--continuous cryo-pumping surfaces, no need for baking, simple design and minimal running cost, for example. On the other hand, desorption coefficients as high as 10^5 from cold surfaces have been reported, which raises the possibility of a run-away phenomenon similar to that which has affected operation of the ISR. Analyses of cryo-systems carried out independently at LBL and Rutherford indicate that pumping speed is probably adequate to maintain good vacuum and so we have tentatively chosen to follow the cold-bore route for the proton ring. In the neighborhood of the interaction regions the pumping capacity would probably have to be increased, perhaps by a permanent electro-deposit of porous silver or by a replaceable condensation of CO_2. Gas loads that could enter from the electron ring or pass from the straight sections into magnet sections can be intercepted by short lengths of tubular cryo-pumps that are easily cycled.

(c) Radio-Frequency Systems

Because of the limited vertical clearance, special problems arise in designing the rf systems. In the electron ring, fortunately, a cost optimization study leads to a choice of about 350 MHz for the frequency, and, as a result, the cavities are small enough to clear the proton ring. In the proton ring, the frequencies of the accelerating and bunching systems are 13 and 53 MHz, respectively, the bunching frequency being determined by requiring that the final desired bunch length should occupy about one-fourth of the bucket length. It is visualized to use a single set of structures in the proton ring for both modes; it would consist of a number of tubes which would act as frequency modulated drift tubes during acceleration and initial bunching and as half wave transmission lines at the higher frequency. The requirement of 6 MeV/turn could be met by using 17 tubes, occupying a total length of 50 meters and consuming about 2 MW of parer in the CW mode. They would be located in two of the 28 meter straight sections, separated in azimuth from the electron rf straight sections.

Conclusion

The design presented in this paper is subject to further modification and optimization. The procedure has been to evolve a conceptual design on which to base the Stage I proposal, and to consider detailed design of the final PEP complex only to the point of satisfaction that the two are indeed compatible. An obvious next step is to demonstrate the feasibility of a superconducting accelerator and storage ring; the LBL project, ESCAR,[6] is directed toward that end, including also the development of a suitable vacuum system. There are numerous questions in beam dynamics, particularly in the area of collective effects, which require additional study before we can feel confident that the operating specifications can be realized. This work will continue in parallel with the detailed work required for the construction of Stage I.

It is believed that the total PEP complex will provide one of the most important facilities for future research in high energy particle physics. In addition to the extremely important physics results expected from the electron-positron collisons, the provision for electron (or positron) collisions with protons, outlined here, will permit an enormous extension of parameters in traditional electron machine experiments (inelastic electron scattering, photoproduction, etc.,), and in addition will open the field of weak interactions to practical experimentation with a well-understood, well-controlled probe--the electron.

Acknowledgment

The work reported here is that of the members of the LBL-SLAC Joint Study Group. The author is their spokesman.

References

1. C. Pellegrini, J. Rees, B. Richter, M. Schwartz, D. Möhl, and A. Sessler, Proceedings of the VIII International Conference on High Energy Accelerators, CERN, 1971, p. 153.

2. Particle physics with Positron-Electron-Proton Colliding Beams, LBL-SLAC Study Group, LBL-750 or SLAC-146, April 1972.

3. J. Rees, The PEP Electron-Positron Ring, Proceedings of the IX International Conference on High Energy Accelerators, Stanford, May 1974.

4. A Prooosal for a Positron-Electron Colliding Beam Storage Ring Project, SLAC-LBL Joint Study Group, April 1974.

5. Refrigeration System for the NAL Energy Doubles, Cryogenic Consultants Incorporated, April 26, 1973 (unpublished).

6. T. Elioff, et al., Experimental Superconducting Accelerator Ring (ESCAR), Proceedings of the IX International Conference on High Energy Accelerators, Stanford, May 1974.

TABLE I

Lattice Parameters

Average Radius	R		345	m.
Number of Interactlon Points	N_I		6	
Radius of Circular Sextant	R_n		220	m.
Straight Insertion Length	L_s		130.5	m.
Interaction Region Free Space	L_I		20	m.
Vertical Separatlon of Rings	h		0.8	m.
Number of Cells	N_c		48	
Cell Length	L_c		28.8	m.
		Proton	Electron	
Dipole Length	ℓ_d	4.96	5.56	m.
Quadrupole Length	ℓ	1.20	0.78	m.
Dipole Peak Field	B_o	44	2.94	kG
Quadrupole Peak Gradient	$\lvert B'_o \rvert$	560	55.4	kG/m.

TABLE II

Operating Parameters

		High-Energy Mode		Low-Energy Mode		
		Proton	Electron	Proton	Electron	
Momentum	P	200	15	50	5	GeV/C
Number of Particles	$10^{-13}N$	3.6	0.7	3.6	1.06	
Number of Bunches	n_B	24	24	40	48	
Beam Power Radiated	P_B	--	4.9	--	2	MW
Luminosity/crossing	$\mathcal{L}$			2.1 x 10^{31}		$cm^{-2}s^{-1}$
Momentum Width = $\left(\frac{\Delta p}{p}\right)_{rms}$	σ	.047	.094	.188	.031	%
Bunch Length (rms)	σ_ℓ	25	2.6	25	2.6	cm
Interaction Point:						
rms beam width	σ_x^*	.064	.067	.128	.117	cm
rms beam height	σ_y^*	.021	.012	.043	.021	cm
β-function horizontal	β_x^*	3.25	1.05	3.3	3.2	m
β-function vertical	β_y^*	1.42	0.34	1.45	1.05	m
Dispersion	$\eta_x^* = \eta_y^*$	0	0	0	0	
Normalized Emittance (95% beam)						
Horizontal	$\beta\gamma\epsilon_x/\pi$	.016	7.52	.016	2.51	cm-rad
Vertical	$\beta\gamma\epsilon_y/\pi$	.004	.752	.004	.251	cm-rad
Beam-Beam Tune Shift						
Horizontal	$\Delta\nu_x$	.002	.045	.002	.050	
Vertical	$\Delta\nu_y$	.005	.049	.005	.050	
Betratron Function (Max)	β_{max}	771	352	750	100	m
Chromaticity	$\xi = -\left(\frac{p}{\nu}\right)\left(\frac{d\nu}{dp}\right)$					
Horizontal	ξ_x	4.1	3.8	4	4	
Vertical	ξ_y	3.7	5.0	4	4	
Betatron Tune	$\nu_x = \nu$	15.75	15.75	15.75	12.75	
Dipole Field (Cells)	B_0	44.0	2.94	11.0	.98	kG
Quadrupole Gradient (Cells)	$\lvert B'_0 \rvert$	560	55.4	140	15.0	kG/m
Transition Energy	γ_τ	14.5	13.2	14.5	10	

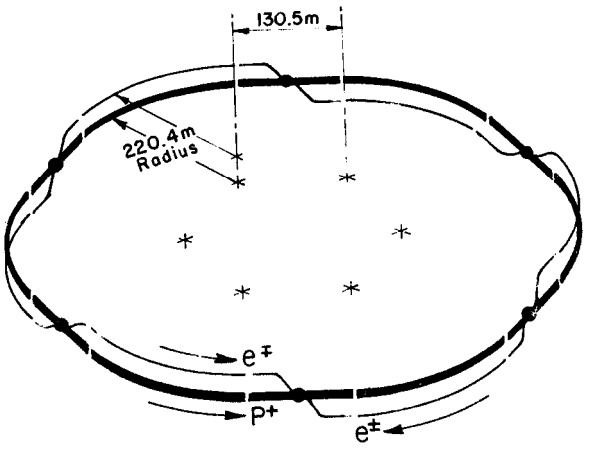

Fig. 1. PEP schematic.

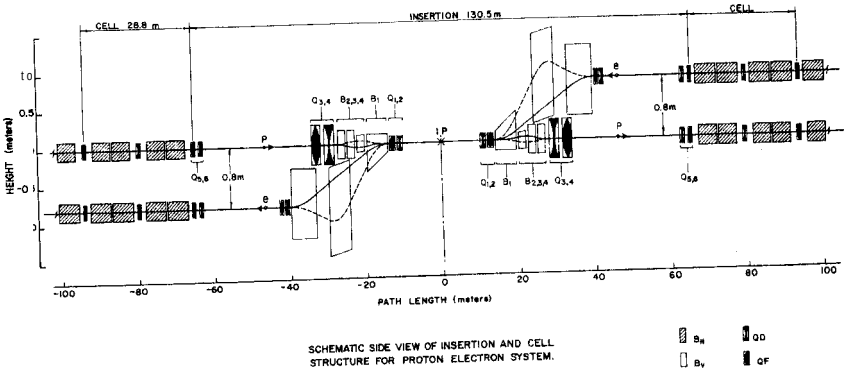

Fig. 2. Schematic side view of insertion and cell structure for proton electron system.

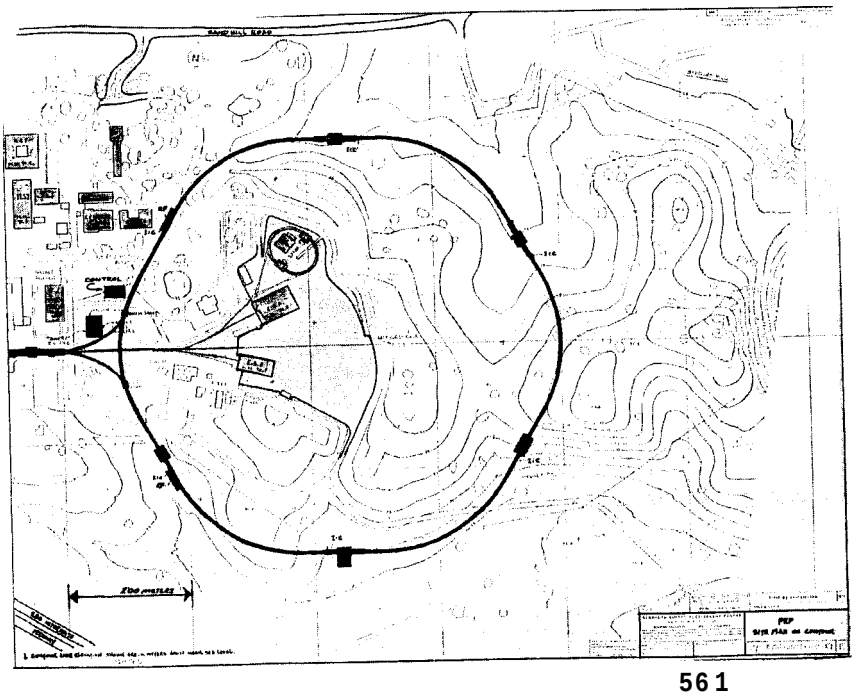

Fig. 3. Aerial view of SLAC site.

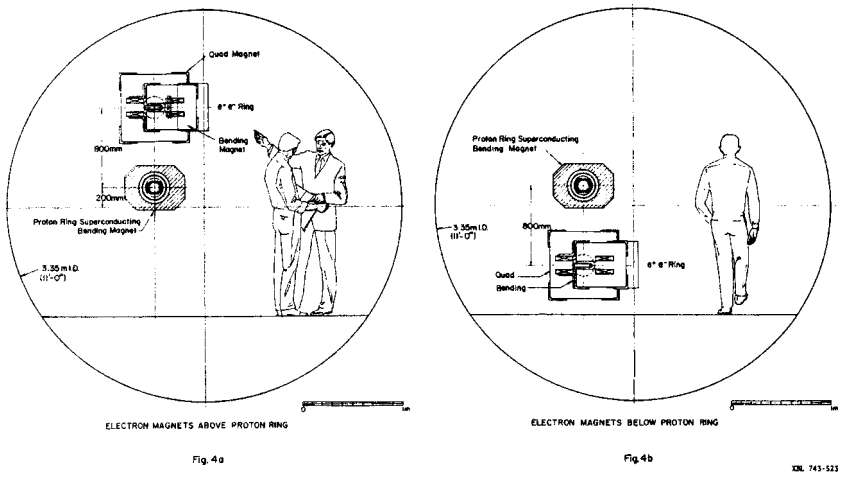

Fig. 4. Tunnel cross sections.

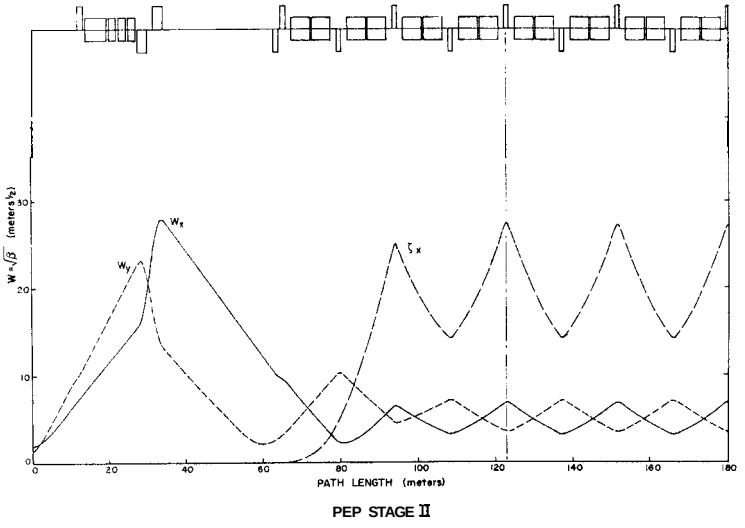

Fig. 5. Proton betatron functions through half sextant.

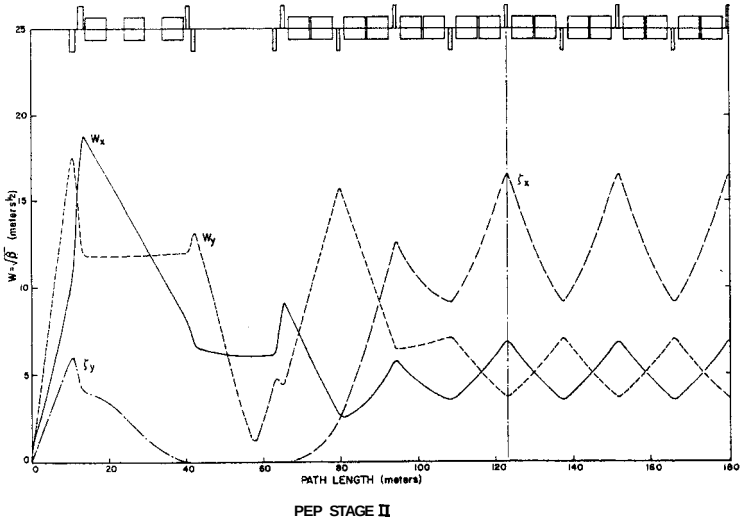

Fig. 6. Electron betatron functions through half sextant.

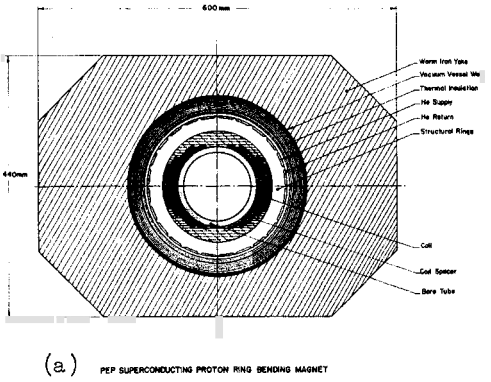

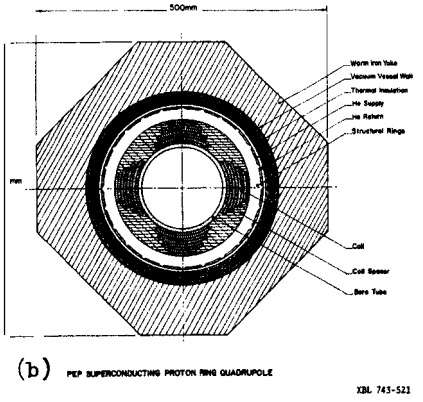

Fig. 7. (a) PEP superconducting proton ring bending magnet.
(b) PEP superconducting proton ring quadrupole.

Alessandro Ruggiero **(NAL):** Do you have any idea of the stability of a bunched proton beam at this current level and would you expect bunch lengthening phenomena?

Lloyd Smith (LBL): We don't know. This is an example for the reasons why we wanted to put off the proton part of this proposal for some time. There are many things of this nature that have to be understood. I think it was quite clear from some of the talks given yesterday that we will have to be extremely careful about the environment and coupling impedances. All this remains to be worked out.

Lee Teng (NAL): I have two questions about the general ring geometry. First, I noticed that you crossed over on the inside for electron–positron injection and, second, your straight sections are quite a bit shorter than those in other devices, especially for 20–GeV protons.

Smith: The short straight sections follow directly from the cross–over feature. It's one virtue of this design that we can get rid of a lot of magnets in that region, leading to a shortening of that insertion. About the first subject, John Rees will talk.

John Rees (SLAC): I'd like to answer it now. The injection as done in most electron–positron storage rings places some very tender elements at the mercy of synchrotron radiation and cooling is the outstanding problem. It is completely solved by injecting from the inside. The arrangement of the beam crossing over or under and then bringing it in parallel is a straightforward mechanical problem.

David Gray (Rutherford): What energy variation are you allowing in the e–p mode of operation?

Smith: You saw the two extreme cases in the so–called typical operating parameters 15 on 200 and 5 on 50 GeV.

Gray: Can you match the circulation times over that energy range?

Smith: Yes, that's pretty much what determines the range. In the insertion, there is actually a loop up and back to push it as far as possible.

Darrell Drickey **(UCLA)**: Isn't it, in principle, possible to increase luminosity by going, for example, to 5 on 200 GeV?

Smith: It's quite possible. I emphasize again that the operating parameters would actually run over a whole range. I might say that because protons and electrons behave differently, it is not possible to construct simple scaling laws as in electron rings and the mentioned energies represent the best combinations we could come up with, again blaming the $\Delta\nu$ being independent of gamma.

THE PEP ELECTRON-POSITRON RING -- PEP STAGE I*

J. R. Rees
LBL-SLAC Joint Study Group
Berkeley and Stanford, California

Summary

The first stage of the positron-electron-proton (PEP) colliding-beam system which has been under joint study by a Lawrence Berkeley Laboratory-Stanford Linear Accelerator Center team for the past two years, will be the electron-positron storage ring. The physics justification for the e^+e^- ring is summarized briefly and the proposed facility is described. The ring will have six arcs having gross radii of about 220 m and six interaction regions located at the centers of straight sections about 130 m long. The longitudinal distance left free for experimental apparatus around the interaction regions will be 20 m. The range of operating beam energies will be from 5 GeV to 15 GeV. The design luminosity at 15 GeV will be $10^{32}cm^{-2}s^{-1}$, and the luminosity will vary approximately as the square of the beam energy. Alternative methods under consideration for adjusting the beam cross-section are discussed. The designs of the storage ring subsystems and of the conventional facilities including the experimental halls at the interaction regions are described.

1. Introduction

In the preceeding report presented to this Conference by L. Smith, the evolution of the PEP system was described.[1] In the autumn of 1973, following the 1973 PEP Summer Study, the two cooperating laboratories, LBL and SLAC, reached the conclusion that the electron-positron storage ring component of the system, operated at beam energies up to 15 to 20 GeV and capable of yielding high luminosity in electron-positron collisions, was a straightforward extension of techniques already successfully used in several laboratories and that such a ring could be designed and built immediately with confidence. For the proton ring, superconducting-magnet technology offered the promise of achieving high beam energy with economical size and with low power consumption; however, there appeared to be some technical uncertainties yet to be resolved. In the meantime electron-positron rings operating in Europe and the U.S. had revealed that a wealth of new and previously unexpected high-energy physics information concerning the structure of elementary particles, both leptons and hadrons, was forthcoming from electron-positron collisions. These experiments suggested that it was urgent to move on higher energies than those available from existing machines.

With these facts in mind, LBL and SLAC jointly decided to propose the immediate design and construction of the 15-GeV electron-positron storage ring, PEP Stage I, and to defer the proposal of the proton storage ring until further development of superconducting technology had taken place. The two laboratories agreed to locate PEP at SLAC and to design the electron-positron ring and its housing to be compatible with the future addition of a 200-GeV proton ring such as that described in the preceding paper.[1] The two universities signed an agreement in February, *1974,* outlining joint financial and management arrangements for the project.

The main component of the proposed facility is an electron-positron storage ring having six bending arcs and six long straight sections. The major diameter of the ring is about 700 m and the radius of the arcs is about 220 m. The facility is shown in Fig. 1. The electrons and uositrons are produced in the SLAC linac and introduced into the storage ring via two beam transport paths emanating from the end of the two-mile

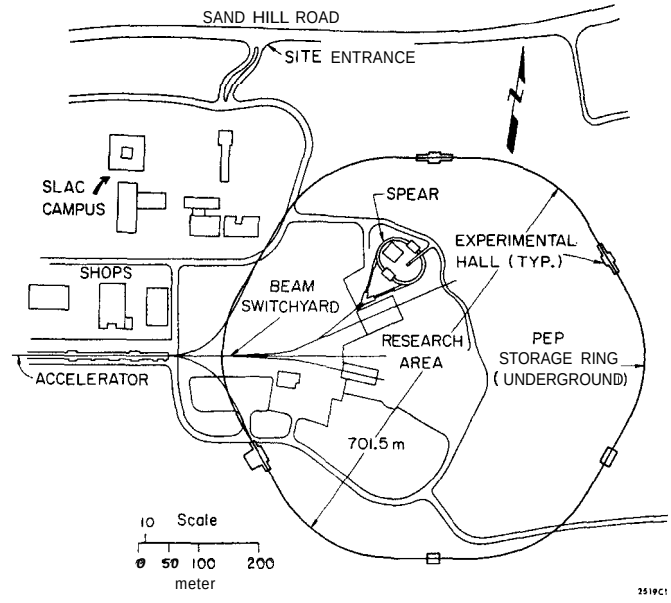

Fig. 1. Layout of the PEP ring superimposed on an aerial view of the SLAC site.

accelerator and joining the storage ring in the northwest and southwest straight sections. Beam of energies up to 15 GeV can be injected and stored, and, at a future date, components could be added to permit stored-beam energies as high as 20 GeV. Also provisions are made in the design of the ring housing so that a synchrotron-radiation research facility could be added in the future.

The energy lost from the beams by synchrotron radiation is restored by a high-power radiofrequency accelerating system which employs klystrons to drive the accelerating structure at a frequency of about 360 MHz and which is capable of delivering several megawatts of power to the beams. Since this power appears as synchrotron radiation which strikes the outer wall of the (mostly aluminum) vacuum chamber, that wall will be water-cooled. The radiation-desorbed gases will be pumped away very rapidly by means of long, narrow sputter-ion pumps located in the vacuum chamber in the bending magnets directly alongside the beams to sustain pressures of about 10^{-8} Torr which must be maintained in the vacuum chamber to achieve adequate beam lifetimes (several hours) and low experimental background counting rates.

The proposed storage ring is designed to generate a luminosity of $10^{32}cm^{-2}s^{-1}$ per interaction region at a beam energy of 15 GeV. This luminosity appears adequate to support a vigorous experimental program. To achieve this performance, it is necessary to store a current of about 100 mA in each beam. Based on the expected performance of the SLAC two-mile accelerator in filling SPEAR II,[2] the filling time for PEP will be ten to fifteen minutes, which is a comfortably short period compared to the storage time of several hours, and ensures that storage ring operations will consume only a small fraction of the linear accelerator beam time.

The fundamental limitation on the performance of existing electron-positron storage rings is the transverse beam-beam limit which imposes an upper limit on

* Work supported by the U.S. Atomic Energy Commission

the current density of the beams where they collide.[3] The magnetic guide field of PEP is designed to attain the specified performance, as described in Section 3, within the limitations established by this instability.

Each counter-rotating beam will be concentrated into three bunches, each a few centimeters long, equally spaced around the ring, and the bunches will collide only at the centers of the six long straight sections. Five of these interaction regions will be housed in experimental halls of various designs for high-energy physics experiments. These designs are discussed in Section 4. The sixth interaction region (northwest) will be reserved for accelerator physics measurements and experiments.

The construction schedule calls for completion of the facility four years after full authorization so that experimental physics could begin in 1980 if full authorization occurs in 1976. The total cost is estimated to be $53.3 million plus escalation.

2. High-Energy Physics with Electron-Positron Colliding Beams

High-energy electron-positron colliding-beam storage rings have opened up a new physical region for the study of elementary particles and their interactions, the region in which a state of pure energy is produced by the annihilation of the colliding electron and positron. This state comes into being only when a particle strikes its anti-particle and therefore does not occur when primary beams from conventional accelerators strike material targets or when protons collide with protons in a proton-proton storage ring system. The energy can rematerialize into combinations of all of the presently known elementary particles. Thus data can be obtained about the structure and interactions of these particles in a new experimental regime.

The results from entering this new region have been surprising and profound. As the energies of the colliding beams have been increased, the results of experiments done with them have become more and more difficult to understand in terms of present models of elementary-particle structure and interactions. Most recently, new experiments from the SPEAR facility at SLAC and the CEA facility in Cambridge have given results which flatly contradict the predictions of the theoretical ideas involving substructure within the nucleon which had been so successful in explaining a host of experiments done with conventional accelerators, and the resolution of this contradiction seems certain to lead to a far deeper understanding of elementary-particle physics. With the PEP storage ring we shall extend the available reaction energy in electron-positron collisions to 30 GeV, thus greatly expanding our reach into the annihilation region.

The range of experimental studies opened up by PEP is extremely rich and varied, spanning the entire field of elementary-particle physics including the strong interactions, the electromagnetic interactions and the weak interactions. In the field of strong interactions, reactions leading to mesons and nucleons in the final state will reveal new and vital information about the structure and sub-structure of the elementary particles. For example, a conceptually simple experiment, the measurement of the total reaction cross section for producing strongly interaction particles by electron-positron collisions, tests some very basic hypotheses about the structure of the particles produced. These hypotheses have failed the tests of experiments with the present generation of electron-positron rings, and experiments at higher energy may demand entirely new theoretical constructs.

In the field of pure electromagnetism, processes with only electrons, mu-mesons and gamma rays as reaction products can be studied. The theory of the electromagnetic interaction, quantum electrodynamics, is the only successful field theory in particle physics in the sense that all experimental tests to date agree with its predictions. PEP will greatly increase the energy limits to which this theory can be tested. Particularly exciting is the fact that, if present trends in the hadron production observed in e^+e^- colliding beams continue to the maximum PEP energy, and if our present concepts of the way these reactions take place have any validity, then quantum electrodynamics must break down in the PEP energy region.

In the study of the weak interaction, PEP will open new vistas. For example, the colliding electron-positron pair can transform itself into a mu-meson pair either by the weak or by the electromagnetic interaction, and the energy-dependences of these two processes are such that the weak interaction amplitude becomes more and more competitive with the electromagnetic amplitude the higher the energy. At PEP energies, the interference between the two should become observable. Particle physicists are now seeking a unified picture of the weak and electromagnetic interactions and PEP offers the possibility of testing various unifying concepts from a new experimental vantage point.

Theoretical calculations based on current ideas and models indicate that luminosities in the range $10^{31}\text{cm}^{-2}\text{s}^{-1}$ to $10^{32}\text{cm}^{-2}\text{s}^{-1}$ are required to carry out a comprehensive program of studies in weak, strong and electromagnetic interactions.

In summary, PEP offers the possibility of the study of a very broad range of fundamental questions in particle physics in a new and presently inaccessible energy region. The mysteries unveiled in the present generation of electron-positron colliding-beam facilities lead us to expect new phenomena to be uncovered with this device. These experiments, together with the complementary experiments with protons, neutrinos and mesons at the highest-energy proton accelerators, offer great promise of leading to a new depth of understanding of elementary particles and the fundamental laws of physics.

3. Description of the Electron-Positron Storage Ring

Magnetic Focusing System for the Storage Ring

Tables of Parameters. Table 1 presents a summary of general parameters and lattice parameters of the PEP e^+e^- storage ring, and Table 2 gives typical beam parameters for 15-GeV operation. Emittances are defined as (σ_β^2/β).

Table 1

Genera1 Parameters

Beam Energy, E		
Nominal Maximum	**15**	**GeV**
Minimum	**5**	**GeV**
Design Luminosity per Interaction Region, $\mathscr{L}_{max}$		
At 15 GeV	$10^{32}\text{cm}^{-2}\text{s}^{-1}$	
Below 15 GeV	$10^{32}(E/15)^2\text{cm}^{-2}\text{s}^{-1}$	
Nominal Crossing Angle, 2δ	**0**	**radians**
Number of Interaction Regions		
Total (superperiodicity)	**6**	
Available for High-Energy Physics	**5**	
Reserved for Machine Physics Studies	**1**	
Number of Stored Bunches, N_b	**3**	
Available Length at Each Interaction Region	**20**	**m**

Lattice Parameters

Straight Section Length	**130.416**	**m**
Gross Radius of Arcs	**220.337**	**m**
Magnetic Bending Radius	**169.916**	**m**
Maximum Diameter of Ring	**701.505**	**m**
Circumference of Ring	**2166.912**	**m**
Cell Length	**28.842**	**m**
Total Number of Cells	**48**	
Number of Standard Cells	**36**	
Effective Length of Bending Magnets	**5.561**	**m**
Effective Length of Cell Quadrupoles	**0.780**	**m**
Bending Field at 15 GeV	**2.9447**	**kG**
Maximum Quadrupole Field at Bore Radius	**<7.5**	**kG**

Table 2

Typical Beam Parameters at 15 GeV

Total Betatron Tunes			
Horizontal	18.75		
Vertical	18.75		
Momentum Compaction	0.00455		
Transverse Damping Time	0.00823		s
x-y Coupling Coefficient	0.280		
Horizontal Emittance	2.3	x 10^{-5}	cm-rad
Vertical Emittance	1.8	x 10^{-7}	cm-rad
Number of Stored Particles (each beam)	4.44	x 10^{12}	
Synchrotron Radiation Power (each beam)	2.6		MW
Linear Tune Shifts per Interaction Region			
Horizontal, $\Delta\nu_x$	0.06		
Vertical, $\Delta\nu_y$	0.06		
Luminosity (each interaction region), $\mathscr{L}$	1.0	x 10^{32}	$cm^{-2}s^{-1}$
Cell Parameters			
Horizontal Phase Advance	97.0°		
Vertical Phase Advance	82.3°		
Maximum Horizontal Beta	48.2		m
Maximum Vertical Beta	50.2		m
Maximum Momentum Dispersion	2.24		m
Interaction Region Parameters			
Horizontal Beta, β_x^*	4.0		m
Vertical Beta, β_y^*	0.20		m
Momentum Dispersion, η^*	-0.73		m
Beam Size (r.m.s.)			
Horizontal Betatron, σ_x^*	0.096		cm
Horizontal Dispersion, σ_{xE}^*	0.072		cm
Total Horizontal, σ_x^*	0.12		cm
Total Vertical, σ_y^*	0.006		cm

Choice of General Parameters. The primary design goals set for the PEP storage ring were: (1) to cover the range of beam energies from 5 GeV up to 15 GeV in order to provide a range of center-of-mass energies extending approximately from those expected to be available at other smaller e^+e^- colliding-beam machines up to those available at the largest proton accelerators; (2) to maintain luminosities around $10^{32}cm^{-2}s^{-1}$ over this range in order to provide experimentally useful reaction rates with the expected cross sections; (3) to furnish an adequate number and variety of experimental halls (interaction regions) to permit a vigorous and varied national program of experimentation and (4) to ensure compatibility of the housings and experimental halls with the possible future addition of a superconducting 200-GeV proton storage ring for e-$ collisions, another 15-GeV electron ring for e-e- or e e^+ collisions, or both additional rings. These goals together with the size, shape and geophysical characteristics of of potential locations at SLAC led us to the choice of the six-sided storage ring shown in Fig. 1. With a radiofrequency power of about 5 MW available to the beams and with the arrangements for controlling the cross-sectional area of the beams described below, the storage ring should achieve a peak luminosity of $10^{32}cm^{-2}s^{-1}$ at a beam energy E of 15 GeV, and a variation of luminosity approximately proportional to E^2 below that energy. It may also be possible to operate the storage ring at energies somewhat higher than 15 GeV with reduced luminosity. The design-luminosity curve is shown in Fig. 2.

The arc radius and the straight-section length are the two most influential parameters in determining the performance of the storage ring. The arc radius should be as large as possible to minimize synchrotron radiation power. Component-free drift spaces 20 m long centered at the interaction regions have been reserved for experimental purposes. The rest of the space in the straight section is used for injection systems, rf

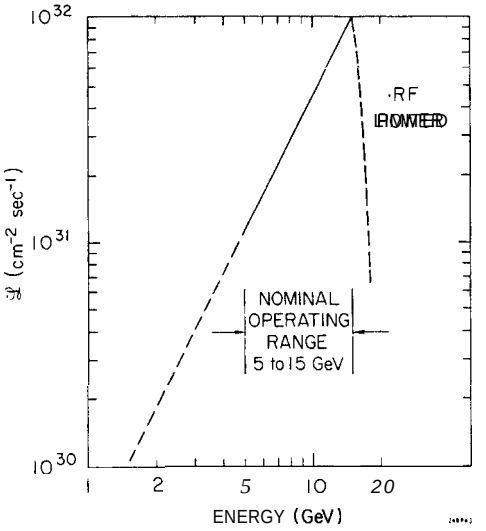

Fig. 2. Design luminosity as a function of beam energy showing the nominal operating range and the upper limit imposed by the available rf power.

cavities and various beam-control elements.

In order to attain high luminosity, it is necessary to collide intense beams within a small cross-sectional area. However, the number of particles which can be collided within a given area is limited by the incoherent beam-beam interaction;[3] this limit is usually characterized by the small-amplitude vertical and horizontal tune shifts $\Delta\nu_y$ and $\Delta\nu_x$. It is well known that, when beam currents are limited by the beam-beam interaction, the maximum theoretical luminosity $\mathscr{L}_{max}$ may be increased if the beam size is enlarged. If one operates a storage ring at different energies under the same focusing configuration, the transverse beam dimensions vary directly as energy E, the maximum (tune-shift-limited) number of storage particles as E^3; thus the luminosity varies as E^4 and drops off very rapidly at lower energies. If, however, the focusing configuration is changed as the energy is lowered in such a way that beam size remains essentially constant, approximately filling the aperture, then the maximum number of stored particles varies as E and luminosity as E^2. This E^2 luminosity is quite acceptable, because most reaction cross sections increase at lower energies. Above the design energy, luminosity will be rf-power-limited, and will drop precipitously, cutting off at an energy of around 18 GeV.

Several different methods for beam size control will be provided. These include varying the momentum dispersion function at the interaction point as in SPEAR,[2] unmatching the momentum dispersion function so that it does not repeat periodically from cell to cell and varying the betatron tune.[4] Vertical size will be adjusted by means of variable horizontal-vertical betatron-oscillation coupling. Using combinations of these techniques, it should be possible to reach, or at least approach, the luminosity shown in Fig. 2 at all operating energies.

Variation of the betatron tune gives a contribution to $\mathscr{L}_{max}$ which varies as ν_{xA}^{-3}, where ν_{xA}^{-3} is that part of the radial tune which comes from the bending arcs. Momentum dispersion at the interaction region gives a contribution proportional to η^{*2}/β_x^*, where η^* and β_x^* are respectively the momentum dispersion function and the betatron amplitude function at the interaction point. An unmatched dispersion function η gives a luminosity increment proportional to η_1^2/β_x^* where η_1 is a measure of the mismatch in the bending cells.

A lattice in which the arcs consist of doublet

cells and are joined by comparatively simple insertions was chosen.[5] Preliminary studies showed that the natural beam size would be about right to give the peak design luminosity if the bending part of the lattice contained between *40* and 50 cells operating with a betatron phase advance per cell of around 90° in both the horizontal and vertical planes. For convenience, the number of cells was chosen to be *48*, or eight cells per 60-degree arc. The nominal phase advance of 90° per cell allows considerable latitude in varying the tune, since doublet cells work reasonably well at phase advances from below 45° to above 135°. A conventional separated-function bending cell, shown in Fig. 3, provides independent control of the total betatron tunes

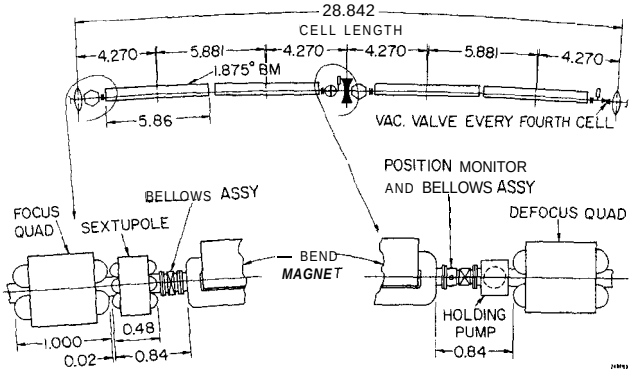

Fig. 3. A standard cell is shown between the quadrupole centerlines. Dimensions are in meters.

ν_x and ν_y by means of the independently controllable focusing and defocusing quadrupoles. The spaces between the quadrupoles and bending magnets provide room for various devices including the sextupoles, which are necessary to control chromaticity.

Each insertion consists of a straight section, shown in Fig. *4*, of approximately *130* m in length, and

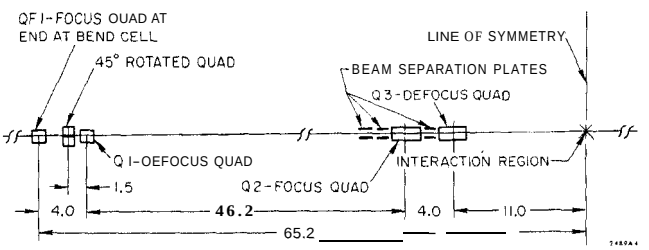

Fig. *4*. The straight insertion, which is symmetric about the interaction point, is shown from the centerline of the cell quadrupole to the interaction point. Dimensions are in meters.

two modified bending cells which have standard dimensions but independently-powered quadrupoles. Suitable configurations have been found over a considerable range of values of tunes, β_x^*, β_y^*, η^* and η_1 (the η-mismatch amplitude). These configurations include ranges for the various beam-enlargement schemes which are adequate to produce the design luminosity over the designated operating range of 5 to 15 GeV. Solutions which are favorable for injection also have been found.

Apertures and Magnet Design

The "beam-stay-clear", or minimum unobstructed lateral region around the design orbit, is a roughly elliptical figure with diameters

$$a_i = 20\,\sigma_i + 2\ \text{cm}$$

where a_i is the vertical or horizontal aperture diameter, σ_i is the vertical or horizontal rms beam radius and the subscript denotes the particular location on the circumference. The factor of 20 allows sufficient, but not overly conservative, clearance to give good beam lifetimes according to experience at SPEAR; the additional *2* cm is a margin for orbit distortions and misalignments. The actual bore clearance of the magnets will include an additional allowance for vacuum chamber walls, installation tolerances and for a possible bake-out mantle.

The magnet system is being designed to minimize the installed cost plus 10-years' operating cost at 15 GeV. Prudent attention was given to reducing energy consumption. The magnets themselves will be capable, nevertheless, of operation at *20* GeV. Laminated magnets were selected for the main ring elements in order to minimize capital costs and to ensure sufficient uniformity magnet-to-magnet.

Radiofrequency System

General. The energy radiated per turn by a 15-GeV electron circulating in the PEP ring is 26 MeV. In order to achieve a reasonable quantum lifetime, an overvoltage which depends on the lattice parameters and radiofrequency is required. At a frequency of 358 MHz (chosen for reasons discussed below), a peak rf voltage of *44* MV is sufficient. In order to reach the design luminosity of $10^{32}\text{cm}^{-2}\text{s}^{-1}$, the required circulating current is 100 mA for this same lattice. The radiated power is therefore 2.6 MW per beam, or 5.2 MW total. In addition, another 2.0 MW is dissipated in the rf structure. At lower energies, the rf power requirements are lower.

It is proposed that the required rf power of 7.2 MW be supplied by *24* klystrons, each delivering a CW output power of 300 kW to an accelerator section 2.1 m in length, comprising five cavities. The accelerator sections will be arranged in two groups of 12 sections each, located at the ends of the southern-most straight section, shown in Fig. 1. Allowing space between sections for flanges, bellows, etc., the overall length of each group will be about 30 m. Rf power will be supplied to the cavities through waveguides running down vertical penetrations from the klystrons which will be housed above ground for ease of maintenance. A list of the principal parameters for the rf system is given in Table 3.

Table 3

General Rf System Parameters

Frequency	358.6	MHz
Energy Loss per Turn	26	MeV
Peak Rf Voltage[1]	*44*	MV
Particles per Beam	*4.4* x 10^{12}	
Circulating Current per Beam	100	mA
Synchrotron Radiation Power (total)	5.2	MW
Total Accelerating Structure Length	60	m
Active Accelerating Structure Length	50	m
Total Shunt Impedance (V_p^2/P_c)	950	MΩ
Total Cavity Power Dissipation	2.0	MW
Total Rf Power	*7.2*	MW
Conversion Efficiency at Design Current[2]	*70*	%
Number of 300-kW Klystrons	*24*	
Total Power Input to Rf Power Supplies[3]	**11**	MW

[1] For a quantum lifetime of 12 hours.

[2] Ratio of radiated power to total rf power.

[3] Based on klystron efficiency of **70%** and a power supply efficiency of 95%

Choice of Frequency. Although operation at frequencies below 100 MHz has some advantages, the attainable shunt impedance per unit length of the cavities is low. In order to attain the high peak voltages required for PEP using such cavities, the length of the rf structure would need to be several hundred meters. By using a higher frequency, the geometric shape of the cavities can be optimized and the shunt impedance per unit length can be increased dramatically. On the other hand, as the operating frequency is increased, the overvoltage ratio (peak voltage divided by the synchrotron radiation loss per turn) required to give a reasonable quantum lifetime also increases. Taking these two competing factors into account, it can be shown that there is a rather broad optimum for PEP in the frequency region 100 to 400 MHz.

Within this frequency region, economic and engineering considerations dominate the choice of frequency. The structure diameter, weight and cost become unreasonably large below about 200 MHz. A careful study of the comparative advantages of klystrons vs gridded tubes indicated that klystrons were superior to tetrodes with respect to initial and annual operating costs, reliability and expected life. Klystron size and cost are lowest at the upper end of the 100-400 MHz frequency range. This factor, together with the decrease in structure costs with increasing frequency, led to a choice of 358 MHz for both PEP and SPEAR II.[2] Before PEP is constructed, operational experience with the new SPEAR II rf system will have served as a test of the proposed design.

System Design. Further details on the PEP rf system design are described in another report to this Conference.[6]

Vacuum System

Introduction. The vacuum system proposed for PEP will be similar in design, construction and operation to the system currently in successful use at SPEAR.[7] The vacuum chamber in the bending magnets will be an 11-m-long, 6061-T4 aluminum extrusion with an internal cross section, shown in Fig. 5, designed to accommodate

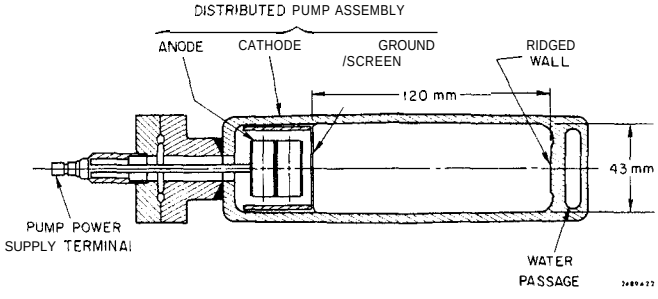

Fig. 5. Cross section of the vacuum chamber for the bending magnets. The vacuum pump which operates in the fringing-field region of the magnet is shown with one of the high-voltage terminals.

the beam-stay-clear region required by beam dynamics. The synchrotron-radiation absorbing wall will be approximately 10 mm thick. The absorbing surface will be ridged as in the SPEAR chambers in order to minimize the synchrotron-radiation-induced gas desorption. A cell vacuum chamber will consist of two bending magnet chambers and two quadrupole chambers. The quadrupole chambers will accommodate the required expansion bellows, position monitors, gauging, etc.

Synchrotron Radiation. The surfaces which are subjected to synchrotron radiation require cooling. At 15 GeV and 100 mA dc in each beam, the total power radiated per beam will be 2.6 MW. The maximum linear heat flux is 35 W/cm for a single electron or positron beam and 45 W/cm for both beams. The synchrotron radiation consists of photons with a spectral energy distribution up to well above 80 keV.

The main gas load during operation is due to synchrotron-radiation-induced desorption which is dominated by a two-step process in which a photoelectron is ejected from the vacuum chamber wall by a synchrotron-radiation photon and subsequently desorbs a gas molecule upon reentering the wall. This gas load is concentrated in the arcs where the synchrotron radiation is produced. Data from SPEAR indicate that it is conservative to extrapolate the desorption rate linearly with beam energy. The total photon desorbed gas load for the entire ring is estimated to be 10^{-5} Torr-ℓ/mA-s at 15 GeV.

Vacuum Pumps. The vacuum system is conductance-limited in the bending magnet chambers where the bulk of the outgassing occurs. Distributed sputter-ion pumps of the type which were developed and used for SPEAR will therefore be installed inside the vacuum chamber within the bending magnets. These pumps are rated at 300 ℓ/s per m of pump length. Commercially available 100-ℓ/s ion pumps will be mounted at each quadrupole and will maintain the system at a base pressure of 1×10^{-9} Torr without a stored beam. Based on the above estimate for the total gas load, the maximum pressure will be 5.0×10^{-8} Torr and the average pressure will be 2.5×10^{-8} Torr.

In the insertions, which will be fabricated of 300-series stainless steel tubing, the main gas load will be due to thermal outgassing. Initially, a system of commercially available ion pumps will be installed to maintain an average pressure of 5×10^{-9} Torr. Extra pumping ports will be provided so that added pumps could lower the average pressure in the insertions to 5×10^{-10} Torr if required by experimental conditions.

Electron and Positron Injection

The six PEP interaction regions are illuminated by three equally-spaced bunches in each beam which are filled selectively by gating the SLAC linac gun. The rf frequency of 358 MHz implies that the rf phase (time) acceptance will be of the order of nanoseconds.' A special new electron gun has been installed on the two-mile accelerator to provide very high peak currents in the short (—1.4 ns) pulses necessary for injection into both SPEAR II and PEP. Figure 6 is a plot showing the PEP filling time vs injection energy. The line shows the predicted injection times based on a conservative 50% injection efficiency and the expected yields of electrons and positrons with the new gun. For good operating efficiency, the filling time should not exceed ten or fifteen minutes. From Fig. 6, it can be seen that this can be achieved at energies above approximately 10 GeV up to the maximum positron energy from the two-mile accelerator, which coincidentally is 15 GeV, the design energy of the ring. The maximum injection repetition rate, which is used at the highest injection energies, is 360 pps, the full SLAC rate. At lower filling energies, the damping rates of horizontal betatron oscillations and the energy oscillations require that the filling repetition rate be reduced. The design of the injection system permits the filling of an adjacent bunch while a previously injected bunch is damping, and the curve in Fig. 6 reflects this mode of operation.

For storage ring operation at energies below reasonable injection energies, especially below 10 GeV, the beam will be stored at the injection energy and then the ring magnets will be ramped down to the operating energy.

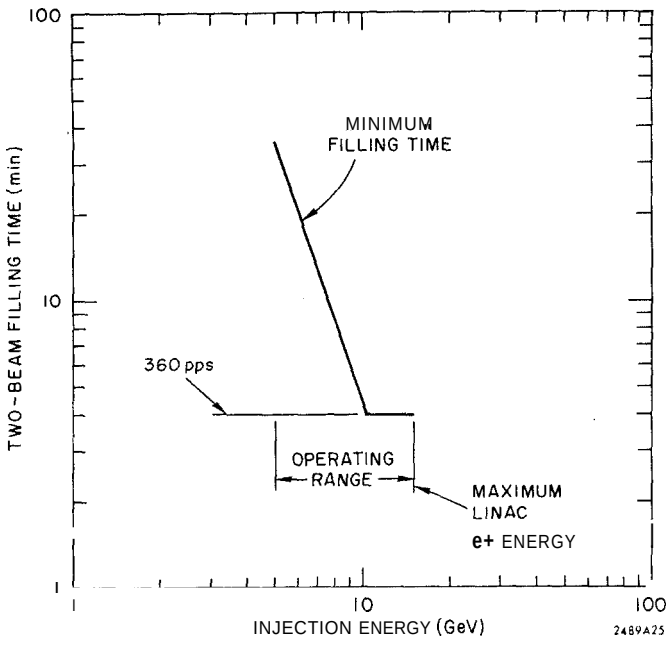

Fig. 6. Filling time vs injection energy. Filling time is the time required to fill both the electron and positron beams to a current of 100 x E(GeV)/15 mA from a beam of 20 mA e^+ and 40 mA e^- in a 1.4 ns pulse with 50% capture efficiency.

Instrumentation Monitoring and Control

The storage ring system, like the linear accelerator, is too spread out for a single data-collection point to be practical. Data will, therefore, be collected at a number of places, edited and compressed as much as possible and then transmitted to the control room. The control room will be located to permit a short path for direct transmission of fast monitoring signals from the injection lines. To reduce the amount of cabling, signals generated within the bending sextants will be wired to instrumentation racks in the nearest data center. Interlock signals will be summarized and then wired directly to the equipment they must control. The remaining signals will be edited by a small computer and sent by serial link to the control room.

The central element of the control system will be a "large mini-computer" which will provide task synchronization between the peripheral elements and manage intercommunication. It need not have elaborate computational ability. It will have three types of "peripherals". The first type is the "data-collection" computer, at least one per interaction area, which provides all connections to the real world. The second type is the console manager which provides all operator interfaces. The third peripheral will be a moderately-sized computational computer which will carry out large-scale calculations and provide file management and programming aids.

Control of Beam Instabilities

Transverse Instabilities. In the design of this storage ring it has been assumed that the maximum luminosity obtainable is determined by the beam-beam incoherent limit and that it is possible to store beams of sufficient intensity to reach this limit. The various transverse instabilities that can occur with large bunched beams and can jeopardize their storage may be categorized into three types: those that are determined by the average circulating current, those that are present because there are multiple bunches in the ring and those that depend upon the peak current in a single bunch.

The present PEP design appears to be rather conservative in requiring an average single-beam current of 100 mA in three bunches. Many electron storage rings have stored such currents at much lower energies where the transverse instabilities are generally much more troublesome. While multiple-bunch transverse instabilities have been predicted, they have not been observed in rings having only a few bunches. Also, because the bunch spacing in PEP is large and fixed, it seems feasible to build a feedback system to damp each bunch individually. The only multiple-bunch motion that has been observed in SPEAR is the coherent motion between two colliding beams. This coupled motion does not seem to be of major concern and its effect is ameliorated by use of electric quadrupoles which are planned for inclusion in the PEP lattice.

The head-tail instability has been the most important single-beam transverse instability observed in electron storage rings and it has been controlled through the chromaticities. In the PEP design it will be possible to vary the value of the chromaticity by means of the sextupole fields which are distributed throughout the lattice without producing destructive non-linear resonances.

The peak current required in PEP is not substantially different from that already attained in single beams in SPEAR.

Longitudinal Instabilities. The six circulating bunches in PEP will have six coherent normal modes. The in-phase oscillations of the bunches can be controlled by a feedback loop coupling a signal picked up from the beam back to a varactor-diode phase modulator in the input drive to one or more of the klystron groups. In order to damp the other five possible modes, a high-frequency cavity will be installed to split the synchrotron oscillation frequencies.

Three potential longitudinal instabilities which can arise out of the b am-beam interaction have been suggested and studied.' The first occurs only when the colliding beams cross at an angle, which is not the case in PEP. The second is due to a non-zero value of the η-function at the interaction region η^*. It places an upper limit of the value of η^* above that at which PEP will operate. The third occurs when the bunch length is large compared to the value of the β-function at the interaction region. This will not be the case in PEP.

A potential problem in the design of the PEP rf system is the additional power loss due to the excitation of higher-order cavity modes. Both theoretical and experimental approaches are planned in attacking this problem, and it is expected that by proper structure design, the enhanced power loss due to the excitation of higher-order cavity modes can be held to a tolerable level.

4. Physical Plant

Ring Housing and Shielding

The ring will be located symmetrically about the axis of the SLAC two-mile accelerator with the western-most point approximately 100 m downstream from the end of the accelerator. The terrain slopes downward from the accelerator axis in both north and south directions so that the interaction regions, which are off the axis, will generally lie in areas of lower elevation. Some segments of the ring will be in areas low enough to permit cut-and-cover construction. Those parts deeper underground will require bored tunnels.

The ring, which is horizontal, will be housed in a tunnel at an elevation of approximately 65 m above mean sea level. It crosses under the SLAC beam switchyard about 11 m below the accelerator beam. As shown in Fig. 1, the ring will circumscribe the present research yard. The beam transport tunnels, through which electrons and positrons are brought into the ring, will start at the end of the linear accelerator and branch away and downward, crossing over the ring to insertion points from the inside of the ring, as shown in Fig. 1.

The electron-positron storage ring will be positioned high in the tunnel and suspended from the concrete lining. The tunnel design provides for eventual inclusion of a proton ring. The proton storage ring would occupy a middle height and the electron-positron storage ring would be remounted to alternate above and below it, crossing it in a vertical plane at the interaction points. In the bored tunnel areas a circular housing will be constructed *3.3* m in diameter, as shown in Fig. 7. A rectangular section *3.3* m wide by 2.7 m

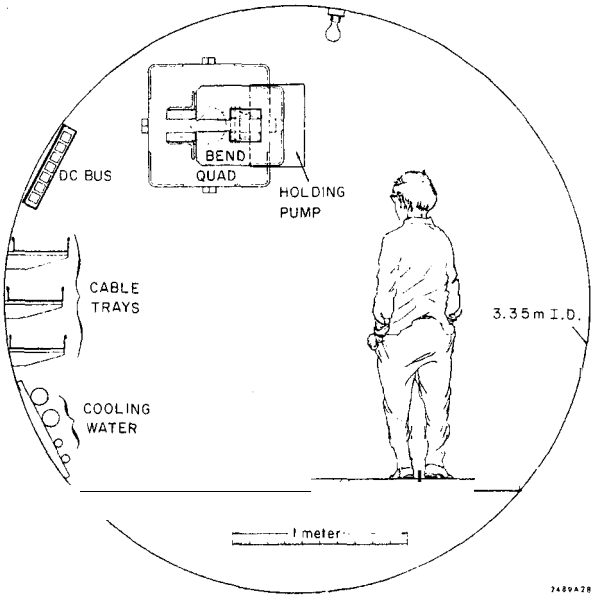

Fig. 7. Cross section of the PEP housing.

high is planned in the cut-and-cover areas. The access aisle will be on the outside of the ring. Because the production of neutrons by proton interactions is some three orders of magnitude greater than that due to electron interactions, and, in addition, because the energy of stored protons will be about 200 GeV as compared to 15 GeV for the stored electrons and positrons, the total shielding requirements will be determined by beam losses from the future proton storage ring.

Experimental Areas

The planned site for PEP offers convenient access to five of the six interaction regions. Thus, it is proposed that five experimental areas be developed in a manner suitable for experiments in the first stage of PEP. The sixth one will have access for only relatively small experimental setups such as those needed for accelerator physics and luminosity monitoring.

The complement of experimental areas is regarded as typical; however, a Summer Study will be held in 1974 on the subject of PEP experimentation, and the details of the experimental areas may change.

The primary constraint on the experimental areas, imposed by the magnet configuration, is the length of the interaction region drift section, which will be 20 m. This is the distance between the final focusing elements of the storage ring and is the space in which most experimental equipment will be mounted.

It is proposed that two of the experimental areas be of the basic design shown in Fig. 8. These so-called

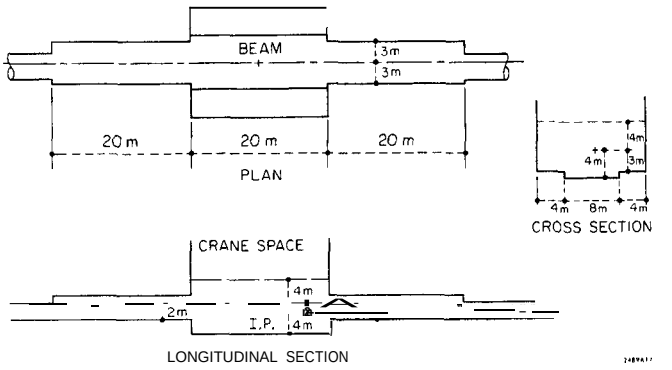

Fig. 8. "Standard" interaction area with alcove.

"Standard" areas are seen as general purpose facilities which will accommodate many of the experiments planned for PEP, including those involving a future proton ring. The basic design consists of an 8-meter-by-20-meter pit with 4 m of clearance above and below the beam Line. On either side of the pit is a platform *4* m wide and *3* m below beam elevation and extending along the beam line are 20-meter alcoves 6 m wide. These dimensions are determined by examining some of the experiments envisaged for standard areas, such as tests of quantum electrodynamics, various studies of hadron production and searches for weak interaction effects.

The third area will have the same transverse dimensions as that described above, but the pit will be extended along the beam direction to a total length of *30* m and the forward-angle alcoves will be omitted. This extension is provided mainly for weak interaction experiments where there may be significant interference between the single-photon exchange amplitude and weak amplitude in the forward direction for processes such as muon pair production. Rather involved forward-angle experiments providing for ranging out muons (using 10-15 m of iron) to measure their polarization are accommodated by this area.

The fourth experimental area is the largest and could be dedicated to a large 4π-steradian magnetic detector or some other large device as yet unconceived. The layout of the experimental pit area at the interaction region is largely determined by the geometry of a large cylindrical magnetic detector similar to the one in current use at SPEAR, except with a superconducting coil and possibly also provisions for calorimetry to give additional information on energetic hadrons. The pit region has clearances of ± 6 m vertically, and horizontally 8 m and 12 m on either side of the center line.

The fifth area is designated with an eye to future potential expansion. Initially, it will have the same dimensions as the Standard experimental area except that the alcoves will be omitted. In addition, the ends of the pits will be made in such a manner that either one or both can later be easily extended to provide additional experimental space downstream of the proton beam for various possible e-p devices.

Power and Cooling

The maximum power demand of the electron-positron

storage ring and experimental apparatus is estimated to be 26 MW. The installed capacity will be 36 MW. While the distribution system can provide 3 MW to each of the five experimental areas, it is expected that the total experimental-equipment load will not exceed 5 MW at any time.

Except for experimental areas, low-conductivity water (LCW) will be provided for the installed power capacity. One megawatt of cooling capacity will be installed at each experimental area. Cooling will be done by relatively small local LCW systems exchanging heat with cooling tower water which will be distributed around the ring to cool the closed-loop LCW systems.

Acknowledgements

The work reported in this paper is that of the members of the LBL-SLAC Joint Study Group; the author is only their spokesman. Special thanks, however, are due W. B. Herrmannsfeldt and C. S. Nissen.

References

1. L. Smith, "The Proton-Electron-Positron Project - PEP", invited paper at this conference.
2. J. Paterson, "SPEAR, Status and Future Developments", invited paper at this conference.
3. F. Amman, IEEE Trans. Nucl. Sci. NS-20, No. 3, 858 (1973).
4. R. H. Helm, M. J. Lee and J. M. Paterson, report to this conference;
   M. Bassetti, report to this conference.
5. R. H. Helm and M. J. Lee, report to this conference.
6. M. A. Allen and P. B. Wilson, report to this conference.
7. U. Cummings et al., J. of Vac. Sci. and Tech. 8, *348* (Jan.-Feb. 1971).

DISCUSSION

Alessandro Ruggiero (NAL): The proposed ring encircles the present research yard. Do you anticipate any interference with potential expansion of the research yard or any other conflict?

John Rees (SLAC): The answer is no, we don't expect to expand the research yard in the easterly direction because the huge backstop is required to stop the radiation from the linear accelerator and the level of the storage ring is way below ground there and does not interfere with the normal operation in any way. We even expect to be able to tunnel under the linac without disturbing it except when we have *to* open the enclosure to bring out the injection beams. Dr. Panofsky points out that the linac works well at a magnitude 5 earthquake and the same can be said for SPEAR. We had a stored beam and it didn't even dump.

Melvin Month (BNL): Is the luminosity quoted per interaction region and has each bunch **six** interactions per revolution?

Rees: Yes. The revolution is quoted per interaction region **and** each bunch has six interactions per revolution. Being in the same plane, they can't get by each other.

ISABELLE ANTIPROTON OPTION*

C. Baltay
Columbia University, New York, New York
R. Chasman, H.W.J. Foelsche, H. Hahn, M. Month, and A. van Stienbergen
Brookhaven National Laboratory
Upton, New York

Summary: The possibility of colliding antiprotons in ISABELLE has been investigated. Protons are accelerated on the second harmonic to 200 GeV in one of the rings and are extracted into a bypass during flat top, The 30 GeV antiprotons from a target placed at a low-β point in this bypass are transported to the second ring where they are injected and matched into a bucket of a 10th harmonic rf system. This procedure is repeated until all the buckets are filled. The antiprotons are then accelerated to 200 GeV. Protons are now stacked in the first ring in the opposite direction, accelerated to 200 GeV and made to collide with the antiprotons. $p-\bar{p}$ luminosities up to $\sim 10^{29}$ cm^{-2}sec^{-1} seem feasible.

Introduction

The attractiveness for intersecting storage rings such as ISABELLE would be further enhanced if they would provide interactions of a variety of particles besides proton-proton interactions. Ever since the ISABELLE Summer Study some design effort has been directed towards exploring such possibilities. As a result several options have emerged and special care was taken in the basic ISABELLE design to allow for their addition at a later time at minimum cost. The antiproton option, to be described here, involves accelerating and storing a $\sim$ 1 mA antiproton beam and colliding it at 200 GeV with 10 A ISABELLE proton beam. A pp luminosity of the order of 10^{29} cm^{-2}sec^{-1} is obtained.

Choice of Method

Various methods of accumulating large antiproton densities in storage rings have been studied in the past.

The most straightforward mechanism for $\bar{p}$-production is to target protons outside the storage ring and to inject the produced antiprotons into the ring. In this case the number of antiprotons collected in the ring depends on the production cross section as well as on the longitudinal and transverse acceptances of the ring. In previous studies, such a procedure alone has resulted in rather small p intensities. To increase those, several methods have been suggested involving repeated injection made possible by transverse phase-space damping or, in other words, by overcoming the limitations imposed by Liouville's theorem. Budker[2] proposed to damp the transverse oscillations of the antiprotons by means of Coulomb collisions with a high quality beam of electrons traveling with the antiprotons. This is technologically complex and not very efficient for the ISABELLE parameters. Recently, van de Meer[3] put forward the idea of damping betatron oscillations by detecting and compensating statistical variations of the beam center. This so-called stochastic cooling is being investigated experimentally at the ISR, but its usefulness is limited by rf noise problems.

A somewhat different way of obtaining a high antiproton intensity is to use antiprotons originating in $\bar{\Lambda}$ decay and again avoid the constraints of Liouville's theory.[4] The antihyperons would be produced at a target in the vicinity of the storage ring and would produce antiprotons by decay in flight inside the aperture. However, in order to reach high intensities with this method, injection times of the order of days are required. Furthermore, very high radiation levels would result near the injection point.[5]

In the ISABELLE antiproton option none of the above-mentioned technically difficult methods are used. A relatively high intensity of circulating antiprotons (– 1 mA) is obtained in the following way: Protons (~ 10 A) are accelerated to 200 GeV in one of the rings by a second harmonic rf system and, while still bunched, extracted in a single turn into a bypass. The 30 GeV antiprotons from a target placed at a low-β point in this bypass are transported to the second ring, where they are injected and stacked in a bucket of a tenth harmonic rf system. This procedure is repeated until all ten buckets are filled, whereafter the antiprotons are accelerated to 200 GeV. Protons are now stacked in the first ring in the opposite direction accelerated to 200 GeV and made to collide with the antiprotons.

Antiproton Intensity

The antiproton yield, for a primary proton energy of 200 GeV, has recently been measured.[6] It has a plateau around 30 GeV with $d^2\sigma/d\Omega dp \approx 0.5$ $\bar{p}$ per interaction/sr (MeV/c). For small forward angles (<10 mrad), the number of 30 GeV antiprotons that can be stacked in the ISA ring is given by:

$$N_{\bar{p}} \cong \frac{d^2\sigma}{d\Omega dp} N_p \frac{C_{ISA}}{M_p \ell_B} \Delta\Omega \Delta p \eta_t \eta_s \quad . \qquad (1)$$

Here N_p is the number of protons in the ISA,

M_p is the number of proton bunches,

C_{ISA} is the ISA circumference,

ℓ_B is the proton bunch length at 200 GeV (antiproton bunch length at 30 GeV),

$\Delta\Omega$ (in steradians) is the solid angle at the target, inside of which antiprotons will be accepted by the ISA ring,

Δp (in GeV/c) is the momentum spread which will be accepted in the ring at 30 GeV,

η_t is the target efficiency including the effect of $\bar{p}$ interactions within the target, and

η_s is the stacking efficiency.

The solid angle $\Delta\Omega$ of the acceptable $\bar{p}$ beam is given by:

$$M = \pi a' b' \quad ,$$

* Work performed under the auspices of the U.S. Atomic Energy Commission.

where a' and b'are half angles of divergence. These are related to the horizontal and vertical betatron acceptances, A_h and A_v, of the machine by

$$a' = \frac{A_h}{\pi a} \quad \text{and} \quad b' = \frac{A_v}{\pi b} ,$$

a and b being the effective half sizes of the $\bar{p}$ source at the target. The effective source dimensions must include an allowance for the divergence of the $\bar{p}$ beam over the finite length, ℓ_t, of the target. It is advantageous, in principle, to make the physical width of the target (or the proton beam size) as small as possible to get close to the limits $a_{min} = \ell a'/2$ and $b_{min} = \ell b'/2$. However, practical considerations limit the effective source dimensions to $a \approx \sqrt{2} a_{min}$ and $b = \sqrt{2}\, b_{min}$ leading to

$$\Delta\Omega = \frac{\sqrt{2}\left(A_h A_v\right)^{+\frac{1}{2}}}{\ell_t}$$

Substituting in Eq. (1), one gets

$$N_{\bar{p}} \cong \frac{d^2\sigma}{d\Omega dp} N_p \frac{C_{ISA}}{M_p \ell_B} \frac{\sqrt{2}\left(A_h A_v\right)^{\frac{1}{2}}}{\ell_t} \Delta p \eta_s \eta_t \quad . \qquad (2)$$

Betatron and momentum acceptances are closely related to the available aperture, which should be as large as possible for maximum $N_{\bar{p}}$. For antiprotons the available aperture can be made larger than that assumed for protons, considering the low $\bar{p}$ intensity ($\sim$ 1 mA). Space-charge effects will be negligible in this case and one can let the beam fill the vacuum chamber horizontally, Furthermore, beam loading problems do not exist. One can use a low cost, rf accelerating system of higher frequency and voltage than what is used for the proton beam. This in turn will make it possible to stack the antiprotons azimuthally rather than in momentum space, gaining both in available aperture and stacking efficiency. At the same time, the voltage can be made high enough so that the rf system will be able to accommodate as large a momentum spread as the vacuum chamber will accept.

Protons in the ISA are accelerated on the second harmonic frequency, resulting in two circulating bunches. On flat top, during which the protons are extracted, 70% of the particles in one bunch lie within 1/10 of the circumference. The antiprotons, produced by the protons, will have the same bunch structure. One of the antiproton bunches will be injected, in the second ring, into a bucket of a 10th harmonic rf system with an efficiency of 70%. Ten ISA proton pulses (the second $\bar{p}$ bunch from each ISA pulse will be dumped) are required to fill the ten buckets with antiprotons.

The horizontal aperture of 8 cm is subdivided in the following way at *30* GeV, assuming a momentum spread of *2.5%* and a horizontal acceptance $A_h = 2\pi \times 10^{-6}$ m.rad (which is matched to the production cone):

Betatron amplitude:	1.9 cm
Phase oscillation amplitude $[X_p(\Delta p/p)]$:	*4.3* cm
Sagitta:	*1.3* cm
Reserve:	*0.5* cm
Total:	8.0 cm

A *4.4* cm long iridium target has an optimum target efficiency of $\eta_t = 1/3$. With these numbers and taking $A_v = A_h$ and $C_{ISA}/M_p \ell_B = 5$, one gets

$$\Delta\Omega = 2 \times 10^{-4} \text{ and } \frac{N_{\bar{p}}}{N_p} \cong 8 \times 10^{-5}$$

Extraction and Targeting of Primary Proton Beam

The 200 GeV proton beam will be extracted in the south experimental insertion (Figs, 1 and 2). The quadrupole magnets in this insertion will be rearranged to give slowly varying β-functions in the central part ($\beta_h \sim 12$ m, $\beta_v \sim 25$ m at the center) and to leave a free space of 100 m there. In the beginning of this 100 m drift space, a 1 mrad horizontal kicker magnet will be installed. The time between proton bunches is about *4* psec so that only very moderate demands are put on the kicker rise time. After a 10 m drift space following this kicker, the beam will be sufficiently displaced to enter the array of 3 septum magnets listed in Table I. They are followed by a *24* m drift space at the end of which the beam will enter a 60 mrad achromatic bend, followed by a triplet that will focus the beam at the target 5 m away. The target is located at a distance of $\sim$ *3.5* m from the ISA ring, which leaves adequate space for shielding,

The beam spot size at the target is only $\sim$ 0.25 x 0.25 mm^2 corresponding to β = 0.60 m. The target will most likely explode from the exposure to 6 x 10^{14} protons and will have to be replaced for each proton pulse,

Table I. Septum Magnets

Septum	Unit	1	2	*3*
Length	(m)	1	1.5	*1.5*
Deflection	(mrad)	1.8	*4.0*	*4.0*
Peak field	(kG)	*12*	18	18
Gap height	(cm)	*1.5*	*1.5*	1.5
Septum thickness	(mm)	*2.5*	*5*	5
Peak current	(kA)	15	22.5	22.5
Current density	(kA/cm^2)	40	30	*30*

Antiproton Beam Transport

Antiprotons emerging from the target will be focused by a strong, large aperture, room temperature triplet located 3 m downstream from the target. Thereafter, they will enter a 21 mrad bending magnet, which will separate them from the protons that were transmitted by the target. The protons will continue into a beam dump while the antiprotons will go into an achromatic bend from which they will emerge parallel to the ISA ring. Two quadrupole doublets will now match the antiproton beam into a transport channel that runs in parallel with the ISA ring and which simulates an ISA octant, with room temperature magnets.

Antiproton Injection and Acceleration

The antiprotons will be injected into the ISA by a fast kicker at the injection insertion ordinarily used for protons. (The rise time of this kicker has to be $\sim$ 150 nsec which is well within the present state of art.) They will be captured and matched into a bucket of a 10th harmonic (1.12 MHz) rf system. The peak voltage per turn required for matching is $\sim$ 150 kV, which is also suitable for 2 min acceleration to 200 GeV, using a synchronous phase of 5°. Because of the low antiproton intensity, the rf system can have high impedance resulting in low power demands.

$\bar{p}$-p Luminosity

The expected luminosity for p-$\bar{p}$ collisions has been calculated. It is limited by beam-beam interaction and it has been assumed that the maximum permissible tune shift for the antiprotons is $\Delta\nu = 0{,}005$. For a 1.7 mrad horizontal crossing geometry with $\beta_v = 2.5$ m and $\beta_h = 5$ m at the intersection point, assuming a 10 A proton beam with an emittance of $0.4\pi\ 10^{-6}$ m.rad at 30 GeV, one gets

$$L_{p\bar{p}} \simeq 8 \times 10^{28} cm^{-2} sec^{-1}$$

Acknowledgments

The authors are greatly indebted to Dr. G.K. Green for valuable discussions.

References

1. ISABELLE Design Study, in press.
2. G.I. Budker, Sov. J. Atomic Energy, 22, 438 (1967)
3. S. van der Meer, Report CERN/ISR-PO/72-31, (1972).
4. G.K. O'Neill, Princeton-Pennsylvania Accelerator Report PPAD 415D (1961).
5. K. Hübner, Report CERN/ISR-TH73/-19 (1973).
6. W.F. Baker, et al., NAL-Pub-74/13-EXP (submitted to Phys. Rev. Lett;) (1974).

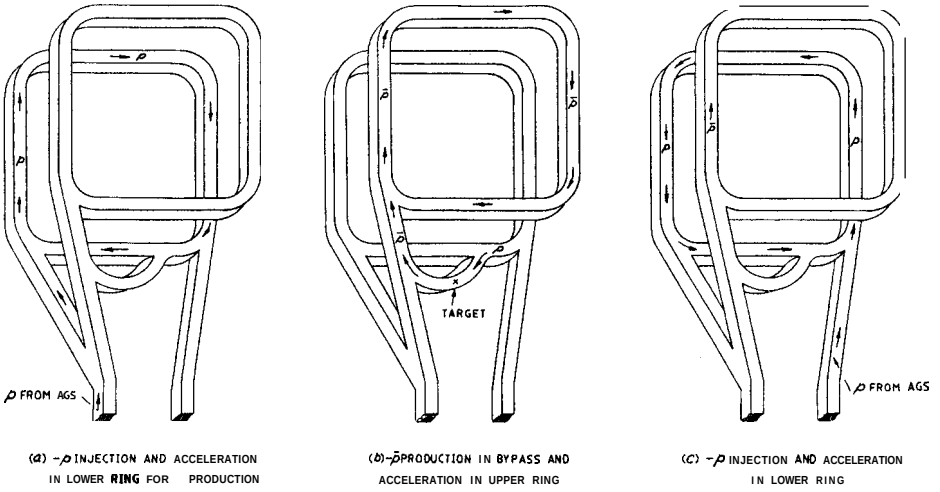

Fig. 1.

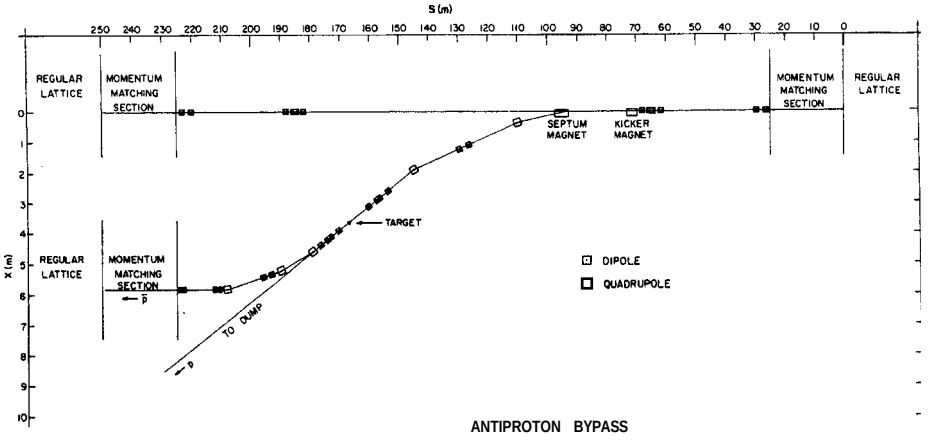

Fig. 2.

Andrei Kolomensky (Lebedev Institute): What is the main limitation for increasing the luminosity: Is it a tune process or something else?

Renate Chasman (BNL): It's the tune. The antiprotons will see a very dense proton beam and will experience the ordinary beam-beam interaction.

Kolomensky : So this figure 0.005 is the main limitation?

Chasman: Yes.

James Allaby (CERN): At what energy are the antiprotons injected?

Chasman: At 30 GeV, where the yield reaches a plateau so that the intensity is really proportional to the momentum bite.

Marshal King (Rutherford): The bypass presumably is superconducting. Have you thought about the effects of scattering downstream of the target, particularly in comparison with the dipole value?

Chasman: No, the entire bypass from the target downstream will be at room temperature.

SLED. A METHOD OF DOUBLING SLAC's ENERGY*

Z. D. Farkas, H. A. Hogg, G. A. Loew and P. B. Wilson

Stanford Linear Accelerator Center
Stanford University, Stanford, California 94305

Introduction

Over the past few years, several schemes for making significant increases in the energy of the SLAC beam have been proposed. Two of the proposals, namely the use of superconducting accelerating sections[1] and recirculation of the beam for a second pass through the existing accelerator,[2] have been abandoned for technical and economic reasons after extensive investigation. An on-going method of gradually raising the beam energy is the development and installation of 30- and 40-MW klystrons by the SLAC Klystron Group. It is clear, however, that the accelerator would have to be completely refitted with klystrons producing about 100 MW in order that the present machine energy be approximately doubled. While such an approach is not inconceivable,[3] the realization of such klystrons and the modulators needed to drive them would require further years of development and a high initial capital investment.

Since the accelerator energy is determined by the peak RF input power, and since many experiments are not now limited by average beam power, it was felt that some method for enhancing peak RF power at the expense of RF pulse width might be the answer for increasing SLAC's energy without at the same time increasing the average input power consumption. Standard pulse compression schemes were considered and rejected. One approach that seemed to hold promise, however, came as a result of our experience at SLAC with superconducting cavities. In the course of making measurements on superconducting cavities, it is a common observation that the power radiated from a cavity that is heavily overcoupled approaches four times the incident generator power immediately after the generator has been switched off. Normally this radiated power travels as a reverse wave back toward the generator. There are, however, several microwave networks which can direct this radiated power into an external load; for instance, two identical cavities attached to a 3-db coupler, as shown in Fig. 1. Using overcoupled cavities, we have in principle a

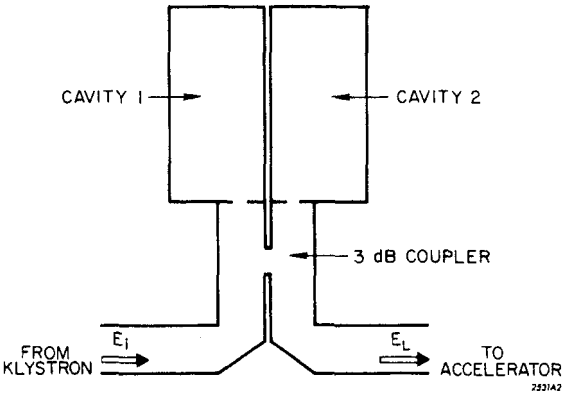

FIG. 1--Schematic drawing of the SLED microwave network.

power multiplier which can enhance peak power by up to a factor of four. This is accomplished, of course, at the expense of pulse width, since the radiated power decays away with a time constant given by the cavity filling time. A further development which enhances the viability of the SLED concept is the observation that if the RF source is reversed in phase rather than simply being switched off, the peak power can be increased by up to a factor of nine. How this comes about is described qualitatively in the following section.

Qualitative Description of SLED

In the case of the present SLAC accelerator, klystrons provide a 2.5 psec RF output pulse which travels, through a waveguide directly into the accelerating sections as indicated schematically at the top of Fig. 2. In the case of SLED, the

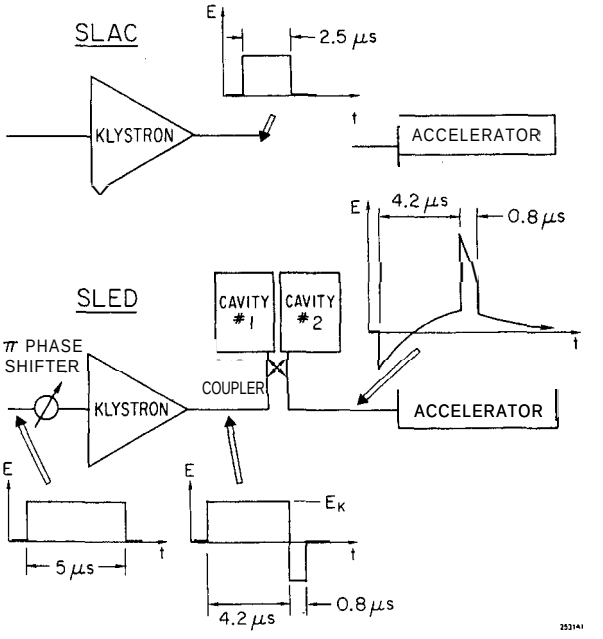

FIG. 2--A comparison of the present SLAC and SLED RF systems.

high-power waveguide system is broken near the klystron and the power divider/dual-cavity assembly shown schematically in Fig. 1 is inserted. The cavities are assumed to be identical and tuned to resonance. After the RF pulse is turned on, the fields in the cavities build up and a wave of increasing amplitude is radiated from the coupling apertures of each cavity. The two emitted waves combine so as to add at the accelerator port of the 3-db coupler, while they cancel at the klystron port. In addition to the wave emitted from the cavities, a wave travels directly from the klystron to the accelerator. This direct wave, which is just the wave that would appear at the accelerator if both cavities were detuned, is opposite in phase to the combined emitted waves. If the cavities are overcoupled, the emitted wave grows in time to an amplitude which is larger than the direct wave. The net field at the input to the accelerator, which is the sum of the direct and emitted waves, then goes through a phase reversal as shown at the right-center of Fig. 2. One accelerator filling time (0.8 psec) before the end of the RF pulse, the π phase shifter reverses the phase of the output wave from the klystron as shown by the waveform at the bottom of Fig. 2. Immediately after this phase reversal, the emitted and direct waves add in phase at the accelerator, since the emitted wave (which is proportional to the stored fields in the cavities) cannot change instantaneously. Therefore, when the klystron phase is reversed, the field at the input to the accelerator increases by two units (assigning one unit to the

*Work supported by the U. S. Atomic Energy Commission.

direct wave, E_K), since at any instant the load wave is the sum of the direct and emitted waves. Following the phase reversal, the fields in the cavities (and hence the emitted wave also) decrease rapidly as the cavities try to charge up to a new field level of opposite phase. The resultant wave at the accelerator decreases also, as is shown qualitatively in Fig. 2. At the end of the RF pulse, the direct wave goes to zero and the emitted wave only is present at the accelerator. It then decays to zero with a time constant given by the cavity filling time.

Theory

In order to understand the theory of SLED in detail, it is helpful to consider the transient behavior of the reflected and stored fields for a single resonant cavity. As discussed previously, the field which would normally be reflected back toward the generator in the case of a single resonant cavity is directed into the load by means of the microwave network shown in Fig. 2. In analyzing the behavior of a single cavity, it is convenient to consider the net reflected field as the superposition of a wave E_e emitted from the coupling aperture, and a reverse wave E_K which is equal in magnitude to the incident wave E_i from the generator (klystron), and which is reflected from the waveguide-cavity interface with a 180^o-phase reversal. If at any instant the generator is turned off, the field traveling away from the cavity is equal to E_e, which in turn is proportional to the stored field inside the cavity at that time. If, on the other hand, at any instant the cavity could be emptied of stored energy (by, for example, instantaneously detuning it) then the reverse wave traveling back toward the generator would be just E_K. By conservation of power,

$$P_K = P_L + P_c + dW_c/dt \quad ,$$

where P_K is the incident power, P_L is the net reflected power (the power delivered to the load in the case of the SLED network shown in Fig. 2), P_c is the power dissipated in the cavity and W_c is the energy stored in the cavity at time t. *Using* $P_c = \omega W_c/Q_0$, together with the fact that power is proportional to the square of the field, ($P = kE^2$), the above relation becomes

$$E_K^2 = (E_e + E_K)^2 + E_e^2/\beta + (2Q_0/\omega\beta)E_e dE_e/dt \quad .$$

A cavity coupling coefficient β has also been defined, such that $kE_e^2 = \beta P_c$. If at any instant the generator is turned off, β is given by the ratio of the power emitted from the coupling aperture to the power dissipated in the cavity walls. If we now introduce the cavity filling time $T_c = 2Q_L/\omega = 2Q_0/[\omega(1+\beta)]$, the preceding expression can be rearranged to give

$$T_c dE_e/dt + E_e = -\alpha E_K \quad , \qquad (1)$$

where $\alpha = 2\beta/(1+\beta)$.

Equation (1) can now be solved for the generator waveform E_K shown at the top of Fig. 3. For convenience, we take E_e to be initially positive, and since initially E_e and E_K must be opposite in phase, we take E_K to be -1. At time t_1 the phase of the generator wave is reversed, and $E_K = +1$. At time t_2 the incident power is turned off. By solving Eq. (1), the following expressions for the emitted field in the three time intervals A, B and C shown in Fig. 3 are obtained:

$$E_e(A) = -\alpha e^{-\tau} + \alpha \quad ; \qquad E_{e_1} = -\alpha e^{-\tau_1} + \alpha \quad ; \qquad (2a)$$

$$E_e(B) = \gamma e^{-(\tau-\tau_1)} - \alpha \quad ; \qquad E_{e_2} = \gamma e^{-(\tau_2-\tau_1)} - \alpha \quad ; \qquad (2b)$$

$$E_e(C) = E_{e_2} e^{-(\tau-\tau_2)} \qquad (2c)$$

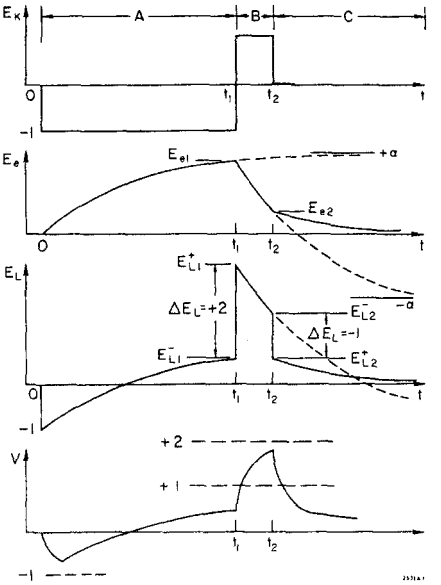

FIG. 3--Direct wave E_K, emitted wave E_e, and net load wave E_L for SLED.

where $\tau \equiv t/T_c$, $\gamma \equiv \alpha(2 - e^{-\tau_1})$ and E_{e_1} and E_{e_2} are the values of E_e at t_1 and t2. The variation in E_e as a function of time is shown in Fig. 3 for the case $\beta = 5$, $\tau_1 = 2$ and $\tau_2 = 2.4$. The load waveform, given by $E_L = E_K + E_e$, is also shown in Fig. 3. The load fields are:

$$E_L(A) = E_e(A) - 1 = -\alpha e^{-\tau} + (\alpha - 1) \qquad (3a)$$

$$E_L(B) = E_e(B) + 1 = \gamma e^{-(\tau-\tau_1)} - (\alpha - 1) \qquad (3b)$$

$$E_L(C) = E_e(C) = \left[\gamma e^{-(\tau_2-\tau_1)} - \alpha\right] e^{-(\tau-\tau_2)} \qquad (3c)$$

The field on a traveling-wave constant-gradient accelerating section is given by $E(z,t) = E[0, t - \Delta t(z)]$, where $\Delta t(z)$ is the length of time it takes for a wave to propagate from the input of the structure to position z on the structure. For a constant-gradient structure, in which the group velocity varies linearly with z according to $v_g(z) = v_{g0}(1 - gz/L)$, the propagation time to position z is given by

$$\Delta t(z) = \int_0^z \frac{dz}{v_g(z)} = \int_0^z \frac{dz}{v_{g0}(1 - gz/L)} \quad .$$

Defining $z' = z/L$, where L is the length of the accelerating structure, and integrating the above expression, we obtain

$$\Delta t(z') = T_a[\ln(1 - gz')/\ln(1 - g)] \qquad (4)$$

where $T_a = \Delta t(1) = (L/gv_{g0})\ln[1/(1-g)]$ is the filling time for the structure. The field $E(z,t)$ along the structure is now obtained by substituting $t - T_a[\ln(1 - gz')/\ln(1 - g)]$ for t in Eqs. (3). The result is:

$$E(A) = -\alpha e^{-\tau} f(z') + (\alpha - 1) \qquad (5a)$$

$$E(B) = \gamma e^{-(\tau-\tau_1)} f(z') - (\alpha - 1) \qquad (5b)$$

$$E(C) = \left[\gamma e^{-(\tau_2-\tau_1)} - \alpha\right] e^{-(\tau-\tau_2)} f(z') \qquad (5c)$$

where $f(z') = (1 - gz')^\nu$ and $\nu = (T_a/T_c)[\ln(1-g)]^{-1}$.

In using these relations, the fact must be taken into account that there are discontinuities in the field along the accelerating structure corresponding to discontinuities at

times $t_d = 0$, t_1 and t_2 in the field as a function of time at the input to the structure. In general, a field discontinuity will occur at a position z'_d along the structure for a discontinuity at time t_d in the waveform at $z=0$, where

$$z'_d = (1/g)\left[1 - (1-g)^{(t'-t'_d)}\right] \quad . \tag{6}$$

This expression is obtained by solving Eq. (4) for z', defining also a normalized time by $t' = t/T_a$, and setting $\Delta t = t - t_d$. For example, in the time interval $0 < t < t_1$, the field is zero for $z' > z'_d$, where z'_d is obtained using $t'_d = 0$ in Eq. (6). For $z' < z'_d$, the field is given by Eq. (5a).

The accelerating voltage is now obtained by integrating the field from $z' = 0$ to $z' = 1$, taking into account the location of the field discontinuities and using the appropriate fields given by Eqs. (5) up to and following each discontinuity. Thus the energy gain V for the interval $t_1 < t < t_2$ is given by

$$V = \int_0^{z'_{d_1}} E(B)\, dz' + \int_{z'_{d_1}}^{1} E(A)\, dz' \quad ,$$

where z'_{d_1} is given by Eq. *(6)* with $t'_d = t'_1$. The energy gain is by definition unity after one filling time for a direct wave $E_K = 1$, which would be present with the cavities detuned. Since $f(z')$ is common to all of the energy gain integrals, the calculation is simplified by defining

$$F_1(z'_d) = \int_0^{z'_d} f(z')\, dz' = \left[1 - (1-gz'_d)^{1+\nu}\right]\left[g(1+\nu)\right]^{-1} \quad ;$$

$$F_2(z'_d) = \int_{z'_d}^{1} f(z')\, dz' = \left[(1-gz'_d)^{1+\nu} - (1-g)^{1+\nu}\right]\left[g(1+\nu)\right]^{-1}$$

Thus, during $t_1 < t < t_2$,

$$V = \gamma e^{-(\tau-\tau_1)} F_1(z'_d) - (\alpha-1) z'_{d_1}$$

$$- \alpha e^{-\tau} F_2(z'_d) + (\alpha-1)(1-z'_{d_1})$$

Similar expressions can be derived for time intervals A and C. A plot of the normalized energy gain as a function of time is given at the bottom of Fig. 3. The maximum energy is obtained after one filling time, by letting $t = t_1 + T_a$ (or $t' = t'_1 + 1$) and $z'_{d_1} = 1$. For this special case,

$$V_{max} \equiv M = \gamma\, e^{-T_a/T_c}\left[1 - (1-g)^{1+\nu}\right]\left[g(1+\nu)\right]^{-1} - (\alpha-1) \quad . \tag{7}$$

Further details of the SLED theory are given by Farkas[4] and Wilson.[5] The effect of cascading several of the microwave networks shown in Fig. 1 was calculated[4] in the hope of obtaining flatter output pulses and perhaps still higher values for the energy multiplication factor. Somewhat flatter output pulses were predicted, but not higher multiplication factors in the examples investigated. The possibility cannot be ruled out, however, that other more favorable configurations might be found.

Choice of Parameters

An analysis of Eq. (7) shows that the maximum energy gain M approaches 3 if $\beta \gg 1$, $T_c \gg T_a$ and $t_1 \gg T_c$. Since $T_c(1+\beta) = 2Q_0/\omega$, it is impossible to have both a large filling time and a large coupling coefficient unless the unloaded Q of the cavities can be made arbitrarily large. However, the unloaded Q of a practical room-temperature resonator is limited to about 10^5. The RF pulse length is also limited by practical considerations. The present pulse length, t_2 of SLAC is 2.5 psec. It is reasonable to consider doubling %is pulse length to 5.0 psec. Figure 4 shows the

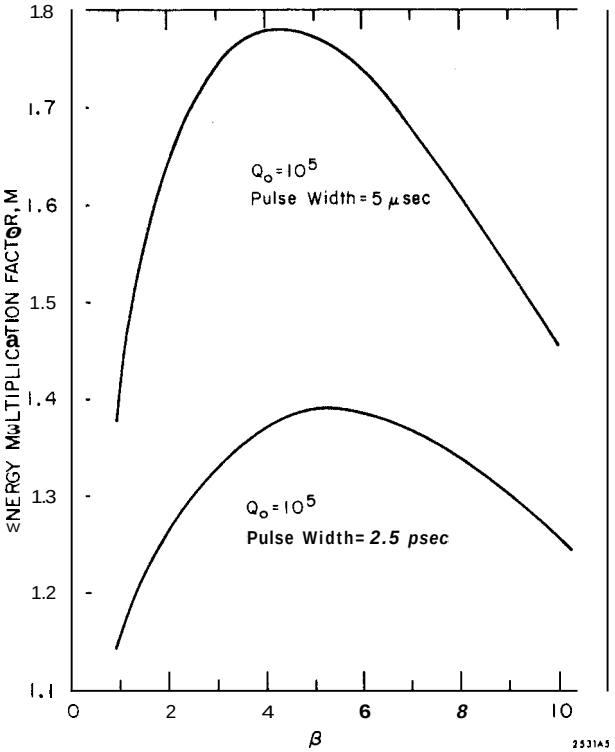

FIG. 4--Energy multiplication factor as a function of cavity coupling coefficient.

energy multiplication factor as a function of the cavity coupling coefficient for these two pulse lengths with $Q_0 = 10^5$. It is seen that the energy gain is maximum for a coupling coefficient in the range $\beta = 4$ to 5. Figure 5 shows the energy multiplication factor M as a function of unloaded Q for various values of RF pulse length, and Fig. *6* gives M as a function of pulse length for various values of Q_0. The coupling coefficient has been optimized at each point on the curves in both figures to give the maximum energy gain. It is seen that the longer the pulse length and the higher the unloaded Q, the greater is the energy gain.

As a result of a number of practical and economic considerations, the parameters proposed for SLED are $Q_0 = 10^5$, $t_2 = 5.0$ psec and $\beta \approx 4.5$. The energy multiplication factor for these values is 1.78. Figure 7 shows the RF power output from the SLED microwave network as a function of time for these parameters. The "pulse compression" effect of the SLED network is clearly seen.

Beam Loading

Figure 8 shows the unloaded relative energy gain as a function of time in the region of peak energy for the SLED parameters as chosen in the previous section. It is clear that the pulse length of a beam accelerated near peak energy will necessarily be short compared to the structure filling time. The unloaded energy is seen to be increasing as a function of time as peak energy is approached. By turning on the beam prior to reaching peak energy, the transient energy droop due to beam loading can be used to produce a rough compensation for the rising unloaded energy gain, resulting in a considerably tighter energy spectrum. For SLAC, the transient beam

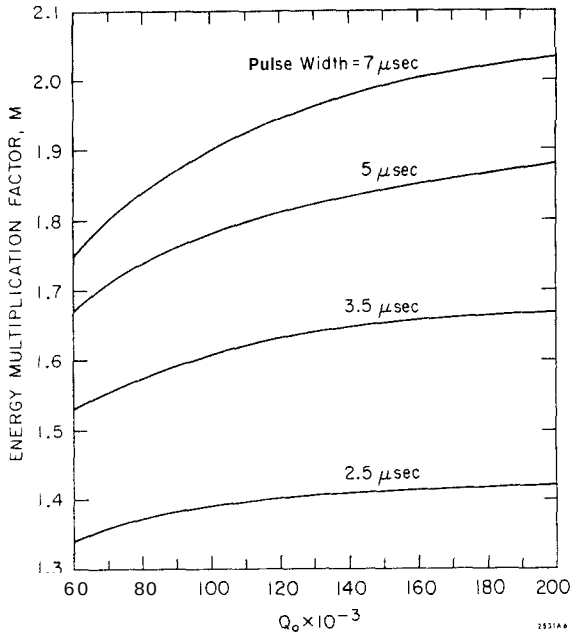

FIG. 5--Energy multiplication factor as a function of unloaded Q.

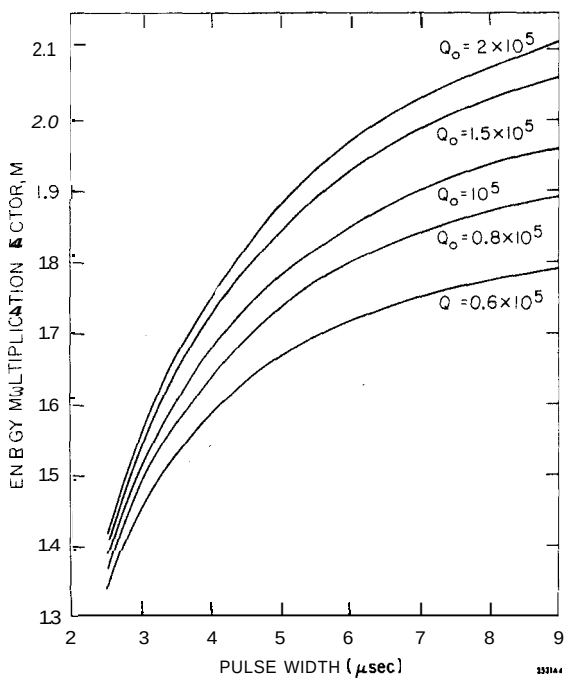

FIG. 6--Energy multiplication factor as a function of pulse width.

loading voltage is given, to the accuracy required here, by

$$V_b(MV) = 35iP\left[2\Delta t/T_a - (\Delta t/T_a)^2\right] ,$$

where i_p is in milliamperes and Δt is the time after the beam has been switched on. Figure 8 also shows the transient variation in the relative beam loading as a function of time for a maximum unloaded energy of 46 GeV and a peak current of 200 mA, assuming that the beam is switched on 0.35 psec before the peak energy is reached. The curve of the resultant beam energy shows that beam loading compensation has reduced the variation in energy gain over this time interval from 10% to about 24%. Table I gives the

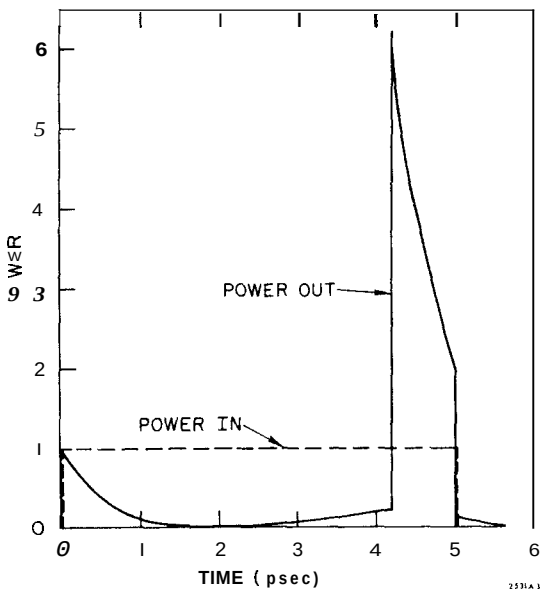

FIG. 7--Input power to and output power from the SLED microwave network as a function of time.

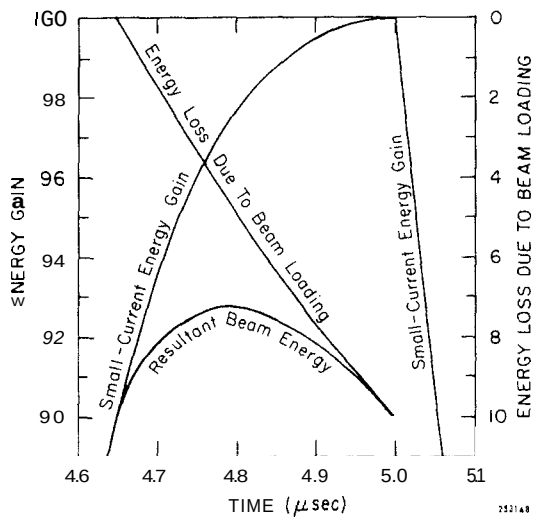

FIG. 8--Unloaded energy gain, energy droop due to beam loading and resultant beam energy for a beam pulse length of 0.35 μsec.

loaded energy V, the peak current i_p, the average current i_{ave} and the energy spectrum width $\Delta V/V$ for various values of the beam pulse length T_b. For each value of T_b, the peak current has been chosen so that the beam energy is the same at the beginning and end of the pulse. The maximum unloaded energy is taken as 46 GeV, which would be obtained from the SLAC linac for an energy multiplication factor of 1.78 and a klystron power of 30 MW. A repetition rate of 180 pps has been assumed in computing the average current.

By shaping the current pulse as a function of time, the energy spectrum widths can in principle be reduced considerably below the values given in Table I for a constant pulse current. Likewise, by advancing the triggers to a fraction of the klystrons along the machine, the peak current for a given beam pulse length can be reduced below the values shown in Table I while still maintaining a tight energy spectrum. The peak pulse current for SLED will in practice be limited by beam breakup. For the present SLAC focusing

Table I

SLED Beam Loading Characteristics (30 MW klystrons)

T_b (μsec)	V (GeV)	i_p (mA)	i_{ave} (μA)	$\Delta V/V$ (%)
0	46.0	0	0	0
0.10	45.8	31	0.6	0.15
0.15	45.4	54	1.5	0.4
0.20	44.8	80	2.9	0.7
0.25	44.0	110	4.9	1.1
0.30	43.0	143	7.7	1.7
0.35	41.8	181	11.4	2.4
0.40	40.3	224	16.2	3.3

configuration and beam energy, beam breakup limits the peak current to 160 mA for a beam pulse length of 0.3 psec. At a final energy of 40 GeV, a pulse current on the order of 250 mA could be accelerated at this pulse length, assuming a reasonable increase in the strength of the focusing along the accelerator.

In Table 11, the parameters for the present SLAC accelerator and for SLED are summarized for a beam-loaded

Table II

Comparison of SLED and Present SLAC Parameters

		Present SLAC (30 MW klystrons)	SLED (30 MW klystrons)	SLED (40 MW klystrons)
Unloaded Energy	(GeV)	26	46	53
Loaded Energy	(GeV)	23.5	41.5	48
Repetition Rate	(pps)	360	180	180
RF Pulse Length	(μsec)	2.6	5.0	5.0
Beam Pulse Length	(μsec)	1.6	0.36	0.36
Average Current	(μA)	40	12.5	14.5
Peak Current	(mA)	10	190	220
Electrons per Pulse		7×10^{11}	4.5×10^{11}	5×10^{11}
Duty Cycle		6×10^{-4}	6.5×10^{-5}	6.5×10^{-5}
Energy Spread	(%)	~1.0	< 1.0*	< 1.0*
Average Beam Power	(kW)	950	520	700

*Assumes current pulse shaping (e g , 230 mA for the first half of the pulse, then 160 mA for the second half for the case of 30 MW klystrons) For constant peak current, estimated energy spread is 2 5%.

energy 10% below the unloaded energy. Parameters for SLED are given for both 30 and 40 MW klystrons; at the time SLED becomes operational, the average peak klystron power per station is expected to lie between these limits.

SLED Cavity Design

As noted in the previous sections, cavities with Q_0 on the order of 10^5 are needed to obtain a power multiplication factor high enough to be of interest. This Q_0 can be obobtained in copper cavities operating at or somewhat above room temperature if a higher-order resonant mode is employed. Considerations of cost, mechanical stability and frequency separation of competing modes make it desirable to choose the mode with the smallest cavity volume for a specified Q_0. Modes which are members of the TE_{01n} family have this desirable characteristic. The value n=5 was chosen as optimum for our purposes. The ratio of diameter D to length L for the cavity remained to be determined. A value of D/L less than unity (which gives maximum Q_0) was chosen on the basis of material availability. A smaller diameter also reduces the deformation of the end-plates due to atmospheric pressure loading. The exact ratio (D/L = 0.611) was selected to maximize frequency separation from competing modes. The TM_{115} mode, which is normally degenerate with the TE_{015} mode, was lowered approximately 24 MHz by cutting a circular groove at the outer diameter in one end-plate. This groove does not disturb the TE_{015} mode field pattern or frequency. In summary, the selected parameters for the SLED prototype cavity are:

Diameter = 20.51 cm
Length = 33.59 cm
*Q_0 = 1.08×10^5

*Theoretical Q for copper at f_0 = 2856 MHz

The rate of change of frequency with temperature is -48 kHz/°C for copper construction.

Preliminary analysis has indicated that a cavity tuning error of 10 degrees is acceptable. Assuming $Q_0 = 10^5$ and $\beta = 5$, the loaded Q is $Q_L = 1.6\times10^4$. Thus the cavity half-bandwidth, $\frac{1}{2}$BW, is approximately 90 kHz . If Af is the difference between the driving frequency and the cavity resonant frequency, the cavity tuning angle is given by $\psi = \tan^{-1}[\Delta f/(\frac{1}{2}BW)]$. Thus, if ψ is to be limited to ±10 degrees, Af must not be greater than 16 kHz. From the tuning rate with temperature given above, this implies that the cavity temperature must be held constant to within 1/3°C. The existing accelerator cooling water system holds temperature fluctuations to better than ±0.15°C, which would appear to be adequate. However, the RF power dissipated inside each cavity, which is calculated to be about 2 kW average for a 30 MW klystron source, will raise the metal temperature on the order of 1.4°C. This temperature change will shift the resonant frequency by 67 kHz and introduce a tuning error of 37 degrees. Although the cavities may be pre-tuned to 2856 MHz at the equilibrium temperature with the RF power on, there will still be a phase- and amplitude-drift period during warm-up following each RF shutdown. The severity of this problem will be gauged during prototype tests. The concept of a mechanically temperature-compensated cavity has been suggested and will be tried if necessary.

A cross-sectional drawing of the prototype assembly is shown in Fig. 9. The cavity cylinders are made from copper forgings, machined to 9.5 mm wall thickness. The inner surface finish is better than 0.15 microns (RMS). Water-cooling tubes are brazed on in pairs covering the five zones of maximum heat dissipation along each cylinder. The cavities are fine-tuned by distorting the thin-wall endplate using a differential screw. The tuning range is approximately ±1 MHz. Coupling between the cavity and waveguide magnetic fields is achieved through circular apertures in the end-plates. A 2.77 cm diameter aperture in a 4.06 mm thick wall gives the desired β value for $Q_0 = 10^5$.

It is anticipated that there will be frequent need to run the accelerator in the present non-SLED mode; that is, with the flat-topped RF pulse from the klystron transmitted without distortion to the accelerator. This can be done by detuning the SLED cavities, which then appear as short-circuits across two ports of the 3-db hybrid coupler. Under these conditions, the klystron pulse is transmitted through the SLED network without significant reflection or loss. The design requirements placed upon the detuner are quite severe. Primarily, when it is moved from the "detuned" to the "tuned" position, it must return the cavity to the same resonant frequency to within a few kilohertz. Also, in the "tuned" position, it must not degrade the cavity Q_0 nor introduce any frequency modulation due to mechanical vibration. A prototype detuner has been designed which consists

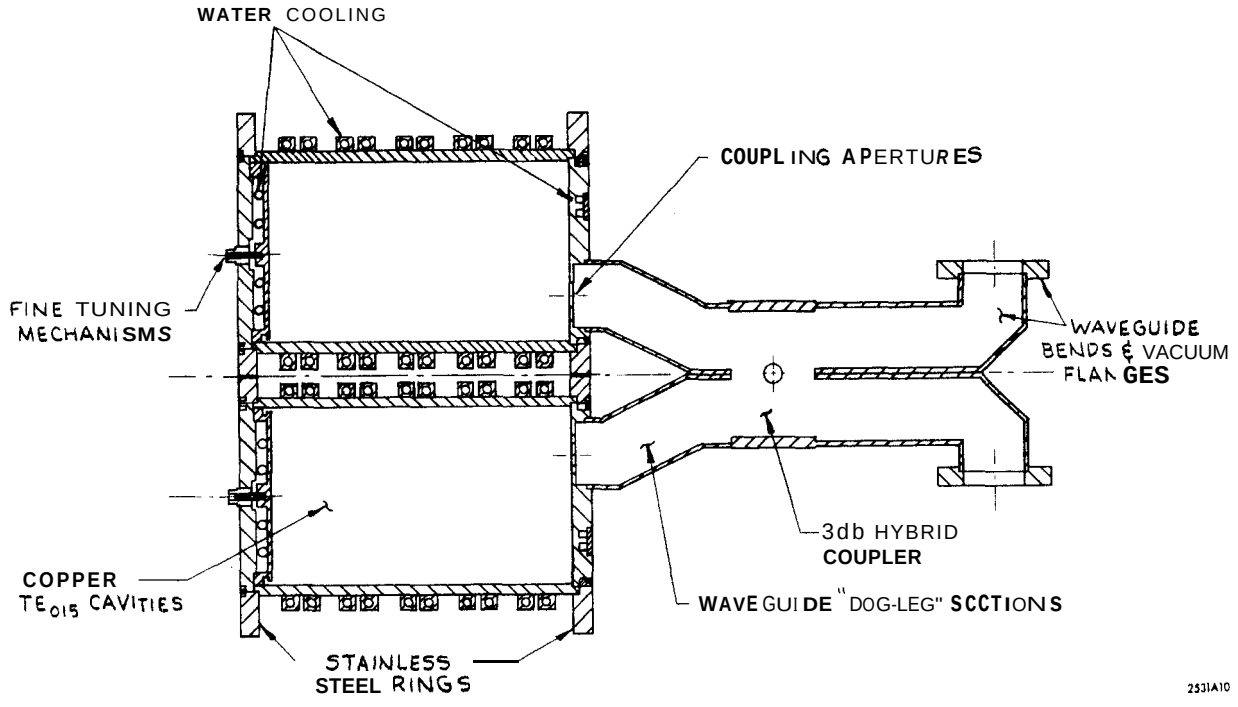

FIG. 9--Assembly drawing of the prototype microwave network for SLED.

of a stainless steel needle 1.52 mm in diameter inserted into the TE_{015} cavity through a 2.03 mm hole in the cavity wall. This hole enters the cavity on a current node and thus causes negligible perturbations of f_0 and Q_0. The needle enters at an angle such that when fully inserted, its tip reaches a circle of maximum azimuthal E field. In this way a detuning of 18 MHz, or approximately 100 bandwidths, is achieved. In its fully retracted position, the needle is decoupled by at least 90 db from the cavity fields and has no residual effect upon f_0 and Q_0.

The SLED prototype assembly described above has performed very well in low-power tests at room temperature. The "detuned" and "tuned" output waveforms follow very closely the "Power In" and "Power Out" curves, respectively, shown in Fig. 7. High-power tests into a matched load are presently in progress. In September of this year, the prototype cavity-hybrid unit will be installed as shown in Fig. 10 on a klystron station near the accelerator injector to allow tests to be made with a beam.

If SLED is to be a viable means for increasing the energy of the SLAC linac, it must be shown that the klystrons can operate satisfactorily at the 5.0 psec RF pulse length and 180 pps repetition rate required. Initial tests at the longer pulse length indicate that the klystron fault rate is somewhat higher than is the case at the present 2.5 psec pulse length, but there is no evidence that the klystrons will not operate satisfactorily under the SLED conditions.

SLED Modes of Operation and Physics Possibilities

Boosting the energy of the present SLAC accelerator into the 40- to 50-GeV range by means of SLED makes available a number of new operating modes for the machine and a corresponding variety of possibilities for the high energy physics program. The full exploitation of the SLED idea requires that all 245 high-power klystron stations be equipped with microwave cavity networks; new pulse-forming networks and pulse transformers must be added to the modulators as well. The combination of these two features gives

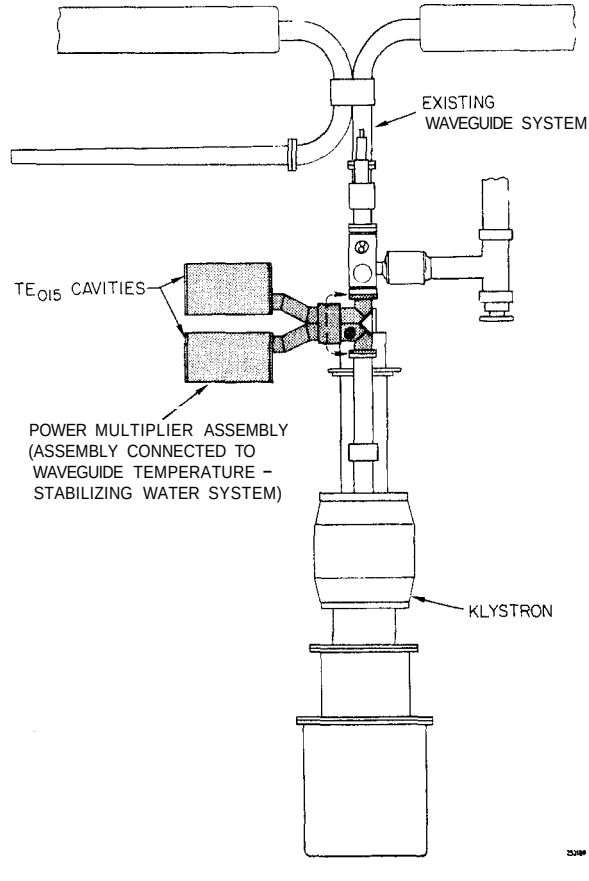

FIG. 10--Proposed installation of the SLED microwave network at a typical station in the Klystron Gallery.

a 5 psec RF pulse at the output of each klystron and boosts its effective peak power from 30 to 100 *MW*. This enhancement in peak power is achieved at the cost of reducing the repetition rate from 360 pps to 180 pps and the beam duty cycle by a factor of 10. The present plan is to make these modifications reversible. The cavity detuners which have been described above can be inserted in a fraction of a second. This results in a possible machine operating mode at the present energy (−23 GeV) but with a beam pulse length of 4.2 psec, giving an improvement in duty cycle over present operation (at 360 pps) of over 30%. This mode of operation cannot be interlaced on a pulse-to-pulse basis with the SLED high-energy mode, but is obtainable after a short switch-over time. It will be used for phasing the machine, possibly for injection of 1.5 GeV electrons and positrons into SPEAR, and for −20 GeV beams for experiments such as LASS (Large Aperture Solenoidal Spectrometer). An alternate method of obtaining low-energy beams might be to inject electrons on an early part of the energy gain waveform. Early injection will be made possible by not installing SLED cavities on the injector klystrons, thereby having a flat 5 psec RF pulse available for capture. When the present mode of operation at 360 pps needs to be restored, this will be done by halving the lengths of the new pulse-forming networks in the modulators. The switch-over might be done by remote control. Even if done manually, the operation should not take more than an hour or so for the entire machine. It is important to point out that none of these modes of operation require an increase in average power for the accelerator above the −25 *MW* that is presently used.

A full discussion of the physics possibilities opened by SLED is beyond the scope of this report. Only a few general remarks will be made here. It appears that End Station A would continue to be the main experimental center for electron scattering and photoproduction physics. In order to bend the 40- to 50-GeV beams into the A-line, three out of the five 0.1° pulsed magnets at the apex of the beam switchyard (BSY) would be replaced by stronger magnets and power supplies. The eight 3° bending magnets which make up the 24° A-bend would also be replaced by stronger magnets. The A-beam dump magnets used for photon experiments would be upgraded. What modifications would be made in the spectrometers is not yet clear.

The main "ecological" change in the research yard would take place in the mix of experiments between End Stations B (ESB) and C (ESC), For higher-energy RF-separated $K^{\pm}$ and antiproton beams, there is insufficient drift distance behind ESB in the Research Yard. For this reason, it has been proposed that the RF separators be moved to the present C-beam, which would be rebuilt with the target moved up by about 100 m. This change might eventually cause LASS and/or the bubble chamber to be moved to the C-beam. The K^{o}-decay experiments in ESB may not require higher energies than at present (and therefore no modifications), but production experiments with K^{o}'s may be exploitable. It is also possible that higher-energy primary e^{-} or photon beams may be of interest to LASS in its present location (or in ESC). In any case, upgrading the 12° B-line would be fairly inexpensive because one would simply add some of the 3° magnets available from the A-line. ESC, on the other hand, would be more drastically modified, but at relatively low cost since no large-angle bends would be involved. The proposed plan would be to create three independent channels by means of a magnetic slit located downstream of the present tune-up dump. The pulsed magnets at the apex of the BSY would aim the electron beam from the accelerator into any one of these three channels. The central beam would be charged (separated beams mentioned above), and the other two would be neutral. One of these neutral beams might consist of photons derived from the collision of electrons with a beam of photons from a laser or from coherent bremsstrahlung; it would be used by the streamer chamber. The other might be a K^{o} beam.

The present cost estimates for SLED (at FY 1974 rates, excluding project indirects, design and engineering, and contingency) break down roughly as follows:

Microwave System	$\sim$1 M
Modulator Modifications	~1.9 M
Instrumentation and Control	−0.5 M
Beam Switchyard Modifications	−1.6 M
Total	$ 5.0 M

Acknowledgements

The authors acknowledge the work that has been carried out by the SLAC Klystron Group, under J. Lebacqz, to test and evaluate the performance of the SLAC klystrons at the longer pulse length required by SLED. C. Olson and the Accelerator Electronics Group have made design and engineering studies of the modifications required to increase the pulse length of the SLAC modulators, and have carried out those modifications on an initial unit for long pulse klystron tests. A. Lisin and R. Sandkuhle have been responsible for the mechanical design of the SLED prototype assembly. Fabrication and scheduling were directed by H. Zaiss. K. Mallory has studied the instrumentation and control problems associated with SLED, and D. Walz has investigated the changes required to upgrade the beam switchyard. J. Murray and L. Keller with many others have studied the high energy physics possibilities opened up by SLED. H. Deruyter has been responsible for all microwave measurements involved in the development and testing of the cavity-hybrid microwave network.

References

1. P. B. Wilson et al., Particle Accelerators 1, 223 (1970).
2. W. B. Herrmannsfeldt et al., Proc of the 8th Int. Conf. on High Energy Accelerators (CERN-Scientific Information Service, Geneva, 1971), p. 563.
3. G. A. Loew, "Electrons, the Energy Crisis and the Possibilities of RF power," SLAC RLA Note 52, Stanford Linear Accelerator Center, Stanford University, Stanford, California (June 1973), unpublished.
4. Z. D. Farkas, "Power Multiplier," Technical Note SLAC-TN-73-8, Stanford Linear Accelerator Center, Stanford University, Stanford, California (September 1973), unpublished.
5. P. B. Wilson, "SLED: A Method for Doubling SLAC's Energy," Technical Note SLAC-TN-73-15, Stanford Linear Accelerator Center, Stanford University, Stanford, California (December 1973), unpublished.

DISCUSSION

Herbert Lengeler (CERN): How are you going to realize a cavity at room temperature with a Q value of 10^5?

Farkas: We use a TE_{115} cavity which just happens to have a Q of 10^5. It's not very big, 8 inches in diameter and 13 inches high.

Helmut Herminghaus (Mainz): Couldn't you have rather severe mismatch during some part of the pulse and if so, how are the klystrons protected?

Farkas: Yes, that is something we worry about. As I mentioned in the talk, the reasons for the 3DB hybrid is to take all the energy reflected from the cavities and channel it into the accelerator section. Another possibility of

separating incident from reflected power at any place would be to use circulators which obviously is not practical at these very high power levels. There is yet another possibility, using resonant rings, which poses other problems.

Andrei Kolomensky (Lebedev Institute): You have three times less average current and you inject less current?

Farkas: Right, we inject over a shorter time.

Kolomensky: Why don't you use some current to excite the cavities? Put the total current at 40 mA and use some of it for excitation.

Farkas: I don't know whether we can use that current. However, it might not be entirely useless. As a matter of fact, there is acceleration at other times than during the 0.2 to 0.3 μs interval of peak acceleration and you might use current at those times for some other purpose.

Raphael Littauer (Cornell): What is the estimated cost of the SLED project?

Farkas: Five million dollars, about two for the cavities and network, another *two* for modifying the modulators, and about one million for instrumentation and control, including the switchyard.

A PRELIMINARY DESIGN OF TRI-RING INTERSECTING STORAGE ACCELERATORS IN NIPPON, TRISTAN

Tetsuji Nishikawa
National Laboratory for High Energy Physics
Oho-machi, Tsukuba-gun
Ibaraki-ken, Japan

Introduction

When the present KEK proton synchrotron project was originally proposed, it was expected to bring up the Japanese high-energy physics program to the present frontier of the world high energy physics. However, a shortcut of the budget forced the project to start with a lower energy accelerator and extend it to a higher energy range. Thus the future extension of the presently constructing 12 GeV proton synchrotron is taken into consideration even at the initiation of the present project?) Several possible extension schemes such as a large conventional synchrotron in the energy region of 80 ~ 100 GeV have been considered as a long range plan of the KEK project. At present, however, the future plan of the KEK synchrotron is concentrated on *a* plan of tri-ring intersecting storage accelerators for various types *of* colliding beam experiments as $e^{\pm}p$, pp, $e^{+}e^{-}$ and $\bar{p}p$ at very high center of mass energies. This project is nicknamed as TRISTAN (Tri-Ring Intersecting Storage Accelerators in Nippon) and a preliminary design study is undertaken in the KEK Accelerator Department in cooperation with the university scientists and the cryogenic specialists. This is a report on the present status of the preliminary design study of the TRISTAN.[2)]

Outline of TRISTAN

The site of KEK is a land area of approximately 220 hectares in Tsukuba District, Japan. The present 12 GeV proton synchrotron project is in progress at the middle of the site, so that there remains a space enough to build a larger ring with more than 2 Km in its circumference. Thus, as ISABELLE:) PEP,[4)] and EPIC[5)] projects, with a superconducting magnet system we will be able to construct a proton storage ring of 150 ~ 200 GeV inside the site boundary.

The presently constructing synchrotron will be used as the injector of the storage accelerator. Since, however, to raise up the proton energy from 12 GeV to a 100 GeV range a large superconductor magnetization is required, the application of superconducting magnets to the storage accelerator would suffer from technical difficulties unless a new superconducting technique could be developed. Therefore, we are planning to install another conventional ring in the same enclosure as a booster between the present synchrotron and the superconducting rings. It accelerates protons to about 50 GeV and its guiding field is inverted in order to provide the protons for another intersecting ring so as to run in opposite direction. The conventional ring will also be used as an electron or a positron storage ring after it acted *as* a proton booster between the present main ring and the superconducting rings. Furthermore, as a future option, this ring may be used to produce antiproton beams which will be accelerated and stored in one of the superconducting rings. So we will be able to carry out various types of colliding beam experiments as pp, $e^{\pm}p$, $e^{+}e^{-}$, $p\bar{p}$ and $e^{\pm}\bar{p}$ by choosing different sets of three rings. The particles accelerated in a ring which is free of colliding beam experiments can be extracted toward an experimental hall and used for stationary target experiments.

A preliminary outline plan of the TRISTAN is shown in Fig.1. Two diamond-shape rings (solid lines) are superconducting proton rings intersecting each other at four interaction points in a horizontal plane. The conventional ring (broken line) will be installed above or below the two superconducting rings and intersect them vertically at the beam-transfer or interacting points. Several experimental halls for stationary target experiments are also shown.

Table I. PRELIMINARY PARAMETERS OF TRISTAN pp RINGS

Injection Energy	12-50 GeV
Maximum Final Energy(Each Ring)	*180* GeV
Number of Intersecting Points	*4*
Average Radius(Curved Section)	204 m
Long Straight Section Length	150 m
Short Straight Section Length	30 m
Total Circumference(6×12 GeV Ring)	2035 m
Maximum Magnetic Field	50 kG
Total Stored Energy	-70 MJ
Acceleration Time	-100 sec
Number of Betatron Oscillations	22.25
Cell Structure Separated Function	FODO
Number of Cells(Each Ring)	80
Cell-Length	-16.4 m
Full Vacuum Chamber Aperture	6 cm
Crossing Angle	40 mrad
Total Charge(Each Ring)	6×10^{14}
Circulating Current(Each Ring)	15 A
Luminosity(180 GeV)	7.5×10^{31} $cm^{-2}sec^{-1}$
Maximum Luminosity for Collinear Crossing	10^{34} $cm^{-2}sec^{-1}$

TRISTAN pp System

A set of preliminary parameters of TRISTAN pp rings is given in Table I. The average radius of TRISTAN rings is taken as six-times of the present main ring or approximately 324 m.

First, six pulses from the present main ring are injected into the TRISTAN conventional ring to fill up its total circumference leading to 6×10^{13} particles per turn. Then the protons are accelerated upto about 50 GeV and transfered into one of the superconducting rings. From the expected beam characteristics of the present synchrotron, the emittances of the 50 GeV beam would be 0.4 and 2.8 πmm·mrad in vertical and horizontal directions, respectively. Using a set of skew quadrupoles in the beam transport line, we interchange horizontal and vertical phase space of the 50 GeV beam before injection. By means of transverse stacking method we can accommodate some ten pulses of the 50 GeV beam in a useful half-aperture of about 3 cm. Thus 6×10^{14} protons or a 15 A proton beam will be stacked and accelerated in each superconducting ring. The filling time needed for the whole stacking process is about 100 seconds for each, and acceleration takes place in the following -100 seconds. The vertical and horizontal emittances at 180 GeV are estimated to be $\varepsilon_V \approx 0.8$ πmm·mrad and $\varepsilon_H \approx 0.35$ πmm·mrad.

In Fig.2 and Fig.3 we show the proposed lattice for TRISTAN superconducting rings with the cell structure of a separated function FODO system. Taking the length of each long straight section as 150 m, we get the average radius of curved section as *204* m. The total cell number of 80 is chosen with betatron oscillation frequen-

cy in neighborhood of 20 and the phase advance of each cell of about 90°. A quadrant of each ring consists of 19 normal cells and one half bending-magnet cell (HBM cell). As is shown in Fig.2, the HBM cell of either ring is located in the down- (or up-) stream in a quadrant of two intersecting rings. Thus the superperiod of each ring is 2 forming a diamond-shape lattice in which each diamond crosses another diamond at a crossing angle of 2°14'. However, the crossing angle can be taken at any degrees by using an appropriate set of deflecting magnets in the position of the missing magnets of the HBM cells or in the long straight sections. In these lattice configurations, we can obtain proton energies of 150 GeV at the bending field of 40 kG and 180 GeV at 50 kG.

The luminosity for a horizontal crossing of the unbunched beams is given by

$$L_{pp} \approx \frac{fN_p^2}{b_p \theta C} ,$$

where N_p is the total number of protons stored in each ring, $2b_p$ the full vertical beam height, θ the crossing angle, C the circumference and f the revolution frequency. Letting $N_p = 6 \times 10^{14}$, $b_p = \sqrt{\varepsilon_v \cdot \beta_v} = 0.9$ mm ($\beta_v = 1$m), $\theta = 2°14'$ and C = 2035 m, we obtain

$$L_{pp} = 7.5 \times 10^{31} cm^{-2} sec^{-1} .$$

If we use a quasi-collinear crossing of the bunched beams, then the luminosity will be improved leading to the maximum luminosity corresponding to the maximum allowable tune shift of Avo,

$$L_{pp\ max} = \frac{\beta_p \gamma_p}{2 r_p} \Delta\nu_0 \doteq 10^{34} \quad cm^{-2} sec^{-1} , \quad (1)$$

where we take the 8-function as $\beta_p (\beta_v = \beta_H) = 1$m, $\gamma_p = 190$ (180 GeV), the classical proton radius $r_p = 1.5 \times 10^{-18}$ m and $\Delta\nu_0 = 0.02$. In this expression, the proton bunch length ℓ_p is assumed to be $\ell_p << 2\beta_p$.

Table II

PRELIMINARY PARAMETERS OF TRISTAN ep RINGS

Maximum Electron Energy	17 GeV
Maximum Proton Energy	180 GeV
Length of Interaction Region	150 m
Bending Radius (Electron)	124 m
Maximum Bending Field (Electron)	4.5 kG
Total Circumference	2035 m
Center of Mass Energy	110 GeV
R.F. Frequency (Electron)	~1200 MHz
Maximum R.F. Voltage (Electron)	100 MV/turn
Electron Current	30 mA
Power radiated by Electrons	1.5 MW
Maximum Luminosity	1.5×10^{31} $cm^{-2} sec^{-1}$
Crossing Angle	≲30 mrad
Injector	1 GeV Electron Linac
Injection Field (Electron)	265 G

TRISTAN ep SYSTEM

In Table II are shown preliminary design parameters of TRISTAN ep system. The center of mass energy of the ep colliding system is 110 GeV with the electron energy of 17 GeV and the proton energy of 180 GeV.

We have considered several schemes for storage of electrons including its injector and RF acceleration system. Because of strong synchrotron radiation along a curved orbit, energy and intensity of the electron beam is limited by feasible RF techniques. In this respect, of the schemes proposed the one preferable is that in which an electron linac is used both as the injector and the ring RF acceleration system!) The total length of the electron linac is about 100 m and it is installed in one of the long straight sections of the TRISTAN conventional ring. As the injector the linac works at a pulsed operation and provides about 10^{12} electrons with a single turn injection. Immediately after this the electron linac is turned into a ring RF system which works, in a sense, at a CW operation. The energy loss per turn for an electron circulating the storage ring is about 35 MeV for a 15 GeV beam and 50 MeV for a 17 GeV Including effect of quantum fluctuations, about twice of these figures are required for the RF peak voltage. Considering the power and aperture requirements, we tentatively choose the RF frequency of the linac at L-band region and divide the total length into 10 sections. With a shunt impedence of about 50 MΩ/m, values of necessary RF power are listed in Table III both for the injector and the storage ring operations. It is shown that RF power tubes with a peak RF power of ~30 MW and with an average power of ~350 kW are required, which, however, would not be far beyond from the present available techniques.

In addition to the RF power requirements, some problems associated with this system should be mentioned. First, the linac RF system has the advantage of achieving a 100 % RF capture of the injected beam. However, about 200 mA·μs peak current of the linac at injection is required for providing a 30 mA circulating current in the ring since the revolution frequency of electrons is 150 kHz. This figure is around the maximum current achieved up to the present in the existing linacs. Furthermore, for obtaining a higher luminosity it is favorable that the electron bunches are arranged so as to be separated from one another at a distance equal to the separation of proton bunches. During the period of synchrotron accelerations, the RF acceleration voltage has to be programmed in a range from some hundred kV to a hundred MV. For this, we probably need to excite each section successively with a feed-back RF control system. In addition, a transverse focusing system along the linac should be matched to the ring lattice system. Preliminary orbit analysis shows that the transverse motion is quite feasible throughout the whole process including injection, acceleration and storage. Finally, if we wish to storage positrons as well as electrons in the same ring, we may need to build another relatively small ring which is provided for injection of positrons at a sufficient intensity.

Table III RF POWER OF ELECTRON LINAC PROPOSED FOR TRISTAN INJECTOR AND RF ACCELERATING SYSTEM

Function	Injector	Storage Ring RF (15 GeV)	Storage Ring RF (17 GeV)
Energy Gain	1 GeV	35 MeV	50 MeV
Operation Mode	Pulsed	CW	CW
Peak RF Voltage (Each Section)	100 Mv	6MV	10 MV
Wall Loss (Each Section)	20 Mw	70 kW	200 kW
Beam Loading (Each Section)	10 MW	100 kW	150 kW
RF Power (Each Section)	30 MW	170 kW	350 kW
Total Power	300 MW	1.7 MW	3.5 MW

The maximum luminosity for ep colliding experiments will be determined by the maximum allowable tune shift for electrons per intersection. For a quasi-collinear crossing, following relations between the length parameters may be assumed as a practical case.

i) The electron bunch length is short enough while the possible shortest proton bunch length could be 0.3 m.

ii) The β function are assumed to be $\beta_V = \beta_H$ and vary as $\beta_{e,p}(s) = \beta_{e,p} + \frac{s^2}{\beta_{e,p}}$ in the interaction region. The β-function for the electron ring at the center of the interaction region is much shorter than that for the proton ring or $\beta_e << \beta_p$.

iii) The proton bunch length (or the length of the interaction region of an unbunched proton beam), ℓ_p, could be longer than or comparable to the β_e value, while it is short enough compared to the β_p value, i.e. $2\beta_e \lesssim \ell_p << 2\beta_p$.

iv) The electron beam radius is narrower than the proton beam radius.

On the assumption of these relations, it is shown[1]) that the tune shift, $\Delta\nu_e$, has a minimum when the following condition is satisfied between the proton bunch length (or the interaction length) and the electron-ring β-function as

$$\ell_p = 2\sqrt{3}\,\beta_e \quad . \tag{2}$$

Taking $\Delta\nu_{e\ min} = \Delta\nu_0$ (maximum allowable tune shift), we can obtain an expression for the maximum luminosity,

$$L_{ep\ max} = \frac{f N_e \gamma_e}{4\beta_e r_e}\,\Delta\nu_0 \ , \tag{3}$$

where N_e is the total number of stored electrons and r_e the classical electron radius. It is noted here the luminosity is one half of the usual expression for extremely short bunches, because the proton bunch length (or the optimum interaction length of an unbunched proton beam) is longer than β_e-value (see equ.(1)). For an unbunched proton beam as given in the pp colliding system, the optimum interaction length is estimated to be $\ell_p = 1$ m and, from equ.(2), the optimum β_e-value is about 0.3 m. Letting $f = 1.5 \times 10^5$ Hz, $N_e = 1.3 \times 10^{12}$ (30 mA), $\gamma_e = 3.3 \times 10^4$ (17 GeV), $r_e = 2.8 \times 10^{-15}$ m and $\Delta\nu_0 = 0.025$, we get

$$L_{ep}\ (\text{unbunched p}) \fallingdotseq 5 \times 10^{30}\ \text{cm}^{-2}\text{sec}^{-1} \ .$$

If we can bunch the proton beam as short as 0.3 m, then the corresponding optimum β_e-value is about 0.1 m and the maximum luminosity will become three-times higher, or

$$L_{ep\ max} \fallingdotseq 1.5 \times 10^{31}\ \text{cm}^{-2}\text{sec}^{-1} \ .$$

Time Schedule and Possible Phase I Project

The time schedule and cost estimates of the TRISTAN project should depend upon many unknown factors as the operation experience of the present machine, the future development of accelerator arts, the national economy, the man-power plan, the supply and power problems, etc. A tentative schedule presently seen is as follows:

1973 ~ 1975	Design study and fundamental research on superconducting magnets.
1975	Completion of the present machine.
1975 ~ 1977	Developments of superconducting magnets for storage rings and technical feasibility study.
1978	Construction started
1982	Completion of the conventional ring.
1985	Completion of the superconducting rings.

A rough total construction cost is estimated to be around 10^4 M yen, and, since this figure may be beyond a growth rate of our research budget, we had better divide the TRISTAN project into two stages, Phase I and Phase II. At present, we are considering two possible courses on the process from Phase I to Phase II. The one is that in which we construct the conventional ring in Phase I and use it as a storage accelerator both for protons and electrons. The construction of the accelerator enclosure for the whole project should also be included in Phase I. The conventional ring will accelerate protons to some ten GeV and electrons over ten GeV. Besides, this ring itself may be used as a 12 GeV electron-proton colliding beam machine. In this option, electrons as a starter are injected, accelerated and stored at about 13 GeV. Subsequently, 12 GeV protons accelerated by the presently constructing synchrotron are injected and stored in the same ring rotating in opposite direction. By a small momentum difference or an application of an electric field, we could separate electron and proton orbits except the interaction regions, so that we can devise a bypass or an interacting region without difficulty (Fig.4)[2]) The ep colliding experiments at 25 GeV in center of mass energy will be performed with a maximum attainable luminosity of about 10^{31} $\text{cm}^{-2}\text{sec}^{-1}$.

The other course from Phase I to Phase II is to build double conventional rings in Phase I and replace one of them by a superconducting ring in Phase II. By means of taking this course, we can perform ep colliding experiments at a center of mass energy as high as 50 ~ 60 GeV; i.e. the energy at which weak processes involving neutrinos would become comparable to electromagnetic processes or large momentum-transfer strong interactions. Design of accelerator and the experimental facilities in Phase I will also become simple and more flexible, provided a little additional construction money should be financed.

Acknowledgement

Many colleagues in the KEK Accelerator Department and other laboratories have contributed to promote the design study reported here. In particular, the discussions with Professor K. Huke, Institute for Nuclear Study, University of Tokyo, Professor K. Kikuchi and Dr. T. Suzuki, KEK Accelerator Department should be acknowledged.

References

1. T. Nishikawa: Proc. 9th Intn'l Conf. on High Energy Acc., SLAC, 1974, p.

2. T. Nishikawa: Proc. U.S.-Japan Seminar on High Energy Accelerator Science, 1973, KEK, p.209

3. 200-GeV Intersecting Storage Accelerators, ISABELLE, A Preliminary Design Study, ed. by J.P. Blewett and H. Hahn, Brookhaven Rept. BNL 16716, May 1972

4. The LBL-SLAC Storage Ring Study Group: Proton-Electron Positron Design Study, IEEE Trans. NS-20 (1973) 1039, see also Pellegrini et al., Proc. of 8th Intn'l Conf. on High Energy Acc., 1971, CERN, p.153

5. D.A. Gray: Proc. U.S.-Japan Seminar on High Energy Accelerator Science, 1973, KEK, p.492

6. A Similar idea is proposed by I. Sato: Genshikaku Kenkyu 17 (1972) *441* (a Japanese Circular published from Institute for Nuclear Study, University of Tokyo)

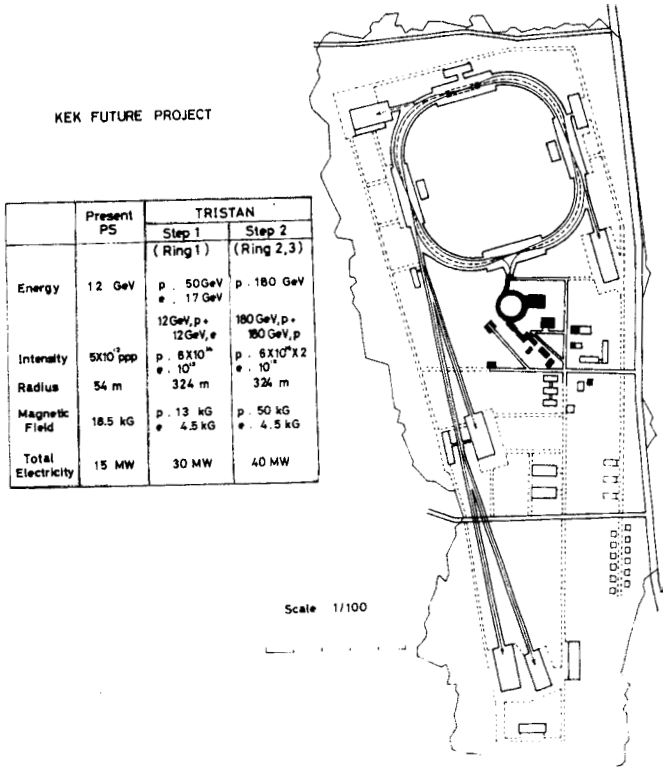

	Present PS	TRISTAN	
		Step 1 (Ring 1)	Step 2 (Ring 2,3)
Energy	12 GeV	p . 50GeV e . 17 GeV	p . 180 GeV
Intensity	$5X10^{12}$ ppp	12GeV, p + 12GeV, e p . $8X10^{10}$ e . 10^{12}	180GeV, p + 180GeV, p p . $6X10^{10}X2$ e . 10^{11}
Radius	54 m	324 m	324 m
Magnetic Field	18.5 kG	p . 13 kG e . 4.5 kG	p . 50 kG e . 4.5 kG
Total Electricity	15 MW	30 MW	40 MW

Fig.1 Plan View of **TRISTAN**

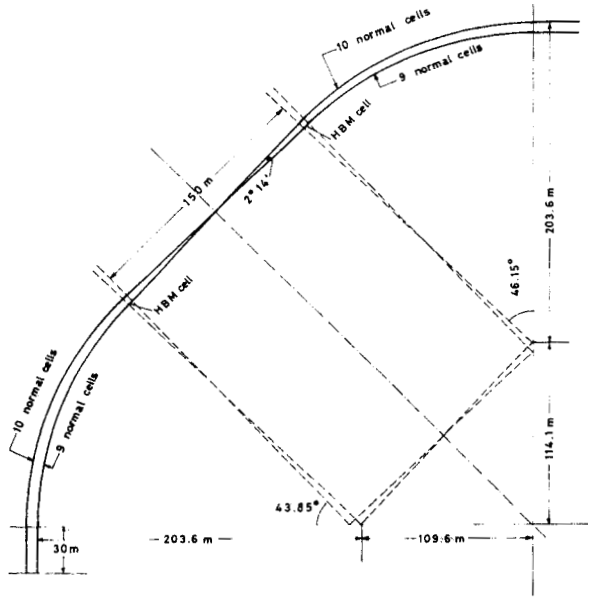

Fig.2 Quadrant of **TRISTAN** pp Rings

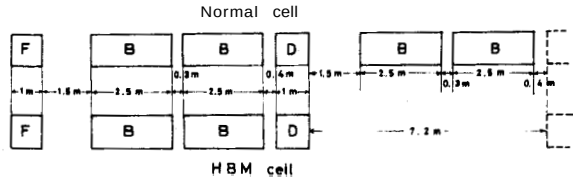

Cell Lrngth		16.4 m
Cell Numbers	Normal cell	76
	HBM cell	4
Radius of Curvature in Bending Magnet		124.0 m
Maximum BM Field (180 GeV)		50 kG
Maximum QM Gradient (180 GeV)		10.4 kG/cm
Phase Advance per cell		82° 7'
β Functions and X_p in regular cell		
β_{max}		26 m
β_{min}		6 m
$(X_p)_{max}$		2.4 m

Fig.3 Cell Structure of **TRISTAN** pp **Rings**

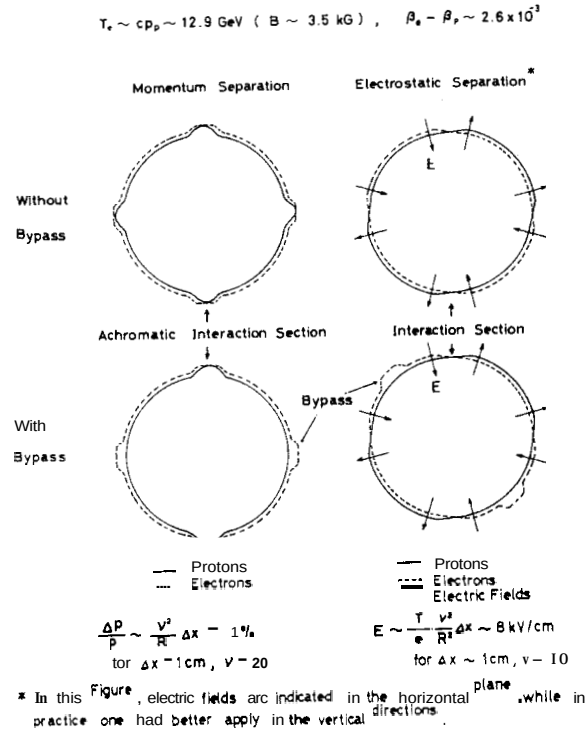

Fig.4 Possible Single Ring ep Colliding Beam System for **TRISTAN** Phase I.

THE SUPER-ADONE ELECTRON-POSITRON STORAGE RING DESIGN

F. Amman, M. Bassetti, A. Cattoni, R. Cerchia, V. Chimenti, D. Fabiani, A. Marra, M. Matera, C. Pellegrini, M. Placidi, M. A. Preger, A. Renieri, S. Tazzari, F. Tazzioli and G. Vignola

Laboratori Nazionali di Frascati del CNEN

Frascati, Italy

Abstract.

The results of a design study[1] for a high energy electron-positron storage ring to be built at the Frascati National Laboratories are summarized.

1. - Introduction.

Super-Adone (SA) is a 10 GeV single-ring machine. Luminosity per crossing is $5\times10^{31} \div 10^{32}$ in the energy range from 5 to 10 GeV with one bunch per beam; multi-bunch operation is envisaged, to increase luminosity at energies lower than 5 GeV.

The design aim is to achieve good performances at relatively low cost; the following assumptions have been made : maximum RF power transferred to the beam 1.4 MW; maximum current per beam 200 mA; approximate linear tune shift per crossing 0.08; two interaction regions; maximum number of bunches per beam eight.

The limit on the current per beam is imposed by filling time since it is assumed to use ADONE as a booster with relatively minor changes to its injector,

The experimental regions are only two. The addition of two more experimental regions would increase costs (two more experimental halls, two more special "low-β" insertions) while four experimental apparatus would anyway not be able to run at the same time in the single bunch mode. At present it is considered more convenient to design the experimental halls in such a way as to guarantee a fast turn-over time for the experiments installed on the machine, rather than to have more straight sections.

As far as beam behaviour in a storage ring is concerned, the operation of existing storage rings allows to draw the following conclusions :

1) operation with charges per bunch of a few 10^{11} $e^{\pm}$ per bunch and peak currents of about 30 A has been achieved;
2) coherent single beam instabilities have been interpreted and cured;
3) the transverse incoherent beam-beam limit[2] is reasonably well explained by current models and numerical computations: the maximum linear tune shift per crossing obtained is about 0.08 (ADONE and SPEAR); a possible explanation for the γ^7 luminosity dependence observed at ADONE at energies lower than 1 GeV, could be a diffusion process in competition with radiation damping; the interpretation is not inconsistent with existing data, and would give, for Super-ADONE, the $\gamma^{7\div4}$ law for luminosity at energies below 2 GeV;
4) anomalous bunch lengthening has not been, so far, clearly interpreted, and although some light has come from the recent SPEAR results[3], extrapolation to new machines and higher peak currents is still difficult;
5) low-β operation has been proved possible and in agreement with expectation[5,10];
6) experimental information on the longitudinal beam-beam limit is not complete[2]; data obtained with ADONE will be used in the following (although the actual limit might be somewhat higher).

The most relevant difference between the new generation of storage rings and the present one, is the required charge per bunch which is typically one order of magnitude higher; this represents the major unknown of these projects and requires careful studies to determine possible coherent losses in RF structures and bunch lengthening effects, The operation of DORIS and SPEAR II will cast some light on these phenomena and will allow to bridge at least part of the gap in terms of charge per bunch and peak current.

Another problem of the new generation of storage rings is the accumulation of intense positron beams in a single bunch; it turns out that an injection system consisting of a linear injector and a booster is the most convenient solution to keep filling times within tolerable limits and to avoid saturation in the stored current.

2. - Design criteria.

The very strong dependence of radiation loss on energy ($\propto E^4$), at fixed bending radius makes the optimum radius a sharply peaked function of energy. The solution described here has not been carefully optimized and corresponds to an energy somewhat higher than the optimum value for the bending radius chosen.

Assuming that the maximum value of the approximate linear tune shift due to beam-beam interaction, ξ_m, is a constant, the specific luminosity (for $\beta_z \leq \beta_x$) at the beam-beam limit, is given by

$$L/I = 2.17\times10^{32}\ \xi_m E \frac{k}{\beta_z} \quad (cm^{-2}s^{-1}A^{-1}) \quad (1)$$

with β_z in m; k, in the present design, ranges from 1.07 to 1.2 (in general: $k_{max} = 2$ for $\beta_x = \beta_z$ at crossing).

Equ. (1) shows that specific luminosity depends only on the operating energy and the minimum β, ξ_m being constant. The β value cannot be made much smaller than the bunch length for the assumed value of ξ_m; very small β's at the crossing entail very large values of the same quantity in the quadrupoles adjacent to the straight section, with the consequent complications of large aperture and very high sensitivity to errors in the focusing field.

We assume β_z = 0.2 m; from ADONE and SPEAR results we take ξ_m = 0.08 and obtain, with k=1.1.

$$L/I = 0.95 \times 10^{32} E_{GeV} \quad (cm^{-2}s^{-1}A^{-1}) \qquad (2)$$

In the choice of the total current per beam three variables have to be taken into account:

a) maximum RF power to the beams;
b) maximum current that can be stored in a reasonable time;
c) limit set by the transverse and longitudinal beam-beam effects on the beam transverse density.

Point b) sets an absolute limit on the maximum luminosity that can be achieved with a given injection system; a) influences the luminosity at the maximum energy and c) luminosity at low energies, both through economical factors (cost of the RF power and cost of the ring aperture). For a luminosity of 5×10^{31} cm^{-2} s^{-1} at 10 GeV, 50 mA per beam are required, and the RF power transferred to the two beams is 1.4 MW; at constant RF power to the beams and at a total current per beam smaller than 200 mA the allowed beam current is :

$$I = 50 \times (10/E_{GeV})^4 \text{ mA} \qquad \text{for } E \geq 7 \text{ GeV},$$

$$I \leq 200 \text{ mA} \qquad \text{for } E < 7 \text{ GeV}.$$

Transverse and longitudinal beam-beam effects limit the current per beam to :

$$I = 48.7 \cdot h \cdot \xi \frac{E^3_{GeV}}{} H^* \qquad (3)$$

where h is the number of bunches per beam and H^* is a quantity depending on the ring magnetic structure and related to the r.m.s. beam radial dimension σ_x at the interaction point; in the optimum condition of $\xi_x = \xi_z = \xi_m$, and for negligible coupling :

$$\sigma_x = a^p \sqrt{2 \beta_x H^*} \propto E \sqrt{\beta_x H^*}$$

Eqs. (1) and (3) show that for a given magnetic structure (i.e. given H') and number of bunches, the luminosity L is proportional to E^4; if one wants to keep I constant, and therefore obtain $L \propto E$, the product hH^* has to vary like E^{-3}. A possible choice is that of varying the number of bunches; in a double ring the method is easy and the most convenient; in a single ring multiple bunch operation is conceivable, with an upper limit for the number of bunches per beam of 4 to 8.

Many different ways have been devised to increase H^*:

a) use of high dispersion function ψ at the crossing, within the longitudinal beam-beam limit[6];
b) variation of the betatron wavenumber Q_x with energy[7,8];
c) use of special magnetic lattices that allow a continuous variation of H^*[9].

The present design is based on method a) and multibunch operation, with vertically separated beams (except in the interaction regions) and $h \leq 8$. Method b) makes injection somewhat more complicated, while method c) may turn out to be the most flexible and convenient; a more systematic analysis is needed to make the final choice.

A plot of the expected luminosity versus energy is shown in Fig. 1.

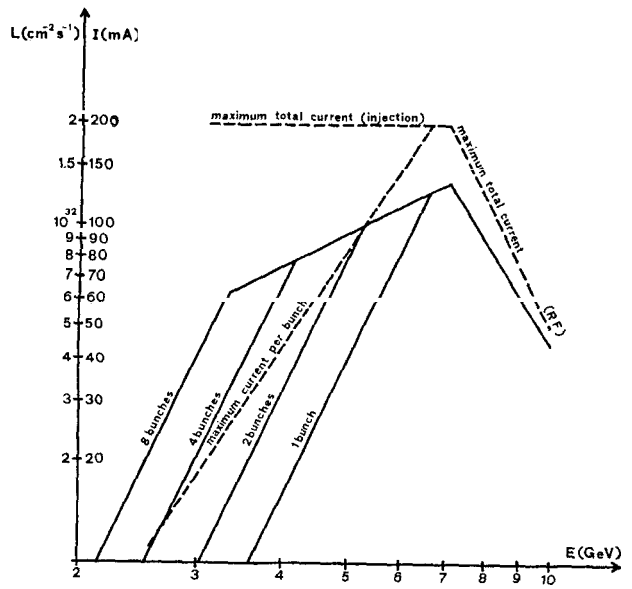

Fig, 1 - Luminosity and current dependence on energy.

As far as injection is concerned, an injection system consisting of a linac and an intermediate energy booster has many advantages : the number of pulses injected on the same stored beam is small (order of $10^2 \div 10^3$); the number of pulses to be transferred from the booster to the main ring is quite low (order of 10') so that the booster energy need not to be very high; the linac energy can be in the 500-1000 MeV range.

In the present design it is foreseen to use ADONE as a booster, operating with six bunches that can be individually extracted; to keep the total filling time within one hour, or one tenth of the lifetime in the main ring at 1.5 GeV, the linac energy has to be increased to 500 MeV with the addition of 4 accelerating sections (two klystrons).

The overall positron filling time is about 45 minutes for 200 mA of positrons and the electron filling time is about 10 minutes. The damping time for betatron oscillations in the main ring is 1.3 sec at 1.5 GeV which allows a maximum repetition rate for successive injection pulses on the same RF bucket of 1 pulse per second.

3. - Lattice description.

The lattice consists of 24 normal cells and 2 low-β insertions each containing 8 magnets: the magnetic elements of a half-insertion are shown in Fig. 2. The experimental straight section is 7 m long, and the distance between its center and the first magnet is 18.1 m. Each half-insertion has 10 independent quadrupoles and 4 magnets.

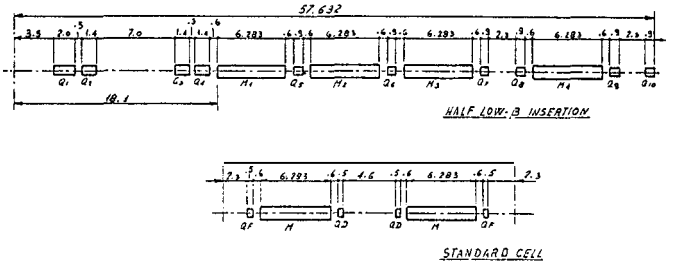

Fig. 2 - Magnetic structure.

The standard cell structure

$$\frac{0}{2}; QF; M; QD; 0; QD; M; QF; \frac{0}{2}$$

is symmetric with respect to the center of the 4.6 m straight section; most of the straight sections are occupied by RF cavities, and all of them contain a sextupole for the correction of chromaticity. Optimization of luminosity as a function of energy requires ψ^2/β_x at the crossing point $(\psi^2/\beta_x)_I$, the number of bunches per beam (h), and the coupling between radial and vertical betatron oscillations (ε) to be adjustable.

Four values of $(\psi^2/\beta_x)_I$ have been chosen, which define four configurations S_A, S_B, S_C, S_D, the number of bunches can be 1, 2, 4, 8 and ε is varied continuously within a given configuration ($\varepsilon_{min} \cong 0.2$). The optical parameters of the standard cell end of the low-β insertion for the 4 configurations S_A, S_B, S_C, S_D are given in Table I.

TABLE I

E_m = 10 Gev τ_x^o = 4.3 msec $\tau_x = \tau_x^o(E_m/E)^3$ $\sigma_x = \sigma_x^o(E/E_m)$ ν_x = 9.2

$A = A^o(E/E_m)^2$ τ_z^o = 4.1 msec $\tau_z = \tau_z^o(E_m/E)^3$ $\sigma_z = \sigma_z^o(E/E_m)$ ν_z = 9.2

σ_p^o = 1.1 x 10^{-3} τ_y^o = 2.0 msec $\tau_y = \tau_y^o(E_m/E)^3$ $\sigma_p = \sigma_p^o(E/E_m)$

Configuration	$a = \frac{\Delta l}{l}\frac{\Delta E}{E} \times 10^3$	β_x^I (m)	β_z^I (m)	ψ^I (m)	H (m)	H° (m)	$A^o \times 10^3$ (m)	σ_x^o out of coupling: cross-sing point (mm)	σ_x^o out of coupling: max (mm)	σ_x^o on coupling: cross-sing point (mm)	σ_x^o on coupling: max (mm)	σ_z^o on coupling: cross-sing point (mm)	σ_z^o on coupling: max (mm)	$C_x = \frac{\Delta\nu_x}{\nu_x}\frac{\Delta E}{E}$	$C_z = \frac{\Delta\nu_z}{\nu_z}\frac{\Delta E}{E}$
S_A	1.5	1.00	.20	0	.31	.31	.72	.8	9.7	.6	6.9	.26	6.4	- 2.1	- 2.4
S_B	1.3	1.00	.20	.98	.26	.74	.60	1.3	9.3	1.2	6.8	.24	6.3	- 2.1	- 2.4
S_C	1.3	2.16	.20	2.33	.26	1.52	.62	2.7	10.8	2.6	8.6	.24	4.8	- 2.3	- 3.5
S_D	1.2	1.25	.20	2.90	.54	3.91	1.28	3.3	15.0	3.2	11.9	.35	6.9	- 2.9	- 3.6

Figs. 3 and 4 shows the optical functions β_x, β_z and ψ for configurations S_A and S_D respectively.

While it is not possible to pass continuouslyfrom S_A and S_B to S_C and S_D, it is possible to pass from S_A to S_B and from S_C to S_D: only two injection configurations are therefore needed. The two injection structures have β_z^I = 1 m and ψ^I = 0.

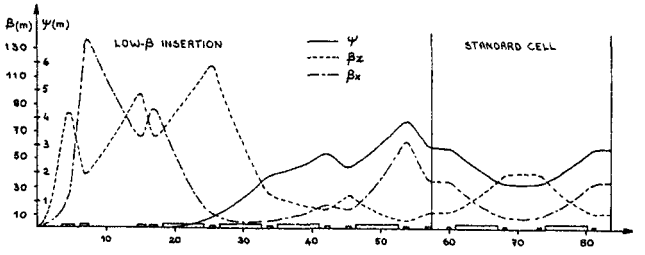

Fig. 3 - Optical functions for configuration SA.

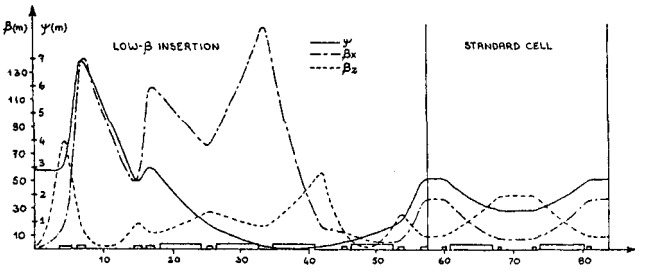

Fig. 4 - Optical functions for configuration S_D.

Operation with more than one bunch per beam can be obtained by separating the beams at all crossing points in the vertical plane (except for the experimental straight sections) using three independent pairs of electrostatic plates in each quarter of the machine.

There will be three kinds of quadrupoles having the following half-apertures (A): A = 105 mm (Q_2, Q_6); A = 90 mm (Q_3, Q_4, Q_5, Q_9); A = 75 mm (Q_1, Q_7, Q_8, Q_{10} and periodic cell) and two different kinds of magnets (the 16 low-β insertion magnets(b), and the 48 magnets of the periodic cells(a)), having the following characteristics:

	Gap height	Useful field region	total gap width
(a)	110	120	285
(b)	150	170	425

All magnets and quadrupoles will have laminated structures, assembled from precision-punched steel laminations. Magnets will be of the "C" type for ease of access and to make vacuum chamber assembly easier. With laminated cores "C"-type magnets are cheaper than "H"-type ones.

4. - Injection system.

For injection it is proposed to use ADONE as a booster. Injection in ADONE will be at 0.5 GeV over six equally spaced (58 ns) bunches which can be individually extracted after acceleration to 1.5 GeV.

A schematic diagram of the injection equipment connecting SA to the Linac/Adone facility is shown in Fig. 5.

Extraction from ADONE requires a slow "bumper", a fast kicker magnet and two septum magnets. The kicker magnet will occupy one of the interaction straight sections. The beam transport system both matches the ADONE emittance to the acceptance of SA and allows for a compensated deflection in the vertical plane. The overall system is achromatic to first order.

For injection into SA a perturbed closed orbit is excited by means of a bumper coil (EB) located in the high β_x section preceding the (I)sections, and switched off with two similar coils (SB) in the following high β_x sections. To achieve a complete compensation, in position and angle, of the perturbed closed orbit, two correcting bumps (CB) will be put in sections (I) near the deflectors D_1, D_2.

The same bump excites the perturbations for both injected beams making the overall number of oc-

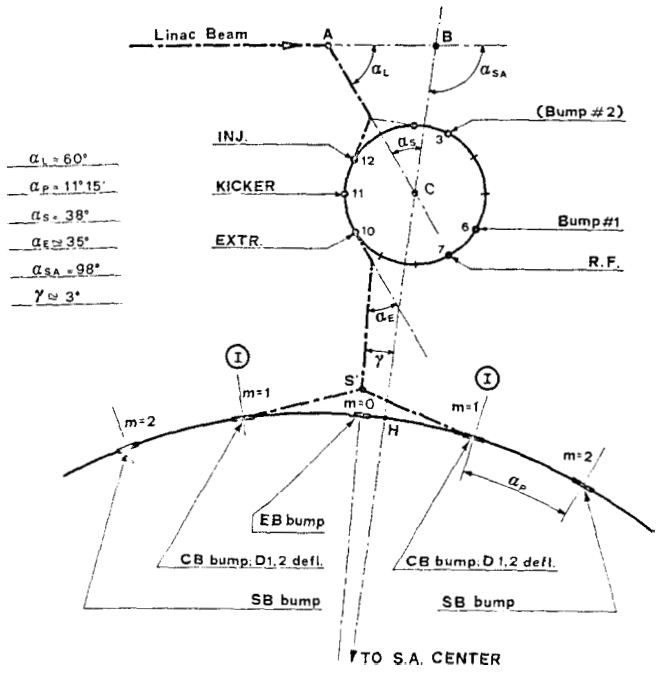

Fig. 5 - Injection system.

cupied high-β_x sections equal to 5.

The final deflection onto the right injection orbit is accomplished by means of two pairs of septum deflectors D_1, D_2 placed in sections (I).

5. - Radiofrequency system.

A reasonable choice for the RF frequency is 102.8 MHz, twice the frequency of the new ADONE RF system. At 102.8 MHz, 20 MV per turn are needed to ensure the required beam lifetime. We assume the shunt impedance per cavity to be 3 MΩ and the maximum voltage per cavity *to* be 0.**36** MV. There are therefore 56 cavities (two per straight section). The power lost in the cavities is 1.2 MW at 20 MV, and power to the beam is 1.4 MW at 10 GeV, totalling 2.6 MW.

The cavities are normal reentrant resonators, under vacuum. Cavities only will be placed in the tunnel, while power amplifiers (one per cavity) will be located in nearby buildings and connected to the cavities through power coaxial cables.

6. - Vacuum system.

The system is designed for an average pressure of 10^{-9} Torr, with two 200 mA beams at 10 GeV. Pressure in the experimental sections will be 10^{-10} Torr.

The vacuum chamber material is S. S. AISI **304** L; its surface area is: chamber 13.4×10^6 cm^2, cavities 5×10^6 cm^2; the volume is: chamber 16×10^3 liters, cavities 90×10^3 liters.

Details on the required vacuum equipment, which includes distributed pumping in all magnets, can be found in the following 'parameter summary'.

Parameter summary.

Beam

Energy (GeV)	5	7	*10*
Luminosity $\times 10^{-32}$ (cm^{-2}s^{-1})	**0.96**	**1.3**	**0.43**
Current (mA)	200	200	50
Number of bunches per beam	4	1	1
Radiation loss per turn (MeV)	0.**86**	**3.**3	13.8
R. m. s. dimensions at interaction point (mm)			
radial uncoupled	**1.6**	0.9	0.8
radial coupled	**1.6**	0.**85**	**0.6**
vertical coupled	**0.17**	**0.16**	0.3
azimuthal [radiation]	50	**70**	**75**
Lifetime (hours)	~21	~14	~9

Magnetic structure

Central orbit length (m)	857
Average radius (m)	**136.51**
Experimental straight section total length (m)	2 x 7
Number of periodic cells	24
Periodic structure	0/2-F-B-D-0-D-B-F-0/2
Period length (m)	26.166
Bending magnet radius (m)	64
Bending magnet length (m)	64 x 6.283
Maximum field (Tesla)	0.**52**
Periodic cell quad length (m)	96 x 0.5
Maximum gradient (Tesla/m)	5
Weight (Tons) magnets	Fe 900 Cu 120
quadrupoles	Fe 185 Cu 40
Magnet gap aperture (cm^2)	
periodic cell	28.5 x 11
insertion	42.5 x 15
Quadrupole maximum inner radius (cm)	
periodic cell	7.5
insertion	10.5

Focusing characteristics

Periodic cell	$\beta_{x,z}$ (m)	max	35÷37; **39÷41**
		min	8÷9 ; 10÷12
	ψ(m)	max	2.90÷3.10
		min	1.60÷1.80
	α R (m)		1.61÷2.*08*
Insertion	$\beta_{x,z}$ (m)	max	140÷170; 80÷140
	ψ(m)	max	3.5÷7
Interaction point	$\beta_{x,z}$ (m)		1.0÷2.2; 0.2
	ψ(m)		0÷2.9
Natural chromaticity : radial			**-2.16** -2.9
vertical			-2.4÷ -3.6
Betatron frequency : radial			9.2
vertical			9.2
Revolution frequency (MHz)			0.35

Radiofrequency system

Frequency (MHz)	**103**
Harmonic number	294
Number of cavities	56
Number of amplifiers	*56* (2 x 28)
Maximum power to the beam (MW)	2 x 0.7
Total R.F. power (MW)	2.6
Peak voltage (MV)	20

Vacuum system

Number of 200 l/s Ti-pumps	120
Number of 270 l/s turbomolecular pumps	32

Distributed pumps :	
pumping speed (l/s.cm)	10
length (m)	400
Pressure with beam in the experimental straight section (Torr)	10^{-10}

Injection

Extracted beam emittance (mmxmrad):	
horizontal	~5
vertical	3
Average injection rate (A/hour)	e^+ 0.2; e^- 1÷2
Injection energy in SA (GeV)	1.5
Injection energy in Adone (GeV)	0.5
Injection rate in Adone (p.p. s.)	5

7. - Buildings and utilities.

The tunnel will be built under ground between section 1 and section 5; the remaining part will be built at surface level. Two experimental halls ($20 \times 40 m^2$ x x 16 m height) will cover the experimental sections.

The maximum required electric power is 25 MVA including spare power, and is no problem,

The required cooling water flow is about 12.5 l/sec and could also be easily available.

A simple building, serving the machine and plants, will collect the electric, water, cooling, heating and conditioning stations tohether with the' machine services; control and data rooms will be put in a connected building.

The RF final stages will be accomodated in a different building.

8. - Higher energy ring.

A very preliminary study of the maximum dimersion ring that can be built in the Frascati National Laboratories area shows that a circular ring with mean radius of 340 in (or a race-track with a total length of about 2. 500 m) is feasible.

The storage ring energy could be 15-16 GeV, and the corresponding energy loss per turn would be (25-33) MeV/turn; the RF power transferred to the beams, required to obtain a luminosity of 5×10^{31} $cm^{-2}s^{-1}$ at the maximum energy would be (1.75÷2.3) MW. The injection system discussed above could be adequate, if a slight reduction in luminosity (8×10^{31} max, at 10÷11 GeV) is accepted.

References

I - Super-Adone, Internal document of the Italian Institute of Nuclear Physics (INFN) and of the Frascati National Laboratories (1973).

2 - F. Amman, Beam-beam limits, 1973 Particle Accelerator Conference, IEEE Trans. on Nuclear Science NS-20, 858 (1973).

3 - M. A, Allen et al., Some observations on bunch lengthening at SPEAR, Report SPEAR-171 (1974).

4 - F. Amman et al., Remarks on two beam behaviour of the 1.5 GeV electron positron storage ring Adone, Proc. VIII Intern. Conf. on High Energy Accelerators, CERN (1971).

5 - SPEAR storage ring group, Operating resultsfrom SPEAR, 1973 Particle Accelerator Conference, IEEE Trans. on Nuclear Science NS-20, 752 (1973).

6 - SLAC storage ring group, The SLAC storage ring project SPEAR, Proc. VIII Intern. Conf. on High Energy Accelerators, CERN (1971), pag. 145.

7 - J. Rees et al., Preliminary design of a 15 GeV electron-positron variable tune storage ring, Report SPEAR-167 (1973).

8 - G. H. Rees et al., Variable damping and tunes in the e- ring, Report EPIC/MC/39 (1974).

9 - M. Bassetti, Resonant methods for beam size control in storage rings, This Conference.

10 - R. Averill et al., Colliding electron and positron beams in the CEA bypass, Proc. VIII Intern. Conf. on High Energy Accelerators, CERN (1971), pag. 140.

DISCUSSION

John Rees (SLAC): When you put more than one bunch in each orbit, how do you keep them apart except at the interaction region?

Sergio Tazzari (Frascati): We have a system of electrostatic plates that allows us to separate them.

James M. Paterson (SLAC): This is the same question put a different way. When you have multi-bunching and have the bunches separated in the other part of the ring, what is the typical beta function where the bunches pass?

Tazzari: The maximum beta function on the standard cell is about 50 meters.

Kjell Johnsen (CERN), Session Chairman: I thank the last speaker and I'd also like to thank the other speakers. I think many realistic projects have been presented to us this morning. It's probably too much to hope that all will be funded before we meet again at the Accelerator Conference, but I think we should hope, and have good reason to hope, that a few will have been started before the next conference.

BUNCHED BEAM INTERSECTING STORAGE ACCELERATORS FOR PROTON-PROTON COLLISIONS*

M. Month
Brookhaven National Laboratory
Upton, New York

Abstract

A set of parameters suitable for the operation of a bunched beam storage device for head-on proton-proton collisions is developed. The use of superconducting magnets allows a high energy/circumference ratio as well as a high magnet aperture/power consumption ratio as compared to conventional magnet designs. Using the AGS as injector, a beam-beam limited luminosity of 10^{32} cm^{-2} sec^{-1} at *200* GeV can be achieved using "single-turn" injection, this a consequence of the high intensity (0.7 A), low density AGS beam. The beam-beam tune shift limit is taken to be 5×10^{-3}. Acceleration from 30 to 200 GeV in *2.3* min. is obtained with a *27* MHz, *33* kV (peak) rf system with modest power dissipation. Various parameters, e.g. tune, chromaticity, nonlinear detuning and synchrotron frequency are discussed in terms of their influence on beam stability. In particular, the longitudinal stability of the bunches, the phase area growth due to rf noise, the transverse resistive wall instability, the head-tail effect, and beam stability against nonlinear resonances, specifically those arising from the beam-beam interaction, are discussed. It is found that the parameter set proposed is consistent with beam stability against these effects.

1. Introduction

We propose a pair of intersecting storage accelerators capable of colliding bunched proton beams head-on.[1] We will discuss the performance of such a device in terms of attainable energy and luminosity. The energy that is achievable follows directly from the choice of the ring circumference and the dipole magnetic field. The luminosity, on the other hand, is determined by the average current, the value of β^* at the collision point, the bunch length, and the beam-beam tune shift. Thus, we have 6 primary parameters upon which the ultimate performance is based.

Actually, we must consider a third performance characteristic, the beam lifetime, by which we mean the time during which there exist collisions providing usable experimental information. We can interpret this characteristic in terms of a luminosity duty factor. Since a deteriorating beam must be dumped and then the rings refilled, we can define the duty factor as the fraction of total operating time that beams capable of giving acceptable data persist.

We must ask, therefore: How much time during a given operating period will a beam be utilized for experimental purposes? And how much time will be spent dumping and refilling? The answer to the first question is the beam lifetime, which involves an understanding of various beam stability phenomena. The answer to the second is related to practical considerations: that is, it is the specific time required for dumping, obtaining a new beam, injecting, and setting up for collisions.

As we will see, the basic thrust of our suggestion will be a bunched beam with low momentum spread and large betatron emittance. This immediately differentiates our design from momentum stacked storage devices, such as the CERN ISR, used for colliding coasting proton beams.[2] In this latter case, large momentum spread is required for beam stability, small betatron emittance to maximize luminosity. In the bunched beam case, we want a small momentum spread in order to control linear tune spread at small values and we want large emittance to keep the transverse beam density low so that the beam-beam limit is not exceeded, Thus, for bunched beams, the preferred stacking mode is in betatron phase space. However, given the AGS as an injector, we find that the beam characteristics are not too far removed from optimal. We therefore suggest, for an initial design, the extremely simple operating procedure of taking the AGS bunches as they are, transferring them to the storage device (of course, we need as many AGS pulses as is required to fill the circumference of the ISA), accelerating and colliding them. That is, we suggest initially a no-stacking-operating mode.

To be specific, we will use for our lattice, the configuration proposed for the BNL ISA project.[3] This provides the basis for obtaining three fundamental parameters: the circumference, the vacuum chamber aperture, and the attainable energy. The particular values for these parameters are intimately tied to the question of whether to use a conventional magnet design or a superconducting one. Disregarding the technical feasibility of the superconducting design, which is extensively discussed in Ref. (3), the latter, superconducting magnet choice has two distinct advantages. First, there is the obvious fact that for a given machine radius, the higher magnetic field gives a higher energy. Secondly, for a given power consumption (in the superconducting design, heat leaks require power dissipation), the conventional design is severely limited by magnet gap, meaning greatly reduced vertical aperture as compared to the superconducting magnet design. As will become apparent, the larger aperture significantly improves beam stability and performance, the latter ultimately translating into higher luminosity. For this study, we will adopt a somewhat large aperture, which greatly simplifies the design effort. This implies the use of superconducting magnets, unless, of course, there is a willingness to lift the stringent limitation on magnet power consumption, thereby allowing the gap of the conventional dipoles to substantially increase.

Although we will not consider vacuum pumping and electron clearing here, we point out that requirements on these functions should be substantially reduced by the low average current and bunch structure.

In Section *2*, we discuss the performance capability of the bunched beam ISA, specifically the energy and luminosity. In Section **3**, the matching conditions for the bunched beam transfer are given, and we consider the acceleration and storage of the beam, including the stability of the bunches. Section *4* will deal with the nonlinear beam-beam interaction. As we will see, the synchrotron motion coupled with the beam-beam interaction imposes a strong constraint on the linear tune spread (e.g. that tune spread arising from momentum spread through the machine chromaticity). This connects the nonlinear constraints with transverse beam stability arising from collective beam effects. As it turns out, both the harmful consequences of the beam-beam nonlinearities and the transverse instabilities can both be suppressed by having a nonlinear tune spread in addition to the linear one. Both these aspects will be discussed together in Section *4*. Table I provides a list of parameters that are developed over the length of this paper.

* Work performed under the auspices of the U.S. Atomic Energy Commission.

TABLE I. PARAMETERS FOR A BUNCHED BEAM ISA

Basic Parameters

Average Radius, R (m)	*428.2*
Final Energy, E (GeV)	*201.4 (302.1)*
Magnetic Field, B (kG)	*40 (60)*
Average Current, I (A)	*0.72*
β at Collision Point, β^*(m)	*3.0*
Beam-Beam Tune Shift, $\Delta\nu_{bb}$	5×10^{-3}
Luminosity Per Collision Region (cm^{-2} sec^{-1})	1.04×10^{32} *(1.56×10^{32})*

Lattice†

Vertical Beam Separation (cm)	*46.0*
FODO Cell Length (m) (no.)	*25.7 (48)*
Maximum β (m)	*43.0*
Maximum Dispersion $X_{p,max}$ (m)	*1.7*
Multipurpose Insertion (straight) Length (m) (no.)	*40.0 (4)*
Experimental Insertion (straight) Length (m) (no.)	*200.0 (4)*
Dipole Filling Factor in Curved Portions	*61%*
Bending Magnet Length (m) (no.)	*4.11 (256)*
Symmetry	*4*

Beam Transfer and Rf Parameters

Kicker Rise Time (μsec) (Inj. & Ej.)	0.22
V_{rf} (Peak Voltage/Turn, kV)	*32.7*
f_{rf} (Frequency, MHz)	*26.8*
Bunching Factor, B, During Storage (Length/Separation)	*0.063* (15.78:1)
Q (Quality Factor)	*70*
$\lvert Z_s \rvert$ (Shunt Impedance) (kΩ)	*20*
Rf Power (kW)	*26.7*
Acceleration Time (min.)	*2.29*
Synchrotron Wave Number, ν_s	1.39×10^{-4}

Beam Characteristics at Injection (Matched From AGS)

AGS Intensity (Protons Per Pulse)	1.2×10^{13}
Protons Per Bunch, N_B	10^{12}
AGS Longitudinal *95%* Emittance (eV-sec/bunch)	1.0
AGS Transverse *95%* Emittance (Area/π at *30* GeV, rad.m)	*2.35×10^{-6}*
Injection Energy (GeV)	*30*
Total Fractional Momentum Spread	*2.04×10^{-3}*
Bunching Factor, B, at Injection	*0.093* (10.81:1)

Beam and Chamber Characteristics

At Cell β_{max}, β_{max}= 43.0m, X_p=1.7m, Vertical Half Beam Size (cm) *(30, 201.4 GeV)*, b	*1.00, 0.39*
Horizontal Half Beam Size (cm) *(30, 201.4 GeV)*, a	*1.17, 0.43*
Total Fractional Momentum Spread (Final Energy)	*4.45×10^{-4}*
Total Bunch Length (m) *(4 X rms length)*	*4.26*
Central Tune	*19.381*
Chromaticity (u' = pdν/dp) (Final Energy)	*+ 2.25*
Linear Tune Spread (via Chromaticity) (Final Energy)	
Nonlinear Tune Spread (Detuning Effect)	10^{-2}
Space Charge Tune Shift *(30, 201.4 GeV)*	*6.64×10^{-4}, 2.18×10^{-5}*
Chamber Radius, r (cm)	*4.0*

†See Ref. (3).

2. Performance: Energy and Luminosity

Energy

The attainable energy is simply determined from the amount of circumference available for bending and the maximum dipole field. Subtracting the straight parts of the circumference (used for injection, ejection, rf stations, and experiments), and using a *61%* dipole filling of the curved portions[3], we have,

$$p(\mathrm{GeV/c}) = 5.035\ B(\mathrm{kG}) \quad . \qquad (2.1)$$

This means at a *40* kG field, the maximum energy is *201.4* GeV, while for a *60* kG field, this increases to *302.1* GeV.

Luminosity

Under certain conditions, the luminosity and the limiting beam-beam tune shift can be very simply expressed. If the beams are nearly round in the transverse plane and if the rms bunch length is sufficiently less than the value of β^*, then we have[4] for the luminosity, L, and tune shift, Δ_{bb},

$$L = \left(\frac{I}{e}\right) \frac{\gamma}{r_p} \frac{\Delta\nu_{bb}}{\beta^*} \quad , \qquad (2.2)$$

$$\Delta\nu_{bb} = \frac{r_p \beta^* N_B}{4\gamma ab} \quad , \qquad (2.3)$$

where a,b are the horizontal and vertical 1/2 beam sizes *(95%* sizes), γ is the energy in proton mass units, e is the electron charge, r_p is the classical proton radius, I is the average beam current, and N_B is the number of protons per bunch. The bunch length constraint is

$$\ell_p < 4\ \beta^* \quad . \qquad (2.4)$$

Neglecting the small horizontal size arising from dispersion, we see that for a given beam-beam limit, *(2.3)* fixes the transverse bunch density. If we take $\Delta\nu_{bb}$ = 5×10^{-3}, and γ = *214.7*, we find

$$\frac{N_B}{\epsilon} = 2.62 \times 10^{18}\ \mathrm{m}^{-1} \quad .$$

The number of protons per bunch, corresponding to an average current of *0.72* A, is $N_B = 10^{12}$. This is a reasonable assumption as to what the AGS, as an injector, can provide. This then gives a required emittance, ϵ = *0.38×10^{-6}* rad.m (at *201.4* GeV). This corresponds to ϵ = *2.35×10^{-6}* rad.m at 30 GeV, which is in fact very close to the measured AGS emittance.[5] Using I = *0.72* A, and β^* = *3* m, then L = *1.04×10^{32}* cm^{-2} sec^{-1}. The *95%* bunch length is restricted to ℓ < 12 m, which is well within our design bunch length.† The emittances assumed correspond to beam sizes small compared to our design vacuum chamber radius.

The possibility of increasing the luminosity exists, but involves complications. The current can be increased by injecting more than one turn in betatron phase space, complicating our simple one turn matched transfer scheme. The value of β^* can be reduced; however, this ultimately has the effect of increasing the chromaticity and making quadrupole tolerances more stringent. It further requires a lower bunch length, which means higher voltage and power consumption. Thirdly, for the bunched beam, it is conceivable, because of the small linear tune spread, that the beam-beam tune shift limit is larger than 5×10^{-3}. That is, by placing the beam in tune space far from low order resonances (e.g. away from *4* through 10), the beam-beam limit may be less than for stacked coasting beams, where

because of the large linear tune spreads, low order resonances (e.g. 5th) must be nearby.[6] To take advantage of this possibility however, what is required is a higher transverse beam density, i.e. for the same current, a lower emittance.

3. Beam Transfer and Rf Parameters

For an ISA circumference 3-1/3 times the circumference of the AGS, 40 AGS bunches would be needed to fill the ISA.[3] If 4 AGS pulses are used, each contributing 10 bunches (with 2 removed), the fast kicker requirement in the AGS is relaxed. In the ISA, the rise time of the fast kicker is determined by the distance between bunches, d. Since, in the AGS, we have 12 equally spaced bunches, the distance between bunches is $d = C_{AGS}/12 = 67.3$ m, since $C_{AGS} = 807.2$ m. Thus, the ISA kickers must be capable of rising and falling in roughly $t_r = d/c = 0.22$ μsec. The matched bunches will be injected in one of the multipurpose insertions, as shown in Ref. (3).

If we transfer matched bunches in stationary buckets, the matching condition is

$$\left(Vh\right)_{ISA} = \left(Vh\right)_{AGS} \frac{\eta_{ISA} R^2_{ISA}}{\eta_{AGS} R^2_{AGS}} \qquad (3.1)$$

where $\eta = \frac{1}{\gamma_t^2} - \frac{1}{\gamma_{INJ}^2}$, γ_t is the transition energy (in proton mass units), γ_{INJ} is the injection energy, V is the peak rf voltage, and h is the harmonic number of the respective rf systems. With $V_{AGS} = 384$ kV/turn, $h_{AGS} = 12$, $\eta_{AGS} = 0.0137$, $R_{ISA} = \frac{10}{3} R_{AGS}$, and $\eta_{ISA} = 0.0021$ (i.e. $\gamma_t = 18$, $\gamma_{INJ} = 32$), we have, for matching

$$\left(Vh\right)_{ISA} = 7848.2 \text{ kV/turn} \quad . \qquad (3.2)$$

From the point of view of bunched beam stability, it is desirable to have a high frequency rf system (i.e. high h).[7] However, this, coupled with the matching constraint (3.2), which would require a "lower" voltage, means that the bucket rapidly shrinks around the bunch. Thus, given the matching constraint, there is a limit on h. The bucket area is given by

$$A_b = \frac{4\sqrt{2}\sqrt{E_o}}{\pi\sqrt{\pi} f} \sqrt{\frac{V\gamma}{\eta h^3}} \quad , \qquad (3.3)$$

where f is the revolution frequency and E_o is the proton rest energy.

To clarify this point about high rf frequency (i.e. high harmonic number, h), we will develop the current limit arising out of the bunched beam space charge frequency shift, which is the most stringent limit on current. If the chamber wall is perfectly conducting, then the image force induced on the beam is non-resistive. Although no growth can result, a non-resistive force can drive the beam into a condition of latent instability, which could then be activated by the chamber resistivity or resonant structures in the ring. The condition for the current limit can be derived from the Landau damping criterion which states essentially that the frequency shift resulting from the force must be less than the spread in synchrotron frequency for the bunches, or[8]

$$\frac{\Delta\omega_{sc}}{\Omega_s} < \frac{S}{4\Omega_s} \quad , \qquad (3.4)$$

where $\Delta\omega_{sc}$ is the space charge frequency shift, $\Omega_s = 2\pi f\upsilon_s$ is the central synchrotron frequency, υ_s is the synchrotron wave number, and S is the spread in synchrotron frequency in a bunch. If the bunches are well within the bucket, then S comes primarily from the octupole component of the synchrotron force, i.e.,

$$\frac{S}{\Omega_s} = \frac{\pi^2 h^2 B^2}{16 M^2} \quad , \qquad (3.5)$$

where M is the number of (equally spaced) bunches (note that $h \geq M$), and B is the bunching factor (length/separation). The real space charge frequency shift can be written,[7]

$$\frac{\Delta\omega_{sc}}{\Omega_s} = (0.152) \frac{\pi^3 E_o Z_o}{16 f^2} \frac{g_c I B}{\gamma\eta A^2 M^2} \quad , \qquad (3.6)$$

where I is the average beam current, A is the invariant bunch area (in eV-sec), Z_o is the free space impedance ($Z_o = 377$ ohms), g_c is a geometrical factor,

$$g_c = 1 + 2\ln(r/b) \quad , \qquad (3.7)$$

and r,b are the vacuum chamber radius and beam radius respectively. Taking $r/b \approx 4$, we obtain from (3.4),

$$I < 4.9 \times 10^{-3} \gamma\eta A^2 h^2 B \quad , \qquad (3.8)$$

which is dependent on h, not M. For elliptical bunches, the peak voltage, V, and bunching factor, B, are related by,

$$Vh = \frac{8 f^2}{\pi^3 E_o} \frac{\eta A^2 M^4}{\gamma B^4} \quad . \qquad (3.9)$$

At injection, taking M = 40, A = 1.0 eV-sec (a realistic value for the AGS at $N_{AGS} \approx 1.2 \times 10^{13}$ ppp),[5] and Vh from (3.2), we find from (3.9), $B^{-1} = 10.81$. If h = M, the current limit from (3.8) is $I < 0.049$ A, which is more than an order of magnitude less than the design current of 0.72 A. To stabilize the beam at injection, we use a higher rf frequency. Taking h = 6 M = 240 (corresponding to an rf frequency, $f_{rf} = 26.76$ MHz), the current limit increases to $I < 1.76$ A. The matching peak voltage can be found from (3.2): V = 32.7 kV/turn. The bucket area at injection is, from (3.3), $A_b = 1.68$ eV-sec, which results in a bucket filling of $A/A_b = 60\%$.

The process of increasing h and decreasing V is clearly an effective stabilizing technique. After matching, the voltage can be increased (adiabatically) in order to decrease the bucket filling factor. Then, of course, the bunches become tighter and the current limit is slightly reduced.

At high energy, the current limit is greatly increased. With $\gamma = 214.7$, $\eta = 0.0031$, we find $B^{-1} = 15.78$, $A_b = 2.13$ eV-sec, giving a bucket filling of 47%, and a space charge current limit, $I < 11.9$ A.

It is thus clear that in the storage phase, the limitation to bunch stability derives from the interaction with resonant structures.[7] For each such structure, there will be a limit on its shunt impedance. For example, consider a structure, capable of inducing a dipole mode beam oscillation at a frequency, $f_{RES} \approx 50$ MHz, near the "critical frequency". We find a shunt impedance limit, $R_s < 3$ kΩ. However, for such a structure, if the shunt impedance is 100 Ω above the limit, we estimate a growth time on the order, $\tau \approx 10$ sec. Such a short growth time reflects the importance of achieving the required stability limit for each resonant structure.

The bunch characteristics during storage can be found from:

(1) bunch length, $\ell_p = \frac{2\pi RB}{M}$, **(3.10)**

(2) total momentum spread,

$$\frac{\delta p}{p} = \frac{2\pi \nu_s B}{M\eta} \qquad (3.11)$$

(3) central synchrotron frequency,

$$\nu_s = (Vh\eta/2\pi\gamma E_o)^{\frac{1}{2}} \qquad (3.12)$$

Using V_{rf} = 32.7 kV/turn, f_{rf} = 26.8 MHz (h = 240), B^{-1} = 15.78 (A = 1.0 eV-sec), we have ν_s = 1.39 X 10^{-4}, ℓ_p = 4.26 m, $\Delta p/p$ = 4.45 X 10^{-4}.

After matching, the 40 bunches in the ISA can be directly accelerated. Acceleration is governed by the equation

$$p = eV \sin\phi \quad f \quad , \qquad (3.13)$$

where ϕ_s is the rf stable phase angle. Thus, the time to accelerate an amount δp is

$$6t = \frac{\delta p}{f\ eV\ \sin\phi_s} \quad . \qquad (3.14)$$

With $\delta p = p_{Final} - p_{INJ}$ = 171.4 GeV/c, V = 32.7 kV, and $\phi_s = 20^o$, we have δt = 2.29 min.

The proton bunches must be stored for long periods of time in order to sustain a high luminosity duty factor. Since there is negligible radiation damping of synchrotron oscillations for protons, rf noise, which can couple to this motion, can induce a diffusive growth in the synchrotron amplitude. In particular, we will limit ourselves here to an estimate of the longitudinal phase space area growth due to fluctuations in the rf voltage. It has been shown that for a mean square voltage fluctuation

$$\langle u^2 \rangle = \left\langle \left(\Delta V/V\right)^2 \right\rangle \quad , \qquad (3.15)$$

the mean diffusion time for growth of the synchrotron amplitude is [9]

$$\tau = \frac{h}{\pi f\ Q\ \nu_s^2 \langle u^2 \rangle} \quad , \qquad (3.16)$$

where Q is the quality factor for the accelerating cavity. If we take h = 240, $\langle u^2 \rangle$ = 0.76 X 10^{-6} (corresponding to an error in stable phase angle of 0.05 degrees), f = 111.5 kHz, ν_s = 1.39 X 10^{-4}, and Q = 70 (consistent with a shunt impedance, R_s = 20 kΩ and a peak beam current, I_{peak} = 11.4 A), we find a growth time on the order of years.

4. Tune, Tune Spread and the Beam-Beam Interaction

The fundamental limit to the performance of a storage device arises from the fact that during collisions, the electromagnetic forces between two sufficiently intense beams induce beam growth and ultimately beam loss at the aperture boundary. A measure of the strength of the interaction is the beam-beam linear tune shift, Δ_{bb}, although the beam-beam interaction is in fact a highly nonlinear one. There is disagreement about whether the observed beam loss can be explained using traditional resonance concepts or whether some new multiresonance picture must be used, with resonances combining to cause quasi-random, i.e. diffusion-type beam behavior. We are not here concerned with this aspect of the beam-beam interaction. We simply accept the existence of such a limit, though we might mention the point that if the beam-beam limit is tune sensitive" as appears to be the case and, further, if closeness to low order nonlinear resonances (i.e. of order 4 or 5, rather than 11 or 12) enchances the loss phenomenon, then bunched beams could have a beam-beam limit higher than coasting beams since the tune spread is far less and the working line (really a working point in the bunched beam case) can be set away from the low order resonances. Thus, we choose a rather conservative beam-beam limit, Δ_{bb} = 5 X 10^{-3}. But, since our working point can be removed from all resonances up to, say, the 13th order, then it is not inconceivable that for bunched proton beams, the limit would be considerably higher.

However, with bunched beams, particles execute synchrotron motion. Through the machine chromaticity, this time variation of momentum translates into a dynamic tune oscillation. Particles can thus "pass through" high order resonances and the possibility of "lock-in" emerges.[10] The beam-beam interaction is by far the most dangerous source of nonlinear resonances," and we will therefore attempt to set up stability criteria for these nonlinearities in the presence of synchrotron motion. We will do so by treating the nonlinear resonances in the traditional manner as isolated entities. In doing this, we are making the implicit assumption that the dynamic tune variation caused by the synchrotron motion does not significantly alter the beam-beam limit, or that, in any case, we are operating below the true limit.

The basic stabilization criteria are related to (1) control of the central tune away from the "low" order nonlinear resonances, (2) maintenance of small linear tune spread (equivalent to the maximum tune variation per synchrotron period) for essentially the same reason, (3) introduction of sufficient nonlinear detuning (e.g., 0th azimuthal harmonic octupole), and (4) an upper bound on the resonance excitation strength. We confine ourselves to one-dimensional resonances. Analogous criteria for coupling resonances are more complicated, but not conceptually different.

The tune of the ISA is $\nu \sim$ 19-20. If our particular choice is ν = 19.3810, then we are very close to a 21st order resonance (8/21). The nearest resonances of lower order are the 13th (5/13) and the 8th (318). The distance from these resonances are 0.0036 and 0.006 respectively. This gives us a feeling for the required control on ν spread, $\overline{\Delta\nu}$. With $\overline{\Delta\nu}$ = 10^{-3}, we can essentially neglect these resonances. Note that this type of control is required during collisions where the high order resonances may be dangerous. Thus, we need such control only under static magnetic and rf conditions.

Although tune control as described here might be sufficient to stabilize a beam against beam-beam nonlinearities, we can place some limit on resonance excitation in the event that in practice the tune control is not as fine as prescribed. To derive the nonlinear stability criteria, we will use the quasi-static (adiabatic) picture of "lock-in" or "particle trapping". Under such circumstances, we can derive two simple constraints. First, by including sufficient nonlinear detuning, any particle trapped will not reach an aperture. If we let Δ_{NL} represent the nonlinear (octupole) detuning strength at the rms beam amplitude, then the amplitude range for "lock-in" is given approximately by

$$\Delta\epsilon = \frac{\overline{A_L}}{\Delta_{NL}} \epsilon_B \quad , \qquad (4.1)$$

where ϵ_B is the rms beam emittance, and $\Delta\epsilon$ is the "lock-in" range in emittance units. If we have Δ_{NL} = 10^{-2} and $\overline{\Delta_L}$ = 10^{-3}, then we see that the range $\Delta\epsilon$ is 1/10 of the beam emittance. It should also be remembered that since trapped particles do not reach an aperture limit, they simply oscillate within the range $\Delta\epsilon$ and, to lowest order, there is no effect of the nonlinear "lock-in"

process on the beam.

The condition *(4.1)* is independent of the exciting resonance. For strong excitation strengths, this will cease to be the case. One can picture the effect in the particle phase space. Unstable fixed points, which for small excitation widths are outside the machine aperture, begin to move toward the beam. When they are near the beam, particle motion becomes dominated by these unstable fixed points and the particles will begin to move on outward (in amplitude) moving trajectories. To prevent this, we set a limit on the resonance excitation width, Δ (evaluated at the beam rms emittance):[6]

$$\Delta < \Delta_{NL} \left(\frac{\epsilon_B}{\epsilon_{AP}}\right)^{(p-4)/2} , \qquad (4.2)$$

where ϵ_{AP} is the emittance corresponding to the aperture, and p is the order of the resonance ($p > 4$). For $\Delta_{NL} = 10^{-2}$, this condition will be easily satisfied, even for the strong beam-beam interaction.

For a weak resonance (Δ_e small) or high synchrotron frequency, our adiabatic assumption will begin to break down. Actually, we can picture this breakdown qualitatively as follows: If the tune variation is slow, the particle trapping is efficient. As the tune rate increases, the buckets trapping the particles move through the phase space faster and become "leaky". The trapping efficiency of these buckets decreases. However, since the bucket motion within the phase space is a distance in amplitude only a fraction of the beam size, we expect no significant distortion of the beam distribution.

With the parameters we have chosen, we find that for the beam-beam interaction, adiabatic conditions essentially do prevail--the adiabatic condition being

$$\bar{\Delta}_L \lesssim 2\pi \Delta_e \Delta_{NL}/\nu_s , \qquad (4.3)$$

where ν_s is the synchrotron wave number, and where it is understood that *(4.3)* represents an "order-of-magnitude" criterion.

Using the calculations for resonance excitation widths given in Ref. (12), we can give an example of the use of the foregoing expressions for a typical case. Take the 10th order resonance, with $\Delta_e = 10^{-3}\,\Delta_{bb}$. With $\Delta_{bb} = 5 \times 10^{-3}$, $\Delta_e = 5 \times 10^{-6}$. If we have the aperture at $\epsilon_{AP} = 10\,\epsilon_B$, *(4.2)* for $p = 10$ is $\Delta_e < 10^{-5}$. This means that for the 10th order resonance, the unstable fixed points are outside the aperture, but not by much. The implication of this is that if the beam-beam tune shift increases, and if Δ_{NL} remains the same, these unstable fixed points will enter the machine vacuum chamber. Thus, the aperture limit, or sink for particle loss, will occur inside the chamber. Of course, this is only a real limit on Δ_{bb} if we are forced to choose a tune in the vicinity of this resonance and if Δ_{NL} is not large enough.

We conclude that the group of parameters $\{\bar{\Delta}_L = 10^{-3}, \Delta_{NL} = 10^{-2}, \Delta_{bb} = 5 \times 10^{-3}, \nu_s = 1.39 \times 10^{-4}\}$ represents a consistent, stable set.

Because the transverse density varies along the bunch, the space charge tune shift is coupled to the synchrotron motion and therefore adds to the tune variation during synchrotron motion. The circular geometry implies no image contribution at the chamber center. We therefore have for the incoherent tune shift,[13]

$$\Delta\nu_{sc} = \left(\frac{I}{e}\right) \frac{r_p R}{\pi\nu f B \gamma^3} \frac{1}{b(a+b)} . \qquad (4.4)$$

With $I = 0.72$ A, $R = 428.2$ m, $\nu = 19.381$, $B^{-1} = 15.78$, $\gamma = 214.7$, $a = 0.43$ cm, $b = 0.39$ cm, we have $\Delta\nu_{sc} = 2.18 \times 10^{-5}$. This is negligible as a contribution to the range of tune through a synchrotron period.

Since we have stated both linear and nonlinear tune spreads, we must examine their consistency with stability against the transverse resistive wall instability.[14] Landau damping stabilization can be derived from linear and/or nonlinear tune spread. Note that the synchrotron frequency is sufficiently small that the linear tune and tune spread are well defined characteristics in the adiabatic sense and the latter provides an effective means of Landau damping. In this case, we can write two separate expressions for the required spread, one relating to image forces created in the chamber and the other dependent on the beam characteristics. Of course, both must be satisfied. We have, approximately, for the criterion dependent only on the image force,

$$\delta\nu > \frac{4 r_p R^{5/2}}{e\nu\gamma r^3} I \sqrt{\frac{2\epsilon_o \rho_e}{c|k-\nu|}} , \qquad (4.5)$$

where $\delta\nu$ is the full width of the betatron tune distribution, k is the azimuthal mode number ($k > \nu$), r is the chamber radius, ρ_e is the chamber resistivity (in ohm-m), and ϵ_o is the free space dielectric constant ($\epsilon_o = 10^{-9}/36\pi$ sec/ohm-m); while the beam dependent criterion is approximately,

$$\delta\nu > \frac{4 r_p R^2 I}{e\nu c \gamma^3 B b^2} , \qquad (4.6)$$

where b is the 1/2 beam size.

Take k = 20 (lowest mode), $\rho_e = 1.6 \times 10^{-8}$ ohm-m. (Aluminum), and $r = 4$ cm, then (4.5) gives at injection ($\gamma = 32$) $\delta\nu > 1.03 \times 10^{-4}$. At high energy, the criterion becomes $\delta\nu > 1.54 \times 10^{-5}$. For the beam dependent term, we require $\delta\nu > 2.88 \times 10^{-3}$ at injection; while at high field, the fall-off with γ is rapid, leading to the requirement $\delta\nu > 9.15 \times 10^{-5}$. Thus, the linear tune spread, $\bar{\Delta}_L = 10^{-3}$ will be more than adequate during storage. At injection, effective damping of the resistive wall instability will result if we combine the linear tune spread with the rather large nonlinear spread, $\Delta_{NL} = 10^{-2}$.

The head-tail instability[15] is stabilized (1) by having positive chromaticity and (2) by having sufficient nonlinear tune spread. Our design value, $\nu = +2.5$, stabilizes azimuthal oscillation modes up to the 8th at injection and higher at the final energy. The large nonlinear tune spread, $\Delta_{NL} = 10^{-2}$, means that the beam should be stable against the head-tail effect for all modes.

5. Conclusions

We have developed a set of parameters suitable for the operation of a bunched beam storage device for head-on proton-proton collisions. The use of superconducting magnets allows a high energy/circumference ratio as well as a high magnet aperture/power consumption ratio as compared to conventional magnet designs. With the AGS as injector, we can achieve a respectable luminosity with "single-turn" injection as a consequence of the high intensity, low transverse density AGS beam. At an energy of 200 GeV, and an average current of *0.72* A, our estimated beam-beam limited luminosity is 10^{32} cm^{-2} sec^{-1}. The beam-beam tune shift limit has been taken to be 5×10^{-3}. Acceleration from 30 to 200 GeV in *2.3* min can be obtained with a *27* MHz, *33* kV (peak) rf system with modest power dissipation.

Beam stability plays an especially important role in storage ring design. Various parameters, e.g. tune, chromaticity, nonlinear detuning and synchrotron frequency have been discussed in terms of their influence on beam stability. In particular, we have considered the longitudinal stability of the bunches, the phase area growth due to rf noise, the transverse resistive wall instability, the head-tail effect, and beam stability against nonlinear resonances, specifically those arising from the beam-beam interaction. We have found our proposal parameter set to be consistent with beam stability against these effects.

References

1. M. Month, BNL Informal Report, CRISP 73-20 (1973).
2. "The Design Study of Intersecting Storage Rings (ISR) for the CERN Proton Synchrotron", CERN Report AR/Int. SG/64-9 (1964).
3. "200-GeV Intersecting Storage Accelerators-ISABELLE", A Preliminary Design Study, BNL Report 16716 (1972); and subsequent revised edition, 1974, to be published.
4. M. Sands, Stanford University Report, SLAC-121 (1970).
5. The AGS parameters have been obtained privately from M.Q. Barton, J.C. Herrera, E.C. Raka and A. van Steenbergen.
6. M. Month, BNL Informal Report, CRISP 73-24 (1973).
7. M. Month, BNL Informal Report, CRISP 73-23 (1973).
8. F.J. Sacherer, Proc. 1973 Particle Accelerator Conference, San Francisco, p. 825, March 1973.
9. E. Hartwig, V.K. Neil, and R.K. Cooper, Proc. 1973 Particle Accelerator Conference, San Francisco, p. 833, March 1973.
10. See, for example: SPEAR Storage Ring Group, p. 752; and Orsay Storage Ring Group, p. 768, Proc. 1973 Particle Accelerator Conference, San Francisco, March 1973.
11. A. Schoch, CERN Report, CERN 57-23 (1958).
12. E. Keil, CERN Reports CERN/ISR-TH/72-7 and 72-25 (1972).
13. L.J. Laslett, Proc. 1963 Summer Study on Storage Rings at Super-High Energies, (J.W. Bittner, ed.), BNL Report 7534, p. 324 (1963).
14. L.J. Laslett, V.K. Neil and A.M. Sessler, Rev. Sci. Instrum. 36, 436 (1965).
15. C. Pellegrini, Frascati Report, LNF-69/45 (1969); M. Sands, SLAC Reports SLAC-TN-69/8, 69/10 (1969); and B. Zotter, CERN Report, CERN/ISR-TH/69-60 (1969).

INSERTIONS FOR COLLIDING-BEAM STORAGE RINGS

W.W. Lee and L.C. Teng
National Accelerator Laboratory*
Batavia, Illinois

Abstract

A new approach is presented for the design of the beam-collision straight sections of high-energy colliding-beam storage rings. Interchangeable special function lattice insertions are used to obtain local beam characteristics at the collision point to meet the requirements of individual experiments. Other insertions are used to adjust the phase advance and the orbit-length dispersion to optimize the performance of the rings. These insertions are modularized in length and matched to one another in optics and dispersion functions so that they can be inserted or joined together with maximum flexibility. Examples are given for 1000 GeV-1000 GeV superconducting magnet proton storage rings.

Introduction

The magnet rings of colliding-beam storage rings can be considered as being composed of two types of sections serving different functions. These can roughly be identified as the inactive curved sections and the active straight sections. In straight sections beams are injected and made to collide, and experiments are performed. Curved sections serve only to transport the beams from one straight section to the next. The design of the inactive curved sections is based only on beam stability and economy, and is generally the concern of the accelerator builders alone; whereas the design of the active straight sections is crucial to both the builders and the users.

The conventional procedure for designing the straight sections is to first assemble the builders and the users in study sessions. Plans of all conceivable colliding-beam experiments are made. Each straight section is designed for one or a group of these hypothetical experiments. These straight sections are then incorporated as integral parts of the magnet lattice of the storage rings. In contrast, for conventional experiments using the external beam from an accelerator, because of the flexibility in the interposing beam lines the design of specific experiments have much less influence on the design of the magnet lattice. We suggest here a parallel interpretation of colliding-beam experiments which restores to some degree the decoupling between the machine and the experiments and leads to a different approach for design of the straight sections in storage rings.

When the beam in a storage rings exits from a curved section it can be considered as having been extracted from the machine. A tailor-made line is provided to transport the "external" beam to the experimental target (the collision point) for the specific experiment. After going through the very thin target (the other beam) the beam unaffected by the target is transported "back" by another tailor-made beam line to be reinjected and recirculated in the following curved section. The design approach suggested by this interpretation consists in modularizing and specializing segments (insertions) of the straight-section ("external") beam lines of storage rings in such a way that all segments are mutually matched and hence mutually interchangeable, Specific modules are joined together to transport the beams to the Collision point with the characteristics appropriate to the specific experiment. Other appropriate modules joined together then transport the beam onward to the next curved section properly matched for recirculation. In this manner the flexibility in the external beam lines of an accelerator could, to a large extent, be retained for the straight-section beam lines of storage rings. The parallelism is broken only by the needs of recirculation which impose the following additional constraints on the straight-section beam lines for storage rings:

(a) For an accelerator the length of the external beam line is to some extent flexible. For storage rings the length of the straight-section beam line constrained between curved sections is fixed.

(b) The phase advance in the transport line which is of little consequence for the external beam of an accelerator must be considered for the straight-section beam lines of storage rings.

(c) We need a standard recirculating line which simply transports the beam across a straight section and properly matched for recirculation without "targeting" for experiments.

(d) Since the target is the other beam the same consideration of matching and recirculation applies also to the "target" beam.

Examples

To demonstrate the practicality of this approach we will use as an example two 1000-GeV proton colliding-beam storage rings using superconducting magnets. In each ring the curved sections are composed of 100 curved separated-function FODO cells each 60 m long and having a phase advance of 90°. The parameters of such a cell are given in Fig. 1. The curved sections of the two rings are assumed to be stacked one above the other with a vertical separation of 0.3 m between beams. In or near the beam-collision point it is likely that some quadrupoles will be used in common by both beams. These quadrupoles will have opposite focal actions on the two beams traveling in opposite directions. Thus, the

*Operated by Universities Research Association, Inc. under contract with the U.S. Atomic Energy Commission.

simplest lattice arrangement is such that all adjacent quadrupoles between the two rings have opposite focal actions on the two beams, hence the same field-gradient polarity.

As initial steps in the development of this approach we assume:

(a) The simplest standard recirculating line would consist of straight cells formed by leaving out the dipoles in the curved FODO cells. A series of a multiple of 4 of these straight cells would have unity transfer matrices in both the horizontal and the vertical planes and would hence match both optics and dispersion. The straight-section length could therefore be 240 m, 480 m, etc.

(b) The lengths of the modular insertions should be multiples of the half-cell length of 30 m. Since the length of the straight sections is fixed insertions should be kept as short as possible.

(c) As standard transport elements for the straight-section beam lines we will use 1.1 m quadrupoles and 6.2 m dipoles. These turn out to be convenient choices of lengths. The currents in these magnets are adjusted to give the required strengths in the same manner as for transport elements in external beam lines of accelerators.

(d) Although not demanded in principle, matching for recirculation would be greatly simplified if the phase advances in the horizontal and the vertical planes are identical in all insertions. This is automatically guaranteed by making all insertions antisymmetric such that the two planes are longitudinal reflections of each other.

We now give a few examples of specific insertions. Optics and dispersion matching is obtained by first using the "thin" version of the computer program MAGIC' in which all magnet elements are assumed to be of zero length. The results are then used as trial input to the "thick" version of the program to give the final physical parameters. For simplicity, when several standard transport elements must be strung together to give the required strength we have not included the short drift spaces between the elements necessary to accommodate the end structures and connections.

A. Dispersion Modifying Insertion

As examples we give here two zero-dispersion insertions (dispersion function = η = 0) which reduce the horizontal dispersions at the ends of curved sections to zero. If the curved section ends in an F quadrupole where the dispersion is large the insertion would have to be 2 cells in length and look like that shown in Fig. 2. Four 24.67 mrad dipoles introduced into the normal straight cells produce a local horizontal orbit displacement of 0.740 m and a horizontal dispersion to cancel that from the curved section. There does not seem to be any advantage in modifying the optics by rearranging the quadrupoles. If the curved section ends in a D quadrupole where the dispersion is small the insertion could be reduced to 1½ cell long by first modifying the optics in the insertion (still matched to that of normal cells at the ends) and then introducing four 12.44 mrad dipoles. The local orbit displacement is reduced to 0.228 m. This insertion is shown in Fig. 3. Identical insertions would be used in reverse at the downstream end of the straight sections to rematch dispersion for recirculation.

Conventionally, zero dispersion in the straight section is obtained by modifying the ends of the curved sections as an integral part of the ring lattice. These insertions illustrate the basic departure of the present approach. They can be inserted or withdrawn freely without affecting the operation of the ring.

B. Beam-Size Modifying Insertion

As an example we show in Fig. 4 a low-β insertion (β = amplitude function). This insertion is conventional except that it is antisymmetric, matched to the normal cell optics at the ends, and has a length modularized to 2½ cell lengths. The 8-value β^* at the central collision point is 1 m in both planes. The total free drift space on either side of low-β point is 25 m long. The free drift-space length could be substantially increased for higher low-β values. For extremely long drift spaces the insertion would be 3½ cells in length. Presumably several insertions with different β^* values (including high-β values) would be needed.

C. Phase Adjusting Insertion

To make it possible to freely interchange insertions having different phase advances we need an insertion with a phase advance which is adjustable over a wide range. Evidently this insertion would be used to adjust the betatron tune of the ring. In other cases one may also use it to adjust the phase advance across a single straight section to a desired value. An example of this insertion which is antisymmetric and matched to the normal cell optics is shown in Fig. 5. The phase advance is adjustable from 100° to 300°. The field-gradient settings of the quadrupoles are plotted against the phase advance. It should be possible to program these curves into the control computer so that the phase advance can be adjusted by turning a single knob.

D. Orbit-Length Dispersion Adjusting Insertion

This is an obvious companion to the phase adjusting insertion. To be useful the insertion should be rather long. The simplest would be a 4-cell long antisymmetric insertion with 360° phase advance. By varying the field-gradients of the quadrupoles but keeping the phase advance at 360° one can very the orbit-length dispersion $\frac{\Delta \ell}{\ell} / \frac{\Delta p}{p}$ without affecting the optics and dispersion matching at the ends. No example is given for this simple insertion. The utility of this insertion is less obvious than that of the phase adjusting insertion, but clearly it could be used to adjust the transition energy of the ring.

E. Beam Crossing ("Targeting") Insertion

The beams traveling in opposite directions in the two rings stacked one on top of the other are separated by 0.3 m. These two beams can be displaced vertically to come together to collide head on in a half-cell by three vertical dipoles as shown in Fig. 6. These dipoles must have a vertical good field aperture of more than 50 mm. It is likely that the standard transport dipoles turned vertical would have an adequate aperture. Several remarks should be made for this insertion.

(1) This insertion is generally followed by a beam size modifying insertion. The vertical dipoles in this insertion should be trimmed to give the appropriate small beam separation and angle at the entrance to the following insertion such that the beams would cross each other at the proper location (e.g. the low-β point) and at the desired small angle. Furthermore, the vertical dipoles could easily have an adequate trimming range to accommodate either the cross-over geometry (the upper beam becomes the lower beam in the following curved section) or the no-cross-over geometry.

(2) The small vertical dispersion introduced by the vertical bends will make the distance over which the beams collide longer hence extending further away from the low-β point. The resulting reduction in luminosity is generally quite small, especially if the horizontal dispersion is made zero in the collision region.

(3) This short insertion occupying only a drift space is not a true insertion in the dispersion-optical sense. In some cases it can be merged into the ends of other insertion, i.e. the vertical dipoles can be placed in a drift space of adequate length in any insertion.

With the sample insertions given above we can now put together an example of a complete straight-section beam line. To get the maximum luminosity we would want zero-dispersion and low-β at the beam-collision ("targeting") point. This could be obtained from the string of insertions shown in Fig. 7. The total length is 7½ cells or 450 m.

Similar exercises in putting together other complete straight-section beam lines indicate that a straight-section length of 4 cells or 240 m (in 1000-GeV storage rings) is too short for full exploitation of the flexibility inherent in this scheme. A straight-section length of 8 cells (480 m) or greater would be more appropriate. This study also shows that the straight-section length should be measured in terms of the betatron oscillation wave length in the curved section which is in turn governed by the available dipole and quadrupole strengths for the specified beam energy. One wave length is too short, two or more wave lengths would be adequate.

An obvious criticism for this design approach is that the flexibility is bought at the expense of longer straight sections. However, comparison with conclusions of design studies for Isabelle and PEP indicates that, in fact, the additional length required is rather small. Recalling the parallelism invoked in the Introduction we observe further that even with the slightly longer length these straight-section beam lines are much shorter than the conventional external beam lines of an accelerator at the same energy. This parallelism also provides a basis for the choice of the number of straight sections. Accelerator facilities in which experiments are performed mainly in external beams typically have 4-6 external beam lines. A similar number of straight sections in a colliding-beam storage ring facility is thus appropriate.

References

1. M.J. Lee, W.W. Lee and L.C. Teng, "Magnet Insertion Code (MAGIC)", Note-61, 1973 PEP Summer Study Report (1973).

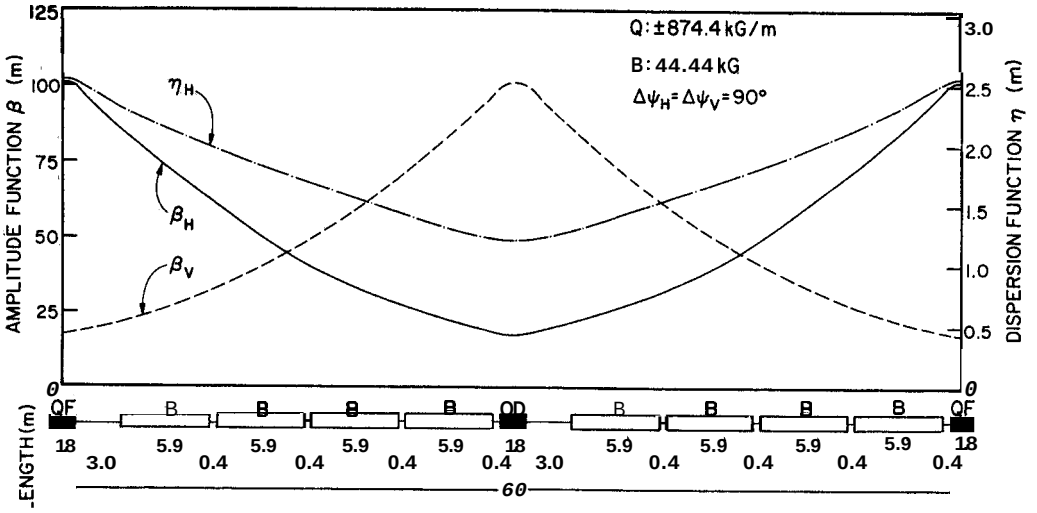

Figure 1. Normal curved cell

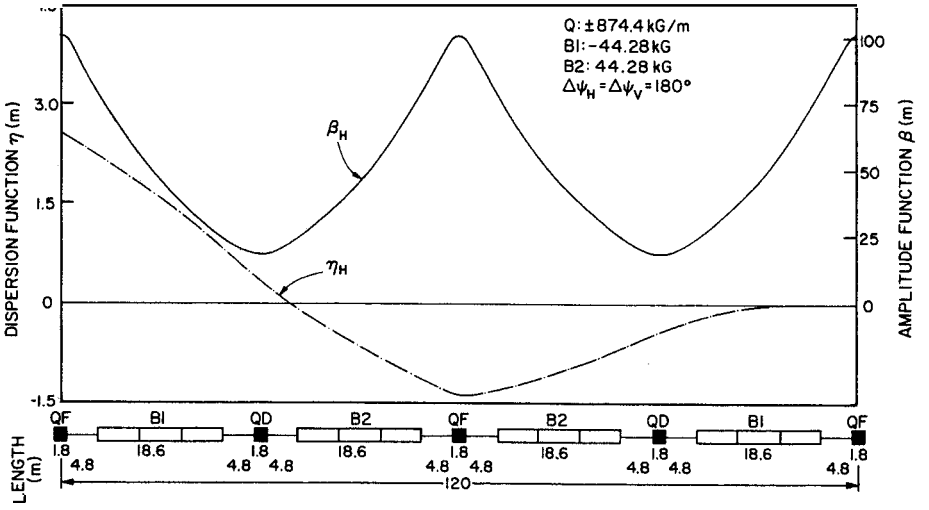

Figure 2. Zero-dispersion insertion (F type)

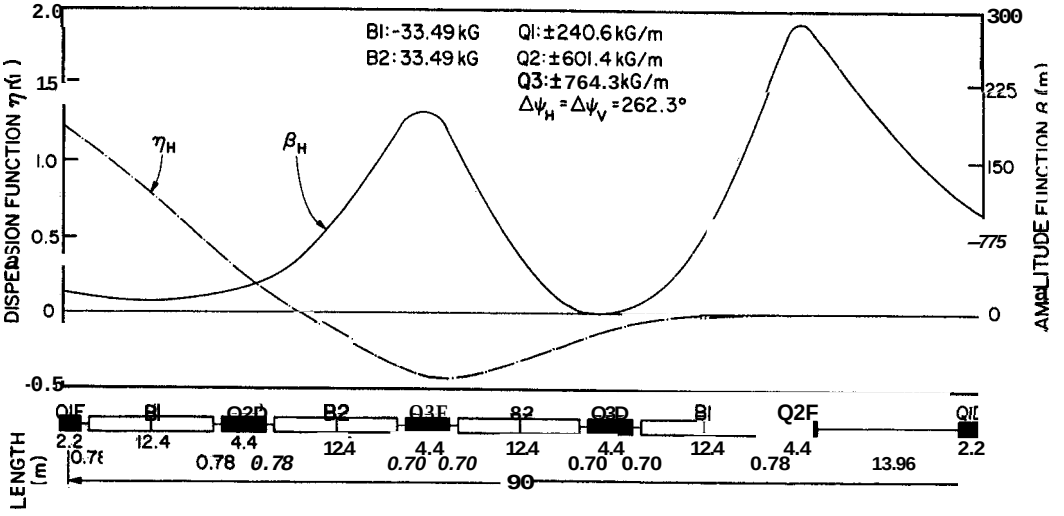

Figure 3. Zero-dispersion insertion (D type)

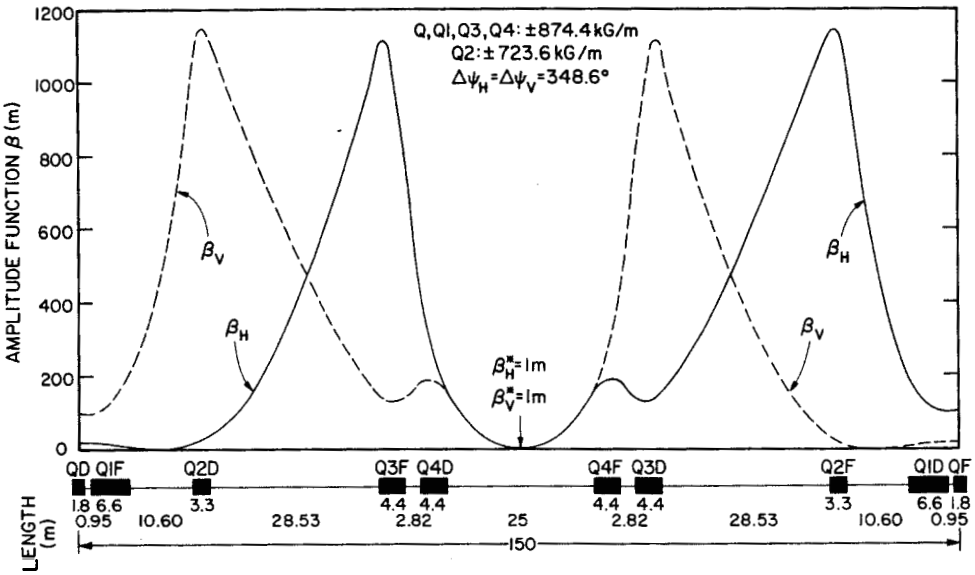

Figure 4. Low-β insertion

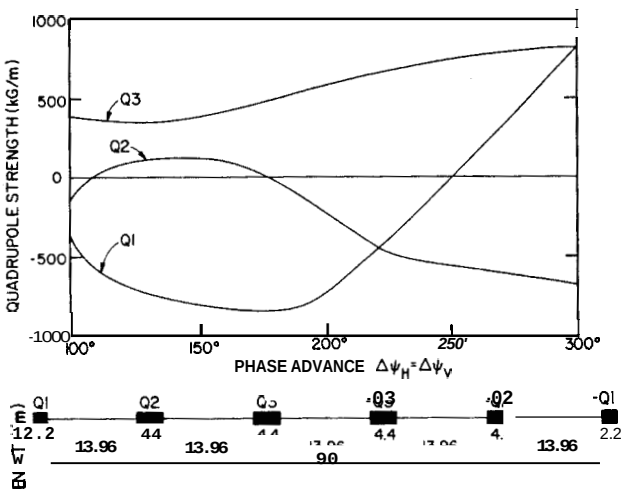

Figure 5. Phase adjusting insertion

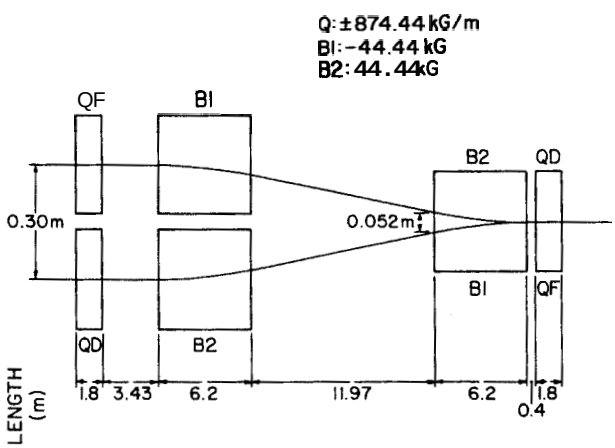

Figure 6. Beam crossing insertion

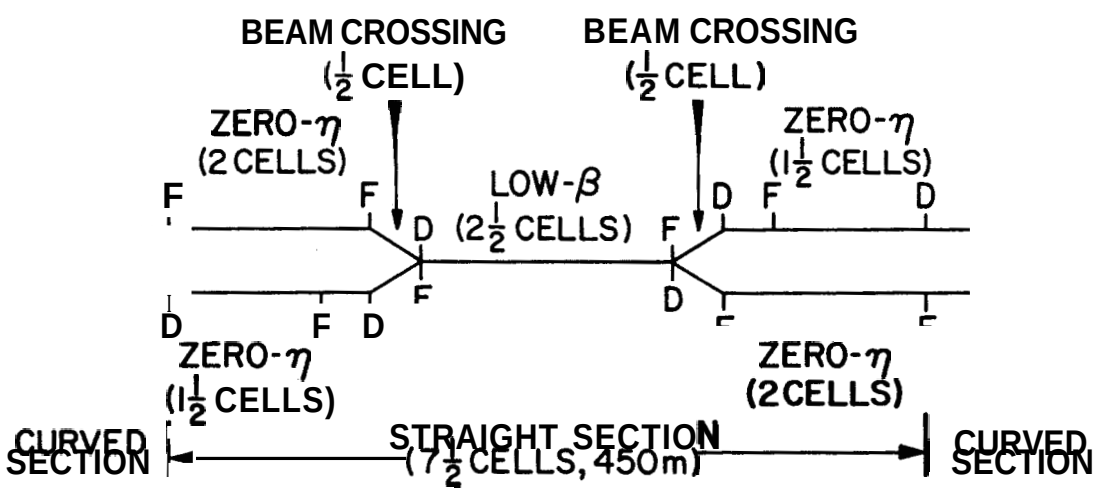

Figure 7. High luminosity straight section

-RESONANCE CROSSING IN A PROTON SYNCHROTRON; APPLICATION TO ISABELLE*

R. Chasman
Brookhaven National Laboratory
Upton, New York

A. Garren
Lawrence Berkeley Laboratory
Berkeley, California

R.L. Gluckstern
University of Massachusetts
Amherst, Massachusetts

and

F.E. Mills
National Accelerator Laboratory
Batavia, Illinois

Summary. We have investigated the effect on the transverse properties of a beam in the presence of a nearby nonlinear resonance, periodic variation of the betatron tune as a result of synchrotron oscillations leading to periodic resonance crossing, and a zeroth harmonic octupole term (or other multipole) which makes the betatron frequency depend on transverse amplitude. Depending on whether the product of the resonance strength and the zeroth harmonic octupole component is small or large, one gets one of the following two pictures for fast resonance crossing: a) A pattern of resonances and side bands the side bands being separated by ν_s/n (ν_s is the synchrotron frequency, n the order of the resonance). Detailed consideration of the betatron phase change between consecutive crossings leads to prediction of an odd-even dependence of the beam growth on the side band number. Computer runs yield phase-space trajectories which confirm these predictions in detail. b) A diffusion-like process, the betatron tune shift between crossings resulting from the amplitude change now being larger than the spacing of side bands. The diffusion picture also holds whenever ν_s/n is smaller than the betatron tune stability. These effects are observed in computer runs and lead to design tolerances for the resonance terms. When nonlinearities are present that are larger than these tolerances, azimuthally distributed multipoles have to be introduced to tune out the resonances. The multipole distributions required to do so have been calculated.

Introduction

In a proton storage ring accelerator such as ISABELLE~large currents (~ 10 A) are accelerated for times of the order of minutes. The beam must have a spread both in momentum and betatron frequency to stabilize against longitudinal and transverse instabilities. The spread in betatron frequency is achieved by a momentum dependent ν-value or chromaticity. Under these conditions the w-value of individual particles will vary periodically with time while the beam is accelerated, as a result of synchrotron oscillations. This leads to repeated crossings of those nonlinear resonances included in the particles v-swing. During acceleration the excitation of nonlinear resonances is due primarily to magnet imperfections because the beams in the two rings are separated and the relatively Large nonlinear effects originating in beam-beam interaction are absent.

The present paper deals with the transverse beam behavior under the following conditions: a) A nearby single nonlinear resonance, due to magnet nonlinearities, b) periodic variation of the betatron tune as a result of synchrotron oscillations leading to periodic crossing of the nonlinear resonance, c) a zeroth harmonic octupole term which makes the betatron frequency depend on the transverse amplitude.

Several authors[2,3] have dealt with the transverse motion of particles under similar conditions. However, their treatments are generally limited to a single synchrotron period and fail to make detailed predictions for the transverse beam behavior resulting from many repeated resonance crossings. In this paper, theory and computer simulations have been extended to cover many synchrotron periods. All calculations are one-dimensional, but a generalization to both transverse dimensions is straightforward. Fast crossings only (see below) have been considered.

Theory

General Case

The one-dimensional equation of the betatron motion of a particle in a nonlinear perpendicular field B in a synchrotron is given by:

$$\frac{d^2x}{ds^2} + K(s)x = \frac{1}{\rho}\left(b_2x^2 + b_3x^3 + b_4x^4 + \ldots.\right) \qquad (1)$$

Here $B = B_0(1 + b_1x + b_2x^2 + b_3x^3 + b_4x^4 + \ldots.)$, K(s) includes the linear part of B and ρ is bending radius. Introducing the variables $\eta = \beta^{-\frac{1}{2}}x$ and $\sigma = \frac{1}{\nu}\int ds/\beta$ one gets[4]:

$$\frac{d^2\eta}{d\sigma^2} + \nu^2\eta = \frac{\nu^2\beta^{3/2}}{\rho}\sum_{n=3,\ldots} b_{n-1}\beta^{(n-1)/2}\eta^{n-1}$$

where β is the Courant-Snyder β-function and ν is the betatron tune.

An additional transformation to amplitude phase variables I and φ given by $I = \eta'^2/\nu^2 + \eta^2$, $\varphi = -\arctg \eta'/\nu\eta$ (or $\eta = \sqrt{I}\cos\varphi$, $\eta' = -\sqrt{I}\nu\sin\varphi$) yields

$$I' = -\frac{2\sqrt{I}\nu\sin\varphi}{\rho}\sum_{n=3,\ldots} b_{n-1}\beta^{(n+2)/2}\eta^{n-1}$$

$$\varphi' = \nu - \frac{\nu\cos\varphi}{\rho\sqrt{I}}\sum_{n=3,\ldots} b_{n-1}\beta^{(n+2)/2}\eta^{n-1}\ .$$

One can set $\eta = \sqrt{I}\cos\varphi$ on the right-hand side of these expression and gets:

Work performed under the auspices of the U.S. Atomic Energy Commission.

$$I' = -\frac{2\nu}{\rho}\sin\varphi \sum_{n=3,\ldots} b_{n-1}\beta^{(n+2)/2} I^{n/2}\cos^{n-1}\varphi$$

$$\varphi' = \nu - \frac{\nu}{\rho}\cos\varphi \sum_{n=3,\ldots} b_{n-1}\beta^{(n+2)/2} I^{(n-2)/2}\cos^{n-1}$$

Near an isolated nonlinear resonance of order n, $\nu = r/n + \Delta_o$ where r is an integer and $\Delta_o \ll 1/n$. Fourier analyzing the nonlinear field coefficients $b_i = \Sigma b_{ir}\cos r(\theta + \theta_r)$, keeping only the octupole zeroth harmonic component and neglecting rapidly oscillating terms one obtains in the smooth approximation with $\beta = R/\nu$ and $\sigma = \theta$ (R is the average radius of the machine, θ the regular length):

$$I' = -\frac{2\nu}{}\left(\frac{R}{}\right)^{(n+2)/2} I^{n/2}\sin[n\varphi - r(\theta+\theta_-)]$$

$$\varphi' = \nu - \frac{\nu}{2^n\rho}\left(\frac{R}{\nu}\right)^{(n+2)/2} b_{n-1,r} I^{(n-2)/2}\cos[n\varphi - r(\theta+\theta_r)].$$

Substituting $\chi = n\varphi - r(\theta+\theta_r)$, $B_n = -\nu/(2^n\rho)(R/\nu)^{(n+2)/2} b_{n-1,r}$ and $A = -(3\nu/8\rho)(R/\nu)^3 b_{3,0}$ one finally gets:

$$I' = 2B_n I^{n/2}\sin\chi \qquad (2a)$$

$$\chi' = (n\nu - r) + nAI + nB_n I^{(n-2)/2}\cos\chi \,. \qquad (2b)$$

For a constant betatron tune these equations lead to the usual invariant of motion for a nonlinear resonance. Fixed points are obtained from $I' = 0$, $\chi' = 0$. The nonlinear resonance widths are given by $\pm B_n I^{(n-2)/2}$. In the appendix, a Hamiltonian, valid for any order resonance, is derived from which Eq. (2) can be obtained. More exact expressions for B_n and A are also given.

The θ-dependence of ν will be written as

$$\nu(\theta) = \frac{r}{n} - \frac{\Delta}{n}(\cos\nu\theta - \cos\nu_s\theta_o) \,,$$

where $A > 0$, Δ/n is the half-swing of the betatron frequency ν and ν_s is the synchrotron frequency. Δ_o/n, defined as $\Delta/n\cos\nu_s\theta_o$, is the difference between the average frequency $r/n + \Delta/n\cos\nu_s\theta_o$ and the resonance frequency r/n. $\nu(\theta)$ will be equal to r/n whenever $\theta = \pm\theta_o + 2j(\pi/\nu_s)$ where j is any integer and $0 \le \nu_s\theta_o \le \pi$.

Setting $\chi_\pm = \chi(\pm\theta_o)$, where χ_+ and χ_- are the values of χ at the upward and downward resonance crossings, one has near $\theta = \pm\theta_o$:

$$\chi = \chi_\pm + \chi''_\pm \frac{(\theta \mp \theta_o)^2}{2}$$

Assuming the condition for fast crossing in which $n\nu$ varies much more rapidly than the two other terms, nAI and $nB_n I^{(n-2)/2}\cos\chi$, on the right-hand side of Eq. (2b), one can write $\chi'' = \nu_s\Delta\sin\nu_s\theta$, $\chi''_\pm = \chi''(\theta_\pm) = \pm\nu_s\Delta\sin\nu_s\theta_o$. The change ΔI and $\Delta\chi$ in I and χ during one synchrotron period (assuming AI is small) are then obtained from Eq. (2) in the following way:

$$\Delta I = 2B_n I^{n/2}\left[\int_{-\infty}^{\infty}\sin\left[\chi_+ + \chi''_+\frac{(\theta-\theta_o)^2}{2}\right]d\theta + \int_{+\infty}^{\infty}\sin\left[\chi_- + \chi''_-\frac{(\theta+\theta_o)^2}{2}\right]d\theta\right] .$$

$$\Delta\chi = (\Delta_o + nAI)\frac{2\pi}{\nu_s} + nB_n I^{(n-2)/2}\left[\int_{-\infty}^{+\infty}\left[\chi_+ + \chi''_+\frac{(\theta-\theta_o)^2}{2}\right]d\theta + \int_{+\infty}^{-\infty}\cos\left[\chi_- + \chi''_-\frac{(\theta+\theta_o)^2}{2}\right]d\theta\right] .$$

Evaluation of the integrals in the expressions of AI and $\Delta\chi$ leads to

$$\Delta I = 4CB_n I^{n/2}\cos\left(\frac{\chi_+ - \chi_-}{2} + \frac{\pi}{4}\right)\sin\frac{\chi_+ + \chi_-}{2}$$

$$\Delta\chi = (A + nAI)\frac{2\pi}{\nu_s} + 2CB_n I^{(n-2)/2}\cos\left(\frac{\chi_+ - \chi_-}{2} + \frac{\pi}{4}\right)\cos\frac{\chi_+ + \chi_-}{2} .$$

where $C = \sqrt{\dfrac{2\pi}{\nu_s A \sin\nu_s\theta_o}}$.

Noticing that $\Delta\chi_+ = \Delta\chi_- = \Delta\chi$, one can go to a new variable $\bar{\chi} = (\chi_+ + \chi_-)/2$, leading to

$$AI = 4CB_n I^{n/2}\cos\left(\frac{\chi_+ - \chi_-}{2} + \frac{\pi}{4}\right)\sin\bar{\chi} \qquad (3a)$$

$$\Delta\bar{\chi} = (\Delta_o + nAI)\frac{2\pi}{\nu_s} + 2CB_n I^{(n-2)/2}\cos\left(\frac{\chi_+ - \chi_-}{2} + \frac{\pi}{4}\right)\cos\bar{\chi} \qquad (3b)$$

I and $\bar{\chi}$ get impulses at $\theta = \pm\theta_o + 2\pi j/\nu_s$. One can therefore write $I'(\theta)$ in the following way:

$$I'(\theta) = 2\frac{\nu_s}{2\pi}CB_n I^{n/2}\sum_{j=-\infty}^{\infty}\left\{\sin\left[\chi_+^i + \frac{2\pi j}{\nu_s}\Delta_o + \alpha(\theta) + \frac{\pi}{4}\right]\delta\left(\theta - \theta_o - \frac{2\pi j}{\nu_s}\right) + \sin\left[\chi_-^i + \frac{2\pi j}{\nu_s}\Delta_o + \alpha(\theta) + \frac{\pi}{4}\right]\delta\left(\theta + \theta_o - \frac{2\pi j}{\nu_s}\right)\right\} .$$

Here χ_+^i and χ_-^i are the initial values of χ_+ and χ_-, $\alpha'(\theta) = nAI + nB_n I^{(n-2)/2}\cos\chi$ and $\alpha(\theta) = \int_o^\theta \alpha'(\theta)d\theta$. After some manipulation of the δ-functions one finally gets with $F_j = \cos[(\chi_+^i - \chi_-^i)/2 + \pi/4 - (\Delta_o - \nu_s j)\theta_o]$:

$$I'(\theta) = 4\frac{\nu_s}{2\pi}CB_n I^{n/2}\sum_j F_j\sin[\bar{\chi}^i + (\Delta_o - \nu_s j)\theta + \alpha(\theta)] . \qquad (4a)$$

Similarly it can be shown that

$$\bar{\chi}'(\theta) = \Delta_o + nAI + 2\frac{\nu_s}{2\pi}CB_n I^{(n-2)/2}\sum_j F_j\cos[\bar{\chi}^i + (\Delta_o - \nu_s j)\theta + \alpha(\theta)] . \qquad (4b)$$

Side Band Approximation

In the case that $\Delta_o = \nu_s\ell + \varepsilon$, where $\varepsilon \ll \nu_s$ and $\alpha'(\theta) \sim$ const, the term with $j = \ell$ in Eq. (4a and b) will always be the slowest varying one, permitting the neglect of the other more rapidly oscillating terms. With the additional transformation $\Phi = \bar{\chi} + \nu_s\ell\theta$, one gets:

$$I' = 4\frac{\nu_s}{2\pi}CB_n I^{n/2}F_\ell\sin\Phi \qquad (5a)$$

$$\Phi' = (\Delta_o - \ell\nu_s) + nAI + 2\frac{\nu_s}{2\pi}CB_n I^{(n-2)/2}F_\ell\cos\Phi \,. \qquad (5b)$$

These equations are now identical in form to those which were obtained earlier for $\nu(\theta) = \text{const}$ (see 2a and b) with the exception that $(\nu - r/n)$ has been replaced by $\Delta_o - \ell\nu_s$ and B_n by $2(\nu_s/2\pi)CB_nF_\ell$. Varying the betatron tune with the synchrotron frequency hence causes the resonance at $\nu = r/n$ to be replaced by a series of resonances (or side bands) at $\nu = r/n + \nu_s\ell/n$ where *d* is any

integer. The width of these resonances are $\pm 2(\nu_s/2\pi)$ $CB_nF_\ell I^{(n-2)/2}$ compared to $B_nI^{(n-2)/2}$ obtained at $\nu=r/n$ in the case of $\nu(\theta)$ = const. In the side approximation then the particle motion will follow invariants in I,Φ phase space given by

$$\text{Const.} = (\Delta_o - \ell\nu_s)I + \frac{nAI^2}{2} 2\frac{\nu_s}{2\pi} CB_nF_\ell I^{n/2} \cos\Phi \quad . \qquad (6)$$

Fixed points are obtained from $I' = 0$, $\Phi' = 0$. The dependence of the side band width $\pm 2(\nu_s/2\pi)$ $CB_nF_\ell I^{(n-2)/2}$ on the side band order ℓ is contained in $\sin \nu_s\theta_o$ and Fg. While $\sin \nu_s\theta_o$ varies monotonically with ℓ, F_ℓ exhibits an odd-even dependence for side bands near—the central resonance, which comes from the fact that γ changes by $\sim \pi/2$ when ℓ changes by 1.

Diffusion Approximation

The assumption used to obtain the side band picture was $\alpha'(\theta)\approx$const, where $\alpha'(\theta)=nAI+nB_nI^{(n-2)/2}\cos\chi$. If $\Delta\alpha'(\theta)$ the change in $\alpha'(\theta)$ over one synchrotron period, is comparable to ν_s, then terms with different j's will dominate in the sums in Eq. (4a and b) at different values of θ and one cannot approximate these sums by the same $j=\ell$ term at all values of θ. To first order in $B_nI^{(n-2)/2}$, $\Delta\alpha'(\theta)\approx nA\Delta I$. Taking ΔI from Eq. (3a) one gets that $\Delta\alpha'(\theta)\ll\nu_s$ implies $|4ACB_nI^{n/2}|\ll\nu_s$ and one expects that the side band picture should no longer be valid if $|4ACB_nI^{n/2}|\gtrsim\nu_s$. In order to see how the amplitude I will vary with θ or (time) in this regime one has to go back to Eq. (3a) which gives the change in I over one synchrotron period. If one assumes that will now vary randomly with θ (or time) one gets a diffusion-like rms-type growth of I expressed by: $dI^2/dt = (\Delta I)^2\nu_s/T_{rev}$, where T_{rev} is the revolution time around the machine and $(\Delta I)^2$ is the average value of $(\Delta I)^2$. One obtains for the doubling time t_d for the rms value of I:

$$t_d = \frac{\alpha_n \Delta T_{rev}}{8B_n^2 I_o^{n-2}\pi} \qquad (7)$$

where $\alpha_n = \frac{4^{1-n/2} - 1}{1 - n/2}$ and I_o is the initial value for I.

As can be seen from Eq. (7) t_d is independent of the synchrotron frequency and the zeroth harmonic octupole component and inversely proportional to the square of the resonance width. However, ν_s and A (or $b_{3,0}$) enter into the condition $|4ACB_nI_o^{n/2}|\gtrsim\nu_s$ under which diffusion-type emittance growth can occur.

Computer Calculations

Computer calculations have been performed aimed at testing the theoretical predictions for the transverse beam behavior presented in the previous section. Some results obtained in these simulations will be given below.

The transverse particle motion corresponding to a single machine revolution was calculated by a linear transformation followed by a nonlinear kick. The ν-value entering the linear transformation, varied with time with the synchrotron frequency and was shifted by an amount $-(3\nu/8\rho)(R/\nu)^3 b_{3,0} I$, where I is the particle amplitude.

The following parameters were kept fixed in all computer runs: R = 382 m, ρ = 167 m, A/n = 0.03 and ν_s = 0.001. The resonance betatron tunes were kept close to 21.

Figures 1 through 4 refer to a third order resonance. In Fig. 1 particle trajectories in I, Φ space are shown for four different average betatron tunes corresponding to $\nu = 1/3(r + \ell\nu_s)$ where r = 62 and ℓ = 0,1,2 and 3. The zeroth harmonic octupole component is small and the side band picture should hold. The trajectories clearly follow invariants of the form given in Eq. (6). This figure also exhibits the odd-even dependence of F_ℓ on ℓ, which was mentioned earlier, and the amplitudes corresponding to the stable fixed points agree well with theory. Similar trajectories are shown in Fig. 2 for different average betatron tunes slightly off the central band and again seem to verify the predictions expressed in Eq. (6).

In Fig. 3 the amplitude of a single particle is plotted as function of revolution number for different values of the zeroth harmonic octupole component $b_{3,0}$. The initial amplitude is 2×10^{-6} m in all runs. When $b_{3,0}$ is small the particle amplitude varies periodically with time as can be expected from the phase-space trajectories shown in Figs. 1 and 2. However, when the $b_{3,0}$ is increased, the simple periodic time dependence deteriorates and a more random behavior sets in, indicating that the side band picture no longer holds. The necessary condition, stated earlier in this paper for the side band model to be valid was $|4ACB_nI^{n/2}| \ll \nu_s$. With the numerical values used here this is equivalent to $|b_{3,0}| \ll 10\ m^{-3}$, in good agreement with the results shown. In Fig. 4 the rms amplitude of 10 particles starting out with $I = 2 \times 10^{-6}$ m but different values of $\bar{\chi}$ is plotted as function of revolution number under similar conditions. When $b_{3,0}$ is small the rms amplitude fluctuates with time but no growth pattern can be seen. For large octupole components the diffusion picture predicts an amplitude doubling time of 1.4 sec, corresponding to 175 000 revolutions. This is in fair agreement with the numerical results shown here for a statistical sample of only 10 particles.

Results obtained with a fifth order resonance are contained in Figs. 5 and 6. Particle trajectories in the I, Φ phase plane, obtained with a small zeroth harmonic octupole component, are shown in Fig. 5 for three different average betatron tunes, $\nu = 1/5(r + \ell\nu_s)$, corresponding to r = 104 and ℓ = 0,1 and 2. The odd-even dependence of the factor Fg entering into the expression for C in Eq. (6) is again obvious. For the conditions referring to Fig. 5 an unstable fixed point exists, but it occurs at an amplitude above the range of I included there. Figure 6 shows the rms amplitude of 10 particles as function of revolution number for a small and large value of $b_{3,0}$. As in the case of a third order resonance, no steady rms amplitude growth can be seen for the small zeroth harmonic octupole term while a diffusion-type growth shows up when this term becomes large. Again, the amplitude doubling time is within the range of theoretical predictions.

Discussions of Results and Application to ISABELLE

Both theoretical and numerical calculations presented in this paper indicate that fast crossing of nonlinear resonances with an amplitude dependent betatron tune leads to two different patterns of transverse beam behavior.

When the effective betatron tune (including the amplitude dependent part) is constant within a range small compared to ν_s/n, particles move along phase-space trajectories predicted by a simple resonance theory involving side bands. For a given nonlinear resonance strength one can then limit the transverse beam growth by adjusting both the distance of the average Linear betatron tune to the nearest side band and the strength of the zeroth harmonic octupole component. In the case that the variation of the effective betatron tune is of the order ν_s/n and more, the beam no longer follows the resonance pattern. A diffusion-like emittance growth sets in, which one should be able to avoid by resonance compensation.

In an ideal machine, where the average linear betatron tune is constant, the variation of the effective ν-value comes from its amplitude dependent part. One then gets diffusion-like behavior only when a large zeroth harmonic octupole (or other multipole which makes the betatron frequency depend on transverse "amplitude") component exists. Nonideally, however, there most probably will be a variation in the average linear betatron tune and for small values of ν_s one will have beam growth even in the absence of strong octupoles. Computer results, not shown here, confirm this.

In ISABELLE ν_s is of the order of 10^{-5} and, even with weak octupoles, one might get diffusion-like beam growth from nonlinear resonance crossings. The emittance doubling times have been calculated from Eq. (7) for different order resonances assuming the nonlinearities that are to be expected in the ISABELLE magnets. The results are given in the following table together with the nonlinear field coefficients:

n	b^r_{n-1}	t_d(sec)
3	0.005 m^{-2}	0.58
4	0.095 m^{-3}	680
5	1.7 m^{-4}	7.4×10^5
6	31.2 m^{-5}	1.0×10^9
7	521 m^{-6}	2.8×10^{12}

For an acceleration time of a few minutes nonlinear resonances of the order 5 and higher appear harmless. The third and fourth integral resonances can be avoided by proper placement of the working line and no resonance compensation seems to be required.

Acknowledgments

The authors wish to thank Dr. Lloyd Smith for valuable discussions regarding resonance compensation.

Appendix

Equations for Transverse Motion in Angle-Action Variables with Resonant Perturbations when the Tunes Vary Due to Synchrotron Oscillations

For completeness we include a derivation of the equations for amplitude and phase in the vicinity of a single resonance that, we believe, clarifies the proper arguments to use in thetrigonometric functions of the relevant Fourier coefficients, and that takes account of the slow variation of the tunes due to the synchrotron oscillations. The treatment applies to any resonance, horizontal, vertical, or coupled.

We start with a Hamiltonian for the motion of x,z, $p_x = dx/ds$, $p_z = dz/ds \equiv x_1, x_2, p_1, p_2$ in terms of the path length s, where x and z are the horizontal and vertical displacements from the instantaneous closed orbit. We have[5]

$$H = H^{(0)} + H', \quad H^{(0)} = \frac{1}{2}\Sigma\,(p_i^2 + K_i x_i^2),$$

$$H = \sum_{n=2}^{\infty} H^{(n)}, \quad H^{(n)} = \frac{B_o}{B\rho} \sum_{L+M=n} \frac{n!}{L!M!n}\, c^M_{n-1} x^L z^M .$$

The K_i and c^M_{n-1} are defined in terms of median-plane expansions of the magnetic field

$$B(x,z=0) = B_o(1 + b_1 x + b_2 x^2 + \ldots),$$
$$B(x,z=0) = B_o(a_0 x + a_1 x^2 + \ldots),$$
$$K_x = \frac{B_o b_1}{B\rho} - \frac{1}{\rho_o^2}, \quad K_z = -\frac{B_o b_1}{B\rho};$$

$$c^M_{n-1} = \left[(-1)^{M/2} b_{n-1},\ (-1)^{(M+1)/2} a_{n-1} \right] \text{ for M even, odd.}$$

We then replace x_i, p_i by phase and amplitude variables Ψ_i, J_i using the (instantaneous) betatron functions β_i, α_i (Ref. 4):

$$x_i = \sqrt{2J_i\beta_i}\cos\Psi_i, \quad p_i = -\sqrt{2J_i/\beta_i}\,(\sin\Psi_i + \alpha_i\cos\Psi),$$

by use of the generating function $F_1 = -\Sigma(x_i^2/2\beta_i)(\tan\Psi_i + \alpha_i)$. The transformation equations $p_i = \partial F_1/\partial x_i$, $J_i = -\partial F_1/\partial\Psi_i$, $H_1 = H + \partial F_1/\partial s$ and the relations $d\beta_i/ds = -2\alpha_i$, $d\alpha_i/ds = K_i\beta_i - (1+\alpha_i^2)/\beta_i$, give $H_1 = \Sigma(J_i/\beta_i) + H'(\Psi_i, J_i)$. We investigate the resonance arising from the $x^L z^M$ term in H' that oscillates as $\cos\Psi_{\ell m}$, where

$$\Psi_{\ell m} = \ell\Psi_x + m\Psi_z; \quad \ell = L, L-2, \ldots; \ \ell \geq 0; \ m = M, M-2, \ldots, -M.$$

This term has the form $h\, c^M_{n-1}(J_x\beta_x)^{L/2}(J_z\beta_z)^{M/2}\cos\Psi_{\ell m}$, with h a constant. It causes a resonance when the tunes $\nu_i = \nu_i^o$, where $\nu^o_{\ell m} \equiv \ell\nu_x^o + m\nu_z^o = r$ = integer.

We now make a second transformation to variables μ_i, $\bar{J}_i$:

$$\mu_i = \Psi_i - \Phi_i, \quad \Phi_i = \int ds \left[\frac{1}{2\pi}\left(\frac{\nu_i}{R} \right) \right], \quad \bar{J}_i = J_i .$$

in which ν_i depends on s due to the synchrotron oscillations. The generating function, $F_2 = \Sigma J_i(\Psi_i - \Phi_i)$, gives $\mu_i = \partial F_2/\partial\bar{J}_i$, $J_i = \partial F_2/\partial\Psi_i$, $H_2 = H_1 + \partial F_2/\partial s$. In addition we change to $\theta = s/R$ as independent variable and get

$$H_2(\mu_i, J_i, \theta) = \Sigma(\nu_i - \nu_i^o)J_i + R\,h\,c^M_{n-1}(J_x\beta_x)^{L/2}(J_z\beta_z)^{M/2}\cos(\mu_{\ell m} + \Phi_{\ell m})$$
$$\mu_{\ell m} = \ell\mu_x + m\mu_z, \quad \Phi_{\ell m} = \ell\Phi_x + m\Phi_z .$$

Since μ_i, J_i vary slowly we average the other factors over one turn, and obtain

$$H_2(\mu_i, J_i) = \Sigma(\nu_i - \nu_i^o)J_i + D^{LM}_{\ell m} J_x^{L/2} J_z^{M/2}\cos(\mu_{\ell m} + \gamma^{LM}_{\ell m}),$$

where $$D^{LM}_{\ell m} = \left[\left(A^{LM}_{\ell m} \right)^2 + \left(B^{LM}_{\ell m} \right)^2 \right]^{\frac{1}{2}},$$

$$\gamma^{LM}_{\ell m} = \tan^{-1}\left(B^{LM}_{\ell m}/A^{LM}_{\ell m} \right),$$

$$\left\{A^{LM}_{\ell m}, B^{LM}_{\ell m}\right\} = Q^{LM}_{\ell m}\frac{B_o}{B\rho}\int_o^{2\pi R} ds\, c^M_{n-1}\beta_x^{L/2}\beta_z^{M/2}\left\{\cos\Phi_{\ell m}, \sin\Phi_{\ell m}\right\}$$

$$Q^{LM}_{\ell m} = \epsilon_{\ell m}(n-1)!/\left[2^{n/2}\pi \left(\frac{L+\ell}{2}\right)!\left(\frac{L-\ell}{2}\right)!\left(\frac{M+m}{2}\right)!\left(\frac{M-m}{2}\right)! \right], \quad n = L + M$$

and $\epsilon_{\ell m} = \frac{1}{2}$ if $\ell = m = 0$; $\epsilon_{\ell m} = 1$ otherwise. To suppress the resonance, $c^M_{n-1}(s)$ must lead to $D^{LM}_{\ell m} \approx 0$.

*For example a sextupole to second order.

Finally we transform to variables $\bar{\mu}_i, \bar{J}_i$:

$$\bar{\mu}_1 = \mu_{\ell m} + \gamma^{LM}_{\ell m} = \ell\mu_x + m\mu_z + \gamma^{LM}_{\ell m}, \quad \bar{\mu}_{12} = m\mu_x - \ell\mu_z,$$

$$\bar{J}_1 = (\ell J_x + m J_z)/(\ell^2 + m^2), \quad \bar{J}_2 = (m J_x - \ell J_z)/(\ell^2 + m^2),$$

using the generating function $F_3 = (\ell\mu_x + m\mu_z + \gamma^{LM}_{\ell m})\bar{J}_1 + (m\mu_x - \ell\mu_z)\bar{J}_2$. The new Hamiltonian is

$$H_3(\mu_i, J_i, \theta) = \Sigma(\bar{\nu}_i - Ti)\bar{J}_i +$$

$$D^{LM}_{\ell m}(\ell\bar{J}_1 + m\bar{J}_2)^{L/2}(m\bar{J}_1 - \ell\bar{J}_2)^{M/2}\cos\bar{\mu}_1$$

$\bar{\nu}_1 = \ell\nu_x + m\nu_z$, $\bar{\nu}_2 = m\nu_x - \ell\nu_z$, $\bar{\nu}_1^{\theta} = \nu_{\ell m} = r$ = integer.

Since H_3 is independent of μ_2, J_2 is a constant, and the equations for μ_1, J_1 are $d\mu_1/d\theta = \partial H_3/\partial J_1$, $dJ_1/d\theta = -\partial H_3/\partial\mu_1$.

For the multiple crossing of a horizontal resonance: $L = \ell = n$, $M = m = 0$, in the presence of a 0-th harmonic octupole term, the motion follows from the Hamiltonian

$$H_3(\bar{\mu}_1, \bar{J}_1, \theta) = (n\nu_x - r)\bar{J}_1 + D^{n0}_{n0}(n\bar{J}_1)^{n/2}\cos\bar{\mu}_1 + D^{40}_{00}(n\bar{J}_1)^2 .$$

The equations of motion, Eq. (2), are obtained from H_3 by substituting

$$\bar{J}_1 = J_x/n = I/2n, \quad \bar{\mu}_1 = \chi, \quad B_n = nD^{n0}_{n0}/2^{n/2}, \quad A = D^{40}_{00} .$$

As for the phases $\Phi_{\ell m}$ that enter the formulas for $A^{LM}_{\ell m}$, $B^{LM}_{\ell m}$, if we evaluate them at the resonance, then $\Phi_i = \int_o^s (ds/\beta_i)$ which is the Courant-Snyder phase σ_i. If we evaluate them at another momentum, say P_1, then $\Phi_i = \nu_i(\sigma_i - \theta) + \nu_i^o\theta$. The term $\nu_i(\sigma_i - \theta)$ oscillates about zero in each period on the lattice; the $\nu_i^o\theta$ term contributes $r\theta$ to $\Phi_{\ell m}$, which is the factor often used, incorrectly, in place of the complete $\Phi_{\ell m}$. It is probably safe to ignore the variation of $D^{LM}_{\ell m}$ with momentum, but all of the terms involved must be taken at one momentum value in evaluating this number.

References

1. H. Hahn and M. Plotkin, Eds. "Design Study of 200 GeV Intersecting Storage Accelerators" (in press).

2. A.A. Kolomensky and A.N. Lebedev, Theory of Cyclic Accelerators, Chapter 3, 38 (1966).

3. M.H.R. Donald, RHEL/M/NIM (1973). (See also other references in this paper)

4. E.D. Courant and H.S. Snyder, Ann. Phys. 3, 1-48 (1958).

5. G. Guignard, CERN Report CERN/SI/Int. DL/70-3 (1970).

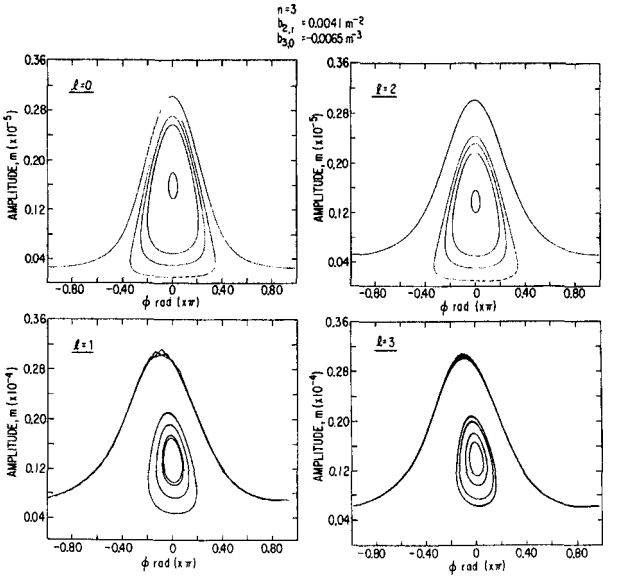

Fig. 1. Particle trajectories in I-Φ space for different side bands of a third order resonance. (Note the difference in vertical scale for even and odd band.)

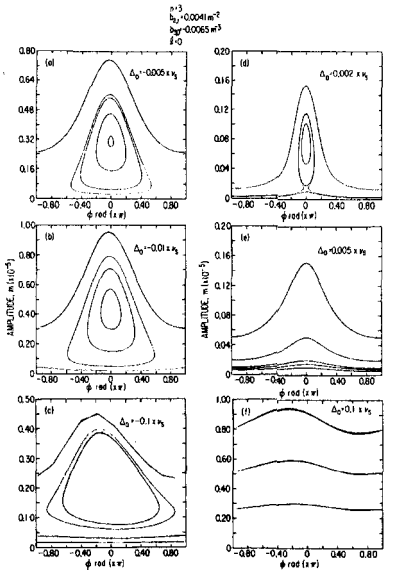

Fig. 2. Particle trajectories in I-Φ space near the central ($\ell = 0$) side band of a third order resonance.

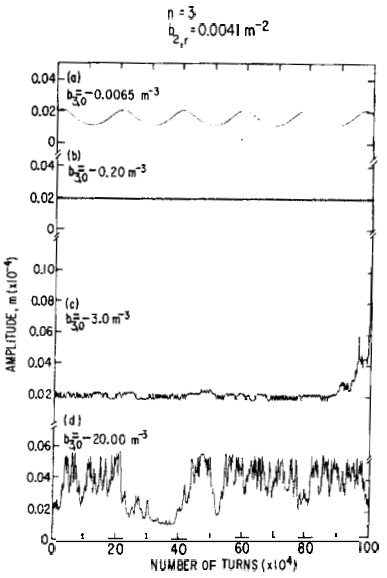

Fig. 3. Single particle amplitude as function of revolution number, for different zeroth harmonic octupole components, near a third order resonance.

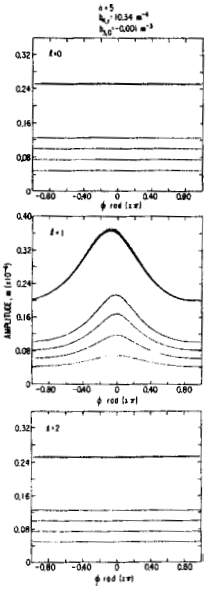

Fig. 5. Particle trajectories in I-Φ phase space for different side bands of a fifth order resonance.

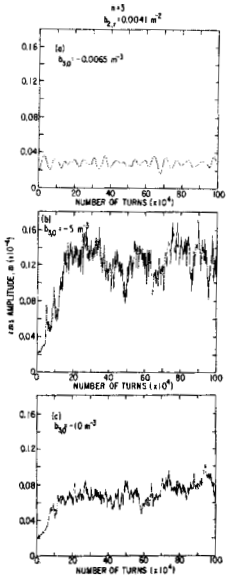

Fig. 4. rms amplitude of 10 particles as function of revolution number, for different zeroth harmonic octupole components, near a third order resonance.

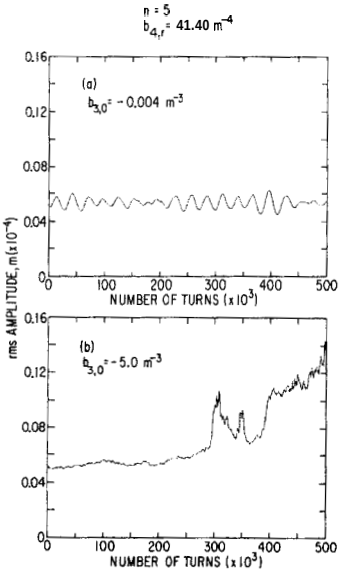

Fig. 6. rms amplitude of ten particles as function of revolution number, for different zeroth harmonic octupole components, near a fifth order resonance.

MAIN RING MAGNET SYSTEM OF KEK PS

A. Ando, K. Endo, T. Kasuga, M. Kihara and E. Takasaki
National Laboratory for High Energy Physics
Oho-machi, Ibaraki, Japan

Summary

Results of the field measurement on the quadrupole and bending magnets for the main ring of KEK 12 GeV proton accelerator are shown. The design of secondary magnets is reported.

Introduction

The main ring of the KEK 12 GeV proton accelerator is the separated function synchrotron with the four long straight sections? There are *48* bending magnets and 56 quadrupole magnets in the ring, and two quadrupole magnets and one bending magnet, which serve as the reference magnets for the main ring B-clock system, are set up in the power house.

All magnets have already been set into the tunnel by March and the precise alignment is now going on. The magnetic field measurement on the quadrupole magnet was performed before installed into the tunnel. On the bending magnet, however, the field measurement is in progress inside the main ring tunnel.

The design of the secondary magnets has already finished. The following secondary magnets are installed in the main ring; the horizontal and vertical steering magnets, the trimming quadrupole magnets, the skew quadrupole magnets, the sextupole magnets, and the octupole magnets.

The steering magnets are always used in dc excitation. The other correction magnets are also energized by dc power supplies in the initial operation of the main ring, so as to provide correction only at injection, although magnets themselves are designed to permit future pulsed operation with the full excitation at the maximum energy. All magnets are excited by individual power supplies to generate harmonics with changeable amplitude and phase.

In this report, the results of the field measurements on the quadrupole and bending magnets, and the design of the secondary magnets are given.

Magnetic Field Measurements

Quadrupole magnet

Magnetic field measurements were performed on 60 quadrupole magnets before installed in the main ring tunnel. As the basic measurements on each magnet, the excitation curve of the field gradient, the transversal distributions of the field gradient at the center of magnet and the effective gradient length $(1/B')\int B'ds$ on the magnet axis were measured at eight excitation levels from 0.13 kG/cm to *2.04* kG/cm.

These field measurements were done under the dynamic operation by using two digital integrators connected with the conventional twin coils and the reference coil. The long coil 10 cm long was used for measurements of the effective gradient length. In order to check the stability of the measuring system, one particular magnet was chosen as the standard magnet, on which the above-mentioned quantities were frequently measured. The results of this measurement have shown the rms statistical error to be less than 0.02 % for both the field gradient and the effective gradient length at all excitation levels.

The remanent field was also measured by the Hall generator after exciting the magnet up to 2.0 kG/cm. The relative error for the remanent field gradient is less than *4* %, and the accuracy in its absolute value is estimated to be at most 7 %.

The radial distributions of the effective gradient length on the standard magnet are shown in Fig.1. As the result of the multipole expansion, the effective gradient length contains the 12th multipole as the main higher component, rather than the octupole as shown in Table 1. It is the particular feature of using the oriented steel that the higher multipole components in the effective length do not change appreciably with the field strength.

The histograms of the field gradient, the effective gradient length and the integral of field gradient $\int B'ds$ are shown in Fig.2. The average value and the standard deviation for these quantities are given in Table 2. The fluctuation in $\int B'ds$, which is the most interesting quantity from the viewpoint of the operation of the machine, is less than 8×10^{-4} at all excitation levels.

The average value of the remanent field gradient is *0.58* G/cm with the fluctuation of *0.04* G/cm. This fluctuation corresponds to 3×10^{-4} at injection field of 150 G/cm. In Table 2, the effect of the remanent field is added to the field gradient produced by the exciting current, for B' = 0.128 kG/cm.

Bending magnet

Magnetic measurements on the *48* bending magnets have not yet been finished. In this section, the measured results on one bending magnet are reported.

The bending magnet is measured under the dynamic operation by using the same measuring system as that for the quadrupole magnet. The remanent field is also measured by the Hall generator after pulsing the magnet up to 17.5 kG.

As reported in the previous paper: a slight amount of gradient exists in the field produced by the exciting current. The k-value at the injection field is -0.017 m^{-1} and it decreases with increasing field strength to reach an almost constant value of -0.005 m^{-1} above a certain field level. This variation of the field gradient may be attributed to the systematic gap opening during welding, the gap deformation due to the magnetic force and the core saturation.

The remanent field on the magnet centerline is 6.6 G and the gradient is 12 G/m. This can be partly cancelled by the field gradient produced by the exciting current (i.e. B' = −25.5 G/m at the injection field).

The radial distribution of the effective length was measured at 1.5, 7.5, 12.2 and 15.8 kG along the coordinate system shown in Fig.3. At low fields, the integral of the field strength over the central part of magnet is little dependent on the radial position. Therefore, the multipole components included in the effective length are mainly governed by the contribution from the fringing field at both ends. Above the medium fields, however, the field integral over the central part of the magnet is dependent on the position. The multipole components included in the effective length are listed in Table 3.

Although the power supply capability limited the maximum excitation to 15.8 kG for full scale magnet, we have roughly estimated the effective length from the data of the half-length magnet. The effective length for the half-length magnet is 1614.9 mm and the sextupole coefficient a_2/a_0 is $-1.2\ m^{-2}$. Considering that the sextupole component of the field strength at the magnet center is $-1.1\ m^{-2}$, the sextupole component included in the effective length for the full scale magnet can be approximated to be $a_2/a_0 = -1.13\ m^{-1}$.

Design of Secondary Magnets

The secondary magnets consist of 56 steering magnets, 16 trimming quadrupole magnets, 8 skew quadrupole magnets, 8 sextupole magnets and 16 octupole magnets. They are installed in the midi straight sections after F and D quadrupole magnet, in such a manner that they have the same superperiodicity as the main lattice.

Although strict tolerances were imposed on the main magnets, the variation in field strength and the misalignment of magnets yield the closed orbit distortion, which is estimated to be 13 mm in the horizontal plane and 6 mm in the vertical plane. Also, the variation in the field gradient and the field imperfections caused by the fringing field and the saturation effect excite the linear and non-linear resonances.

In Table 4 are summarized the principal parameters of the secondary magnets, and the proposed location for these magnets is shown in Fig.4. The secondary magnets are energized by dc power supplies, in the initial operation of the accelerator, to provide the correction only at injection. However, these magnets except for the steering magnet are made of laminated cores to permit future pulsed operation.

Steering magnet and closed orbit correction

The closed orbit distortion is caused by misalignment and random variation in field strength of the main magnets. The correction is done by the steering magnets at injection, and the displacement of the main quadrupole magnets at high fields.

The steering magnets are placed after every quadrupole magnet; 28 horizontal steering magnets follow the main F quadrupoles and 28 vertical ones the main D quadrupoles. The position of the closed orbit is measured with 56 beam position monitors which are fixed at the downstream end of every main quadrupole magnet. The field strength of the steering magnets listed in Table 4 is sufficient for providing the local closed orbit bump less than the half-aperture in both planes.

Current of the steering magnets is ad'usted with a method based on the least squares theory? The correcting deflections represented by a vector $\vec{\theta}$ are related to the measured distortion $\vec{x}$ in the following form;

$$\vec{x} + A\vec{\theta} = 0 , \qquad (1)$$

where A is a matrix constructed from the betatron oscillation variables. Since the solution of the above equation suffers from sensor error, besides A has no inverse matrix, it is relevant to treat eq.(1) as the least square problem in which the norm $||\vec{x} + A\vec{\theta}||^2$ is minimized. After simple manipulations, we get

$$\vec{B} + M\vec{\theta} = 0 ,$$

where $\vec{B} = A^T \vec{x}$ and $M = A^T A$. The matrix M is symmetric and has real and non-negative eigenvalues. The eigenvectors with low eigenvalue give only minor effects on the closed orbit and can be deleted from the solution?

In Fig.5 the eigenvalues are arranged in order of their dominant frequency, showing a resonant sensitivity to distortions with frequency near the ν value.

Fig.6 shows examples of closed orbit correction, assuming that the original closed orbit has the distorted sinusoidal form with frequency of 7.25. The effect of monitor failure has been studied by letting the distortion at thefailedmonitor be zero. In order to reduce the maximum closed orbit distortion by a factor of 2 or 3, it is sufficient to select 10 eigenvectors even in the presence of 3 failed monitors.

The closed orbit correction at high fields is performed in the similar way by replacing the deflection $\vec{\theta}$ by the displacement of the main quadrupole magnets and constructing a new matrix A.

The power supplies for the steering magnets will permit independent control of individual current. A block diagram for this system is shown in Fig.7. Information such as magnet location and current is transmitted to each power supply in the digital form through transmission lines. Each magnet current is changed after converting the digital settings into an analogue value.

Trimming quadrupole magnet

The trim quadrupole magnets are used for independent tuning of the horizontal and vertical betatron frequencies and exciting the 15th harmonic to cancel the stopband of the half integer resonance at $\nu = 7.5$. The error quadrupole field comes from the variations in the gradient length $\int B'ds$ of the quadrupole magnet and the k-value in the bending magnet.

Correcting sextupole and octupole magnets may be the source of gradient error when the excursion of closed orbit from the center of magnets is present. Similarly, the higher multipole components in the bending magnet yield the same effect.

In the "fine tuning" mode, the trim quadrupole should not excite any harmonics in the neighbourhood of $2\nu_x$ and $2\nu_z$, such as 14th, 15th and 16th. As the trim quadrupoles have the same periodicity as the main lattice, the harmonics of multiple of 4 are excited. To eliminate the 16th harmonic, the current of the quadrupoles in one superperiod must be properly modulated. Although the complete elimination is impossible with 4 quadrupoles, the stopband can be suppressed to 0.08 for the tune shift $\Delta\nu = 0.1$, for the proposedarrsngement. Since the betatron frequencies can be tuned by the main quadrupoles, the trim quadrupoles are used for fine tuning of $\Delta\nu$ less than 0.2.

The stopband width which is expected from the gradient error in the main magnets is 0.016, assuming the variation of 30 % in the k-value of the bending magnet (Table 5). At 12 GeV, however, the closed orbit excursion (5 mm rms) in the bending magnet produces the stopband width of the same amount. Contribution from the correcting sextupole magnets may be even larger. In the "15th excitation" mode, two quadrupole pairs at the opposite side of the ring are excited with the same gradient but in opposite sign, so as not to excite such harmonics as Oth, 14th and 16th. In order to change the amplitude and phase of the 15th harmonic independently in both planes, eight quadrupoles are used to generate cos and sin functions.

The trim quadrupole magnets are designed to be excited up to 4 T/m, which corresponds to the tune shift $\Delta\nu = 0.1$ for the maximum energy. At first, however, the trim quadrupoles are excited by dc power supplies up to 0.7 T/m which will provide the tune shift $\Delta\nu = 0.2$ at

the injection field. The required strength for the 15th harmonic excitation is smaller than this, so that both modes are easily superimposed.

Skew quadrupole magnet

Sources of the skew quadrupole field are the roll of the quadrupole magnets and the vertical closed orbit deviation in the presence of the sextupole field. If an increase of 10 % in emittance due to the coupling oscillation at $\nu_x = \nu_z$ is allowed, the tolerable limit is given by $B_x' = 1.6 \times 10^{-5}$ T/m at injection and 1.9×10^{-4} T/m at 12 GeV, for $\nu_x - \nu_z = 0.005$. These values correspond to the average roll error of 10^{-5} rad.

The main quadrupole magnets were settled in the tunnel with the roll error less than 10^{-4}. Here, assuming the mean value of roll error to be 5×10^{-5}, the required strength of the skew quadrupole field is obtained as listed in Table 4. Such field is provided by the special windings on the octupole magnet described later.

Sextupole magnet

Sextupole magnets are used for narrowing the stopband of the third order resonance and compensating the chromatic aberration. Source of the sextupole field is mainly the fringing field and the saturation effect in the bending magnet. The sextupole field produced by eddy current in the vacuum chamber is less important in our case because the injection field is high.

The stopband width for each resonance line, which is estimated by using the data of the field measurement, is summarized in Table 5. Here we assumed the roll error of the bending magnet is 10^{-4} rad. As seen in the table, the dangerous resonance is $3\nu_x = 22$ which is near the working point.

The tune shift due to momentum error is $\Delta\nu_x = -0.04$ and $\Delta\nu_z = -0.02$ for $\Delta p/p = 0.3$ % at injection. At 12 GeV, it becomes $\Delta\nu_x = -0.002$ and $\Delta\nu_z = 0$ since $\Delta p/p = 0.1$ %. To compensate this tune shift, especially $\Delta\nu_x$, eight sextupole magnets are used. The required strength is given in Table 4. The field strength required to cancel the 22nd harmonic of sextupole field is smaller than that for compensation of the tune shift.

Octupole magnet

Octupole magnets are used for narrowing the stopband of the fourth order resonance induced by both magnetic imperfections and the space charge force.

The main source of the octupole component is the fringing field and saturation effect of the main quadrupole magnet. Amplitude dependent tune shift due to the octupole field is less than 10^{-3} for the horizontal emittance of $\varepsilon_H = 80\ \pi$ mm-mrad. The stopband width is given in Table 5.

In the presence of momentum spread, the betatron frequency oscillates around a central ν value by virtue of the synchrotron oscillation. When the beam crosses the fourth order resonance lines many times during the acceleration period, the horizontal and vertical emittance growth occurs. Since the growth rate at each traversal of the stopband depends on its width, it should be eliminated by the correcting octupole magnets.

Octupole magnets are also used to provide octupole field with appropriate amplitude and phase for the half integer resonant extraction.

The coupled motion induced by space charge forces drives $2\nu_x - 2\nu_z = 0$ resonance which will result in the emittance blow-up! This can be compensated by the octupole field with the zeroth harmonic. For the intensity of 5×10^{12} protons in the ring, the required strength is 30 G/cm^3 at 12 GeV. This field strength is sufficient for the correction of field error and the half integer resonant extraction.

Acknowledgements

The authors wish to thank Professor T. Nishikawa for many fruitful discussions and continuous support. Thanks are due to Messrs. A. Araki, T. Igarashi and S. Ochiai for preparing the field measurement equipments and carrying out the numerical computation.

References

1. K. Endo and M. Kihara, Proc. 4th Int'l Conf. on Magnet Technology, BNL, 1972, p.363.

2. M. Kihara, Proc. U.S.-Japan Seminar on High Energy Accelerator Science, Tokyo and Tsukuba, 1973, p.134.

3. G.R. Lambertson and L.J. Laslett, Proc. 5th Int'l Conf. on High Energy Accelerators, Frascati, 1965, p.26.

4. G. McD. Bingham, NAL internal report TM-200 (1970).

5. A.G. Ruggiero, NAL internal report TM-348 (1972).

6. B.W. Montague, CERN 68-38 (1968).

7. G. Guignard, CERN 70-24 (1970).

Table 1. Multipole coefficients for the effective gradient length of the quadrupole magnet ($\ell_G = \sum_{n=0}^{14} a_n x^n$)

B' (kG/cm)	0.128	1.777	1.927
a_0 (mm)	615.48	604.15	602.70
a_1/a_0 (m^{-1})	0.029	0.018	0.013
a_2/a_0 (m^{-2})	0.16	−0.21	−0.39
a_3/a_0 (m^{-3})	−11.7	6.1	8.4
a_4/a_0 (m^{-4})	−2040	−2360	−2300
a_5/a_0 (m^{-5})	5100	−20200	−22800

Table 2. Average values and standard deviations of $\frac{dB}{dx}$, L_G and $\int\frac{dB}{dx}ds$ for the quadrupole magnet

$\frac{dB}{dx}$ (kG/cm)	$\sigma(\frac{dB}{dx})$ (%)	L_G (mm)	$\sigma(L_G)$ (%)	$\int\frac{dB}{dx}ds$ (kG)	$\sigma(\int\frac{dB}{dx}ds)$ (%)
0.128	0.047	615.66	0.050	7.832	0.059
1.268	0.058	610.65	0.055	77.40	0.075
1.777	0.058	603.76	0.076	107.26	0.079
1.927	0.050	602.24	0.088	116.02	0.047

Table 3. Multipole coefficients for the effective length of the bending magnet

$$(\ell_B = \sum_{n=0}^{5} a_n x^n)$$

B	(kG)	1.5	7.5	12.2	15.8
a_0	(mm)	3257.0	3254.4	3243.7	3228.8
a_1/a_0	(m^{-1})	-0.0067	-0.0037	-0.0043	0.002
a_2/a_0	(m^{-2})	-0.24	-0.18	-0.24	-0.47

Note that, as seen in Fig.3, the fluctuation in measured values at 1.5 kG is somewhat larger.

Table 4. Principal parameters of the secondary magnets

	Number	Length (m)	Field strength at injection	Field strength at 12 GeV	Power supply
Steering magnet					
horizontal	28	0.15	920 G	-	dc
vertical	28	0.15	370 G	-	dc
Trim quadrupole	16	0.15	70 G/cm	0.4 kG/cm	pulsed
Skew quadrupole	8	0.2	9 G/cm	100 G/cm	pulsed
Sextupole magnet	8	0.4	8 G/cm^2	190 G/cm^2	pulsed
Octupole magnet	16	0.2	0.25 G/cm^3	30 G/cm^3	pulsed

Table 5. Total stopband width

N	n_1	n_2	injection	12 GeV		
2	2	0	0.016	0.008	$\langle \Delta B'/B' \rangle = 8\times10^{-4}$ for QM	
	1	1	1.8×10^{-6}	5.7×10^{-7}	$\langle \Delta B' \rangle$ = 8 G/m (inj)	} for BM
	0	2	0.016	0.008	30 G/m (12 GeV)	
3	3	0	0.027	0.039	B'' = 0.07 T/m^2 (inj)	} for BM
	2	1	3.3×10^{-6}	4.6×10^{-6}	4 T/m^2 (12 GeV)	
	1	2	0.033	0.046		
	0	3	1.2×10^{-6}	1.7×10^{-6}		
4	4	0	1.4×10^{-3}	1.5×10^{-4}	B''' = 0.6 T/m^3 (inj)	} for QM
	3	1	4.7×10^{-8}	4.4×10^{-9}	8 T/m^3 (12 GeV)	
	2	2	6.3×10^{-4}	5.7×10^{-5}		
	1	3	3.3×10^{-8}	3.1×10^{-9}		
	0	4	3.3×10^{-4}	3.3×10^{-5}		

Roll error is assumed to be 5×10^{-5}rad and 10^{-5}rad for QM and BM. < > means rms error.

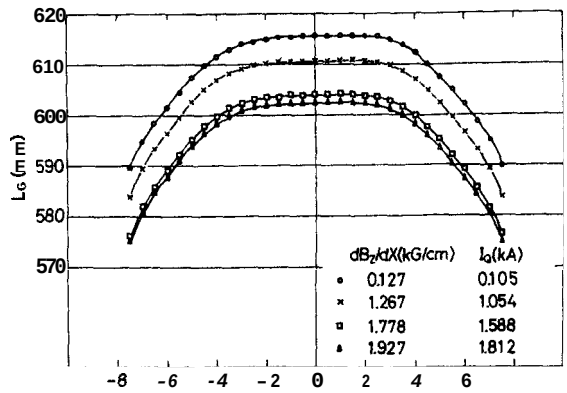

Fig.1 Radial distributions of the effective gradient length of the quadrupole magnet.

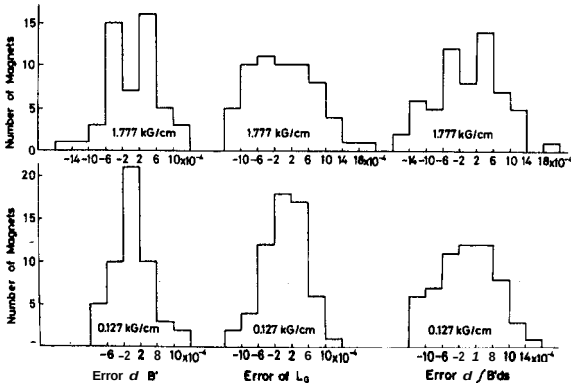

Fig.2 Deviations in $\frac{dB}{dx}$, L_G and $\int\frac{dB}{dx}ds$ of the quadrupole magnet.

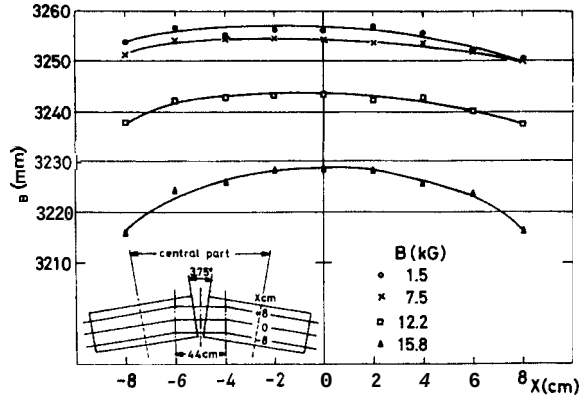

Fig.3 Radial distributions of the effective length of the bending magnet.

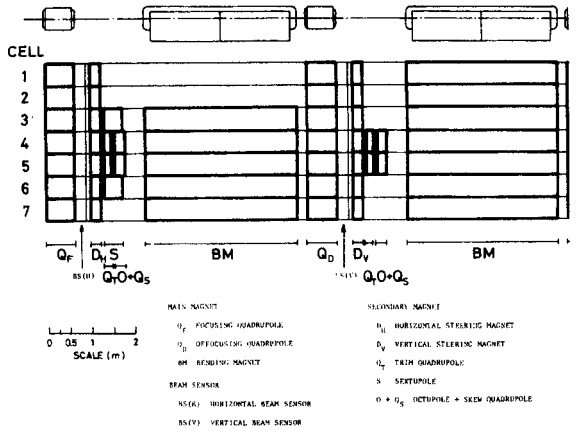

Fig.4 Secondary magnet locations.

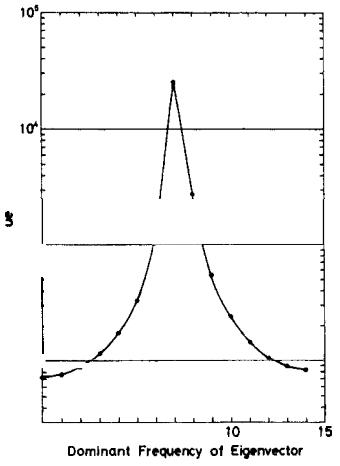

Fig.5 Eigenvalues arranged in order of dominant frequency of eigenvectors. They are doubly degenerated except for both ends.

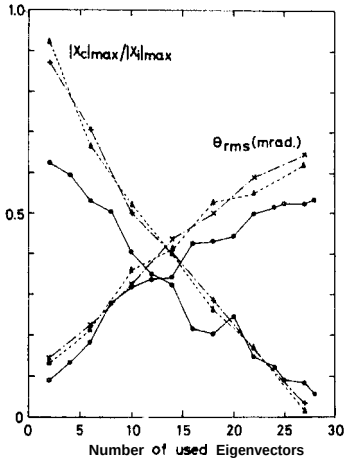

Fig.6 Ratio of the maximum orbit distortion after and before correction, and rms value of correcting deflections as the function of number of used eigenvectors. Solid lines: no monitor failure. Dotted lines: three monitors in failure. Dash-dotted lines: three consecutive monitors in failure.

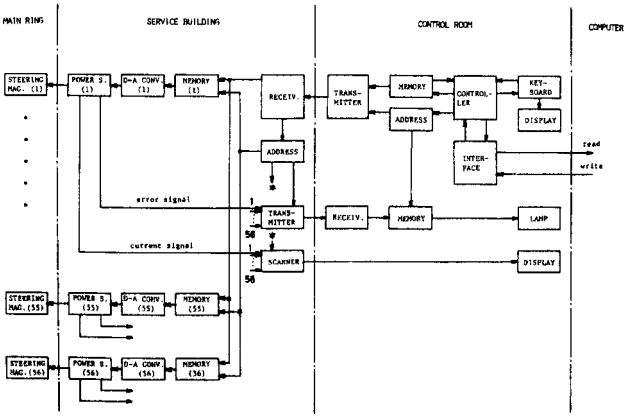

Fig.7 Block diagram of the control system for the steering magnet power supply.

SATURNE II : PROPOSAL OF A RENOVATED PROTON FACILITY AT SACLAY

H. Bruck, J. -L. Laclare, G. Leleux
Section d'Optique Corpusculaire, Centre d'Etudes Nucldaires de Saclay
and the "GERMA" group*

Abstract.

The Saclay proton synchrotron Saturne will be transformed into a strong focusing machine to be used essentially for nuclear spectroscopy. The advantages of a circular machine for such a purpose are underlined. The shortcomings of weak focusing are analysed and essential parameters of the transformed machine are given.

1 - Generalities.

The Saclay proton synchrotron Saturne is 16 years old. But there are still long range programs for use of this machine in the field of nuclear physics, with heavier or polarized particles, for medical purposes, but mostly for proton nuclear spectroscopy.

For the latter purpose, a circular machine, even when compared to the Linac in Los Alamos, seems also attractive. It has less intensity but higher energy and less energy dispersion. Furthermore, the extraction mechanism analyses the energy, making therefore a separate energy analyser unnecessary.[1,2]

	$\bar{I}$	E_c	$\Delta p/p$ total	$\Delta p/p$ analysed
Los Alamos	$6.\,10^{15}$	0.8 GeV	10^{-2}	----
Saturne II (expected)	$2.\,5.\,10^{12}$	2.7 GeV	$3.\,10^{-4}$	

At present, the beam gets progressively unreliable with intensities approching $N_{acc} \longrightarrow 10^{12}$ accelerated protons, the horizontal emittance of the extracted beam being $(\varepsilon_x)_{ext} \sim 30\ \pi$ mrd. mm.

More particles in a much smaller emittance are expected from a modern machine.

It has been decided to renovate Saturne. Preliminary studies led to the recommandation to keep the present 20 MeV injector, the magnet power supply and the building, but to set up a new strong focusing, separated function magnet structure around the old magnet (fig. 1). Construction of this machine has started and will be completed in 1977. The cost is evaluated at $33.6\ 10^6$ french francs. The expected performance characteristics of the transformed machine are :

	(old machine) Saturne I	(new machine) Saturne II
E_c	3 GeV	2.7 GeV
N_{acc} at 1 GeV	$\lesssim 10^{12}$	2.5 1012
T_c	3 sec	0.9 sec
A	15 %	30 %
$\frac{dN_{ext}}{d\varepsilon_x}$ x 5 π mrd. mm	$3.\,10^{10}$	$2.25\ 10^{12}$
$\left(\frac{\Delta p}{p}\right)_{ext}$	$2.\,10^{-3}$	some 10^{-4}

for meaning of symbols see section 3.

2 - Essential improvement factors.

Apparently the difficulties to get a reliable beam of high intensity in the present machine are related to resistive wall instabilities and to enlargement of the beam by betatron resonances.[3] The importance of these effects is inherent in the weak focusing principle : in order to get a beam steady with respect to transverse resistive instability, the betatron wave numbers ν_x and ν_z have to cover finite domaines $\delta\nu_{x,z} \gtrsim (\Delta\nu_{x,z})_{sc}$, where $\Delta\nu_{sc}$ is the space charge displacement of the wave numbers. Therefore with growing intensity the required values of $\delta\nu_x$ and $\delta\nu_z$ grow and cover a growing number of resonance lines.

Now, not only at given beam density, $\delta\nu_x$ and $\delta\nu_z$ are large in a weak focusing machine (because $\Delta\nu_{sc} \propto 1/\nu$), covering many resonance lines, but at given magnet field quality, the band width of these lines is also much larger than in a strong focusing machine.

In renovating Saturne, it therefore appears as most essential to introduce strong focusing with as high as possible wave numbers. A strong focusing separated function structure has been designed having betatron wave numbers $\nu_x = \nu_z = 3.6$, physical radius R = 16.8m and long straight sections, each ~10m long as required for easy extraction (fig. 1).

* "Groupe d'Etude et de Rdalisation de la Machine" in charge of future development and carrying the proposal into effect. This group comprises staff members of CEA and IN2P3 ; R. Vienet is in charge of this group.

Comparing the old machine to the new one at the same relative field errors $\langle \delta B' \rangle / B$; $\langle \delta B'' \rangle / B$; $\langle \delta B''' \rangle / B$, the respective theoretical stop band width are reduced to 1/50 ; 1/6 ; 1/10.

Because of its higher wave numbers, this machine furthermore accelerates polarized protons without crossing low harmonic depolarizing resonances.[4]

Another essential improvement of performance characteristics will result from further reducing magnet field fluctuations.

Owing to strong and only slowly decreasing eddy currents inside the 10 mm thick iron sheets of the present magnet core, the field strength would be depressed at beginning of extraction flat top by $\Delta B/B = 10^{-2}$ with time constant $\tau \sim 1/10$ sec, whereas a field constant to at least 10^{-5} is required. This defect will be cured by an entirely new magnet, decided upon for various reasons and having sheet thickness of 1.5 mm.

Furthermore, the ripple of the power supply is at present $\Delta I/I$ = some 10^{-3} during field rise and $\Delta I/I$ = some 10^{-4} during flat top, whereas ten times less must be achieved. The appropriate technology has not been decided upon yet. Use of the present magnet as a filter is contemplated.

3 - Parameters.

a) Orbit. "Missing magnet" lattice.

Maximum kinetic energy(proton)	E_c = 2.7 GeV
Physical radius	R = 16.8 m
Magnet radius	ρ = 6.34 m
4 long straight sections, each of length	L = 10.3 m
Magnet field index	n = 0
Maximum quadrupole strength	$(G\ell)_F$ = 4.12 T
	$(G\ell)_D$ = 4.49 T
Betatron wave numbers	$\nu_x \approx \nu_z \approx 3.6$
Natural wave number dispersion	$k = d/(dp/p)$
	$k_x = -4.8$; $k = -4.8$
Orbit parameters	$(\beta_x)_M$ = 17.4 m ; $(\beta_x)_m$ = 1.47 m
	$(\beta_z)_M$ = 16.0 m ; $(\beta_z)_m$ = 1.78 m
Momentum compaction	α = 0.017
Local momentum compaction	Rg_M = 6.77 m ; Rg_m = -4.76 m

b) Injection.

Energy(protons)	E_i = 20 MeV
Number of turns	n_i = 200
Injected number of particles	N_i = $6 \cdot 10^{12}$
Space charge displacement at injection	$(\Delta\nu_{ce})_x$ = 0.17
	$(\Delta\nu_{ce})_z$ = 0.17
Emittances	$(\varepsilon_x)_i$ = 90 π mrd. mm
	$(\varepsilon_z)_i$ = 200 π mrd. mm
Energy dispersion	$(\Delta p/p)_i = \pm 8 \cdot 10^{-3}$
Maximum beam dimensions	$(x_M)_i = \pm 8.2$ cm ; $(z_M)_i = \pm 6.8$ cm

c) Acceleration.

Peak voltage	$\hat{V}_{RF}$ = 14 kV
Harmonic number	k_{RF} = 3
Speed of magnet field rise	$\dot{B}$ = 3.5 T s^{-1}
Number of accelerated particles	N_{acc} = 2.5. 1012
Kinetic transition energy	$E_{c,tr}$ = 6.36 GeV

d) Extraction (1 GeV)

Number of particles	$N_{ext} = 2.\ 25.\ 10^{12}$
Emittances (total)	$(\mathcal{E}_x)_{ext} \leq 7\ \pi$ mrd. mm ; $(\mathcal{E}_z)_{ext} = 25\ \pi$ mrd. mm
Energy dispersion (total)	$(\Delta p/p)_{ext} \gtrsim \pm 145\ 10^{-4}$
Energy resolution	$(\Delta p/p)_{res} \simeq 10^{-}$
Duration of one cycle	$T_c \approx 0.9$ sec
of flat top	$\tau \approx 0.3$ sec
Duty cycle	$A \approx 30\ \%$

References.

1. R. Beurtey and J. Faure,
Private communication.

2. H. Bruck, J.-L. Laclare and G. Leleux,
General properties of slowly extracted beam,
present proceedings.

3. J. Faure, G. Leleux and R. Vienet,
Instabilities detected in Saturne,
present proceedings.

4. J. Faure, A. Hilaire and R. Vienet,
Acceleration of polarized protons in Saturne,
Particle Accelerators *3* (1972) pp 225.

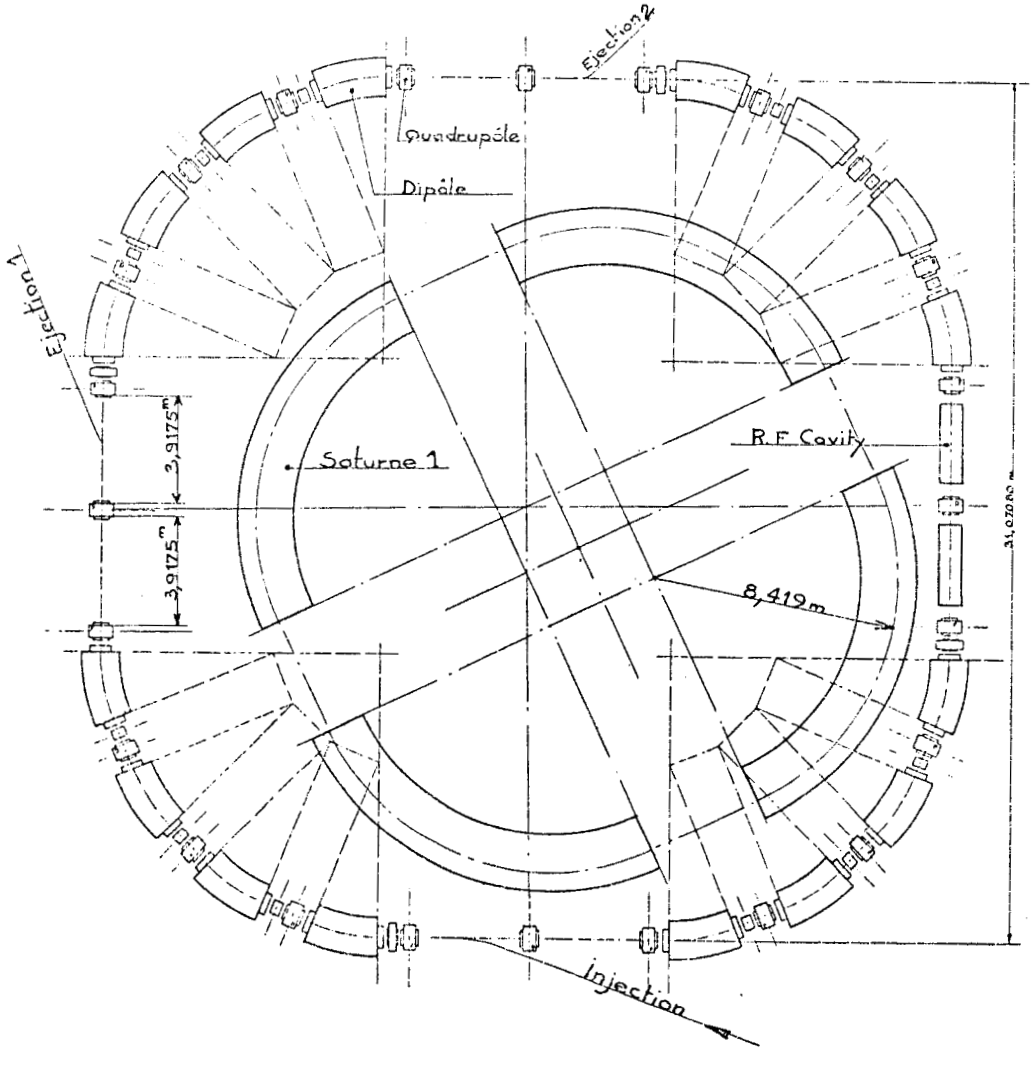

THE ELECTRON PULSE STRETCHER EROS

N. R. Heese and R. Servranckx
Saskatchewan Accelerator Laboratory,
University of Saskatchewan, Saskatoon, Canada, S7N 0W0

1. Introduction

The Electron Ring of Saskatoon is designed as a pulse stretcher whose purpose is to bring the duty factor of the 250 MeV electron linear accelerator at Saskatoon from a value of 6.25×10^{-4} to a value of 0.8 or more. The ring, into which the 1 μs long linac pulse is injected, is a racetrack shape of 73 m circumference. The electrons are then slowly extracted between linac pulses utilizing a resonance phenomenon. The reader is asked to consult Refs. 1 and 2 for a complete description of the design.

2. Optimization of the Design

In 1973 an optimization of the design, as regards to cost, was undertaken. It appeared immediately that the most expensive elements of the design were the quadrupoles and hexapoles, particularly those of the curved sections. Their aperture was over 10 inches. As suggested by K. Brown of SLAC, we examined the possibility of increasing the horizontal tuning, ν_x, from a value of 3 1/3 to 5 1/3. The change might reduce the aperture required since the chromatic excursion is proportional to $1/\nu_x^2$. However, to achieve this, we had to change the structure and increase the number of units in the curved sections and also modify the structure of the straight sections. Figure 1 shows the present layout of the ring: A more detailed analysis of the considerations involved in the modification can be found in Ref. 3.

Figure 2 shows the graphs of the beam dynamic functions β_x, β_z and the chromatic excursion function $g = dx_{co}/d\delta$, where x_{co} denotes the closed orbit, $\delta = p - p_o/p_o$, p is the momentum of the particle, and p_o is the nominal momentum.

A further delicate adaptation of the straight and curved sections allowed a reduction in the aperture of all quadrupoles by a factor of at least two.

3. Monochromatic Extraction

The extraction process adopted is based on the 1/3 resonance which has been extensively described in the literature (see Ref. 1). Previous to this an achromatic extraction process was considered. A modification of the chromatic parameters of the ring enabled us to achieve a monochromatic extraction of the beam.

The area of the extraction triangle is plotted on the graph in Fig. 3. From this graph it can be seen that the particles along the curved segment from B to C are extracted. They cover an energy spread of 0.08%. If by some deceleration process (radiation, RF, betatron core) the stable particles of the beam can lose energy with time, they will be extracted at the same energy and within the same energy spread while the tuning of the machine remains constant.

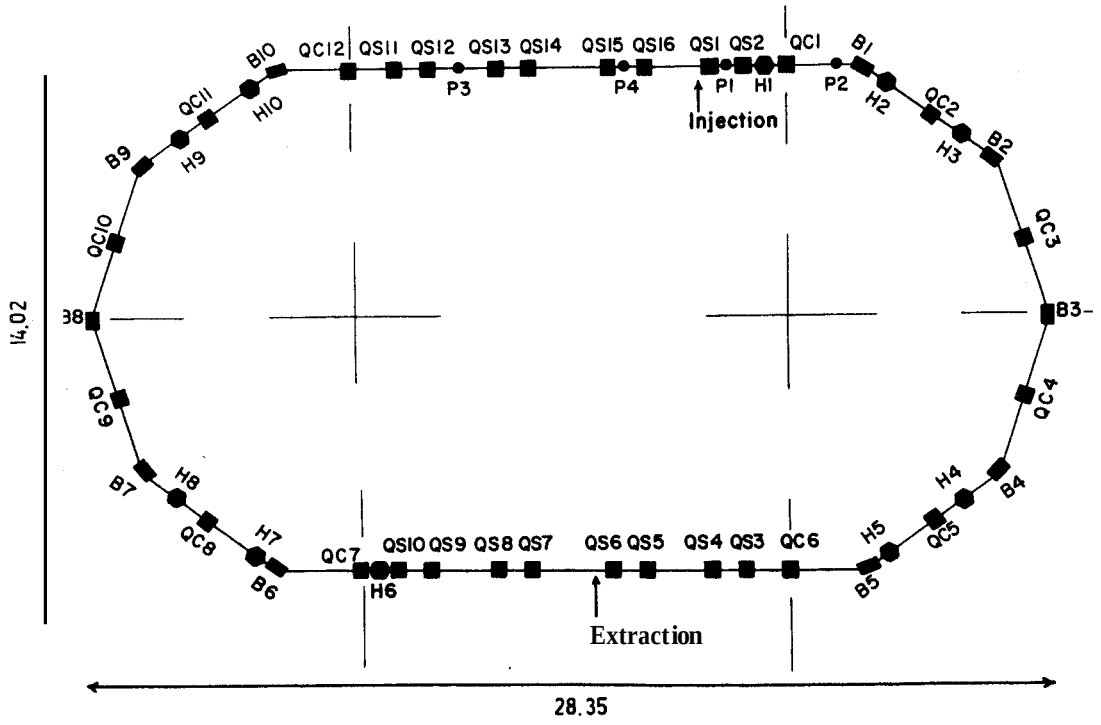

Fig. 1 EROS ring layout

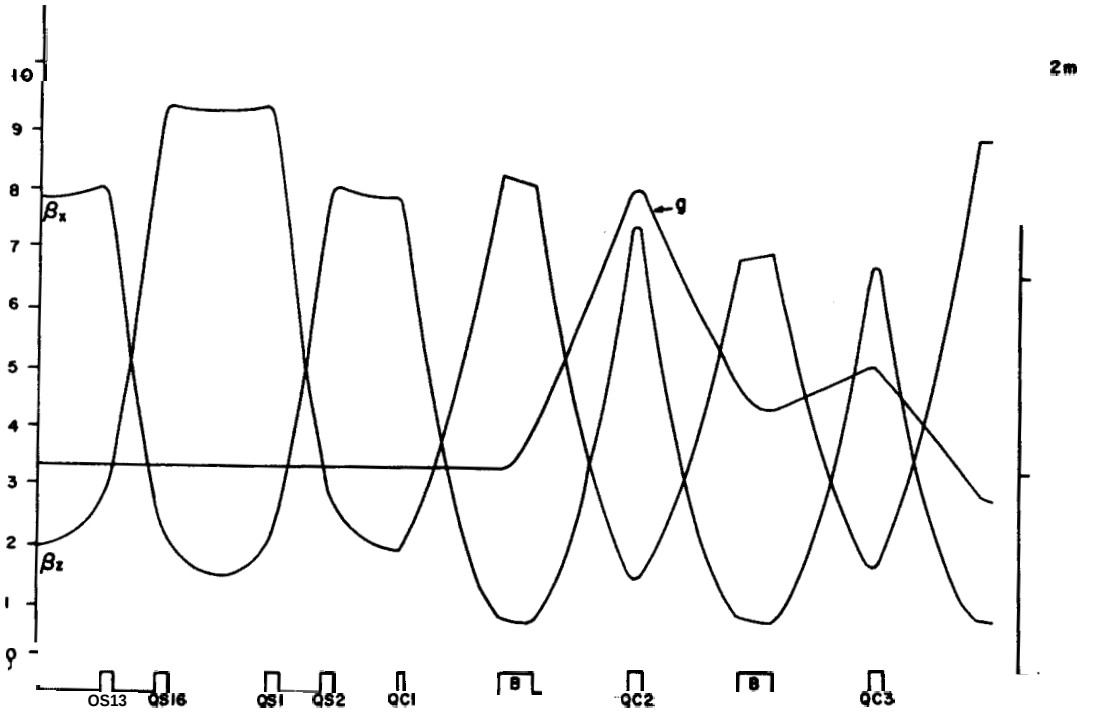

Fig. 2 β_x, β_z, g-function in half a curved section.

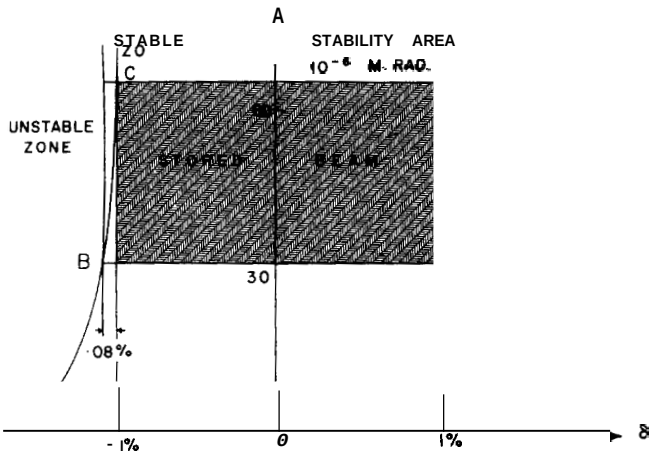

Fig. 3 Area of extraction triangle.

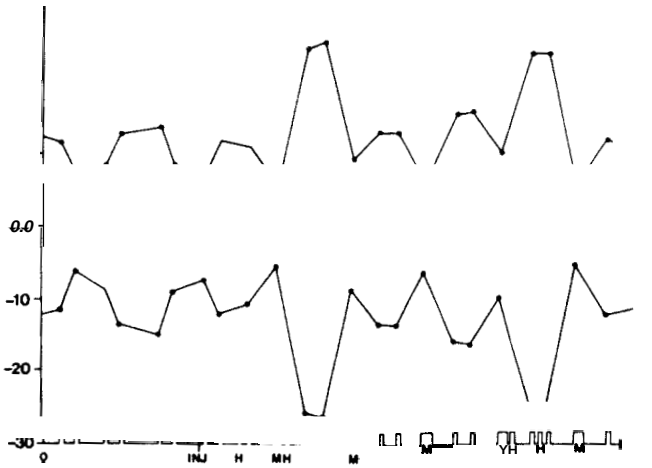

Fig. 4 Stored beam horizontal envelope.

Detailed calculation of particle tracing[4] shows this process works very well and leads to a beam size much in favor of the monochromatic extraction. The beam obtained by this extraction process is expected to have the following characteristics:

Energy range	150 to 250 MeV
Energy spectrum	0.08%
Beam emittance - horizontal	3 mm-mrad
- vertical	25 mm-mrad

The beam envelopes around the ring are as shown on Figs. 4, 5 and 6. In such an extraction the ring acts as a monochromator.

Extraction of the particles results from energy loss due to synchrotron radiation. The energy loss per turn is given by

$$\Delta E(\text{keV}) = 88.5 \frac{E^4(\text{GeV})}{m} .$$

Assuming the energy spread is 1%, the energy to be lost for complete extraction is $\Delta E(\text{keV}) = 1 \times 10^4\ E(\text{GeV})$. The number of turns needed to lose this energy is then

$$N = \frac{1 \times 10^4\ R(m)}{88.5\ E^3(\text{GeV})} = 113 \frac{R(m)}{E^3(\text{GeV})} .$$

Table 1 illustrates some values for our ring (remember R = 1 m). Since the ring is 73 m long, one turn takes 243.3 ns so that the total time (T) for full extraction can be computed and the allowable maximum repetition rate (Rm) for complete extraction is obtained easily (the accelerator natural repetition rate is 625 pps).

A pulsed betatron core could be used to increase the energy loss. The technical feasibility of this device is being studied.

We are also examining the use of a radio frequency cavity to achieve the required loss. One possible method is similar to that used on the ISR at CERN where they managed to accelerate particles by moving empty RF buckets through the beam.

Table 1
Radiation Losses and Repetition Rate in EROS

E (GeV)	ΔE_{tot} (MeV)	N	T (ms)	Rm (pps)
0.1	0.058	113 × 103	27.5	36.4
0.15	0.294	33 × 103	8.0	125
0.2	0.931	14 × 103	3.4	294
0.25	2.27	7.2 × 103	1.75	571
0.3	4.71	4.2 × 103	1.02	980

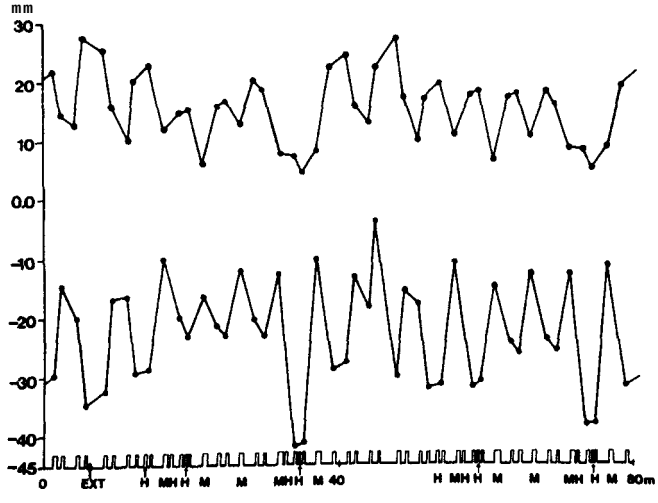

Fig. 5 Horizontal envelope during extraction.

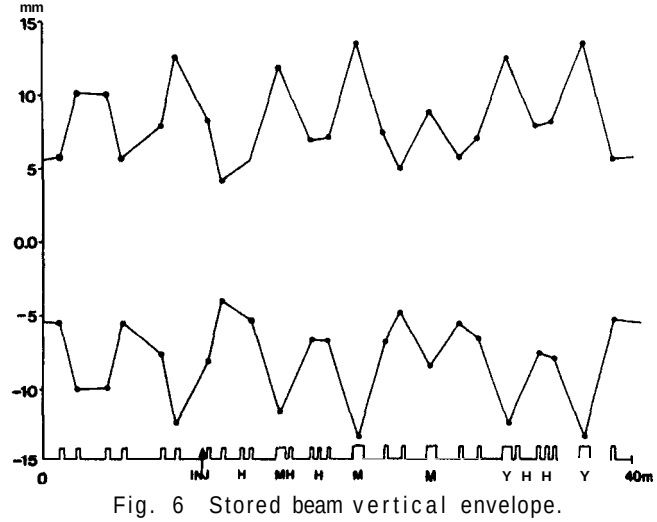

Fig. 6 Stored beam vertical envelope.

4. Main Magnetic Components of EROS

The perturbation of the ring design effected in 1973 by the presence of Karl Brown had a vast and beneficial impact on the magnetic components. The apertures of the quadrupoles and hexapoles were reduced from 10 inches in some parts of the ring to a uniform 4 inches all around. The bending magnets, although increasing in number from eight to ten were reduced considerably in size which allowed us to design them as rectangular units. The aim of the magnet design has been to achieve the required performance while keeping the construction as simple as possible.

Bending Magnets

Table 2 shows the parameters that must be satisfied for the bending magnets. Using a gap height of 5 cm (leaving a little room for error in the placement of the vacuum box and anticipating larger vertical oscillations during tune-up), it was found that a pole width of 17.78 cm (7 in.) would be more than adequate, provided small rectangular shims were used at the sides of the pole to extend the width of the useable field. The computer program TRIM5 was used extensively in the magnet design, and Fig. 7 shows a cross section of the proposed magnet, with the shaded area in the gap depicting the region of acceptable field levels (as ascertained by TRIM). The iron length of the magnet was evaluated using fringing fields given by TRIM and

Table 2
Bending Magnet Requirements

Field required for 250 MeV	8333 G
Deflection angle	36°
Effective length	61.808 cm
Poleface entrance angle	18°
Poleface exit angle	18°
Field index	0
Beam envelope in bending magnets:	
Max. vertical space occupied by beam	2.80 cm
Max. horizontal space occupied by beam	3.51 cm (including extraction)
Sagitta of 36° bend	4.90 cm
Width of good field required	8.41 cm
Definition of "good field"	± 0.05%
Power supply stability	± 0.005% (long term)
Field difference between any two magnets	< 0.1%

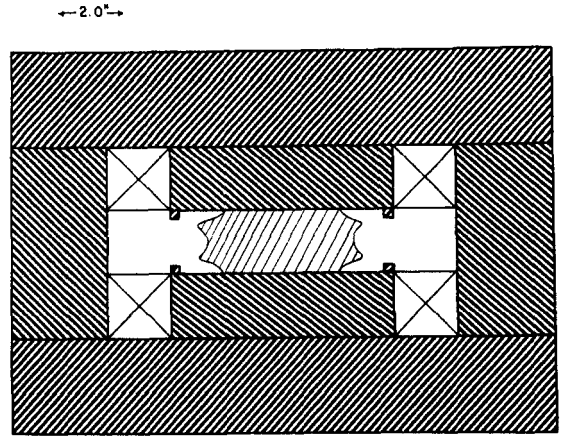

Fig. 7 Cross section through bending magnet.

Table 3
Quadrupole Requirements

1)	Strength	$-1.828\ m^{-2}$
	Effective length	0.25 m
	Aperture	12.7 cm (5 in.) diam.
	Max. field gradient	15,233 G/m
	Max. poletip inductance	967.4 G
	Number required	8
	Designation	5 QS 1.2
2)	Strength	$1.922\ m^{-2}$
	Effective length	0.25 m
	Aperture	12.7 cm (5 in.) diam.
	Max. field gradient	16,017 G/m
	Max. poletip inductance	1016.9 G
	Number required	8
	Designation	5 QS 1.2
3)	Strength	$1.778\ m^{-2}$
	Effective length	0.25 m
	Aperture	12.7 cm (5 in.) diam.
	Max. field gradient	14,817 G/m
	Max. poletip inductance	941.0 G
	Number required	4
	Designation	5 QC 1.2
4)	Strength	$3.556\ m^{-2}$
	Effective length	0.25 m
	Aperture	12.7 cm (5 in.) diam.
	Max. field gradient	29,633 G/m
	Max. poletip inductance	1882.0 G
	Number required	8
	Designation	5 QC 2.4
	Total integrated harmonic content at 4 in. aperture	1%
	Field difference between any two quadrupoles (tracking)	< 0.1%
	Power supply stability	± 0.005% (long term)

Table 4
Sextupole Requirements

1)	Strength	$-6.0\ m^{-3}$
	Effective length	0.2 m
	Aperture	12.7 cm (5 in.) diam.
	Poletip inductance	242 G
	Number required	2
	Designation	5 S .4
2)	Strength	$-7.65\ m^{-3}$
	Effective length	0.2 m
	Aperture	12.7 cm (5 in.) diam.
	Poletip inductance	305.7 G
	Number required	4
	Designation	5 S .4
3)	Strength	$0.318\ m^{-3}$
	Effective length	0.2 m
	Aperture	14.0 cm(5.5 in.)diam.
	Effective poletip inductance (these are air-core magnets)	15.6 G
	Number required	4
	Designation	5.5 S .016
	Total integrated harmonic content permissible at 4 in. aperture	10%
	Magnetic field stability	0.1%

a simple ray tracing program, and it turned out to be 56.64 cm. The flux in the return yoke was 13.6 kG at a thickness of 7.5 cm; the reluctance of the iron was 3% of the total, and the magnet requires 35,000 At at maximum field.

Quadrupoles

Table 3 shows the requirements for quadrupole magnets. Although an aperture of 10 cm would have been sufficient to handle the maximum extent of the beam in the ring, the aperture was increased to 12.7 cm for two reasons: (i) since the ring is designed to handle electrons of 100 MeV or less, the poletip inductance of the quads at this energy would have been very low (300 gauss or less), and remanent field problems would probably be encountered which would jeopardize the fine tuning of the ring. (ii) The first harmonic produced in a quadrupole due to the non-infinite extent of the magnet and to the non-hyperbolic shape of the poles is the 12-pole (n = 6, which decreases with the fifth power of the radius as one moves inward), thus an increase in aperture to 12.7 cm would considerably decrease the harmonic content at the normalizing aperture of 10 cm. The pole pieces can thus be cut from 6 inch diameter circular steel rods, which simplifies the construction considerably. Further reduction of harmonic content can be achieved by careful assembly and machining, chamfering the pole-edges at the exit and entry planes of the magnet and using mirror-plates (field-clamps) with adjustable studs.[6] Prototype magnet tests will reveal if these steps are necessary.

To meet ring tuning requirements, the quadrupoles must be driven in four groups (three groups of eight magnets and one group of four). The poles of all the magnets of one group must therefore be driven in series by one power supply. Since we wanted to avoid high voltages, we decided to use small water-cooled coils of low impedance.

Sextupoles

The requirements for sextupoles are outlined in Table 4. It can be seen that the poletip inductance of the iron magnets is quite low even after an increase in aperture; thus for low energy operation, remanent field problems could occur. Only experience will show the necessity of adding a degaussing cycle to the power supplies that drive them. Harmonic content should not be a problem, due to the increased aperture in both the iron-core and air-core magnets. The magnet coils are air-cooled and all of the magnets in each of the three groups indicated in Table 4 will be driven in series.

References

[1] R. Servranckx, Proceedings of the International Conference on Photonuclear Reactions and Applications, Asilomar, Calif., p.1039 (1973).
[2] Saskatchewan Accelerator Laboratory, Internal Reports SAL-RING-16 to -25, -27 (unpublished).
[3] Saskatchewan Accelerator Laboratory, Internal Report SAL-RING-28 (unpublished).
[4] R. Servranckx, Particle Accelerators (in press).
[5] J. S. Colonias and J. H. Cole, Proceedings of the International Symposium on Magnet Technology, Stanford University, p.188 (1965).
[6] W. V. Hassenzahl, Proceedings of the International Conference on Magnet Technology, Brookhaven, p.469 (1972).

PRELIMINARY DESIGN CONSIDERATIONS FOR THE STAGE I PEP LATTICE+

R. H. Helm and M. J. Lee

Stanford Linear Accelerator Center
Stanford University, Stanford, California 94305

Description and Summary

A general description of the proposed PEP e^+e^- storage ring may be found elsewhere[1,2] and in these Proceedings.[3] In the present paper, we discuss the lattice and its operating characteristics in more detail, show how the design luminosity and other criteria may be met and outline the limits of the operative regions of the beam parameters in several modes of operation.

The relevant design parameters are:

Beam Energy, E (each beam)	5 to 15 GeV
Luminosity per Interaction Regions at 15 GeV, $\mathscr{L}$	10^{32} cm^{-2}sec^{-1}
Number of Superperiods (number of interaction regions)	6
Number of Stored Bunches, N_b (each beam)	3
Available Length per Interaction Region	20 m
Length of Straight Sections	130.416 m
Gross Radius Arcs	220.337 m

Figure 1 depicts schematically the basic elements of the lattice as presently conceived and shows typical betatron and dispersion functions. The 60° arc of each superperiod contains eight cells, of which six are standard while in the two end cells the quadrupoles are independently variable. The structure is symmetric about the interaction points and about the centers of the 60° arcs. The proposed Stage I of PEP lies in a horizontal plane, although a future Stage II option with an added 200 GeV proton ring would involve vertical as well as horizontal bends.[4] Qualitatively speaking, the four independent quadrupoles in the straight sections Q3, Q2, Q1 and QF1 (see Fig. 1) provide matching of the betatron functions from the interaction point to the cells; the two modified cell quadrupoles QD1 and QF2 provide for dispersion matching; and the two sets of standard cell quadrupoles QD and QF allow adjustment of the betatron tunes.

Design Requirements

Luminosity Considerations. In order to define the lattice requirements imposed by the luminosity specification, we consider an idealized situation in which the stored e^+ and e^- beams are equal, and the coupling between horizontal and vertical betatron oscillations is adjusted so that the horizontal and vertical beam-beam tune shifts are equal ($\Delta\nu_x = \Delta\nu_y = \Delta\nu$). It then follows from simplified theory[5,6] that

$$\mathscr{L}_{max} = \frac{\pi}{r_e^2 m_e^2} f_0 N_b (\Delta\nu)^2 E^2 \left(\frac{1}{\beta_y^*} + \frac{1}{\beta_x^*}\right)\left(\epsilon_0 + \frac{\eta^{*2}}{\beta_x^*}\frac{\sigma_E^2}{E^2}\right). \quad (1)$$

Further, if the bending magnets are of equal strength and zero-gradient,

$$\mathscr{L}_{max} = \frac{55\pi}{32\sqrt{3}} \frac{\hbar c/e^2}{r_e m_e^4} \frac{f_0 N_b (\Delta\nu)^2 E^4}{P\rho} \left(\frac{1}{\beta_y^*} + \frac{1}{\beta_x^*}\right)\left(\langle \overline{H} \rangle + \frac{1}{2}\frac{\eta^{*2}}{\beta_x^*}\right), \quad (2)$$

where $\mathscr{L}_{max}$ is the maximum luminosity at the beam-beam tune shift $\Delta\nu$, $\hbar c/e^2 = 137.0$, r_e is the classical electron radius, m_e is the electron rest energy, f_0 is the orbital frequency, N_b is the number of bunches in each beam, E is the energy of each beam, β_x^* and β_y^* are the horizontal and vertical betatron functions at the interaction point, $\epsilon_0\pi$ is the total transverse emittance (i.e., the sum of the areas in radial and vertical phase space), η^* is the dispersion function at the interaction point, σ_E/E is the relative energy spread due to quantum excitation,, ρ_0 is the magnetic radius of the bending magnets and $\langle H \rangle$ is defined by

$$\langle \overline{H} \rangle = \frac{1}{2\pi\rho_0} \sum \int_i \frac{1}{\beta_x} \left[\eta^2 + (\beta_x \eta' - \frac{1}{2}\beta_x' \eta)^2\right] ds \quad (3)$$

where $\int_i$ denotes integration over the i-th bending magnet and Σ denotes summation over all bending magnets.

The luminosity is limited by the maximum tolerable beam-beam tune shift which is typically $\Delta\nu_{max} = 0.025$ to 0.08 per interaction point in e^+e^- storage rings.[7,8] It is evident from Eqs. (1) and (2) that the interaction betatron functions should be as small as possible. The minimum value of β_y^* has been chosen to be around 0.2 meters because it is felt that the maximum β-value at the nearest quadrupole, 10 meters from the interaction point, should be not much greater than 500 meters in order to keep apertures and chromaticity within tolerable bounds. The minimum value permitted for β_x^* is considerably larger because of the D-F configuration of the Q3-Q2 doublet. (See Fig. 1.) As will be seen later, useful ranges of β_x^* for the present design lie in the range of ~3 to 5 meters.

Aperture Limitation. Equation (2) shows that for a fixed lattice, luminosity varies as E^4 and therefore falls off very rapidly at low energy. However, it is possible to modify the lattice so that the beam size is kept essentially constant as a function of energy; then luminosity varies only as E^2, as may be seen from Eq. (1). In the PEP design, the apertures are chosen for the design energy and luminosity at 15 GeV and the luminosity is therefore aperture-limited at lower energies with an approximate E^2 dependence.

Beam Enlargement. Several schemes for beam enlargement* have been studied for lower energy operation. Some of the important features of these schemes are described below.

(1) Variable Tune. It can be shown that, approximately, $\epsilon_0 \propto N_c \psi_{xc}^{-3} E^2$ where N_c is the number of bending cells and ψ_{xc} is the horizontal betatron phase advance per cell.[2]

† Work supported by the U. S. Atomic Energy Commission.

* For another discussion of beam enlargement see Ref. 9.

Thus in order to keep ϵ_0 constant for different energies we wish to make the lattice operable over some range of values of ψ_{xc}. In this design study we have considered only cases with $\nu_x \times \nu_y$ and also have assumed that the vertical tunes should be just slightly above an integer or half-integer per superperiod.[10,11] This means that for the PEP lattice with superperiodicity of 6, the desirable tunes are, e.g., $\nu_{x,y} \approx 12, 15, 18, 21, \cdots$. In the present PEP design, the horizontal phase advance in the straight insertion is always close to 360°, so that the design values of phase advance per cell are $\psi_{xc} \approx 45^0, 62.5^0, 90^0, 112.5^0, \cdots$.

(2) Energy Disperiosn (High η^*). A variable value of the interaction point dispersion function η^* alters the luminosity limit through the factor η^{*2}/β_x^* [Eqs. (1) and (2)]. This scheme has been used successfully, e.g. at SPEAR.[7]

(3) Mismatched Dispersion Function. In common practice the momentum dispersion function is matched so that it repeats periodically from cell to cell in the standard cells. We may, however, for low energy operation mismatch the dispersion function in the standard cells as described by

$$\eta(s) = \eta_0(s) + \eta_1(s),$$

where $\eta_0(s)$, the matched dispersion function, is periodic from cell to cell, and $\eta_1(s)$, the mismatch component, is oscillatory at the betatron wavelength. As is shown elsewhere, this results in an increase in the function $\langle \overline{H} \rangle$, described roughly by[6]

$$\langle \overline{H} \rangle = \frac{1}{\beta} (\eta_{0s}^2 + \eta_1^2 \qquad (4)$$

where the subscript s denotes the symmetry point (midpoint) of the bending arc. That is, the emittance is quadratic in the mismatch amplitude.

A fourth method of beam enlargement, mismatching the betatron function β_x, also affects the quantity $\langle \overline{H} \rangle$. This scheme was considered briefly in the PEP study but seemed to offer no obvious advantages. It may be studied further if serious difficulties arise in other schemes.

Another possible method of beam enlargement consists of altering the damping partition number J_x, since $\epsilon_0 \propto \langle \overline{H} \rangle / J_x$. In order to avoid complexity and expense, no special insertion is planned for damping modification as is planned in EPIC.[12] However, it still would be possible to vary J_x by varying the rf frequency from its nominal value; it may be shown that the PEP lattice would require a frequency change of about 2 parts in 10^5, resulting in a maximum orbit shift of less than a centimeter, to reduce J_x to zero.

Since the variable tune and the dispersion-mismatch methods increase the transverse emittance they increase the aperture requirements everywhere in the lattice. The high-η^* method, on the other hand, enlarges the beam in only the few quadrupoles nearest the interaction points, which may be a significant advantage in terms of sensitivity to orbit distortions. However it has been shown that the high-η^* configurations may lead to a longitudinal instability if η^* is too large.[8]

We expect that practical operating configurations will consists of combinations of variable-tune and high-η^*, or of high-η^* and mismatched-η, although other combinations may prove useful. Some of these configurations are discussed in a later section.

First Order Design

Summary of Constraints. The lattice requirements that have been discussed so far imply that the values of β_x^*, β_y^*, η^* and the tunes ν_x and ν_y should be independently adjustable. In addition, the symmetry of the ring requires that the slopes of the betatron and dispersion functions vanish at the interaction regions; i.e., $\beta_x'^* = \beta_y'^* = \eta'^* = 0$. Thus, eight mathematical constraints are imposed on the focusing strengths, requiring at least eight independently variable sets of quadrupoles. A number of other important constraints must also be considered. A twenty meter drift space is required for experiments at each interaction region. The maximum values of the p-functions and η-function must be kept everywhere within reasonable bounds in order to minimize aperture requirements and to reduce chromaticity and other aberrations. Magnetic field values must be kept within conservative limits. Furthermore, sufficient drift space must be reserved for various components such as rf cavities, injection components (septum magnets and kickers), rotated quadrupoles, sextupoles, beam monitors and control devices, electrostatic plates for separating the beams and so on.

The geometry of the ring has been fixed by considerations discussed in Ref. (1). Once the quadrupole locations have been fixed and the quadrupole strengths have been specified to satisfy the eight mathematical constraints mentioned above, it will not always be possible for all configurations to satisfy the additional constraints imposed by aperture and quadrupole strength limits. Hence in the present study we have mapped out the regions of beam parameters within which all of the constraints are satisfied. Some of the results will be described in a later section.

Computational Methods. Solutions for the quadrupole settings under a variety of focusing configurations as specified by the values of β_x^*, β_y^*, η^*, η_s, ν_x and ν_y have been found by use of the magneto-optic programs MAGIC[13] and TRANSPORT.[14] MAGIC employs thin-lens approximations for the transport elements, but has great flexibility and speed, and has been used to survey a wide range of configurations. TRANSPORT has been used to obtain more precise thick-lens solutions in a number of cases, and the beam tracing program SYNCH[15,16] has been used to generate emittances, beam sizes, luminosities, etc., from the TRANSPORT solutions. In all cases which have been checked, the thin-lens MAGIC results* agree with the thick-lens TRANSPORT-SYNCH results to within 5 to 10% in betatron functions, damping rates, emittance and luminosity.

Typical Configurations. The MAGIC program has been used to survey a large number of possible configurations. Some of the interesting results are shown in Figs. 2 through 6.

*Figures 2, 3 and 4 show the operative regions in the (β_x^*, η^*) plane at several different tunes in the matched-η mode. The tunes of 18.75, 15.75 and 12.75 have been chosen for illustrative purposes; in practice, of course, ν_x and ν_y would be split to avoid the linear coupling resonance, and neither would be exactly on the quarter integer. The operative regions in these plots are limited by regions in which either the beam size becomes too large (aperture limit) or in which there are no mathematical solutions to the non-linear set of equations which relate the constraints to the variable quadrupole strengths. The luminosity contours are plotted for the nominal energies of 15, 10 and 5 GeV, respectively; the beam-beam tune shifts per interaction region are assumed to be $\Delta\nu_x = \Delta\nu_y = 0.06$. Note that the design luminosities given by $\mathscr{L}_{max} \propto E^2$ are respectively 1.0, 0.44 and 0.11 (in units of 10^{32}cm^{-2}sec^{-1}) for 15, 10 and 5 GeV. For other values of tune shift and energy the value of luminosity may be scaled according to Eq. (2).

The luminosity contours and boundaries of the operative region in the (β_x^*, η^*) plane may be shifted somewhat by different choices of β_y^*.

* In the computation a pair of thin lenses is used for each quadrupole magnet with a short focal length such as Q2 and Q3. The thin lenses are symmetrically located about the center of the magnet and separated by 1/2 of magnet length.

Table I shows values of some of the beam and machine parameters for three typical matched-q configurations, as obtained by TRANSPORT and SYNCH.

Figure 5 illustrates the operative region in the (η_s, η^*) plane for the mismatched-q mode of operation, for $\nu = 18.75$, $\beta_x^* = 4.0$ m and $\beta_y^* = 0.2$ m. The contours represent the energies at which $\mathscr{L}_{max} = 10^{32}(E/15\ \mathrm{GeV})^2$ (in $\mathrm{cm}^{-2}\mathrm{sec}^{-1}$) at tune shifts of $\Delta\nu_x = \Delta\nu_y = 0.06$. Note that the full design energy range of 5 to 15 GeV is covered in one continuous region of the (η_s, η^*) plane, but that non-zero values of η^* as well as η-mismatch are required at the lower energies. In the right-hand portion of Fig. 5, the beam size at the interaction point is dominated by the dispersion term for configurations near the lower operative boundary, and by emittance (enhanced by the η-mismatch) near the upper boundary.

Figure 6 shows how the parameters α (momentum compaction) $\sigma_{x\beta}$, σ_{xE}, and the energy for design luminosity vary with the η-mismatch, along the particular path designated as Path A in Fig. 5.

Second-Order Design

Chromaticity. Sextupole magnets will be placed near some of the standard cell quadrupoles in order to control the chromaticity. The uncorrected chromaticities when the tunes are around 18 are $\xi_x \approx -35$, $\xi_y \approx -100$ where the definition is

$$\xi = E_0 \frac{\partial \nu}{\partial E} .$$

Overcorrection of the chromaticities by 10 to 20% will probably be used as at SPEAR, in order to take advantage of the fast damping effect for coherent oscillations.[17] The sextupole strengths required for this correction have been found to be quite modest.

Non-linear Stopbands. The sixfold symmetry of the ring will tend to produce large sextupole Fourier coefficients with indices which are multiples of 6. These will strongly excite the stopbands at tunes 12 and 18. To suppress these coefficients we probably will need additional sextupoles in the straight sections; e.g., near QF1 and Q3.

Damping Variation with Frequency. The damping partition numbers (J_x and J_E) for an off-energy particle are determined by the value of the quantity

$$D = D_0 + D_E \frac{\Delta E}{E_0} + \cdots ,$$

where, for a machine using rectangular zero-gradient bending magnets,[18]

$$|D_0| << 1$$

and

$$D_E \approx \frac{2\oint \eta^2 G^2 ds}{\oint B^2 ds} ,$$

in which G is the local quadrupole gradient and B is the bending field. The damping rates,

$$\alpha_x \propto J_x = 1 - D \qquad \text{and} \qquad \alpha_E \propto J_E = 2 + D$$

are affected very little by the natural energy spread of the beam because ΔE goes through many synchrotron oscillations during a damping period. However, if the equilibrium closed orbit is shifted by a change in orbital frequency (or equivalently rf frequency), we have

$$D_f \equiv f_0 \frac{\partial D}{\partial f_0} = -\frac{D_E}{\alpha}$$

or

$$D \approx -\frac{D_E}{\alpha}\frac{\Delta f_0}{f_0}$$

where α is the momentum compaction factor. Thus a shift in the rf frequency does affect the damping rate.

In the matched PEP configurations, we typically have $D_E \sim 250$ to 300, with α ranging from -0.004 at tune 18 to -0.02 at tune 12. Hence the frequency change to produce $D \sim 1$ is $\Delta f_0/f_0 \gtrsim 2 \cdot 10^{-5}$. In the unmatched-configurations, however, D_E can be an order of magnitude greater, and the frequency stability required to keep the damping rate constant may be a problem.

Conclusions

The present version of the PEP lattice is capable of reaching the theoretical design luminosity by means of several alternative operating configurations, at least according to first-order theory. Investigation of non-linear effects may further delimit the choice of favorable operating configurations.

Acknowledgments

Many of the features of the lattice design originated with A. Garren, W. Herrmannsfeldt, P. Morton, B. Richter and J. Rees. We are indebted to A. King and B. Woo for computer programming assistance.

References

1. PEP Study Group, A Proposal for a Positron-Electron Colliding Beam Storage Ring Project, ed. J. Rees and W. B. Herrmannsfeldt, Stanford Linear Accelerator Center Report No. 171, Stanford Linear Accelerator Center, Stanford, Calif. (1974).
2. J. Rees and B. Richter, "Preliminary Design of a 15-GeV Electron-Positron Variable-Tune Storage Ring," PEP-NOTE 69, 1973 PEP Summer Study Report (unpublished).
3. J. Rees, "The PEP Electron Positron Ring — PEP Stage I," invited paper to this conference.
4. L. Smith, "The Proton-Electron-Positron Project — PEP," invited paper to this conference.
5. M. Sands. "The Phvsics of Electron Storage Rings, an Introduction," Proceedings of the International School of Physics "Enrico Fermi", Course XLVI, ed. B. Touschek (Academic Press, 1971); also Stanford Linear Accelerator Center Report No. 121.
6. R. H. Helm, M. J. Lee and J. M. Paterson, "Beam Enlargement by Mismatching the Energy-Dispersion Function," published report to this conference.
7. J. Paterson, "SPEAR, Status and Future Developments," invited paper to this conference.
8. F. Amman, "IEEE Trans. Nucl. Sci. NS-20 No. 3, 858 (1973).
9. M. Bassetti, "Beam Dimension Control in Storage Rings," CNEN, Frascati Laboratories, published report to this conference.
10. M. Bassetti, Proceedings of V International Conference on High Energy Accelerators, Frascati, 709 (1965).
11. B. Richter, "Design Considerations for High Energy Electron-Positron Storage Rings," Proceedings of the International Symposium on Electron and Positron Storage Rings (1966).
12. G. H. Rees, "Aspects of PEP as Compared to EPIC," PEP-NOTE 51, 1973 PEP Summer Study (unpublished).
13. M. J. Le. W. W. Lee and L. C. Teng, "Magnet Insertion Code," PEP NOTE 61, 1973 PEP Summer Design Study (unpublish).
14. K. L. Brown, and S. K. Howry, "TRANSPORT/360 A Computer Program for Designing Charged Particle Beam Transport System," Stanford Linear Accelerator Center Report No. 91 (1970).

15. **A. A.** Garren and **A.** S. Kenney, "A Computer Program for Synchrotron Design and Orbit **Analysis,**" Internal note LBL 1968 (unpublished).
16. J. S. Colonias, "Particle Accelerator Design; Computer Programs," Book, Academic Press (1974).
17. ***SPEAR*** Group, "Fast Damping of Transverse Coherent Dipole Oscillations in SPEAR," published report to this conference.
18. H. Wiedemann, "Scaling *of* FODO-CELL Parameters," PEP-NOTE 39, 1973 PEP Summer Study (unpublished).

TABLE I

Typical Beam Parameters

		5 Gev	10 Gev	15 GeV	
Total Betatron Tune					
Horizontal	ν_x	12.75	15.75	18. 75	
Vertical	ν_y	12.75	15.75	18. 75	
Momentum Compaction		0. 01668	0. 00759	0.00455	
Transverse Damping Time	τ_x, τ_y	0.222	0.0278	0. 00823	sec
x-y Coupling Coefficient	κ	0.249	0.294	0.280	
Horizontal Emittance	ϵ_x	1.730×10^{-5}	2.149×10^{-5}	2.297×10^{-5}	cm-rad
Vertical Emittance	ϵ_y	1.072×10^{-6}	1.858×10^{-6}	1.796×10^{-6}	cm-rad
Number of Stored Particles (each beam)	N	1.252×10^{12}	3.055×10^{12}	4.44×10^{12}	
Synchrotron Radiation Power (each beam)	P_{rad}	0.0090	0.353	2.596	MW
Linear Tune Shifts per Interaction Point					
Horizontal	$\Delta\nu_x$	0. 06	0.06	0. 06	
Vertical	$\Delta\nu_y$	0. 06	0. 06	0. 06	
Luminosity (each interaction point)	$\mathscr{L}$	0.117×10^{-32}	0.462×10^{32}	1.008×10^{32}	$cm^{-2}sec^{-1}$
Cell Parameters					
Horizontal Phase Advance	ψ_x	48.9^o	72.9^o	97.0^o	
Vertical Phase Advance	ψ_y	29.9^o	56.5^o	82.3^o	
Maximum Horizontal Beta	$\beta_{x\,max}$	50.1	45.1	48.2	m
Maximum Vertical Beta	$\beta_{y\,max}$	78.8	53.9	50.2	m
Maximum Momentum Dispersion	η_{max}	6.38	3.34	2.24	m
Interaction Region Parameters					
Horizontal Beta	β_x^*	4.6	4.0	4.0	m
Vertical Beta	β_y^*	0.16	0.20	0.20	m
Momentum Dispersion	η^*	-2.40	-1.20	-0.73	m
Horizontal Beam Size (betatron)	$\sigma_{x\,\beta}^*$	0. 0892	0.0927	0.0959	cm
Horizontal Beam Size (dispersion)	$\sigma_{x\,E}^*$	0. 0789	0.0789	0.072 0	cm
Horizontal Beam Size (total)	σ_x^*	0.1191	0.1217	0.1199	cm
Vertical Beam Size	σ_Y^*	0.00414	0.00610	0. 00600	cm

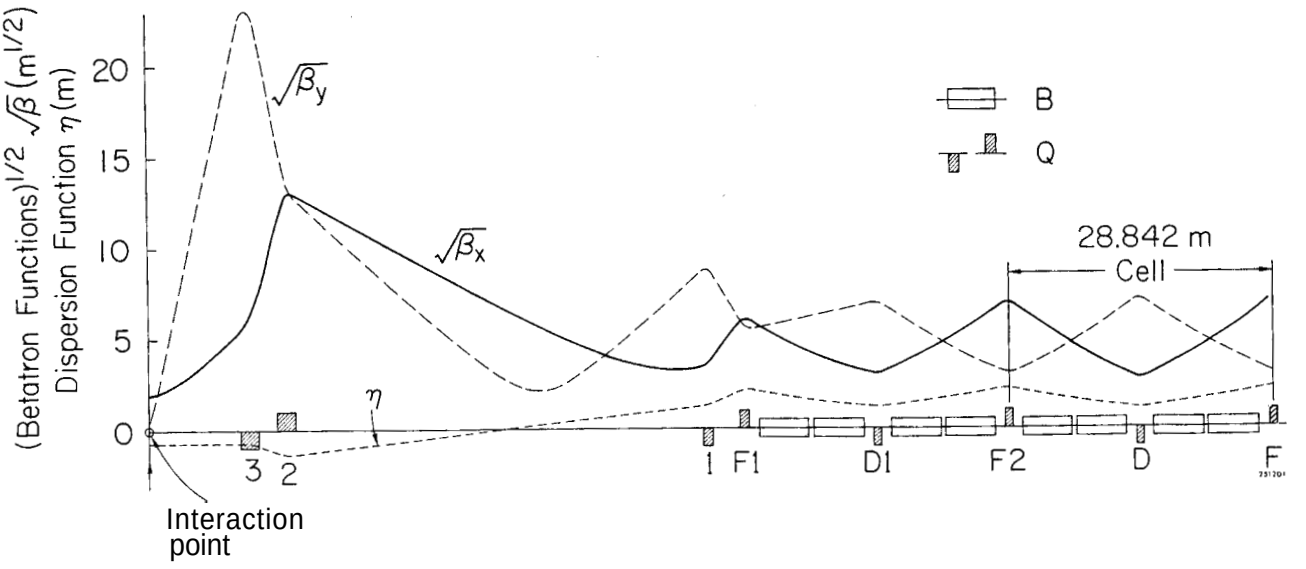

FIG. 1--Schematic of PEP lattice. The typical betatron functions shown are for a matched-q configuration (see text for definition) with $\beta_x^* = 4.0$ m, $\beta_y^* = 0.2$ m, $\eta^* = -0.73$ m, $\nu_x = \nu_y = 18.75$.

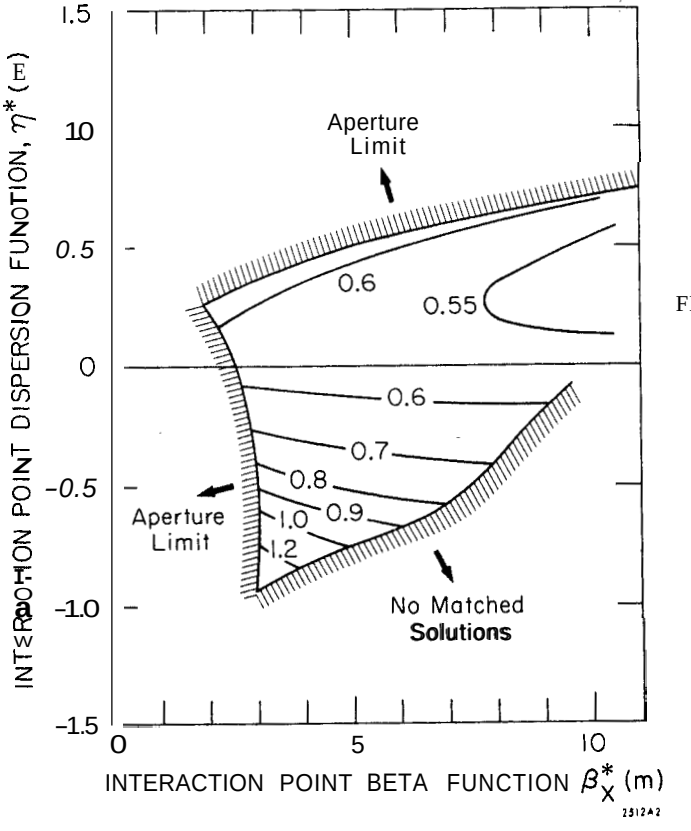

FIG. 2--Matched-η mode operative region in the (β_x^*, η^*) plane with $\nu_x = \nu_y = 18.75$, $\beta_y^* = 0.20$ m. The contours are luminosities in units of 10^{32}cm^{-2} sec^{-1}, computed at energy E = 15 GeV and beam-beam tune shifts $\Delta\nu_x = \Delta\nu_y = 0.06$.

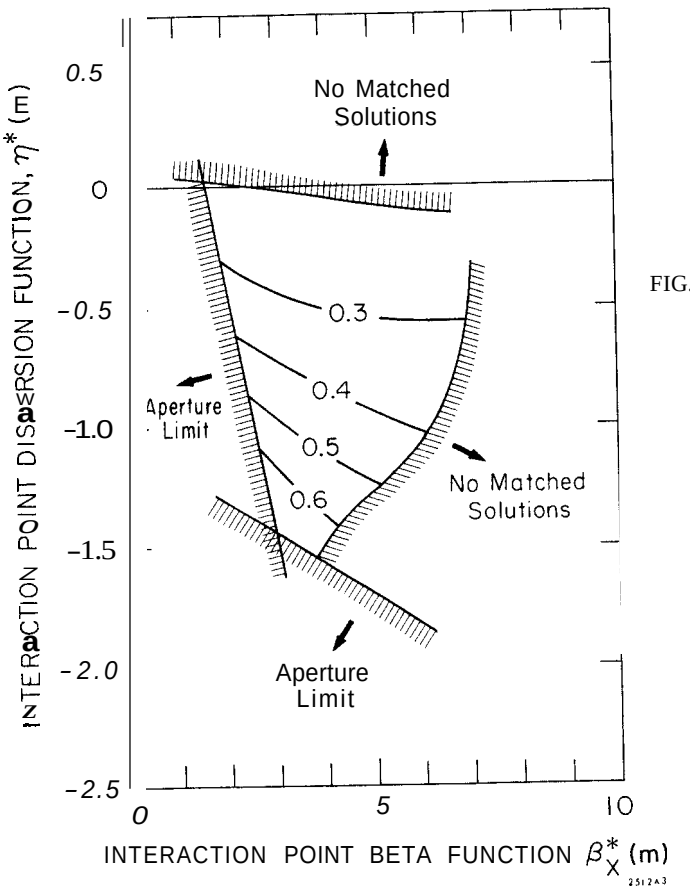

FIG. 3--Matched-η mode operative region in the (β_x^*, η^*) plane with $\nu_x = \nu_y = 15.75$, $\beta_y^* = 0.18$ m. The contours are luminosities in units of 10^{32} cm^{-2} sec^{-1}, computed at energy E = 10 GeV and beam-beam tune shifts $\Delta\nu_x = \Delta\nu_y = 0.06$.

FIG. 4--Matched-η mode operative region in the (β_x^*, η^*) plane with $\nu_x = \nu_y = 12.75$, $\beta_x^* = 0.16$ m. The contours are luminosities in units of 10^{32}cm^{-2} sec^{-1} computed at energy E = 5 GeV and beam-beam tune shifts $\Delta\nu_x = \Delta\nu_y = 0.06$.

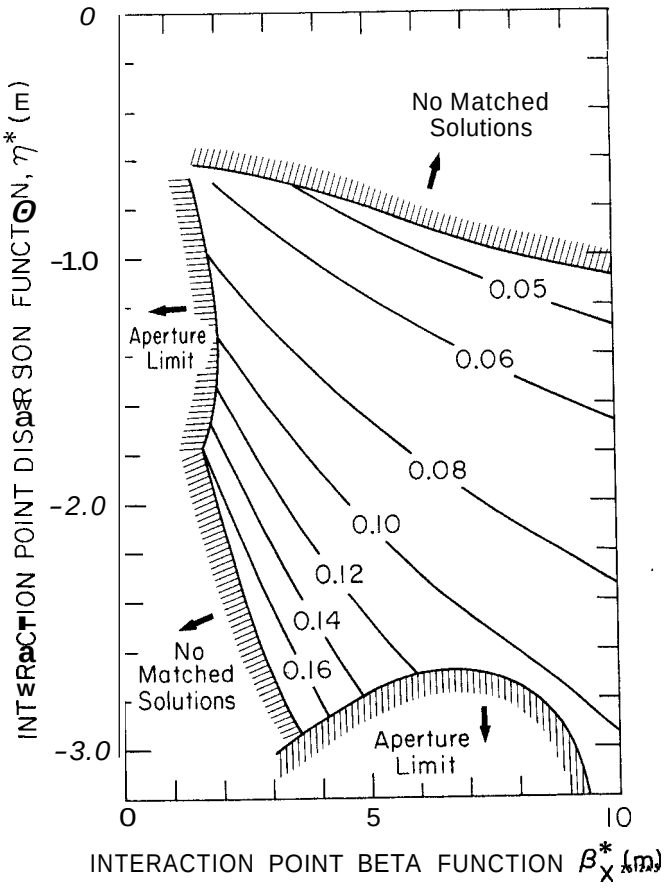

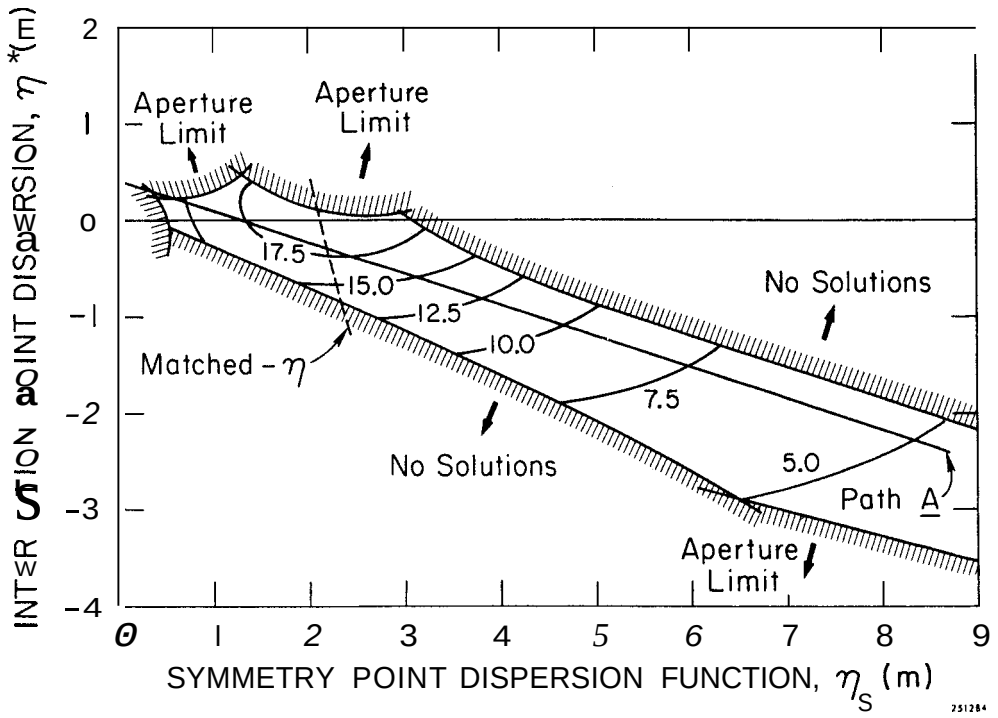

FIG. 5--Mismatched-η mode operative regions in the (η_S, η^*) plane with $\nu_x = \nu_y = 18.75$, $\beta_x^* = 4.0$ m, $\beta_y^* = 0.20$ m. The contours are the energies E_L (GeV) corresponding to luminosities given by $\mathscr{L}_{max} = 10^{32}(E_L/15\ \text{GeV})^2$ (in units of $\text{cm}^{-2}\text{sec}^{-1}$), with $\Delta\nu_x = \Delta\nu_y = 0.06$. The dashed curve labeled "η-matched", near $\eta_S = 2$, represents solutions for which the dispersion function is periodic within the standard cells. The line labeled "Path A" is for reference in Fig. 6.

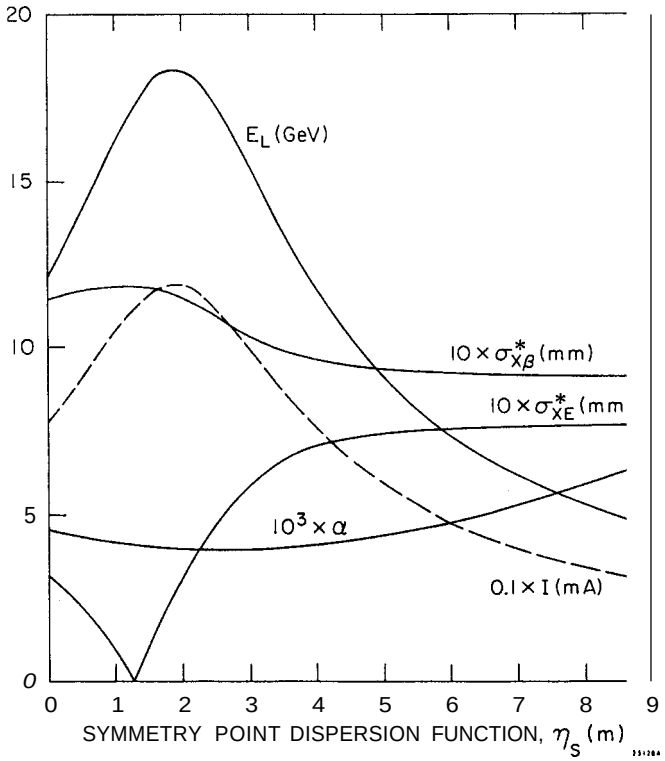

FIG. 6--Variation of beam parameters for different mismatched-η configurations along Path A in Fig. 5 $\sigma_{x\beta}$ is rms beam amplitude due to betatron motion; σ_{xE} is rms beam amplitude due to compaction factor; and I is the current in each beam and $\mathscr{L}_{max} = 10^{32}(E_L/15\ \text{GeV})^2$.

DESIGN CONSIDERATIONS FOR A HIGH ENERGY ELECTRON POSITRON STORAGE RING

H. Wiedemann
Deutsches Elektronen-Synchrotron DESY
Hamburg, Germany

The successfull operation of the electron positron storage ring - SPEAR - in the multi-GeV-range encouraged the accelerator physicist to think about the next generation of storage rings for energies Of more than 10 GeV. We have learned from the presently working storage rings that it seems not practical to assume an artificial beam enlargement as an essential design aspect. As is well known this artificial beam enlargement was needed to get high luminosities at medium energies where the beam intensities are limited by the beam beam interaction at the collision points. Therefore we have to find other means to increase the luminosity in this energy regime. One possible way is to vary the focusing of the periodic cell structure of a storage ring with energy, thus varying the quantum excitation of betatron oscillations [1),2)]. This brings us to the point where we should discuss more general the influence of the beam optics in the periodic cell structure on relevant storage ring parameters. In this note this influence on the energy will be discussed. This can be done in rather general terms since the special design of the long straight section on both sides of the interaction point has no effect on the beam parameters except the amplitude functions at the point where the beams collide. For these amplitude functions we assume values which we know can be realized. Throughout this note we assume only one ring where the two beams counterrotate in the same vacuum pipe and collide head on in the interaction points.

I. Storage Ring Parameters for Numerical Calculations

For numerical calculations in this note we assume the following storage ring parameters which are close to parameters assumed in different laboratories for electron-positron storage ring studies of the next generation:

circumference of the ring	C	= 2304 m
bending radius	p	= 206.8 m
average radius of the arcs	R	= 256.7 m
installed rf-power	P_{rf}	= 5.0 MW
totallength of cavities (copper)	L_c	= 240 m
shunt impedance of the cavities at 500 Mc	R_c	= 10 MΩ/m

II. Maximum Energy of the Storage Ring

The maximum energy of a storage ring is given when the total installed rf-power is dissipated in the cavities. These cavity losses depend on the cavity length, the shunt impedance per unit length, the rf-frequency and on the necessary rf-voltages as given by the focusing of the periodic cell structure.

The amount of cavity length depends on the amount of money one wants to spend for them. It is not intended to use this length as a parameter here but rather use one length for which the necessary free length in a ring of 2 km circumference can be realized. The shunt impedance per unit length for 500 Mc is conservatively assumed to be 10 MΩ/m which could be increased somewhat using other than iris structures e.g. trift tube cavities. Since the production of the latter are more costly one has to find a cost optimum for the product $R_c \cdot L_c$. The effect of the rf-frequency has been studied in detail [3)] with the result of a very flat optimum in the range of 200 to 700 Mc depending somewhat on the energy for which the design is made. In this note we assume 500 Mc. For these rf-parameters the maximum achievable energies as a function of focusing power are calculated. The focusing is varied by varying the cell length keeping the phase advance per cell constant at 90°. This 90° degree phase advance per cell is an essential for the multibunch operation which is discussed later. Characterising the focusing by the transition energy γ_{tr} the maximum achievable energies using copper rf-cavities are shown in fig.1. It becames clear from fig.1 that the transition energy should be about 20 or larger in order not to loose to much energypotential of the ring. However, the gain between $\gamma_{tr} = 20$ and $\gamma_{tr} = 30$ is only 1 GeV if we use copper cavities.

Designing storage rings of the next generation it might be reasonable also to have a look at the next generation technology which in our case means superconducting cavities. In this case the energy isn't limited by cavity losses any more but by the minimum reasonable luminosity which falls off like E^{-10} in this energy regime. If we exchange the 240 m copper cavities by 240 m of superconducting cavities the maximum energy for a luminosity of $L = 10^{31}\ cm^{-2}sec^{-1}$ is computed and shown in fig.2. Here we find a rather steep increase in energy versus transition energy which calls for the maximum reasonable focusing.

III. Luminosity

It has been shown that increased focusing in the periodic cell structure leads to higher achievable energies. This is a true reflection of the fact that at a fixed energy in the rf-power limited case an increased focusing also results in higher luminosities (fig.3).

At lower energies however, there is the problem of the beam beam incoherent limit. So far it was assumed that each beam is made up by only one bunch *or* in case of more than two interaction points by half as many bunches as there are interaction points. In this case the bunches meet only at the interaction points and nowhere else in the arcs where the beta-functions and by this the beam beam effect is larger. In fig.3 the circles ○ show the maximum luminosities for one bunch. For energies lower than those indicated by the crosses the beam beam effect is effective. Here the luminosity scales like $L \sim A \cdot \gamma^2$, where A is the beam cross section at the interaction point. If natural beam sizes are used - $A \sim \gamma^2$ - the luminosity scales like $L \sim \gamma^4$. To avoid this fast drop of the luminosity toward lower energies the variation of the focusing was proposed [1)2)]. In this note another mode of operation is proposed.

For this we divide the whole energy regime into three parts:

1) J. Rees, B. Richter, Preliminary design of a 15 GeV Electron-Positron Variable Tune Storage Ring, PEP-Note 69; 1973 PEP-Summer-Study
2) H. Wiedemann, e-p Luminosity for different energies in PEP, PEP-Note 58, 1973 PEP-Summer-Study
3) M. Allen, G. Rees, CRISP-Note 72-68, Brookhaven

1. The rf-power limited regime

Here the luminosity is given by: [4]

$$(1)\quad L_1 = \frac{1}{4e^2 f}\,\frac{P_B^2}{U^2 R\cdot B}$$

where: P_B the rf-power available per beam, U the energy loss per turn, f the revolution frequency; A the beam cross section and B the number of bunches. It is clear that the number of bunches should be as small as possible e.g. B = 1. Also the beam cross section should be minimized which requires strong focusing as has been already discussed. Using the scaling laws for FODO-Cell structures [5] the luminosity scales like $L_1 \sim \gamma_{tr}^4$.

2. The rf-power and tune shift limited regime

In this case the beam current per bunch is limited by the incoherent beam beam effect.

$$(2)\quad \Delta\nu = \frac{r_e}{2ef}\,\frac{I\beta}{\gamma AB} = \frac{r_e}{2ef}\,\frac{P_{rf}}{\gamma U}\cdot\frac{\beta}{AB} \le 0.05$$

(β: amplitude function at the interaction point, B number of bunches).
Together with eq. (1) the luminosity is given by

$$(3)\quad L_2 = \frac{f\Delta\nu^2}{r_e^2}\,\frac{A}{\beta^2}\,B\gamma^2$$

Since we assume natural beam sizes the number of bunches B has to be varied according to eq.(2) like:

$$(4)\quad B = \frac{r_e}{2ef}\,\frac{P_{rf}}{\gamma U}\,\frac{\beta}{A} \sim \gamma^{-7}$$

If we find a way to increase the number of bunches considerably the luminosity scales like $L_2 \sim \gamma^{-3}$ in this regime. Here we neglected the rf-cavity losses. Since it seems very advantageous to increase the number of bunches, a way to do this is discussed in this note. As a result of this discussion we find a maximum number of bunches B_{max} which is much smaller than the harmonic number.

3. The tune shift limited regime

At lower energies where we always have the maximum number of bunches the total beam current is limited only by the incoherent beam beam limit and the luminosity is given by:

$$(5)\quad L_3 = \frac{f\Delta\nu^2}{r_e^2\beta^2}\,\gamma^2 A B_{max}$$

Since there is no easy way to have many bunches and a variable focusing the beam sizes are given by the quantum excitation e.g. $A \sim \gamma^2$ and the luminosity then scales as $L_3 \sim \gamma^4$.

Since this multi bunch mode requires only a phase advance of 90° per cell in the arcs the luminosity can be increased at very low energies by turning off every second quadrupole in the arcs thus increasing the cell length by a factor of two. By this the product $A\cdot B_{max}$ can be increased as will be shown later. In principle this can be continued to increase the luminosity at very low energies but doing *so* the aperture limit is reached very fast.

4) M. Sands, Physics of Electron Positron Storage Rings, SLAC-121

5) H. Wiedemann, Scaling of FODO-Cell Parameters, PEP-39, 1973 PEP-Summer-Study

IV. Beam Separation

If we use many bunches per beam we have to separate them outside the interaction points. This can be done with an appropriate number of electrostatic separating plates. Many and strong fields however, are needed if we do not match the separation to the focusing structure of the ring. Since there is a small beam beam effect left even if the beams are separated one would like to have the points where the bunches meet at similar places from the beam optics point of view. The easiest way of separating the two beams is given in the case where the phase advance per cell is just 90°. An electrostatic field introduces a regular closed orbit oscillation with a wavelength equivalent to two cell lengths (fig.4). The distance between bunches cames out to be one cell length or a multiple of that length. While for the arcs only one separating plate on either end is needed one may need some more in the straight sections due to the nonregular structure there.

The circumference of the storage ring has to be a multiple of the cell length. Also the distance from any "pass by point" in the arcs to the interaction point has to be a multiple of one half cell length.

In the numerical example a transition energy of γ_{tr} = 31 is realized by a cell length of L = 14.4 m. The maximum number of bunches then is 160.

V. Beam-Beam-Effect

Even with beam separation there is still an electromagnetic interaction of one beam on the particles of the other beam the socalled long range forces. It is well known from experience of running storage rings that the beam separation has to be large compared to the standard beam width (a horizontal beam separation is considered). In this note a beam separation is assumed large enough that one beam sees only a force from the other beam which falls off like the inverse of the separation, $F \sim 1/x$. This means the separation x is at least $10\sigma_x$. For that large separations the linear tune shift turns out to be: [6]

$$(6)\quad \delta\nu = 9.6\times10^{-9}\,\frac{\beta_x I\cdot C}{cp\ x^2}$$

where β is the betatron amplitude at the "pass by points", I the total beam current in amps, C the ring circumference, cp the beam energy and x the beam separation (C,β,x in meters).

To achieve the shown luminosity in fig.3 for γ_{tr} = 31, a maximum current of I = 140 ma at 15 GeV and β_x = 11.1 m at a pass by points the linear tune shift is $\delta\nu\cdot x^2 = 0.023\ cm^2$. For a separation of x = 1 cm which is equivalent to a separation of $x = 20.5\ \sigma_x$ the total linear tune shift outside the interaction points is only $\delta\nu = 0.023$. The total beam beam effect at a separation of $x \approx 20\ \sigma_x$ is very much reduced to a mere linear tune shift which can easy be corrected by electrostatic quadrupoles. The nonlinear part of the beam beam effect can be neglected for the magnitude of separation discussed here [6].

The total aperture requirement in this case is only $A = x + 14\ \sigma_x$ = 17 mm. This seems very little however, one needs more at higher energies. At 22 GeV which is the highest energy where the beams have to be

6) SPEAR-Group, Beam Beam Coupling in SPEAR, Proceedings of this conference

separated the standard width is σ_x = 0.71 mm. A separation of x = 1 cm corresponds still to 14 σ_x and the aperture requirement is only A = 20 mm. This small aperture requirements show that the beam separation may be easily increased to twice the assumed value to be safe.

At energies below 15 GeV it is advantageous to double the cell length by turning off every second quadrupole which gives a γ_{tr} = *15.4*. Here the maximum number of bunches is 80 and the maximum current at 12 GeV is I = 290 ma. With β_x = 33.2 m and x = 2 cm corresponding to 10 σ_x the linear tune shift is $\delta\nu$ = *0.044*. In this case the maximum luminosity is 2×10^{32} $cm^{-2}sec^{-1}$ for a total installed rf-power of 5 MW (fig.3).

VI. Conclusion

To achieve the highest possible energy for a given installed rf-power the focusing in the periodic cell structure should be as strong as possible. For lower energies where the beam beam effect is effective the total beam current can be pushed up by filling many bunches in one beam, which requires beam separation outside the interaction points. The total linear tune shift due to long range forces is small. Even with beam separation the required apertures seem not to be excessive due to the small beam sizes produced by the strong focusing.

Acknowledgement

The author wishes to thank G.A. Voss for many helpfull discussions.

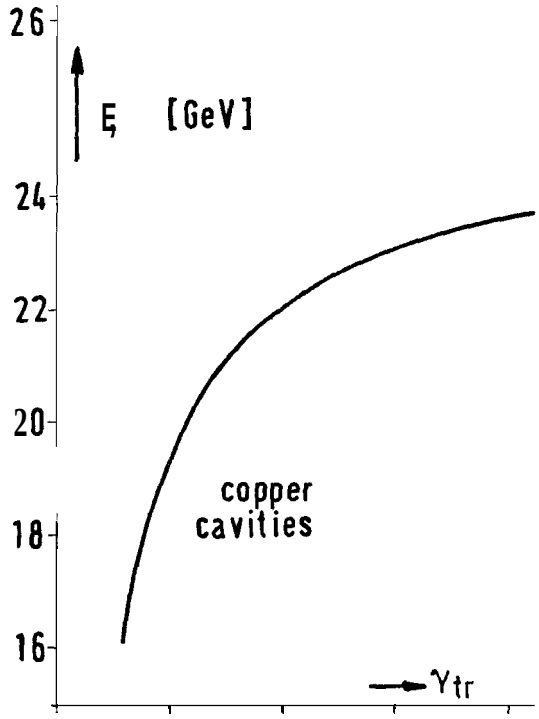

Fig.1: Maximum storage ring energy vs transition energy,

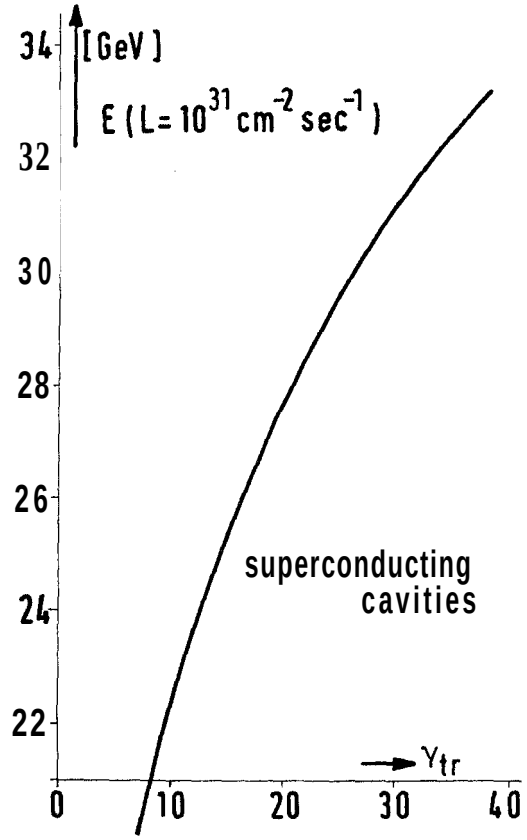

Fig.2: Maximum energy for a luminosity of L = 10^{31} $cm^{-2}sec^{-1}$ vs. transition energy.

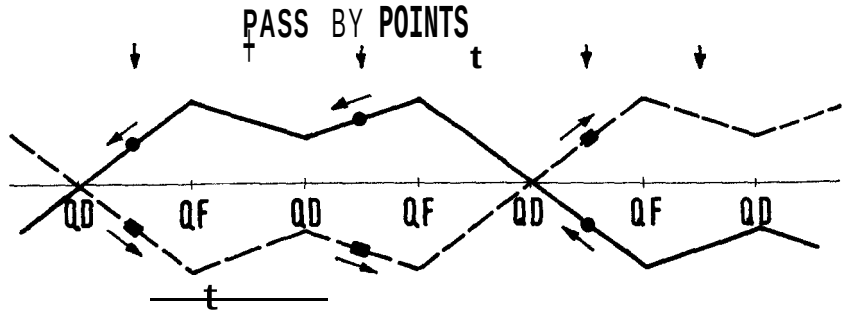

Fig.4: Separation of the beams in the multibunch mode.

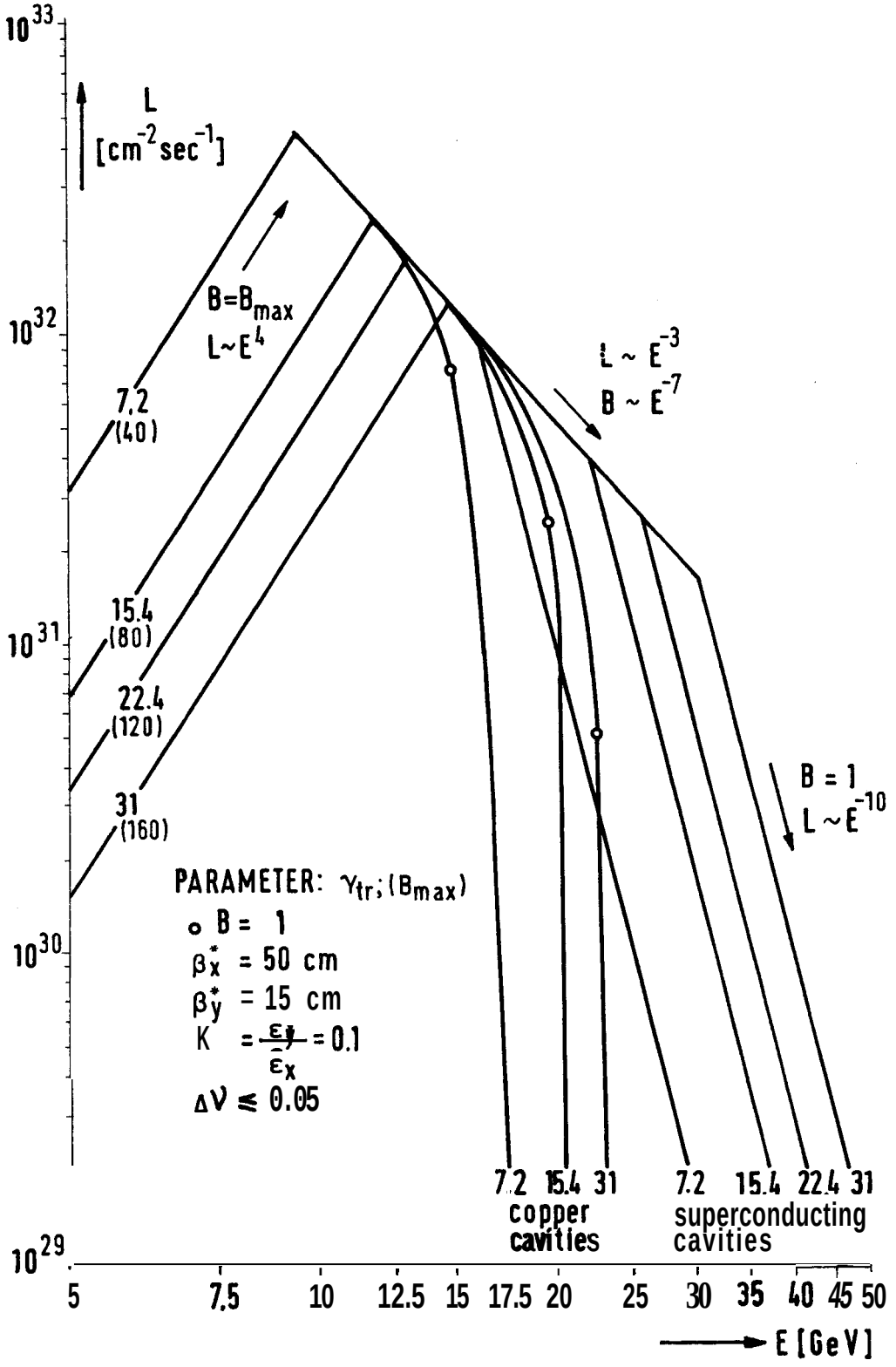

Fig.3: Luminosities for different transition energies and numbers of bunches.

HIGH-INTENSITY STORAGE RINGS FOR MESON FACTORY

Batskikh G.I., Vasiliev A.A., Kuzmin A.A., Meshcherov R.A.,
Murin B.P., Rybalko V.S.

Radiotechnical Institute of the USSR Academy of Sciences
Moscow, USSR

Stavisskiy Yu.Ya.

Institute of Physics and Energetics

Abstract

Design aspects and basic parameters of storage rings are considered. Storage rings are designed to stretch and to bunch the beam of the high-intensity linac-meson factory. Continuous beam as well as intense short (25 nsec) proton pulses are provided. Beam duty factor varies from 10^{-5} approximately up to 1. Peak current of stored beam reaches 50 A.

A 600-MeV Linac (meson factory) will provide at its output high intensity beams of accelerated protons and negative hydrogen ions H^- with macropulse current of 50 mA and 5 mA respectively, repetition rate of 100 Hz and duty factor of 1% [1]. In future it is supposed to increase H^--ions current up to the value of proton current.

In some physics experiments, where counters are used, high beam pulse intensity is not acceptable due to counting channels overloading. For such experiments it is desirable to have a time-stretched beam with duty factor aproaching 100%. At the same time a number of important applications is based on pulsed modes of accelerator operation, when practically the whole beam intensity is concentrated in short bursts. To such applications one can attribute.

1. Neutron physics
2. Study of fast processes, induced by protons, mesons, neutrons.
3. Rare process experiments limited by background, not assosiated with the accelerated beam.

In connection with the development of the atomic power production and adjacent technology, the role of applied neutron studies is increased.

The most effective methods of neutron studies are based on the "time of flight" technique, wich needs pulsed neutron sources of high intensity. From this point of view the linac current macropulse duration (100 psec) is too large, and it is necessary to use some equipment to form short intense bursts.

This report describes the principles of construction and main parameters of storage rings [2] wich will make it possible to change linac beam duty factor in wide range and to provide both practically continuous beam and intense short pulses of 25 nsec.

Storage ring-buncher

For neutron experiments based on the "time of flight" technique, it is supposed to use a strong focusing storage ring of relatively small diameter. The magnet system of such a storage ring-buncher should first of all be compact, and at the same time it should provide sufficient space for various systems, necessary for beam injection, bunching, diagnostics and extraction.

Fig. 1 shows the chosen structure of the magnet period, the amplitude functions βx, βz and the closed orbit displacement for an off-momentum particle $(\Delta p/p=0.01)$. The magnet period consists of three strong fo-

cusing magnets, placed side by side (a triplet with combined functions of focusing and bending fields), and a free straight section of 2.38 m length.

Fig. 2 presents layout of main systems and components of the storage ring–buncher. The magnet system comprises 11 periods of the mentioned type. In free straight sections one can see the components of the charge-exchange injection and fast extraction system, RF bunching cavities and scrapers for removing the beam "halo". In this figure there are also shown the main components of the systems for beam diagnostics and correction.

For the chosen circumference the proton revolution period is equal to 200 nsec. The injected H^--beam macropulse duration equals to 100 μsec, that is the charge–exchange injection occupies 500 turns.

The H^--beam is supposed to be bunched at the linac input and to be accelerated in groups of bunches, the frequency of groups being equal to 40 MHz. Each group at the same time consists of five bunches in correspondence with the frequency of the 1-st linac stage accelerating field (~200 MHz). In order to avoid excessive momentum spread of stored protons and, consequently increase of beam radial dimension, it is expedient to choose the frequency of the bunching voltage in the storage ring–buncher equal to 200 MHz. In this case each bunch will be injected into a single bucket of RF field, each five filled buckets being accompanied by five empty ones. Thus four 25–nsec groups of bunches are stored within the chamber of the storage ring.

In order to decrease the amplitude of the RF cavity voltage, a debuncher is installed at the output of the linac. The debuncher decreases the injected beam momentum spread down to $\pm 0.1\%$.

The main problem of the injection is the heating of the charge–exchange carbon film target, installed at some distance from the chamber axes. In order to decrease the heating it is necessary to limit the time of the stored beam passage through the target. It is achieved by two pulsed magnets which provide beam bump at the target position. When the magnets are switched on the beam orbit is shifted onto the target. At the end of the injection cycle the pulsed magnets are switched out and their magnetic fields decrease down to zero simultaneously during 10–20 μsec. Thus an adiabatic and at the same time relatively fast removal of stored beam from the charge–exchange target is provided. Calculations demonstrate, that the carbon target temperature will increase by 1200–1500°C per one injection cycle at the injected beam pulse of 50 mA. During intervals between injection cycles the target is qooled down by heat radiation, but the target maximum temperature can tise up to 2000–2500°C. That is why a possibility is provided to change the target after each injection cycle, for instance, by using a set of films, mounted on a rotating disc [3].

In the storage ring–bunchex two independent extraction lines are provided.Fast extraction of the beam or the single group of bunches into each line is achieved by two kickers and a septum magnet (Fig. 2). The distance between kickers equals to half of the wavelength of betatron oscillations, so kicker pulses have opposite polarities. A matched two–units ferrite deflector with travelling wave is used as a kicker magnet.These units are powered from special pulsed generators including a double pulse forming line and a shock ferrite line. Hydrogen thyratrons are supposed to be used as current switches.

The chosen storage ring structure makes it possible to use different modes of fast extraction. The minimum burst duration (25 nsec) is provided when extraction repetition rate is 400 Hz. High value of peak and average power, commutated in the pulsed generators, are needed for small rise and decay time in kickers (20 nsec) and for high repetition rate of cycles. Thus the extraction system is one of the most complicated and powerful systems of the storage ring–buncher.

During designing of the vacuum chamber and RF system the main attention will be paid to the problem of the intense beam interaction

with RF cavities and other chamber components.

The pumping system must provide 10^{-8} torr pressure within the chamber. The main parameters of the storage ring–buncher are presented in Table I.

TABLE I

Main parameters of the storage ring–buncher

N,N:	Parameter	Unit	Value
1.	Energy of stored protons	MeV	600
2.	Orbit length	m	47.5
3.	Number of magnet periods	-	11
4.	Betatron oscillation number	-	2.75
5.	Induction of magnetic field on the equilibrium orbit	kG	72
6.	Radius of orbit curvature	m	3.39
7.	Magnetic field index	-	19.3
8.	Proton revolution period	nsec	200
9.	Injected H^--beam duration	μsec	100
10.	Injection cycles repetition rate	Hz	100
11.	H^--beam pulse current	mA	5–50
12.	Charge–exchange target thickness (carbon)	$\mu gr/cm^2$	200
13.	Charge–exchange injection efficiency	%	95
14.	Proton current in storage ring	A	2.4–24
15.	Incoherent betatron frequency shift due to space–charge effect	-	0.02–0.2
16.	Injected beam emittance	rad.m	$1.7\pi.10^{-5}$
17.	Stored beam emittance		
	a) horizontal	rad.m	$5\pi.10^{-5}$
	b) vertical	rad.m	$4\pi.10^{-5}$
18.	Vacuum chamber aperture		
	a) horizontal	cm	12
	b) vertical	cm	7

The stored beam is extracted from the storage ring–buncher on the external uranium target in pulses with duration and repetition rate near to optimum for neutron experiments. In future it is supposed to store protons during two injection cycles by very careful design of the main systems of the storage ring. Thus the stored beam intensity can go up to 50 A.

Construction of storage ring–buncher in the meson factory complex will provide pulsed neutron sources with neutron fluxes exceeding those of the best installations, now operating or being under construction.

Storage ring–stretcher

A possibility to stretch the meson factory beam by means of a special storage ring–stretcher was discussed earlier [2]. The main parameters of such an installation are presented in Table II. In the storage ring–stretcher a passibility is provided to store intense beams at different energies in the range of 300–600 MeV with following slow extraction during the intervals between linac acceleration cycles. Thus a practically continuous beam with duty factor of 98–99% is achieved.

In the storage ring–stretches it is also supposed to use very thin internal targets, which will be repeatedly crossed by the stored beam. This will make if possible to perform thorough study of nuclear reactions by observation of the yield of heavy nuclei with short tracks in the target.

A peculiar feature of the storage ring–stretcher magnet system is its four matched straight sections, the total. length of which equals aproximately to the half ring circumference. In two of them, where charge–exchange target of the injection system and internal targets for nuclear–physics experiments are installed, there is a deep minimum of the amplitude function in both transverse directions with values of $\beta_{min}=0.1\beta_{av}$, where β_{av} - average value of amplitude function in normal period. Thus the influence of the multiple scattering of protons in the target on the stored beam emittance is essentially reduced.

TABLE II

Main parameters of the storage ring–stretcher

N, N:	Parameter	Unit	Value
1.	Energy of stored protons	MeV	300–600
2.	Orbit length	m	236
3.	Extracted beam mean intensity	A	45
4.	Duty factor	%	98
5.	Proton current in the storage ring	A	0.38–0.46
6.	Number of turns injected	-	80–100
7.	H^--beam pulse current	mA	5
8.	Momentum spread (after debuncher)	%	± 0.2
9.	Charge–exchange target thickness	$\mu gr/cm^2$	120–180
10.	Charge–exchange efficiency	%	93
11.	Emittance increase due to the multiple passage through the target	rad.m	$(0.2-0.13)2.5\pi \cdot 10^{-5}$
12.	Number of magnet structure superperiods	-	2
13.	Number of normal periods (structure with separated functions)	-	16
14.	Number of matched sections	-	4
15.	Maximum magnetic field induction in dipole magnets	kG	8.864
16.	Field gradient in quadrupole lenses	kG/m	50.6
17.	Betatron oscillation number	-	5.75
18.	Vacuum chamber aperture		
	a) in bending magnets		
	horizontal	cm	15
	vertical	cm	7
	b) in quadrupoles–circular	cm	15

The most effective method of educing particle losses at extraction without increase of the vacuum chamber aperture in the main part of the ring is introduction of special matched straight section where maximum of β-function in the extraction plane is much more than the amplitude function value in the main structure. The storage ring–stretcher has two such straight sections ($\beta_{max} \simeq 5\beta_{av}$), and an electrostatic septum of the extraction system is installed in one of them.

For slow extraction the 3-d order ($Q_x = m/3$) nonlinear resonance excited by the m-th harmonic of the sextupole component of the magnetic field, is supposed to be used. A specific feature of the storage ring–stretcher slow extraction is the significant effect of the space-charge forces on the process of resonant excitation. Particles, oscillating with increasing amplitude, are moving in an essentially nonlinear field of the central beam region, remaining in the nonlinear resonance separatrix. This induces nonlinear frequency shift, which essentially reduces the orbit separation at septum at the beginning of extraction. In order to reduce these limitations and achieve the extraction efficiency near to 100% a special octupole correction is introduced in the storage ring–stretcher. A possibility of a partial compensation of the stored beam space-charge by means of electrons is also under consideration.

While choosing the parameters of the storage ring–stretcher, the future possibility to use it for development of *an* accelerating complex based on the linac in order to rase the proton energy up to 5–6 GeV by a superconducting linac or by a "fast" proton synchrotron with charge-exchange injection is also taken into consideration.

The authors are grateful to V.A.Aksenov, N.Ya.Basalaeva, V.A.Vizir, A.I.Dzergach, N.I.Kuzmina, V.A.Osipova, V. A. Skuratov and A. P. Fedotov for several discussions.

References

1. Murin B.P. "Proc.of the 8-th Int.Conf.on High-Energy Acc.", CERN, Geneva, 1971, p.540.
2. Batskikh G.I. et al. "Proc.of the III Soviet Union Conf.on Acc.of charged particles" (in Russian) Moscow, 1973, v.II, p.249.
3. Gorka A.J. IEEE Trans. on Nucl. Sci. v.NS-20, N 3, 1973, p. 387.

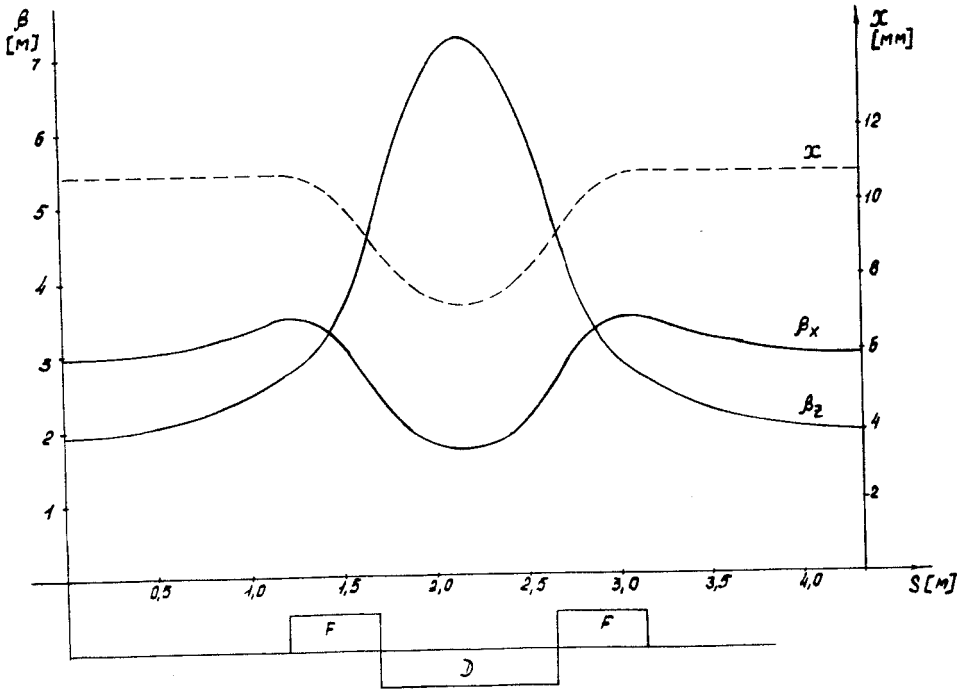

Fig. 1. Magnet period structure and calculated parameters of betatron oscillations (F, D - focusing and defocusing magnets, βx, βz - amplitude functions for horizontal and vertical oscillations, X - closed orbit displacement for particles with $\Delta p/p=0.01$).

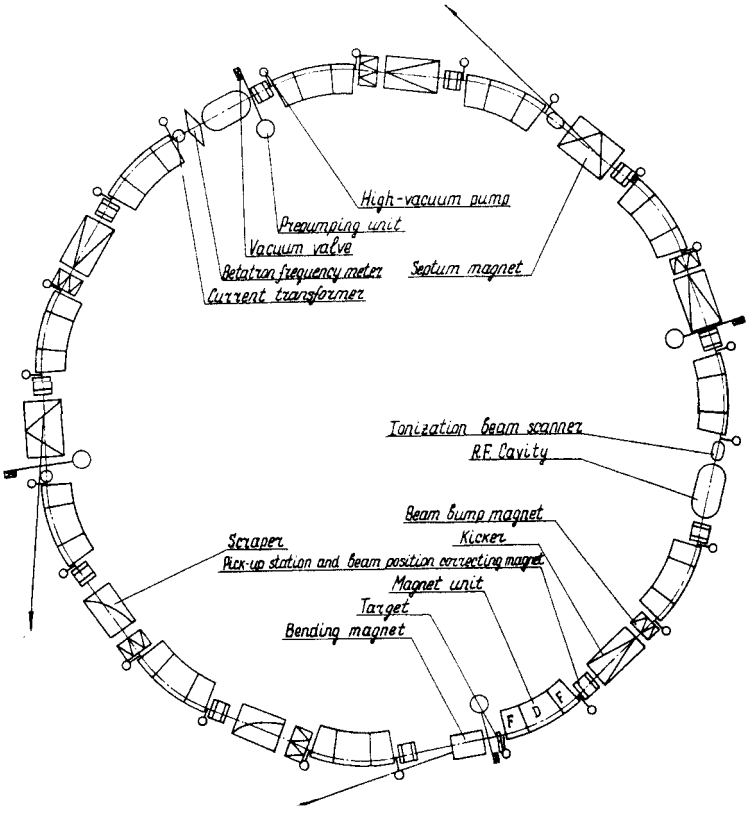

Pig. 2. Layout of the main components of the storage ring-buncher

TRENDS OF THE DEVELOPMENT OF STRONG CURRENT CYCLIC ACCELERATORS - MESON FACTORIES

V.P.Dzhelepov, V.P.Dmitrievsky, V.V.Kolga
Joint Institute for Nuclear Research, Dubna, USSR

I.Introduction

The available experimental results and the requirements of the modern theory of various nuclear processes in the energy region below 1 GeV convincingly show that it is necessary to further increase the intensities of both primary proton beam and secondary particle beams (neutron, pion and muon ones) produced by accelerators[1].

A group of scientists of the Laboratory of Nuclear Problems, JINR, has been studying 700-900 MeV strong current proton cyclic accelerators.

Here the basic results as well as the conclusions on these studies are given. The future development of this branch of accelerators has been considered on the present day level. The results of investigations on linear accelerators are compared.

II.Strong Current Phasotrons

The beam intensities of the 500-1000 MeV operating phasotrons are within 1-3 μA.

The current limit at such intensities appears in the accelerator central region where the axial rigidity dependent on the magnet system is minimal, while the beam particle density(χ) is maximal. In order to consider the theoretically possible ways of increasing phasotron intensities, let us analyze the expression determining the phasotron beam current

$$I = e \times R \dot{R} \propto Z \Delta t/T \qquad (1)$$

In the nonrelativistic approximation the limit particle densities determined by the accelerator magnet system

$$\chi = \frac{\varepsilon_0}{m_0} Q_z^2 B^2 \qquad (2^*)$$

does not depend on the accelerator regime. Here m_0 is the rest mass of the given particle, ε_0 is the vacuum dielectric permiability, α is a bunch angular width determined by the angular size of the separatrix.

The axial size of the beam (Z)is determined by the effective aperture of the magnetic field, which does not exceed some cm in the area of the shimmed fringing field. The magnitude $R\dot{R} = \frac{E\dot{E}}{e^2c^2B^2(1+n)}$ is proportional to the voltage amplitude over the accelerating electrode (V) and is practically independent of the magnetic field configuration since $0.25 > |n| > 0$ for all phasotrons, where $n = \frac{R}{B}\frac{dB}{dR}$.

The efficiency of capturing to the accelerator phasotron regime which depends on the capture time(Δt) vs the modulation period (T) is determined by the phase mode and is increased proportionally to V/K, where

$$K = -\frac{E}{\omega}\frac{d\omega}{dE} = 1 - \frac{\nu}{1+n} \frac{1}{\beta^2} ,$$

* B is the induction of the magnetic field in T, Q is the axial frequency of free oscillations for the beam whose amplitude is small compared to the transversal dimensions.

For phasotrons having the azimuthally homogeneous magnetic field the magnitude "n" is varied in the above range and the magnitude K is practically the same along the radius for all the accelerators of the given energy.

Thus, the problem of increasing the phasotron intensity is only to increase the amplitude of the accelerating voltage across the dee since the limit particle density in the central region (χ) does not depend on the character of the magnetic field variation (2).

This method for increasing the intensity has been used for CERN phasotron conversion[2], where the intensity may be increased according to the $V^{3/2}$ as it follows from (1).

The second important improvement of phasotrons is to increase the beam extraction efficiency which is based on the use of current and iron-current magnetic channels. The septum (the thickness of the front plate) of such channels does not exceed 3 to 6 mm, which provides the 50-60% coefficient of beam extraction from the accelerator chamber when using the regenerative system.

Such channels are under development now for the CERN, Columbia University[4] and Dubna[5] phasotrons.

As the analysis of expression (1) shows, there is another way to increase phasotron intensities which consists in approximating the structure of the phasotron magnetic field to that of the isochronous cyclotron. The degree of this approximation is characterized numerically by the parameter "K" whose value for the increasing average magnetic field along the radius is always smaller than unity.

The increasing of the value "K" along with increasing the capture efficiency results in decreasing the range of accelerating frequency B_0/B_c times, where B_0 and B_c are the induction in the centre of the accelerator before and after the magnetic system conversion (with the fixed final particle energy).

This reduction of the frequency range considerably simplifies the problem of increasing the amplitude of the accelerating voltage across the dee which is the basic problem for phasotrons having the azimuthally homogeneous field, when rearranging the frequencies of the accelerating voltage about $f_0/f_K \approx 2$, the mechanical units of the frequency rotary capacitor puts the limit to obtaining the required voltage amplitudes. The increase of the average induction of the magnetic field along the phasotron radius to a necessity of using the space variation of the field intensity in order to provide the axial stability of particles in acceleration.

The stability theories for such field structures have been described in many publications[6]. The spiral structures of magnetic fields are used in the conversion of the Dubna phasotron and the Nevis Laboratories (New York) on0 too. The theoretical consideration shows that the application of spiral structure magnetic fields as a means for increasing

the current of accelerated particles is quite promising. This principle can be used for creating accelerators having the quasi-continuous regime of acceleration. This regime is possible for the case when the law of varying the average induction of the magnetic field along the radius is quite close to the isochronous field. If B_i is a function corresponding to the isochronism of closed orbits for the whole energy range, B is the deviation from this law in the phasotron regime of acceleration along the radius, it is easy to see that with $K < 1$ we have

$$\frac{\Delta B}{B_i} = \frac{1}{2} K \eta_i \qquad (3)$$

where

$$\eta_i = \frac{\beta^2}{1-n^2}$$

If K is not larger than

$$K \leq \zeta \frac{eV}{E\beta^2} \qquad (4)$$

where ζ is the factor of the unity scale, we have the quasi-continuous phasotron regime of acceleration[8].

The main peculiarities of such cyclotron-phasotron regime of acceleration are its non-critical behaviour towards the amplitude of the accelerating voltage (within inequality (4)) and the extremely narrow band of frequency modulation:

$$\frac{\Delta f}{f} = \frac{1}{2} K \beta^2 \qquad (5)$$

which in many cases can be achieved by means of electronics.

Now there are no available experimental results on the abovesaid acceleration regime.

III. Strong Current Isochronous Cyclotrons

The abovesaid possibilities which can be expected from the phasotron method of acceleration allow even nowadays to increase the average particle current in such accelerators up to 20-50 μA.

The approximation to the cyclotron-phasotron regime will increase this limit about an order of magnitude. A further increase of intensity in phasotrons having a Ω-shaped magnet meets principal limitations which are due to the effects of the beam space charge.

In order to reduce this limit a new type of accelerators, the so-called strong-focusing cyclotron[9], has been suggested at the Laboratory of Nuclear Problems and a possibility of combining the isochronism of closed orbits and strong focusing*) has been proven[10] for the wide energy range.

The basic results of theoretical studies are as follows. In the magnetic fields of the type:

$$B_z = B(r)\left[1 + \varepsilon F(r,\gamma)\right] \qquad (6)$$

where ε is the field variation widths, $F(r,\gamma)$ is the periodic functions on r and γ is the dynamics of particle motion in azimuthally-homogeneous fields.

The main features are as follows:

a) the increase of maximal energy of transversal oscillations with a fixed amplitude (rigidity increase);

b) the comparison of accelerated particle pulses which results in the increase of the pulse range in the given volume of the magnetic field;

c) the weakening of the relations between ion rotation on closed orbits and stability conditions.

These theoretical conclusions have been confirmed by two models of the isochronous cyclotron with spiral structure magnetic field constructed at the Laboratory of Nuclear Problems, Dubna, USSR.

The first model was used to accelerate deuterons up to 12 MeV, the minimal r.f. amplitude across the dee was only 2 kV [11].

Thus, the possibility of cyclic acceleration during over 2000 revolutions was confirmed experimentally at the present day level of shimming and magnetic field stabilization. The general view of the pole piece of this accelerators is shown in Fig. 1.

The second model, an electron strong focusing cyclotron, was aimed at experimental testing the possibility to accelerate the proton beam in the cyclotron regime up to 100 mA. The general view and model windings are shown in Figs. 2 and 3.

In a static case the dynamic similarity of the proton and the electron in the magnetic field is based on the motion equation:

$$\frac{d\bar{\beta}}{dt} = e\left[\bar{\beta}\cdot\frac{\bar{B}}{m}\right], \quad \bar{\beta} = \frac{\bar{v}}{c} \qquad (7)$$

and hence

$$\left(\frac{\bar{B}}{m}\right)_e = \left(\frac{\bar{B}}{m}\right)_p \qquad (8)$$

for the whole range of the velocity module $|\bar{v}|$

The Coulomb field and the acceleration process taken into account make this similarity criterion more complicated. However, for each limiting mechanism it can be formulated at the confidence level of the effect under study. Thus, if one assumes that the basic effect limiting the beam density is the transversal repulsion by the Coulomb field, then with the equal strength and geometry of the beam the similarity criterion for this effect will be

$$\frac{i_p}{i_e} = \frac{V_p f_p}{V_e f_e}. \qquad (9)$$

With the current of 1 mA [12] produced by the electron model of the strong focusing cyclotron, as it follows from ref.[9], it is possible to generate currents up to 200-300 mA without the "transversal" space charge effect limitation.

The limit beam intensity of 100 mA below 1 GeV results in the appearence of a number of specific problems. Among them is the problem of 100% beam extraction from the accelerator chamber, since the beam achieves hundreds MW.

The effect of expanding the closed orbits in the periodic magnetic field [13] will allow to solve this problem. This effect is based on the dependence of the closed orbit expansion ($\rho/L \; d\rho/dL$) upon the magnetic field

*) The strong focusing magnetic system is that for which Q_r and Q_z are larger than unity.

variation ($\mathcal{E}(z)$, $d\mathcal{E}/dz$) where $\mathcal{L}$ is the length of the closed orbit.

In the magnetic fields of (6) type the main radius of the closed orbit for the particle having the momentum P is obtained from the expression

$$P = e\,B\,(R_m)\,R_m\,\lambda, \qquad (10)$$

where R_m is the mean radius of the closed orbit; λ is the parameter determined by the Periodic (N) part of the field structure (6) and can be as follows:

$$\lambda = \frac{1}{2} + \sqrt{\frac{1}{4} + \frac{\mathcal{E}^2}{2N^2}\left(\frac{3}{2} + n + \frac{d\mathcal{L}\mathcal{E}}{d\mathcal{L}z}\right)_{z=R_m}} \qquad (11)$$

When determining the length of the closed orbit by means of the mean radius from (11) it follows that

$$\frac{\rho}{\mathcal{L}}\frac{d\mathcal{L}}{d\rho} = \frac{1}{1 + n + \frac{z}{\lambda}\frac{d\lambda}{dz}\Big|_{z=R}} \qquad (12)$$

The result shows the possibility of considerable controlling the coefficient of orbit expansion near the following values:

$$\frac{R}{\lambda}\frac{d\lambda}{dz}\Big|_{z=R_m} \approx -(1+n)_{z=R_m}$$

In the static regime the separation of closed orbits is increased 20–50 times. Thus, this regime allows to expand the closed orbit without varying the shape of the beam emittance When the resonance method of extraction[14] is used, as is known, the shape of emitaance is changed.

The dynamic regime of this effect differs somewhat from the static one, however, the main conclusion on the possibility of increasing the energy step of the closed orbit 20–50 times is conserved.

A further important problem of such strong-focusing accelerators is the efficiency For powers of the accelerated beam close to 100 MeV this efficiency will be completely determined by the r.€. power. The contributions of all auxiliary energy systems (the magnet, the vacuum system, etc.) are negligibly small. The efficiency of modern lamp generators in the frequency range of interest is 70-75%[15]. The r.f. losses in cavities with the amplitude of 200–400 kV of accelerating voltage are not larger than 50–200 KW and this is negligibly small compared to that transferred to the beam. Thus, the efficiency of the ring isochronous cyclotron with strong focusing must be close to that of the r.f. generator.

The similar parameters of the accelerated beam can be obtained at proton linear accelerators of continuous operation. It is known that the best linear proton accelerators even at present have pulse currents of about 200 mA[16]. However, pulse losses for such accelerators are 40 MW[17], which considerably affects the accelerator efficiency and the cooling systems in the continuous acceleration regime.

Both for ring and linear machines there arises a problem of phasing the accelerating cavities at large beam loads. This problem, to our mind, can be solved considerably easier €or ring machines than for linear ones due to some reasons:

a) the number of cavities is 50-100 times smaller;
b) the amplitude of accelerating voltage is several times smaller;
c) the cavity self frequency is small.

These considerations have been laid in the basis of the studies in the development of the 800 MeV strong-focusing cyclic meson factory - a "supercyclotron", the proton beam intensity being 10–100 mA.

A linear accelerator of continuous operation is assumed to be used as an injector for this accelerator[18].

IV. "K" Meson Generators

The absence of dynamic similarity of orbits in isochronous cyclotrons considerably complicates their use in the 1.6 GeV energy region. The attempt to pass integral resonance in particle acceleration is due to considerable increase of the r.f. power system of the accelerator which should provide in this case the energy gain scores MeV at each turn. The creation of the system of some successive accelerators of the energy gain 1 GeV raises the whole cost too much.

However, there is a certain possibility to be considered separately, if the problem of strong current K-meson factories becomes important. This possibility is also based on the properties of closed orbits in the periodic structures having the magnetic field variation $\mathcal{E}(r)$.

The main contribution to the violation of dynamic similarity in acceleration is made by the variation of "n", which is determined by the requirement of isochronism in closed orbits

Usually for isochronous cyclotrons a direct problem is put forward: with increasing the mean value of the induction field along the accelerator radius the mean value of the induction field along the accelerator radius the proper $\mathcal{E}$ F function (see (6)) is chosen such that the space stability should appear. However, for smaller changes of "β" a reverse problem is possible when the condition n = constant is the basic requirement with which the dynamic similarity of orbits is obtained (Q_r, Q_z = const.). In this case the condition of isochronims of closed orbits is based on the choice of the function F and is determined by the variation of the shape and the coefficient of stackening closed orbits at various radii:

$$\frac{\lambda_0}{\lambda}\left(\frac{\sigma}{\sigma_0}\right)^{n+1} = \frac{\sigma_0}{\sigma}\left(\frac{\beta}{\beta_0}\right)^{n} \qquad (13)$$

where $\sigma = \frac{1}{\sqrt{1-\varepsilon^2}}$; $L = 2\pi R_m \sigma$, σ is the coefficient of orbit lengthening due to the periodic field structure.

As has been shown in ref.[19] such a possibility exists and can be implemented in strong current K.meson factories.

V. Conclusion

The present paper is not intended for covering all the variety of problems arising in the development of strong current meson factories. It concerns the basic, in the

authors' opinion, problems on particle acceleration physics. A lot of technical problems have not been touched upon. However, the experience of developing meson factories shows that they can be solved at the present day level.

Table 1

Accelerated proton energy (MeV)	800	Number of accelerating gaps	8
Accelerated proton current (MA)	10-100	Voltage across the cavity(kV)	250
Injected proton energy (MeV)	50	R.F. Power (MW)	76
Axial oscillation frequency	1.3-1.4	Number of sectors	8
Radial oscillation frequency	$2r_0 > 1$	Yoke magnet diamter (cm)	1900
Injection radius (cm)	240	Magnet height (cm)	560
Mean field at the injection radius (Gauss)	4270	Magnet weight (t)	3450
Full radius (cm)	650	Magnet power supply (KW)	1750
Mean field at the injection radius (G)	7500	R.F. losses in cavities (kW)	1000
Energy gain per revolution (MeV)	2.0	Beam power (MW)	8-80
Ion rotation rate (MHz)	6.2	Efficiency of beam extraction from the accelerator chamber (%)	100
Acceleration voltage frequency(MHz)	49.6	Beam intensity losses in acceleration	10^{-4}

References

1. V.G.Vasilkov,V.I.Goldansky,V.P.Dzhelepov, V.P.Dmitrievsky. JINR Publication P9-5285(1970).
2. G.Brianti,E.G.Michaelis, SC Improvements, Rep. M53(1966).
3. V.P.Dmitrievsky, B.I.Zamolodchikov, V.V.Kolga. AE, 9,303,1960.
4. K.Ziegler, E.Martin, R.Cohen. V Int.Cyc. Conf., Oxford (1969) p.226.
5. N.L.Zaplatin, A.F.Chesnov.Proc.III Nation. Conf. on Accelerators,Moscow,1972.
6. V.P.Dzhelepov, V.P.Dmitrievsky,B.I.Zamolodchikov,V.V.Kolga. UFN,85,651,1965.
7. John A.Matrin. V Int. Cyc. Conf. (1969)p.3 R.Cohen, E.Martin, S.Rainwater,K.Schneider, K.Ziegler,S.Ohnuma.V Int.Cyc.Conf. Oxford (1969)p.699.
8. V.P.Dzhelepov, V.P. Dmitrievsky. Proc. III National Conf. on Accelerators, Moscow,1972
9. V.P.Dzhelepov et al. Int.Conf. on Isochronous Cyclotrons. Gatlinburg, USA (1966)p. 215.
10. V.N.Anosov,A.A.Glazov,Yu.N.Denisov et al. AE,25,539(1968).
11. A.A.Glazov,V.I.Danilov,V.P.Dzhelepov et al. 8, No. 3,189 (1960).
12. A.A.Glazov,V.P.Dzhelepov et al. JINR Publication P9-6214(1972).
13. V.P.Dmitrievsky,V.V.Kolga,N.I.Polumordvinova. JINR Publication P9-6733(1972).
14. W.Jogo.V Int.Cyc.Conf.,Oxford(1969)p.159. J. Reginald Richardson,M.K.Craddock,Oxford (1969)p.85.
15. K.L.Erdman,R.Roirier,O.K.Fredriksson, S.F.Welton,W.A. Grundman. VI Int.Cyc.Conf. Vancouver,1972.
16. I.Kapchinsky, V.A.Batalin,A.A.Kolomiets, B.K. Kondratiev,R.P. Kuida, PTW, 5,17(1972).
17. D.C.Hagerman,IEEE Trans. on Nucl.Sci., NS.13(4)p.277.
18. V.A.Teplikov,A.P.Maltsev,S.M.Ermakov, A.V.Zotov,V.A.Yurchenko. IFVE Ing-68-35-K (1968).
19. V.P. Dmitrievsky, V.V.Kolga, N.I. Polumordvinova. the VIIIth International Confer. on High Energy Accelerators. CERN (1971), p.518.

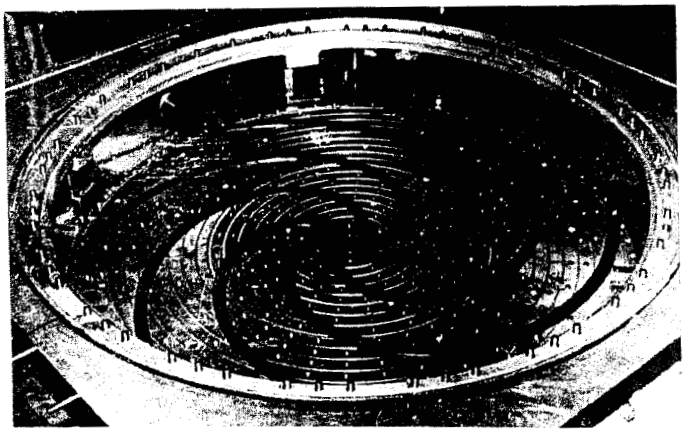

Fig. 1
The general view of the accelerator pole piece

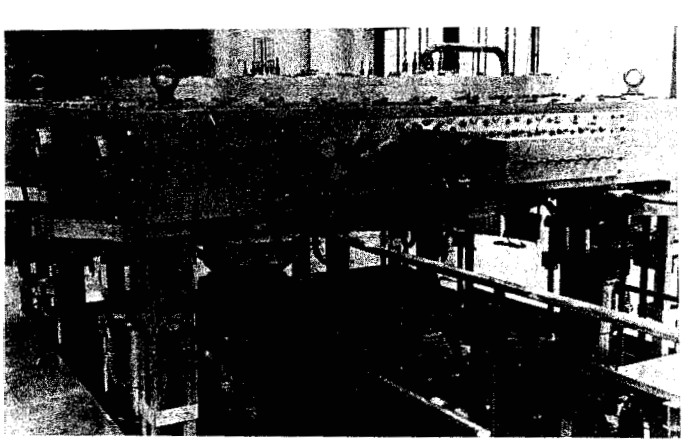

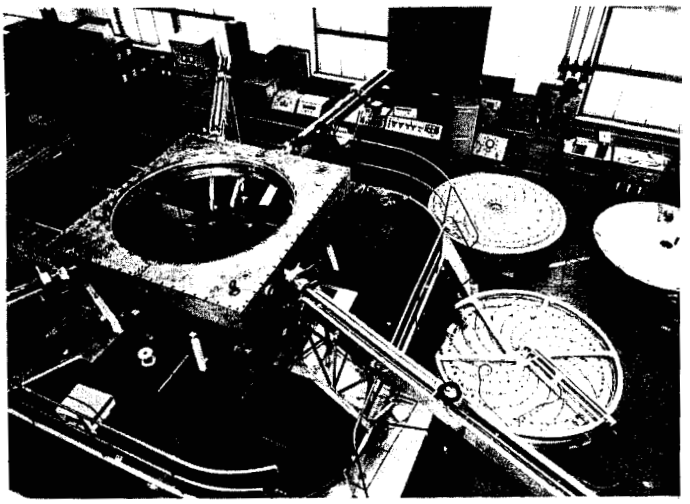

Figs. 2, 3
The general model view and the model windings

FIRST BEAM TESTS WITH THE 590 MeV RING CYCLOTRON AT SIN

J. -P. Blaser, H. A. Willax

'Swiss Institute for Nuclear Research, Villigen, Switzerland

Abstract

At the beginning of this year a few tests were performed with the SIN ring cyclotron, the first isochronous cyclotron accelerating protons successfully in CW-mode to truly relativistic energies ($\gamma = 1.6$ 3). The extracted proton beams, though still low in intensity, were used for production of pions at an external target. The results of these early tests are presented and discussed.

Introduction and Brief History of the Project

In the early sixties studies were started at ETH (Swiss Federal Institute of Technology in Zurich) about a high intensity proton accelerator in the "intermediate energy" range (0.5 - 1 GeV). The idea was to develop research in the overlapping region of nuclear and particle physics by making available very intense beams of pions and muons. This new field, also potentially rich in applications, e.g., chemistry, solid state physics, biology and medicine, was considered very suitable for a new national research facility in Switzerland in order to continue a valuable tradition in nuclear physics and to stimulate participation at CERN. A small team at the physics department of ETH investigated different accelerator types primarily for production of pion beams of high intensity and good experimental quality. [1] In 1962 - 1963, a proposal for a double stage isochronous cyclotron, a "meson factory", capable of providing 500 MeV p in an external CW beam of up to 100 μA, was worked out. [2]

The concept of a ring cyclotron with separated magnets, several re-entrant RF cavities providing high accelerating voltages and "free sections" inserted between the magnets, appeared beneficial for the following reasons: At proposed energies the loss of beam within the machine and beam transport systems has to be minimized. Optimal beam transmission through the accelerator and high extraction efficiency are main design goals. The large operating radius of the ring combined with a high energy gain per particle revolution lead to the high extraction efficiency achievable in such a machine. [3] Good focusing properties of small gap magnets as well as possibilities for tailoring the beam before injection aid beam transmission. The "open structure" eases maintenance and repairs of activated machine components.

In the meantime, a committee of CERN member states (ECFA) had recommended a series of future accelerators in Europe. Complementing large projects to be realized on an international scale, smaller accelerators in national centers were considered as essential backup for the international effort to assure the scientific resources, available at the universities. Among these proposals a "meson factory" along the line of the ETH studies was proposed.

Results of early beam dynamics studies and model work on main components of the proposed accelerator were encouraging enough to submit a project proposal to the Swiss Government in 1965. A development and construction budget of 92 MSfr. was granted in 1966. The decision on starting construction, however, was delayed until late 1968, when a practical solution was worked out for a modification of the first cyclotron stage (the injector cyclotron) to a multiparticle variable energy machine. In the design of this cyclotron, two modes of operation had to be considered:

a) the injector mode, in which a 72 MeV p beam of high quality and intensities up to 100 μA had to be delivered at 50 MHz pulse frequency (the correct frequency for full acceptance in the ring cyclotron), and
b) the variable energy mode providing beams of d, He_3, a, heavy ions and polarized p and d to be directly used for nuclear physics experiments.

The difficult task of building this machine was taken up by Philips-Company Eindhoven in fall of 1968.

At that time the development of main components of the ring cyclotron, carried out by the cyclotron group of ETH [4] had progressed so far that procurement could be started. The laboratory became an annex institution of ETH with the name SIN (Swiss Institute for Nuclear Research). In 1969, after good results with full scale prototypes of a main magnet and an accelerating cavity had been achieved and after a thorough beam dynamical study [5] indicated stability limits, it was decided to increase the final energy from 520 to 590 MeV without altering the design geometry of the ring cyclotron as frozen in 1967. A calculated risk was taken with this decision since it entailed two possible problems:

1) The betatron oscillations had to pass the condition of the non-linear coupling resonance $\nu_r = 2\,\nu_z$ at least twice at rather high energies, and
2) the magnets (already in process of being ordered) had to provide more flux, so that critical areas in the yoke cross section became saturated.

In spring of 1969 the building construction program started at Villigen with a tight schedule; the initial assembly work of both accelerators began by summer 1971. A carefully scheduled mounting and testing period of two years lead to the final assembly of the machines by summer 1973. Already in fall 1972 the testing and debugging of subsections of the ring machine were started' (1/4 ring tests). The final corrections of the magnetic field by careful shimming of the individual magnet sectors required special efforts in summer 1973, concentrated around the injection and extraction region where perturbing effects of magnetic beam guiding elements had to be compensated. While the injector cyclotron [7] achieved first internal beam on August 1, 1973 without the extraction elements installed, the ring cyclotron and beam transport systems were made ready for first beam tests scheduled for October 1973. A delay in the fabrication of the magnetic deflector coil of the injector cyclotron's extraction system brought a 3 month delay in testing the accelerator system with proper beam (72 MeV p at 50 MHz). In November 1973, a few preliminary tests of the beam transport system and injection into the ring were performed successfully with low energy particles (20 and 17 MeV p, 33 MeV d) which could be extracted from the first stage cyclotron without the magnetic deflector coil being mounted.

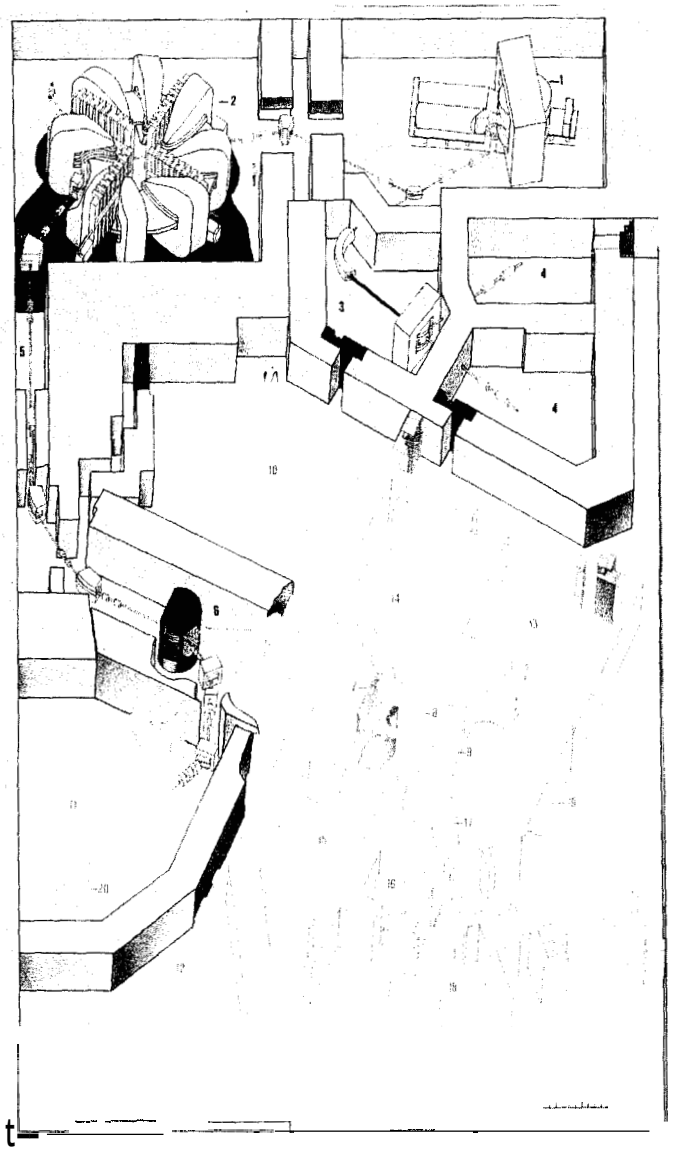

Fig. 1 SIN Experimental Hall
Scheme of the status of assembly during the first test period between January and April 1974 is marked by heavier contours. The lighter contours demonstrate the assembly goals of the end of 1974.

1) Injector cyclotron (2. 5 m pole diam)
2) Ring cyclotron (15 m outer diam)
3) Analyzing system for low energy beams
4) Experimental areas for low energy beams
5) 590 MeV p beam line
6) Pion production target "M" (thin target)
7) Local shielding for thick target "E"
8) Secondary beam bending magnet
9) Beam dump
10) Experimental area for pion work
11) Experimental area, used for first pion detection and experiments (πM3)
12) Low intensity p beam (future)
13, 14) Pion experimental area
15) Biomedical pion beam area
16) Muon experimental area
17) Superconducting muon channel
18) Muon experimental area
19) Opening for neutron beam
20) μ -neutrino mass experiment

With the beginning of this year an experimental p beam of proper injection energy (between 70. 5 and 72 MeV) and pulse frequency (50.7 MHz) could be extracted at intensities of 1 - 2 μA. This test beam was used in six major test runs to learn about the principle functioning of the accelerator system, the two last runs also including the use of the first pion production target with one secondary beam transport channel (πM3).

Beam Tests with the SIN Ring Cyclotron

In Fig. 1 is seen the status of assembly in the experimental hall of SIN Villigen during the first test period between January and April 1974. The injector cyclotron, during this period still under responsibility of Philips, is shown in Fig. 2. Its properties and technical features are described elsewhere.[7] For the initial tests with a p beam of approximately correct injection energy and a pulse frequency corresponding to the 3rd harmonic mode, this machine still had an improvised shorting bar, providing the 50 MHz resonant structure within the main vacuum chamber. It had to be separately mounted and manually adjusted to the right position for the exact isochronous frequency (theoretical value 50.680 MHz). The magnetic deflector coil, the second essential element of the beam extraction device, had just been installed in December 1973. Operational experience on extracted beam and its quality still had to be gained in the time period discussed below. The ring cyclotron, as described elsewhere[6] and shown in Fig. 3, was already equipped with all essential elements, including beam probes and deflection devices. A double set of carbon collimators limiting the free vertical beam aperture to 25 mm at injection radius and to 15 mm over a radial range from 490 to 590 MeV were installed for protection of critical components. There was no operational experience yet on the long term stability of all four cavities working simultaneously, or the RF induced perturbing signals on the probes.

The first experimental test runs were handicapped by the following factors:
- limited time periods of simultaneous operation of all accelerating cavities in use, with interruptions when a cavity fell back into a multipactoring condition. In the course of the runs, however, the average "on-off"-

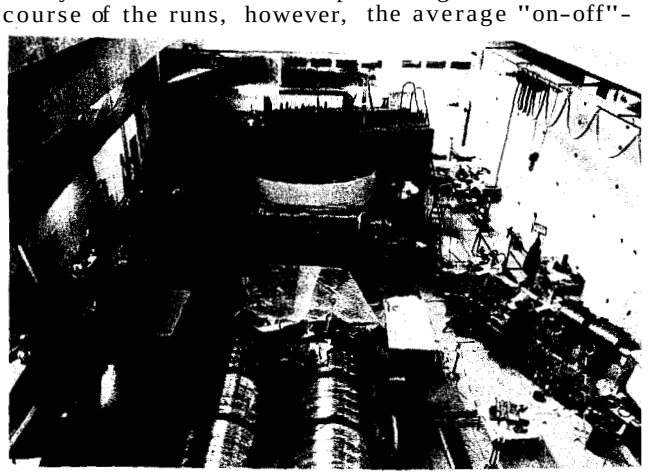

Fig. 2 Injector Cyclotron
Situation shortly before final assembly in summer 1973. The dee (under plastic cover) and the connected RF resonators for variable frequency are withdrawn from the main vacuum chamber.

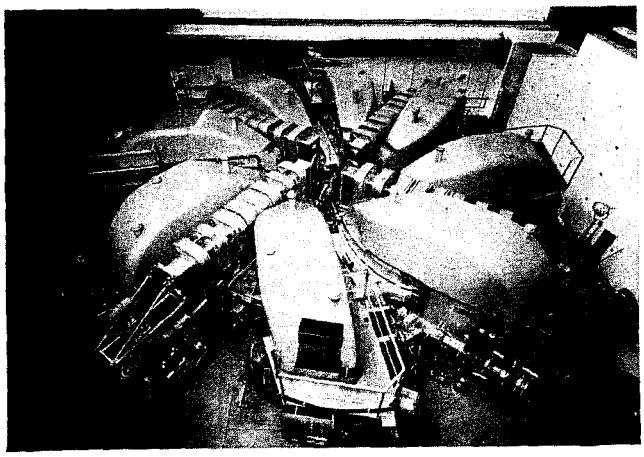

Fig. 3 590 MeV Ring Cyclotron
Situation during final assembly in summer 1973. Between the eight 250 t sector magnets are four RF cavities providing voltages up to 650 kV at 50 MHz. The extraction beam path (right foreground) is being installed.

time ratio changed from typically 50 % to 90 % taken over 20 hours, with periods of uninterrupted operation of up to 6 hours.
- perturbing signals on probe current readings, induced by the cavities operating at high voltages. Some of the effects could be eliminated or diminished during the course of the tests.
- uncertainities in the absolute value of the energy of the injector beam of ± 1 MeV, and uncertainities in the reproduction of the injector settings, leading to a defined energy and optical beam characteristics. Those changes in initial conditions usually caused time consuming experimental search for the proper settings of the beam transport system and the ring injection parameters.
- fluctuations in intensity and (sometimes) in the intensity distribution within the useful emittance, especially noticed when the ion source of the injector was set for low intensities. This effect, in many cases, made optimizations on certain parameter settings very time consuming.

In the first night of tests with a 1 μA beam of the proper injection energy (= 72 MeV) and the required pulse frequency (50.7 MHz) on January 11/12, 1974, the beam transfer from the injector to the center of the ring cyclotron could be accomplished with a 60 - 70 % transmission. Before injection into the ring, the proper position of the main injection elements first had to be determined. The vertical alignment of the beam was found to be critical. We succeeded in detecting the beam over the first 5 to 7 accelerated revolutions. However, coherent oscillations of 10 - 15 mm amplitude in both directions were observed. In the following night (January 12/13, 1974), the settings of injection parameters were improved. RF pickup on two essential probes made measurements difficult. With the remaining, unaffected probe, the beam was finally detected over the range from 72 - 92 MeV. Fig. 4 shows the radial intensity distribution taken by the 1 mm radial differential probe. Except for the two innermost revolutions the turn spacing corresponds to a "peak to peak" accelerating voltage in each cavity of 480 kV. This is within the 10 % uncertainity of the voltage calibration of the cavities, which were set for 500 kV.

In the second test run of January 17/18, the failure of an RF power feed-through made it necessary to attempt acceleration in the ring with three cavities only. Even though under those conditions (with the injection elements adjusted to an "uncentered" equilibrium orbit) the problem of the first internal beam clearing all obstacles is not trivial, this run was successful. With a 1 - 1.5 μA beam delivered from the injector, the transmission through the beam line could be brought up to 80 - 90 %. At injection a typical loss of 20 % had to be taken into account. Immediately after the centering problems had been solved experimentally, a beam of up to 0.7 μA could be brought out to approximately 540 MeV without trim-coil corrections to the main field. Some trim-coil adjustments were necessary to take the beam further out. A current of 0.4 μA was achieved at 570 MeV. However, a drastic decrease in beam intensity, starting about 2 cm before extraction radius, could not be overcome. At the nominal extraction radius, 5 - 10 nA of circulating beam remained. The attempt to extract part of that beam was successful: 4 nA of 585 MeV p were measured at the temporary beam dump, installed in the cyclotron vault 5 m downstream from the last extraction magnet. The reason for the drastic intensity drop shortly before extraction radius was found during the following visual inspection of the ring. Vertical beam clipping had occured due *to* a Paulty mount of a single trim-coil plate in one sector magnet. This fault was quickly repaired and the broken RF feed-through was replaced by a spare unit.

For the third major beam experiment on February 7/8, the injector beam quality had improved, and higher beam intensities could be achieved. With a stable 1.5 μA beam delivered from the injector and the four ring cavities operating stably over periods of several hours, transfer and injection of the beam into the ring presented no basic problems. Even though some initial coherent beam oscillations in the ring could not completely be eliminated, a 0.2 - 0.3 μA beam was accelerated to extraction radius, the transmission from injection to extraction being approximately 75 %. About 80 % of this beam was extracted and measured at the temporary external beam dump in the cyclotron vault. For a short time the injector beam intensity was increased, and 0.6 μA were registered at this beam dump.

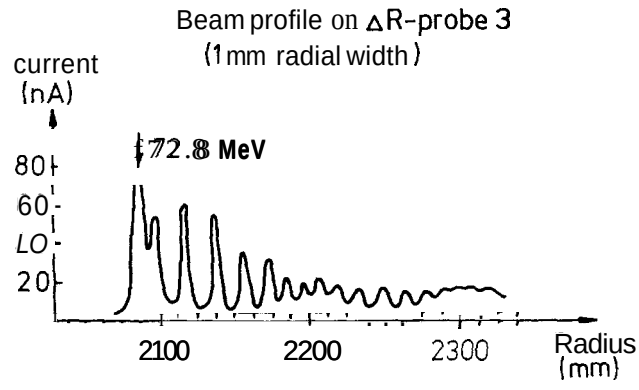

Fig. 4 Profile of separated beam revolutions as measured with a differential beam probe of 1 mm when acceleration from 72 to 92 MeV was achieved for the first time.

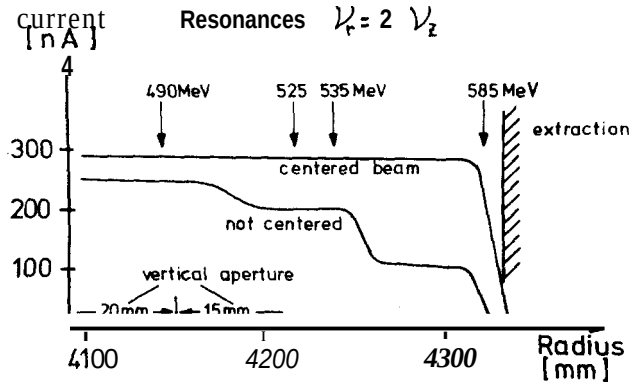

Fig. 5 Radial beam profiles at high energies. This plot shows the internal beam current versus radius for a well centered and a non-centered beam. Initially, the beam was injected excentrically into the ring cyclotron, giving radial oscillations of about 15 mm amplitude. These radial oscillations were converted into vertical oscillations at the coupling resonance $\nu_r = 2\ \nu_z$ which occurs at four different energies before extraction. Due to the small vertical aperture of beam collimators there resulted a noticeable beam loss after each crossing of a resonance. After centering the injected beam by adjusting the electrostatic inflector voltage no beam loss was observed.

The fourth experiment, carried through on February 15, was mainly aimed at closer investigations of the ring internal beam behaviour. With a typically 0.5 - 1 μA beam, the build-up of coherent beam oscillations and their effect on total transmission through the ring was measured. The following results could be stated:

- A first harmonic horizontal field component on the order of a few G in the magnetic field near injection radius causes difficulties with the vertical alignment of the beam in the ring.
- Depending on the centering of the beam at injection (initiating coherent horizontal oscillations), the transmission of beam to extraction radius may be affected by the coupling resonance $\nu_r = 2\nu_z$ which, in our case, without trim-coil corrections, occurs at energies of 490, 525 and 535 MeV. In Fig. 5 beam intensity profiles versus machine radius are shown for the two typical cases of a well centered beam, and a beam with initial coherent radial amplitude of ∿ 15 mm.

For the beam tests on February 23/24 and March 16/17, the p beam line of 40 cm length, leading from the ring to the first pion production target (housed in heavy local shielding) was installed and operable. The first pion channel πM3 with the length of 15 m was also ready for transmitting beam (see Fig. 1). During tune-up on February 23, again one cavity of the ring cyclotron failed due to a fault in the grid circuit of the power amplifier. With three cavities operating stably at operating voltages between 450 and 500 kV per cavity, a loss of 30 - 40 % at injection had to be taken into account. A coherent radial oscillation had to be eliminated by excitation of pole face windings in two adjacent magnets. Since the main goal of the experiment was the first production of pions in an external target, not much time was spent to optimize injection parameters. A beam of 0.1 - 0.2 μA was brought to extraction radius and with an extracted beam of 50 - 100 nA, the 590 MeV p beam line was tested for the first time. The beam immediately was brought on target, a 0.5 cm carbon plate. Due to a slight misalignment of a temporary collimator the transmission in the p beam line could not be improved beyond 50 % that day, However, with a 50 - 100 nA beam on target in a spot size of ∿ 1 cm^2, the first pions were detected behind the pion channel, which was set to a momentum of 300 ± 3 MeV/c. In more than six hours of beam on target, several very informative first measurements on pion production rates, π - μ - e ratios and the effectiveness of shielding could be made. After readjustments of the machine settings and an increase of injector beam intensity to ∿ 5 PA, a beam of 0.8 - 1 μA was extracted from the ring and 0.3 μA were used on target for a short while.

For the following test on March 16/17, all four RF cavities were operational. For injection, acceleration and extraction, no pole face windings had to be used. However, this time the injector beam showed a large horizontal emittance (probably due to a large dispersion). 50 % of the beam available at the injection point were lost within the injection channels of the ring (whereas the transmission through those channels was more than 80 - 90 % in previous runs). Intensities had to be kept low for this reason. For a period of almost 12 hours, beam of varying intensities between 50 - 300 nA was delivered for optimization of the 590 MeV p beam line (which could be brought up to over 90 % in rather short time) and for pion production on target M. The emittance of the 590 MeV beam was measured to be typically:
A_x = π x 12 mm mrad, A_z = π x 4 mm mrad. A result of measurements on the pion range taken after the pion channel (set for 200 MeV/c) is shown in Fig. 6.

Towards the end of this experimental "production run", the intensity of the injector beam increased to 10 μA. With a circulating beam of 4 - 5 μA on the first orbit in the ring, a 2 μA beam of 590 MeV was extracted and used for a short time on target M for measurements on background radiation.

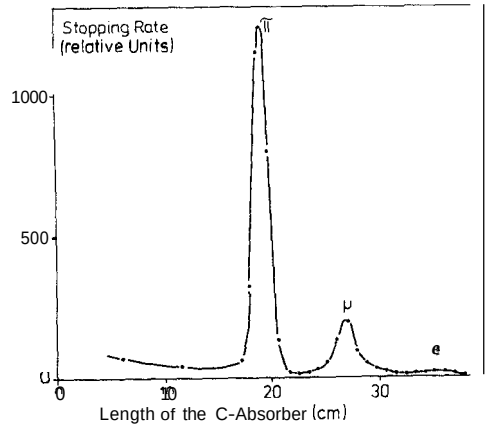

Fig. 6 Differential Range Curve (p_π = 200 MeV/c)
A range curve was taken as a quick test of the predicted momentum resolution and intensity of the pion beam in the πM3 area. The predictions were confirmed within 30 %.

p intensity	: 200 nA during 1 1/2 h
pion production target	: 0.96 g/cm^2 of carbon
pion stop rate	: 370 stops/s in 1.4 g/cm^2 of carbon
momentum resolution	: 2 % FWHM

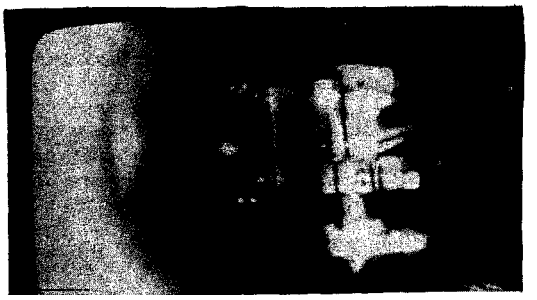

Fig. 7 590 MeV p Beam
Trace of a 1 μA p beam observed through TV on a movable quartz plate in front of the entrance to the second internal deflection element of the ring cyclotron (a magnetic quadrupole channel of 15 mm free aperture). The spot size is about 6 mm x 8 mm. This beam is well separated from the internal circulating beam, having passed the electrostatic deflector channel 45° upstream. The quadrupole channel had to be positioned slightly above midplane for good transmission through the following elements.

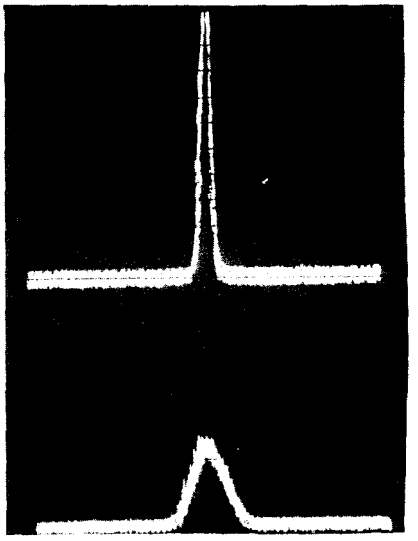

Fig. 8 590 MeV p Beam
The intensity distribution of 1μA beam in the horizontal plane, measured by two "profile monitors" (metal plates of 1 mm thickness sweeping through the beam), about 3 and 6 m after extraction from the ring.(Calibration on abscissa in cm).

After this preliminary test period, in which the injector cyclotron under the responsibility of Philips has produced valuable test beam with increasing reliability and quality, this machine was prepared for acceptance tests. On March 26, 1974 for the first time it produced slightly more than 100 μA extracted beam in the injector mode. On April 18, measurements on the beam extracted from this machine at 72 MeV and 50.65 MHz showed the following results:

Current	: 105 μA
Emittance A_x, A_z	: Π x 5 mm mrad (80 % of beam)
Energy spread Δ E	: 200 keV (FWHM)
Phase width	: 20° RF at 50.65 MHz

Further Procedure

While the definite version of the 50 MHz shorting bar system is being installed in the injector at present, the ring is being prepared for the next operating period scheduled at the end of May 1974. During the summer of this year the following main activities are planned:

- Education and training of personnel for operation and maintenance of the accelerator system.

- Beam development on both accelerators with the special aim of improvement of the total transmission.

- Delivery of low intensity beam (up to a few μA) on pion production target M (thin target) for pion experiments.

- Installation of target E (thick target), the corresponding secondary beam lines and the beam dump.

After a longer shut-down in the late summer of 1974, it is expected to bring the whole facility to a condition where more than 10 μA can be usefully produced.

Acknowledgment

As the main reason for a first success in the start-up of this accelerator facility we consider the excellent work and high motivation of all the staff members involved during its development, construction and beginning operation, as well as their dedication to their tasks, which often were difficult. We hope the spirit of this great team can be kept up during the difficulties of beginning operation. The great effort of some industrial firms which undertook to supply us with reliable components of unconventional features needs to be mentioned as an essential part of the success. We thank our authorities for their confidence and steady support in all phases of the project.

References

1. J. P. Blaser and K. Steimel
Nucl. Instr. and Methods 18/19, p. 417 (1962)

2. H.A. Willax
CERN 63-19, p. 386 (1963)

3. G. Tripard, W. Joho
Nucl. Instr. and Methods 79, p. 293 (1970)

4. H.A. Willax
Proc. Oxford Cyclotron Conference, p. 58 (1969) (Butterworth, 1971)

5. W. Joho, Thesis (May 1970)
"Extraction of a 590 MeV Proton Beam from the SIN Ring Cyclotron" (SIN Report TM-11-8)

6. H. A. Willax
IEEE Trans. Nucl. Sci., NS 20 (3), p. 202 (1973)

7. A. Baan et al
IEEE Trans. Nucl. Sci., NS 20 (3), p. 257 (1973)

BASIC DESIGN CONSIDERATIONS ON AN ELECTRON BEAM STRETCHER

H. Herminghaus
Institut fur Kernphysik, D-6500 Mainz, West-Germany

This paper gives a brief description of some less conventional schemes for injection, extraction and spill out control to be used with an electron beam pulse stretcher ring.

In designing an electron beam stretcher for the 300 MeV Electron Linac of Mainz University the **main** effort was made to get low transversal beam emittance of the extracted beam and to provide some means for flattening the beam intensity. To be compatible with later recycling of the linac the stretcher should be able to operate up to 600 MeV. The magnet ring will mainly consist of two 180^{o} bending systems connected by two long straight sections. In this paper, however, only some as we think rather unconventional details will be discussed.

Since the emittance of the extracted beam is in part determined by the emittance of the circulating beam we consider it to be of advantage to use a longitudinal stacking in order to keep the emittance as small as possible. The stacking procedure is as follows: The beam is swept between two deflecting cavities of mutual distance L through the aperture of a focussing lens, the focal length of which is L/4. By correct phasing of the RF the beam will not move downstream the device (Fig. 1). The linac beam is fed in obliquely through the first deflector and bent to a regular orbit by

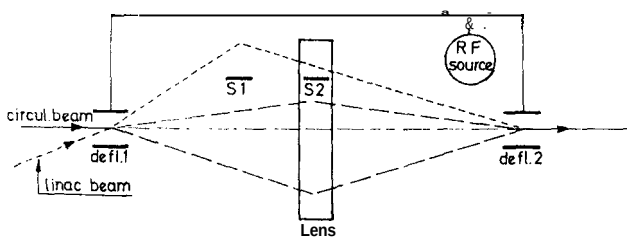

FIG. 1--longitudinal stacking scheme.

means of two septa. In this manner it is achieved that injection is not affected by the performance of the RF, provided only that the beam passes behind the septa at inflection and in front of it at the successive turns. This scheme should work with reasonable margins for bunch lengths of less than 10^{o} over 6 turns of injection. To preserve the bunch structure sufficiently during injection the momentum compaction factor should be less than 10^{-3} if an energy range of 2.5% is to be captured. After about 100 turns after injection the original bunch structure may be considered to be totally lost. It is reckoned with a maximum injected linac beam of 170 mA, leading to a maximum circulating beam of about 1A.

For extraction at some location of the ring dispersion will be provided and it shall have there a large horizontal but small vertical β-function. This gives a flat beam, the position of which is dependent of energy (Fig. 2). At the low

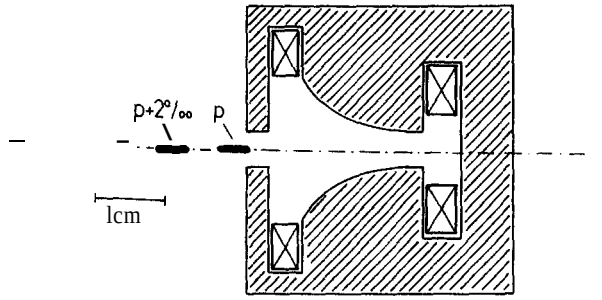

FIG. 2--Semiquadrupol used for extraction. Beam dimension and dispersion in correct scale.

energy side a small semiquadrupole is situated inside the vacuum (gap width about 5 mm). If the energy of the beam is lowered slowly it drifts into the gap of the semiquadruple and is bent out subsequently. Final extraction is done by a magnetic septum a few meters downstream. The semiquadrupole is acting at a small fraction of the beam at a time only, causing a large Q-shift there of about 0.15 over a few mm. It is believed that this extraction scheme is scarcely affected by field errors in the ring.

The extraction has been computed by tracing many particles by a computer program, taking into account a field distribution in the semiquadrupole as measured at a conductive paper model. Figure 3 gives an example for such a computation. The extracted phase space shown had been obtained

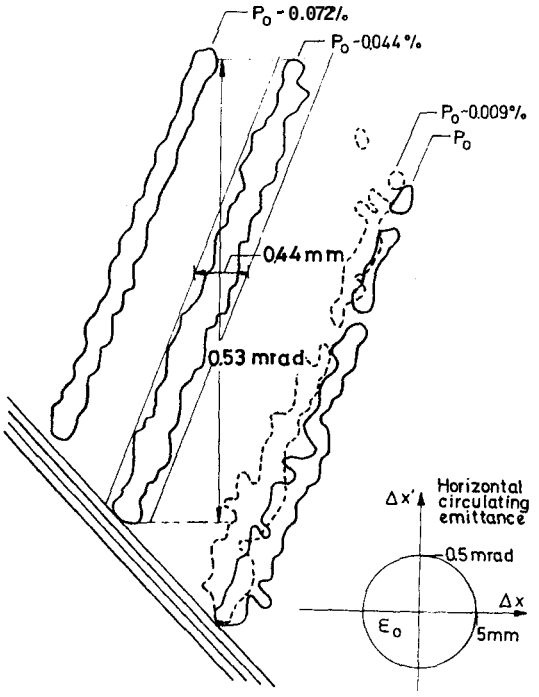

FIG. 3--Phase space of extracted beam at location of semiquadrupole. Each area encloses electrons of equal energy. The beam at lower left represents the shadow of the septum. The dimensions of the phase space areas as indicated by arrows in the figure represent 3% of the circulating emittance. Dispersion is assumed to be 4.5 cm/%. Total momentum spread of extracted beam is less than 0.08%.

with $Q_H = 0.15$, $Q_V = 0.26$, all other parameters as indicated in the figure. The emittance of any monochromatic part of the extracted beam is about 3% or less of the emittance of the circulating beam in horizontal direction, while vertically the emittance is enlarged by a factor of about 1.3. Extraction efficiency is about 90%. Since all monochromatic parts can be arranged to be of equal length and parallel in phase space as shown in Fig. 3 they can easily be brought to complete coincidence by a chromatic deflection system. So the overall emittance is substantially less than the emittance of the injected linac beam.

The slow energy shift necessary for extraction may be done by synchrotron radiation loss at an energy range of

about 250 to 330 MeV.[1] Below 250 MeV the electrons lose their energy too slowly. This may be cured by inserting a small accelerator cavity in the ring which will periodically accelerate and decelerate the electrons. Those particles that have suffered enough deceleration will be extracted, the others will remain in the ring until, by a small phase slip per turn, these will meet a decelerating field, too. The process is controlled by proper variation of both amplitude and phase of the RF, thus providing flattening of the extracted beam intensity. At energies higher than 330 MeV, the following scheme may be used to compensate for too quick energy loss by synchrotron radiation: In a RF separator structure there are always transversal and axial forces related by

$$F_{tr} \sim j \cdot \text{grad } F_{ax} \ ,$$

j indicating a 90^{0} phase shift in time.[2] Thus, the inflecting device shown in Fig. 1 may be converted into an accelerating mechanism by inserting a third cavity between the two others. This cavity should be phased in such a way that particles which have suffered maximum deflection in the first cavity meet the accelerating field off axis in the middle one at its maximum value. In this case, any closed orbit particle being deflected at all will be accelerated. By providing a certain RF phase slip between turns a very smooth acceleration of all closed orbit particles may be achieved and it is easily estimated that even for particles undergoing betatron oscillations the energy gain comes to an average rather quickly. Thus, the device described may be used to accelerate an unbunched beam. Though the achievable acceleration is very modest, it is sufficient in our case to compensate the radiation loss which amounts to about 6 keV per turn for electrons at 600 MeV with 2 m bending radius. The RF power requirement of the deflector cavities is in our case mainly determined by the necessity to avoid transverse beam instabilities and amounts to several tens of kilowatts each. Moreover, the interaction of the beam with the two outer deflectors tends to disturb the proper distribution of RF power in these cavities. It is desirable, therefore, to find a similar mechanism using less cavities. At the moment, schemes are investigated in which the setup of a small betatron oscillation by the transverse field of the RF separator mode is used subsequently for acceleration by the axial field of the same mode in a second cavity.

I am greatly indebted to Messrs. K. H. Kaiser, W. Manz and H. Schier for their great help in doing the numerical computations.

REFERENCES

1. R. Servranckx, Proc. Int. Conf. on Photonuclear Reactions and Applications, Asilomar, Calif., March 1973, p. 1039.
2. H. Hahn, Rev. Sci. Instr., Vol.34 No.10 (1963) p.1094.

THE NEXT STEP: ACCELERATORS VERSUS STORAGE RINGS

Leon M. Lederman
Columbia University, New York, New York, 10027

The reason I was willing to accept the invitation of Dick Neal to come here was largely because of the opportunity it gave me to collectively pay homage to the community of accelerator scholars for all the magnificent instruments which have been provided to me and presumably the users I represent here. Perhaps he picked me because I am old enough to have been through so many of these things, starting with a Nevis Cyclotron, and progressing through the Cosmotron and the AGS, and recently, the ISR, and the Fermi National Accelerator Lab with even occasional forays to the Bevatron and PPA. The teamwork of the users and the builders is part of our profession. We work hard in mutual stimulation. You make the machines, and we try to use them so well that the need for more machines becomes self-evident. Both of us, of course, working so that Gell-Mann and his friends become more and more famous. (That is not really fair. It is really an unholy trinity, engaged in a more or less honorable endeavor, the significance of which for history and for the future we do not have to elaborate here.)

My subject is to put the thing in perspective, and I have a slide here for people who do not travel so much. This is a picture of the Fermi National Accelerator Laboratory (Fig. 1) where I have been spending most of my time. Let me just

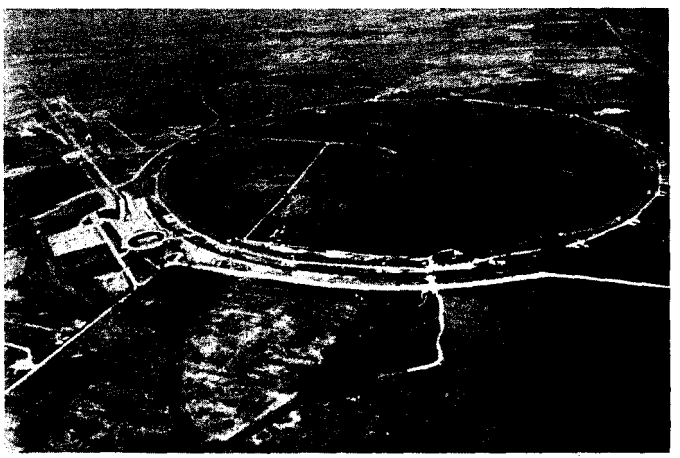

FIG. 1--Air view of the Fermi National Accelerator Laboratory.

say that I am very poorly prepared for these remarks, largely because of the fault of some of you here. I had planned to prepare this talk in some detail during the breakdowns of the FNAL accelerator, and for the last six weeks or so there have been so few.. .. It is really a thing of great beauty. We sit three kilometers from the accelerator and watch a beam sit steadily on a target which is only about 0.4 mm in transverse dimension, and with a duty cycle and intensity which is just positively embarrassing. This is, though, the last word in accelerators, and I always wondered what future archeologists might make of this — and to illustrate that I have another slide, which might surprise you (Fig. 2). It is clear to me the mystery of Stonehenge is solved! Some of you might even appreciate the next figure (Fig. 3), which shows how this was built. You see your progenators, the accelerator builders of an early day — I do not know if you recognize anybody.

In considering my assignment, The Next Step, I decided to be as general as I could, considering configurations that are thinkable in my lifetime as a physicist, which might not last more than another fifteen or twenty years. In reviewing

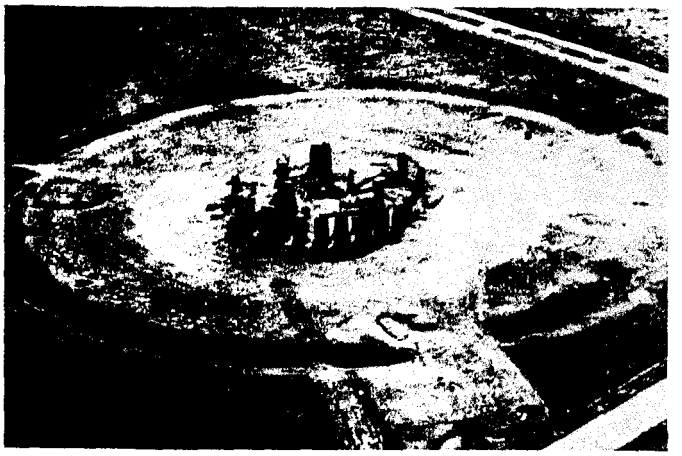

FIG. 2--Air view of Stonehenge.

FIG. 3--Construction of Stonehenge.

the history, there were always two arguments used for a new accelerator. One was to answer existing questions of the kind Gell-Mann reviewed for us in beautiful detail, and the other was that the accelerator should permit the kind of exploration that has always led to totally new questions — even undreamed of, like CP violation, or strangeness, or some of the many other discoveries that were made in a totally

surprising context. And both these steps are quite important. I might give an example of something which is a little bit out of context of here, but something I would like to bring to the attention of this gifted group. Some of us, a few years ago, wrote little notes on the interest that might accrue to collisions of high energy uranium with uranium. I wrote such things, stimulated by some work we did with antiproton production far below thresholds, a nuclear physics question, and then I read a note by Francis Farley, who took off on some speculations of Cocconi about the virtues of complexity. These are highly speculative things, and therefore there was no dream that one should actually spend real money on accelerating uranium to very high energies. But recently, starting from very abstract theoretical ideas, Lee and Wick have produced a nuclear physics theory which has greatly stimulated the idea of going to many GeV per nucleon. It is just these kinds of connections — remote connections — which have made our subject so interesting.

Let me now talk about more relevant things. I was asked to talk about storage rings versus accelerators, And much to my surprise, I found that the ISR has been, in a sense, too successful. Because if one looks at the current listing of unfunded projects, one finds six storage rings — that is something people are thinking about — five are electrons, one is a proton-proton storage ring, and no conventional accelerators! How could this be? What happened to the conventional accelerator? Is a new, conventional accelerator unthinkable in the time scale of the next ten-fifteen years? Thus, in the time I had to prepare this, I considered whether this is a wise thing — is it wise to forgo the opportunity for conventional accelerators?

In Fig. 4, we have a review of all possible experiments, trying not to omit anything. We have lepton-lepton, lepton-hadron, hadron-hadron interactions. We write "storage" where it seemed obvious that a storage ring was the right thing, and "accelerator or storage" when that is possible, and accelerator clearly when you require secondary beams. Now it could be that $p\bar{p}$ could also go in storage rings, but that is somewhat of a quibble. Here is then an almost complete list of the kinds of experiments you can do unless somebody finds something which is different from a hadron or a lepton. (I teach physics for poets, and I got an examination paper last week in which a hadron was defined as "a no longer active particle physicist.")

lepton-lepton	lepton-hadron	hadron-hadron
e^+e^-, e^-e^- : S	ep A or S	pp A or S
	PP A	$\bar{p}p$, πp, Kp, Yp : A
	νp A	

S = Storage
A = Accelerator

But there are alternative reactions, e.g.

$$\left.\begin{aligned} \mu^+ + Z &\to \mu^+ + \mu^- + \mu^+ + Z \text{ (tridents)} \\ &\to e + \mu + Z \\ \nu + Z &\to \mu^+ + \mu^- + \nu + Z \end{aligned}\right\} \text{A}$$

or

$$p + p \to \ell^+ + \ell^- + \text{junk} \qquad \text{A or S}$$

FIG. 4--All possible experiments to do at accelerators and storage rings.

There are alternative reactions (Fig. 4) sometimes, which are not totally obvious, but which permit the study of lepton-lepton scattering using nuclei as observers — this works if the incident energy is high enough. There are also some interesting experiments certainly, like neutrinos going to muon pairs, and other experiments which involve lepton-lepton interactions, as we will see, where the leptons come out of some complex and maybe not so pretty initial state.

In looking at these experiments, one must remember that there are deep interconnections — for example, there are three which study hadronic electricity: the e^+e^- goes to hadrons, which is of enormous current interest today — it is worked on at SPEAR; the deeply inelastic scattering; and perhaps electron pairs coming out of what you have in the way of hadrons, say proton-proton collisions. If you want to test the complete theory of the electrical structure of hadrons, presumably you need information on all three kinds of reactions. And then, again, looking at e^+e^- goes to hadrons, the data look very much like pp goes to hadrons. The hadronic things coming out look so much like the yields we see at the ISR, that clearly there is an important connection, and that further investigations of both will have *to* go hand-in-hand.

I will now survey briefly a set of experiments which one would like to do. Most of these are extrapolations of currently active experiments. The extrapolations of expected cross sections are made here in these next few charts, on the basis of data at lower energies, on the basis of models, and sometimes dimensional scaling, and then maybe sometimes on the basis of just nothing at all. In contrasting storage rings and accelerators, I take 5 TeV as a thinkable accelerator, largely because it fits on the Fermi National Accelerator site — and has roughly the same relation to a thinkable storage ring (and here we have had a great deal of thought) as ISR and FNAL, which are the complimentary accelerators we are working with today. And clearly, as we study FNAL and ISR, and the relationships of the two kinds of experiments, we will learn more about the validity of the kind of comparison I am doing now. So my thinkable accelerators from the point of view of hadron collisions are a storage ring of at least 200 GeV against 200 GeV, for Super **ISR,** and say roughly 5 TeV for Super FNAL. These are arbitrary numbers, if you like, but thinkable in the time frame of the next ten or so years and at costs which very probably do not exceed the annual construction costs we have already inflicted on the U. S. taxpayers. I have made up a report card, Table I, (this being the end of the semester),

TABLE I

Report Card

	Super ISR (SISR)	Super FNAL (SNAL)
• $\sqrt{s}$	$\geq$ 400	~ 100
• usable $\sqrt{s}$	depends	100
• usable luminosity[a]	$\to 5 \times 10^{7}$	10^{12} [b]
• dwell time[c]	B-	B+
• experimental area's flexibility, cost	A	C-
• particle identification	B-	A?
• backgrounds	D	D
• secondary beams	F	P
• interaction of expt. and machine	C-	A-
• sociology	B	A+

Table I (cont'd)

(a) But don't forget Fermi motion.

(@)Only for pp experiments.

(c) Compromises — energy, intensity, special tricks, unequal energies.

---

where some entries are in the form of numbers and some are just letter grades. In some cases, we use the pass–fail option. The first entry is $\sqrt{s}$ which is a ridiculous notation for the energy available in the collision. Super ISR is listed as more than 400 GeV and Super FNAL (5 TeV) about 100 GeV. But I also made a note here, "Do not forget about Fermi motion", because for some special experiments 100 GeV can go surprisingly high paying a price in luminosity. Another entry is usable energy in the center of mass. Usable energy is not always all of the available energy and this depends, again, very much on the kind of experiment you do, and also on what comes next, which is luminosity. I think it is fair to say that a conventional accelerator can probably exploit the full energy available, 100 GeV. It has not yet been established at FNAL, but we will see that it is not terribly far away. For the ISR, whether you can use the full square root of s depends upon what you are talking about. Certainly for the exploration of totally new physics, production processes, it does not seem as if you will ever use the full energy unless luminosities are much, much higher than are being talked about. On the other hand, for tests of scaling, where you have various scaling parameters, for example $2p/\sqrt{s} \equiv x$, you want to make this vary over a very large range — then the mere fact that energy is available is useful.

The next entry in Table I is luminosity and I took for this what might be plausible, namely a beam of a few 10^{13} ppp which gives $\sim 10^{12}$ interactions per second for SNAL. For the Super ISR, Iassumed $\sim 10^{33}\,\mathrm{sec}^{-1}$, which gives 5×10^{7} interactions per second. That is luminosity. On the other hand, usable luminosity is a different thing. Usable luminosity for a conventional accelerator is relevant to experiments using primary protons which, if we look at FNAL, is a small fraction of all the experiments. Most of the luminosity at NAL is being used to generate secondary particles. That is how you can compensate for the fact that you have to build a 5 TeV machine to get a mere 100 GeV available. You make lots of secondary particles. Of course at the ISR you use the full luminosity — to date only $\sim 5\times 10^{5}$ interactions/sec. Experimental techniques for surviving at the projected SISR rates are in principle on hand but have yet to be proved practical.

Again, even in pp experiments, it is not at all clear that the full luminosity at NAL is usable. At NAL recently, when the beam intensity reached 10^{13} particles, it was at times embarrassing, because if the proper experiments, for example neutrino experiments, are not running, even though the beam is split many ways, there are many experiments that cannot use the full luminosity. The apparatus just does not work. It is not easy to make full use of primary protons at the full intensity — you have to use tricks. However, it has been done in special cases and the important thing to note is that the intensity is there,

There are other entries like dwell time — how long do you sit to do an experiment. You sit as the ISR a long time because there are lots of compromises. Since you have many experiments around the ring, if one experiment wants high energy, and another experiment wants low energy, clever as the people at the ISR are, they have not yet been able to change the energy as one goes from one crossing region to the other. (I have a lot of confidence in them, and I expect that one of these days, they will solve the problem.) But until they do, it is a problem and so you have meetings at which one has to make a compromise, and at the ISR it is usually what Carlo Rubbia wants. To get your particular spectrum of conditions you have to wait a long time. Someone every once in a while comes in and he says, "I only want 1 A today." If he is convincing, we have to wait; there's the usual compromise. Now at NAL, for example, there is the new technique of the front porch, where several energies might be available at one time; this can certainly be a great help, and source intensities are no problem — many more groups can more or less control their own intensity, although that still needs some improvements. SNAL gets good grades for this.

Then there are things like experimental areas and flexibility, which are really quite a problem at a conventional accelerator. The bigger the accelerator, the bigger the problem. The experimental areas are complex, and costly, and not nearly as flexible as people hoped, certainly for NAL. Whereas relatively, I think, the experimental areas at the ISR are fairly simple — they are much smaller, physically, and more easy to rearrange. They also cost less.

Particle identification in doing experiments is a problem. Using a many TeV beam, if one scales Cerenkov counters, for example, one finds enormous lengths. A several mile long Cerenkov counter boggles the mind a bit. On the other hand, there may be other techniques that are, or may become much more useful at SNAL, e.g., the relativistic rise in the ionization loss, or perhaps transition radiation; there are techniques which are being developed and there is clearly a lot of interaction between instrumentation and the exploitation of accelerators. Particle identification at the ISR is easy in the forward direction because you can use Cerenkov counters of moderate length. Here, what is relevant is that at SNAL you are dealing with particles of many TeV, whereas at SISR one deals with particles of merely 100 GeV; now we have learned how to deal with those particles. On the other hand, the need to exploit the limited luminosity at ISR requires large aperture equipment and this means that it is much more difficult, say, at 90°, to do particle identification; most of the good particle identifiers have small apertures.

Backgrounds: Well, I find everywhere I go there are lots of backgrounds. I do not give good marks to any machine. This is probably my problem. Maybe electron machines are better. On the other hand, most of the cross sections I will show you that are of interest at NAL, or SNAL, are a much smaller fraction of the total cross section than they would be at SISR; so just the energy gives you a better grade for ISR's.

There is one thing that gives ISR types a bad grade, and that is the interaction of the experiment and the machine — what I call "real life at the ISR". You are very much coupled in with the machine at an ISR. It is well known that you cannot keep these clumsy experimentalists away from the machine, and every once in a while they knock something over, and the machine goes out for months — that is hard to avoid. Whereas at NAL, close contact between experimentalists and the accelerator proper is at a minimum.

Sociology in Table I just means how many physicists can you employ, and it is amazing how well the ISR does. But that is also because it is in Europe, where large groups were pioneered. We once counted 200 Ph.D.'s working at one time, and I do not think that NAL can beat that, although in principle it should. So I gave that a better mark anyway.

Well, now I want to sort of back up this report card with some information. The effect of Fermi motion, if you like, or essentially the nuclear physics boost you get from hitting a nucleus instead of a free proton, scaled up from the work we did at PPA and the Bevatron to NAL, is given in Fig. 5. In one collision out of 10^{5}, the 28 GeV that is usually available from a 450 GeV accelerator goes way up to 40 or 50 GeV. This is not an unmixed blessing, It is interesting for certain explorations if you have a good signal you can then ask about

a particle whose mass is 40 GeV. The same considerations will enable SNAL to go to ~140 GeV.

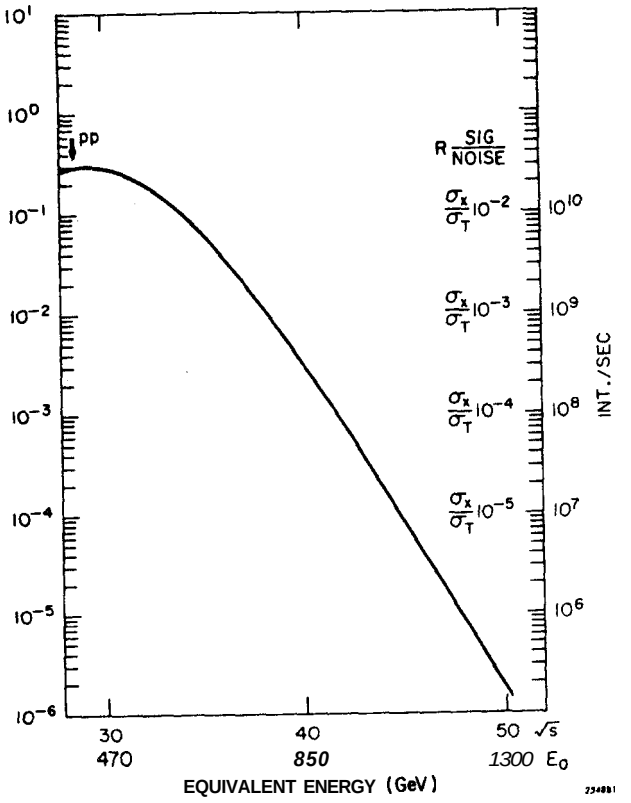

FIG. 5--"Fermi motion boost" at NAL (450 GeV).

I talked about usable luminosity, or using luminosity that is available. Let me *go* through a quick history of the ISR to illustrate this. Shown in Fig. 6 is a charged particle spectrometer, the Saclay-Strassbourg spectrometer, which has produced some nice results on charged-particle yields at 90^{o}. You see the crossing region and you see the spark chambers and the magnet, more spark chambers, and other identifiers. The total solid angle of this apparatus is of the order of 0.01 steradian. I would like to contrast it with another approach at the ISR, which was the so-called CCR experiment, which insisted on having *a* very large coverage, about 1.0 steradian on each side, This experiment was interested in large, transverse momentum π^{o}'s, and tracked a yield curve out to a transverse momentum of ~9 GeV. It stopped running at the end of 1972, and here it is in 1974 and the spectrometers, of which there are several working at the ISR (one is shown in Fig. 7), have still not really gone beyond about 4 or 5 GeV, to my knowledge. *So* the use of the luminosity is not a trivial thing, and one pursues this problem.

Here is a picture of what our groups hopes to do next at the **ISR,** which is essentially a 2π spectrometer (Fig. 8). This is a now super-conducting magnet, with spark chambers inside, and glass outside to look at γ rays, and a wall thickness of only ~1 radiation length, so that one does not disturb the photons too much. This would help the ISR in achieving luminosity times solid angle, which might *go* up by a factor of ~50 or so above the previous generation of experiments.

The same sort of thing happens at NAL. The next figure, Fig. 9, is useful for comparing SNAL against the SISR. Here is a Cronin-Piroue data on production of pions. Note that they have, in fact, a rather small aperture but still they are able, with some trouble, to achieve cross sections of the order of $<10^{-37}$. In terms of exhausting the kinematic limit you see data out to $x_{\perp} \sim 0.7$ where the maximum value of the accelerator is 1; you see they are not too far away.

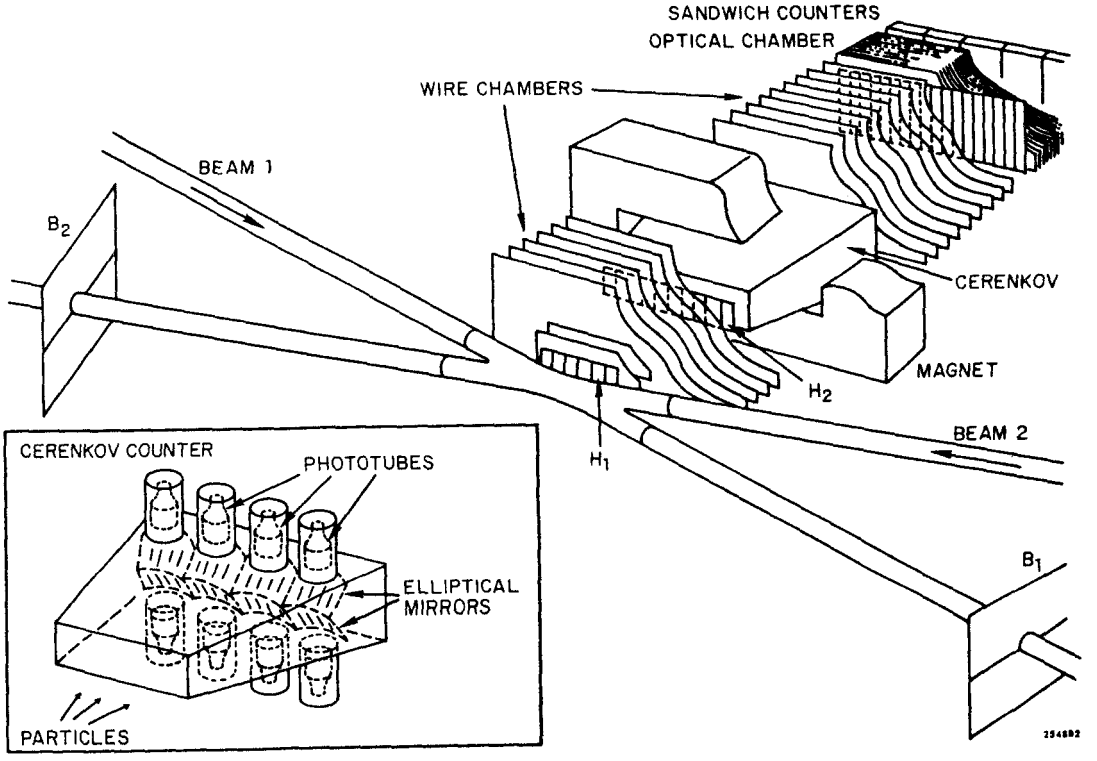

FIG. 6--The Saclay-Strassbourg Spectrometer at ISR.

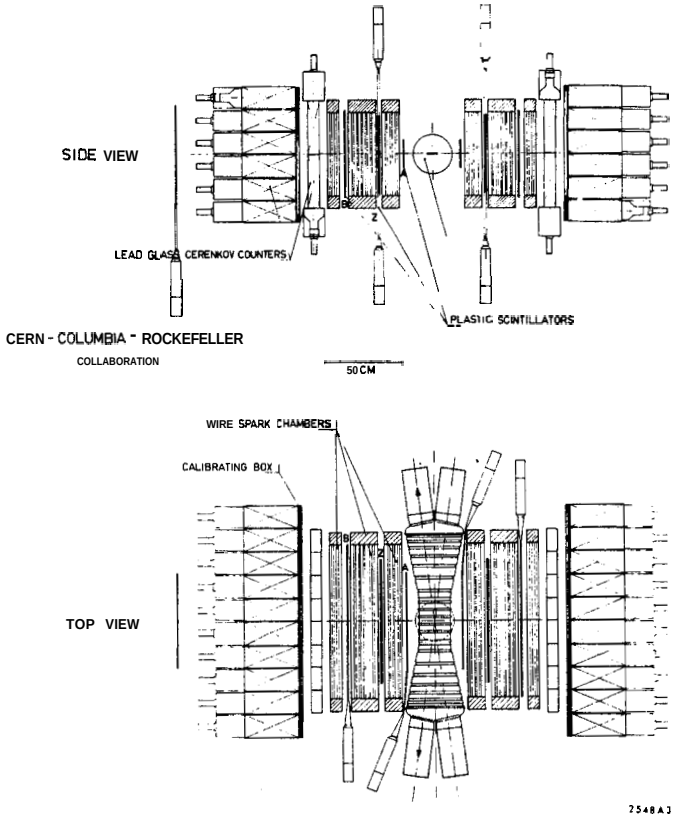

FIG. 7--The CCR Experiment Spectrometer at ISR.

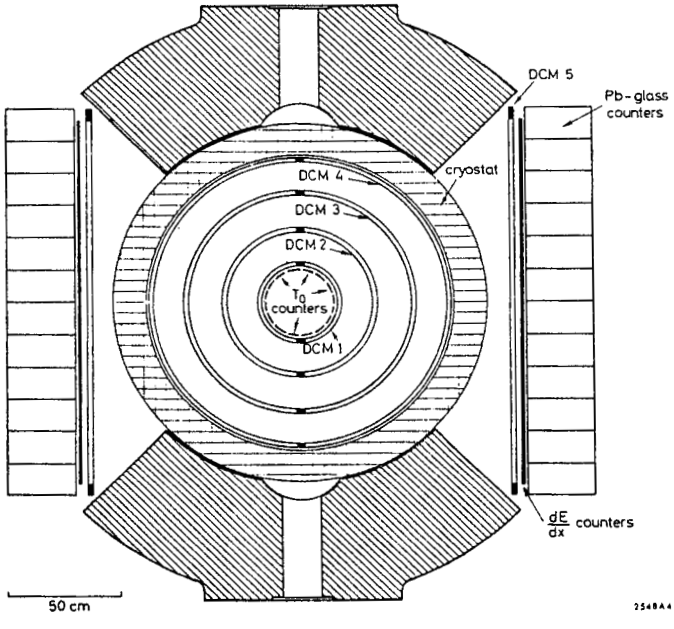

FIG. 8--A planned 2π Spectrometer at ISR.

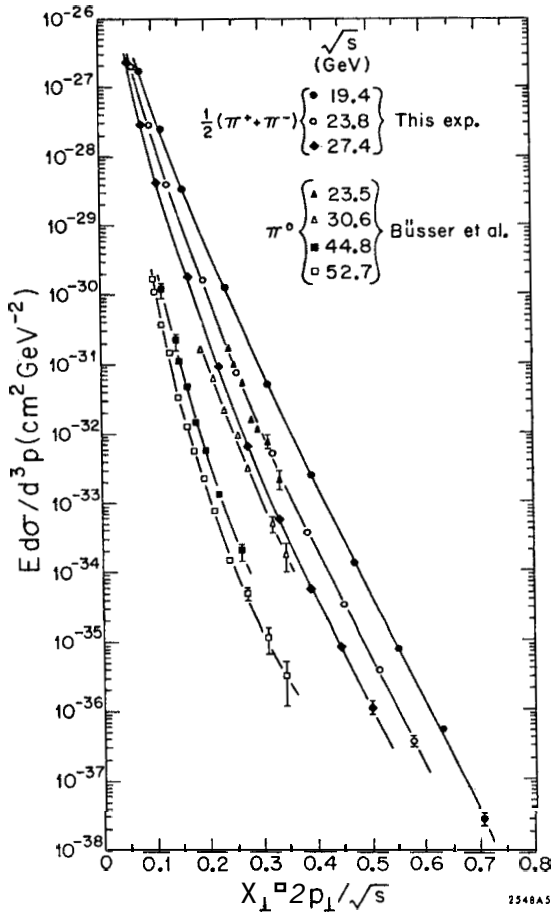

FIG. 9--Cronin-Piroue data on pion production.

And this is a very early NAL experiment. The comparison with data taken at ISR is given in Fig. 9, where even though the ISR energy is much higher, the luminosity is such that with a reasonably good solid angle, one could not go above $x_\perp \sim 0.4$. This is a good example. Energy you have, but limited luminosity prevents you from exploiting it fully. Of course, that was one stage. One hopes one will be able to go on, in both experiments. We will always be more inhibited at the ISR. This is the luminosity price.

Now let me go on to some other experiments. Figure 10 is the famous rising total cross sections. There is some bubble chamber data from NAL and there are the famous ISR experiments showing this rising cross section. New data from the total cross section group at NAL have experimental points which also show a rise with statistical errors in this region of the order of one or two-tenths of a percent. So here, again, you see a comparison between an ISR experiment where you have difficult experiments with fairly large error bars, but a big handle in s, as opposed to very precise experiments over a more limited range of s. What is even more interesting about the NAL approach is that they also have cross sections (Fig. 11, 12), for π's K's, and anti-protons, incidentally all of which look as if they were rising

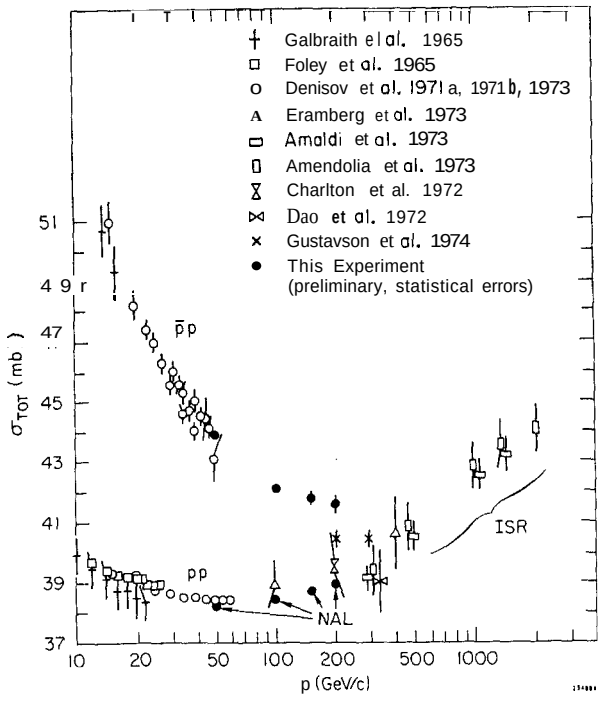

FIG. 10--The proton-proton total cross section.

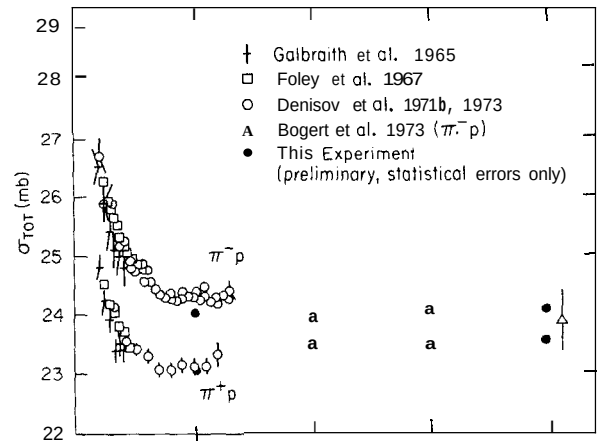

FIG. 11--The $\pi^{\pm}$p total cross sections.

in this region. And it seems to me that in any incisive elucidation of this phenomenon, the need for secondary particle cross sections is also important. And perhaps I ought to leave this as a question: would theory be totally happy having only the proton-proton data?

The next Figure **(13)** deals with an extrapolation of total *cross* sections under various current theories and some possible SNAL and SISR "results". Following this (Fig. **14)** is a multiplicity extrapolation and then (Fig. **15)** a slope parameter in elastic scattering. The "stretch" in rapidity for ISR, SNAL and SISR in two current models is given in Fig. 16. Here was a clear ISR break since the NAL parameter s cannot extend far enough — only the ISR could discover the "central plateau".

Let me go on to some other experiments, and extrapolations thereof. Figure 17 is a strong interaction experiment which is a continuation of high p perpendicular, proton plus proton goes to pion plus anything. This is an extrapolation of

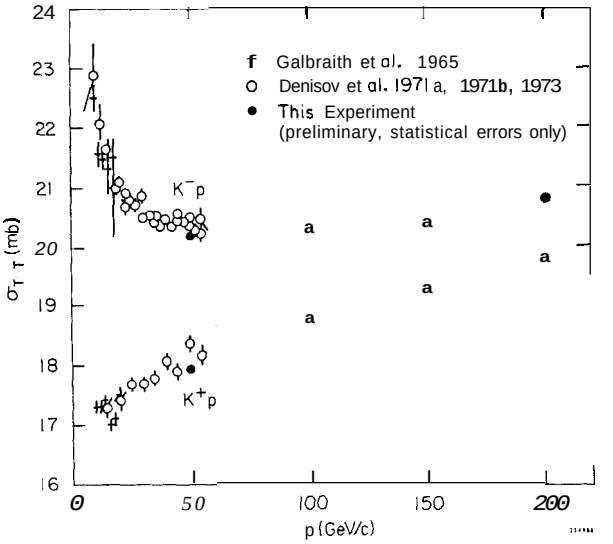

FIG. 12--The $K^{\pm}$p total cross sections.

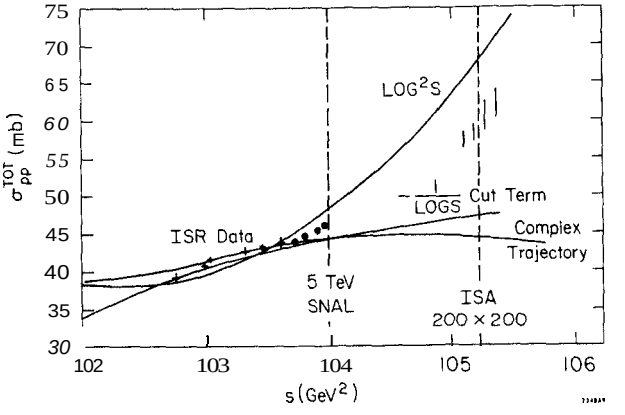

FIG. 13--Model-dependent extrapolation of the proton-proton total cross section.

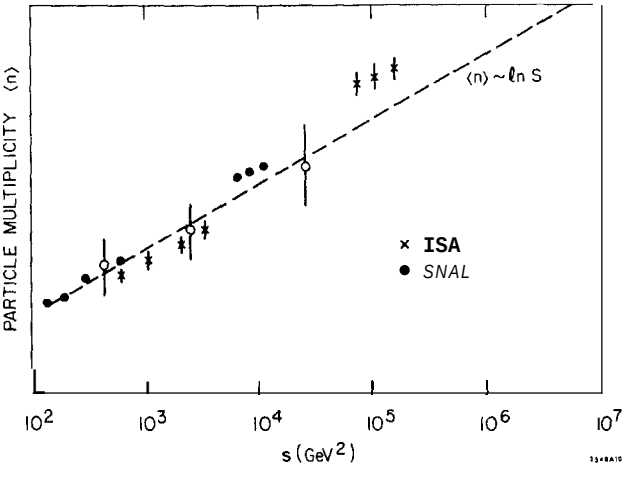

FIG. 14--ln s extrapolation of the particle multiplicity.

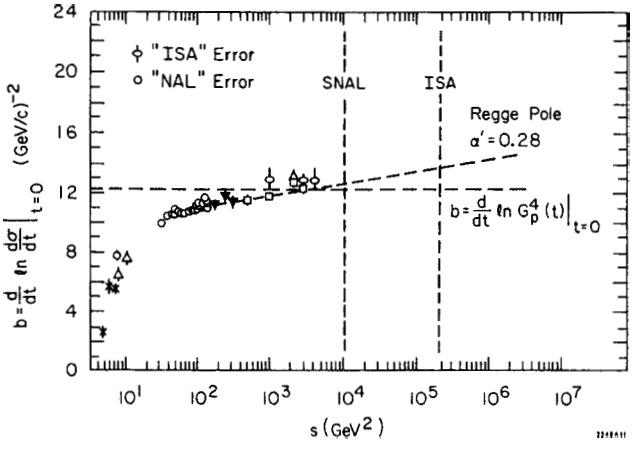

FIG. 15--Slope parameter in proton-proton elastic scattering.

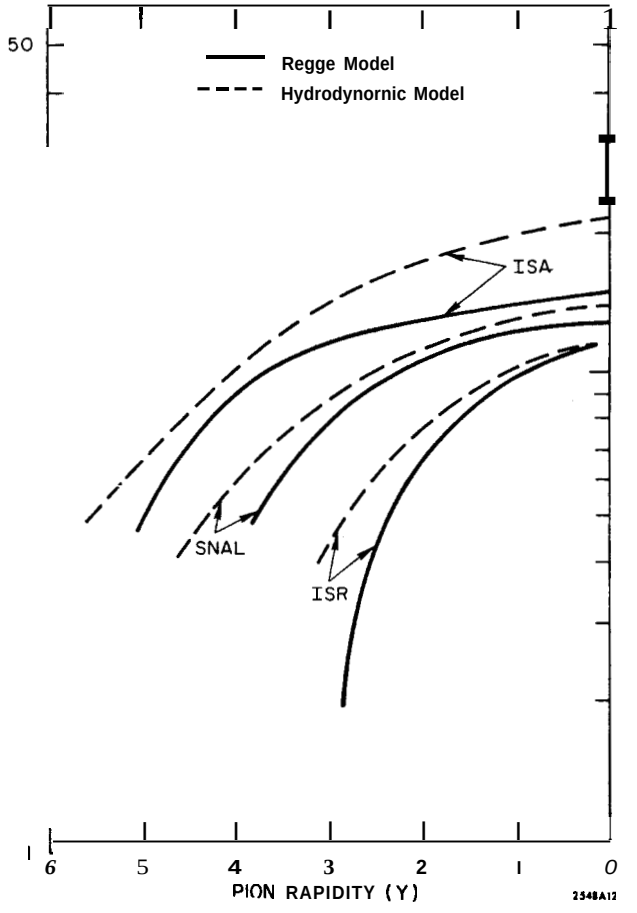

FIG. 16--Two model-dependent extrapolations of the pion rapidity distribution at **ISR,** Super NAL, and ISA.

ISR data, to SNAL and **SISR** and you see that 20 GeV/c is observable if one can go to cross sections like 10^{-39}, and I think that is certainly possible for SNAL. On the other hand, for an **ISR** I think it is very hard to go say, below 10^{-37}, but this also gets to ~20 GeV/c.

The two machines in this particular piece of physics, where the s dependence is not very dramatic, are roughly equivalent. SNAL however permits additional information to come from incident pions, **kaons,** and $\bar{p}$'s. On the other hand, one of the things which is most intriguing to me in high

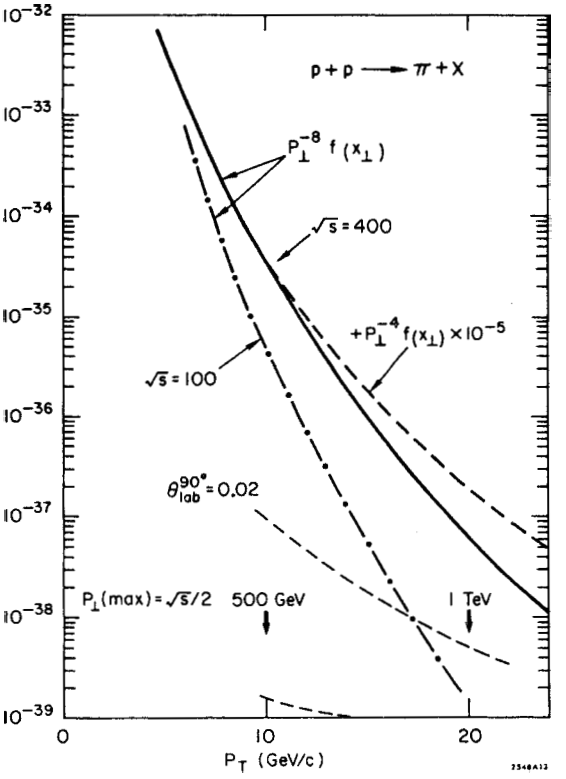

FIG. 17--Cross sections at $\theta_{cm} = 90^{o}$ for inclusive production of π mesons, as a function of the transverse momentum of the π meson.

$P_\perp$ phenomena is the possibility of observing interference effects between strong and electromagnetic, or between strong and weak interactions. One does not really know where those interference effects take place — they may take place near $P_\perp \sim 15$ GeV/c, or maybe a little bit beyond. And here you might, then, look at strong interactions for violation of discrete symmetries in order to detect such interference. You might look for, say, parity violation, and so on. For that reason, you are certainly led to a greater interest in the high energy. And that will be primarily true, in general, for weak interactions.

Figure 18 shows another way to look at it. This is a sort of kinematic region from the point of view of testing any scaling laws for deep inelastic stuff, and clearly **SISR** takes you out a long way in s; on the other hand, SNAL covers a big chunk too.

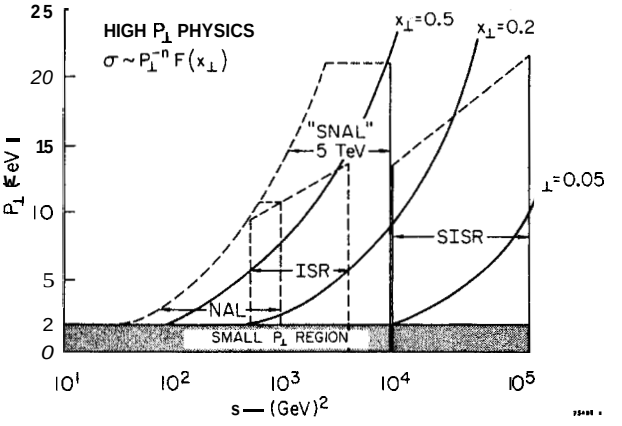

FIG. 18--Regions in $s(GeV^2)$ and $P_\perp$ (GeV) available to NAL, **ISR,** Super NAL, and Super **ISR.**

Figure 19, shows a case of looking at electromagnetic interactions with proton machines, again in a large storage ring, one can (if one believes in these extrapolations which are admittedly model dependent, maybe totally wrong, but which are at least thinkable) explore masses, look for things

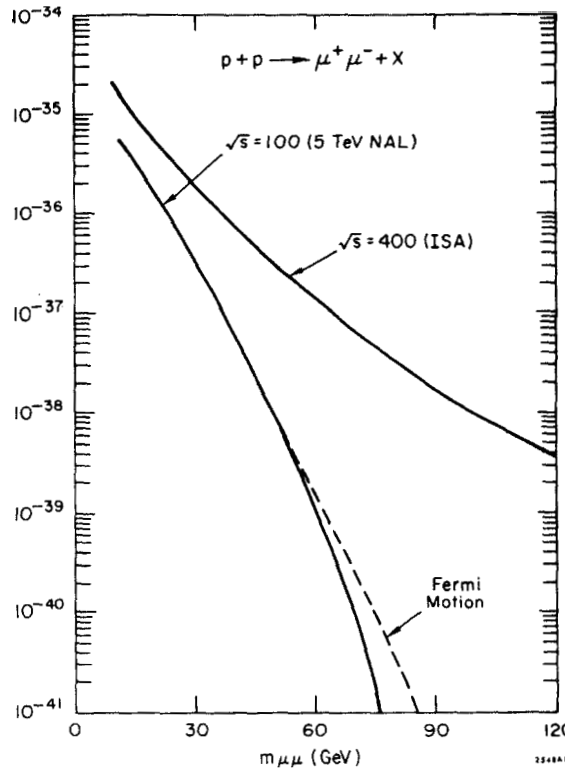

FIG. 19--Electromagnetic interactions with a proton machine; μ-pair production at a 5 TeV NAL and ISA.

up to enormously large masses, because again if we can reach 10^{-37} we seem to have sensitivity out to about 60 GeV of mass. Again, though, if you look down here at 10^{-39}, you see that you have about the same limit with a conventional accelerator. Why would you want to do this sort of thing? Well, there are several reasons. One is, you would like to look for bumps, you would like to look for the Z_0's, and a Z_0 on a background of this kind would presumably show up as some resonance in the effective mass of $\mu\mu$ or ee or whatever lepton pair you look for. Also, if the continuum does have some size which can be measured, one wants to answer questions of scaling, and you might also want to calibrate the search for intermediate bosons, which presumably have the same hadronic part but an interesting and new leptonic part. Figure 20 shows one of a long series of things that can be made with the virtual photon flux discovered in Fig. 19. These are heavy leptons. These curves are steep and so **SISR,** for the first time, really takes over (up to $m_L \sim 80$ GeV). Other "things" calibrated by Fig. 19 are quarks, monopoles and, in fact, anything that can be pair produced at say, PEP. We DO NOT discuss the relative experimental problems without bullet proof vests.

We now come to what could be the most interesting point: weak interactions, The main point about pp collisions is, of course, that you have such high energy. Somehow we have to be freed of the tyranny of doing neutrino physics. At the moment we are stuck with it, but it may be that one can never do weak interactions with protons because the effective signal is too small. One does not know yet. In perhaps two or three years, one will know whether this is a feasible reaction. There are two ends here: one is actual production of the intermediate boson, and the other is weak interactions without an intermediate boson.

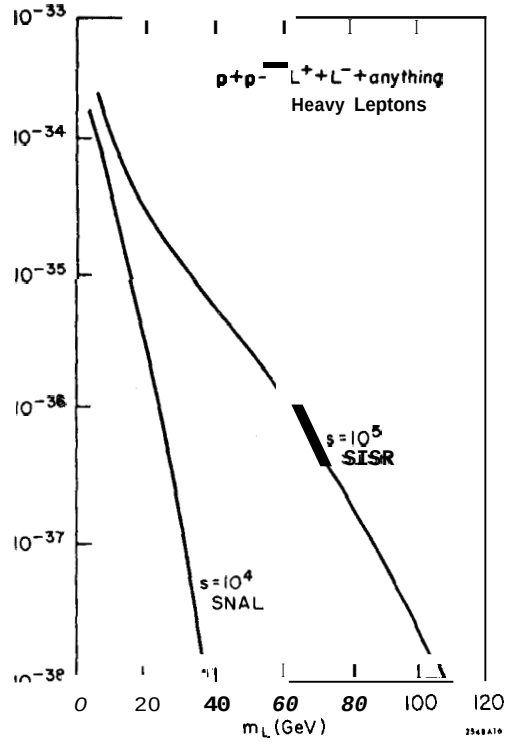

FIG. 20--Heavy lepton production as a function of lepton mass at Super NAL and Super ISR.

Figure 21 shows that, at $\sqrt{s} = 400$ you have a signal which might be measurable out to beyond $Q^2 = (100\ \text{GeV})^2$. Remember that in number of events, one multiplies by 10

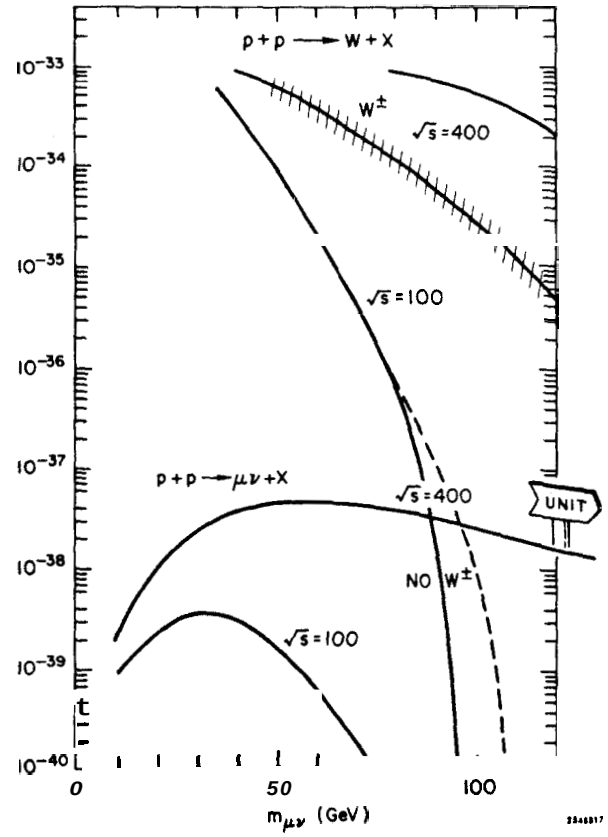

FIG. 21--Production of W boson or $\mu\ \nu$ in proton-proton scattering.

if one takes a reasonable bite in Am. So there are of the order of a hundred events per day, and one can track this thing out and answer one of the crucial questions of weak interactions as to what happens at very, very high values of the effective lepton mass. Strictly, there is no unitarity limit in this reaction. On the other hand, one knows that for a four fermion interaction at a center of mass energy of some hundreds of GeV, unitarity breaks down. Whatever physics intercedes should show up in a reaction of this kind at high masses. That is the force of this kind of research. All of this is to say that ISR's may be useful for weak interactions. They may even be useful for such esoteric things as neutral currents, e.g., interference between virtual Z^0 and γ's to produce lepton pairs. We know NAL type machines can also study these questions, but not much beyond ~50 GeV. Experimentally, there is reasonable hope that backgrounds of ~100 GeV/c transverse momentum objects from non-weak sources will be manageable. Missing transverse momentum signalling a neutrino will also be helpful.

We now go to the report card about secondary beams. There is simply an enormous amount of stuff that still wants to be done at the next level of energies. For example (see Fig. 22), elastic scattering of secondary particles, total cross sections, hyperon interactions, high $P_\perp$ events for not

1. π, K, $\bar{p}$ elastic
2. π, K, $\bar{p}$ total
3. hyperon-nucleon scattering
4. high $P_\perp$ for $\pi p \rightarrow$ hadron + anything
5. resonances $Kp \rightarrow$ hadron + anything
6. K^0 physics pp — hadron + anything $\sqrt{s} \sim 80$ GeV
7. muon beams — 10^7/sec up to 3 TeV

   μp scattering

   Brems. (QED)

   μ^* Prod.

   Universality etc.
8. electron beams — prob. similar
9. y-beams, even polarized!
10. neutrino beams E_ν — 2 TeV

    very high σ will permit

    more civilized detectors

    But: shielding! up ve!

FIG. 22--Secondary beam possibilities at Super NAL.

only protons but also the other particles because the quantum number effects may be revealing. The resonances are things which have to be pursued and which with storage rings will be very difficult. There is K^0 physics, and maybe some elucidation of the CP problem, maybe that we are stuck with K mesons and have to do more experiments of that kind. Then going to electromagnetic interactions there are photon beams of interesting intensity and these may even be polarized by crystal techniques. There are muon beams of the order of 10^7/sec, up to perhaps 3 TeV. Now that should be a very beautiful thing for scattering, for tests of QED, at center of mass energies of the order of 100 GeV, for perhaps searches for heavy leptons, and tests of μe universality. And for some sort of clue to the Bjorken formula we saw before. Presumably at these accelerators you could also make electron beams, like muon beams, with similar intensities. Then, of course, in weak interactions there are neutrino beams, and to have a 2 or 3 TeV neutrino beam with the consequently much higher cross sections might permit more civilized detectors, detectors which may not be so big. There is, of course, the problem of shielding, which I have not solved with these high energy machines, but somebody will solve them.

Let me discuss electron-proton scattering. I did say that ep can be done two ways — storage mechanism or via conventional accelerator. One usually looks at a kinematic domain, q^2 vs u where we compare a 15 GeV e against 200 GeV p storage ring solution to the problem, with muon beams of 3 TeV. Using 10^7 muons and a reasonable target I get a muon luminosity of 5×10^{33}, roughly get a factor of 50 improvement over storage ring in luminosity. Off hand, in Fig. 23, it looks as if a very large kinematic range is

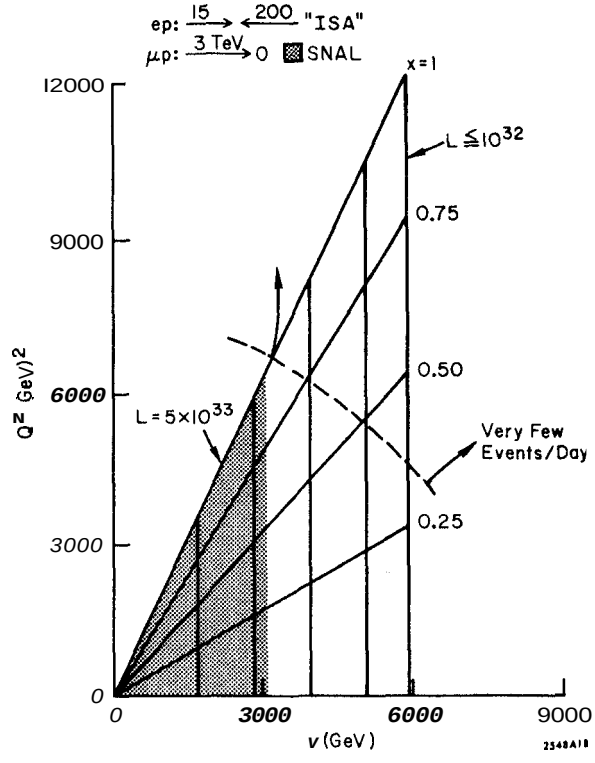

FIG. 23--Availalbe ν (GeV) - Q^2 (GeV^2) regions in lepton-proton scattering: comparison of ep storage ring (ISA) and μp conventional accelerator (Super NAL).

exposed by ep storage rings. On the other hand, if one looks at the numbers, one finds that in a large part of this plot the number of events per day is very small. So if one says, "Well, one can do good physics with a very small number of events per day", then of course the whole thing is relevant. If one says, "You really cannot learn anything very incisive from a very small number of events per day", then the two experiments look more competitive, with greater flexibility, e.g. in secondary particle detection, going to the muon approach.

I briefly considered alternatives to the e^+e^- storage question and could only come up with the "Fermi accelerator" Fig. 24 to compete with 15 GeV × 15 GeV e^+e^-. Conventional magnets are used. Rumor has it that Wilson wants the real estate for 100 kG superconducting magnets. This way he would feel challenged. For storage rings of course.

My conclusions are that a ~10 year program must include both proton storage rings and a fixed target proton accelerator. The graphs here indicate that a good match would have the Super ISR with ~6 -10 times the $\sqrt{s}$ as

FIG. 24

a "conventional" Super-NAL, that is, the example I chose finds the two machines too closely matched. Costs become a crucial matter. We need e^+e^-, and probably in the form of storage rings. As NAL and ISR develop, in the next few years we will see how sound the comparisons made here turn out. I hope that in the next few years, also, that we will find enough things to shake what I thought was the great complacency of Gell-Mann in saying that he sees in the air the ultimate theory. I hope we can spoil that. We will surely try.

DISCUSSION

Murray Gell-Mann,(California Institute of Technology): Can you give some idea of the cost?

Lederman: You want to know how much a 5 TeV accelerator will cost. I have no idea. I don't think a reasonable estimate is possible. I can give you a number that no one can prove that's impossible, a number like 200 million dollars can not be proven an impossible number.

PERSPECTIVES ON COLLIDING BEAMS

E. Keil
CERN
Geneva, Switzerland

Summary

The design and performance of colliding beam devices is restricted by two different kinds of limitations: those due to technology and funds, and those due to space charge phenomena. Among the technological limitations are maximum magnetic fields, RF power, and the stored energy of the beams. The space charge limits are determined by single-beam and beam-beam phenomena, such as the stability of coherent longitudinal and transverse oscillations, or the incoherent beam-beam tune shift. The aim in the design of a colliding beam device is to achieve the best possible luminosity within all these limits. Procedures for determining appropriate machine parameters which include all constraints from the beginning, have been developed. The resulting parameter sets will be compared to those of machines under study at present. The design procedures also allow predictions how the parameters and luminosity of future colliding beam devices would change if some or all of the technological limitations were to occur at a different level.

1. Introduction

The beam dynamics and technology on which the design of storage rings is based are essentially the same for both electron and proton machines. There are, however, important differences such as synchrotron radiation. The discussion will be presented under two main headings

- electron storage rings
- proton storage rings.

Since no electron-proton machine has as yet been built it would appear too early to make predictions for the parameters of the next generation of these machines.

For each kind of machine, the requirements which have to be satisfied in order to achieve a high luminosity will be reviewed first. They can be cast into a series of design equations which link their design parameters. It turns out that a fairly detailed picture can be obtained by choosing a rather small number of parameters. Their choice is guided by extrapolation and scaling from existing machines. Finally, examples of machines beyond those presently contemplated will be shown which are designed according to these principles.

2. Electron storage rings

The principles for the design of an electron storage ring have been known for a long time[1]. The storage ring SPEAR[2] has been designed accordingly. The operating experience with ADONE[3] and SPEAR' has recently led to some changes in the design principles[5] which are being incorporated in the design of the electron-positron part of PEP[6]. The following presentation follows essentially Ref. 5. It is assumed that the electron and positron bunches collide head-on, i.e. they follow the same trajectory in opposite directions in the vicinity of the interaction point.

2.1 Luminosity and beam-beam tune shift

Apart from the energy of the colliding particles, the luminosity per intersection L is the most important parameter of a storage ring as far as its usefulness for colliding beam physics is concerned. It is given by

$$L = \frac{N^2 f}{4\pi k \sigma_x^* \sigma_Y^*} \tag{1}$$

N is the total number of particles in one beam, f is the revolution frequency, σ_x^* and σ_Y^* are the rms beam horizontal (x) and vertical (y) radii at the interaction point, k is the number of bunches in one beam. In (1), the rms bunch half length σ_ℓ does not appear because it has been assumed that it is smaller than the amplitude functions β_x^* and β_Y^* at the intersection point.

The beam-beam interaction at the crossing points is usually accompanied by the electromagnetic effect of one beam on the other. It has become customary to describe the strength of this essentially non-linear perturbation by the linear tune shift given to particles close to the axis of the other beam.

The beam-beam tune shifts in the two directions are given by

$$\Delta Q_y = \frac{N r_e \beta_y^*}{2\pi k\, (\sigma_x^* + \sigma_y^*)\, \sigma_y^* \gamma} \tag{2}$$

$$\Delta Q_x = \frac{N r_e \beta_x^*}{\pi k\, (\sigma_x^* + \sigma_y^*)\, \sigma_x^* \gamma} \tag{3}$$

Here, r_e is the classical electron radius and γ is the usual relativistic parameter,

The recent treatment[5] differs from the previous one[1] by assuming head-on collisions and, consequently using products of beam radii in (2) and (3). This reflects the experimental observation in ADONE[3] and in SPEAR' that crossings at an angle do not yield a higher luminosity although in this case the product of beam radii is replaced by a - bigger - effective beam cross section.

It is most instructive to eliminate one power of N, from (1) by using (2). This manipulation yields

$$L = \frac{N f \gamma \Delta Q}{2 r_e \beta_y^*} \tag{4}$$

It has been assumed that $\sigma^* >> a_Y^*$.

Equation (4) holds for any N and any ΔQ_y provided that the approximations used in its derivation are satisfied. However, it gains its full significance by interpreting it in the following manner: if ΔQ_y is replaced by its maximum permissible value ΔQ, and if the beam dimensions at the interaction point are chosen such that (2) and (3) hold then (4) gives the maximum luminosity which can be achieved in an electron storage ring with N electrons in each beam.

It is interesting to note how little one has to know about a storage ring in order to estimate its luminosity. The maximum beam-beam tune shift ΔQ is believed to be a universal constant. There are two lower limits for β_y^*, the bunch length and high values of β_y at the ends of the intersection region which are a consequence of low values of β_y^*. The most important outstanding parameter is N which is entirely determined by single beam phenomena.

Looked upon in a different way, *(4)* is just a formal expression which relates the luminosity to a small number of as yet unknown parameters. All the difficulties of designing storage rings are hidden in these parameters.

2.2 Synchrotron radiation

In electron machines the synchrotron radiation is by far the most important single beam phenomenon. The power loss P which has to be compensated is given by[1]:

$$P = \frac{4\pi}{3} r_e m_e c^2 \gamma^4 N f \rho^{-1} \tag{5}$$

Here ρ is the bending radius of the electron beam and $m_e c^2$ is the electron rest mass. It is customary in electron storage ring design to use *(5)* to eliminate Nf from *(4)*. In this case the luminosity becomes:

$$L = \frac{3}{8\pi} \frac{\Delta Q \rho P}{r_e^2 m_e c^2 \gamma^3 \beta_Y^*} \tag{6}$$

The interpretation of this equation is the same as that of *(4)*.

Clearly, there are many space charge phenomena in electron storage rings which have caused difficulties in their initial operation, but, which on the whole have been overcome later on. For this reason, they have not been included in the design procedure.

2.3 Design procedure

2.3.1 Outline

For a given energy y, the luminosity (6) depends only on *4* parameters: ΔQ, ρ, P, β_y^*. Fixing all of them determines L. If R/ρ is fixed, N follows from (5). Fixing k and imposing upper limits on ΔQ_y and ΔQ_x, gives, from *(2)* and (3), upper limits on $\beta_y^*/(\sigma_x^* \sigma_y^*)$ and on β_x^*/σ_x^{*2}. These expressions are taken at the interaction point. In order to obtain a machine design, they have to be related to the beam size and lattice parameters in the normal machine lattice. If one assumes that there are no dispersive elements - and also no dispersion matching - between the machine lattice and the interaction point, then the ratio β_x/σ_x^2 is an invariant. It is, in fact, given by quantum fluctuations in synchrotron radiation and becomes approximately[1]

$$\frac{\sigma_x^{*2}}{\beta_x^*} = \frac{\sigma_x^2}{\beta_x} = \frac{3C_q}{2} \cdot \frac{R}{Q^3} \frac{\gamma^2}{\rho} \tag{7}$$

where $C_q = 3.84 \times 10^{-13}$ m. Since all parameters in (7) except Q are known, this equation determines the maximum Q-value Q_{max} in the machine lattice. The actual value of Q must be smaller than Q_{max} and be compatible with the requirements on the working point.

In addition, there is the contribution to Q from the insertions which is not included here.

For a given Q and a chosen phase advance per period, the parameters of the period are completely determined, such as β_{max}, β_{min}, length, and quadrupole focal length. The radial beam size in the cells follows from (7). To complete the description of the machine, $\sigma_{y_{max}}$ and β_x^* are still to be determined. They are related by (2) and the usual scaling of σ and β, $\sigma \sim \beta^{1/2}$:

$$\frac{\beta_y^*}{a_x^* \sigma_y^*} = \frac{\beta_{max}}{\sigma_{x_{max}} \sigma_{y_{max}}} \left(\frac{\beta_y^*}{\beta_x^*} \right)^{1/2} \tag{8}$$

If r is defined so that $\sigma_{y_{max}} = r\sigma_{x_{max}}$, (2), (7) and (8) can be manipulated to give

$$r^2 \beta_x^* = \beta_y^* \left(\frac{Q}{Q_{max}} \right)^6 \tag{9}$$

Since only the product $r^2\beta_x^*$ is fixed by (9), r and hence the vertical beam size can be chosen freely, and β_x^* fixed afterwards to maximize the luminosity. In order to save vertical aperture, $\sigma_{y_{max}}$ is fixed at $\sigma_{y_{max}} = 1$ mm, resulting in a vertical aperture A_y of *40* mm, half of which is for closed orbit errors. Allowing 20 $\sigma_{y_{max}}$ for the beam gives a good beam lifetime and ample allowance for the change in the beam size due to the beam-beam interaction. The horizontal aperture A_x is determined in the same way.

The peak RF voltage V required is determined by the radiation loss/electron U which follows from the total power P and the number of electrons. V has to be higher than U by the overvoltage ratio q required to achieve a given quantum lifetime τ_q. The latter is related to the damping time τ_s by a pair of transcendental equations[1].

2.3.2 Results

A machine designed according to the procedure just described is the preliminary design of a 15 GeV electron-positron storage ring[5] which is compatible with the current PEP design[6]. Its parameters are summarized in Table I.

In order to demonstrate where electron storage ring design may lead to in the future, the parameters of this machine are scaled to an even higher energy. Consider a step in energy by a factor $10^{1/2}$, i.e. from 15 to about 50 GeV. In order to keep the luminosity constant which is the bare minimum in view of the rapid decrease of most of the cross sections involved, the radius of the machine is assumed to go up by a factor of $10^{3/4}$, and the RF power by a factor $10^{3/4}$. This choice fixes the machine design apart from the RF parameters which are chosen to yield a constant quantum lifetime. The results are also shown in Table I.

TABLE 1

Comparison of electron storage ring parameters

E/GeV	15	50
$L/cm^{-2}s^{-1}$	10^{32}	10^{32}
R/m	220	1240
R_0/m	318	1790
ρ	0.75R	0.75R
ΔQ_y	0.06	0.06
ΔQ_x	$\leq$ 0.06	$\leq$ 0.06
k	2	2
f/kHz	150	26.7
β_y*/m	0.2	0.2
P/MW	2.77	15.6
σ_x^{*2}/β_x/cm	$\geq 5.4 \times 10^{-5}$	3.0×10^{-5}
$\sigma_x^*\sigma_y^*/\beta_y$/cm	$\geq 5.4 \times 10^{-5}$	3.0×10^{-5}
N	4.25×10^{12}	7.56×10^{12}
Q	10	27
β_{max}/m	59	127
β_{min}/m	10.1	21.8
$\sigma_{x_{max}}$/mm	6.3	6.2
$\sigma_{y_{max}}$/mm	1	1
β_x*/m	5.21	6.21
A_x/mm	146	144
A_y/mm	40	40
τ_s/ms	3.7	3.7
τ_q/s	10^4	10^4
U/MeV	27	480
q	2.2	1.36
V/MV	60	650

It may be seen that a machine at 50 GeV energy requires a very large RF voltage and RF power, and that it has a very large radius. This may indicate that the technological limit for electron storage is below 50 GeV. Since this limit is so much influenced by synchrotron radiation it appears rather difficult to overcome.

3. Proton storage rings

Practical experience on proton storage rings is available from a single machine, the ISR[7]. In addition, there have been a few design studies[8,9,10], but there is no established design procedure for this type of machine. Below, an outline of such a procedure is presented. It is assumed that the proton beams are unbunched and collide at a small angle.

3.1 Luminosity and beam-beam tune shift

When the proton beams collide at an angle such that they are well separated at the ends of the free intersection space, the luminosity L obtained is given by:

$$L = \frac{c\lambda^2}{\pi^{\frac{1}{2}}\sigma^*\alpha_0} \tag{10}$$

Here c is the velocity of light, λ is the line (number) density of protons, and α_0 is the crossing angle. It has been assumed that the rms beam radii σ_x^* and σ_y^* are equal to σ^*.

Under the same assumptions, the beam-beam tune shift in the x direction is:

$$\Delta Q = \left(\frac{2}{\pi}\right)^{\frac{1}{2}} \frac{\lambda r_p \beta^*}{\gamma\sigma^*\alpha_0} \tag{11}$$

Here, r_p is the classical proton radius and β^* is the value of β_x and β_y at the interaction point. It has been assumed that the crossing takes place in the vertical plane. In this case $|\Delta Q_y| \leq |\Delta Q_x|$ always holds for a round beam.

The above expressions are all approximations. They are valid for beams which are well separated at the end of the free space around the intersection point, and for values of β^* which are not too small. The optimum choice of β^* will be discussed below. Accurate formulae for round beams[11,12] and for elliptic beams[13] are available.

If the tune shift (11) is again used to replace one power of A in (10) the following formula is obtained:

$$L = \frac{c\gamma\ \lambda\ \Delta Q_x}{2^{\frac{1}{2}}\ r_p\ \beta^*} \tag{12}$$

Although this is valid for all values of λ and ΔQ_x it may again be interpreted as an expression for the maximum value of the luminosity which can be obtained in a proton machine, if the crossing angle and/or the beam dimensions are adjusted so that (11) holds with ΔQ_x replaced by its maximum permissible value.

It can be shown[12] that the luminosity L reaches an asymptotic value when β^* decreases, and that 2/3 of that luminosity are obtained when β^* is chosen as follows:

$$\beta^* = \left(\frac{\Delta Q_x E_t\ \ell}{8\pi\ \lambda\ r_p}\right)^{\frac{1}{2}} \tag{13}$$

Here $E_t = 4\pi\beta\gamma\sigma^{*2}/\beta^*$ is the normalised transverse emittance, and ℓ is the free length around the interaction point. With the choice (13) for β^* the luminosity becomes:

$$L = \frac{4}{3} c\gamma \left(\frac{\pi\lambda^3\ \Delta Q_x}{E_t\ \ell\ r_p}\right)^{\frac{1}{2}} \tag{14}$$

3.2 Single beam limits

In proton machines there is no one phenomenon which is clearly more important than all the others. Therefore it is appropriate to include many of them in the design procedure right from the start and to let the latter itself find out which are the most important. The discussion below is based on present knowledge of these phenomena, i.e. any new developments which may make them less severe are not taken into account.

3.2.1 Incoherent tune shift

In the highly relativistic limit where the contribution of the direct space charge effect to the incoherent tune shift is negligible compared to the contribution of images, the standard formula[14] may be written as follows:

$$\Delta Q_I = \frac{N r_p R}{\pi Q \gamma}\left(\frac{E_1}{h^2} + \frac{\rho}{R}\,\frac{E_2}{g^2}\right) \tag{15}$$

Here, h is the half aperture of the vacuum chamber and g is the half height of the magnet gap, and magnets are supposed to occupy only a fraction ρ/R of the circumference. E_1 and E_2 are image field coefficients which depend on the shape of the vacuum chamber and magnet polepieces, respectively. For the parallel plate geometry of a separated function machine one has[14]:

$$E_1 = \frac{\pi^2}{48} \qquad E_2 = \frac{\pi^2}{24} \tag{16}$$

Assuming that g and h are equal and calling the half aperture b, (15) can be brought into the form:

$$\Delta Q_I = \left(\frac{\pi^2}{24}\,\frac{r_p E_p}{e^2 c^2}\right)\frac{I}{B_M b^2}\cdot\frac{R}{Q}\,\frac{R}{\rho}\left(1 + \frac{2\rho}{R}\right). \tag{17}$$

Here $E_p = m_p c^2$ is the rest energy of the protons and B_M is the field strength in the bending magnets. The somewhat strange form of (17) is chosen because it will turn out to be rather convenient to write the design constraints in a form which links the beam dynamics parameters directly to engineering parameters which by experience only take values within rather narrow limits.

It will turn out throughout that the aperture of the vacuum chamber and hence of the magnets is not determined by the space required for the beam proper or for closed orbit errors, but is necessary to remove the walls far enough from the beam so that their effects become small. This, naturally, leads to a circular or nearly circular vacuum chamber. Its cross section should have as few variations as possible in order to avoid the inductive impedances and the cavity resonances associated with them.

In the case of a beam centered in an exactly circular chamber the first term in the bracket vanishes. Hence (17) is pessimistic. This has been confirmed by a recent calculation[15] of the image field coefficient E_1 for a beam with an arbitrary position in an elliptic chamber.

In the design of a storage ring one wants the single beam tune shift to be below a given limit. Hence (17) is a design constraint which the machine parameters must satisfy. In particular, it may be considered as an equation for the current I_q which can be stored in a machine.

3.2.2 Transverse resistive wall instability

The resistive wall instability[16] is the best known example of a transverse coherent instability. The stability criterion can be expressed in the following form[17]:

$$|Z_\perp| \le \frac{E_p}{e}\,\frac{\pi Q}{IR}\left|(n-Q)\eta + Q'\right|\frac{\Delta p}{m_p c} \tag{18}$$

Here the amplitude function has already been replaced by its average value R/Q, $\eta = \gamma_t^{-2} - \gamma^{-2}$, γ_t is the γ-value at transition, $Q' = dQ/dp/p$ is the absolute chromaticity and Δp is the momentum spread in the beam. The above equation must be satisfied for the total transverse impedance $Z_\perp$ in the machine, for all combinations of I and $\Delta p/m_p c$ which occur during its filling, and for every $n > Q$. If stacking in momentum space is used, as in the ISR, then I and $\Delta p/m_p c$ grow roughly in proportion and in (18) may be interpreted as the total current and the total momentum spread in the beam.

In the special case of the resistive wall impedance the following expression applies, neglecting the smaller capacitive impedance:

$$|Z_\perp| = 2^{\frac{1}{2}}\, R\, Z_0\, \delta/b^3 \tag{19}$$

Here Z_0 is the impedance of free space and δ is the skin depth measured at the frequency $\omega = (n-Q)\,c/R$ and hence:

$$|Z_\perp| = \frac{2}{b^3}\left(\frac{R^3 Z_0}{(n-Q)\sigma}\right)^{\frac{1}{2}} \tag{20}$$

σ is the conductivity of the vacuum chamber material. At low mode numbers n, just above Q, the Q' term in (18) dominates and the tune spread required to Landau damp the instability becomes:

$$\delta Q = Q'\,\frac{\Delta p}{p} \ge \frac{2}{\pi c}\left(\frac{Z_0 E_p}{ec}\right)^{\frac{1}{2}}\frac{R}{Q}\left(\frac{R}{\rho B_M}\right)^{3/2}\frac{I}{b^3}\left(\frac{\gamma}{(n-Q)\sigma}\right)^{\frac{1}{2}} \tag{21}$$

In a real machine, the tune spread which can be accommodated is below a given limit. Hence (21) is another design equation for it, giving the current I_t which is transversely stable.

In an actual machine there are many more transverse impedances apart from the resistivity of the vacuum chamber walls. In principle, all have to be included in the stability considerations and designed accordingly. However, there is this difference between isolated objects and the vacuum chamber that the former can be modified as required whereas the latter cannot easily be changed.

In the ISR, a transverse feedback system has been used successfully[18] to counteract the effect of the wall impedance for the two lowest modes. A similar system could also be used in future machines.

3.2.3 Longitudinal resistive wall instability

The traditional stability criterion for the resistive wall instability[19] can be written in the following form[20,21]:

$$\left|\frac{Z}{n}\right| \le \left(\frac{E_p}{e}\right)\frac{\eta}{I\gamma}\left(\frac{\Delta p}{m_p c}\right)^2 \tag{22}$$

Here Z is the tolerable coupling impedance, and n is the mode number. Ap is the full width of the momentum spread at half height of the distribution function. Again, ***(22)*** must be fulfilled for all combinations of I and Ap which occur during the filling process. When stacking in momentum space is used the most severe conditions apply to the beginning of the filling.

For a beam in a circular vacuum chamber of radius b, the coupling impedance, neglecting the small capacitive contribution and putting in the worst n = 1, is given by:

$$\left|\frac{Z}{n}\right| = \frac{1}{b}\left(\frac{RZ_0}{\sigma}\right)^{\frac{1}{2}} \qquad (23)$$

Assuming that the current/pulse is I_p, the momentum spread necessary for longitudinal stability of a single pulse becomes, combining ***(22)*** and ***(23):***

$$\left(\frac{\Delta p}{m_p c}\right)^2_s = \left(\frac{Z_0 R}{\sigma}\right)^{\frac{1}{2}} \frac{e}{E_p} \frac{I_p Q^2 \gamma}{b} \qquad (24)$$

In the derivation it has been assumed that $\gamma >> \gamma_t$ and hence $\eta \simeq Q^{-2}$ has been used.

If one assumes that the aperture taken by the momentum spread of the stacked beam should not exceed the vacuum chamber radius b (this leaves another radius b for manipulations, betatron oscillations, closed orbit distortions etc.), then one can calculate an upper limit I_ℓ for the stored current which is longitudinally stable:

$$I_\ell = \frac{bQ^2 I_p \gamma}{R(\Delta p/m_p c)_s} \qquad (25)$$

This is the third design constraint for a proton machine. In an actual machine there are many more longitudinal impedances apart from the resistivity of the vacuum chamber, the most conspicuous of these being the shunt impedance of the RF system. The RF system of the ISR contains a feedback loop[22] which reduces its shunt impedance at the cavity resonances by a large factor. The elements in question must be designed so that their total impedance is small compared with the vacuum chamber walls or their impedances have to be included.

3.2.4 Synopsis of single beam limits

Many single beam phenomena have been considered which limit the total current which can be stored in a proton storage ring. There are even more phenomena which have not been mentioned at all. Hopefully, they are less restrictive than those mentioned. However, the important thing to be demonstrated was that one should adopt an open-ended approach to the design of these large machines which has been shown here by way of a few examples.

3.3 Technical limits on proton storage rings

The question arises whether there are technical phenomena in proton machines which take the place of the synchrotron radiation in electron machines. It turns out that the stored energy in the beam may be such a phenomenon. It will be considered below.

Furthermore, all the collective effects mentioned have in common that, when the other parameters are fixed, then the aperture radius b must be bigger than some limit. Hence, for a given wavelength there is always an aperture radius b for which the machine works,

The question arises quite naturally whether there are upper limits to the aperture. It turns out that the maximum poletip field of the quadrupoles is one of them.

3.3.1 Stored energy in the beam

If one considers proton machines at several hundred GeV energy and with several amperes of circulating current one finds that the stored energy of the beams may take values which are much bigger than those in the ISR[23] or the large proton synchrotrons at NAL or at CERN. It therefore appears most suitable to include it as a design constraint. It is given by the following expression:

$$W = 2\pi\left(\frac{m_p c}{e}\right)^2 \frac{R}{\rho} \frac{I\gamma^2}{B_M} \qquad (26)$$

There are two reasons why the stored energy in the beam may be dangerous. In emergency cases, the beam must be deflected in a beam dump system by fast ejection and the whole energy in the beam is deposited in a long thin cylinder of material creating problems of local heating and stress. Water has been suggested as a possible material for the absorber[24].

In superconducting machines, in particular, the beam power deposited near to the vacuum chamber is equal to the stored beam energy divided by the beam lifetime. If this power has to be removed at cryogenic temperatures it may constitute a significant heat load. Attempts to localize the beam loss have not yet been successful in the ISR.

The stored energy equation ***(26)*** may be considered as an equation for the maximum current I_W which can be stored in a machine.

3.3.2 Limits on the quadrupole strength

Calculating the properties of a separated function FODO lattice in thin lens approximation[5], one finds that for 90° phase advance per period the focal length of the quadrupoles is given by

$$f = \ell_p/2\sqrt{2} \qquad (27)$$

Here R_p is the length of a period which is related to R/Q by

$$\ell_p = \frac{\pi}{2}\frac{R}{Q} \qquad (28)$$

The relation between focal length and gradient is

$$f = \frac{B\rho}{\ell_Q}\left(\frac{dB}{dx}\right)^{-1} = \frac{B\rho}{\ell_Q}\frac{b}{B_Q} \qquad (29)$$

where $B\rho$ is the magnetic rigidity of the protons, and ℓ_Q is the length of the quadrupoles, and B_Q is their field at a distance b from their centre. Since the value of R/ρ has already been used in several places, the quadrupole length ℓ_Q cannot exceed the space left free by bending magnets. One can introduce an adjustable

parameter C_Q which just describes the fraction of the straight sections in a period occupied by the quadrupoles.

The above formulae can be combined and manipulated to finally take the form:

$$b = \left(\frac{ec}{E_p}\right)\frac{\pi^2}{2^{\frac{1}{2}}16}\left(\frac{R}{Q}\right)^2 \frac{B_Q C_Q}{\gamma}\left(1 - \frac{\rho}{R}\right) \qquad (30)$$

In a real machine, an upper limit for B_Q is determined by the type of magnets used for the construction of the magnet lattice. Therefore (30) is an upper limit for the aperture radius b, and as such it complements the design equations given by the collective phenomena.

It may be considered a fortunate accident that the upper limit for b (30) increases more steeply with R/Q than the lower limits for b determined by the collective phenomena (17) and (21). Hence there is always a solution to the combined equations.

3.4 Proton storage ring design

3.4.1 Outline of the procedure

The design equations (17), (21), (25), (26) and (30) involve only 16 parameters which can be grouped as follows:

i) Machine energy γ

ii) Injected beam parameters, given by injector: I_p, E_t, $(\Delta p/mPc)_i$

iii) Magnet lattice parameters R/ρ, B_M, B_Q, C_Q, b, W_{max}

iv) Space charge parameters σ, n-Q, δQ_{max}, ΔQ_{1max}

v) Intersection parameters ℓ, ΔQ_{2max}

The most transparent way of proceeding consists in choosing first these parameters, then to calculate the maximum currents I_q, I_t, I_ℓ, I_n permitted by (17), (21), (25), (26) and the corresponding luminosities. This yields a clear picture of which luminosity can be obtained with a given set of machine parameters. It is then quite easy to choose a good set of parameters for which many more derived quantities can be obtained.

3.4.2 Choice of parameters

The choice of the parameters must be guided by extrapolation and scaling from existing proton synchrotrons and storage rings. As examples, machines will be used which are under study at CERN, using the CERN SPS as an injector, and therefore operating with known and fixed injected beam parameters. The choice of the magnet lattice parameters R/ρ, %, B_Q, C_Q can be guided by a comparison with the large proton synchrotrons at NAL and CERN, for a conventional copper-steel magnet system. For the supraconducting magnet system, parameters in the vicinity of the ISABELLE proposal[25] are used.

The aperture radius b and the stored energy in the beam W_{max} are used as parameters for the time being. They will be fixed later.

The choice of the vacuum chamber material fixes σ, the conductivity. It is advantageous to work in the half-integral range of Q just above an integer. Hence n-Q = $^3/_4$. Experience with the ISR suggests that non-linear resonances must be avoided in order to obtain a good lifetime of the stored beam, and a low background from beam-wall events in the experiments. The working space in the tunes is restricted to the range between the 5th order resonances at Q = n + $^3/_5$ and the 3rd order resonances at Q = n + $^2/_3$. This leaves a free space of $\Delta Q = {}^1/_{15}$ which includes the 8th order resonances at Q = n + $^5/_8$.

This free space must be large enough to include the tune spread required for transverse stability, the tune spread in the single beam and the sum of all the tune spreads due to the beam-beam interactions. Replacing the tune spreads by the corresponding tune shifts yields roughly

$$\Delta Q \geq \delta Q_{max} + \Delta Q_{1_{max}} + N_2\, \Delta Q_{2_{max}} \qquad (31)$$

Here N_2 is the number of crossing points. On the basis of this argument, the values $\delta Q_{max} = \Delta Q_{1max} = 0.02$ were used in the examples.

The maximum permissible value ΔQ_{2max} for the beam-beam tune shift has been the subject of much speculation[26,27,28]. Experimental information from the ISR suggests that no bad effects are observable with $\Delta Q_2 \simeq 7 \times 10^{-4}$ if the tunes are chosen as described above. In addition, a special experiment at 2 GeV/c[29] has shown that there is no detectable lifetime reduction for a beam lifetime of about 30 minutes at $\Delta Q_2 \simeq 5 \times 10^{-3}$. In this experiment the short lifetime was entirely due to single beam effects, most likely intra-beam scattering[30,31]. An experiment using a non-linear lens to simulate the second beam has not yet given conclusive results.

Choosing $\Delta Q_{2max} = 0.005$ has become standard practice[6,25,32].

Choosing the same size of the working region as in the ISR and the standard value for the beam-beam tune shift is not necessarily a satisfactory method of extrapolation. An argument against this choice is that a beam-beam effect which is an order of magnitude stronger will excite non-linear resonances more strongly and hence the invisible 8th order resonances may become harmful. There are two arguments in favour of this scaling: Firstly, future machines will have a higher luminosity than the ISR at roughly the same number of protons, and are, therefore, relatively less sensitive to beam-wall background. Secondly, the "feeding" of particles into the resonances by intra-beam scattering is slower at higher energies. The balance between the arguments against and in favour of the choices made can only be arrived at by more detailed calculations.

The last parameter to be fixed was the free length around the crossing points. It was chosen as ℓ = 30 m.

3.4.3 Results

Using these parameters, the stored current and the luminosity were calculated, employing the accurate formulae[12] for the beam-beam tune shift and the luminosity. The results are displayed in Figs. 1 to 4. The energy (γ) is used as abscissa. Each graph contains 4 sets of curves. One set has W as a variable parameter, the other 3 sets the aperture radius b; they apply to the single beam tune shift, and the transverse and longitudinal stability limits. For smaller values of γ, the longitudinal phase space density limit may be independent of b.

This means that the momentum spread of the injected beam is stable and hence no aperture dependent blow-up is required.

It may be seen that usually the single beam tune shift and the stored energy in the beam present the most serious limitations. A superconducting machine needs a smaller stored energy in the beam and a smaller aperture radius b for the same luminosity than a conventional copper-steel magnet machine.

Proton machines in the energy range up to 1000 GeV which correspond to accelerators in the energy range up to *2130* TeV appear to be technically feasible. However, they are very large and correspondingly expensive.

In order to simplify the presentation, the operation at only one energy has been considered. This excludes machines such as ISABELLE[25] in which the stored beam has to be accelerated to the design energy, and the operation of a given machine over an extended energy range. Both these problems can be tackled within the formalism presented by scaling the parameters y, B_M and B_Q accordingly. It turns out that the stored current is proportional to γ when the tune of the machine is kept constant. According to *(14)* this would result in a luminosity variation like $\gamma^{5/2}$. The operating range of the machine can be extended towards lower energies by using a larger aperture than is required at maximum energy.

3.4.4 Specific machines

On the basis of the results displayed in Figs. 1 to *4* a parameter list for a *400* GeV/c conventional machine has been worked out which is being used to design this machine in more detail. It is shown in Table 11. All the derived parameters can be obtained from the formulae given earlier in this paper. For comparison, I have included the parameters of a superconducting machine with the same energy and luminosity. In these machines, round numbers were chosen for the aperture such that the actual values of AQ, and δQ were below the limits imposed.

The important conclusion from Table II is that it is possible to design stable machines with a good luminosity. They compare favourably with the ISR because the collective effects are of the same order of magnitude and the luminosity is much higher.

Comparing the conventional and superconducting machines in Table II shows that in the latter one reaches the same luminosity with a smaller radius, aperture and stored energy.

Much work still has to be done before the feasibility of these machines can be established, in particular in the following areas: design of intersection regions, RF acceleration, beam transfer from the SPS and injection, beam dumping, and site layout.

TABLE II

Comparison of *400* GeV proton storage ring parameters using conventional and superconducting magnet

		conv,	s.c.	
Maximum momentum	p	*400*	*400*	GeV/c
Maximum field in bending magnets	B_M	1.8	*4.0*	T
Maximum poletip field in quadrupoles	B_Q	*0.6*	2.0	T
Circumference factor	R/ρ	*1.3*	*1.6*	
Bending radius	ρ	*741*	*333*	m
Average radius	R	*964*	*533*	m
Quadrupole filling factor	C_Q	*0.5*	*0.2*	
Aperture radius	b	*30*	*20*	mm
Average wavelength	R/Q	*36.4*	*17.9*	m
Betatron wavenumber	Q	*26.5*	29.8	
Phase advance/period	μ	π/2	*n12*	
Period length	a_P	*57.2*	28.1	m
Quadrupole length	a_Q	*3.3*	*1.1*	m
Injected current/pulse	I_P	*0.07*	*0.07*	A
Injected phase space density	D	1.3×10^{20}	1.3×10^{20}	m^{-3}
Injected normalised beam emittance	E_t	$30\pi\cdot10^{-6}$	$30\pi\cdot10^{-6}$	m
Stored current	I	*5*	*5*	A
Number of injector pulses		*72*	*72*	
Stored energy in the beam	W_B	*40*	22	MJ
Single beam tune shift	ΔQ_1	0.015	0.008	
Vacuum chamber conductivity	σ	10^6	10^6	A/Vm
Resistive wall mode number	n-Q	*0.75*	*0.75*	
Required tune spread in beam	δQ	*0.007*	*0.005*	
Total stored momentum spread	Δp/p	3.6×10^{-3}	4.2×10^{-3}	
Free length in crossing regions	ℓ	*30*	*30*	m
Amplitude function at crossing point	β_0	*2.0*	*2.0*	m
Rms beam radius at crossing point	σ_0	*0.2*	*0.2*	mm
Beam-beam tune shift/crossing	ΔQ_2	0.005	*0.005*	
Crossing angle	α	1	1	mrad
Luminosity/crossing	L		10^{33}	$cm^{-2}s^{-1}$

4. Conclusions

A comparison between the extrapolations for electron and proton machines in Tables I and II shows that an electron machine at 50 GeV is significantly bigger than a proton machine at 400 GeV. This is even more true when one considers the superconducting version of the latter. Hence, there is a distinct difference in the maximum energy which one can hope to achieve in electron and proton machines. Whether this difference is significant or not must be decided on the basis of experiments which can be performed with these machines.

References

1) M. Sands in "Physics with Intersecting Storage Rings", editor B. Touschek, Academic Press, New York (1971)

2) J. Rees et al., 8th Int. Conf. High Energy Acc., CERN, 143 (1971)

3) F. Amman, 8th Int. Conf. High Energy Acc., CERN, 63 (1971)

4) H. Wiedemann et al., 1973 Particle Acc. Conf., San Francisco, 838 (1973)

5) J. Rees and B. Richter, SPEAR-167 (1973)

6) L. Smith, this conference

7) K. Johnsen, this conference

8) Proton-Proton Colliding-Beam Storage Rings for the Natl. Acc. Lab., Design Study 1968

9) J.P. Blewett and H. Hahn, editors, BNL 16716 (1972)

10) A.N. Skrinsky et al., 8th Int. Conf. High Energy Acc., CERN, 72 (1971)

11) E. Keil, C. Pellegrini and A.M. Sessler, to be published in Nucl. Instr. and Meth.

12) E. Keil, Nucl. Instr. and Meth. 113, 333 (1973)

13) B.W. Montague, private communication

14) L.J. Laslett, BNL 7534, 324 (1963)

15) B. Zotter, Report CERN/ISR-TH/74-11 (1974)

16) L.J. Laslett, V.K. Neil, A.M. Sessler, Rev. Sci. Instr. 36, 436 (1965)

17) H.G. Hereward, private communication

18) L. Thorndahl and A. Vaughan, 1973 Particle Acc. Conf., San Francisco, 807 (1973)

19) V.K. Neil and A.M. Sessler, Rev. Sci. Instr. 36, 429 (1965)

20) V.K. Neil, D.L. Judd and L.J. Laslett, Rev. Sci. Instr. 32, 267 (1961)

21) E. Keil and W. Schnell, Report CERN/ISR-TH-RF/69-48 (1969)

22) F.A. Ferger and W. Schnell, USSR 2nd Natl. Conf. Particle Acc., Moscow, Vol. 2, 128 (1972)

23) A. Delizée et al., 7th Int, Conf. High Energy Acc., Yerewan, Vol. 2, 183 (1969)

24) B.W. Montague, private communication

25) H. Hahn, this conference

26) B.V. Chirikov, Inst. of Nucl. Phys., Novosibirsk, Preprint 267, Section 4.3 (1969)

27) E. Keil, 8th Int. Conf. High Energy Acc., CERN, 372 (1971)

28) L.J. Laslett, this conference

29) K. Hübner, this conference

30) C. Pellegrini, Frascati Report LNF-68/1 (1968)

31) A. Piwinski, this conference

32) G.H. Rees, this conference

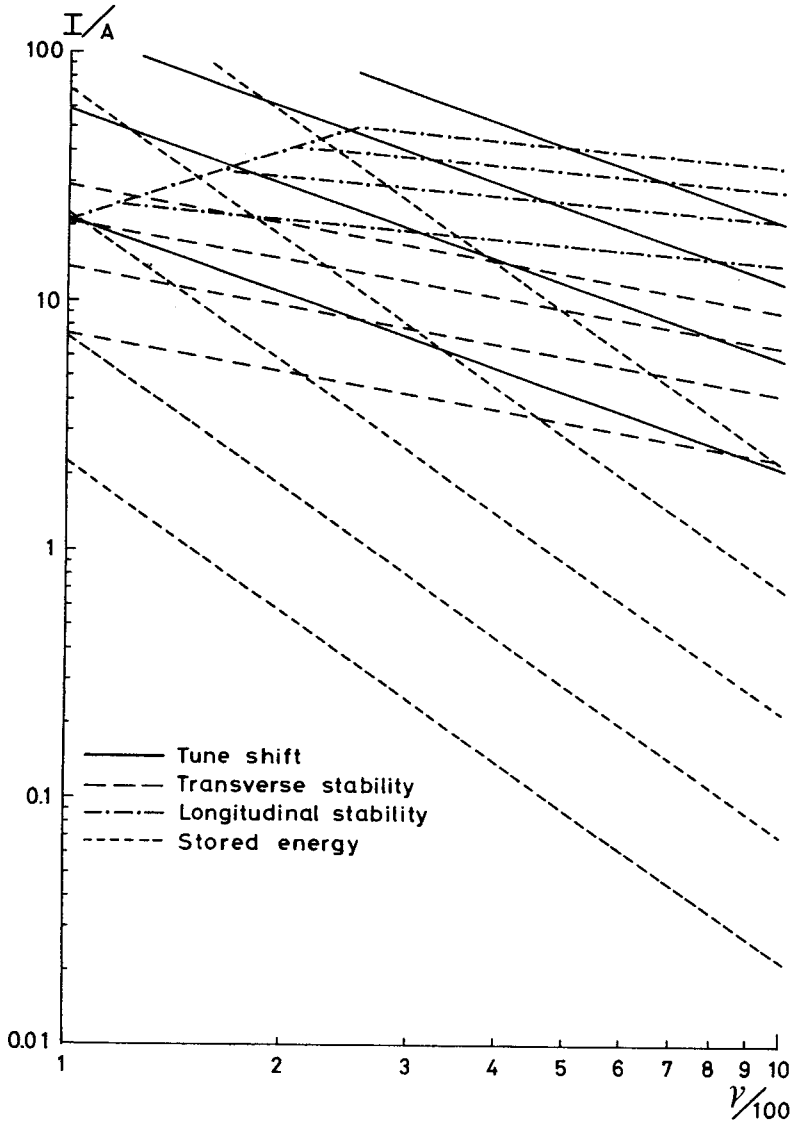

Fig 1 - Circulating current I vs energy γ

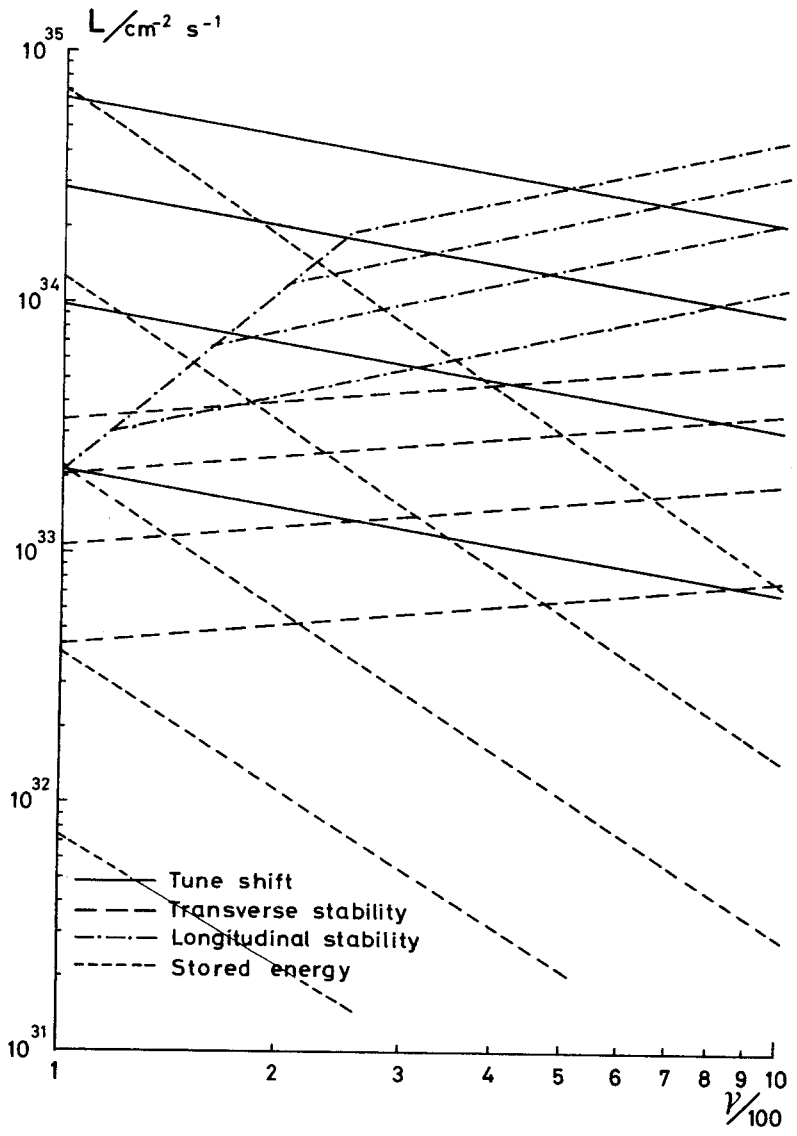

Fig 2 - Luminosity/crossing L vs. energy γ

The parameters used in the figures are: $R/\rho = 1.3$, $B_M = 1.8$ T, $B_Q = 0.6$ T, $C_Q = 0.5$, $n\text{-}Q = 0.75$, $\ell = 30$ m, $\Delta Q_1 = 0.02$, $\Delta Q_2 = 0.005$, $\delta Q = 0.02$, $\Delta(\beta\gamma)_i = 0.013$, $E_t = 29.6\pi \times 10^{-6}$ m, $\sigma = 10^6$ A/Vm, $I_p = 70$ mA. The curves for tune shifts, transverse and longitudinal stability are drawn for an aperture radius b = 20, 30, 40, 50 mm. The curves for the stored energy in the beam are drawn for W = 1, $10^{\frac{1}{2}}$, 10, $10^{\frac{3}{2}}$, 100 MJ.

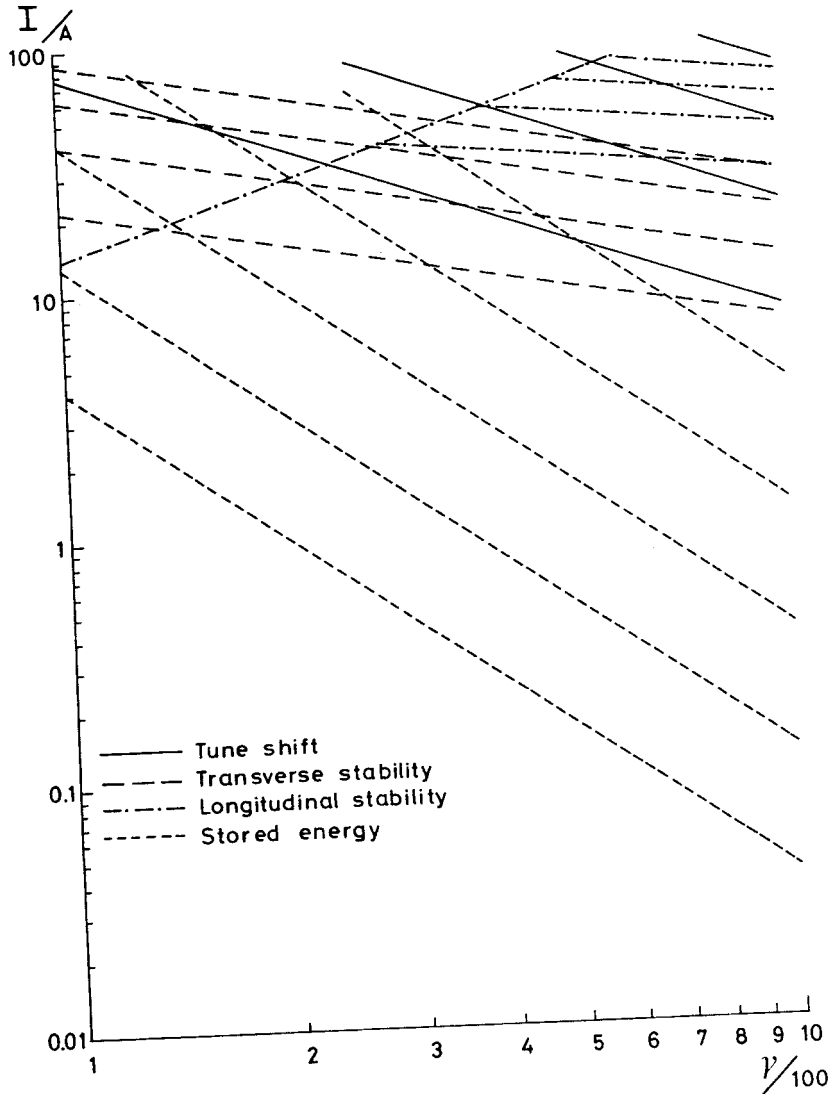

Fig. 3 - Circulating current I vs energy γ

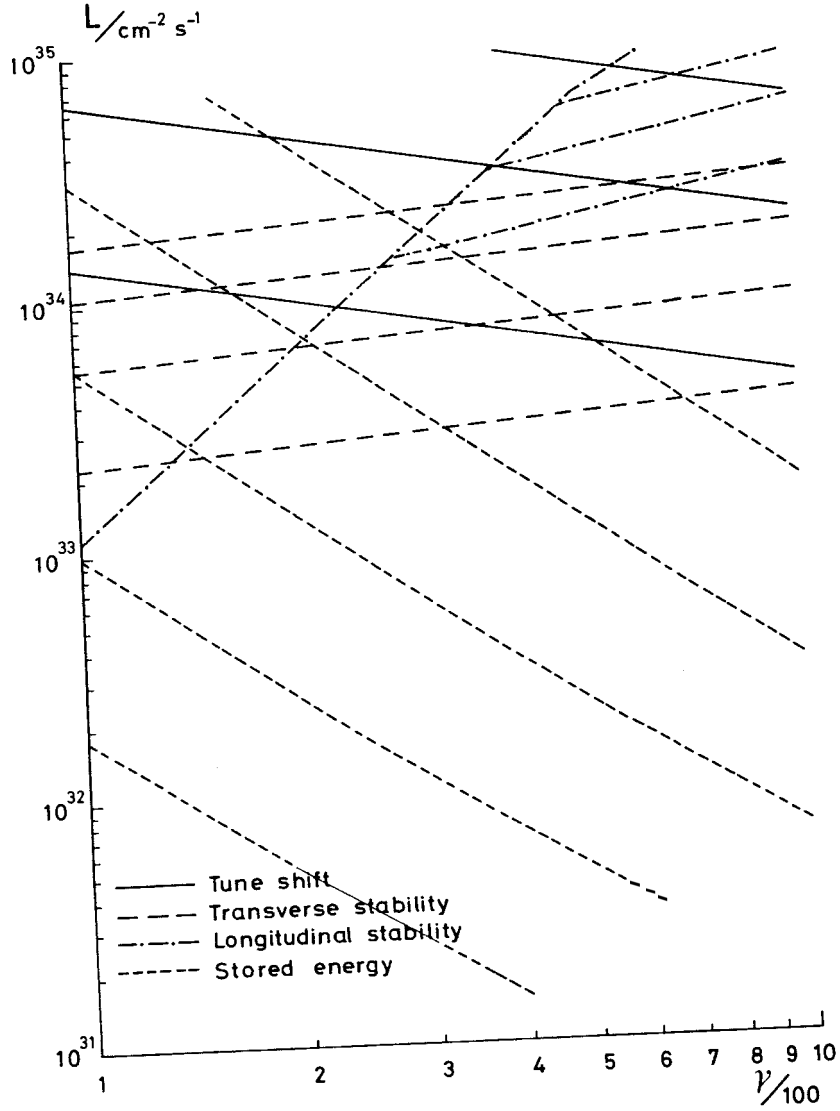

Fig. 4 - Luminosity/crossing L vs energy γ

The parameters used in the figures are: $R/\rho = 6$ $B_M = 4$ T, $B_Q = 2$ T, $C_Q = 0.2$, $n\text{-}Q = 0.75$, $\ell = 30$ m, $\Delta Q_1 = 0.02$, $\Delta Q_2 = 0.005$, $\delta Q = 0.02$, $\Delta(\beta\gamma)_i = 0.013$, $E_t = 29.6\pi \times 10^{-6}$ m, $\sigma = 10^6$, $I_p = 70$ mA. The curves for tune shifts, transverse and longitudinal stability are drawn for an aperture radius b = 20, 30, 40, 50 mm.. e curves for the stored energy in the beam are drawn for $W = 1, 10^{\frac{1}{2}}, 10, 10^{\frac{3}{2}}, 100$ MJ.

Rae Stiening (NAL): How does one avoid 5th-order resonances—in other words, can you make magnets of good quality at that high energy?

Keil: That is a good question. I'll answer the second part first. I don't think that the magnet tolerances influence the order of resonances which one can stand in a machine more than the beam-beam effects in the machine; that is to say that if you make a lousy magnet, then you may get single-beam difficulties. However, if you want to run the machine as a colliding beam device,. then the two-beam situation is bound to be worse even under these conditions.

Matt Allen (SLAC): Just an engineering detail—the 50-GeV machine would need about 1km of RF cavities. The wall losses would be about 20 MW for copper cavities. This might be a possible application for superconducting cavities which would require a lot of niobium.

SYNCHROTRON RADIATION SOURCES

S.P.Kapitza (presented by V. V. Elyan)
Institute for Physical Problems
Moscow, USSR

Summary. Synchrotrons and storage rings as synchrotron radiation sources in the vacuum ultraviolet and soft X-ray region are discussed. Comparative consideration of several special projects of dedicated SR storage rings is given.

Synchrotron radiation (SR) is well known to the accelerator community mainly as an unwelcome refuse of synchrotrons and electron storage rings. Following the modern trend in utilizing all products that appear in an industrial process much use has been recently found for this by-product of accelerator technology.

SR spans a very broad band of the electromagnetic spectrum practically starting in the infrared and usually terminating somewhere in the X-ray region. Certainly from the point of view of energy 10 keV quanta, even 100 keV ones cannot compete with the GeV's and TeV's that tend to dominate the minds of those present, But it is the technology and expertize developed for high energy physics that compels us to consider SR sources. Thus a new challenge to the accelerator designer is open and a new dimension for the use of high energy particle accelerators is added in providing a most powerful tool of research in a diverse number of fields.

May be it is this diversity of applications that presents one of the major difficulties, for we could certainly leave the development of this field to the future user who could make the decision, what sort of machine is considered to be the best. But when a number of fields from solid state physics to biology, from diagnostic medicine to astrophysics are involved, who then should take the lead? In this case I think it is for the machine builder to get an understanding of the users' needs and by combining them with the current possibilities of accelerator technology make the proper step in building a new machine. Before considering this next step I will start with reminding you of the main properties of SR.

SR is primarily produced when a fast electron with an energy $E \gg E_0 = mc^2$ is deflected in a strong magnetic field H. Radiation is emitted tangentially to the orbit and is spacially confined to a small angle $\vartheta \approx 1/\gamma = E_0/E$ typically less than 1 mrad for energies above 1 GeV. The spectrum is continuous, passing through the millimeter, submillimeter, IR, optical, UV into the X-ray region. The number of quanta gradually decreases with photon energy ξ as $\xi^{1/3}$ up to a Cut off frequency, where the spectrum is rapidly terminated, The cut of wave length λ_{max} is determined by the electron energy E (GeV) and the radius R(m)

$$\lambda_{max} = \frac{1{,}7R}{\gamma^3} \qquad (1)$$

We will consider λ_{max} the wave length at the maximum of the power spectrum as the main parameter of the SR spectrum, rather than the critical wave length $\lambda_c = 2{,}42\,\lambda_{max}$ introduced in most theoretical papers on SR.

SR is highly polarized, its plane of polarisation being that of the orbit. In a full revolution of a charge $\frac{2\pi}{137}\cdot\gamma$ quanta are emitted with a total radiation loss of ΔE

$$\Delta E\,(kev) = 88{,}5\,\frac{E^4\,(Gev)}{R\,(m)} \qquad (2)$$

Thus the SR power is $P_s = I\,\Delta E$, where I is the electron beam current. For all practical purposes the electron spin and quantum phenomena do not affect the SR spectrum, although the beam cross section is determined by quantum fluctuations. The classical electrodynamic theory is in full agreement with all observations and the appropriate treatment can be found in most modern textbooks (see also [1]).

SR from a high energy electron beam presents a source of highly collimated, polarized radiation with a well defined continuous spectrum. Its spectral intensity in the UV and X-ray region is far greater than that of any other sources. Moreover, even in the infrared the intensity is higher than that of heated bodies usually used as sources in IR spectroscopy. These well defined properties of SR have led to consider an electron beam radiating in a magnetic field as a primary radiation standard, being at 1 GeV more or less similar to a black body at a temperature $\sim 10^7$°. SR standards are finding use in calibrating UV and X-ray instruments for space astronomy.

Most of the work with SR has been done on existing synchrotrons and storage rings. This extensive experience is well summed up in a number of conference reports [2] and references can be found in an extensive bibliography [3]. The first experiments were mainly done parasitically on large synchrotrons, the most prominent being the DESY 7 GeV synchrotron at Hamburg. Later a substantial project had also been started at Daresbury on the NINA 4 GeV synchrotron where a national SR facility is now operating.

Although much work is still being done on most electron synchrotrons, SR facilities are now provided also on the large modern electron storage rings. The Stanford SR Project (SSRP) at SPEAR described in detail elsewhere in these Proceedings [4] provides a national US facility mainly for the VW and X-ray region with a high flux down to 1 Å. Up to seven experiments can share a beam run, which accepts 11,5 mrad SR emitted horizontally. A broad ranging program of research will be pursued including studies of UV and X-ray photoelectron spectroscopy, extended X-ray absorption edge fine structures, X-ray diffraction on biological system, Compton scattering X-ray absorption, X-ray induced luminiscence, sub-nanosecond time constant measurements on solids, chemical kinetic studies and UV reflectivity, thus covering most of the problems requiring the short wavelength part of the SR spectrum.

A most powerful facility is to be provided at the DESY-DORIS storage ring, where

two large SR bunkers are built in addition to those that were primarily used on the DESY synchrotron. One of these new bunkers is operated by the European Molecular Biology Organization (EMBO) and will be devoted to studies of complex biological structures - enzimes, muscles, etc.

Parasitic SR facilities are also envisaged on the new 1,7 GeV DCI storage ring at *Orsay* (France) operated by the Laboratoire pour l'Utilisation du Rayonnement Electromagnetique (LURE) group, working at present on the 550 MeV ACO ring. From 1975 ACO will be used only for SR work.

In the Soviet Union at Novosibirsk SR work is actively being done both on the 670 MeV VEPP-2M storage ring and the large VEPP-3 complex. A summary of data on these machines that all provide parasitic SR facilities is given in the first half of Table I.

The work on these machines will certainly lead to rapid and immediate progress in the whole field of SR research. This will provide for a new opportunity to reaccess the merits of various SR sources and will contribute to the demands that a SR source should comply with, although even now we can consider these demands and envisage the parameters of a dedicated SR source.

The future SR source will certainly be a storage ring. Work on storage rings has shown them to be ideal sources of radiation. They are fret: from vibrations that so complicates experiments on large synchrotrons, provide great spacial and temporal stability of the beam, little if *any* radiation danger, which is a constant hazard on lar e synchrotrons. On large synchrotrons the R beam is practically available some 20 to 30 meters from the beam, when with storage rings work in the immediate vicinity of the machine is possible.

At present the only storage ring fully committed to SR work is the Wisconsin Tantalus I facility[7]. Its remarkable success in the SR field down to ~100 Å has led to a project of converting the old 180 MeV NBC synchrotron into a 240 MeV storage ring, described in more detail in these Proceedings[8]. The conversion will include a 10 MeV injector microtron, a new vacuum chamber, coils and supplies necessary for the operation of the synchrotron as a storage ring. A 300 MeV SR storage ring is being currently built in Japan. These SR sources will provide for work in the low energy part of the spectrum, down to ~100 Å, whereas the large colliding beam machines will be supplying the shorter wave lengths down to ~1 Å.

The next step is the design of dedicated SR storage rings, producing SR down to the shortest limit of practical importance should now be considered. A critical accessment of λ_{max} in this case leads one to the conclusion that 1,5 ± 1 Å is the limiting value, this figure being of crucial importance for the design of a SR storage ring.

The next parameter of importance in the design is the magnetic field. Modern trends in the designing of high energy synchrotrons and storage *rings* favor low fields. In the case of SR sources just the opposite is right- the field should be as high as possible.

The storage ring is best conceived as a separated function machine[7]. Moreover, the separation of functions takes a step futher by introducing special magnets designed solely for the production of SR. These multiple gap magnets - wigglers were first introduced to increase SR damping in the CEA colliding beam experiment. Now these magnets operated at as high a field as reasonable will be used as a local means of generating SR. Thus the magnetic system is to be made up of bending dipole magnets, focussing quadrupoles and SR magnets, plus auxiliary magnets for tuning the system and compensating higher order gradients. The focussing lattice of the magnetic system is of rather straightforward design that allows one to adjust the β-function and ν_z and ν_x within certain margins. The main bending magnets are to be of the C-type where access to the vacuum chamber and SR light tubes is simpler. This concept is used in all three major projects of SR sources which we will now consider in more detail (see Table I).

The most ambitious project is the 2 GeV electron storage ring, proposed by the Daresbury laboratory group to take place of the NINA synchrotron 8,9. This large storage ring is designed to run with a 1A current and will certainly be the most powerful dedicated SR source with 240 kw in SR power. Using a 5 T superconducting wiggler insert the λ_{max} can be shifted down from 2,5 Å to 0,8 Å with a corresponding increase in flux. The design of superconducting wigglers using the available superconducting cables is quite straightforward for fields up to 5 T and may be 6 T. Future developments will make the construction of wigglers with fields up to 10 T possible.

At least 10 beam lines are envisaged with the machine that will use most of the support facilities of the NINA synchrotron. The SR storage ring is suitably placed in the hall that at present houses the main NINA magnet. The injector to the storage ring is to be a booster 500 MeV synchrotron with electrons primarily accelerated by a 8 MeV microtron or linear accelerator.

Next one should mention the Tantalus II, the first large dedicated SR facility, a project that was proposed by the Wisconsin University Group[10]. At first this project tnat draws much from the experience gained with the 240 MeV Tantalus I ring was designed for 960 MeV, but later the energy was increased to 1760 MeV with a corresponding increase in size[11]. The bending field is rather low 1,2T and nigh field wiggler sections are also envisaged. The circulating current is to be 100 mA and the injector to the storage ring will be a 35 MeV microtron.

The project proposed in the design study by *our* group at the Institute for Physical Problems follows a similar pattern.[12] It is to be a separated function machine operating at 1,35 GeV with a rather high bending field of 1,8 T. As a next step in the development program superconducting high field section8 are also suggested. We plan for a 100 mA circulating current and propose to use a 30 MeV microtron injector. The general design has some similarity to the VEPP-2M storage ring and will draw on the experience with that machine.

In comparing the intensity of SR sources it is important to note that the effective SR luminosity is directly proportional to the current, rather than the number of particles

circulating, and inversely proportional to the beam hight. The beam cross section is ultimately dependent on the beam current, tuning of the ring and coupling of vertical and horizontal motion, so it is rather difficult to calculate the effective SR luminosity of a storage ring and the flux finally enter ing the detector of the experimental set up. That is why only the total SR power is given in Table I without taking into account the beam size and the divergence of the electron beam in the SR storage ring as determined by its β -function, To get an idea of the intensities available, recent experiments on VEPP-3 have shown that with only a 20 mA stored beam and operating at 3 m from the electron beam at least a 100 fold decrease in exposure time was obtained in a comparative experiment on molecular biology X-ray structure work at 1,5 A that was to determine the relative merit of storage rings as compared to modern high intensity fine focus rotating anode X-ray tubes. The optical brightness of the electron beam SR source can be enhanced by adjusting the local β value so that the beam will converge at the point of origin of the SR. The image of the radiating beam can be transported by an optical ellipsoid mirror reflecting X-rays at grazing incidence and leading to a great increase in flux available for experiments.

The vacuum systems of all projects propose to use the now standard all metal techniques developed on storage rings that can lead to an expectant beam life time of some hours at high energies and beam currents, requiring a base pressure of 10^{-9} torr.

Berillium windows can be used to separate the storage ring vacuum system for X-rays shorter than 4 7 Å. For experiments with longer wave lengths up to 1050 Å where optical LiF windows become transparent a common vacuum system for the user and the machine becomes necessary. It may be worth noting that much surface physics and other work also demands ultra high vacuum conditions, compatible with that of a storage ring, and appropriately dealt with in all the design studies.

We thus see that all these projects have much in common, the differences mainly stemming from prototypes used and technical circumstances of secondary importance that govern the detailed decisions made.

These projects do not approach the limit of modern storage ring design, for both in current and energy they are surpassed by the most advanced existing electron storage rings, where the operation is futher complicated by all the problems brought in by a colliding beam experiment.

These specialized storage rings may be Considered as radiation devices where the active body is a highly confined relativistic electron beam. It is fascinating to inquire on other possibilities of inducing this highly excited state of matter to radiate. One of these possibilities is the undulator, consisting of an extended region of a periodic magnetic field. If the period of the field along the beam is ℓ , the wiggling motion of the electron leads to a dipole radiation whose wave length is primarily determined by a Doppler effect shortening

$$\lambda = \frac{\ell}{2\gamma^2} \sim \frac{\ell}{1-\beta\cos\vartheta} \qquad (3).$$

For a 2 GeV electron and $\ell = 1\,cm$, $\lambda = 3\,Å$. For a pure dipole radiation pattern the magnetic field has to be less than the field that produces the same SR, in this case less than 0,6 T. At higher fields the radiation pattern is complicated by local synchrotron radiation, that can also be considered as Doppler shifted multiple radiation. In the case of strong fields the momentary synchrotron radiation pattern manages to develop and the whole device can be considered really to be a wiggler. Unfortunately the radiation from the undulator is not monochromatic, being broadened by the angular Doppler effect factor.

It has also been suggested to use Compton scattering from laser beams. In this case the scattered beam wave length is primarily determined by a formula similar to *(3)*

$$\lambda \approx \frac{\lambda_\ell}{4\gamma^2} \qquad (4).$$

Thus for a CO_2 C.W. laser $\lambda_\ell = 10^{-3}\,cm$ and already with a beam of electron at E = 100 MeV one obtains λ = 0,6 Å. The angular dependence term again leads to a rather broad spectrum, influenced also by the angular convergence of the laser beam as determined by the diffraction pattern of the optical beam forming system in setting up a spacial standing wave pattern interacting with the stored electron beam.

Unfortunately the intensity from all these C.W. devices is not large. Without going into detailed calculations it is worth noting that all processes considered could really be thought of as different cases of Compton scattering. Compton effect is the basic interaction of an electromagnetic field with the free electron. SR radiation can also be considered as Compton scattering in a frame of reference where the electromagnetic wave has been transformed to a constant magnetic field. At present a constant magnetic field provides the greatest macroscopic density of electromagnetic energy and thus it is the best means for producing scattered radiation, in this case SR. May be in the future high power c.w. laser technology will provide a better opportunity but at present superconducting coils seem to be the best way of producing the high field interacting with the electron.

Certainly the most fascinating thing to do would be to make coherent synchrotron radiation, but no one has yet suggested a way of doing this with fast electrons, although devices that can be considered as SR lasers, or rather masers, operating in the millimeter and submillimeter band have been described.

SR storage rings at present should be considered as a multiple purpose broad band sources of radiation. For this new generation of machines one can suggest the building of a rather simple storage ring that will lead to immediate progress in a diverse number of fields. Moreover, in analysing the possibilities of these facilities it seems that the new techniques and instrumentation which will have to be developed will demand more effort and even greater expenses than the design and operation of a SR storage ring. Mirror for collecting and focussing the SR from the Orbits have to be designed. New monochromators will have to be developed, new opportunities in X-ray diffraction work explored. The pola-

risation of SR may lead to new possibilities in ESCA work, as better monochromatisation will lead to greater details in the electron spectrum studied. The benefit of the fine adjustment of the wave length near the K-edge of a scattering atom may lead to methods of determining the phase of the diffracted wave in X-ray crystal studies, eliminating the phase ambiguity in reconstructing the structure. I will not dwell on the possibilities of greatly enhancing the contrast in medical diagnostic work that seems so promising by operating near the K-edge of iodine, iron or other elements, nor on the fascinating development of a novel X-ray scanning microscope.

Much will depend on the extent to which SR research will develop and will the necessity in a SR storage ring lead to recognize it as a facility similar to nuclear research reactors, powerful electron microscopes, etc.

It will be greatly surprising if a source of radiation many orders of magnitude more powerful will not lead to new departures in science and may be the most exciting uses of SR are still not recognized for it is in principle impossible to plan for the unknown.

In all dedicated storage ring projects considered the primary flux and intensity of SR will be less-than 'that immediately available in existing high power storage rings, operating as centralized facilities, producing may be the shortest wave length and/or the greatest flux. But parasitic operation will always limit the opportunities of an enterprising experimentalist, for in these conditions it is difficult to adjust the β - function or introduce special SR magnets without drastically interfering with the intricate adjustments needed for colliding beam experiments. A dedicated machine offers greater freedom for SR research, freedom that will surely lead to new and unexpected developments.

The SR storage ring is a specialized machine. a source of auanta that can be aptly called a photon factory. In spite of its size and complexity it will certainly produce more photons at a cheaper price than any existing device. From a human point of view atoms and molecules, not to speak of the complex structures discovered in modern molecular biology in these fields are just as fundamental as the remote depths of space and inanimate matter penetrated by our most powerful machines of research: telescopes and accelerators. In SR one can see a novel agent that strangely unites these frontiers of scientific adventure made possible by the advances of modern technology.

Storage Rings as SR Sources Table 1.

Facility	E GeV	H T	$\lambda_{max.}$ A	I mA	ΔE keV	P_{SR} kw	$R_{bend.}$ m	D m
SPEAR	2,5	0,65	2	250	270	65	12,7	60
DORIS	1,75 3,5	0,48 0,96	5,3 0,65	6000 200	70 1100	420 220	12,1	55
D C I	1,8	1,6	1,5	500	240	120	3,8	30
VEPP-3	2,25	1,26	1,2	200	375	75	6	23,6
Tantalus I	0,24	1,5	90	10	0,55	0,0055	0,54	3
N B S	0,24	0,96	140	100	0,35	0,035	0,83	3
VEPP-2M	0,67	1,8	10	100	15	1,5	1,22	5,7
Tantalus II	1,76	1,24	2	100	180	20	4,5	26
New NINA	2	1,2	1,6	1000	240	240	5,55	30
I P P	1,35	1,8	2,4	100	110	10	2,5	10

REFERENCES

1. A.A.Sokolov and I.M.Ternov. Synchrotron Radiation, Pergamon Press, 1960.
2. Notes of the Annual SR Users Group Conference published by the SR Center, Physical Sciences Laboratory. University of Wisconsin, 1968-1973.
3. DPNL Synchrotron Radiation Bibliography, 1972.
4. H.Winick. The Stanford Synchrotron Radiation Project (SSRP), These Proceedings, 1974.
5. E.M.Rowe and F.E.Mills. Tantalus I: A dedicated storage ring SR source, Particle Acc., 211-227, 4, 1973.
6. E.M.Rowe, M.A.Green. W.S.Trzeciak, W.R.Winter Jr. The conversion of the NBS 180 MeV electron synchrotron to a 240 MeV storage ring for SR research, These Proceedings, 1974.
7. S.Kapitza. Synchrotron radiation as a new tool of research, in Russ., Priroda, 10, 1971. See also Proc. III All-Union Part. Acc.Conf.,Moscow, oct.,1972,v.I,pp.11-16.
8. P.J.Thompson. DNPL, TM-105, 1973.
9. D.J.Thompson, G.Saxon, N.Marks, V.P.Suller and T.E.Swain. A 2 GeV 1A electron storage ring dedicated to the production of SR. These Proceedings, 1974.
10. E.Rowe et al. IEEE Trans.on Nucl.Sci.NS-18, 3,210-212, 1971.
11. E.Rowe. Proc. III All-Union Part.Acc.Conf., Moscow, October 1972, v.1, pp. 25-30.
12. S.Kapitza, L.Lugansky, L.Zikin. Design study of a 1,35 GeV synchrotron radiation source, Proc. III All-Union Part.Acc.Conf., Moscow, October 1972, v.1, pp.82-84.

ASTROPHYSICS AND ELEMENTARY PARTICLE PHYSICS*

Remo Ruffini†
Joseph Henry Laboratories, Princeton University, Princeton, New Jersey 08540

ABSTRACT

Recent developments of relativistic astrophysics allow the observation of regimes in which all existing field theories have never been tested. In the description of these regimes, unreachable in any experiment performed in a laboratory on the Earth, our current knowledge of electrodynamics or elementary particle physics has to be extrapolated by many orders of magnitude. For the first time, we are able to observe phenomena in which a fully relativistic treatment of gravitational interactions is mandatory.

1. INTRODUCTION

There is a major difference between astrophysics and usual experimental physics. In the usual experiments performed in a laboratory on the Earth, a physical phenomenon is isolated from all kinds of inessential and competing processes and reproduced in its most simple and clear form in order to be directly submitted to measurement and inquiry. Once the possibility of a new physical phenomenon is theoretically envisaged, a suitable experiment is designed in order to focus on this specific process. The strength and power of an experiment is such that on the basis of its result, the theory is confirmed or disproved. The success of an experiment is greater the most scientists succeed in focusing on a direct and clear measurement of the effect under consideration. In this interplay between the theory and the experiment and their possible feedback lies the entire dynamics of human scientific knowledge as postulated by Galileo.

In astrophysics, this program cannot be applied straightforwardly, mainly because some of the phenomena we are interested in do take place on time scales much too long to be recorded by a human observer (the lifetime for the thermonuclear evolution of a star of one solar mass is expected to be $\sim 10^{10}$ years!) and the size of the "objects" under investigation involves masses orders of magnitude larger than that of the earth ($M_\odot \sim 2 \times 10^{33}$ gr mass of a galaxy $\sim 10^{12} M_\odot$, estimated mass of a quasar $\sim 10^{10}$ Mg). The corresponding densities and pressures reach limits unthinkable in any earth-bound experiment (the core of a massive neutron star can reach hundred times nuclear densities).

However, although the approach is here different, yet the final result, namely the "isolation" of a specific phenomenon in an "experiment" is quite the same. In astrophysics, we are dealing with a very large number of entities (10^{12} stars in a galaxy, 10^4 galaxies in a cluster of galaxies, etc.). Between these entities, we can make classifications and divide them with respect to some "equivalence relation" into "equivalence classes." In the case of stars, e.g., these equivalence relations can be the mass, the luminosity, the surface temperature, the radius of the star, any special periodicity or any combination of these parameters. From these classifications, a certain regular pattern often emerges and relations can be established between the different equivalence classes. By far the most successful of these classifications in the case of stars has resulted in the Hertzsprung-Russel diagram. In the case of stars after the endpoint of thermonuclear evolution, a corresponding diagram is currently being constructed from a direct observation of pulsars and binary x-ray sources.

One of the greatest successes of theoretical astrophysics has been to relate through detailed theoretical models the regular pattern appearing in the classification with the temporal evolution of a star. It is difficult to overemphasize the importance of this essential step. Thanks to this, it is then possible to reconstruct the effective evolution of a single star by observing stars belonging to different equivalence classes. Although, therefore, we will never be able to follow each star (or galaxy or quasar) through its evolution, we can in principle, by looking at a large enough sample of stars, find one which at the moment of observation indeed performs for us the "experiment" we are interested in, in order to isolate and probe a new physical phenomenon. This, in a few words, is the methodology which govern the dynamics in the processes of acquiring knowledge in astrophysics.

The recent enormous success of this entire field of research stems from the very important interplay between so many different experimental techniques ranging from observatories working at radio and optical wavelengths on the Earth and telescopes for γ and x-ray observations on artificial Earth satellites, to the field of burst astronomy which is still in its infancy. Still all these observations would have produced very small progress if a deep theoretical understanding of these experimental data would not have occurred simultaneously—that is, if the theoretical framework would not have made comparable progress. Essential in the interplay between theoretical work and experimental research has been a very effective use of numerical analysis on computers which on one side has allowed a drastic reduction in the time of analysis of the experimental results and on the theoretical side has enabled one to overcome at once some of the gravest difficulties in the solution of the field equations governing the phenomena.

In particular, in the last forty years, the profound progress made in nuclear physics has allowed one to gain a much deeper understanding of thermonuclear evolution of stars. It has also become clear that during its entire thermonuclear evolution, a star radiates on the order of a few percent of its mass by burning light elements (H, He) into heavier elements. Only in the last four or five years, however, it has become clear that by far the most energetic epoch of the life of a star is reached after the exhaustion of its thermonuclear sources of energy has occurred and the star has undergone gravitational collapse. The interest in the latest stages of the evolution of a star is also dictated by the large amount of the new physical processes expected to be encountered in the description of gravitationally collapsed objects. Magnetic fields of the order of 10^{12} gauss are expected to be developed in the magnetosphere of a neutron star. During the few milliseconds in which gravitational collapse occurs of the order of 10^{57} nucleons are expected to undergo at once transformations dominated by weak interactions of the form

$$e^- + p \rightarrow n + \nu_e$$
$$n \rightarrow p + e^- + \bar{\nu}_e$$
$$e^+ + n \rightarrow p + \bar{\nu}_e$$

The neutron star, expected to be the outcome of this process, has an average density which can be as high as ten times nuclear densities. This density, together with the fact that the material in the star is degenerate ($T = 0$), implies that the Fermi energy of the particles is so high as to generate all the resonances and particle spectra observed in earth-bound accelerators (CERN or other). The other aspect, of course, which has generated so much interest, stems from

*Summary of a talk delivered at the International Accelerator Conference at the *Stanford* Linear Accelerator Center, May 1974. An extended version is to appear in the "American Scientist."

†Work partially supported by NSF Grant GP30799X to Princeton University.

the possibility of being for the first time ultrarelativistic gravitational fields at work and have not only the first clear evidence for the existence and possibility of a direct detection of gravitational radiation but also the formation of a completely collapsed object or a "black hole." We have, therefore, the opportunity of testing the validity, under a variety of regimes, of the two best field theories known in theoretical physics: Maxwell's theory of electromagnetism and Einstein's theory of gravitation. On the other hand, we have the possibility of learning much new physics about the weak and strong interactions from the analysis of neutronization of matter and the equilibrium configurations of neutron stars.[1,2]

In all these respects, the process of gravitational collapse and the physics of gravitationally collapsed objects has an enormous potential for a deeper understanding of nature and physical processes. A comparable amount of knowledge could be gained, in principle, only from another phenomenon: the collapse or the initial explosion of the Universe itself.

2. THE BASIC THEORETICAL WORKS ON GRAVITATIONAL COLLAPSE

The entire area of research of the physics of collapsed objects was started by a few fundamental works both in the theoretical and experimental fields. Nothing can illustrate better the motivation behind these pioneering theoretical works than the words of Landau[3] at the beginning of his classic paper, "On the Theory of Stars," "The astrophysical methods usually applied in attacking the problems of stellar structure are characterized by making physical assumptions chosen only for the sake of mathematical convenience . . . It seems reasonable to try to attack the problem of stellar structure by methods of theoretical physics, i.e., to investigate the physical nature of stellar equilibrium. For that purpose we must at first investigate the statistical equilibrium of a given mass without generation of energy . . ."

This way of attacking the problem of the equilibrium configuration of a star at the endpoint of thermonuclear evolution by using the tools of quantum mechanics and Fermi statistics was first proposed by R. H. Fowler[4] and E. C. Stoner[5] but it was not until the decisive contributions of Chandrasekhar' and Landau[7] that the central role played by special relativity in the solution of this problem was recognized. The understanding of this key factor led directly to the novel concept of a critical mass against gravitational collapse.

We can here summarize the main points of the reasoning that led to this conclusion. The description of a star in this approach follows very much along the lines of the Thomas–Fermi treatment of an atom.[7] In the model of the atom, the electrons are described by a degenerate Fermi gas constrained to a finite volume by the Coulomb attraction of the nucleus.[4]

At the endpoint of thermonuclear evolution, the composition of a star is expected to be of nuclei embedded in a gas of electrons (all the orbitals having been detroyed by the great compression of the material, white dwarf star $\rho \sim 10^5$ gr/cm) or, alternatively, a gas of neutrons, protons, and electrons in beta equilibrium (the matter having undergone neutronization under the effect of pressure, neutron star $\rho \sim 10^{15}$ gr/cm^3). In both cases, the material of the star is simply describable by a degenerate Fermi gas, constrained to a finite volume by the self-gravitation of the system. The pressure to keep the system from collapsing is simply given, in both cases, by the quantum pressure due to the Pauli exclusion principle.[7] In the case of the white dwarf stars, the pressure is mainly due to the gas of degenerate electrons while the nuclei mainly contribute to the density distribution; in the case of neutron stars, both pressure and density are generated by the gas of neutrons.[1,2]

The main formulae can be obtained most straightforwardly.

For a degenerate Fermi gas, the density of particles is simply given by

$$n = \frac{N}{V} = \frac{8\pi}{h^3} p^2 \, dp$$

and the Fermi momentum

$$P_F = \left(3\pi^2 \hbar^3 N/V\right)^{1/3} .$$

The kinetic energy of a particle is given by

$$E = p^2/2m . \qquad (1)$$

The total energy is then, simply,

$$\int_0^{P_F} \frac{4\pi}{h^3} \frac{p^4}{} \, dp$$

and the pressure[8]

$$P = -\partial E/\partial V = \left(3\pi^2\right)^{2/3} \left(\hbar^2/5m\right) (N/V)^{5/3} \qquad (2)$$

If, however, the kinetic energy at the top of the Fermi sea becomes comparable to the rest energy of the particle, then the particle energy is no longer given by Eq. (1) but by the usual relativistic relation

$$E = c\left(p2 + m2\, c2\right)^{1/2}$$

or in the extreme relativistic regime by

$$E = c\, p . \qquad (3)$$

The pressure is then in this limit given by

$$P = -\partial E/\partial V = \left(3\pi^2\right)^{1/3} (\hbar c/4) (N/V)^{4/3} \qquad (4)$$

The increase of pressure corresponding to an increase in density is clearly much smaller in Eq. (4) than in Eq. (2). To have clearly understood and expressed this relativistic softening of the equation of state and have focussed the essential role the transition to a relativistic regime plays in the physics of a degenerate star have been the basic contribution of S. Chandrasekhar[6] and L. Landau,[3] which led to the revolutionary concept of a critical mass against gravitational collapse.

There exists, therefore, a fundamental difference between the theoretical description of an atom and that of a degenerate star. Never do the electrons in an atom reach energy so relativistic as to be in the regime described by Eq. (4). Their pressure, given by Eq. (2), reacts to a density change in such a way as always to balance the attractive effects of the electromagnetic field of the nucleus. In a star at the endpoint of thermonuclear evolution, on the contrary, the conditions under which Eq. (4) applies are always reached if the star is massive enough as a direct consequence of the non-screening and long-range character of gravitational interactions. The more massive the star is, the more it contracts, the more the spatial volume of the phase space occupied by the system is reduced and correspondingly the volume in the momentum space expanded[8] so that the Fermi momentum of the system can always reach relativistic regimes. In the transition from Eq. (2) to Eq. (4), the pressure dependence on the density softens considerably and the system is not able to hold itself up in equilibrium, then gravitationally collapses. Practically in free fall the star should shrink down to a point, Landau said, if some new physical phenomena would not occur!

Following these pioneering works, the systematic analysis and detailed computations of the configurations of equilibrium of white dwarfs were presented by S. Chandrasekhar[9] and the ones for neutron stars by R. J. Oppenheimer and G. M. Volkoff.[10] The value of the critical mass for white dwarfs was found to be $M_{crit} \simeq 1.39\ M_\odot$, the one for neutron stars $M_{crit} \sim 0.7\ M_\odot$.

What was the relation of these theoretical works with reality? White dwarf stars had indeed been observed for many years[11] and the theoretical work of Chandrasekhar was in splendid agreement with experiments. For the discovery of neutron stars, we have to wait still a few decades (see Section 3). The key idea leading to their identification was presented as far back as 1934 by Baade and Zwicky[12] in a very compact paper.

"With all reserve we advance the view that supernovae represent the transitions from ordinary stars into neutron stars which in their final stages consist of extremely closely packed neutrons."[12]

It was not until 1939 with the work of Oppenheimer and Snyder[13] that attention was focussed not on the stable equilibrium configurations of degenerate matter (neutron stars and white dwarfs) but on the process of gravitational collapse itself. Then for the first time it became self-evident how the analysis of this phenomenon was so important and revolutionary for our understanding of the nature of space and time. It became clear that the phenomenon of gravitational collapse with its processes of time dilatation, light deflection, and gravitational red shifts, was a most unique place where a fully relativistic theory of gravitation could be seen at work and the validity of general relativity confronted with experimental evidence. The work of Oppenheimer and Snyder appears today one of the most important cornerstones of relativistic astrophysics and one of the most mature and profound works ever written in gravitation physics. In that paper, the authors not only give the basis for the entire field of what will be later known as "black hole" physics, but they also give a fully analytic solution of the collapse of a cloud of dust (pressure zero or free fall, very good approximation to a realistic gravitational collapse) with a detailed analysis of the self-closure of the system from a faraway observer as a consequence of the general relativistic effects.

Still more time was needed *to* realize that the process of gravitational collapse was the ideal place to generate a theoretically detectable amount of gravitational radiation.[14] The reason for this delay is simply explained: Since the first days of general relativity, Einstein himself[15,16] had shown that gravitational fields, like any other relativistic mass zero field, had to propagate with the speed of light and that energy could be carried by gravitational waves. It was not conceived, however, even by a gedanken process, how gravitational radiation could indeed be detected. This key, a fundamental contribution, was made by Joseph Weber in 1960.[17] It was in a much detailed article[18] and in an extensive book[19] that Weber presented not only the main principles on which the detectability of gravitational radiation should be based, but also presented the technical details on the ground of which a detector of gravitational radiation could be built. This detector was made operational by Joseph Weber himself.[1] The relevance of this paper, quite apart from its impact on experimental techniques, has been also very large in generating in the theoretical field, in the following years, much thinking on astrophysical processes to produce detectable amounts of gravitational radiation.

With this paper, we can conclude the set of "heroic" works which were destined to open a new era in relativistic astrophysics.

3. THE DISCOVERY OF COLLAPSED OBJECTS

After the flourishing of the fundamental theoretical works between 1931 and 1939, the progress of relativistic astrophysics was dramatically slowed down due to many diverse social and scientific interests. It was not until 1957 that work in this field started again to develop, thanks mainly to the contributions of Ambartsumian,[20] Cameron,[21] Wheeler,[22] Zel'dovich,[23] and their students and collaborators. The major emphasis in their work was directed toward critically reconsidering the assumptions made in the classical works of Oppenheimer and his students.[10,13] Alternative models of neutron stars were advanced, the emphasis being directed at times toward a better treatment of the surface layers, at times toward the understanding of the role played by nuclear interactions in the treatment of the core. Different models lead to different ranges of masses, radii, and density distributions for the neutron stars' equilibrium configurations.[14]

Slowly the maturity of a "critical" interest of research was regained and new fresh ideas started again to flourish.

In 1962 a new program of research started by R. Giacconi, H. Gursky, F. Paolini, and B. Rossi gave the first evidence for the existence of x-ray sources outside the solar system. In 1964 Zel'dovich[24] following an earlier suggestion of Shklovsky developed a model giving a clear evidence for the possibility of x-ray generation by a plasma accreting into a neutron star. Then in 1968, Shklovsky[25] presented a totally new and original idea: Scorpius XI, the first and most powerful source of x-rays observed in the galaxy is most likely, Shklovsky suggested, a close binary system in which one of the members is a neutron star and the other member a cool dwarf star. "A stream of gas flowing out of the second component is permanently incident on the neutron star," this accreting material enormously compressed should then emit x-rays; "the optical object accompanying the x-ray source might be a cool dwarf star with half of its surface heated by a strong flux of hard x-rays from the source." As we shall see, this article will become a few years later the leading work for the understanding of one of the most exciting discoveries of modern astrophysics: the binary x-ray sources.

1968 is the year *in* which an enormous momentum is gained in this entire field of research.. .the first clear evidence for the existence of neutron stars is given. This conclusion clearly follows from the discovery of pulsars[26,27] and the observation of the pulsar NP0532 at the center of the Crab Nebula.[28] The hypothesis advanced in 1939 by Baade and Zwicky[12] of the possible connection between neutron stars and supernova remnants is spectacularly confirmed. This discovery naturally led to an in-depth search for pulsars inside our own galaxy; of the order of 105 of them are kept today under constant observation and much has been learned about their pulsed radiation, spectra, and time variabilities.[29] Unfortunately the theoretical feedback has not yet been as strong as one could have possibly wished. One of the most important by-products of the discovery of pulsars has been, however, to have dramatically brought back to the attention of a large section of theoretical and experimental astrophysicists the basic issues of the physics of gravitationally collapsed objects.

The clear evidence for the existence of neutron stars, together with the unavoidability of the existence of a critical mass against gravitational collapse,[30] made the existence of "black holes" inside our galaxy inescapable. On the other side, the theoretical picture to be expected at this ultimate endpoint of gravitational collapse appeared more and more complex and presented fundamental issues on the physical processes occurring in these ultrarelativistic regimes.[31,32]

From all this naturally developed the need for launching a realistic effort in order to detect and differentiate the two families of collapsed objects: neutron stars and black holes. The simple idea was advanced by Ruffini and Wheeler[32] of capitalizing on the Shkovsky accretion picture not only in the case when a neutron star is a member of a close binary system but also in the case where a black hole attracts and pulls material from the companion star. The short time variability of the x-ray source and the statistical analysis involved would then be a most powerful tool for the determination of the "form factor" of a black hole.[14]

The discovery and systematic analysis of the binary x-ray sources started in 1971 by the group led by Riccardo Giacconi[33] using the Uhuru satellite came in the most mature moment to have the maximum exploitation and better theoretical

understanding of the experimental results.[34] The success of this discovery has been certainly enhanced by the resonance with so many different observational techniques.[35,36]

In the theoretical field, the feedback of these observations has been very impressive. Essential to the understanding of these binary systems is first of all the understanding of the process of gravitational collapse itself through which these systems have to be formed.[37] On the other side, to understand the process of x-ray emission, a fully relativisitic magnetohydrodynamics has to be developed[38] together with more classical analysis of disc-like structures around the collapsed object in equilibrium under the two opposite effects of gravitational attraction and centrifugal forces.[39-41] The physics of binary star systems is essential in reaching the understanding of the evolution of these binary systems.[42] An accurate analysis of the gravitational and electromagnetic structure of the collaped objects is essential for the understanding of the "core" of these x-ray sources. Finally, criteria to differentiate between the two classes of collapsed objects are much needed.[34]

The great progress currently being made in all these theoretical fields, together with the possibility of having in the forthcoming year, satellites with x- and γ-ray telescopes with larger collecting areas and better time resolutions, as well as pointing facilities, make one hope that in the next five, or at most, ten years, a complete understanding of the final configuration of gravitationally collapsed stars will be gained.

Each one of these X-ray binaries is much like a high-energy accelerator. Here the acceleration process is done by gravity and we have to infer from the scattering of the imploding material the "form factor" of the collapsed object.

If we now turn from this program of research to be achieved in the next few years to a much larger program on longer time scales, two different directions of research naturally present themselves to our attention. The first is clearly to try to directly observe the transition from a normal star into a collapsed object by observing "the moment of gravitational collapse." See Figure 1. This program points to the clear need for developing an entirely new branch of theoretical and experimental astrophysics, what we should call "burst astronomy." In this sense, the recent results obtained by I. Strong,[44] the preliminary work of K. Lande and at the University of Torino,[45] the large effort being made in building a new, more sensitive, set of gravitational wave detectors at the Universities of Louisiana, Rome, and Stanford[46] can only be viewed with the greatest expectation and excitement.

The second direction points toward even a larger program: capitalize on what we are learning in the physics of collapsed objects for gaining a deeper knowledge of the fundamental field equations governing physical processes. It is conceivable that the analysis of these fully relativistic processes will be of great help in the understanding of other apparently disconnected fields of physics, like, e.g., elementary particle physics. It is very likely that this will be by far the most exciting long-range frontier!

References

1. For a review of the current status of the theoretical and experimental research in this field, we suggest Black Holes, Gravitational Waves and Cosmology by M. Rees, R. Ruffini, and J. A. Wheeler, Gordon and Breach, New York, London, **1974,** or
2. Neutron Stars, Black Holes and Binary x-ray Sources, H. Gursky and R. Ruffini, eds., Reidel, Dordrecht, Holland, **1974.**
3. L. D. Landau, "On the Theory of Stars," Phys. Zeit. der Sowiet 1, **285 (1932).**
4. R. H. Fowler, "On Dense Matter," Mont. Not. of RAS XXXVII, **114 (1926).**
5. E. C. Stoner, "The Limiting Density in White Dwarf Stars," Philosophical Magazine 77, **63 (1929).**
6. S. Chandrasekhar, Mon. Not. of RAS 91, **456 (1931).**
7. See, e.g., L. D. Landau and E. M. Lifshitz, Mecanique Quantique, MIR, Moscow, **1971.**
8. See, e.g., L. D. Landau and E. M. Lifshitz. Physique Statistique, MIR, Moscow, **1970.**
9. S. Chandrasekhar, Mont. Not. of RAS 95, **207 (1935).**
10. R. J. Oppenheimer and G. M. Volkoff, Phys. Rev. 55, **374 (1939).**
11. See, e.g., A. S. Eddington, The Internal Constitution of Stars, Cambridge University Press, **1926.**
12. W. Baade and F. Zwicky, Phys. Rev. 45, **138 (1934).**
13. J. R. Oppenheimer and R. Snyder, Phys. Rev. 56, **455 (1939).**
14. See, e.g., R. Ruffini, "Neutron Stars, Black Holes and Binary X-ray Sources," invited talk at the **1973** Solvay Conference on Relativistic Astrophysics.
15. A. Einstein, Sitzber. Preuss. Akad. Wiss., **588 (1916).**
16. A. Einstein, Sitzber. Preuss. Akad. Wiss., **154 (1918).**
17. J. Weber, Phys. Rev. 117, **306 (1960).**
18. J. Weber, General Relativity and Gravitational Waves, Interscience Pub., Inc., New York, **1961.**
19. See, e.g., J. Weber, Phys. Rev. Letters 18, **795 (1964).**
20. See, e.g., V. A. Ambartsumian and G. S. Saallyou, Soviet Astr. 6, **601 (1961)** and references mentioned there.
21. A. G. W. Cameron, "Neutron Star Models," Astrophys. J. 130, **884 (1959).**
22. See, e.g., J. A. Wheeler et al. report at the Solvay Conference, **1958.**
23. See, e.g., Ya. B. Zel'dovich, Soviet Phys. J.E.T.P. 14, **1143 (1962).**
24. Ya. B. Zel'dovich, Soviet Phys. Dokl. 9, **246 (1964).**
25. I. S. Shklovskii, Soviet Astron. 11, **749 (1968).**
26. A. Hewish et al., Nature 217, **709 (1968).**
27. T. Gold, Nature 218, **731 (1968).**
28. D. H. Staelim, E. C. Reifenstein, Science 162, **1481** (1968).
29. See, e.g., E. Groth, "Observational Properties of Pulsars" in ref. **2.**
30. The unavoidability of the existence of a critical mass for the equilibrium configurations of neutron stars has been proved independently from any detail of the equation of state at nuclear or supranuclear densities by C. Rhoades and R. Ruffini, Phys. Rev. Letters 32, **324 (1974).**
31. R. Penrose, Rivista del Nuovo Cimento, Numero Speciale, Vol. I, **1969.**
32. R. Ruffini and J. A. Wheeler, Physics Today 24, **30 (1971).**
33. See, e.g., R. Giacconi in "Binary X-ray sources," invited talk delivered at the Solvay conference on relativistic astrophysics, in press, **1974.**
34. See, e.g., R. Ruffini, "The Physics of Gravitationally Collapsed Objects" in ref. **2.**
35. See, e.g., P. Boynton, "Optical Observations of X-ray Sources" in ref. **2.**
36. See, e.g., R. H. Hjellming, Ap. J. Letters 182, **L29 (1973).**
37. See, e.g., S. Colgate, "Supernovae" in ref. **2.**
38. See, e.g., ref. **34** and references mentioned therein.
39. V. F. Schwartzman, Astron. Z. 15, **377 (1971).**
40. J. E. Pringle and M. Rees, Astron. and Astrophys. 21, **1 (1972).**
41. Shakura and Sunyaev, Astron. and Astrophys.
42. See, e.g., R. P. Kraft, "Evolution of Binary Systems: Neutron Stars and Black Holes" in ref. **2.**
43. See, e.g., R. B. Partridge, "Burst Astronomy" in ref. **2.**
44. See I. Strong, "Cosmic Gamma-Ray Bursts" in ref. **2.**
45. See, e.g., Editorial Report in Physics Today, July **1974.**
46. See, e.g., W. Fairbank et al, in the Proceedings of the Varenna Summer School, 1972, B. Bertotti, ed., Academic Press, New York, **1974.**
47. B. Paczynski, Annual Review of Astron. and Astrophys. 9, **183, 1971,** and references mentioned therein.
48. W. D. Arnett, Astrophys. and Space Sci. 5, **180 (1969).**

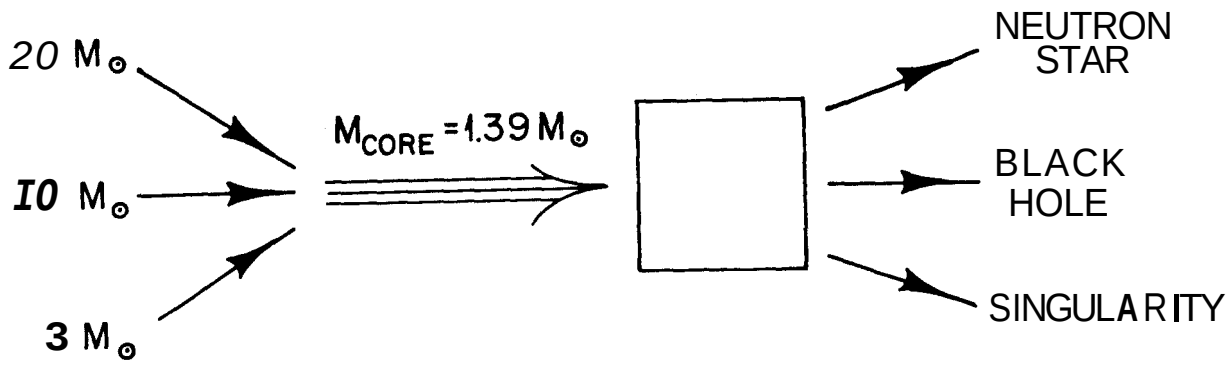

Fig. 1

Figure 1. Recent theoretical work by Arnett[47] and Paczinsky[48] has shown that stars in a large range of masses $2 \lesssim M/M_{\odot} \lesssim 50$ toward the endpoint of their thermonuclear evolution develop a degenerate core of white dwarf material. Once this core reaches the critical value of 1.39 $M_{\odot}$ (Chandrasekhar limit), the star undergoes gravitational collapse. It is extremely important to prove by experimental evidence the validity of this theory postulating a "standard" starting point for the process of collapse to occur. The "moment of gravitational collapse," much shorter than a second, leads the collapsing core either to a neutron star or to a black hole or to a still theoretically unconceived configuration which we label most generally as a "singularity." The key factor in determining which of the different outcomes will in fact occur appears to be more and more controlled by the value of the critical mass of neutron stars. [13]

A 2 GeV 1A ELECTRON STORAGE RING DEDICATED TO THE PRODUCTION OF SYNCHROTRON RADIATION

DARESBURY SYNCHROTRON RADIATION SOURCE DESIGN GROUP*
Daresbury Laboratory,
Daresbury, Warrington, England

Summary

An electron storage ring is being designed to replace the 5 GeV electron synchrotron NINA as a source of synchrotron radiation. The new machine will be used solely for this purpose and its design is being optimized to the needs of the experimenters. The characteristic wavelength of the radiation will be 4 Å and the flux at that wavelength about 3×10^{13} photons/s/mr (horizontal) in 0.1% bandwidth. Design considerations include long beam lifetime, small source size and large available solid angle for most beam lines. Assuming a bending field of 1.2 T the beam in the storage ring will have an energy of 2 GeV and the design value of the circulating current will be 1 A. The mean radius will be about 15 m and there will be at least 10 beam lines. Superconducting wavelength shifters or "wigglers" can be incorporated to extend the usable spectrum on two beam lines to 0.1 Å. The new machine will fit into the existing buildings at Daresbury.

Introduction

At the present time, the 5 GeV electron synchrotron NINA provides two synchrotron radiation beam lines supporting nine experiments. These are parasitic on the high energy physics programme, which is expected to cease in about four years' time. To continue to provide a synchrotron radiation facility it is estimated that a purpose-built dedicated source will not only be more suitable but will be cheaper to operate than a high energy synchrotron, saving the capital cost after about five years of operation. Studies have therefore been carried out to determine the requirements and feasibility of such a machine and a detailed design is now emerging.

Specification

A considerable proportion of experiments use radiation down to 1 Å (0.1 nm) in wavelength, and a few such as scattering experiments and radiometry require wavelengths down to 0.1 A or less.

For reasons of intensity, duty cycle, beam stability, and access, the source should clearly be a storage ring, and it has therefore been designed for a characteristic wavelength (λ_c) of about 4 Å, with the understanding that wavelength shifters[1,2] (or "wigglers") will be inserted in two straight sections to provide shorter wavelengths.

High intensity is most important for many experiments and is necessary to justify the facility. This design will provide 3×10^{13} photons/s/mr (horizontal) in 0.1% bandwidth at 4 Å wavelength and 5×10^{13} at the spectrum peak (10 Å). With a 1.2 T bending field and a 2 GeV beam this will require a circulating current of 1A. Other user requirements are: small beam cross section at the tangent points (~ 2 mm^2); lifetime of stored beam at least 8 hours; facility to circulate only one bunch, for time-resolved measurements in the nanosecond region (at reduced mean intensity); and space for at least 10 beam lines of up to 40 mr horizontal aperture and with good access whilst a beam is circulating (but not necessarily whilst filling).

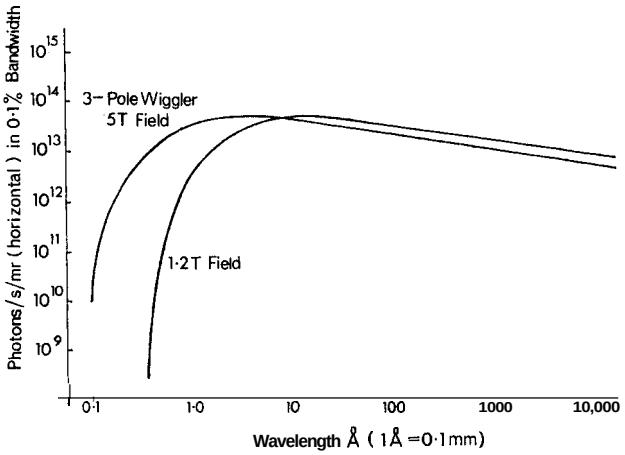

Fig.1 shows the spectra[3] for the two types of beam line.

Some Machine Design Features

Choice of energy and field

Unlike an accelerator or storage ring used for high energy physics, in a synchrotron radiation source it is the characteristic wavelength λ_c rather than the energy which is a prime parameter. The number of photons/s/mr (horizontal) in 0.1% bandwidth at a wavelength λ is given by[3] $N = F(\lambda/\lambda_c) \times$ beam energy (GeV) $\times$ beam current (A), where F is an algebraic function involving no other machine parameters, and $\lambda_c = 18.6/BE^2$ where B is the bending field (T) and E is the energy (GeV).

If the dipole magnetic field is increased, the radiation spectrum can be kept constant by decreasing the particle energy, which results in a reduction in the bending radius and integrated field length of the magnets, though it is also necessary to increase the circulating beam current. The reduction in integrated field length decreases both the capital and running costs of the magnets, and it has been found[4] that the combined costs are a minimum when a dipole field of about 1.7 T is chosen. Above this value saturation effects dominate the magnet design and cause the costs to increase sharply. However the loss of aperture, also due to pole saturation, at fields above 1.4 T cannot be tolerated in an electron storage ring, and the final choice of field will be in the region of 1.2 to 1.3 T. At such levels the loss of aperture *is* small, and the total magnet cost is only 6% above optimum. The higher energy and lower circulating current benefit the r.f. system through reduction of beam loading and provide better high energy flux from a given wiggler magnet. For 1.2 T the energy will be 2 GeV and the bending radius 5.55 m.

*The principal persons concerned with the machine design are:

D. J. Thompson (project leader), V.R. Atkins, J.C. Hopkins, E.A. Hughes, A. Jackson, J.B. Lyall, N. Marks, P. Moore, D.E. Poole, M.W. Poole, G. Saxon, V.P. Suller, T.E. Swain, K. Tarry, D.G. Taylor, B. Trickett.

The magnet lattice

Having chosen the energy and bending radius, the magnet lattice must be selected. A separated function design is essential in a storage ring to provide radial damping. An 8-cell FBODBO lattice (F, D = quadrupoles, B = dipole, O = straight) was chosen for the following reasons :-

it gives good access to the synchrotron radiation,

it has adequate length and numbers of straight sections,

it has economy of components,

it provides ease of chromaticity correction,

it requires reasonable quadrupole field gradients,

the triplet lattice is anti-damping to electrons with relatively small energy deviations.

The requirement for 2.3 m of clear space in each straight section, after allowance for sextupoles, then fixed the mean radius.

There will be 16 sextupole magnets, individually energized, for chromaticity control and for local sextupole field correction. Other correction elements include skew quadrupoles and an octupole magnet.

Stability considerations restrict the Q-values to less than 3.5 Within this region the structure resonances centred on $Q_V = Q_R = 2^2/_3$ (i.e. p = 8) dominate the diagram and need to be avoided. The regions centred on $Q_V = Q_R = 2\%$ and 3% are reasonably free of lower order resonances and in the injection process allow the maximum flexibility in kicker timing. As 2% is much further from the stability limit it is preferred for the storage ring to operate in the region $2\frac{1}{4} < Q_{\cdot} \quad Q_R < 24$. However, the cross-sectional dimensions of the damped beam, which are determined by the quantum excitations resulting from synchrotron radiation emission, and therefore increase with energy, are smaller for a given lattice when operated at higher Q_R values. For this reason the storage ring will be operated at the highest feasible Q_R value. The storage ring will have the capability of operating at any point within the stable area in the Q-diagram so that subject to injection limitations the tune can be changed to find the optimum working point.

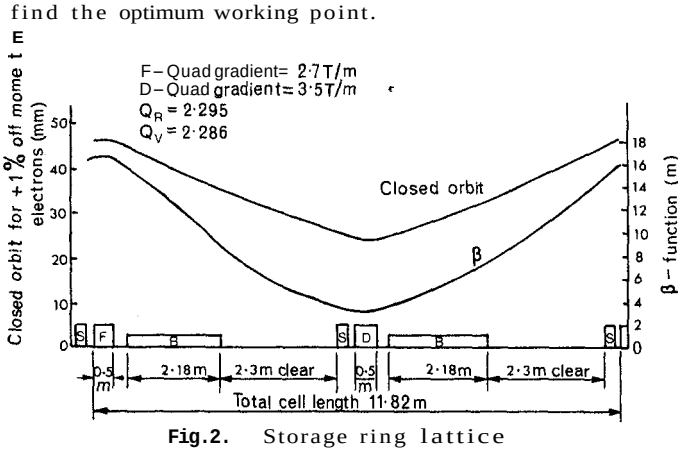

Fig.2. Storage ring lattice

The lattice parameters assuming $Q_V \sim Q_R \sim 2.25$ are shown in fig.2.

The sixteen dipole bending magnets have a magnetic length of 2.18 m and are of a 'C core' design. Whilst this design has a smaller good field aperture and is more susceptible to saturation effects than the 'H' or 'window frame' designs, it is required in order to allow the connection of a large number of beam lines including those from "wigglers". The magnets will be built from thick laminations rather than machined from solid blocks. This not only allows complete shuffling of the steel but also eliminates the small eddy currents which occur in a solid magnet when rise times of the order of a few minutes are used.

The sixteen quadrupoles will also be laminated and there will be separate power supplies for the dipoles and for the focusing and defocusing magnets so as to control the radial and vertical Q values separately.

Injector

In order to accumulate a high circulating current it is essential to inject many pulses into the storage ring. The injection energy must therefore be high enough for radial damping of betatron oscillations to take place between injection pulses. An energy of 600 MeV has been chosen, giving a damping time constant of 400 ms and an adequate Touschek lifetime of 50 mins.

The injection method is a conventional multi-turn system using a septum magnet and a fast localized orbit bump produced by two fast kickers. The exact rate at which injection can take place is determined by the acceptance aperture of the storage ring, the emittance of the 600 MeV beam and the radial Q value at injection. These parameters are not yet finalized, but so far it appears that injection can be at a rate of up to 6 Hz when Q_R is in the vicinity of 2%.

The 600 MeV electrons for injection into the storage ring will be provided by a linear accelerator in the range 10-15 MeV followed by a booster synchrotron. This will have a mean radius one third that of the storage ring. Extraction and transfer to the storage ring will take place over three turns though it is not considered necessary for each injected pulse to fill the storage ring uniformly.

Extraction from the booster will be by a simple shaving technique with a fast orbit bump and a septum magnet. With a circulating current of 20 mA in the booster this will lead to electrons being accumulated in the storage ring at between 1 and 5 mA per pulse, and at a transfer rate of 5 Hz the 1000 mA stored beam will be reached in ∿ 3 minutes.

Alternatively efficient single-turn extraction using an integer resonance system could be developed.

The booster synchrotron is a combined function machine of the FODO type to provide maximum length of useful straight section. It too will contain 8 unit cells and the field on the equilibrium orbit will be 0.785 T. Each magnet will bend through an angle of $22\frac{1}{2}^{\circ}$ and will be curved. The bending radius is 2.546 m and the gaps in the central orbit between the individual laminated blocks reduced by inserting profiled, laminated steel packets, bonded to the nearest magnet block.

The repetition rate of the booster will be 10 Hz, but injection into the storage ring can be at any submultiple by appropriate pulsing of the gun. At 10 Hz it is calculated that both the dipole and sextupole fields due to eddy currents in the corrugated stainless steel vacuum vessel (wall thickness 0.2 mm) will be acceptably small.

The radio-frequency system

Since the beam loss due to synchrotron radiation at 2 GeV, 1A is 255 kW the r.f. system forms a major part of the storage ring equipment. Factors to be taken into account in the design of such a system are i) quantum lifetimes with implications in the choice of cavity voltage in the storage mode; and ii) stability of operating conditions with heavy beam loading. It is also necessary to limit the synchrotron oscillation frequency, particularly at injection.

The radiated beam power will be increased by about 10% if two "wigglers" are added (without reducing the beam current). The total power requirement will therefore be around 400 kW. It is judged prudent not to exceed 50 kW per cavity window, so that there will be 8 separate single cell cavities. In order to maintain the low shunt impedance (10-15 MΩ) required from stability and beam loading considerations at an acceptable peak voltage, the unconventional technique of fabricating the cavities from stainless steel will be adopted, although this increases the difficulty of achieving a high coupling factor to the feeder waveguide. The cavity frequency is not finally decided but will be either 428 MHz or 499 MHz depending mainly on economic considerations relating to r.f. power sources.

For resistive matching the coupling β is $1 + P_b/P_c$ where P_b is the radiated power and P_c is the power dissipated in the cavities. Reactive compensation of the beam loading induced voltage is obtained by detuning the cavity by an amount

$$\Delta f = \frac{f_o I_o \cos \phi_s ZT^2 \ell}{2Q_o V_{ep}} = \frac{f_o P_b \cot \phi_s}{2Q_o P_c}$$

where I_o is the mean beam current, V_{ep} is the effective peak cavity voltage, $ZT^2\ell$ is the total transit time corrected shunt impedance and ϕ_s is the phase angle of the beam relative to the voltage zero.

Ideally the beam loaded cavity should present a match to the amplifier at all energies and beam currents. This can only be achieved if both the cavity tuning and the coupling factor are varied and it is hoped to go some way towards achieving this. It is necessary to work with a system stable in the presence of coherent synchrotron oscillations. To ensure this the 'stability factor' δ must be less than unity. For the resistively matched system $\delta = 1/(1 + 2P_c/P_b)$ which is always less than one if there are cavity losses. If the beam loaded cavity is not resistive then the more general expression for stability is

$$1 + \tan 2\psi - \frac{I \tan \psi \, ZT^2 \ell}{(1 + \beta) V_{ep} \cos \phi} > 0$$

where ψ is the detuning angle. It may be noted that stability is aided by over coupling (high β) and by detuning to a higher frequency (high tan $) than would give exact compensation.

At injection (600 MeV) the beam builds up in small increments to 1A. The beam power is low so stability is easy to achieve. However the beam induced voltage is high and a large cavity detuning must be used. To keep this to a reasonable amount a high cavity voltage must also be employed, with due regard, however, to the frequency and amplitude of the synchrotron oscillations.

On accelerating to 2 GeV the radiated power increases. It is proposed to vary the voltage, the coupling and the detuning during acceleration and fig.3 shows a suitable programme.

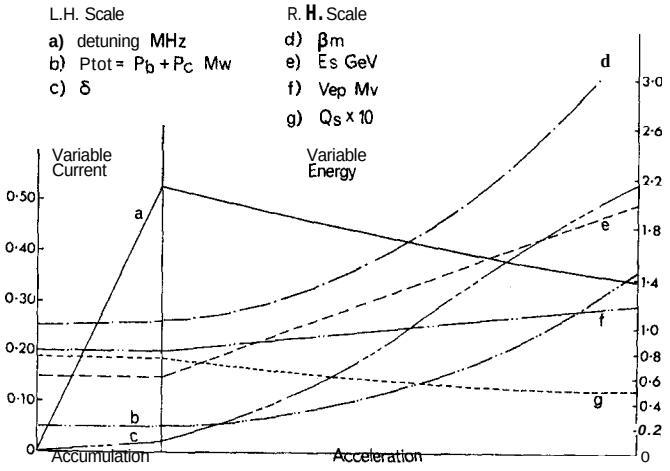

Fig. 3. R.f. parameters

Other Design Features

Vacuum. The high value of radiated power in the storage ring (255 kW excluding wiggler losses) dictates a well-cooled vacuum chamber. Because of the large number of branches, ease of fabrication of complex shapes is essential and stainless steel will be used. Because of lifetime considerations, the emphasis will be on a clean bakeable vacuum system, giving a pressure of 10^{-9} torr at full beam current. There will be differential pumping between the storage ring and each experimental beam line, and in the transfer path from the booster synchrotron. There will be distributed ion-pumping in the dipole magnets giving at least 1000 ℓ/s pumping speed per dipole.

Radiation. Personnel safety presents a problem in that the users must be able to set up equipment whilst a beam is circulating, and be in close proximity to their equipment whilst data-taking. Radiation levels around a storage ring are inherently low except whilst filling, at which time the building will be evacuated. By using scrapers and an emergency beam dump it can be arranged that most of the beam is lost in pre-determined areas which are adequately shielded. The remainder of the ring will have a modest shield wall of lead, iron or concrete, and the vacuum chamber will be designed to prevent high energy photons from going down the beam lines to experiments.

Single Bunch Operation. This will be required by experimenters interested in measurement of lifetimes of excited states. It will provide 300 ns between pulses. It will require a low frequency chopper to inject a short burst of pulses into the synchrotron, followed by a higher frequency device (∿ 35 MHz) to reduce this to a single bunch. Using a suitable synchronizer to trigger the extraction system, a single bunch will be stacked in the storage ring.

Controls. The whole machine complex will be controlled through a network of computers. At the lowest level, three minicomputers, one each for linac, booster synchrotron and storage ring, will be interfaced to the plant via CAMAC. All local controls will operate via these to permit independent testing of the three accelerators. These minicomputers will be connected via parallel data links to a more powerful machine forming the central control facility. This machine will contain the main database for the system, and will support two identical control consoles, aided by a fourth minicomputer. It will also be linked to an on-line task in the Daresbury central computer, an IBM 370/165, which will make very powerful computation facilities available

on-line for accelerator physics work.

The Wavelength Shifter or "Wiggler"

To accommodate the small number of users who require radiation between 0.1 Å and 0.8 Å it is intended to insert "wiggler" magnets[1,2] into straight sections in the storage ring lattice. In view of the development of superconducting technology it is certainly feasible to provide a sufficiently high field over the full aperture. The use of large numbers of poles in these magnets to enhance the radiation intensity is undesirable because of the large increase in r.f. power required. Use of a small number of poles with the highest fields practicable is to be preferred, as this benefits the user at short wavelengths most economically. It is therefore intended initially to use only three poles in each wiggler magnet and to design for a peak field of 5 T. Recent improvements in superconducting coil design indicate that fields in excess of 6 T may eventually be realised, and this will enhance the intensity at 0.1 Å by an order of magnitude. Design work on a superconducting wiggler magnet is proceeding at the Rutherford Laboratory of the Science Research Council. These magnets will be full aperture so as not to affect injection or beam lifetime, but will only be energized after the beam has been stored and accelerated.

Installation

The layout (fig.4) has been chosen with three things in mind - to provide for many experiments with good access, to allow the maximum amount of installation to proceed prior to the cessation of high-energy physics using NINA, and to minimise civil engineering work. All these points result in the storage ring being placed approximately centrally in the "Inner Hall" of the NINA building. At least one quarter of the ring can be constructed without interfering with the operation of NINA. Reduction of the high energy physics experimental areas from five to three will release sufficient space to build the injector (perhaps without all its shielding), and at the same time other space will become available for controls and for some of the ancillary plant before NINA closes down.

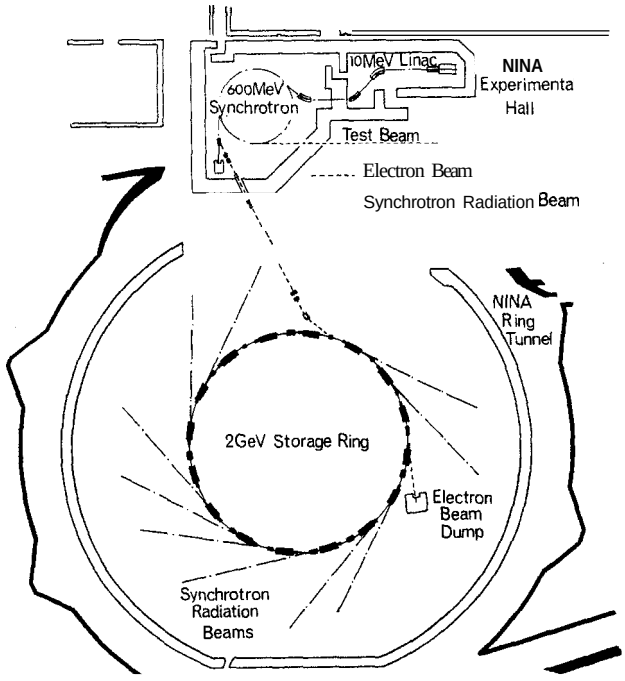

Fig.4. Layout

Parameter List

Injector

Energy	10-15 MeV
Energy spread (maximum)	± 0.5%
Emittance (maximum)	10^{-5} m-r
Current (within above limits)	20 mA

Booster Synchrotron

Peak energy	600 MeV
current	20 mA (∿ 10^{10} e-/pulse)
Peak magnetic field on orbit	0.785 T
Bending radius	2.546 m
Mean orbit radius	5.02 m
Betatron Q-value, both planes	2.25
Period structure	FODŌ (Comb. Func. Lattice)
No. of periods	8
Field index in F-sector	-5.2
Field index in D-sector	6.2
Field gradient in F	2.04% per cm
Field gradient in D	2.44% per cm
Magnetic length of sector magnet	1.0 m
Aperture	120x35 mm (approx.)
Repetition rate	10 Hz
R.f, frequency	428 MHz or 499 MHz
R.f. power	< 1 kW peak

Storage Ring

Energy	2 GeV
Characteristic wavelength	3.88 Å
Maximum current	1 A (∿ 2 x 10^{12} e- stored)
Beam lifetime at maximum current	8 hours
Peak magnetic field	1.2 T
Bending radius	5.55 m
Mean orbit radius	15.05 m
Betatron Q-value (either plane)	2.0 - 3.5
Peak quadrupole gradient	4.5 T/m
Period structure	FBODBO (Sep. Func. Lattice)
No. of periods	8
Dipole magnetic length	2.18 m
Quadrupole magnetic length	0.5 m
No. of sextupoles/period	2
Clear length of straight section	2.3 m (approx.)
Good field aperture	150x40 mm (approx.)
Maximum pressure with 1A beam	torr
Vacuum chamber aperture	200 x 45 mm
Distributed pumping capacity/dipole	1000 l/s
Radiation damping time, 600 MeV	440 ms (radial betatron)
Touschek lifetime, at 600 MeV	50 min
Radiation loss from normal dipoles, at 2 GeV	255 keV/turn
R.f. frequency	428 MHz or 499 MHz
Total r.f. power	∿ 400 kW
No. of cavities	8
Cavity material	Stainless steel
Cavity shunt impedance (transit time corrected)	1.25 to 2.0
Q_s	∿ 0.05

Programme

The official design study of the dedicated Synchrotron Radiation Source will be complete by the end of 1974. It is expected to show that the capital cost will be about £2M (1973 prices). Approval for construction will then be sought, and if the present ideas for the NINA programme turn out to be correct, the SRS

will come into operation during 1979.

References

1. W.S. Trzeciak. "A "wavelength shifter" for the University of Wisconsin electron storage ring". IEEE Trans. Nucl. Sci. NS-18, (1971) 213.

2. R.J. Averill, R.D. Hays and H. Mieras. "Wiggler magnet design". CEAL-TM-199 (January 1973).

3. V.P. Suller. "Comparative Synchrotron Radiation Spectra". Daresbuq Laboratory Internal Report, DL/TM 118 (December 1973).

4. N. Marks and M.W. Poole. "The choice of dipole magnetic field for the SRS". Daresbuq Laboratory Internal Report to be published.

THE STANFORD SYNCHROTRON RADIATION PROJECT (SSRP)†

H. Winick
Stanford University
Stanford, California 94305

Summary

The Stanford Synchrotron Radiation Project is a new national facility for UV and X-ray research using synchrotron radiation from the storage ring SPEAR. This ring now operates in colliding beam mode with E (stored beam energy) varying from 1.5 to 2.5 GeV and with 15 to 45 mA in each beam. Improvements in mid-1974 will raise the energy to $\gtrsim$ 4 GeV with expected currents of up to 100 mA in each beam. The critical energy of the synchrotron radiation spectrum varies as E^3 and is 11 keV for E = 4 GeV. Up to seven experiments can share a beam run which accepts 11.5 mrad of radiation. The UV and soft x-radiation are deflected at grazing incidence on ultrasmooth platinum plated copper blocks and focused on custom built, high vacuum, high resolution monochromators. X-radiation above about 3.5 keV emerges from a 630μ thick beryllium window assembly. Sensors in the beam run detect high pressure or contamination and cause valves to close isolating the beam runs from each other and from the SPEAR vacuum system. Shielding and interlocks permit experimenters to adjust their equipment with beam shutters closed and to be within about 1 m of their equipment during operation with shutters open. A broad ranging program of research will be pursued including studies of UV and x-ray photo-electron spectroscopy, extended x-ray absorption edge fine structure, x-ray diffraction on biology systems, compton scattering, x-ray absorption x-ray induced luminescence, sub-nanosecond time constant measurements on solids, and UV reflectivity.

Introduction

SSRP utilizes synchrotron radiation from circulating electrons in the storage ring SPEAR. SSRP has been funded since June 1973 by the National Science Foundation and is administered by the W. W. Hansen Laboratories of Physics at Stanford University. SPEAR is a high energy electron-positron colliding beam storage ring located at the Stanford Linear Accelerator Center (SLAC), funded by the Atomic Energy Commission. Prospective users of SSRP should contact the Director, Professor S. Doniach or the Deputy Director, Professor W. Spicer, at the W. W. Hansen Laboratories of Physics.

SSRP is open to **all** qualified users. Experimental proposals are reviewed by the Director, advised by a Proposal Review Panel, outside referees, and the SSRP staff. Early submission of proposals is recommended. **SLAC** exercises control over radiation safety and also sets vacuum standards for experiments which will connect on-line to the SPEAR Vacuum System.

Characteristics of SPEAR

Some basic synchrotron radiation relationships are given in Table I. Additional synchrotron adiation relationships are given by Rowel and Winick.[1] The storage ring SPEAR has been described in the literature.[3] The particular parameters of SPEAR that are relevant to synchrotron radiation are listed in Table II. The spectral distribution of the radiation is shown in Fig. 1. The data given in Table II and Fig. 1 are obtained using the result of Mack.[4] SPEAR has a bending radius of 12.7 m The radiation is highly polarized with the E vector in the plane of the acceleration.

BASIC SYNCHROTRON RADIATION RELATIONSHIPS

ELECTRON ENERGY:	**E (GeV)**
RADIUS OF CURVATURE:	**R (METERS)**
ELECTRON CURRENT:	**I (AMPERES)**

$$\frac{\Delta E}{\text{TURN-ELECTRON}} = 88\frac{E^4}{R}\ (\text{keV});\quad \epsilon_c = 2.2\frac{E^3}{R}\ (\text{keV})$$

$$\text{TOTAL RADIATED POWER} = 88\frac{E^4}{R} \times I\ (\text{kW})$$

$$\text{EMISSION ANGLE} \approx \frac{1}{\gamma} = \frac{mc^2}{E} = 2 \times 10^{-4} \text{ at } 2.5 \text{ GeV}$$

$$\frac{N_\gamma}{\text{TURN-ELECTRON}} \approx \frac{\Delta E/\text{TURN-ELECTRON}}{\epsilon_c} = 40E$$

TABLE I

SPEAR now operates for colliding beam experiments with one RF bunch per beam at energies up to 2.5 GeV per beam (limited by RF voltage). The current is limited by the maximum allowable incoherent tune shift ($\Delta\nu \approx .05$) due to beam-beam interaction. This limit increases with increasing energy. With the present SPEAR operational configuration, the currents corresponding to this limit are shown in Table II. Machine studies on SPEAR are in progress to increase the beam cross-section at the interaction point so that larger currents and larger interaction rates (luminosity) can be achieved, especially at the lower energies. Larger currents can of course be stored in a single beam (over 200 mA has been stored in one electron bunch and even more is possible if more of the 40 RF bunches are filled) but present plans call for synchrotron radiation operation only during colliding beam experimental runs. The water-cooling of the SPEAR vacuum chamber is adequate for synchrotron radiation losses of up to 150 kW per beam.

The beam decays with a lifetime that depends on

†Supported by National Science Foundation Grant No. GH 39525, in cooperation with the Stanford Linear Accelerator Center and the Atomic Energy Commission.

energy and current. At 2.5 GeV the lifetime is 2 hours with 45 mA in each beam and increases to 4 hours with 30 mA per beam. Typically it takes 15 to 30 minutes to fill SPEAR with 2 beams, following which beams are stored and made to collide for several hours, after which the cycle is repeated.

PARAMETERS OF SPEAR

	UNTIL 7/74			AFTER 11/74			
ACCELERATING FREQ. (MHz)	51			358			
PULSE DURATION (10^{-10} sec) (FWHM)	8 to 16			1 *to* 2.4			
ORBITAL FREQ. (MHz)	1.28			1.28			
E_e (GeV)	1.5	2.0	2.5	3.0	3.5	4.0	4.5
I_e (mA)	20	25	45	*50*	75	75	45
RADIATION LOSS (kW)	0.70	2.8	12	28	78	135	130
ϵ_c (keV)	0.58	1.4	2.7	4.7	7.4	11	15.7

TRANSVERSE ELECTRON BEAM SIZE AND DIVERGENCE AT SYNCHROTRON RADIATION SOURCE POINT (TYPICAL AT 2.5 GeV)

	x (mm)	x'(mrad)	y (mm)	y'(mrad)
FWHM	3.22	0.566	1.59	0.266

TABLE II

During the summer of 1974 the magnet power supplies and the RF system will be modified to permit beam storage up to 4.2 GeV or more. The new RF system will produce 500 kW at 358 MHz. The present RF system produces 160 kW at 51 MHz. Higher colliding beam currents are possible at the higher energies reaching an expected peak of 100 mA at 3.8 GeV. Above 3.8 GeV the expected beam current falls off due to RF voltage limits. In addition to the dramatic improvement the higher currents and energy will make in synchrotron radiation power and critical energy, ϵ_c, as shown in Table II, the higher frequency will reduce the synchrotron radiation light pulse to $\sim 10^{-10}$ sec making possible experiments requiring fast time correlations.

Plan of the Synchrotron Radiation Facility

A prefabricated steel building 12 m wide, 24 m long and 7.3 m high has been constructed adjacent to SPEAR as shown in Fig. 2 and Fig. 3. The building is well insulated and temperature controlled and has a thick (30 cm) concrete floor for stability. Vibration sources (such as compressors) are located outside the building and decoupled from the building and floor.

About 11.5 mradians of synchrotron radiation, corresponding to 15 cm of curved path in a SPEAR bending magnet, emerges tangentially into a high vacuum pipe. This horizontal fan of radiation is split three ways by reflection at grazing incidence on two remotely movable ultra-smooth platinum-plated copper blocks[5] placed 6.5 m from the source point. One of these mirrors intercepts the outer 2 mrad of synchrotron radiation at a horizontal grazing angle of incidence of 2° resulting in a horizontally focused 4° deflected beam containing photons with energy up to about 2 keV. A plane mirror intercepts the inner 3 to 6 mrad at a vertical grazing angle of incidence of 4° causing the beam to rise at 8° from the median plane. This rising beam contains photons up to 300 eV. Since SPEAR can produce up to 25 W of synchrotron radiation per mrad these mirrors are cooled thermoelectrically.

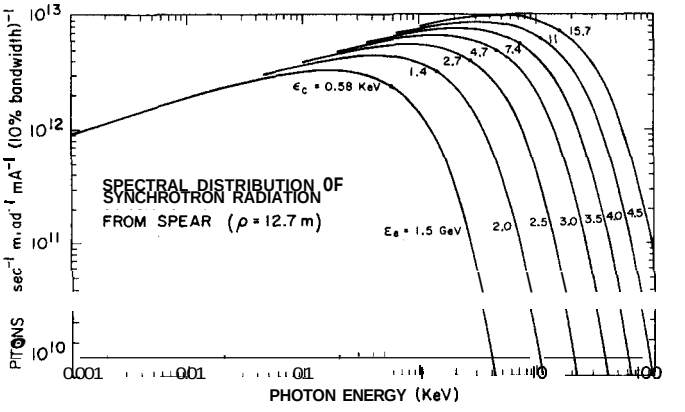

Figure 1

The central part of the beam contains 3 to 10 mrad of radiation which is not deflected by mirrors. This radiation proceeds down the high vacuum beam pipe, passes through a pair of water-cooled 65μ thick beryllium foils and exits from the vacuum system 10.5 m from the source point through a pair of 250μ beryllium windows. Significant transmission begins at about 3.2 keV. This window system has been used successfully over extended running periods with SPEAR operating at 2.4 GeV with currents up to 50 mA. In-vacuum water-cooled carbon foils[6] are being considered to handle the higher power densities that will be present when SPEAR operates at higher energy.

After emerging from the SPEAR vacuum system the x-rays travel in a helium atmosphere into a shielded area in which several crystal monochromators and experiments will be installed. Some of these direct the monochromatic radiation upwards to an upper level experimental area as shown in Fig. 3 and Fig. 4.

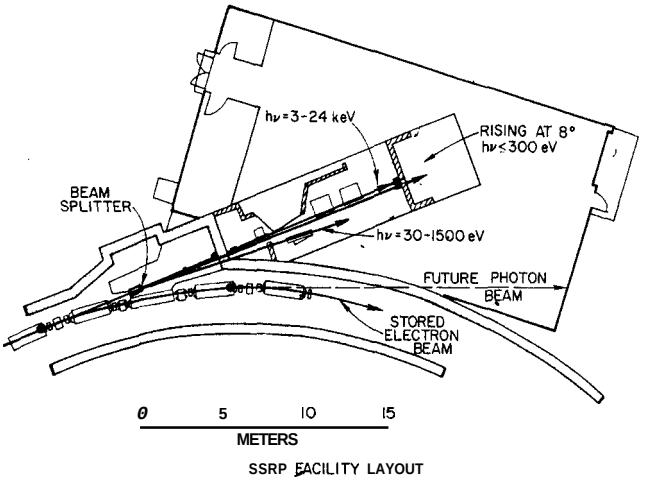

Figure 2

An elevated concrete slab 4.5 m wide, 12 m long, and 2.4 m above the floor serves as a second level for installing experimental apparatus. The rising 8° beam line vacuum pipe penetrates this slab as shown in Fig. 3. Electrical services, compressed air, helium and water services are installed at several locations along the perimeter of the slab. Vacuum controls, radiation protection controls, and signals to and from the SPEAR and SLAC control rooms are centralized in an adjacent control room.

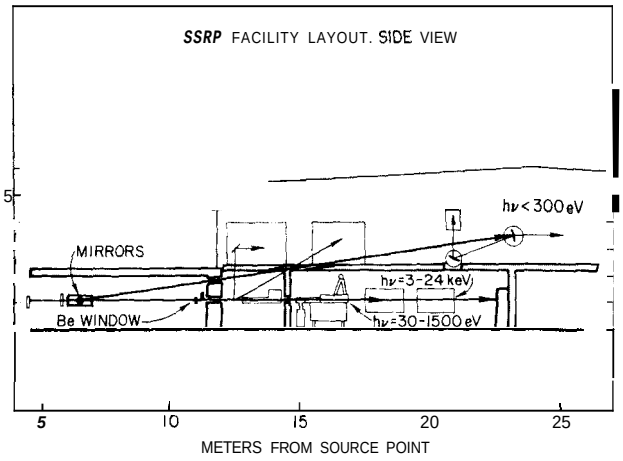

Figure 3

The synchrotron radiation beam can be independently steered so that it can be reproduced spatially, correcting for variations that may occur from run to run, or variations that may be required for positioning the two colliding beam interaction points. This is accomplished by powering steering coils some of which are arranged in pairs to produce local orbit distortions (beam bumps) in the vicinity of the synchrotron radiation source point.

Vacuum System

The vacuum system is built to SLAC specifications[7] and is all metal and bakable. The central beam pipe extends to 10.5 m from the source terminating at the beryllium window assembly within the SPEAR tunnel. The 4° and 8° beam runs continue in vacuum in the synchrotron radiation building and extend to 16 m and 23 m from the source point.

All metal ultra-high vacuum gate valves isolate the beam runs from each other and from the SPEAR vacuum system. Synchrotron radiation strikes only water-cooled surfaces and movable water-cooled absorbers may be remotely inserted to block the radiation.

Ionization gauges and fast sensors[8] are used to detect leaks and desorption diodes[9] sense contamination. These devices are monitored by a vacuum control system which causes valves to close automatically in the event of vacuum problems. Fast isolation from SPEAR is provided by a vane which closes in 30 msec.[10]

Radiation Protection System

A system of beam stoppers, a permanent magnet, radiation monitors and interlocked gates is installed to protect personnel from exposure to synchrotron radiation or the high energy radiation that could result in the worse case event that injected or stored beams are lost in SPEAR in certain critical allocations. With appropriate beam stoppers closed, occupancy is safe in the immediate vicinity of experiments during all phases of SPEAR operation. With beam stoppers open experimenters are able to occupy areas within about 1 m of beam lines. Access to the SPEAR tunnel and to the primary x-ray beam line in the SSRP building is remotely controlled by SLAC operators. Access to small secondary beam areas is experimenter controlled.

Status of the Project

At this writing (April 1974) a pilot project beam run has been in operation since July, 1973, providing radiation to an x-ray photo-electron spectroscopy (XPS) experiment and an extended x-ray absorption fine structure (EXAFS) experiment. This equipment is now being removed and the full facility with all beam runs, control systems, personnel protection systems, shielding, etc., is being installed. Operation with five experiments is planned for May and June, 1974. Following this the SPEAR ring will be down for several months for the improvement program which will allow storage of beams with energy in excess of 4 GeV. Some synchrotron radiation should be available in the latter part of 1974 and routine operation for colliding beam and synchrotron radiation experiments is scheduled to commence in late 1974 or early 1975.

Experimental Program

X-ray Beam Line (hν > 3 keV)

Several different groups will set up spectrometers using the x-rays available in the main beam line. The activities in this beam line include:

X-ray Photo-Electron Spectroscopy (XPS). A 3-crystal monochromator designed to produce intense radiation at 8.0 keV with a bandwidth of 0.1 eV has been built by P. Pianetta of Stanford and has been operated in a double crystal configuration. A high vacuum sample chamber and electron energy analyzer built by I. Lindau of Stanford is also complete. The equipment was used in a pilot project x-ray beam and has produced its first data on the 4f levels of metallic gold.[11] A broad-ranging program of research in the fields of solid state materials science, inorganic and organic chemistry will be led by W. Spicer, I. Lindau and S. Doniach of Stanford.

Extended X-ray Absorption Fine Structure (EXAFS). Initially one EXAFS channel-cut single crystal x-ray spectrometer with associated detectors and data processing equipment is being assembled. Several investigators (including A. Bienenstock, S. Doniach, S. Hunter, B. Kincaid, and M. Weissbluth of Stanford, D. Sayers and E. Stern of the University of Washington, F. Lytle of the Boeing Aerospace Company and P. Eisenberger of the Bell Telephone Research Laboratories) will use EXAFS studies to determine the radial structure functions associated with specific elemental constituents in a variety of complex materials including gases, liquids, glasses and certain complex crystalline materials in which the environment of one particular kind of atom is important; e.g., the iron atom in hemoglobin.

X-ray Diffraction. A group from the California Institute of Technology (J. Baldeschweiler, R. Stroud, and N. Webb) are building a focusing monochromator with low angle diffraction camera for x-ray diffraction studies of biological systems including time dependent diffraction. Samples to be studied include proteins, enzymes, muscle, and membrane systems.

A group consisting of K. Hodgson and E. Shooter of Stanford and L. Jensen of the University of Washington,

Seattle, are proposing to install a diffractometer at the focus of the monochromator to do structural studies on protein single crystals.

Compton Scattering. P. Eisenberger of the Bell Telephone Research Laboratories is planning to build a triple axis monochromator - energy analyzer system to measure x-ray inelastic scattering. This is planned for use in SPEAR II (early 1975). Among other measurements that of the Comptonprofile in solids and molecular systems gives very detailed information aboutelectronic charge distributions which can be used to test specific theories of chemical bonding.

4° Beam Line ($25 < h\nu < 2500$ eV). A flexible facility, entered around a specially designed grazing incidence monochromator with a fixed exit slit, will be set up in this beam line under the direction of F. C. Brown, R. Bachrach, and S. Hagstrom of the Xerox Research Center at Palo Alto and Stanford University. A beam splitting mirror will provide about 2 mrad to this line, focused in the horizontal direction. Research on this beam line will include studies on high resolution soft x-ray absorption spectroscopy, x-ray induced luminescence, photo-emission spectroscopy by time of flight measurement and subnanosecond time constant measurements on solids.

8° Rising Beam Line ($h\nu < 300$ eV). A specially adapted ultra-high vacuum normal incidence monochromator for this energy range is now being built by the McPherson Company under subcontract from China Lake for installation in the beam run. A group from the Michelson Laboratory at China Lake, led by V. Rehn (others include A. Baer, T. Donovan, D. Kyser, and J. Stanford), in collaboration with a Stanford group, will make reflectivity and photo-emission measurements. Differential reflectivity (electro- and piezo-reflectance) measurements are being planned.

Acknowledgments

The dedication of the SSRP staff, R. Dannemiller, A. Golde, and B. Salsburg, together with Mark Baldwin of SLAC, has been vital to the progress of this project. Invaluable assistance has Seen received from many others at SLAC, particularly R. Baker, W. Basinger, M. Beck, R. Filippi, G. Fischer, A. Gallagher, F. Generali, F. Hall, J. Harris, E. Hoyt, B. Humphrey, J. Jurow, R. Larsen, R. Melen, J. Miljan, R. Messimer, W. Milner, H. Morales, J. Paterson, J. Pope, W. Porter, R. Robbers, W. Savage, T. Taylor, A. Tseng, G. Warren, and J. Wehner, The beam line vacuum system was drawn with meticulous care by F. Johnson. Our debt is particularly great to N. Dean for the genuine interest, guidance and support he provided.

References

1. Ednor M. Rowe, IEEE Trans. Nucl. Sci. NS-20, NO. 3, p. 973, June 1973.
2. Herman Winick, IEEE Trans. Nucl. Sci. NS-20, NO. 3, p. 984, June 1973.
3. J. M. Paterson, Proc. of this Conference. *Also* B. Richter, Proc. of 1973 Particle Accel. Conf., San Francisco. IEEE Trans. on Nucl. Sci. NS-20, No. 3, p. 752, June 1973.
4. R. A. Mack, Spectral and Angular Distribution of Synchrotron Radiation, CEAL-1027 (1966).
5. S. Holmes, A. Klugman, and P. Kraatz: Applied Optics, 12, No. 8, p. 113, Aug. 1973.
6. E. W. Hoyt and P. Pianetta, SLAC TN-73-10, Sept. 1973.
7. M. Baldwin and J. Pope, SLAC TN-73-13, Oct. 1973.
8. G. W. McClure, Appl. Phys. L 2, No. 12, p. 233, (1963).
9. E. Garwin, E. Hoyt, J. Jurow, M. Rabinowitz, Proc. 4th International Vacuum Congress, Apr. 1968, Manchester, England.
10. This fast closing vane is of the type used on the ISR at CERN and was kindly supplied to us by CERN.
11. I. Lindau, P. Pianetta, S. Doniach and W. Spicer, X-ray Photo-Emission Spectroscopy at the Stanford Synchrotron Radiation Project. Accepted for publication in Nature.

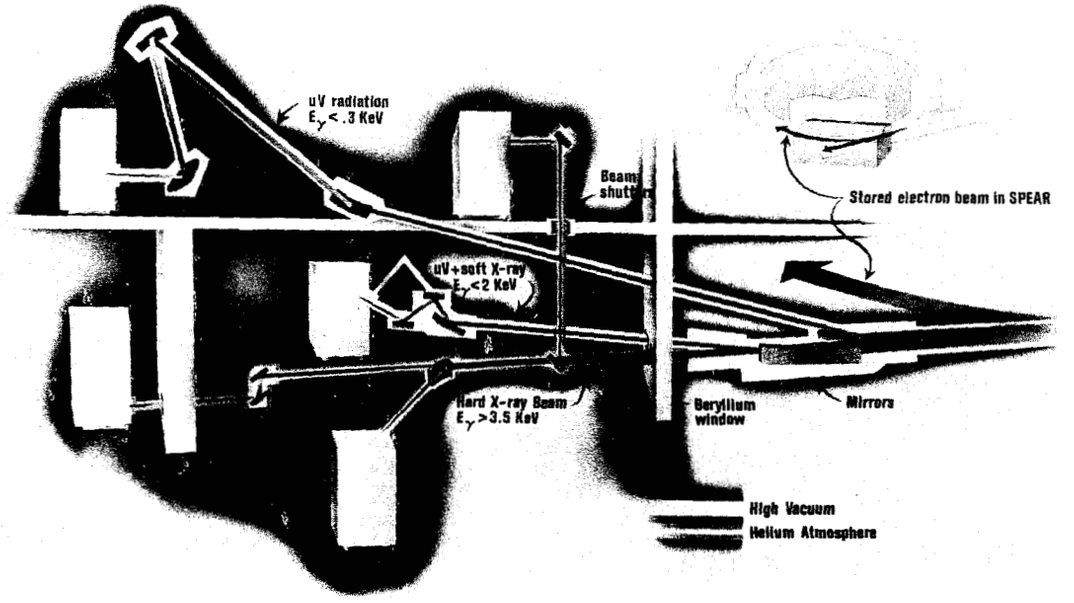

Figure 4

THE CONVERSIONOFTHE NBS 180 MEV ELECTRON SYNCHROTRON TO A 240 MEV ELECTRON STORAGE RING FOR SYNCHROTRON RADIATION RESEARCH

E. M. Rowe, M. A. Green, W. S. Trzeciak, and W. R. Winter, Jr.
Physical Sciences Laboratory - University of Wisconsin
Stoughton, Wisconsin

Introduction

The National Bureau of Standards 180 MeV electron synchrotron was used for the first investigations of the optical and electronic properties of solids, liquids, and gases utilizing synchrotron radiation1. Since the time of this pioneering work, other sources of far greater brightness such as DESY, the Tokyo Synchrotron, and Tantalus I have come into use as synchrotron radiation sources. Thus several years ago, it became evident that in order to maintain a viable vacuum ultraviolet and soft x-ray research program at the NBS utilizing this machine as a synchrotron radiation source a considerable increase in source brightness would be necessary.

Two alternatives were considered. The first of these was to increase the beam brightness through a hundredfold increase in beam current, from 1 mA to 100 mA, by means of a new injector operating at 6 MeV. The machine would have remained a synchrotron and, hence, the duty factor would remain unchanged, i.e. no more than 0.2 assuming that useful synchrotron radiation is produced only at electron energies between 150 and 180 MeV and sinusoidal magnet excitation. The beam cross section area would have been 3π mm^2 at an absolute minimum at full energy and current because only adiabatic damping could occur in this mode of operation.

Operation of the synchrotron as an electron storage ring was then considered. In this mode of operation a beam cross sectional area of less than 0.65π mm^2 could be expected after damping, and the duty factor would be 1.0. A brightness figure of merit, defined by $S = ID/A$, where I is the beam current, D is the duty factor, and A is the electron beam cross sectional area, can be used to compare the two alternatives. Taking a circulating current of 10 mA, and the storage mode duty factor of 1, gives a value for $S = 1.54$ mA/mm^2. A similar calculation for synchrotron operation at 100 mA circulating yields $S = 2.1$ mA/mm^2. Thus, 10 mA at 180 MeV, which represents minimal operation of the machine as a storage ring, would give about the same brightness as synchrotron operation at a very high beam current. Further, whereas 100 mA operation of the machine as a synchrotron is the best that could be expected, operation of the machine as a storage ring would probably not be limited to beam currents of 10 mA. In addition, with relatively simple modifications, the machine energy could be raised, probably to as much as to 240 MeV, which would result in a considerable increase in the range and intensity of the synchrotron radiation spectrum. Finally, the storage mode of operation also offered 10^{-9} to 10^{-10} torr internal pressures and close access to the machine by the investigators; that is right up to the vacuum chamber. These are qualities of synchrotron radiation sources that have come to be expected by vacuum ultraviolet and soft x-ray experimentalists.[2] On the basis of these considerations, the decision was made to proceed with the conversion project.

I. Scope of the Conversion Project

During the study of the conversion project, it became clear that the only component of the original machine that could be preserved was the magnet. Other components such as the magnet coils, radio frequency system, magnet power supply and vacuum chamber could not be used in the converted machine.

Furthermore, the field index of the synchrotron magnet was greater than 3/4, a condition that leads to overdamping of the synchrotron motion and, therefore, antidamping of the radial motion[3]. Thus, besides a higher energy injector and injection system, the project required a vacuum chamber capable of supporting vacuua in the 10^{-9} - 10^{-10} range, a radio frequency system and accelerating cavity, magnet coils and magnet power supply and, finally, means for adjusting the field index of the magnet to a value below .75.

Interestingly, increasing the source brightness of the synchrotron by the first alternative would also have required a new vacuum chamber, accelerating cavity and magnet correction coils. Subsequently, investigation of the condition of the synchrotron indicated that the main magnet coils would also have to be replaced because of their advanced state of deterioration.

A plan view of the converted synchrotron is shown in Fig. 1, and operating parameters are given in Table I. In what follows, the components necessary for the conversion project will be described.

Table I

Converted Synchrotron Parameters

MAGNET	
Field Index	0.70
Radial Tune	0.54
Vertical Tune	0.83
Field at Injection	0.044T
Field at 180 (240) MeV	0.73 (1.0) T
Orbit Radius	0.84 M
Useful Radial Aperture	5.00 cm
Useful Vertical Aperture	2.50 cm
INJECTION	
Type	Multi-turn
Source	10 MeV Microtron
Inflector	Shorted Coaxial Line, 0.15 T, Nominal
Pulsed Field Bump	1.1×10^{-3} TM, Turning Off in 0.12 μsec
RF SYSTEM	
Frequency	113.6 MHz
Harmonic Number	2
Number of Cavities	1
Maximum Volts Per Turn	10 kV
Maximum Power Available	3 kW

Table I (cont'd.)

VACUUM SYSTEM	
Construction	Stainless Steel, Bakeable
Pumps	One 200 ℓ/sec Sputter Ion Holding Pump Plus Sixteen 50 Liter Sputter Ion Pump Elements Mounted Internally
Pressure (average, without beam)	5×10^{-10} Torr

II. Injector

Based on experience gained during the development of the 44 MeV microtron previously constructed at the Physical Sciences Laboratory as an injector for Tantalus I, the decision was made to employ a 10 MeV microtron as the injector for the converted synchrotron. The operating parameters of this machine are given in Table II.

Table II

Microtron Parameters

Accelerating Frequency	2.998	kmHz
Cavity Gradient	515	$kVcm^{-1}$
Repetition Rate	15–60	Hz
Energy Gain Per Turn	1	MeV
Number of Turns	10	
Beam Pulse Length	1	μsec
Pulse Beam Current	30	mA
Vertical Emittance	< 0.13	π mrad cm
Radial Emittance	< 1.1	π mrad cm

The microtron, shown in Fig. 2 with its beam transport line, is mounted vertically so as to present its small vertical emittance to the radial admittance of the converted synchrotron in order to simplify multi-turn injection. Pumping is supplied by four internally mounted sputter ion elements operating in the magnet fringe field. The base pressure achieved with this system is 3×10^{-8} torr.

Radio frequency power for the microtron is supplied by a two MW tunable magnetron (English Electric Valve Co. M5015) driven by a conventional storage line and thyratron modulator. The radio frequency system consists of the magnetron, a 25 db isolator, a remotely controlled attenuator and a dual 70 db directional coupler. The use of the attenuator allows adjustment of cavity excitation while the magnetron operates at fixed output power for frequency stability.

Electrons are supplied by a LaB_6 pellet 2 mm in diameter mounted in a tantalum support which is also the cathode heater. Cathodes, which have a lifetime of approximately 100 hours, can be replaced in less than one hour inclusive of the time required to achieve operating vacuua (10^{-6} torr) in the microtron.

The accelerating cavity is of cylindrical geometry and is constructed of OFHC copper. An unloaded Q of 11,000 was obtained for the cavity in spite of the fact that the front and back cover plates are simply bolted on. A cavity coupling coefficient of $\beta = 3.5$ permits pulse beam currents in excess of 50 mA.

Electrons are extracted from the microtron by means of a compensated iron channel on the tenth orbit with nearly 100% efficiency. The operation of this microtron is characterized by simplicity, reliability and, above all, stability.

III. Beam Transport System

The beam transport system consists of two quadrupole doublets, a beam stop mounted at the focus of the first doublet and a chopper positioned upstream from the beam stop. The chopper deflects the electron beam so as to miss a 5 mm aperture in the beam stop by means of a DC electric field. During injection a radio frequency electric field, synchronized with the storage ring radio frequency accelerating system, is superimposed on the DC field so that approximately 100 pulses of 2.5 nsec length pass through the beam stop aperture to the next doublet and, thence, to the inflector.

IV. Inflector and Pulse Bump System

In order to achieve the design circulating beam current, multi-turn injection will be carried out. The coaxial inflector produces a field of .15 T which is sufficient to bend the electrons through $\pi/4$ radians against the magnetic field of the storage ring and place them on an orbit 2 cm displaced outward from the central orbit. Excitation for the inflector is provided by a thyratron discharging a capacitor through a 48:1 low leakage inductance matching transformer. The current flowing through the inflector during the pulse is 7550 amperes. The current pulse is sinusoidal and its length is 50 psec.

Located diametrically opposite from the inflector is a pulsed magnetic bump capable of displacing the orbit by two cm at the inflector. During injection the bump is pulsed, displacing the orbit so as to be tangential to the inflector. During the decay of the bump field the orbit moves back to its unperturbed position. The time required for the bump field to decay is .12 μsec, during which time twelve beam pulses will be injected. Assuming 25% efficiency for injection and capture, stored beam currents of greater than 15 mA should be possible with a microtron beam current of 30 mA.

The bump field is produced by a thyratron discharging a two section energy storage line of 10Ω impedance through the bump inductance. A capacitor and a 10Ω resistor terminate the circuit and thus reflections are eliminated. Fig. 3 shows the bump structure and Fig. 4 shows the bump magnetic field as a function of time.

V. Vacuum System

In order to achieve the required 10^{-9} range pressures in the storage ring vacuum chamber an all stainless steel system is required. Space limitations in the magnet do not permit bellows, thus the chamber will be a rigid annulus of 1.66 meters mean diameter with a 20 cm × 9 cm rectangular cross section. Sixteen dual sputter ion pump elements will be mounted along the inner wall of the vacuum chamber to handle the synchrotron radiation induced outgassing under stored beam conditions.

To pass photon beams for the two research areas to be serviced by the storage ring, a total of eleven, 4 cm diameter ports, tangential to the central orbit, will be provided. As an aid to injection system adjustment, one of these ports will be positioned so as to allow observation of a BeO_2 scintillator plate which may be positioned by remote control, either directly in front of the inflector so

as to intercept the injected beam or further in so as to intercept the injected beam after one revolution.

VI. Radio Frequency System

The electron revolution frequency in the storage ring is 56.8 MHz. In order that the accelerating cavity, which must be mounted internal to the vacuum chamber, not take up an unduly large portion of the circumference of the vacuum chamber, second harmonic operation of the accelerating system has been chosen. The accelerating cavity, which is a $\lambda/4$ coaxial resonator, is constructed of OFHC copper and exhibits an unloaded Q in excess of 2000. Provisions for cavity tuning by means of a remotely controlled capacitance probe near the accelerating gap have been included and the cavity is water-cooled. The cavity is also shown in Fig. 3.

The power amplifier is a conventional push-pull tetrode amplifier capable of 3 kW output. This is sufficient power to drive the accelerating cavity to voltages in excess of 10 kV. At a beam energy loss of approximately 350 eV per turn at 240 MeV this accelerating potential will insure adequate lifetime against quantum fluctuations and Touschek effect. Beam loading of the cavity at currents as high as 100 mA are not expected to be a problem.

VII. Magnet Correction Coils

To reduce the field index of the synchrotron magnet to a value below 3/4, four pair of coils will be mounted on the magnet pole faces. These coils will be energized independently to maintain a field index of 0.70 over the whole range of magnet excitation. The maximum MMF required of any of the compensating coils is 3000 ampere turns; however, field measurements indicate that at fields greater than about .8 T the current flow in the coils must reverse due to saturation effects in the magnet. Since the rate of rise of the magnet field between injection and full energy will be rather low (0.1 T sec^{-1}), a system utilizing relays rather than bipolar supplies will be used to reverse the polarity of the compensating coils.

Excitation of the compensating coils will be controlled by signals derived from the magnet current.

VIII. Main Magnet Coils and Power Supply

At an energy of 180 MeV the synchrotron magnetic field was at the central orbit .73 T. Since the original coils could not operate continuously at the excitation necessary to produce this field, new field coils were necessary. Because of this and because compensating coils to control the field index were also required, the decision was made to construct field coils capable of operating at an excitation sufficient to produce a field of 1.2 T at the central orbit. Thus, the maximum energy that will actually be reached by the converted synchrotron will depend on the capability of the compensating coils to control the field index.

The magnet coils are excited by an SCR controlled, current regulated power supply. Peak voltage and current ratings of this supply are 1250 amperes at 400 volts. Long term current regulation of the supply is ± 0.01% against line and load fluctuations combined. The control signals for the magnet power supply are generated by digital techniques, thus computer control of the converted synchrotron will be possible.

IX. Current Status of the Conversion Project

The 10 MeV microtron and most of the electron beam transport system are complete and have been tested. The main magnet coils and the compensating coils are also complete. The vacuum chamber and radio frequency accelerating system are under construction. Installation at the National Bureau of Standards of the major components of the converted synchrotron is scheduled to begin in June 1974.

References

1. Madden, R. P. and Codling, K., New Autoionizing Atomic Energy Levels in He, Ne, and Ar, Phys. Rev. Letters, 10, 516 (1963).

2. Rowe, E. M. and Mills, F. E., Tantalus I: A Dedicated Storage Ring Synchrotron Radiation Source, Particle Accelerators 1973, Vol. 4, pp. 211–227.

3. Bruck, H., Accélérateurs Circulaires de Particules, Presses Universitaires de France, 1966, Chap. 24.

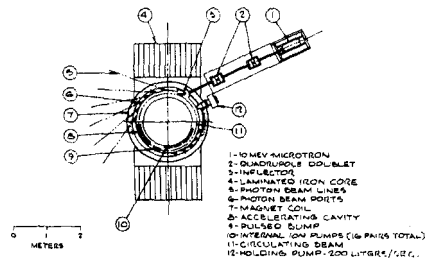

FIG. 1--Plan view of converted synchrotron,

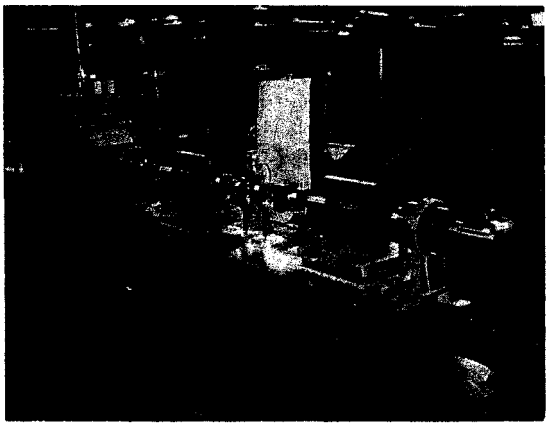

FIG. 2--10 MeV Microtron and beam transport line. Units shown are (from left to right) microtron, steering magnet, chopper, quadrupole doublet, beam stop, beam current monitor transformer, quadrupole doublet and steering magnet.

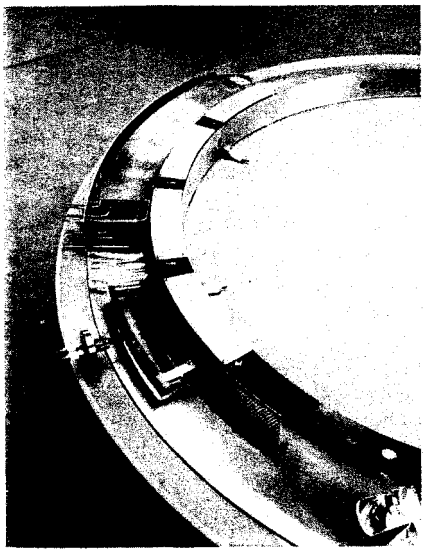

FIG. 3--Section of vacuum chamber during construction showing pulse bump, internal sputter-ion pump elements and radio frequency accelerating cavity.

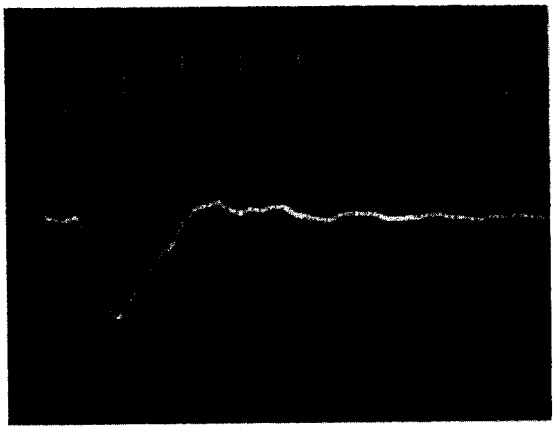

FIG. 4--Pulse bump magnetic field as a function of time. Sweep speed 10^{-7} sec cm^{-1}.

LIST OF PARTICIPANTS BY COUNTRY

AUSTRIA
CERN
Werner Kubischta

International Atomic Energy Agency
Alexander V. Shalnov

CANADA
University of British Columbia
Michael K. Craddock
Bruce L. White

Atomic Energy of Canada, Limited
J.A. Hulbert
Carl H. Westcott

McGill University
Robert B. Moore

University of Saskatchewan
Leon Katz
Roger Servranckx

CERN
James V. Allaby
Frank Beck
Philippe Bernard
Roy Billinge
M. Hildred Blewett
Franco Bonaudi
Michael Crowley-Milling
Fritz Ferger
Hans Fischer
Jacques Gareyte
Werner Hardt
Mervyn Hine
J. Trevor Hyman
Willibald Jentschke
Kjell Johnsen
Eberhard Keil
Herbert Lengeler
Ernest G. Michaelis
Boris Milman
Karl H. Reich
Lorenzo Resegotti
Frank Sacherer
Karl Heinz Schindl
Wolfgang Schnell
Brian Southworth
Peter Wolstenholme

FRANCE
Institute National De Physique
Andre Chabert
Jean Yoccoz

Universite Paris-Sud, Centre D'Orsay
Paul Brunet
Jean Buon
Pierre Lehmann
Marie Paule Level
Pierre Marin
Henri Zyngier

Centre D'Etudes Nucleaires De Saclay
Gaston Bronca
Henri Bruck
Jean Faure
Maurice Gouttefangeas
Marcel Jablonka
Jean-Louis Laclare
Jean-Marie Lefebvre
Francis Netter

EAST GERMANY
Karl-Marx-Universitat
Johannes Ranft

WEST GERMANY
Physikalisches Institut, Bonn
Dirk Husmann
Wolfgang Paul
Helmut Piel

Max-Planck-Institut fur Plasmaphysik
Claus Andelfinger
Peter Merkel

DESY
Donatus Degele
Arno Febel
Horst Gerke
Guenter Hemmie
Anton Piwinski
Klaus Steffen
Gustav-Adolf Voss

Institute fur Experimentelle, Karlsruhe
Anselm Citron
Helmut Krauth
Michael Kuntze
Peter Turowski

Institute fur Kernphysik, Mainz
Helmut Herminghaus

GREECE
N. R. C. Demokritos
Tassos A. Filippas

ITALY
Laboratori Nazionali Di Frascati
Ubaldo Bizzarri
Aldo Cattoni
Massimo Placidi
Alberto Renieri
Sergio Tazzari
Angelo Turrin

JAPAN
National Laboratory for High Energy Physics
Motohiro Kihara
Yoshitaka Kimura
Tetsuji Nishikawa

Institute for Nuclear Study, University of Tokyo
Hiroshi Tsujikawa
Kazuo Huke

NETHERLANDS
I. K. O.
Conrad De Vries

SWEDEN
Chalmers Technical University
Gosta Brogren

SWITZERLAND
Swiss Institute for Nuclear Research
Jean-Pierre Blaser
Rolf Wideroe

UNITED KINGDOM
Daresbury Nuclear Physics Laboratory
Alick Ashmore
David E. Poole
Michael W. Poole
David J. Thompson

Rutherford High Energy Laboratory
James R. J. Bennett
Peter Clee
Martin H. R. Donald
David A. Gray
N. Marshall King
Alfred R. Mortimer
Grahame Rees
David B. Thomas

Hammersmith Hospital
Geoffrey Burton

UNITED STATES OF AMERICA
Argonne National Laboratory
Lowell M. Bollinger
Edwin A. Crosbie
Tat K. Khoe
Robert L. Kustom
Lloyd G. Lewis
Ronald L. Martin
Lazarus G. Ratner
James Simpson

Austin Research Associates Corporation
Millard L. Sloan

Brookhaven National Laboratory
Mark Q. Barton
John Blewett
Renate W. Chasman
Gordon T. Danby
George Kenneth Green
Harold Hahn
Alfred W. Maschke
Melvin Month
George Parzen
Eugene C. Raka
R. Ronald Rau
William B. Sampson
Theodorus J. M. Sluyters
Julius Spiro
Arie Van Steenbergen

California Institute of Technology
Murray Gell-Mann

Lawrence Berkeley Laboratory
University of California
Robert Avery
Warren Chupp
Bruce Cork
Tom Elioff
Robert J. Force
Alper Garren
William Gilbert
Michael Green
Hermann Grunder
Walter Hartsough
Edward Hartwig
John M. Hauptman
Paul Hernandez
David Judd
John A. Kadyk
Dennis Keefe
Glen Lambertson

UNITED STATES OF AMERICA (cont'd)
Lawrence Berkeley Laboratory
University of California
L. Jackson Laslett
Christoph Leemann
Kenow Lou
Richard Mobley
Richard Morgado
Jack Peterson
Joseph B. Rechen
Frank Selph
Andrew M. Sessler
Lloyd Smith
John W. Staples
Lynn Stevenson
Jack Tanabe
Ralph Thomas
Ferdinand Voelker
William Wenzel

Lawrence Livermore Laboratory
University of California
V. Kelvin Neil

University of California, Los Angeles
Darrell Drickey

University of California, Santa Cruz
Matthew Sands

Columbia University
Leon Lederman

Laboratory of Nuclear Studies
Cornell University
Joseph L. Kirchgessner
Raphael M. Littauer
Boyce McDaniel
Gerald Rouse
Ronald M. Sundelin
Maury Tigner

Harvard University
Karl Straucb

University of Illinois
Alfred O. Hanson

Meson physics Facility
Los Alamos Scientific Laboratory
Donald C. Hagerman
James Halbig
Willard E. Jule
Edward Knapp
James E. Spencer

University of Maryland
Martin P. Reiser
Gus T. Zorn

University of Massachusetts
Robert Gluckstern

Cyclotron Laboratory
Michigan State University
Henry G. Blosser

National Accelerator Laboratory
Francis Cole
Donald A. Edwards
Helen Edwards

UNITED STATES OF AMERICA (cont'd)
National Accelerator Laboratory
H. Eugene Fisk
James E. Griffin
Edward Hubbard
Philip V. Livdahl
Frederick E. Mills
Shigeki Mori
Shoroku Ohnuma
Curtis W. Owen
Robert Peters
Paul Reardon
Alessandro Ruggiero
Rae Stiening
Lee C. Teng
Donald E. Young

Oak Ridge National Laboratory
Charles M. Jones
Robert S. Livingston

Physics International
Bruce Ecker
Sidney Putnam

Princeton University
Remo Ruffini
Milton G. White

Plasma Theory Division
Sandia Laboratories
Glenn Kuswa
Craig L. Olson

Stanford Linear Accelerator Center
Stanford University
Matthew A. Allen
Joseph Ballam
Karl Brown
Joseph K. Cobb
Kenneth F. Crook
Sidney D. Drell
Z. David Farkas
Gerhard E. Fischer
John L. Harris
Richard H. Helm
William B. Herrmannsfeldt
Harry A. Hogg
Roland F. Koontz
Charles J. Kruse
Jean V. Lebacqz
Martin J. Lee
Alexander V. Lisin
Gregory A. Loew
Kenneth B. Mallory
Roger H. Miller
Philip L. Morton
Richard B. Neal
Wolfgang K. H. Panofsky
James M. Paterson
Vernon G. Price
Daryl D. Reagan
John R. Rees
Burton Richter
Andrew P. Sabersky
Steven J. St. Lorant
Richard Taylor
Dieter Walz
Alan Wilmunder
Perry B. Wilson

UNITED STATES OF AMERICA (cont'd)
Stanford High Energy Physics Laboratdry,
Stanford University
Ilan Ben-Zvi
Robert Hofstadter
Michael S. McAshan
Roy E. Rand
H. Alan Schwettman
Todd Smith
John P. Turneaure
Herman Winick

U. S. Atomic Energy Commission
Division of Physical Research
John Teem
George Wheeler
William A. Wallenmeyer

National Bureau of Standards
Center for Radiation Research
James E. Leiss

Texas Instruments
Richard Sah

University of Wisconsin
Ednor M. Rowe

Yale University
Klaus Peter Schuler

UNION OF SOVIET SOCIALIST REPUBLICS
Institute of High Energy Physics
Serpukov
Yuri Ado

Institute of High Energy Physics, Moscow
USSR Academy of Sciences
Nicolai V. Lazarev
Leonid Ivanovich Sokolov

Joint Institute for Nuclear Research, Moscow
Vatali P. Dmitrievsky
Vladislav P. Sarantsev

P. N. Lebedev Institute, Moscow
USSR Academy of Sciences
Andrei A. Kolomensky

Physical Engineering Institute, Moscow
USSR Academy of Sciences
Oleg A. Valdner

Radiotechnical Institute, Moscow
USSR Academy of Sciences
Vladimir V. Elyan

LIST OF PARTICIPANTS - ALPHABETICALLY

Yuri Ado
Institute of High Energy Physics
Moscow District
Serpukov, USSR

James V. Allaby
NP Division - CERN
1211 Geneva 23
Switzerland

Matthew Allen
Stanford Linear Accelerator Center
P.O. Box 4349
Stanford, California 94305

Claus Andelfinger
Max Planck Institut Fur
Plasmaphysik
8046 Garching
Germany

Alick Ashmore
Daresbury Nuclear Physics
Laboratory
Daresbury, Near Warrington
Lancs., Great Britain

Robert Avery
Lawrence Berkeley Laboratory
University of California
Berkeley, California 94720

Joseph Ballam
Stanford Linear Accelerator Center
P.O. Box 4349
Stanford, California 94305

Mark Q. Barton
Brookhaven National Laboratory
Upton, Long Island
New York 11973

Frank Beck
Laboratory II - CERN
1211 Geneva 23
Switzerland

James R. J. Bennett
Rutherford High Energy
Laboratory
Chilton, Didcot
Berkshire, England

Ilan Ben-Zvi
Stanford High Energy Physics
Laboratory
Stanford University
Stanford, California 94305

Philippe Bernard
TC Division - CERN
1211 Geneva 23
Switzerland

Roy Billinge
Laboratory - CERN
1211 Geneva 23
Switzerland

Ubaldo Bizzarri
Laboratori Nazionali Di Frascati
Box 70
Frascati 00044, Italy

Jean-Pierre Blaser
Ecole Polytechnique Federale
Institut De Physique
CH-5234 Villigen, Switzerland

John Blewett
Brookhaven National Laboratory
Upton, Long Island
New York 11973

M. Hildred Blewett
ISR - CERN
1211 Geneva 23
Switzerland

Henry G. Blosser
Cyclotron Laboratory
Michigan State University
East Lansing, Michigan 48823

Lowell M. Bollinger
Argonne National Laboratory
9700 South Cass Avenue
Argonne, Illinois 60439

Franco Bonaudi
ISR - CERN
1211 Geneva 23
Switzerland

Gosta Brogren
Chalmers Technical University
Gothenburg, Sweden

Gaston Bronca
Centre d'Etudes Nucleaires
de Saclay
BP no. 2
F-91-Gif-sur-Yvette, France

Karl Brown
Stanford Linear Accelerator Center
P.O. Box 4349
Stanford, California 94305

Henri Bruck
Centre d'Etudes Nucleaires
de Saclay
BP no. 2
F-91-Gif-sur-Yvette, France

Paul Brunet
Lab. de l'Accelerateur Lineaire
Universite Paris-Sud, Centre
d'Orsay, Batiment 200
F-91405 Orsay, France

Jean Buon
Lab. de l'Accelerateur Lineaire
Universite Paris-Sud, Centre
d'Orsay, Batiment 200
F-91405 Orsay, France

Geoffrey Burton
Hammersmith Hospital
Synchrotron Unit
London, England

Aldo Cattoni
Laboratori Nazionali Di Frascati
Box 70
Frascati 00044, Italy

Andre Chabert
Institut National de Physique
11, Rue Pierre-et-Marie-Curie
F-75231 Paris Cedex 5, France

Renate W. Chasman
Brookhaven National Laboratory
Upton, Long Island
New York 11973

Warren Chupp
Lawrence Berkeley Laboratory
University of California
Berkeley, California 94720

Anselm Citron
Institut Fur Experimentelle
Kernphysik
Postf. 3640
Karlsruhe, Germany

Peter Clee
Rutherford High Energy
Laboratory
Chilton, Didcot
Berkshire, England

Joseph Cobb
Stanford Linear Accelerator Center
P.O. Box 4349
Stanford, California 94305

Francis Cole
National Accelerator Laboratory
P.O. Box 500
Batavia, Illinois 60510

Bruce Cork
Lawrence Berkeley Laboratory
University of California
Berkeley, California 94720

Michael K. Craddock
Physics Department
University of British Columbia
Vancouver 8, British Columbia

Kenneth Crook
Stanford Linear Accelerator Center
P.O. Box 4349
Stanford, California 94305

Edwin A. Crosbie
Argonne National Laboratory
9700 South Cass Avenue
Argonne, Illinois 60439

Michael Crowley-Milling
CERN
1211 Geneva 23
Switzerland

Gordon T. Danby
Brookhaven National Laboratory
Upton, Long Island
New York 11973

Donatus Degele
DESY
Notkestieg 1
Hamburg 52, Germany

Conrad De Vries
I. K. O. Oosterringdijk 18
Amsterdam-0, Netherlands

Vitali P. Dmitrievsky
Joint Institute for Nuclear Res.
101000 Moscow Head Post Office
P.O. Box 79, USSR

Martin H. R. Donald
Rutherford High Energy
Laboratory
Chilton, Didcot
Berkshire, England

Sidney D. Drell
Stanford Linear Accelerator Center
P.O. Box4349
Stanford, California 94305

Darrell Drickey
Department of Physics
University of California
Los Angeles, California 90024

Bruce Ecker
Physics International
2700 Merced St.
San Leandro, California 94577

Donald A. Edwards
National Accelerator Laboratory
P.O. Box500
Batavia, Illinois 60510

Helen Edwards
National Accelerator Laboratory
P.O. Box500
Batavia, Illinois 60510

Tom Elioff
University of California
Lawrence Berkeley Laboratory
Berkeley, California 94720

Vladimir V. Elyan
Radiotechnical Institute
USSR Academy of Sciences
125083, Moscow, USSR

David Farkas
Stanford Linear Accelerator Center
P.O. Box 4349
Stanford, California 94305

Jean Faure
Centre d'Etudes Nucleaires
de Saclay
BP no. 2
F-91-Gif-Sur-Yvette, France

Arno Febel
DESY
Notkestieg 1
Hamburg 52, Germany

Fritz Ferger
ISR - CERN
1211 Geneva 23
Switzerland

Tassos A. Filippas
N. R. C. Mocritus
Aghia Paraskevi-Attikis
Athens, Greece

Gerhard E. Fischer
Stanford Linear Accelerator Center
P.O. Box 4349
Stanford, California 94305

Hans Fischer
TC Division - CERN
1211 Geneva 23
Switzerland

H. Eugene Fisk
National Accelerator Laboratory
P.O. Box 500
Batavia, Illinois 60510

Robert J. Force
Lawrence Berkeley Laboratory
University of California
Berkeley, California 94720

Jacques Gareyte
MPS Division - CERN
1211 Geneva 23
Switzerland

Alper Garren
University of California
Lawrence Berkeley Laboratory
Berkeley, California 94720

Murray Gell-Mann
California Institute
of Technology
Pasadena, California 91109

Horst Gerke
DESY
Notkestieg 1
Hamburg 52, Germany

William Gilbert
University of California
Lawrence Berkeley Laboratory
Berkeley, California 94720

Robert Gluckstern
University of Massachusetts
Amherst, Massachusetts 01002

Maurice Gouttefangeas
Centre d'Etudes Nucleaires
de Saclay
BP no. 2
F-91-Gif-Sur-Yvette, France

David A. Gray
Rutherford High Energy
Laboratory
Chilton, Didcot
Berkshire, England

George Kenneth Green
Brookhaven National Laboratory
Upton, Long Island
New York 11973

Michael Green
Lawrence Berkeley Laboratory
University of California
Berkeley, California 94720

James E. Griffin
National Accelerator Laboratory
P.O. Box 500
Batavia, Illinois 60510

Hermann Grunder
University of California
Lawrence Berkeley Laboratory
Berkeley, California 94720

Donald C. Hagerman
Los Alamos Scientific Laboratory
Meson Physics Facility
Los Alamos. New Mexico 87544

Harold Hahn
Brookhaven National Laboratory
Upton, Long Island
New York 11973

James Halbig
Los Alamos Scientific Laboratory
Meson Physics Facility
Los Alamos, New Mexico 87544

Alfred O. Hanson
University of Illinois
Urbana, Illinois 61801

Werner Hardt
MPS Division - CERN
1211 Geneva 23
Switzerland

John Harris
Stanford Linear Accelerator Center
P.O. Box 4349
Stanford, California 94305

Walter Hartsough
University of California
Lawrence Berkeley Laboratory
Berkeley, California 94720

Edward Hartwig
University of California
Lawrence Berkeley Laboratory
Berkeley, California 94720

John M. Hauptman
Lawrence Berkeley Laboratory
University of California
Berkeley, California 94720

Richard Helm
Stanford Linear Accelerator Center
P.O. Box 4349
Stanford, California 94305

Guenter Hemmie
DESY
Notkestieg 1
Hamburg 52, Germany

Helmut Herminghaus
Institut Fur Kernphysik
Postf. 3980
Mainz, Germany

Paul Hernandez
Lawrence Berkeley Laboratory
University of California
Berkeley, California 94720

William Herrmannsfeldt
Stanford Linear Accelerator Center
P.O. Box 4349
Stanford, California 94305

Merrvyn Hine
CERN
1211 Geneva 23
Switzerland

Robert Hofstadter
Stanford High Energy Physics
Laboratory
Stanford University
Stanford, California 94305

Harry Hogg
Stanford Linear Accelerator Center
P.O. Box4349
Stanford, California 94305

Edward Hubbard
National Accelerator Laboratory
P.O. Box500
Batavia. Illinois 60510

Kazuo Huke
Institute for Nuclear Study
University of Tokyo
Tanashi, Tokyo, 188, Japan

J. A. Hulbert
Atomic Energy of Canada, Limited
Chalk River Nuclear Laboratories
Accelerator Physics Branch
Chalk River, Ontario, Canada

Dirk Husmann
Physikalisches Institut
Nussallee 12
Bonn, Germany

Trevor Hyman
Laboratory - CERN
1211 Geneva 23
Switzerland

Marcel Jablonka
Centre d' Etudes Nucleaires
de Saclay
BP No. 2
F-91-Gif-Sur-Yvette, France

Willibald Jentschke
CERN
1211 Geneva 23
Switzerland

Kjell Johnsen
ISR - CERN
1211 Geneva 23
Switzerland

Charles M. Jones
Oak Ridge National Laboratory
Oak Ridge, Tennessee 37830

David Judd
Lawrence Berkeley Laboratory
University of California
Berkeley, California 94720

Willard E. Jule
Los Alamos Scientific Laboratory
Meson Physics Facility
Los Alamos, New Mexico 87544

John A. Kadyk
University of California
Lawrence Berkeley Laboratory
Berkeley, California 94720

Leon Katz
Accelerator Laboratory
University of Saskatchewan
Saskatoon, Saskatchewan S7N OWO
Canada

Denis Keefe
University of California
Lawrence Berkeley Laboratory
Berkeley, California 94720

Eberhard Keil
CERN
1211 Geneva 23
Switzerland

Tat K. Khoe
Argonne National Laboratory
9700 South Cass Avenue
Argonne, Illinois 60439

Motohiro Kihara
National Laboratory for High
Energy Physics
Oho-Machi, Tsukuba-Gun
Ibaraki-Ken, 300-32, Japan

Yoshitaka Kimura
Energy Physics
Oho-Machi, Tsukuba-Gun
Ibaraki-Ken, 300-32, Japan

N. Marshall King
Rutherford High Energy
Laboratory
Chilton, Didcot
Berkshire, England

Joseph L. Kirchgessner
Laboratory of Nuclear Studies
Cornell University
Ithaca, New York 14850

Edward Knapp
Los Alamos Scientific Laboratory
Meson Physics Facility
Los Alamos, New Mexico 87544

Andrei A. Kolomensky
Lebedev Physical Institute
USSR Academy of Sciences
Leninsky Prospect 53
Moscow, USSR

Roland Koontz
Stanford Linear Accelerator Center
P.O. Box 4349
Stanford, California 94305

Helmut Krauth
Institut Fur Experimentelle
Kernphysik
Postf. 3640
Karlsruhe, Germany

Charles Kruse
Stanford Linear Accelerator Center
P.O. Box4349
Stanford, California 94305

Werner Kubischta
CERN
1211 Geneva 23
Switzerland

Michael Kuntze
Institut Fur Experimentelle
Kernphysik
Postf. 3640
Karlsruhe, Germany

Robert L. Kustom
Argonne National Laboratory
9700 South Cass Avenue
Argonne, Illinois 60439

Glenn Kuswa
Sandia Laboratories
Division 5245
Albuquerque, New Mexico 87115

Jean-Louis Laclare
Centre d'Etudes Nucleaires
de Saclay
BPno. 2
F-91-Gif-Sur-Yvette, France

Glen Lambertson
Lawrence Berkeley Laboratory
University of California
Berkeley, California 94720

L. Jackson Laslett
Lawrence Berkeley Laboratory
University of California
Berkeley, California 94720

Nicolai V. Lazarev
Institute for Theoretical &
Experimental Physics
Moscow, USSR

Jean Lebacqz
Stanford Linear Accelerator Center
P.O. Box **4349**
Stanford, California **94305**

Leon Lederman
Physics Department
Columbia University
Irvington-On- Hudson
New York **10025**

Martin Lee
Stanford Linear Accelerator Center
P.O. Box **4349**
Stanford, California **94305**

Christoph Leemann
Lawrence Berkeley Laboratory
University of California
Berkeley, California **94720**

Jean-Marie Lefebvre
Commissariat A l'Energie Atomique
B-P-2 cen-Saclay 91-Gif
Yvette, France

Pierre Lehmann
Lab. del'Accelerateur Lineaire
Universite Paris-Sud, Centre
d'Orsay, Batiment **200**
F-91405 Orsay, France

James E. Leiss, Director
National Bureau of Standards
Center for Radiation Research
Washington, D. C. **20234**

Herbert Lengeler
NP Division - CERN
1211 Geneva **23**
Switzerland

Marie Paule Level
Lab. de l'Accelerateur Lineaire
Universite Paris-Sud- Centre
d'Orsay, Batiment **200**
F-91405 Orsay, France

Lloyd G. Lewis
Argonne National Laboratory
9700 South Cass Avenue
Argonne, Illinois **60439**

Alexander Lisin
Stanford Linear Accelerator Center
P.O. Box **4349**
Stanford, California **94305**

Raphael M. Littauer
Laboratory of Nuclear Studies
Cornell University
Ithaca, New **York** **14850**

Philip V. Livdahl
National Accelerator Laboratory
P.O. Box **500**
Batavia, Illinois **60510**

Robert S. Livingston
Oak Ridge National Laboratory
Oak Ridge, Tennessee **37830**

Gregory A. Loew
Stanford Linear Accelerator Center
P.O. Box **4349**
Stanford, California **94305**

Kenow H. Lou
Lawrence Berkeley Laboratory
University of California
Berkeley, California **94720**

Michael S. Mc Ashan
Stanford High Energy Physics
Laboratory
Stanford University
Stanford, California **94305**

Boyce McDaniel
Laboratory of Nuclear Studies
Cornel1 University
Ithaca, New York **14850**

Kenneth Mallory
Stanford Linear Accelerator Center
P.O. Box **4349**
Stanford, California **94305**

Pierre Marin
Laboratoire de l'Accelerateur
Lineaire
Batiment **200**
Orsay, France

Ronald L. Martin
Argonne National Laboratory
9700 South Cass Avenue
Argonne, Illinois **60439**

Alfred W. Maschke
Brookhaven National Laboratory
Upton, Long Island
New York **11973**

Peter Merkel
Max-Planck-Institut **Fur**
Plasmaphysik
8046 Garching
Germany

Ernest G. Michaelis
MSC Division - CERN
1211 Geneva **23**
Switzerland

Roger Miller
Stanford Linear Accelerator Center
P.O. Box **4349**
Stanford, California **94305**

Frederick E. Mills
National Accelerator Laboratory
P.O. Box **500**
Batavia, Illinois **60510**

Boris Milman
Laboratory II - CERN
1211 Geneva **23**
Switzerland

Richard Mobley
Lawrence Berkeley Laboratory
University of California
Berkeley, California **94720**

Robert B. Moore
Foster Radiation Laboratory
McGill University
Montreal, Quebec
Canada

Melvin Month
Brookhaven National Laboratory
Upton, Long Island
New York **11973**

Richard Morgado
Lawrence Berkeley Laboratory
University of California
Berkeley, California **94720**

Shigeki Mori
National Accelerator Laboratory
P.O. Box 500
Batavia, Illinois **60510**

Alfred R. Mortimer
Rutherford High Energy
Laboratory
Chilton, Didcot
Berkshire, England

Phil L. Morton
Stanford Linear Accelerator Center
P.O. Box **4349**
Stanford, California **94305**

Richard B. Neal
Stanford Linear Accelerator Center
P.O. Box **4349**
Stanford, California **94305**

V. Kelvin Neil
Lawrence Livermore Laboratory
University of California
Livermore, California **94550**

Francis Netter
Centre d'Etudes Nucleaires
de Saclay
BPno. **2**
F-91-Gif-Sur-Yvette, France

Tetsuji Nishikawa
National Laboratory
Of High Energy Physics
Oho-Machi, Tsukaba-Gun
Iboraki-Ken, Japan

Shoroku Ohnuma
National Accelerator Laboratory
P.O. Box **500**
Batavia, Illinois **60510**

Craig L. Olson
Plasma Theory Division
Sandia Laboratories
Albuquerque, New Mexico **87115**

Curtis W. Owen
National Accelerator Laboratory
P.O. Box 500
Batavia, Illinois 60510

Wolfgang K. H. Panofsky
Stanford Linear Accelerator Center
P.O. Box 4349
Stanford, California 94305

George Parzen
Brookhaven National Laboratory
Upton, Long Island
New York 11973

James Paterson
Stanford Linear Accelerator Center
P.O. Box 4349
Stanford, California 94305

Wolfgang Paul
Physikalisches Institut
Nussallee 12
D 5300
Bonn, Germany

Robert Peters
National Accelerator Laboratory
P.O. Box 600
Batavia, Illinois 60510

Jack Peterson
University of California
Lawrence Berkeley Laboratory
Berkeley, California 94720

Helmut Piel
University of Wuppertal
Wuppertal, Germany

Anton Piwinski
DESY
Notkestieg 1
Hamburg 52, Germany

Massimo Placidi
CERN
1211 Geneva 23
Switzerland

David E. Poole
Daresbury Nuclear Physics Lab.
Keckwick Lane
Daresbury, Warrington, 3WA4 4AD
England

Michael W. Poole
Daresbury Nuclear Physics Lab.
Keckwick Lane
Daresbury, Warrington, 3WA4 4AD
England

Vernon G. Price
Stanford Linear Accelerator Center
P.O. Box 4349
Stanford, California 94305

Sidney Putnam
Physics International
2700 Merced St.
San Leandro, California 94577

Eugene C. Raka
Brookhaven National Laboratory
Upton, Long Island
New York 11973

Roy E. Rand
Stanford High Energy Physics
Laboratory
Stanford University
Stanford, California 94305

Johannes Ranft
Sektion Physik
Karl-Marx-Universitat
DDR-701 Leipzig
Linnestr. 5, East Germany

Lazarus G. Ratner
Argonne National Laboratory
9700 South Cass Avenue
Argonne, Illinois 60439

R. Ronald Rau
Director, Physics Department
Brookhaven National Laboratory
Upton, Long Island
New York 11973

Daryl Reagan
Stanford Linear Accelerator Center
P.O. Box 4349
Stanford, California 94305

Paul Reardon
National Accelerator Laboratory
P.O. Box 500
Batavia, Illinois 60510

Joseph B. Rechen
Lawrence Berkeley Laboratory
University of California
Berkeley, California 94720

Grahame Rees
Rutherford High Energy
Laboratory
Chilton, Didcot
Berkshire, England

John Rees
Stanford Linear Accelerator Center
P.O. Box 4349
Stanford, California 94305

Karl H. Reich
MPS Division - CERN
1211 Geneva 23
Switzerland

Martin P. Reiser
University of Maryland
College Park, Maryland 20742

Alberto Renieri
Laboratori Nazionali Di Frascati
Box 70
Frascati 00044, Italy

Lorenzo Resegotti
ISR - CERN
1211 Geneva 23
Switzerland

Burton Richter
Stanford Linear Accelerator Center
P.O. Box4349
Stanford, California 94305

Gerald Rouse
Laboratory of Nuclear Studies
Cornell University
Ithaca, New York 14850

Ednor M. Rowe
University of Wisconsin
P.O. Box6
Stoughton, Wisconsin 53589

Remo Ruffini
Physics Department
Princeton University
P.O. Box 708
Princeton, New Jersey 08540

Alessandro Ruggiero
National Accelerator Laboratory
P.O. Box 500
Batavia, Illinois 60510

Andrew Sabersky
Stanford Linear Accelerator Center
P.O. Box 4349
Stanford, California 94305

Frank Sacherer
CERN
1211 Geneva 23
Switzerland

Richard Sah
Texas Instruments
P.O. Box 5012 Station Z
Dallas, Texas 75222

William B. Sampson
Brookhaven National Laboratory
Upton, Long Island
New York 11973

Matthew Sands
University of California
Santa Cruz, California 95060

Vladislav P. Sarantsev
Joint Institute for Nuclear Res.
101000 Moscow Head Post Office
P.O. Box 79, USSR

Karl Heinz Schindl
MPS Division - CERN
1211 Geneva 23
Switzerland

Wolfgang Schnell
ISR - CERN
1211 Geneva 23
Switzerland

Klaus Peter Schuler
Yale University
New Haven, Conneticut 06520

H. Alan Schwettman
Stanford High Energy Physics Laboratory
Stanford University
Stanford, California 94305

Frank Selph
University of California
Lawrence Berkeley Laboratory
Berkeley, California 94720

Roger Servranckx
Accelerator Laboratory
University of Saskatchewan
Saskatoon, Saskatchewan S7N OWO
Canada

Andrew M. Sessler, Director
University of California
Lawrence Berkeley Laboratory
Berkeley, California 94720

Alexander V. Shalnov, Director
Div. of Research and Laboratories
International Atomic Energy Agency
P.O. Box590
A1011 Vienna, Austria

James Simpson
Argonne National Laboratory
9700 South Cass Avenue
Argonne, Illinois 60439

Millard L. Sloan
Austin Research Associates Corp.
600 W. 28th St.
Austin, Texas 78705

Theodorus J. M. Sluyters
Brookhaven National Laboratory
Upton, Long Island
New York 11973

Lloyd Smith
University of California
Lawrence Berkeley Laboratory
Berkeley, California 94720

Todd Smith
Stanford High Energy Physics Laboratory
Stanford University
Stanford, California 94305

Leonid Ivanovich Sokolov
Institute for Theoretical & Experimental Physics
Moscow, USSR

Brian Southworth
Editor, CERN Courier
CERN
1211Geneva 23, Switzerland

James E. Spencer
Los Alamos Scientific Laboratory
Meson Physics Facility
Los Alamos, New Mexico 87544

Julius Spiro
Brookhaven National Laboratory
Upton, Long Island, New York 11973

John W. Staples
Lawrence Berkeley Laboratory
University of California
Berkeley, California 94720

Klaus Steffen
DESY
Notkestieg 1
Hamburg 52, Germany

Lynn Stevenson
University of California
Lawrence Berkeley Laboratory
Berkeley, California 94720

Rae Stiening
National Accelerator Laboratory
P.O. Box 500
Batavia, Illinois 60510

Steven St. Lorant
Stanford Linear Accelerator Center
P.O. Box 4349
Stanford, California 94305

Karl Strauch
Harvard University
Cambridge, Massachusetts 02138

Ronald M. Sundelin
Laboratory of Nuclear Studies
Cornell University
Ithaca, New York 14850

Jack Tanabe
Lawrence Berkeley Laboratory
University of California
Berkeley, California 94720

Sergio Tazzari
Laboratori Nazionali Di Frascati
Box 70
Frascati 00044, Italy

Richard Taylor
Stanford Linear Accelerator Center
P.O. Box 4349
Stanford, California 94305

John Teem, Director
Division of Physical Research
U. S. Atomic Energy Commission
Germantown, Maryland 20545

Lee C. Teng
National Accelerator Laboratory
P.O. Box 500
Batavia, Illinois 60510

David B. Thomas
Rutherford High Energy Laboratory
Chilton, Didcot
Berkshire, England

Ralph Thomas
Lawrence Berkeley Laboratory
University of California
Berkeley, California 94720

David J. Thompson
Daresbury Nuclear Physics Lab.
Keckwick Lane
Daresbury, Warrington, 3WA4 4AD
England

Maury Tigner
Laboratory of Nuclear Studies
Cornel1 University
Ithaca, New York 14850

Hiroshi Tsujikawa
Institute for Nuclear Study
3-2-1, Midori-Cho, Tanashi
Tokyo, 188, Japan

Peter Turowski
Institut fur Experimentelle Kernphysik
Postf. 3640
Karlsruhe, Germany

John P. Turneaure
Stanford High Energy Physics Laboratory
Stanford University
Stanford, California 94305

Angelo Turrin
Laboratori Nazionali Di Frascati
Box 70
Frascati 00044, Italy

Oleg A. Valdner
Physical Engineering Institute
Imeni A. F. I offe
USSR Academy of Science
Moscow, USSR

Arie Van Steenbergen
Brookhaven National Laboratory
Upton, Long Island
New York 11973

Ferdinand Voelker
Lawrence Berkeley Laboratory
University of California
Berkeley, California 94720

Gustav-Adolf Voss
Desy
Notkestieg 1
Hamburg, 52, Germany

William A. Wallenmeyer
Asst. Dir., High Energy Physics
Division of Physical Research
U. S. Atomic Energy Commission
Washington, D C. 20545

Dieter Walz
Stanford Linear Accelerator Center
P. O. Box4349
Stanford, California 94305

William Wenzel
University of California
Lawrence Berkeley Laboratory
Berkeley, California 94720

Carl H. Westcott
Atomic Energy of Canada, Limited
Chalk River Nuclear Laboratories
Accelerator Physics Branch
Chalk River, Ontario, Canada

George Wheeler
Division of Physical Research
U. S. Atomic Energy Commission
Germantown, Maryland **20545**

Bruce L. White
University of British Columbia
Vancouver 8, British Columbia
Canada

Milton G. White
Princeton University
P.O. Box 708
Princeton, New Jersey **08540**

Rolf Wideroe
Swiss Institute for Nuclear Research
CH **5234** - Villigen
Switzerland

Alan Wilmunder
Stanford Linear Accelerator Center
P.O. Box **4349**
Stanford, California **94305**

Perry B. Wilson
Stanford Linear Accelerator Center
P.O. Box **4349**
Stanford, California **94305**

Herman Winick
Stanford High Energy Physics
Laboratory
Stanford University
Stanford. California **94305**

Peter Wolstenholme
ISR - CERN
1211 Geneva **23**
Switzerland

Jean Yoccoz
Institut National de Physique
11, Rue Pierre-et-Marie-Curie
F-75231 Paris Cedex **5,** France

Donald E. Young
National Accelerator Laboratory
P.O. Box **500**
Batavia, Illinois **60510**

Gus T. Zorn
University of Maryland
College Park, Maryland **20742**

Henri Zyngier
Lab. de l'Accelerateur Lineaire
Universite Paris-Sud, Centre
d'Orsay, Batiment **200**
F-91405 Orsay, France

CATALOGUE
of
High Energy Accelerators

FOREWORD

It has become customary to issue an up-to-date catalogue of the parameters and performance of high-energy accelerators at the time of the International Accelerator Conferences. Accordingly, we have sent out data sheets to the various laboratories, requesting their cooperation in obtaining this information. The forms are identical to those used for the 1971 CERN conference and we thank M. H. Blewett for her kind permission to use them again.

We would like to express our warmest thanks to all those who have returned the filled-out data sheets that include considerable new information.

Unfortunately, sheets for a few of the machines were not returned to us, at least by the publication deadline. Rather than publish out-of-date or incorrect material, we have not included any data for these machines. (They are shown with an asterisk in the Table of Contents.)

In contrast to previous years, you will find in this catalogue a new section listing parameters of a few new major projects that are not yet funded. Realizing that such information is at best tentative, reply to our questionnaire was left as an option for the laboratories contacted and is therefore in no way complete. Further, the authors of these pages which were returned wish us to emphasize that their data is subject to change; however, we feel that this information may reflect the direction in which the High Energy Accelerator field is currently moving.

G. E. Fischer
Ruth Thor Nelson

Note added for revised Proceedings edition:

Since the Conference, we have received two additional data sheets. They are included in this revised Proceedings edition of the Catalogue of High Energy Accelerators. Several data sheets remain outstanding. We regret that we are unable to include a complete listing of the data sheets in this revised edition.

Editors
July 1974

CONTENTS

NAME OF MACHINE: CERN SPS
INSTITUTION: CERN Laboratory II
LOCATION: Geneva - Pays de Gex (F)

PERSON IN CHARGE: J.B. Adams
DATA SUPPLIED BY: G. von Holtey
DATE: January 1974

HISTORY AND STATUS

CONSTRUCTION STARTED (date): 1971
FIRST BEAM OBTAINED OR GOAL (date): end of 1976
TOTAL COST OF FACILITY: 1150 MSF
FUNDED BY: 11 Member States of CERN
TOTAL ACCELERATOR STAFF (now): 360
ANNUAL OPERATING BUDGET: -

ACCELERATOR PARAMETERS

Physical Dimensions (Mean)

RING DIAM. 2200 m; Tunnel sect. Ø = 4 m
MAGNET 80x44 cm; Mag. Gap 15 x 4.5 cm
"DONUT" 34.5x4.5 cm; Aperture 11.0 x 4.3 cm

Injector System

TYPE: improved CPS
OUTPUT (max) 10^{13} ppp at 10 to 14 GeV/c
BEAM EMITTANCE (10 GeV/c) H:2.6π V:3.3π mm-mrad
INJECTION PERIOD 23 usec, or 1 turns
INFLECTOR TYPE: pulsed magnetic kicker

Magnet System

FOCUSING TYPE: AG separate function
No. MAG. UNITS 744+216 Length (ea) 6.26/3.085 m
STRAIGHT SECT. 216 Total S.S. Length — m
FOCUSING ORDER: FODO
BETATRON OSC. FREQ. ν_x 27.6 ν_y 27.55
FIELD, AT INJ. 450 G, at max ca kG
RISE TIME 3.4 sec; Flat-top time 0.7 to 2.0 sec
MAG. WEIGHT (tons) Fe 13500, Cu 1400
POWER INPUT (MW) PEAK 135 MEAN 36

Acceleration System

HARMONIC No. 4620 No. Cavities 2
RF RANGE: 200.2 MHz
ORBIT FREQ.
ENERGY GAIN: 3.6 MeV/turn
RADIATION LOSS - keV/turn
RF POWER INPUT (kW) PEAK 1.0 MW

Other Rekvant Parameters or Notable Features

ACCELERATOR PERFORMANCE

	Normal (or Goal)	Maximum Achieved
ENERGY (GeV)	400	
RESOLUTION ΔE/E (%)		
REPET. RATE (pulse/sec)*	0.17 (0.11)	
PULSE WIDTH		
DUTY FACTOR, macroscopic (%)*	12 (22.5)	
INTERNAL BEAM (part/pulse)	10^{13}	
(part/sec)*	$1.7\ 10^{12}$	($1.1\ 10^{12}$)
CURRENT (mA)	69.5	
BEAM EMITTANCE (mm-mrad)	0.2 π	
SCHEDULED OPERATION (hr/wk)	-	

"ON BEAM" - % OF SCHEDULED TIME

Some Typical External and Secondary Beams

PARTICLE	FLUX (part/sec)	BEAM AREA (cm²)	ENERGY (GeV)	AEIE (%)

RESEARCH PROGRAM

TOTAL EXPERIMENTAL AREA ca 27000 m²
BEAM LINES TO Stations
STATIONS SERVED AT SAME TIME
BEAM SEPARATORS SPECTROMETERS
ON-LINE COMPUTERS WITH Inputs
BUBBLE CHAMBERS, in-house Users'
TOTAL POWER INSTALLED FOR RESEARCH MW
No. USER GROUPS: in-house outside
TOTAL RESEARCH STAFF, in-house outside
ANNUAL RESEARCH BUDGET, in-house
SCHEDULED RESEARCH TIME, hours/week

RECENT IMPROVEMENTS OR MODIFICATIONS TO MACHINE

* for 0.7 sec (2.0 sec) flat top.

Published Articles Describing Machine

The 300 GeV Programme, CERN/1050, January 1972.

NAME OF MACHINE CERN Proton Synchrotron (CPS)
INSTITUTION European Organization for Nuclear Research
LOCATION eyrin, Geneva, Switzerland

PERSON IN CHARGE G.L. Munday
DATA SUPPLIED BY O. Barbalat - L. Hoffmann
DATE February 1974

HISTORY AND STATUS

CONSTRUCTION STARTED (date) 1955
FIRST BEAM OBTAINED, OR GOAL (date) November 24, 1959
TOTAL COST OF FACILITY 200 MFr.Sw. (1954-1959)
FUNDED BY CERN Member States
TOTAL ACCELERATOR STAFF (now) 460
ANNUAL OPERATING BUDGET *** 52 MFr.Sw.

ACCELERATOR PARAMETERS

Physical Dimensions (Mean)

RING DIAM. 200 m; Tunnel sect. 6 x 6 m
MAGNET 1.16,0.94 m; Mag. Gap 10.0 x 15.0 cm
"DONUT 7.4 x15.Qcm; Aperture 7.0 x 14.6 cm

Injector System

TYPE Linac or Booster
OUTPUT 50/300 mA at 50/800 MeV
BEAM EMITTANCE 20 x 20 π / 30 x 13 π mn-mrad
INJECTION PERIOD 20/2.5 usec, or 3/1 turns
INFLECTOR TYPE electrostatic dc and pulsed magnetic kicker or septum and pulsed kicker

Magnet System

FOCUSING TYPE AG Field index, n= 288
No. MAG. UNITS 100 Length (ea) 4.26 m
STRAIGHT SECT. 100 Total S.S. Length 188 m
FOCUSING ORDER FOFDOD
BETATRON OSC. FREQ. ν_H 6.25 ν_V 6.25
FIELD, AT INJ. 147 G, at max 14 kG
RISE TIME 0.7-1.0 sec; Flat-top time 0.5-0.7 sec
MAG. WEIGHT (tons) Fe 3000 , Cu 130
POWER INPUT (MW) PEAK 41 MEAN 2.8

Acceleration System

HARMONIC NO. 20 NO. Cavities 10
RF RANGE. 2.9 to 9.55 MHz
ORBIT FREQ. RANGE 0.145 to 0.478
ENERGY GAIN (max) 80
RADIATION LOSS keV/turn
RF POWER INPUT (kW) PEAK 1000 MEAN 300

Other Relevant Parameters or Notable Features

*** Including developments, Linac and Booster

ACCELERATOR PERFORMANCE

	Normal (or Goal)	Maximum Achieved
ENERGY (GeV)	25	28
RESOLUTION $\Delta E/E$ (X)	± 0.05	
REPET. RATE (pulse/sec)	~ 0.5	
PULSE WIDTH		
DUTY FACTOR. macroscopic (%)	20-25	
INTERNAL BEAM (part/pulse)	$1.5 \cdot 2 \cdot 10^{12}$	$5 \cdot 6 \cdot 10^{12}$ (with Booster)
(part/sec)	10^{12}	$3 \cdot 10^{12}$
CURRENT (mA)		
BEAM EMITTANCE (mn-mrad)	1 π	— —
SCHEDULED OPERATION (hr/wk)	145 (excluding yearly shutdown)	

"ON BEAM" 91 % OF SCHEDULED TIME

Sane Typical External a d Secondary Beams

PARTICLE	FLUX (part/sec)	BEAM AREA (cm^2)	ENERGY (GeV)	$\Delta E/E$ (%)	
Slow ejected protons	$0.5 \cdot 10^{12}$	0.1	24	1.0	on 3 targets
π^-	$4 \cdot 10^5$	1	6	4	
π^+	$1.2 \cdot 10^6$	2	6	2	
$p^+ \pi^+$	$1.6 \cdot 10^6$	2	15	2	
K^+	$2.4 \cdot 10^4$	3	2.8	1.75	
K^-	$2 \cdot 10^3$				

RESEARCH PROGRAM

TOTAL EXPERIMENTAL AREA 20.000 m²
BEAM LINES TO 17 + ISR + 3 tests Stations
STATIONS SERVED AT SAME TIME 10 + ISR + tests
SEPARATED BEAMS 10 SPECTROMETERS 10
ON-LINE COMPUTERS 13
BUBBLE CHAMBERS, in-house 3 Users'
TOTAL POWER USED FOR RESEARCH 27 MW (average)
No, USER GROUPS: mixed 15+5 outside 15 + 40** **
TOTAL RESEARCH STAFF: in-house 190 outside 620 + 500
ANNUAL RESEARCH BUDGET, in-house
SCHEDULED RESEARCH TIME, hours/week 125

** Bubble chamber picture analysis

RECENT IMPROVEMENTS OR MODIFICATIONS TO MACHINE

- 800 MeV Booster Injector
- Transformations for use as SPS injector

* For the whole of CERN

PUBLISHED ARTICLES DESCRIBING MACHINE

Regenstreif,E., CERN 59-29,CERN 60-26, CERN 62-3.
Hine,M.G.N., Int. Conf. Instrum. for High Energy Accel.,LRL,Sept. 60,214-222.
Lapostolle,P.,Onde électrique 40, 489-504(1960).
Adams,J.B., Nature 185,568-72(1960).
Germain,P.,Industries Atomiques 7, 9-10/61-73(1963).
Reich, K. H., Kerntechnik 3, (8)345-55(1961).
Hereward,H.G.,Nucl.Instr.Meth.20,9-11(1963).
Standley,P.H.,Fourth Int.Conf.High Energy Acc. Dubna 1963,99-109 (USAEC Conf.114)
Fifth Int.Conf.High En.Acc.Frascati,1965,80-85.
Eaconnier et al. Seventh Int.Conf.High En.Acc. Erevan 1969, 565-575.
Baconnier et al. U.S.Nat.Acc.Conf.Chicago 1971.

PUBLISHED ARTICLES (cont.)

PS Staff, Ninth Int. Conf. High Energy Accelerators Stanford 1974

NAME OF MACHINE Booster for the CPS (PSB) PERSON IN CHARGE K.H. Reich
INSTITUTION CERN, European Org. Nucl. Res. DATA SUPPLIED BY H. Koziol, K.H. Reich
LOCATION Meyrin, Geneva, Switzerland DATE 8th March 1974

HISTORY AND STATUS

CONSTRUCTION STARTED (date) January 1968
FIRST BEAM OBTAINED. OR GOAL (date) May 1972
TOTAL COST OF FACILITY 60 MFr (Swiss)
FUNDED BY CERN Member States
TOTAL ACCELERATOR STAFF (now) 72
ANNUAL OPERATING BUDGET 8 MFr (including develop,)

ACCELERATOR PARAMETERS

Physical Dimensions (Mean) (width x height)
RING DIAM. 50 m; Tunnel sect. 4.05 x 5.15 m
MAGNET 0.7 x 1.52m Gap 24.1 [1] x 7.0 cm
"DONUT" x cm; Aperture [1] x cm

Injector System
TYPE Improved CERN PS Linac
OUTPUT 50 mA at 50 MeV
BEAM EMITTANCE 30π×30π (95% of beam) mn-mrad
INJECTION PERIOD 100 μsec, or 4 x 15 turns
INFLECTOR TYPE magnetic (1 for multiturn, 1 for monoturn)

Magnet System [2]
FOCUSING TYPE AG, sep. functions; triplets
No. MAG. UNITS 32 Length (ea) (mag.) 1.618 m
STRAIGHT SECT. [3] Total S. s Length [3] m
FOCUSING ORDER ½L1, B, L2, F, L3, D, L4, F, L5, B, ½L1
BETATRON OSC. FREQ. ν_H 4 to 5 ν_V 4 to 5.3
FIELD, AT INJ. 1253 G, at max 5.93 kG
RISE TIME 0.60 sec; Flat-top time 0.08 sec
MAG. WEIGHT (tons) Fe 580, Cu 34.6 (B+F+D)
POWER INPUT (MW) PEAK 5.6 [4] MEAN 1.64 [4]

Acceleration System
HARMONIC NO. 5 No. Cavities 1 per ring:
RF RANGE 2.997 8.033 MHz
ORBIT FREQ. 0.599 1.607 MHz
ENERGY GAIN 1 keV/t
RADIATION LOSS – keV/turn
RF POWER INPUT (kW) PEAK 4 x 7 Mean 4 x 4

Other Relevant Parameters or Notable Features 4 rings stacked on top of each other. Bending magnets and quadrupoles combined to 4-gap units. Linac beam switched to 4 rings by vertical deflector. At 800 MeV the 4 beams are ejected sequentially and combined by vertical bending septum and kicker rnagnets.

Publications describing machine:
Proc. Int. Accelerator Conferences:
VI (Cambridge): Bovet, Reich (p.315)
VII (Yerevan): Bigliani et al. (p.433)
VIII (Geneva): Bovet et al. (p.102, 380)
IX (1974): Baribaud et al.; Reich
Proc. Nat. Accelerator Conference:
4th (Chicago): Asseo et al; Bigliani; Bigliani et al; Brückner; Koziol, Reich; Rufer, Unterlerchner; Sacherer, Sherwood.
5th (San Francisco): Bovet; Baribaud, Metzger; Rabany.

ACCELERATOR PERFORMANCE

(present, at 800 MeV)

	Normal (or Goal)	Maximum Achieved
ENERGY (GeV)	0.800	
RESOLUTION	$\Delta p/p \pm 1.3 \times 10^{-3}$	
REPET. RATE (pulse/sec)	as CPS, max 0.87	
PULSE WIDTH	4 x 0.622	
DUTY FACTOR, macroscopic (%)	$2.16\ 10^{-4}$ %	
INTERNAL BEAM (part/pulse)	7×10^{12} ppp	
(part/sec)	(goal 1.3×10^{13} ppp)	
CURRENT (mA)	400 mA	

BEAM EMITTANCE (nm-mrad) H: 28π; V: 13π
SCHEDULED OPERATION (hr/wk) 1974 : ∿ 3000 h
"ON BEAM" % OF SCHEDULED TIME

Some Typical External and Secondary Beams

PARTICLE	FLUX (part/sec)	BEAM AREA (cm^2)	ENERGY (GeV)	ΔE/E (%)
CPS INJECTOR				

RESEARCH PROGRAM

TOTAL EXPERIMENTAL AREA m²
BEAM LINES TO Stations
STATIONS SERVED AT SAME TIME
BEAM SEPARATORS SPECTROMETERS
ON-LINE COMPUTERS WH Inputs
BUBBLE CHAMBERS, in-house Users'
TOTAL POWER INSTALLED FOR RESEARCH MW
No. USER GROUPS: in-house outside
TOTAL RESEARCH STAFF, in-house outside
ANNUAL RESEARCH BUDGET, in-house
SCHEDULED RESEARCH TIME, hours/week

RECENT IMPROVEMENTS OR MODIFICATIONS TO MACHINE

Mobile console in PSB equipment rooms giving full access to central control computer.

[1]

	section	apert. (und. vac.)
in bend. mag.	13.8x6.8	13.2x6.1
in triplet	13.8x12.4	13.5x12.1
in L1	Ø 12.3	Ø 12.0

[2] Data for quadrupoles

	F	D
number	32	16
magn. length (m)	0.50	0.88
bore radius	0.06	
gradient (T/m)	0.81 (inj)	
	3.83 (max)	

[3] L_1: 16x2.54m; L_2, L_5: 16x0.28m; L_3, L_4: 16x0.59m;
[4] At output of power supply.

Publ. (cont.) Int. Conf. Magnet Technology:
3rd (Hamburg): Asner et al. (p.418)
4th (Brookhaven): Pahud (p.718).

NAME OF MACHINE SATURNE
INSTITUTION C.E.A.
LOCATION SACLAY - FRANCE

PERSON IN CHARGE GOUTTEFANGEAS
DATA SUPPLIED BY
DATE JAN. 1974

HISTORY AND STATUS

CONSTRUCTION STARTED (date) 1955
FIRST BEN OBTAINED. OR GOAL (date) August 1958
TOTAL COST OF FACILITY in 1957 - 87 MF
FUNDED BY C.E.A
TOTAL ACCELERATOR STAFF (now) 192
ANNUAL OPERATING BUDGET

ACCELERATOR PARAMETERS

Physical Dimensions (Mean)

RING DIAM. 22 m; Tunnel sect. m
MAGNET 1.77 2 m; Mag. Gap 17.5 × 52.75 cm
"DONU" 10.648 cm; Aperture 10.6 × 34 cm

Injector System.

Linac
OUTPUT (max) 40mA at 20 MeV
BEAM EMITTANCE 18 mA in 2,8 π mm-mrad
INJECTION PERIOD 600 µsec, or 550 turns
INFLECTOR TYPE. electrostatic V=100 KV E = 66.6 KV/cm

Magnet System

FOCUSING TYPE Weak
No. MAG. UNITS 4 Length (ea) 13.255 m
STRAIGHT SECT. 4 Total S.S. Length 16 m
FOCUSING ORDER
BETATRON OSC. FREQ. ν_H 0.721 ν_V 0.884
FIELD. AT INJ. 771 G, at max 15 kG
RISE TIME 0.87 sec; Flat-top time 0.5 sec
MAG. WEIGHT (tons) Fe 1x080, Cu 55
POYER INPUT (MW) PEAK 24 MEAN 1

Acceleration System

HARMONIC No. 2 NO. Cavities 1
RF RANGE 1.6 8.44 MHz
ORBIT FREQ.
ENERGY GAIN 1.16
RADIATION LOSS keV/turn
RF POUER INPUT (kW) PEAK 36 6

Other Relevant **Parameters** *or* **Notable Features**

acceleration of deutons
5.10^{11} d/pulse at 2,3 GeV

Published Articles Describing Machine

Onde electrique n° 387 (juin 59)

ACCELERATOR PERFORMANCE

	Normal (or Goal)	Maximum Achieved
ENERGY (GeV)	3	3
RESOLUTION ΔE/E ◀▮▶	3.4	
REPET. RATE (pulse/sec)	0.22 with Flat top	
PULSE UIDTH	0.45	
DUTY FACTOR, macroscopic (%)	9	
INTERNAL BEAM (part/pulse)	$1.2 10^{12}$	$1.6 10^{12}$
(part/sec)	$2,6 10^{12}$	$3.5 10^{11}$
CURRENT (mA)		
BEAH EHITTANCE (mm-mrad)	π x28 / π x8	
SCHEDULED OPERATION (hr/wk)	130	168

"ON BEAM" 71 % OF SCHEDULED TIME

Some Typical External and Secondary Beams

PARTICLE	FLUX (part/sec)	BEAM AREA (cm²)	ENERGY (GeV)	ΔE/E (%)
π+	$.6x10^5$	16	2	2
p	$6x10^{10}$	25x12 *	3	0.2
F	$8x10^{10}$	10x15 *	1	0.05
d	$4.4x10^{10}$		2.7	
α	$2x10^9$	350x150 *	0.7	
n	$.5x10^7$	28	2 GeV/c	

RESEARCH PROGRAM (* emittance n 10^{-6})

TOTAL EXPERIHENTAL AREA 3480 m²
BEAH LINES TO 0 Stations
STATIONS SERVED AT SAME TIME 3
BEAM SEPARATORS 0 SPECTROMETERS 2
ON-LINE COMPUTERS WITH 8 Inputs
BUBBLE CHAMBERS. in-house Users'
TOTAL POUER INSTALLED FOR RESEARCH 22 MW
No. USEK GROUPS: in-house 2 outside 12
TOTAL RESEARCH STAFF, in-house outside
ANNUAL RESEARCH BUDGET. in-house
SCHEDULED RESEARCH TIME, hours/week 93

RECENT IMPROVEMENTS OR MODIFICATIONS TO MACHINE

- acceleration of particles *a* $1,2\ 10^{11}$ α/pulse at 1.2 GeV/A
- a superconducting quadrupole doublet OGA permits to increase the number of pions by a factor 4
- A renovation of Saturne is being studied. With a new nasnet and the same injector, one should obtain $1,10^{12}$ p/s external in 3 mmmrad at 1 GeV (max. energy 2.7 - 3 GeV)

NAME OF MACHINE 10 GeV Proton Synchrotron
INSTITUTION Nat.Lab.for High Energy Phys.
LOCATION Tsukuba, Japan

PERSON IN CHARGE T. Nishikawa
DATA SUPPLIED BY
DATE March. 1974

HISTORY AND STATUS

CONSTRUCTION STARTED (date) April, 1971
FIRST BEAM OBTAINED. OR GOAL (date) 1975
TOTAL COST OF FACILITY 4×10^9 Yen
FUNDED BY Javanese Government
TOTAL ACCELERATOR STAFF (now) 65
ANNUAL OPERATING BUDGET 5×10^8 Yen

ACCELERATOR PARAMETERS

Physical Dimensions (Mean)
RING DIAM. 108 m; Tunnel sect. 4.0 x 4.7 m
MAGNET 85 x 70 m; Mag. Gap 5.6 x 14 cm
"DONUT" 5.0 x 14 cm; Aperture 5.0 x 14 cm

Injector System
TYPE 20 MeV Linac + 500 MeV Booster
OUTPUT (max) 1.6×10^{-3} at 500 MeV
BEAM EMITTANCE 75π(H) x 10π(V) mn-mrad
INJECTION PERIOD 5×10^5 μsec, or 9 turns
INFLECTOR TYPE magnetic

Magnet System
TYPE AG separated function
No. MAG. UNITS 48(bng) Length (ea) 3.2 (bng) m
STRAIGHT SECT. 4(long) Total S.S. Length 48.4(ℓ) m
FOCUSING ORDER FODO
BETATRON OSC. FREQ. ν_H 7.25 ν_V 7.25
FIELD. AT INJ. 1.5 kG, at max. 13 (17.5) kG
RISE TIME 0.5(0.85) sec; Flat-top time 0.5 sec
MAG. WEIGHT (tons) Fe 680, Cu 30
POWER INPUT (MW) PEAK 13(25) MEAN 4.5(8.6)

Acceleration System
HARMONIC No. 9 No. Cavities 3
RF RANGE 6.0 to 7.9 MHz
ORBIT FREQ. 0.67 to 0.88
ENERGY GAIN 12.6
RADIATION LOSS 19.1 (16.7) keV/turn
RF POWER INPUT (kW) PEAK 46 mean 26.5

Other Relevant Parameters or Notable Features

ACCELERATOR PERFORMANCE

	Normal (or Goal)	Maximum Achieved
ENERGY (GeV)	8 (12)	
RESOLUTION ΔE/E (%)	0.2 (0.1)	
REPET. RATE (pulse/sec)	1/2	
PULSE WIDTH	0.4	
DUTY FACTOR, macroscopic (%)	25	
INTERNAL BEAM (part/pulse)	$>2 \times 10^{12}$	(10^{13})
(part/sec)	$>10^{12}$	(5×10^{12})
CURRENT (mA)	>280	(1415)
BEAM EMITTANCE (mn-mrad)	$13\pi \times 1.7\pi$	($9\pi \times 1.2\pi$)
SCHEDULED OPERATION (hr/wk)		

"ON BEAM" _____ % OF SCHEDULED TIME

Some **Typical External and Secondary Beams**

PARTICLE	FLUX (part/sec)	BEAM AREA (cm^2)	ENERGY (GeV)	ΔE/E (%)

RESEARCH PROGRAM

TOTAL EXPERIMENTAL AREA 3500 m^2
BEAM LINES TO 3 Stations
STATIONS SERVED AT SAME TIME
BEAM SEPARATORS 3 SPECTROMETERS 2
ON-LINE COMPUTERS WITH 2 Inputs
BUBBLE CHAMBERS, in-house 1 Users'
TOTAL POWER INSTALLED FOR RESEARCH 11 MW
No. USER GROUPS: in-house 3 outside 9
TOTAL RESEARCH STAFF, in-house 25 outside 60
ANNUAL RESEARCH BUDGET. in-house
SCHEDULED RESEARCH TIME. hours/week

RECENT IMPROVEMENTS OR MODIFICATIONS TO MACHM

Published Articles Describing Machine

NAME OF MCHINE Booster Synchrotron for 10-GeV **PS**

INSTITUTION Nat. Lab. for High Energy Phys.

LOCATION Tsukuba, Japan

PERSON IN CHARGE T. Nishikawa

DATA SUPPLIED BY T. Nishikawa

DATE March. 1974

HISTORY AND STATUS

CONSTRUCTION STARTED (date) April, 1971

FIRST BEAM OBTAINED. OR GOAL (date) 1974

TOTAL COST OF FACILITY

FUNDED BY Japanese Government

TOTAL ACCELERATOR STAFF (now) 10

ANNUAL OPERATING BUDGET

ACCELERATOR PARAMETERS

Physical Dimensions (Mean)

RING DIAM. 6 m; Tunnel sect. m

MAGNET 0.7 x 0.8 m; Mag. Gap 7.2 x 14.0 cm

"DONUT 7.0 x 16. cm; Aperture 5.6 x 14.0 cm

Injector System

TYPE Linac

OUTPUT (max) 100 mA at 20 MeV

BEAM EMITTANCE 10π (norm.) mn-mrad

INJECTION PERIOD 5.5 μsec, or turns

INFLECTOR TYPE magnetic

Magnet System

FOCUSING TYPE combined function

No. MAG. UNITS 8 Length (ea) 2.6 m

STRAIGHT SECT. 8 Total S.S. Length 17 m

FOCUSING ORDER FDDFO

BETATRON OSC. FREQ. ν_u 2.25 ν_v 2.25

FIELD, AT INJ. 1.97 G, at max 11.0 kG

RISE TIME 0.025 sec; Flat-top time - sec

MAG. WEIGHT (tons) Fe 88.1, Cu 6.57

POWER INPUT (MW) PEAK MEAN 0.5

Acceleration System

HARMONIC No. 1 No. Cavities 1

RF RANGE 1.616 to 6.077 MHz

ORBIT FREQ. 1.616 to 6.027

ENERGY GAIN max. 7

RADIATION LOSS keV/turn

RF POWER INPUT (kW) PEAK 60 mean 40

Other Rekvant Parameters or Notable Features

ACCELERATOR PERFORMANCE

	Normal (or Goal)	Maximum Achieved
ENERGY (GeV)	0.5	
RESOLUTION ΔE/E (%)	0.3	
REPET. RATE (pulse/sec)	20	
PULSE WIDTH	0.06 μs	
DUTY FACTOR, macroscopic (%)	1.2×10^{-6}	
INTERNAL BEAM (part/pulse)	0.5×10^{12}	(2×10^{12})
(part/sec)	1×10^{13}	(4×10^{13})
CURRENT (mA)	480	(1900)
BEAM EMITTANCE (mn-mrad)	75π(H)x10π(V)	
SCHEDULED OPERATION (hr/wk)		

"ON BEAM" % OF SCHEDULED TIME

Some Typical External and Secondary Beams

PARTICLE	FLUX (part/sec)	BEAM AREA (cm^2)	ENERGY (GeV)	ΔE/E (%)

RESEARCH PROGRAM

TOTAL EXPERIMENTAL AREA m^2

BEAM LINES TO Stations

STATIONS SERVED AT SAME TIME

BEAM SEPARATORS SPECTROMETERS

ON-LINE COMPUTERS WITH Inputs

BUBBLE CHAMBERS. in-house Users'

TOTAL POWER INSTALLED FOR RESEARCH MW

No. USER GROUPS: in-house outside

TOTAL RESEARCH STAFF, in-house outside

ANNUAL RESEARCH BUDGET, in-house

SCHEDULED RESEARCH TIME, hours/week

RECENT IMPROVEMENTS OR MODIFICATIONS TO MACHINE

Published Articles Describing Machine

NAME OF MACHINE NIMROD

INSTITUTION RUTHERFORD LABORATORY
LOCATION CHILTON, DIDCOT, BERKS., UK

PERSON IN CHARGE D A GRAY
DATA SUPPLIED BY D A GRAY
DATE January 1974

HISTORY AND STATUS

CONSTRUCTION STARTED (date) 1957
FIRST BEAM OBTAINED. OR GOAL (date) August 1963
TOTAL COST OF FACILITY £10M to first operation
FUNDED BY Science Research Council
TOTAL ACCELERATOR STAFF (now) 330 incldg expl area
ANNUAL OPERATING BUOGET ~ £8M (Lab. total)

ACCELERATOR PARAMETERS

Physical Dimensions (Mean)

RING DIAM 53.27 m; ~~Circumference~~ Machine Room 61 x 9 m
MAGNET 3.15 x 2.74 m; Mag. Gap 116 x 28.4 cm
"DONUT" x cm; Aperture 100 x 20 cm

Injector System

TYPE Alvarez linac
OUTPUT (max) 45 at 14.9
BEAM EMITTANCE At 18 mA 100% in 50 mn-mrad
INJECTION PERIOD 350 µsec, or 120 turns
INFLECTOR TYPE Electrostatic

Magnet System

FOCUSING TYPE Weak n = 0.6
No. MAG. UNITS 8 Length (ea) 14.751 m
STRAIGHT SECT. 8 Total S.S. Length 30.44 m
FOCUSING ORDER -
BETATRON OSC. FREQ. ν_H 0.71 ν_V 0.87
FIELD, AT INJ. 299 G, at max 14.2 kG
RISE TIME 0.75 sec; Flat-top time Up to 0.95 sec
MAG. WEIGHT (tons) Fe 7,000 , Cu 250
POWER INPUT (MW) PEAK 160 MEAN 2.5

Accelcration System

HARMONIC NO. 4 No. Cavities 1 unit 2 gaps
RF RANGE 1.416 7.980 MHz
ORBIT FREQ. .354 to 1.995 MHZ
ENERGY GAIN 5.5 keV/turn
RADIATION LOSS Negligible keV/turn
RF POWER INPUT (kW) PEAK 45 Mean 20

Other Rekvant Parameters or Notable Features

a) Vacuum vessel is double glass-epoxy laminate system.

b) Magnet is C-type with field correction using 'crenellations'.

Published Articles Describing Machine

i) Nimrod - A 7 GeV proton synchrotron. Ruth. Lab. Report NIRL/R/44 (1965).

ii) The work of the Rutherford Laboratory 1972. Ruth. Lab. Report RHEL/R270 (1973).

ACCELERATOR PERFORMANCE

	Normal (or Goal)	Maximum Achieved
ENERGY (GeV)	7.1	8.0
RESOLUTION ΔE/E (%)	0.015	
REPET. RATE (pulse/sec)	22	
PULSE WIDTH (ms)	450	
DUTY FACTOR, macroscopic (%)	20	
INTERNAL BEAM (part/pulse)	3×10^{12} P	4.2×10^{12} *
(part/sec)	1.1×10^{12}	1.7×10^{12}
CURRENT (mA)	-	-
BEAM EMITTANCE (mm-mrad)		
SCHEDULED OPERATION (hr/wk)	120 average for research and machine development.	

"ON BEAM" 88 % OF SCHEDULED TIME for research.

Some Typical External and Secondary Beams

PARTICLE	FLUX (part/sec)	BEAM AREA (cm²)	Momentum ENERGY (GeV)	ΔE/E (%)	
P	4.5×10^{11}	0.1	7.8	0.7	Zxtracted beam.
π^-, π^+	5×10^7 / 4×10^7	6	1–4 / 0.2	2–10 / 10	
π^-	3×10^3		1.0–2.0	2	
K^+	6×10^3 (K^-)		0.4–1.0	6	
$K^\pm$					

RESEARCH PROGRAM

TOTAL EXPERIMENTAL AREA 7300 m²
BEAM LINES TO 9 Stations
STATIONS SERVED AT SAME TIME 9
BEAM SEPARATORS SPECTROMETERS
ON-LINE COMPUTERS WITH Inputs
BUBBLE CHAMBERS. in-house 0 Users'
TOTAL POWER INSTALLED FOR RESEARCH 24 / 12 MW
No. USER GROUPS: in-house 4 outside
TOTAL RESEARCH STAFF, in-house x outside 141
ANNUAL RESEARCH BUDGET, in-house -
SCHEDULED RESEARCH TIME, hours/week 94 average in 1973

RECENT IMPROVEMENTS OR MODIFICATIONS TO MACHINE

*

1) Second-harmonic cavity commissioned in 1973 gave 40% increase.
Characteristic of cavity:
Harmonic No.8. Drift tube acceleration.
RF Voltage 8 kV peak.
RF power kW 21 peak 12 mean.

2) New 70 MeV injector being built ready for 1975. Should give x 5 beam.

NAME OF MACHINE Zero Gradient Synchrotron
INSTITUTION Argonne National Laboratory
LOCATION Argonne, Illinois USA

PERSON IN CHARGE Ronald L. Martin
DATA SUPPLIED BY Ronald L. Martin
DATE February 1974

HISTORY AND STATUS

CONSTRUCTION STARTED (date) June 1959
FIRST BEAM OBTAINED. OR GOAL (date) Sept. *1963*
TOTAL COST OF FACILITY $50 M
FUNDED BY US AEC
TOTAL ACCELERATOR STAFF (now) 230
ANNUAL OPERATING BUDGET $10.5 M

ACCELERATOR PARAMETERS

Physical Dimensions (Mean)
RING DIAM. 54.7 m; Tunnel sect. 12.7 x 10.4 m
MAGNET 1.4 x 2.6 m; Mag. Gap *14.6* x 136.5 cm
"DONUT" 14.6 x 82.2 cm; Aperture 13.3 x 81.3 cm

Injector System
TYPE Linac
OUTPUT (max) 40 mA at 50 MeV
BEAM EMITTANCE 25 π mm-mrad
INJECTION PERIOD *100* μsec, or 60 turns
INFLECTOR TYPE dc magnetic

Magnet System field index,
FOCUSING TYPE weak n = 0 (wedge foc)
No. MAG. UNITS 8 Length (ea) *16.3* m
STRAIGHT SECT. 8 Total S.S. Length 41.45 m
FOCUSING ORDER
BETATRON OSC. FREQ. ν_H 0.83 ν_V 0.81 (at inj)
FIELD, AT INJ. 482 G, at max 21.5 kG
RISE TIME 0.85 sec; Flat-top time 0-1 sec
MAG. WEIGHT (tons) Fe 4700, Cu 68
POWER INPUT (MW) PEAK 110 MEAN 10

Acceleration System
HARMONIC NO. 8 No. Cavities 1 (3 gaps)
RF RANGE *4.4* to 14.0 MHz
ORBIT FREQ. *0.55* to *1.75* MHz
ENERGY GAIN 10 keV/turn
RADIATION LOSS keV/turn
RF POWER INPUT (kW) P E A K 6 0 Mean 30

Other Relevant Parameters or Notable Features

Only high energy synchrotron using wedge focusing

ACCELERATOR PERFORMANCE

	Normal (~~on Goal~~)	Maximum Achieved
ENERGY (GeV)	12.0	*12.7*
RESOLUTION ΔE/E (%)	±0.01	±0.01
REPET. RATE (pulse/sec)	0.30	0.5
PULSE WIDTH (sec)	0.70	1.0 (max flattop)
DUTY FACTOR, macroscopic (%)	20	20
INTERNAL BEAM (part/pulse) $\times 10^{12}$	2.5	3.8
(part/sec) $\times 10^{12}$	0.8	1.5
CURRENT (mA)	700	1000
BEAM EMITTANCE (mm-mrad) (int)	25 π	150 π
SCHEDULED OPERATION (hr/wk)	80	135 ave for year

"ON BEAM" 90 % OF SCHEDULED TIME

Some Typical External and Secondary Beams

PARTICLE	FLUX (part/sec)	BEAM AREA (cm^2)	ENERGY (GeV)	ΔE/E (%)
π	10^5	1	0.5-8	±(0.75-2)
K	10^3	1	*0.5-6*	±2
K^0	2×10^5	*200*	0.2-2.5	
n	10^6	6	2-11	

RESEARCH PROGRAM

TOTAL EXPERIMENTAL AREA 13000 m^2
BEAM LINES TO 17 Stations
STATIONS SERVED AT SAME TIME 13 peak, 7 average
BEAM SEPARATORS 4 SPECTROMETERS 1
ON-LINE COMPUTERS WITH 5 Inputs
BUBBLE CHAMBERS, in-house 1 Users' 0 (1 streamer chamber)
TOTAL POWER INSTALLED FOR RESEARCH 30 MW
No. USER GROUPS: in-house 5 outside *30*
TOTAL RESEARCH STAFF, in-house outside
ANNUAL RESEARCH BUDGET, in-house $3.5 M
SCHEDULED RESEARCH TIME, hours/week 120 ave.

RECENT IMPROVEMENTS OR MODIFICATIONS TO MACHINE

2 simultaneous external beams
Resonant Extraction - 90% *(40* psec - *700* msec)
Titanium vacuum chamber installed *1972*
Polarized protons to *8.5* GeV/c *1973*
70% polarization - 5 x 10^8/pulse internal
200 MeV injection from booster *1974*

Published Artkles **Describing** Machine

L.C. Teng, "Status of the Argonne 12.5-BeV Zero Gradient Synchrotron," Dubna - *1963* Proceedings, **pp.** 223-232.

NAME OF MACHINE ZGS Booster Synchrotron I
INSTITUTION Argonne National Laboratory
LOCATION Argonne, Illinois USA

PERSON IN CHARGE Ronald L. Martin
DATA SUPPLIED BY James D. Simpson
DATE February 1974

HISTORY AND STATUS

Former 2.2 GeV Cornell Electron Syn.
CONSTRUCTION STARTED (date)
FIRST BEAM OBTAINED, OR GOAL (date) October 1971
TOTAL COST OF FACILITY
FUNDED BY US AEC (Development and AI)
TOTAL ACCELERATOR STAFF (now) 8
ANNUAL OPERATING BUDGET

ACCELERATOR PARAMETERS

Physical Dimensions (Mean)
RING DIAM. 42 m; Tunnel sect. ____ ____ m
MAGNET 0.40x0.55m; Mag. Gap 3.5 x 10.0 cm
"DONUT" 2.5 x8.0 cm; Aperture 2.8 x 6.4 cm

Injector System
TYPE Linac (H^- Ion)
OUTPUT (max) 5mA at 50 MeV
BEAM EMITTANCE 25 mn-mrad
INJECTION PERIOD 200 μsec, or 300 turns
INFLECTOR TYPE None. Strips H to H^+ after injection.

Magnet System
FOCUSING TYPE AG field index, n = 26.1
No. MAG. UNITS 12 Length (ea) 3.16 m
STRAIGHT SECT. ____ Total S.S. Length 13.2 m
FOCUSING ORDER ODFO
BETATRON OSC. FREQ. ν_x 3.375 ν_y 3.375
FIELD, AT INJ. 1.7 H^- kG, at max 3.5 kG
RISE TIME 16 m sec; Flat-top time ____ sec
MAG. WEIGHT (tons) Fe 60, Cu 2.7
POWER INPUT (MW) PEAK ____ MEAN 0.15

Acceleration System
HARMONIC NO. 1 No. Cavities 1
RF RANGE 1.8 to 3.3 MHz
ORBIT FREQ.
ENERGY GAIN 5.5 (max)
RADIATION LOSS ____ keV/turn
RF POWER INPUT (kW) PEAK 50

Other Rekvant Parameters or Notable Features

ACCELERATOR PERFORMANCE

	Normal (or Goal)	Maximum Achieved
ENERGY (GeV)	0.2	0.2
RESOLUTION AEIE (%)		
REPET. RATE (pulse/sec)	30	
PULSE WIDTH		
DUTY FACTOR, macroscopic (%)		
INTERNAL BEAM (part/pulse)	10^{12}	1.5×10^{11} (accel)
(part/sec)		
CURRENT (mA)		
BEAM EMITTANCE (mn-mrad)	5.0 π	
SCHEDULED OPERATION (hr/wk)		

"ON BEAM" ____ % OF SCHEDULED TIME

Some Typical External and Secondary Beams

PARTICLE	FLUX (part/sec)	BEAM AREA (cm^2)	ENERGY (GeV)	AEIE (%)

RESEARCH PROGRAM

TOTAL EXPERIMENTAL AREA ____ m^2
BEAM LINES TO ____ Stations
STATIONS SERVED AT SAME TIME ____
BEAM SEPARATORS ____ SPECTROMETERS ____
ON-LINE COMPUTERS WITH ____ Inputs
BUBBLE CHAMBERS, in-house ____ Users' ____
TOTAL POWER INSTALLED FOR RESEARCH ____ MW
No. USER GROUPS: in-house ____ outside ____
TOTAL RESEARCH STAFF, in-house ____ outside ____
ANNUAL RESEARCH BUDGET, in-house ____
SCHEDULED RESEARCH TIME, hours/week ____

RECENT IMPROVEMENTS OR MODIFICATIONS TO MACHINE

Published Articles Describing Machine

R. L. Martin, Proceedings 1971 Particle Accelerator Conference, Chicago, Illinois, "The Argonne ZGS Booster," p. 957.

NAME OF MACHINE ZGS Booster Synchrotron II
INSTITUTION Argonne National Laboratory
LOCATION Argonne, Illinois USA

PERSON IN CHARGE Ronald L. Martin
DATA SUPPLIED BY James D. Simpson
DATE February 1974

HISTORY AND STATUS Procurement begun

CONSTRUCTION STARTED (date) February 1974
FIRST BEAM OBTAINED. DR GOAL (date) January 1976
TOTAL COST OF FACILITY
FUNDED BY US AEC (AI)
TOTAL ACCELERATOR STAFF (now) 8
ANNUAL OPERATING BUDGET

ACCELERATOR PARAMETERS

Physkal Dimensions (Mean)
RING DIAM. 13.7 m; Tunnel sect. m
MAGNET x m; Mag. Gap 3.1 x 10 cm
"DONUT" x cm; Aperture x cm

Injector System
TYPE Linac (H^- Ion)
OUTPUT (max) 5 mA at 50 MeV
BEAM EMITTANCE 2.5 mn-mrad
INJECTION PERIOD 250 μsec, or 400 turns
INFLECTOR TYPE None. Strips H^- to H^+ after injection.

Magnet System
FOCUSING TYPE AG
No. MAG. UNITS Length (ea) m
STRAIGHT SECT. Total S.S. Length 19.8 m
FOCUSING ORDER FDFODO
BETATRON OSC. FREQ. ν_H 2.2 ν_V 2.32
FIELD, AT INJ. 2.8 kG, at max 10 kG
RISE TIME 16 m sec; Flat-top time sec
MAG. WEIGHT (tons) Fe , Cu
POWER INPUT (MW) PEAK MEAN

Acceleration System
HARMONIC NO. 1 No. Cavities 2
RF RANGE. 2.2 to 5.3 MHz
ORBIT FREQ.
ENERGY GAIN 10 keV/turn (max)
RADIATION LOSS keV/turn
RF POWER INPUT (kW) PEAK 80

Other Rekvrnt Parameters or Notable Features

ACCELERATOR PERFORMANCE

	Normal (or Goal)	Maximum Achieved
ENERGY (GeV)	0.5	
RESOLUTION ΔE/E (%)		
REPET. RATE (pulse/sec)	60	
PULSE WIDTH		
DUTY FACTOR, macroscopic (%)		
INTERNAL BEAM (part/pulse)	5×10^{12}	
(part/sec)		
CURRENT (mA)		
BEAM EMITTANCE (mn-mrad)		
SCHEDULED OPERATION (hr/wk)		

"ON BEAM" % OF SCHEDULED TIME

Some Typical External and Secondary Beams

PARTICLE	FLUX (part/sec)	BEAM AREA (cm^2)	ENERGY (GeV)	AEIE (%)

RESEARCH PROGRAM

TOTAL EXPERIMENTAL AREA m^2
BEAM LINES TO Stations
STATIONS SERVED AT SAME TIME
BEAM SEPARATORS SPECTROMETERS
ON-LINE COMPUTERS WITH Inputs
BUBBLE CHAMBERS, in-house Users'
TOTAL POWER INSTALLED FOR RESEARCH MW
No. USER GROUPS: in-house outside
TOTAL RESEARCH STAFF, in-house outside
ANNUAL RESEARCH BUDGET, in-house
SCHEDULED RESEARCH TIME, hours/week

RECENT IMPROVEMENTS OR MODIFICATIONS TO MACHINE

Published Articles Describing Machlne

NAME OF MACHINE: Alternating Gradient Synchrotron

INSTITUTION LOCATION: Brookhaven National Laboratory, Upton, New York

PERSON IN CHARGE: R.R. Rau

DATA SUPPLIED BY: A. van Steenbergen

DATE: January 28, 1974

HISTORY AND STATUS

CONSTRUCTION STARTED (date): 1953

FIRST BEAM OBTAINED, OR GOAL (date): July 29, 1960

TOTAL COST OF FACILITY: $30.65 M

FUNDED BY: USA-AEC

TOTAL ACCELERATOR STAFF (now): 538

ANNUAL OPERATING BUDGET: $17 M

ACCELERATOR PARAMETERS

Physical Dimensions (Mean)

RING DIAM. 256.9 m; Tunnel sect. 5.49 x 5.49 m

MAGNET 0.84, 0.99 m; Mag. Gap 5.67 x 31.75 cm

"DONUT" 7.9 x 17.4 cm; Aperture 6.35 x 13.33 cm

Injector System

TYPE: Alvarez Linear Accelerator

OUTPUT (max) 100 at 200.3

BEAM EMITTANCE 10 π mn-mrad

INJECTION PERIOD ≤150 μsec, or ≤ 30 turns

INFLECTOR TYPE: pulsed magnetic

Magnet System

FOCUSING TYPE: AG

No. MAG. UNITS 240 Length (ea) 2.28, 1.90, resp. m

STRAIGHT SECT. * Total S.S. Length 270 m

FOCUSING ORDER: (F/2)o(F/2)(D/2)o(D/2)

BETATRON OSC. FREQ. ν_H 8.75 ν_V 8.75

FIELD AT INJ. 251 G, at max 13.1 kG

RISE TIME 0.45 sec; Flat-top time 1.0 sec

MAG. WEIGHT (tons) Fe 4000, Cu 400

POWER INPUT (MW) PEAK 30 MEAN 2.4

Acceleration System

HARMONIC NO. 12 No. Cavities 12 double

RF RANGE, ORBIT FREQ. 2.52 - 4.46 MHz; 0.210 - 0.380

ENERGY GAIN, RADIATION LOSS 192 - keV/turn

RF POWER INPUT (kW) PEAK 1000

Other Relevant Parameters or Notable Features

* 24 X 3 m; 72 X 1.5 m; 144 X 0.6 m

ACCELERATOR PERFORMANCE

	Normal (or Goal)	Maximum Achieved
ENERGY (GeV)		33
RESOLUTION ΔE/E (%)		0.1
REPET. RATE (pulse/sec)		0.5
PULSE WIDTH		1.2 sec flat top
DUTY FACTOR, macroscopic (%)		50
DUTY FACTOR, macroscopic (#/sec)		6 10^{12}
CURRENT (mA)		
BEAM EMITTANCE (mm-mrad)		0.8 π x 3.0 π
SCHEDULED OPERATION (hr/wk)		(6d/7d)

"ON BEAM" 100 % OF SCHEDULED TIME

Some Typical External and Secondary Beams

PARTICLE	FLUX (part/sec)		ENERGY (GeV)	ΔE/E (%)
FEB, Protons	6 10^{12}		28	0.2
SEB, Protons	4 10^{12}		28	0.2
K^+, K^-	10^5, 4 10^4		3	± 1
K^+, K^-	3 10^5, 10^6		1	±
π			3	± 2
$\frac{n}{K^0}$	3 10^7 / 10^6		3-20	

RESEARCH PROGRAM

TOTAL EXPERIMENTAL AREA 15000 m^2

BEAM LINES TO 10 Stations

STATIONS SERVED AT SAME TIME

BEAM SEPARATORS 12 SPECTROMETERS 6

ON-LINE COMPUTERS WITH 2 2 0 Inputs

BUBBLE CHAMBERS, in-house 2 Users' MW

TOTAL POWER INSTALLED FOR RESEARCH 54

No. USER GROUPS: in-house 5 outside 63 involved

TOTAL RESEARCH STAFF, in-house 138 outside -

ANNUAL RESEARCH BUDGET, in-house $5.

SCHEDULED RESEARCH TIME, hours/week 4 weeks 500 hrs.

RECENT IMPROVEMENTS OR MODIFICATIONS TO MACHINE

50-MeV Linac injector replaced by 200-MeV Linac. New magnet system power supply and rf system for doubling repetition rate. New ring vacuum system. Magnet system modularized. New external beam branches, SEB system. Addition of third FEB system for ν physics area.

Published Articles Describing Machine

G.K. Green, E.D. Courant, "The Proton Synchrotron," Handbuck der Physik *44, 218-340 (1959).*

NAME OF MCHINE Revstron
INSTITUTION Lawrence Berkeley Laboratory
LOCATION Univ. of Calif., Berkeley, Calif.

PERSON IN CHARGE Edward J. Lofgren
DATA SUPPLIED BY Kenneth C. Crebbin
DATE February, 1974

HISTORY AND STATUS

CONSTRUCTION STARTED (date) 1949
FIRST BEAM OBTAINED, OR GOAL (date) Feb. 1954
TOTAL COST OF FACILITY $31 M
FUNDED BY USAEC
TOTAL ACCELERATOR STAFF (now) 135
ANNUAL OPERATING BUDGET ∿$5.4 M

ACCELERATOR PARAMETERS

Physical Dimensions (Mean)

RING DIAM. 38.23 m; Tunnel sect. ——— -- m
MAGNET 6.1x2.75 m; Mag. Gap 152 × 30 cm
"DONUT" -- x -- cm; Aperture 112 × 25 cm

Injector System

** TYPE Cockroft-Walton and Linac
OUTPUT (max) 25 (*) (mA) at 19.2(4.8/Amu) MeV
BEAM EMITTANCE 25 mm-mrad
INJECTION PERIOD 600 μsec, or 300 turns
INFLECTOR TYPE 3 Magnet Achromatic + E.S

Magnet System

FOCUSING TYPE Weak Field index n=0.67
No. MAG. UNITS 144 Length(ea) 0.66 m
STRAIGHT SECT. 4 Total S.S. Length 6.1 m
FOCUSING ORDER -----
BETATRON OSC. FREQ. ν_H 0.647 ν_V 0.922
FIELD, AT INJ. 417 G, at max 15.53 kG
RISE TIME 1.7 sec; Flat-top time 0.3 ±2.0 sec
MAG. WEIGHT (tons) Fe 9700, Cu 347
POWER INPUT (MW) PEAK 121 MEAN 6.0

Acceleration System

HARMONIC No. 1 No. Cavities 1 (2 gaps)
RF RANGE 0.24 2.50 MHz
ORBIT FREQ. .497(.252) to 2.47(2.41) MHz
ENERGY GAIN 1.5 (0.75) KeV/turn
RADIATION LOSS ——— keV/turn
RF POWER INPUT (kW) PEAK ——— ----

( )Values for 1 Amu others for protons

Other Relevant Parameters or Notable Features

** Four injector systems. See appropriate one for more details.

ACCELERATOR PERFORMANCE

	Normal (or Goal)	Maximum Achieved
ENERGY (GeV)	5.4-6.1	6.2 (2.75/Amu)
RESOLUTION AEIE (%)	∿0.02	∿0.03
REPET. RATE (pulse/sec)	∿0.2	0.29
PULSE WIDTH	1.5 sec at 5.4 GeV	
DUTY FACTOR, macroscopic (%)	25	
INTERNAL BEAM (part/pulse)	4×10^{12}	6.0×10^{12}
(part/sec)	0.75×10^{12}	1.5×10^{12}
CURRENT (mA)	1.9×10^{3}	2.4×10^{3}
BEAM EMITTANCE (inn-mrad)	∿330 radial	
SCHEDULED OPERATION (hr/wk)	158	

"ON BEAM" 87 % OF SCHEDULED TIME

Some Typical External and Secondary Beams

PARTICLE	* FLUX (part/sec)	BEAM AREA (cm^2)	ENERGY (GeV)	ΔE/E (%)
P	4.5×10^{11}	0.18	6.2	∿0.03
^{2}H	$\sim3.8\times10^{10}$	Minimum	5.5	∿.02
^{4}He	$\sim3.8\times10^{9}$	at	11.0	∿.02
^{12}C	$\sim1.9\times10^{7}$	Peak	33.0	∿.02
^{14}N	$\sim1.0\times10^{7}$	Field	38.5	∿.02
^{16}O	$\sim3.8\times10^{6}$	———	44.0	∿.02
^{20}Ne	$\sim1.9\times10^{4}$	———	55.0	∿.02

"These values for the 19.2 (4.8/Amu) injector.

RESEARCH PROGRAM

TOTAL EXPERIMENTAL AREA ∿7000 m^2
BEAM LINES TO 5 Prim (6 sec from 2 Prim) Stations
STATIONS SERVED AT SAME TIME 3 prim + 6 sec.
BEAM SEPARATORS 11 SPECTROMETERS ---
ON-LINE COMPUTERS 3-PDP-5; 2-PDP-8; 1-PDP-9; 2-PDP-11
BUBBLE CHAMBERS, in-house 0 Users' 0
TOTAL POWER INSTALLED FOR RESEARCH 21 MW
No. USER GROUPS: in-house 10 outside 22
TOTAL RESEARCH STAFF, in-house ——— outside ———
ANNUAL RESEARCH BUDGET. in-house ———
SCHEDULED RESEARCH TIME, hours/week % 142

RECENT IMPROVEMENTS OR MODIFICATIONS TO MACHINE

Installation of cryogenic vacuum pumping reduced base pressure to ∿3×10^{-7} Torr from 2×10^{-6} Torr and reduced pumpdown time required to reach full beam intensity.

With the completion of the Bevalac project, there will be three different injectors available for the Bevatron,

Published Articles Describing Machine

1) F.G.H. Lothrop, D.M.Evans, Digital Control of Bevatron Accel. Cycle, Vol. NS-18 Number 3, June 1971.
2) D.M.Evans, et al, Bevatron Guide Field Control, Vol. NS-18 Number 3, June 1971.
3) R.A.Byrns, J.T.Tanabe, The Bevatron Cryopump, Vol. NS-20 Number 3, June 1973.
4) K.C.Crebbin et al, First Phase of Heavy Ion Acceleration at the Bevatron, Vol. NS-20 Number 3, June 1973.

NAME OF MACHINE 200/500 GeV Synchrotron
INSTITUTION National Accelerator Lab.
LOCATION Batavia, Illinois U. S. A.

PERSON IN CHARGE P. J. Reardon
DATA SUPPLIED BY F. T. Cole/H. L. Allen
DATE March 1. 1974

HISTORY AND STATUS

CONSTRUCTION STARTED (date) 1969
FIRST BEAM OBTAINED, OR GOAL (date) March 1, 1972
TOTAL COST OF FACILITY $230M
FUNDED BY USAEC
TOTAL ACCELERATOR STAFF (now) 275
ANNUAL OPERATING BUDGET

ACCELERATOR PARAMETERS

Physical Dimensions (Mean)

RING DIAM. 2000 m; Tunnel sect. 3.05 2.44 m
MAGNET 0.64x0.35 m; Mag. Gap 13 x 5.2 cm
"DONUT" 12.7 x 5.2 cm; Aperture 12.5 x cm

Injector System

TYPE 8-GeV Booster
OUTPUT (max) 350 at 8-GeV
BEAM EMITTANCE 3π mm-mrad
INJECTION PERIOD twelve 1.6 μsec pulses in 0.8 sec. μsec, or turns
INFLECTOR TYPE Electromagnetic

Magnet System

FOCUSING TYPE AG field index, n = sep fn
No. MAG. UNITS 1014 Length (ea) 6.1 m
STRAIGHT SECT. 50.9 Total S.S. Length 305.4 m
FOCUSING ORDER Q OBBBB Q OBBBB(FODO)
BETATRON OSC. FREQ. ν_H F 19.25 ν_V D 19.25 (300 GeV)
FIELD. AT INJ. 396 G, at max 13.5 kG
RISE TIME 2.4 sec; Flat-top time 1 sec
MAG. WEIGHT (tons) Fe 8000 Cu 850
POWER INPUT (MW) PEAK 60 MEAN 36

Acceleration System

HARMONIC NO. 1113 No. Cavities 15
RF RANGE 53.08 53.10 MHz
ORBIT FREQ. 0.04769 to 0.04771
ENERGY GAIN 2.6 MeV/turn
RADIATION LOSS keV/turn
RF POWER INPUT (kW) PEAK 1800

Other Relevant Parameters or Notable **Features**

ACCELERATOR PERFORMANCE

	Normal (or Goal)	Maximum Achieved
ENERGY (GeV)	300	400
RESOLUTION ΔE/E (%)	1/6	(1/12 at 400 G
REPET. RATE (pulse/sec)	1 sec	1/4 at 200 Ge 1 sec at 300 G
PULSE WIDTH	16%	25% a
DUTY FACTOR, macroscopic (%)	5 x 10^{12}	7 x 1(at 300 GeV
INTERNAL BEAM (part/pulse)		
(part/sec)		
CURRENT (mA)	0.	1.0
BEAM EMITTANCE (mn-mrad)	0.1π	0.1π

SCHEDULED OPERATION (hr/wk) 140 (overall average)
"ON BEAM" 60 % OF SCHEDULED TIME

Some Typical External and Secondary Beams

PARTICLE	FLUX (part/sec)	(cm²)	(GeV)	(%)
π, K	10^7 @ 150	1	to 200	0.1 - 2.1
π, K	10^7 @ 100	1	to 200	0.014 - 1.0
n	10^8/cm²	up	to 300	
K^o	10^6/c			
ν	10^6/m²	up	to 200	5
μ	10^6 @ 150	1	to 150	2
p	Extracted	1	0 - 400	

* Approx. flux 10^{13} interacting protons @ 300 GeV

TOTAL EXPERIMENTAL AREA 10,500 m²
BEAM LINES TO 6 Primary Targets plus 2 Internal Target Stations
STATIONS SERVED AT SAME TIME 7
BEAM SEPARATORS 0 SPECTROMETERS

ON-LINE COMPUTERS WITH Inputs
BUBBLE CHAMBERS, in-house 2 Users n
TOTAL POWER INSTALLED FOR RESEARCH 35
No. USER GROUPS: in-house 15 outside 100
TOTAL RESEARCH STAFF, in-house 120
ANNUAL RESEARCH BUDGET, in-house $5M

RECENT IMPROVEMENTS OR MODIFICATIONS TO MACHINE

Published **Articles Describing Machine**

1. Operating results from NAL, D. E. Young, National Accelerator Conference, IEEE Transactions NS-203, **p.** 191, (1973).

NAME OF MACHINE Booster Synchrotron — PERSON IN CHARGE P. J. Reardon
INSTITUTION National Accelerator Lab. — DATA SUPPLIED BY E. L. Hubbard
LOCATION Batavia, Illinois, U.S.A. — DATE March 1, 1974

HISTORY AND STATUS

CONSTRUCTION STARTED (date) 1969
FIRST BEAM OBTAINED, OR GOAL (date) 1971
TOTAL COST OF FACILITY $17,000,000
FUNDED BY USAEC
TOTAL ACCELERATOR STAFF (now) (Part of NAL
ANNUAL OPERATING BUDGET Accelerator Div.)

ACCELERATOR PARAMETERS

Physical Dimensions (Mean)
RING DIAM. 151 m; Tunnel sect. 3.0 2.4 m
MAGNET 46 x 33 m; Mag. Gap 15.2 x 5.7 cm
"DONUT" none cm; Aperture 16.5 x 4.2 cm

Injector System
TYPE Linear Accelerator
OUTPUT (max) 80 mA at 203 MeV
BEAM EMITTANCE 10π mn-mrad
INJECTION PERIOD 8 μsec, or 3 turns
INFLECTOR TYPE Wire Septum

Magnet System
FOCUSING TYPE Alternating Gradient
No. MAG. UNITS 96 Length (ea) 3.04 m
STRAIGHT SECT. 24 Total S.S. Length 144 m
FOCUSING ORDER FOFDOOD
BETATRON OSC. FREQ. ν_H 6.72 ν_V 6.78
FIELD, AT INJ. 490 G, at max 6.7 kG
RISE TIME .033 sec; Flat-top time none sec
MAG. WEIGHT (tons) Fe 250, Cu 36
POWER INPUT (MW) PEAK 1.8 MEAN 1.3

Acceleration System
HARMONIC No. 84 No. Cavities 16
RF RANGE 30.3 52.8 MHz
ORBIT FREQ. 0.36 0.63 k Hz
ENERGY GAIN 600 keV/turn max
RADIATION LOSS keV/turn
RF POWER INPUT (kW) PEAK 880

Ocher Rekvant Parameters or Notable Features

ACCELERATOR PERFORMANCE

	Normal (or Goal)	Maximum Achieved
ENERGY (GeV)	8	8
RESOLUTION ΔE/E (%)	0.1	
REPET. RATE (pulse/sec)	15	15
PULSE WIDTH (μsec)	1.6	1.6
DUTY FACTOR, macroscopic (%)		
INTERNAL BEAM (part/pulse)	(4 x 10^{12})	1 x 10^{12}
Part/main-ring cycle	(5 x 10^{13}	1 x 10^{13}
CURRENT (mA)	380	100
BEAM EMITTANCE (mn-mrad)	6.5π	
SCHEDULED OPERATION (hr/wk)	164	164

"ON BEAM" 95 % OF SCHEDULED TIME

Some Typical External and Secondary Beams

PARTICLE	FLUX	BEAM AREA (cm²)	ENERGY (GeV)	AEIE (%)
p	1 x 10^{13}	0.3	8	

(Particles/main-ring cycle - main-ring cycle time varies from 3 to 12 sec.)

RESEARCH PROGRAM

TOTAL EXPERIMENTAL AREA none m²
BEAM LINES TO Stations
STATIONS SERVED AT SAME TIME
BEAM SEPARATORS SPECTROMETERS
ON-LINE COMPUTERS WITH Inputs
BUBBLE CHAMBERS, in-house Users'
TOTAL POWER INSTALLED FOR RESEARCH MW
No. USER GROUPS: in-house outside
TOTAL RESEARCH STAFF, in-house outside
ANNUAL RESEARCH BUDGET, in-house
SCHEDULED RESEARCH TIME, hours/week

RECENT IMPROVEMENTS OR MODIFICATIONS TO MACHINE

Published Artkles Describing Machine

1. Booster Synchrotron, E. L. Hubbard, ed., National Accelerator Lab. Report **TM-405 (1973)**

2. The NAL Booster Synchrotron Magnet Power Supply Servo, A. R. Donaldson and R. A. Winje, National Accelerator Conference, IEEE Transactions NS-20, 3, **p. 409, (1973)**

3. Synchronous Transfer **of** Beam from the NAL Fast Cycling Booster Synchrotron to the NAL Main Ring System, **J.** A. Dinkel, J. E. Griffin, E. L. Hubbard, R. E. Peters, and L. C. Teng. National Accelerator Conference, IEEE Transactions NS-20, 3, p. 409, (1973)

76-GeV IHEP

NAME OF MACHINE Proton Synchrotron — PERSON IN CHARGE Yu.M.Ado

INSTITUTION Institute of High Energy Ph. — DATA SUPPLIED BY E.F.Trojanov

LOCATION Serpukhov, USSR — DATE February, 1974

HISTORY AND STATUS

CONSTRUCTION STARTED (date) 1962

FIRST BEAM OBTAINED, OR GOAL (date) October, 1967

TOTAL COST OF FACILITY —

FUNDED BY —

TOTAL ACCELERATOR STAFF (now) —

ANNUAL OPERATING BUDGET —

ACCELERATOR PARAMETERS

Physical Dimensions (Mean)

RING DIAM. 472 m; Tunnel sect. 6 × 8 m

MAGNET — × — m; Mag. Gap — × — cm

"DONUT" 195×11.5m; Aperture 17 × 11.5 cm

Injector System

TYPE Linac

OUTPUT (max) 120 mA at 100 Mev

BEAM EMITTANCE 10π (90%) (norm) mn-mrad

INJECTION PERIOD 36 μsec, or 3 turns

INFLECTOR TYPE electrostatic

Magnet System

FOCUSING TYPE AG Field Index n=443

No. MAG. UNITS 120 Length (ea) 72x10.4+48x9.3m

STRAIGHT SECT. 120 Total S.S. Length 287.5 m

FOCUSING ORDER F O D O

BETATRON OSC. FREQ. ν_x 9.80 ν_y 9.85

FIELD AT INJ. 76 G, at max 13 kG

RISE TIME 2.5 sec; Flat-top time 2 sec

MAG. WEIGHT (tons) Fe 20,000, Al 700

POWER INPUT (MW) PEAK 80 MEAN 15

Acceleration System

HARMONIC No. 30 No. Cavities 52

RF RANGE 2.6 to 6.1 MHz

ORBIT FREQ. 0.086 to 0.202 MHz

ENERGY GAIN 180 kev/turn

RADIATION LOSS — keV/turn

RF POWER INPUT (kW) PEAK 300 mean 80

Other Relevant Parameters or Notable Features

There are 12 superperiods and in each there are 2 long straight sections, each 4.86m long,

Published Articles Dercribing Machine

ACCELERATOR PERFORMANCE

	Normal (or Goal)	Maximum Achieved
ENERGY (GeV)	70	76
RESOLUTION ΔE/E (%)	0.03	—
REPET. RATE (pulse/sec)	1/8	—
PULSE WIDTH	—	2.0sec
DUTY FACTOR, macroscopic (%)	25	—
INTERNAL BEAM (part/pulse)	2.2×10^{12}	~~2.7×10^{12}~~
(part/sec)	2.7×10^{11}	~~3.4×10^{11}~~
CURRENT (mA)	—	—
BEAM EMITTANCE (mn-mrad)	1π	—
SCHEDULED OPERATION (hr/wk)	90(average for year)	

"ON BEAM" — % OF SCHEDULED TIME

Some **Typical External and Secondary Beams**

PARTICLE	FLUX (part/pulse)	BEAM AREA (cm²)	ENERGY (GeV)	AEIE (%)
π^-	10^4-10^6	4	30-65	1
$\pi^+ + p$	10^6	1	40-70	2
π^-	$>10^6$	1	20-50	1
e^-	10^4-10^6	4	20-45	2
K^+	5-10	—	17-40	0.25
$\bar{p}$	5-10^6	—	10-25	0.5
μ^-	$>10^6$	900	20-40	—

RESEARCH PROGRAM

TOTAL EXPERIMENTAL AREA 23,300 m²

BEAM LINES 13 Stations

STATIONS SERVED AT SAME TIME —

BEAM SEPARATORS 2 SPECTROMETERS 5

ON-LINE COMPUTERS WITH 5 Inputs

BUBBLE CHAMBERS, in-house — Users' 2

TOTAL POWER INSTALLED FOR RESEARCH 30 MW

No. USER GROUPS: in-house 6 outside 6

TOTAL RESEARCH STAFF, in-house-outside —

ANNUAL RESEARCH BUDGET, in-house —

SCHEDULED RESEARCH TIME, hours/week —

RECENT IMPROVEMENTS OR MODIFICATIONS TO MACHINE

Fast beam extraction system is operating on 3 directions.

There is neutral beam with intensity 10^6-107 ppp.

NAME OF MACHINE ITEP P.S.
INSTITUTION ITEP
LOCATION Moscow, USSR

PERSON IN CHARGE Goldin L.L.
DATA SUPPLIED BY Goldin L.L.
DATE February 1974

HISTORY AND STATUS

CONSTRUCTION STARTED (date) 1956 1961 1973*
FIRST BEAM OBTAINED. OR GOAL (date)
TOTAL COST OF FACILITY
FUNDED BY
TOTAL ACCELERATOR STAFF (now)
ANNUAL OPERATING BUDGET

ACCELERATOR PARAMETERS

Physical Dimensions (Mean)

RING DIAM. 80 m; Tunnel sect. ____ ____ m
MAGNET 2 x 2 m; Mag. Gap ____ x ____ cm
"DONUT" ____ x ____ cm; Aperture 11 x 8 cm

Injector System

TYPE Linear Accelerator
OUTPUT (max) 200mA at 24.6 MeV
BEAM EMITTANCE 60 nm-mrad
INJECTION PERIOD 4 μsec, or 1 turns
INFLECTOR TYPE lectrostatic

Magnet System

FOCUSING TYPE Strong
No. MAG. UNITS 96 Length (ea ... I,910 m
STRAIGHT SECT. 2.35 M Total S.S. Length 37.6 m
FOCUSING ORDER FODFODFDFDFD
BETATRON OSC. FREQ. ν_H 9.3 ν_V 9.
FIELD. AT INJ. 240 G, at max 12 kG
RISE TME 0.8 sec; Flat-top time 0.3 sec
MAG. WEIGHT (tons) Fe 3000, Cu 500
POWER INPUT (MW) PEAK ____ MEAN 3.5 MWT

Acceleration System

HARMONIC No. ____ No. Cavities 5
RF RANGE 1.09 - 4.77 Mt
ORBIT FREQ. 0.252 - 1.19
ENERGY GAIN 15 KeV
RADIATION LOSS ____ keV/ rn
RF POWER INPUT (kW) PEAK 12-KW/cavity

Other Rekvant **Parameters or Notable Features**

ACCELERATOR PERFORMANCE **

	Normal (or Goal)	Maximum Achieved
ENERGY (GeV)	10	10.4
RESOLUTION ΔE/E (%)		
REPET. RATE (pulse/sec)		
PULSE WIDTH		
DUTY FACTOR, macroscopic (%)		
INTERNAL BEAM (part/pulse)		
(part/sec)		
CURRENT (mA)		
BEAM EMITTANCE (nm-mrad)		
SCHEDULED OPERATION (hr/wk)		

"ON BEAM" ____ % OF SCHEDULED TIME

Some Typical External a d Secondary Beams

PARTICLE	FLUX (part/sec)	BEAM AREA (cm^2)	ENERGY (GeV)	AEIE (%)

RESEARCH PROGRAM

TOTAL EXPERIMENTAL AREA 7000 m^2
BEAM LINES TO ____ Stations
STATIONS SERVED AT SAME TIME ____
BEAM SEPARATORS ____ SPECTROMETERS ____
ON-LINE COMPUTERS WITH ____ Inputs
BUBBLE CHAMBERS, in-house ____ Users' ____
TOTAL POWER INSTALLED FOR RESEARCH ____ MW
No. USER GROUPS: in-house ____ outside ____
TOTAL RESEARCH STAFF, in-house ____ outside ____
ANNUAL RESEARCH BUDGET, in-house ____
SCHEDULED RESEARCH TIME, hours/week ____

RECENT IMPROVEMENTS OR MODIFICATIONS TO MACHINE

* After reconstruction
** The accelerator is in tne course of ajustement after reconstruction.

Published Artkles Describing Machine

NAME OF MACHINE 10 GeV proton Synchrophazotron — PERSON IN CHARGE A.M.Baldin
INSTITUTION Joint Inst.for Nucl. Research — DATA SUPPLIED BY I.N.Semenyushkin
LOCATION Dubna, USSR — DATE July 1971

HISTORY AND STATUS

CONSTRUCTION STARTED (date) I952 ~~I957~~
FIRST BEAM OBTAINED, OR GOAL (date)
TOTAL COST OF FACILITY
FUNDED BY
TOTAL ACCELERATOR STAFF (now)
ANNUAL OPERATING BUDGET

ACCELERATOR PARAMETERS

Physical Dimensions (Mean)
RING DIAM. 72 m; Tunnel sect. ____ ____ m
MAGNET 7.553 m; Mag. Gap 40 × 200 cm
"DONUT" ____ × ____ cm; Aperture 35 × I20 cm

Injector System
TYPE Linac
OUTPUT (max) I.0 at 9.4
BEAM EMITTANCE Π IO mm-mrad
INJECTION PERIOD 350 usec, or 50 turns
INFLECTOR TYPE electrostatic

Magnet System
FOCUSING TYPE weak field Index, n=0.66
No. MAG. UNITS 40 Length (ea) 3.7 m
STRAIGHT SECT. 4 Total S.S. Length 32 m
FOCUSING ORDER
BETATRON OSC. FREQ. ν_H 0.626 ν_V 0.892
FIELD, AT INJ. I50 G, at max I2.(kG
RISE TIME 3.0 sec; Flat-top time me 0.[
MAG. WEIGHT (tons) Fe 36000, Cu 2.700
POWER INPUT (MW) PEAK I40 MEAN I3

Acceleration System
HARMONIC NO. I No. Cavitie I
RF QANGE. 0.2 to • MHz
ORBIT FREQ. 0.2 to I.45
ENERGY GAIN 2.4
RADIATION LOSS ____ keV/turn
RF POWER INPUT (kW) PEAK 500 I50

Other Relevant Parameters or Notable Features

Published Articles Dercribing Machine

ACCELERATOR PERFORMANCE

	Normal (or Goal)	Maximum / Achieved
ENERGY (GeV)	IO	
RESOLUTION AEIE (%)	0.08	Achieved 0.II
REPET. RATE (pulse/sec)		0.5
PULSE WIDTH		
DUTY FACTOR, macroscopic (%)	IO	
INTERNAL BEAM (part/pulse)	x10^9 I.0	I2
(part/sec)	x10^9 I.0	I5
CURRENT (mA)	T5Π	v) 80Π (H)
BEAM EMITTANCE (mn-mrad)		
SCHEDULED OPERATION (hr/wk)		I20

"ON BEAM" 90 % OF SCHEDULED TIME

Some Typical External and Secondary Beams

PARTICLE	FLUX (part/sec)	BEAM AREA (cm^2)	ENERGY (GeV)	ΔE/E (%)
Π⁻	~10^4	5	2-7	±I
Π⁺	~10^3	5	2-5	±I
Sep. K,p				
Π⁺ n			I-5	+2

RESEARCH PROGRAM

TOTAL EXPERIMENTAL AREA 2700 m^2
BEAM LINES TO ____ Stations
STATIONS SERVED AT SAME TIME 3
BEAM SEPARATORS ____ SPECTROMETERS ____
ON-LINE COMPUTERS WITH ____ Inputs
BUBBLE CHAMBERS, in-house I Users' 26 I
TOTAL POWER INSTALLED FOR RESEARCH
No. USER GROUPS: in-house-outside
TOTAL RESEARCH STAFF, in-house ____ outside
ANNUAL RESEARCH BUDGET, In-house
SCHEDULED RESEARCH TIME, hours/week

RECENT IMPROVEMENTS OR MODIFICATIONS TO MACHM

acceleration of deuterons up to IO GeV I=IO pulse, He^2_4 up to 20 BeV I=10^7 ~/p

Slowly extraction of beem from synchrophazotron (τ =400 msec, efficiency 94%;)

NAME OF MACHINE: 1 GeV Model of Cybernetic Accelerator
INSTITUTION: Radiotech.Inst.of Ac.Sci
LOCATION: Moscow, USSR
PERSON IN CHARGE: G.I.Batskikh
DATA SUPPLIED BY: G.I.Batskikh
DATE:

HISTORY AND STATUS

CONSTRUCTION STARTED (date): 1961
FIRST BEAM OBTAINED, OR GOAL (date): 1967
TOTAL COST OF FACILITY:
FUNDED BY:
TOTAL ACCELERATOR STAFF (now): 12 p.
ANNUAL OPERATING BUDGET:

ACCELERATOR PARAMETERS

Physical Dimensions (Mean)

RING DIAM. 12 m; Tunnel sect. ____ ____ m
MAGNET ____ x ____ m; Mag. Gap ____ x ____ cm
"DONUT" ____ x ____ cm; Aperture 1,6 x 2,2 cm

Injector System

TYPE: Van de Graaf
OUTPUT (max) 5 mA at 1.0 MeV
BEAM EMITTANCE 10 π mn-mrad
INJECTION PERIOD ____ μsec, or 1 turns
INFLECTOR TYPE: electrostatic

Magnet System

FOCUSING TYPE: strong n=191,3
No, MAG. UNITS 100 Length (ea) ____ m
STRAIGHT SECT. ____ Total S.S. Length ____ m
FOCUSING ORDER: FODO
BETATRON OSC. FREQ. ν_H 6,25 ν_V 6,25
FIELD, AT INJ. 250 G, at max 10 kG
RISE TIME 0,5 sec; Flat-top time ____ sec
MAG. WEIGHT (tons) Fe 12, Cu 4
POWER INPUT (MW) PEAK ____ MEAN 30 kW

Acceleration System

HARMONIC No. 5 No. Cavities 13
RF RANGE 1,25 to 25 MHz
ORBIT FREQ. 0,25 to 5,0 MHz
ENERGY GAIN max 2 kV
RADIATION LOSS ____ keV/turn
RF POWER INPUT (kW) PEAK ____ ____

Other Rekvant Parameters or Notable Features

ACCELERATOR PERFORMANCE

	Normal (or Goal)	Maximum Achieved
ENERGY (GeV)	1	1.0
RESOLUTION ΔE/E (%)		
REPET. RATE (pulse/sec)	0,5	
PULSE WIDTH	0,5 sec	
DUTY FACTOR, macroscopic (X)		
INTERNAL BEAM (part/pulse)	1 x 10^10	
(part/sec)		
CURRENT (mA)		
BEAM EMITTANCE (mn-mrad)		
SCHEDULED OPERATION (hr/wk)		

"ON BEAM" ____ % OF SCHEDULED TIME

Sane Typical External and Secondary Beams

PARTICLE	FLUX (part/sec)	BEAM AREA (cm^2)	ENERGY (GeV)	ΔE/E (%)

RESEARCH PROGRAM

TOTAL EXPERIMENTAL AREA ____ m^2
BEAM LINES TO ____ Stations
STATIONS SERVED AT SAME TIME ____
BEAM SEPARATORS ____ SPECTROMETERS ____
ON-LINE COMPUTERS WITH ____ Inputs
BUBBLE CHAMBERS. in-house ____ Users' ____
TOTAL POWER INSTALLED FOR RESEARCH ____ MW
No. USER GROUPS: in-house ____ outside ____
TOTAL RESEARCH STAFF, in-house ____ outside ____
ANNUAL RESEARCH BUDGET. in-house ____
SCHEDULED RESEARCH TIME, hours/week ____

RECENT IMPROVEMENTS OR MODIFICATIONS TO MACHINE

Published Artkks Describing Machine

NAME OF MACHINE Bonn 2.5 GeV Synchrotron
INSTITUTION Physikal. Institut d. Univ.
LOCATION D-53 Bonn, Nussallee 12

PERSON IN CHARGE G. Noldeke, W. Paul, K.H. Althoff, G. Knop,
DATA SUPPLIED BY D. Husmann
DATE 22.1.1974

HISTORY AND STATUS

CONSTRUCTION STARTED (date) April 1965
FIRST BEAM OBTAINED, OR GOAL (date) March 1967
TOTAL COST OF FACILITY DM 12.3 x 10^6
FUNDED BY Federal Rep. of Germany and State of Nordrhein-Westfalen
TOTAL ACCELERATOR STAFF (now) 19
ANNUAL OPERATING BUDGET 1.8 x 10^6

ACCELERATOR PARAMETERS

Physical Dimensions (Mean)
RING DIAM. 22.15 m; Tunnel sect. 2.2 x 4.1 m
MAGNET 695.74 m; Mag. Gap 6 x 20 cm
"DONUT 4.2 x 12.5 cm; Aperture 4 x ____ cm

Injector System
TYPE Linac
OUTPUT (max) 250 at 25
BEAM EMITTANCE 3 inn-mrad
INJECTION PERIOD 1 μsec, or 5 turns
INFLECTOR TYPE septum magnet

Magnet System
FOCUSING TYPE AG $n = +23.26$
No. MAG. UNITS 12 Length (ea) 4.005 m
STRAIGHT SECT. 12 Total S.S. Length 21.48 m
FOCUSING ORDER OFDO
BETATRON OSC. FREQ. ν_μ 3.4 ν_V 3.4
FIELD AT INJ. 110 G, at max 11 kG
RISE TIME 8.8 sec; Flat-top time ____ sec
MAG. WEIGHT (tons) Fe 133, Cu 10
POWER INPUT (MW) PEAK .80 MEAN ____

Acceleration System
HARMONIC No. 116 No. Cavities 1 or 2
RF RANGE 499.67 MHz
ORBIT FREQ. 4.3074
ENERGY GAIN 330 keV/turn
RADIATION LOSS max. 325 keV/turn
RF POWER INPUT (kW) PEAK 80 mean 40

Other Rekvant Parameters or Notable Features

ACCELERATOR PERFORMANCE

	Normal (or Goal)	Maximum Achieved
ENERGY (GeV)	2.3	2.5
RESOLUTION AEIE (%)		0.5
REPET. RATE (pulse/sec)		50
PULSE WIDTH	max.	1 msec
DUTY FACTOR, macroscopic (%)	max.	5
INTERNAL BEAM (part/pulse)		4×10^{10}
(part/sec)		2×10^{12}
CURRENT (mA)		0.32 μA
BEAM EMITTANCE (inn-mrad)		1
SCHEDULED OPERATION (hr/wk)		150

"ON BEAM" 85 % OF SCHEDULED TIME

Some Typical External and Secondary Beams

PARTICLE	FLUX (part/sec)	BEAM AREA (cm^2)	ENERGY (GeV)	AEIE (%)
e^-	10^{12}	0.1	.5 - 2.3	.5
γ	5×10^{11}	eff. qu.	at 2.1 GeV	

RESEARCH **PROGRAM**
TOTAL EXPERIMENTAL AREA 1100 m^2
BEAM LINES TO 6 Stations
STATIONS SERVED AT SAME TIME 2
BEAM SEPARATORS - SPECTROMETERS ____
ON-LINE COMPUTERS XDS 2 with 7 Inputs (total)
BUBBLE CHAMBERS, in-house - Users' -
TOTAL POWER INSTALLED FOR RESEARCH 1.2 MW
No. USER GROUPS: in-house 8 outside 4
TOTAL RESEARCH STAFF, in-house x outside 5
ANNUAL RESEARCH BUDGET, in-house 2.5 x 10^6
SCHEDULED RESEARCH TIME, hours/week 150

RECENT IMPROVEMENTS OR MODIFICATIONS TO MACHINE

Ejection of electrons up to 2.3 GeV
On line computer with CAMAC interface

Published Articles Describing Machine

K.H. Althoff et al. : The 2.5 GeV Electron Synchrotron of the University of Bonn, Nuclear Instr. a. Meth. 61 (1968), 1 - 30

NAME OF MACHINE DESY

INSTITUTION Deutsches Elektronen-Synchrotron

LOCATION Hamburg, Germany

PERSON IN CHARGE H. Schopper

DATA SUPPLIED BY H. Kumpfert

DATE January 1974

HISTORY AND STATUS

CONSTRUCTION STARTED (date) 1959

FIRST BEAM OBTAINED, OR GOAL (date) February 1964

TOTAL COST OF FACILITY 110 MDM (orig.constr.costs)

FUNDED BY Federal Government, City of Hamburg

TOTAL ACCELERATOR STAFF (now) 80

ANNUAL OPERATING BUDGET 6 MDM

ACCELERATOR PARAMETERS

Physical Dimensions (Mean)

RING DIAM. 100.84 m; Tunnel sect. 3.7 x 8.8 m

MAGNET 0.77 x 0.69 m; Mag. Gap 5.6(8.8) x 14.4 (9.0) cm

"DONUT" ___ x ___ cm; Aperture 3.8(7.0) x 20(10.0) cm

Injector System

TYPE Electron/Positron* Linacs**

OUTPUT (max) 200 mA(e^-) at 300 - 500 MeV

BEAM EMITTANCE 2 π mm-mrad

INJECTION PERIOD 1 μsec, or 1 turns

INFLECTOR TYPE septum + fast kicker magnet

Magnet System

FOCUSING TYPE AG Field Index n 69.51 (F) 70.16 (D)

No. MAG. UNITS 48 Length (ea) 4.15 m

STRAIGHT SECT. 48 Total S.S. Length 117.6 m

FOCUSING ORDER FODO

BETATRON OSC. FREQ. ν_y 6.29 ν_x 6.23

FIELD AT INJ. 315(42) G, at max 7.9 kG

RISE TIME 9×10^{-3} sec; Flat-top time max. 3.1×10^{-3} sec

MAG. WEIGHT (tons) Fe 570, Cu 77

POWER INPUT (MW) PEAK ___ MEAN 1.7

Acceleration System

HARMONIC No. 528 No. Cavities 16

RF RANGE 499.666 to 499.645 MHz

ORBIT FREQ. 0.9463

ENERGY GAIN max. 1250 keV/turn

RADIATION LOSS max. 8830 keV/turn

RF POWER INPUT (kW) PEAK 1000 mean 700

Other Relevant Parameters or Notable Features

"Positron Data: 1.6 mA ($|\frac{\Delta E}{E}| \leq \frac{1}{2}$ %) at 380 MeV

**The old 40 MeV-Electron Linac (140 mA max.) is still in use

Published Articles Describing Machine

Die Atomwirtschaft. July 1964

Proc. 1973 US Particle Accelerator Conference, San Francisco, (Improvements)

DESY Annual Reports

ACCELERATOR PERFORMANCE

	Normal (or Goal)	Maximum Achieved
ENERGY (GeV)	7.4	7.5
RESOLUTION ΔE/E (X)	± 0.25	± 0.25
REPET. RATE (pulse/sec)	50	50
PULSE WIDTH	3.1	3.1
DUTY FACTOR, macroscopic (%)	15.4	15.4
INTERNAL BEAU (part/pulse)	$4 \times 10^{**}$	5×10^{11}
(part/sec)	2×10^{13}	2.5×10^{13}
average CURRENT (mA)	64	80
BEAM EMITTANCE (mm-mrad)		
SCHEDULED OPERATION (hr/wk)	168	

"ON BEAM" 90 - 95 % OF SCHEDULED TIME

Some Typical External and Secondary Beams

PARTICLE	FLUX (part/sec)	BEAM AREA (cm^2)	ENERGY (GeV)	ΔE/E (%)
2 x e^-	5×10^{12}		1-7.25	± 0.25
	$\varepsilon_z \approx 0.1\pi$ xmmxmrad			
or	$\varepsilon_x \approx 0.5\pi$ xmmxmrad			
	50 % < η < 85 %			
2 x e+	10^{11}		1-7.25	± 0.25
3 x γ				
3 x converted γ (test beams)				
2 x Synchrotron Radiation				

RESEARCH PROGRAM

TOTAL EXPERIMENTAL AREA 6400

BEAM LINES TO 17 Stations

STATIONS SERVED AT SAME TIME 6 x e^- or γ + test & synchr. rad. beams

BEAM SEPARATORS ___ SPECTROMETERS 11

ON-LINE COMPUTERS WITH 20 Inputs

BUBBLE CHAMBERS: in-house ___ Users' ___

TOTAL POWER INSTALLED FOR RESEARCH 23 MW

No. USER GROUPS: in-house: 3 outside: 2 mixed: 9

TOTAL RESEARCH STAFF: ~~in-house~~ ~~outside~~ 275

ANNUAL RESEARCH BUDGET: in-house 7.5 MDM

SCHEDULED RESEARCH TIME, hours/week 136

RECENT IMPROVEMENTS OR MODIFICATIONS TO MA —

- flat top operation (duty factor 15.4 %)
- 2 e^+/e^- beams (fast extraction) for DORIS
- max. circulating currents (e^-) up to 80 mA average as compared to 30 mA
- e^+ beams (slow extraction) for use in normal e- experimental areas
- additional p^+-acceleration capability expected for 1915

NAME OF MACHINE Electron Synchrotron
INSTITUTION Laboratori Naz.dl CNEN
LOCATION Frascati - Italy

PERSON IN CHARGE Ubaldo Bizzarri
DATA SUPPLIED BY " "
DATE Febrmary 1974.

HISTORY AND STATUS

CONSTRUCTION STARTED (date) January 1956
FIRST BEAM OBTAINED, OR GOAL (date) Feb.9, 1959
TOTAL COST OF FACILITY $ 2.0 M
FUNDED BY CNEN
TOTAL ACCELERATOR STAFF (now) 30
ANNUAL OPERATING BUDGET 150.000

ACCELERATOR PARAMETERS

Physical Dimensions (Mean)
RING DIAM. 8.74 m; Tunnel sect. _____ _____ m
MAGNET 096x08 m; Mag. Gap 8.6 x 23 cm
"DONUT" 7.7x21 cm² Aperture 5.7 x 19.2 cm

Injector System
TYPE Microtron
OUTPUT (max) 30 at 12 4
BEAM EMITTANCE H:8 mn-mrad
INJECTION PERIOD 2 μsec, or 100 *turns*
INFLECTOR TYPE Electrostatic

Magnet System
FOCUSING TYPE weak FIELD INDEX 0.61
No. MAG. UNITS 4 Length (ea) 5.65 m
STRAIGHT SECT. 4 Total S.S. Length 27.4 m
FOCUSING ORDER _____
BETATRON OSC. FREQ. ν_H _____ ν_V _____
FIELD, AT INJ. 110 G. at max 10.2
RISE TIME 23 sec; Flat-top time _____ sec
MAG. WEIGHT (tons) Fe 100, Cu 10.
POWER INPUT (MW) PEAK _____ MEAN 0.150

Accelerator System Magnet supply LC Resonant

HARMONIC No. 4 No. Cavities 1
Rf RANGE 43.7 MHz
10.9
ORBIT FREQ.
ENERGY GAIN ~4
RADIATION LOSS- max-25 keV/turn
RF POWER INPUT (kW) PEAK 10 MEAN 4

Other Relevant Parameters or Notable Features

ACCELERATOR PERFORMANCE

	Normal (or Goal)	Maximum Achieved
ENERGY (GeV)		1.1
RESOLUTION ΔE/E (%)		0.1
REPET. RATE (pulse/sec)		20
PULSE WIDTH		4 msec
DUTY FACTOR, macroscopic (%)		8
INTERNAL BEAM (part/pulse)		2 ± 5.10^{10}
(part/sec)		4 ± 10.10^{11}
CURRENT (mA)		
BEAM EMITTANCE (mm-mrad)		20H 4V
SCHEDULED OPERATION (hr/wk)		141

Extracted bean
"ON BEAM" 75% % OF SCHEDULED TIME

Some Typical External and Secondary Beams

PARTICLE	FLUX (part/sec)	BEAM AREA (cm²)	ENERGY (GeV)	ΔE/E (%)
e⁻	2.10^{11}		0.5±1	<0.5
γ	$1.3.10^{11}$	Qeq	0.4±1	
γ	$0.5.10^{11}$	Qeq	1	
*				

* 30-50% polarized

RESEARCH PROGRAM

TOTAL EXPERIMENTAL AREA _____ m²
BEAM LINES TO 5 Stations
STATIONS SERVED AT SAME TIME 1
BEAM SEPARATORS _____ SPECTROMETERS 1
BEAM SEPARATORS _____ _____ Inputs
ON-LINE COMPUTERS YES
BUBBLE CHAMBERS, in-house 2 Users' _____
TOTAL POWER INSTALLED FOR RESEARCH 2.5 MW
No USER GROUPS. in-house 3 outside 7
TOTAL RESEARCH STAFF, in-house 18 outside 44
ANNUAL RESEARCH BUDGET, in-house _____
SCHEDULED RESEARCH TIME, hours/week 141

RECENT IMPROVEMENTS OR MODIFICATIONS TO MACHINE

Published Articles Describing Machine

- Proc . 2nd UN Conf. Peaceful Uses Atomic Energy Geneva 1958, Paper 15/8/1374, UN, NEw York (1958)
- Nuovo Cimento Suppl. 3, 324 (1959)
- Nuovo Cimento Suppl. 24 (1962)
- Lettese al Nuovo Cimento Vol. 1, 16, 820 (1969)
- Frascati Reports (available on request)

NAME OF MACHINE 1.3 GeV Electron Synchrotron PERSON IN CHARGE K. Huke
INSTITUTION Inst.for Nuclear Study, Univ. DATA SUPPLIED BY K. Huke
LOCATION Tanashi, Tokyo, Japan of Tokyo DATE February 1974

HISTORY AND STATUS

CONSTRUCTION STARTED (date) 1957 January
FIRST BEAM OBTAINED. OR GOAL (date) 1961 (750 MeV)
TDTAL COST OF FACILITY ~ $2M*
FUNDED BY Japanese Government
TOTAL ACCELERATOR STAFF (now) 14
ANNUAL OPERATING BUDGET ~ $ 0.1M*
*(salaries not included)

ACCELERATOR PARAMETERS

Physical Dimensions (Mean)
RING DIAM. 10.9 m; Tunnel sect. 2.8 × (dia)14 m
MAGNET 0.7 x 0.53 m; Mag. Gap 5.4 × 15 cm
"DONUT 4.5 x 15 cm; Aperture 3.5 × 11 cm

Injector System
TYPE Linac
OUTPUT (max) 100 mA at inflector 9 MeV
BEAM EMITTANCE 8 mn-mrad
INJECTION PERIOD 1 μsec, or 10 turns
INFLECTOR TYPE Electro-static plate and pulsed magnets for multi-turn.

Magnet System
FOCUSING TYPE AG
No. MAG. UNITS 8 Length (ea) 3.14 m
STRAIGHT SECT. 8 Total S.S. Length 9.60 m
FOCUSING ORDER 1/2 O, 1/2 D,F, 1/2 D, 1/2 O
BETATRON OSC. FREQ. ν_H ~ 2.25 ν_V ~ 2.25
FIELD, AT INJ. 80 G, at max 11 kG
RISE TIME 20~19 msec; Flat-top time --- sec
MAG. WEIGHT (tons) Fe 53, Cu 79
POWER INPUT (MW) PEAK stored MEAN 0.402
0.18 MJ

Acceleration System
HARMONIC No. 16 No. Cavities 1
RF RANGE ~ 138 fixed MHz
ORBIT FREQ. ~ 8.6
ENERGY GAIN peak 10
RADIATION LOSS 64 (max) keV/turn
RF POWER INPUT (kW) PEAK 20 MEAN 4 ~ 5

Other Relevant Parameters or Notable Features

ACCELERATOR PERFORMANCE

	Normal (or Goal)	Maximum Achieved
ENERGY (GeV)	1.3	1.3
RESOLUTION ΔE/E (X)	0.1	0.1
REPET. RATE (pulse/sec)	22.5	22.5
PULSE WIDTH	1.3	6(max)
DUTY FACTOR, macroscopic (%)	~ 5	10
INTERNAL BEAM (part/pulse) ×10^{10}	2	4 at 1 GeV
(part/sec) ×10^{11}	4	8 at 1 GeV
CURRENT (mA)	30	60
BEAM EMITTANCE (mn-mrad)	5	5
SCHEDULED OPERATION (hr/wk)	144	168

"ON BEAM" 95 % OF SCHEDULED TIME

Some Typical External and Secondary Beams

PARTICLE	FLUX (part/sec)	BEAM AREA (cm²)	ENERGY (GeV)	ΔE/E (%)
e^-	4×10^{11}	0.6×0.8	1	0.3
γ	$e\times10^{10}$	2.2	1.14	brems.
		(at 3.1 m from radiator)		
Soft X-ray				

RESEARCH PROGRAM

TOTAL EXPERIMENTAL AREA 1000 m²
BEAM LINES TO 3 (two γ, one e & γ) Stations
STATIONS SERVED AT SAME TIME max 2
BEAM SEPARATORS none SPECTROMETERS 4(25.18.5,6 tons)
ON-LINE COMPUTERS WITH 2 (TOSBAC 40) Inputs
BUBBLE CHAMBERS, in-house 0 Users' 1
TOTAL POWER INSTALLED FOR RESEARCH 0.45 MW
No, USER GROUPS: in-house 2 outside 5
TOTAL RESEARCH STAFF, in-house 16 outside 45
ANNUAL RESEARCH BUDGET, in-house ~ $ 0.05M*
SCHEOULED RESEARCH TIME, hours\week 132

RECENT IMPROVEMENTS OR MODIFICATIONS TO MACHINE

Epoxy-resin doughnuts were replaced by thin stainless steel bellows.
Add a fast extraction system to supply electrons to the 300 MeV storage ring.

Published Articles Describing Machine

1. H. Kumagai, et al., Japanese J. appl. Phys. 1 (1962) 66.
2. Annual Reports from 1960 to 1973, Institute for Nuclear Study, University of Tokyo.
3. K. Huke, et al., Japanese J. appl. Phys. 7 (1968) 1274.

NAME OF MACHINE Lund Electron Synchrotron
INSTITUTION Univ of Lund. Inst of Phys
LOCATION Lun Sweden

PERSON IN CHARGE Facility: Bengt Forkman Machine: Rune Alvinsson
DATA SUPPLIED BY Rune Alvinsson
DATE January 22, 1974

HISTORY AND STATUS

CONSTRUCTION STARTED (date) 1957
FIRST BEAM OBTAINED, OR GOAL (date) Dec. 1960
TOTAL COST OF FACILITY ~ $ 1 M excl. buildings
FUNDED BY Swedish Atom. Research Council
TOTAL ACCELERATOR STAFF (now) 8
ANNUAL OPERATING BUDGET ~ $ 30 000 excl. salaries

ACCELERATOR PARAMETERS

Physical Dimensions (Mean)

RING DIAM. 10.8 m; Tunnel sect. _____ _____ m
MAGNET 0.55x0.39 m; Mag. Gap 4.6 × 13.5 cm
"DONUT" 4 × 7 cm; Aperture 3.6 × 6.5 cm

Injector System

TYPE Microtron
OUTPUT (max) 75 mA at 10 MeV
BEAM EMITTANCE Hor. 20, vert. 50 mm-mrad
INJECTION PERIOD 5 μsec, or 40 turns
INFLECTOR TYPE Electrostatic

Magnet System

FOCUSING TYPE AG
No. MAG. UNITS 16 Length (ea) 1.4 m
STRAIGHT SECT. 16 Total S.S. Length 11.2 m
FOCUSING ORDER FOFDOD
BETATRON OSC. FREQ. ν_H 1.77 ν_V 1.77
FIELD, AT INJ. 100 G, at max. 11.0 kG
RISE TIME 0.04 sec; Flat-top time _____ sec
MAG. WEIGHT (tons) Fe 24, Cu 11.2
POWER INPUT (MW) PEAK _____ MEAN 0.185

Acceleration System

HARMONIC NO. 45 No. Cavities 2
RF RANGE. 399.10 MHz
ORBIT FREQ. 8.87 MHz
ENERGY GAIN max. 60
RADIATION LOSS max. 50 keV/turn
RF POWER INPUT (kW) PEAK 12 MEAN 3

Other Relevant Parameters or Notable Features

ACCELERATOR PERFORMANCE

	Normal (or Goal)	Maximum Achieved
ENERGY (GeV)	_____	1.2
RESOLUTION ΔE/E (%)	_____	_____
REPET. RATE (pulse/sec)	12.5	_____
PULSE WIDTH	_____	5 msec.
DUTY FACTOR, macroscopic (%)	_____	6
INTERNAL BEAM (part/pulse)	_____	2.4×10^{10} (0.8 GeV)
(part/sec)	_____	3×10^{11} (- " -)
CURRENT (mA)	_____	50 (- " -)
BEAM EMITTANCE (m-mrad)	_____	_____
SCHEDULED OPERATION (hr/wk)	120	_____

"ON BEAM" 85 - 90 % OF SCHEDULED TIME

Some Typical External and Secondary Beams

PARTICLE	FLUX (part/sec)	BEAM AREA (cm^2)	ENERGY (GeV)	ΔE/E (%)
bremsstr.				
synchr. light				

RESEARCH PROGRAM

TOTAL EXPERIMENTAL AREA 300 m^2
BEAM LINES TO 4 Stations
STATIONS SERVED AT SAME TIME 4
BEAM SEPARATORS _____ SPECTROMETERS ~
ON-LINE COMPUTERS WITH 2x16 bit digital inputs
BUBBLE CHAMBERS, in-house 1 Users' 0
TOTAL. POWER INSTALLED FOR RESEARCH 0.8 MW
No. USER GROUPS: in-house 3 outside _____
TOTAL RESEARCH STAFF, in-house x outside _____
ANNUAL RESEARCH BUDGET, in-house $ 25 000 excl. salaries
SCHEDULED RESEARCH TIME, hours/week 112

RECENT IMPROVEMENTS OR MODIFICATIONS TO MACHINE

Published Articles Describing Machine

Wernholm, O., Arkiv för Fysik 27, 527 (1964)

NAME OF MACHINE NINA
INSTITUTION DARESBURY LABORATORY
LOCATION DARESBURY, WARRINGTON, U.K.

PERSON IN CHARGE PROFESSOR A. ASHMORE
DATA SUPPLIED BY D. J. THOMPSON
DATE 21ST JANUARY, 1974

HISTORY AND STATUS

CONSTRUCTION STARTED (date) NOVEMBER, 1963
FIRST BEAM OBTAINED, OR GOAL (date) 2nd DECEMBER 1966
TOTAL COST OF FACILITY £4.5.10^6
FUNDED BY SCIENCE RESEARCH COUNCIL
TOTAL ACCELERATOR STAFF (now) 110 (inc. exp area)
ANNUAL OPERATING BUDGET £1.2 M

ACCELERATOR PARAMETERS

Physical Dimensions (Mean)

RING DIAM. 70 m; Tunnel sect. 6.7 x 5.8 m
MAGNET — x — m; Mag. Gap — x — cm
"DONUT" 17.3 x 5.0 m; Aperture 15.0 x 4.4 F cm
13.5 7.0 11.2 6.1 D

Injector System

TYPE IRIS LOADED WAVEGUIDE LINAC
OUTPUT (max) 500 at 43
BEAM EMITTANCE 3.2 mn-mrad
INJECTION PERIOD 0.73 μsec, or 1 turns
INFLECTOR TYPE PULSED MAGNETIC

Magnet System

FOCUSING TYPE AG
No. MAG. UNITS 40 Length (ea) 3.2625 m
STRAIGHT SECT. 3.5m Total S.S. Length 90 m
FOCUSING ORDER 1.0 m FODO
BETATRON OSC. FREQ. ν_H 5.21 ν_V 5.26
FIELD, AT INJ. 69 G, at max 7.45* kG
RISE TIME 9m sec; Flat-top time — sec
MAG. WEIGHT (tons) Fe 360, Cu 40
POWER INPUT (MW) PEAK — MEAN 0.95

Acceleration System

HARMONIC No. 300 NO. Cavities 5
RF RANGE 407.88 MHz
ORBIT FREQ. 1.76 MHz
ENERGY GAIN 470 (max.) keV/turn
RADIATION LOSS 270Q* keV/turn
RF POWER INPUT (kW) PEAK 480 Mean 150 (rating)

Other Rekvmt Parameters or Notable Features

ACCELERATOR PERFORMANCE

	Normal (or Goal)	Maximum Achieved
ENERGY (GeV)	1.0 to 5.0	5.2
RESOLUTION ΔE/E (%)	—	—
REPET. RATE (pulse/sec)	53	—
PULSE WIDTH	2 msec	~~3 msec~~
OUT-FACTOR, macroscopic (%)	7	11
INTERNAL BEAM (part/pulse)	8.10^{10}	$2.4.10^{11}$
(part/sec)	4.10^{12}	$1.2.10^{13}$
CURRENT (mA)	18	54
BEAM EMITTANCE (mn-mrad)	—	

SCHEDULED OPERATION (hr/wk) 168 hrs/wk 5 wks in 7
"ON BEAM" 82 % OF SCHEDULED TIME for research

Some Typical External and Secondary Beams

PARTICLE	FLUX (part/sec)	BEAM AREA (cm^2)	ENERGY (GeV)	AEIE (%)
Electron	2.10^{12}	0.6	1.0-5.0	—
Photon	3.10^{11}	4.0	0.8-5.0	—
Tagged Photon	10^6	1.0	0.25-4.5	

Two synchrotron radiation beams (λ_c = 0.94 Å*)

RESEARCH PROGRAM**

TOTAL EXPERIMENTAL AREA 3000 m^2
BEAM LINES TO 5 (inc. test beam) Stations
STATIONS SERVED AT SAME TIME 3 (inc. test beam)
BEAM SEPARATORS — SPECTROMETERS 5
ON-LINE COMPUTERS ~~MAIN~~ 6 ~~Inputs~~
BUBBLE CHAMBERS, in-house — Users' —
TOTAL POWER INSTALLED FOR RESEARCH 15 MW
No. USER GROUPS: in-house 2 outside 6
TOTAL RESEARCH STAFF, in-house 35 outside 88
ANNUAL RESEARCH BUDGET, in-house £2.2 M
SCHEDULED RESEARCH TIME, ~~hours/week~~ Year 5900 in 1973
00 in 1976

RECENT IMPROVEMENTS OR MODIFICATIONS TO MACHINE

Published Articles Describing Machine

A.W. MERRISON, CONTEMPORARY PHYS. 8, 4 (1967), p.373
DNPL Reports 1-6 and Annual Reports

* Refers to 5.0 GeV

** Excluding Synchrotron Radiation Facility

NAME OF MACHINE: Cornell 12 GeV Electron Synchrotron
INSTITUTION: Cornell University
LOCATION: Ithaca, N.Y.

PERSON IN CHARGE: Maury Tigner
DATA SUPPLIED BY: M. Tigner
DATE: January, 1974

HISTORY AND STATUS

CONSTRUCTION STARTED (date): April, 1965
FIRST BEAM OBTAINED, OR GOAL (date): May, 1967
TOTAL COST OF FACILITY: $11.5 M
FUNDED BY: National Science Foundat.
TOTAL ACCELERATOR STAFF (now): 45
ANNUAL OPERATING BUDGET: $1 M

ACCELERATOR PARAMETERS

Physical Dimensions (Mean)
RING DIAM. 250 m; Tunnel sect. 2 x 3 m
MAGNET 20 x .29 m; Mag. Gap 2.5/3.7 x 10 cm
"DONUT": none cm; Aperture 2.5 x 5.5 cm

Injector System
TYPE: Varian S-Band TW Linac
OUTPUT (max) 100 MA at 150 MeV
BEAM EMITTANCE .16 mn-mrad
INJECTION PERIOD 2.5 usec. or 1 turns
INFLECTOR TYPE: Pulse Magnetic

Magnet System
FOCUSING TYPE: Alternating Gradient
No. MAG. UNITS 192 Length (ea) 3.4 m
STRAIGHT SECT. 6 Total S.S. Length 48 m
FOCUSING ORDER: FDDF
BETATRON OSC. FREQ. ν_H 10.75 ν_V 10.75
FIELD, AT INJ. 50 G, at max kG
RISE TIME 8×10^{-3} sec; Flat-top time - sec
MAG. WEIGHT (tons) Fe 1800, Cu 25
POWER INPUT (MW) PEAK - MEAN 1

Acceleration System
HARMONIC No. 6
RF RANGE: fixed 714 MHz
ORBIT FREQ. 0.205 MHz
ENERGY GAIN 6 MeV/turn, Max.
RADIATION LOSS 1.8×10^{-4} keV/turn
RF POWER INPUT (kW) PEAK 1500

Other Relevant Parameters or Notable Features

ACCELERATOR PERFORMANCE

	Normal (or Goal)	Maximum Achieved
ENERGY (GeV)	12	12.2
RESOLUTION ΔE/E (%)	.5	.5
REPET. RATE (pulse/sec)	60	60
PULSE WIDTH	2×10^{-3} sec.	2×10^{-3} s
INTERNAL BEAM (part/pulse)	10^{11}	3×10^{10}
(part/sec)	6×10^{12}	1.8×10^{11}
DEAM EMITTANCE (mn-mrad)	-	-
SCHEDULED OPERATION (hr/wk)	144	144

"ON BEAM" 85 % OF SCHEDULED TIME

Some Typical External and Secondary Beams

PARTICLE	FLUX (part/sec)	BEAM AREA (cm^2)	ENERGY (GeV)	ΔE/E (%)
γ	10^{11}	1	12	-
ℓ	10^{12}	.5	12	

RESEARCH PROGRAM

TOTAL EXPERIMENTAL AREA 1400 m^2
BEAM LINES TO 5 Stations
STATIONS SERVED AT SAME TIME 2
BEAM SEPARATORS -; SPECTROMETERS 2
ON-LINE COMPUTERS WITH 2 Inputs
BUBBLE CHAMBERS, in-house none Users' none
TOTAL POWER INSTALLED FOR RESEARCH 3 MW
No. USER GROUPS in-house 4 outside 4
TOTAL RESEARCH STAFF, in-house 25 outside 20
ANNUAL RESEARCH BUDGET, in-house $1.8 M
SCHEDULED RESEARCH TIME, hours/week 135

RECENT IMPROVEMENTS OR MODIFICATIONS TO MACHINE

Published Articles Dercribing Machine

NAME OF MACHINE: Orsay Electron Linear Accelerator

INSTITUTION: Lab. Accelerateur Linéaire *

LOCATION: ORSAY (France)

PERSON IN CHARGE: P. BRUNET

DATA SUPPLIED BY: P. BRUNET

DATE: February 1974

HISTORY AND STATUS

CONSTRUCTION STARTED (date): 1956

FIRST BEAM OBTAINED, OR GOAL (date): 1959

TOTAL COST OF FACILITY: 10^8 F fr

FUNDED BY: National Ministry of Education

TOTAL ACCELERATOR STAFF (now): 50

ANNUAL OPERATING BUDGET: 1.5×10^6 F

ACCELERATOR PARAMETERS

Physical Dimensions

ACCELERATOR LENGTH: 360 m, DIAM.:

TUNNEL SIZE (L×H×W): m^3

Injection System

TYPE: Electron Buncher

OUTPUT: 1000 mA AT 12(1.5μs).20(0.02μs)MeV

BEAM EMITTANCE: 5 mm-mrad

INJECTION PERIOD: 1.5 μs 50 RF cycles

Acceleration System

No. SECTIONS: 1 + 38 length (ea): 6 m

FIELD MODE: π/2 FREQUENCY: 2999 MHz

GROUP VELOCITY: Tapered c; Phase Vel ~ 1.0 c

WAVE TYPE: TM-01 FILLING TIME: 0.7 and 0.9 μsec

SHUNT IMPEDANCE (MΩ/cm): 0.45

ATTENUATION (Np/m): 0.54 and 0.92 (total) to 2.7

IRIS, aperture: 1.8 cm, thickness: 3 mm

IRIS SPACING (cm): 2.5

10.150 and 11.800

POWER UNITS No.: 39 TYPE: Klystrons

POWER RATING (MW/unit): 25 and 20

FEED SPACING (m): 6

RF POWER DEMAND (MW) PEAK: 860 MEAN: 0.13

Focusing System

doublets and triplets

QUADRUPOLES, No.: 13 sets SPACING: 6 to 25 m

GRADIENTS: 11 T/m

Other Relevant Parameters or Notable Features

e^- → e+ converter after

16 sections e.g. ≃ 1.0 GeV

ACCELERATOR PERFORMANCE

	Normal (or Goal)	Maximum Achieved
electrons		
ENERGY (GeV)	2.3	2.1
ENERGY GAIN (MeV/m)	10	10
RESOLUTION ΔE/E (%)		
REPET. RATE (pulse/sec)	1.25 to 50	50
PULSE WIDTH (μs)	0.02&1.5	1.5
DUTY FACTOR, macroscopic (%)	10^{-4}&8.10^{-3}	8.10^{-3}
BEAM CURRENT (μA)	7.5	7.5
BEAM EMITTANCE (inn-mrad)	0.3	

positrons	ACO	DCI
ENERGY (GeV)	0.25	1.3
ENERGY GAIN (MeV/m)	10	10
RESOLUTION ΔE/E (%)	2	2
REPET. RATE (pulse/sec)	50	50
PULSE WIDTH (μs)	1.5	0.02
DUTY FACTOR, macroscopic (%)	8×10^{-3}	10^{-4}
BEAM CURRENT (μA)	2.5×10^{-2}	3×10^{-3}
BEAM EMITTANCE (inn-mrad)	6π	1.6π

Some Typical External and Secondary Berms

PARTICLE	FLUX (part/sec)	BEAM AREA (cm^2)	ENERGY (GeV)	ΔE/E (%)
e^-	1×10^{13}	0.2	1.8	1
e+	3×10^9	0.8	0.25	7 (ACO)

RESEARCH PROGRAM (Linac only)

TOTAL EXPERIMENTAL AREA: 250 m^2

BEAM LINES TO: 5 Stations

STATIONS SERVED AT SAME TIME: 2

BEAM SEPARATORS: 0 SPECTROMETERS: 1

ON-LINE COMPUTERS WITH: Inputs

BUBBLE CHAMBERS, in-house: outside:

TOTAL POWER INSTALLED FOR RESEARCH: MW

No. USER GROUPS, in-house: outside:

TOTAL RESEARCH STAFF, in-house: outside:

ANNUAL RESEARCH BUDGET, in-house:

SCHEDULED RESEARCH TIME, hours/week:

Published Articles Describing Machine

Onde Electrique (juillet 1969)

Recent or Planned Modifications to Machine

- Linac beams are not directly used for physics experiments any more, but only for injection in storage rings : ACO in 74, DCI and ACO in 75.
- The last experimental remaining room can handle a 500 MeV e^- or e^+ beam.

* Université PARIS-SED
Dependent on I.N.2.P.3 (Institut National de Physique Nucléaire et de Physique des Particules).

NAME OF MACHINE Mark III Electron Linear Accelerator
INSTITUTION High Energy Physics Lab.
LOCATION Stanford University, Stanford, Calif. 94305

PERSON IN CHARGE Professor R. Hofstadter
DATA SUPPLIED BY Professor M. [illegible] Yearian
DATE March 1974

HISTORY AND STATUS

CONSTRUCTION STARTED (date) 1949
FIRST BEAM OBTAINED, OR GOAL (date) 1953(280'); 1964(310')
TOTAL COST OF FACILITY $3.5 M (Accel. only)
FUNDED BY [illegible]6-69; ONR, AEC, AFOSR
TOTAL ACCELERATOR STAFF (now) See Note A
ANNUAL OPERATING BUDGET See Note A

ACCELERATOR PARAMETERS

Physical Dimensions

ACCELERATOR LENGTH 100 m, DIAM. 10 cm
TUNNEL SIZE (L×H×W) 150 m (variable H&W) m³

Injection System

TYPE Oxide cathode gun
OUTPUT 300 mA AT 80 keV MeV
BEAM EMITTANCE m-mrad
INJECTION PERIOD 1.5 μs RF cycles

Acceleration System

No. SECTIONS 31 length(ea) 3.0m
FIELD MODE 2π/3 FREQUENCY 2856 MHz
GROUP VELOCITY .01c; Phase Vel. 1.00 c
WAVE TYPE TM 01 FILLING TIME 0.83 μsec
SHUNT IMPEDANCE (MΩ/cm) 360
ATTENUATION (Np/m) 0.19
IRIS, aperture 1.9-2.6 cm, thickness 5.8 mm
IRIS SPACING (cm) 3.50
Q 13 500
POWER WITS, No. 31 TYPE Klystrons
POWER RATING (MW/unit) 20
FEED SPACING (m) 3
RF POWER DEMAND (MW) PEAK 600 MEAN 0.1

Focusing System

QUADRUPOLES, No. 4 pairs SPACING variable
GRADIENTS plus magnetic lenses

Other Relevant Parameters or Notable Features

Note A: Mark III in process of phasing out; staff and operating budget minimal.

*1969 - present - NSF

Published Articles Describing Machine

1. General Description: M. Ghodorow et al., Rev. Sci. Instr. 26, 134 (1955).

ACCELERATOR PERFORMANCE

	Normal (or Goal)	Maximum Achieved
electrons		
ENERGY (GeV)		1.2
ENERGY GAIN (MeV/m)		
RESOLUTION ΔE/E (%)		0.4 - 1.0
REPET. RATE (pulse/sec)		0.1 - 120
PULSE WIDTH		0.8 - 1.3 μsec
DUTY FACTOR, macroscopic (%)		1.6×10^{-2}
BEAM CURRENT (μA)		5
BEAM EMITTANCE (mm-mrad)		
positrons		
ENERGY (GeV)		1
ENERGY GAIN (MeV/m)		
RESOLUTION ΔE/E (%)		1
REPET. RATE (pulse/sec)		60
PULSE WIDTH		1 μsec
DUTY FACTOR, macroscopic (%)		0.6×10^{-2}
BEAM CURRENT (μA)		0.2×10^{-3}
BEAM EMITTANCE (mm-mrad)		

Some Typical External and Secondary Beams

PARTICLE	FLUX (part/sec)	BEAM AREA (cm²)	ENERGY (GeV)	ΔE/E (%)
e^-	3×10^{13}	0.3	1	0.1
e^+	10^9	0.3	0.8	0.5
γ	Depends on radiation thickness			

RESEARCH PROGRAM

TOTAL EXPERIMENTAL AREA 1760 m²
BEAM LINES TO 5 Stations
STATIONS SERVED AT SAME TIME 1
BEAM SEPARATORS None SPECTROMETERS 4
ON-LINE COMPUTERS WITH 3 Inputs
BUBBLE CHAMBERS, in-house None outside
TOTAL POWER INSTALLED FOR RESEARCH 3 MW
No. USER GROUPS, in-house outside
TOTAL RESEARCH STAFF, in-house outside
ANNUAL RESEARCH BUDGET, in-house
SCHEDULED RESEARCH TIME, hours/week
} See Note A

Recent or Planned Modifications to Machine

NAME OF MACHINE Superconducting Mark III Electron Linac
INSTITUTION High Energy Physics Lab.
LOCATION Stanford Univ., Stanford, Ca 94305
PERSON IN CHARGE Mason R. Yearian, Acting Director
DATA SUPPLIED BY R. E. Rand
DATE March 1074

HISTORY AND STATUS

CONSTRUCTION STARTED (date) 1969
FIRST BEAM OBTAINED, OR GOAL (date) 1976
TOTAL COST OF FACILITY $10 M
FUNDED BY ONR & NSF
TOTAL ACCELERATOR STAFF (now) 57 + 13 students
ANNUAL OPERATING BUDGET $ 1 M

ACCELERATOR PARAMETERS

Physical Dimensions
ACCELERATOR LENGTH 150 m, DIAM. Dewar 90 cm
TUNNEL SIZE (L×H×W) 180 x 4 x 4 m³

Injection System
TYPE Superconducting Buncher & Pre-accelerator
OUTPUT 0.1 mA AT 8 MeV
BEAM EMITTANCE 0.5π mm-mrad
INJECTION PERIOD CW μs RF cycles

Acceleration System
No. SECTIONS 8 length(ea) 6 m
FIELD MODE π 12 FREQUENCY 1300 MHz
GROUP VELOCITY 1 c; Phase Vel. 1 c
WAVE TYPE TM-01 FILLING TIME μsec
SHUNT IMPEDANCE (MΩ/cm)
ATTENUATION (Np/m)
IRIS, aperture cm, thickness mm
IRIS SPACING (cm)
Q 10^{10} - 10^{11}
POWER UNITS, No. 8 TYPE Klystron
POWER RATING (MW/unit) 0.015
FEED SPACING (m) 6
RF POWER DEMAND (MW) PEAK 0.36 MEAN 0.36

Focusing System
QUADRUPOLES, No. , SPACING
GRADIENTS

Other Relevant Parameters or Notable Features

Operating temperature = 1.85°K

ACCELERATOR PERFORMANCE

	Normal (or Goal)	Maximum Achieved
electrons		
ENERGY (GeV)	0.7 - 2	
ENERGY GAIN (MeV/m)	12.3	
RESOLUTION AEIE (%)	0.01	
REPET. RATE (pulse/sec)		
PULSE WIDTH		
DUTY FACTOR, macroscopic (%)	100	
BEAM CURRENT (μA)	100	
BEAM EMITTANCE (mn-mrad)	0.1	
positrons		
ENERGY (GeV)		
ENERGY GAIN (MeV/m)		
RESOLUTION ΔE/E (%)		
REPET. RATE (pulse/sec)		
PULSE WIDTH		
DUTY FACTOR, macroscopic (%)		
BEAM CURRENT (μA)		
BEAM EMITTANCE (mn-mrad)		

Some Typical External and Secondary Beams

PARTICLE	FLUX (part/sec)	BEAM AREA (cm²)	ENERGY (GeV)	AEIE (%)
e^-	10^{9}	0.05	2	0.01

RESEARCH PROGRAM

TOTAL EXPERIMENTAL AREA 3000 m²
BEAM LINES TO 5 Stations
STATIONS SERVED AT SAME TIME 1
BEAM SEPARATORS SPECTROMETERS 2
ON-LINE COMPUTERS WITH Inputs
BUBBLE CHAMBERS, in-house outside
TOTAL POWER INSTALLED FOR RESEARCH 6 MW
No. USER GROUPS, in-house outside
TOTAL RESEARCH STAFF, in-house outside
ANNUAL RESEARCH BUDGET, in-house
SCHEDULED RESEARCH TIME, hours/week

Published Articles Describing Machine

Suelzle, L. R., IEEE Trans., June 1971, to be published.

Recent or Planned Modifications to Machine